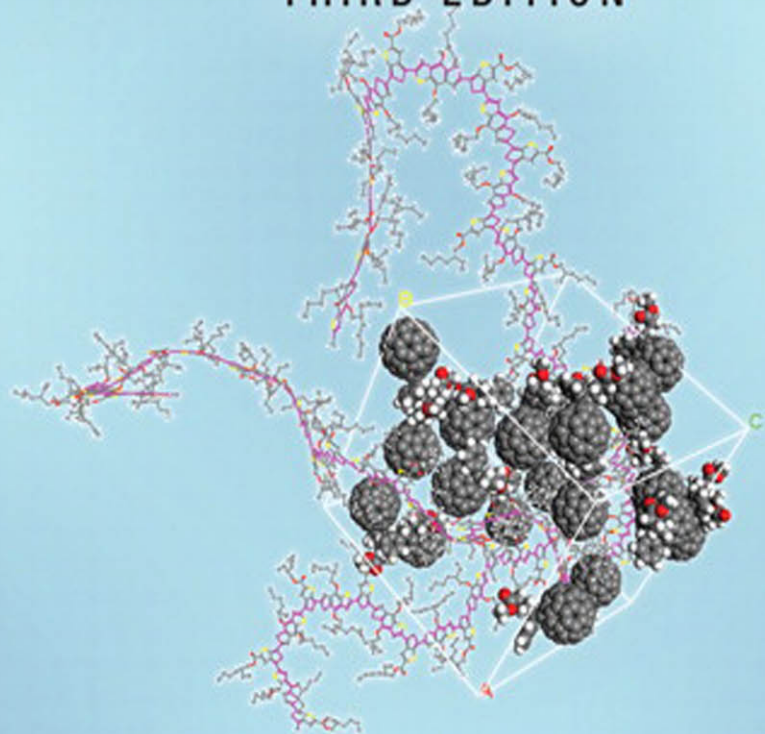


POLYMER SCIENCE & TECHNOLOGY

THIRD EDITION



JOEL R. FRIED

POLYMER SCIENCE AND TECHNOLOGY

Third Edition

This page intentionally left blank

POLYMER SCIENCE AND TECHNOLOGY

Third Edition

Joel R. Fried



PRENTICE
HALL

Upper Saddle River, NJ • Boston • Indianapolis • San Francisco
New York • Toronto • Montreal • London • Munich • Paris • Madrid
Capetown • Sydney • Tokyo • Singapore • Mexico City

Many of the designations used by manufacturers and sellers to distinguish their products are claimed as trademarks. Where those designations appear in this book, and the publisher was aware of a trademark claim, the designations have been printed with initial capital letters or in all capitals.

The author and publisher have taken care in the preparation of this book, but make no expressed or implied warranty of any kind and assume no responsibility for errors or omissions. No liability is assumed for incidental or consequential damages in connection with or arising out of the use of the information or programs contained herein.

For information about buying this title in bulk quantities, or for special sales opportunities (which may include electronic versions; custom cover designs; and content particular to your business, training goals, marketing focus, or branding interests), please contact our corporate sales department at corpsales@pearsoned.com or (800) 382-3419.

For government sales inquiries, please contact governmentsales@pearsoned.com.

For questions about sales outside the U.S., please contact international@pearsoned.com.

Visit us on the Web: informit.com/aw

Library of Congress Cataloging-in-Publication Data

Fried, Joel R.

Polymer science and technology / Joel R. Fried.—Third edition.

pages cm

Includes bibliographical references and index.

ISBN 978-0-13-703955-5 (hardcover : alk. paper)

1. Polymers. 2. Polymerization. I. Title.

QD381.F73 2014

668.9—dc23

2014000967

Copyright © 2014 Pearson Education, Inc.

All rights reserved. Printed in the United States of America. This publication is protected by copyright, and permission must be obtained from the publisher prior to any prohibited reproduction, storage in a retrieval system, or transmission in any form or by any means, electronic, mechanical, photocopying, recording, or likewise. To obtain permission to use material from this work, please submit a written request to Pearson Education, Inc., Permissions Department, One Lake Street, Upper Saddle River, New Jersey 07458, or you may fax your request to (201) 236-3290.

ISBN-13: 978-0-13-703955-5

ISBN-10: 0-13-703955-7

Text printed in the United States on recycled paper at Courier Corporation in Westford, Massachusetts.

First printing, May 2014

*To my parents, who provided the opportunities,
support, and guidance, and to my wife, Ava, and sons,
Marc and Aaron, for their love, patience, and
understanding.*

This page intentionally left blank

C O N T E N T S

PREFACE	xv
PREFACE TO SECOND EDITION	xvii
PREFACE TO FIRST EDITION	xix
ACKNOWLEDGMENTS	xxi
ABOUT THE AUTHOR	xxiii
1 INTRODUCTION TO POLYMER SCIENCE	1
1.1 Classification of Polymers	3
1.1.1 Thermoplastics and Thermosets	3
1.1.2 Classification Based upon the Mechanism of Polymerization	4
1.1.3 Classification Based upon Polymer Structure	7
1.2 Polymer Structure.....	8
1.2.1 Copolymers	9
1.2.2 Tacticity.....	9
1.2.3 Geometric Isomerism	12
1.2.4 Nomenclature	13
1.3 Molecular Weight.....	15
1.3.1 Molecular-Weight Distribution	15
1.3.2 Molecular-Weight Averages	16
1.4 Chemical Structure and Thermal Transitions.....	20
Suggested Reading	22
Problems.....	22
References	24
2 POLYMER SYNTHESIS	25
2.1 Step-Growth Polymerization.....	26
2.1.1 Molecular Weight in a Step-Growth Polymerization	28
2.1.2 Step-Growth Polymerization Kinetics.....	30
2.2 Chain-Growth Polymerization	31
2.2.1 Free-Radical Polymerization and Copolymerization	32
2.2.2 Ionic Polymerization and Copolymerization.....	49
2.2.3 Coordination Polymerization	53
2.2.4 Controlled Radical Polymerizations.....	57
2.3 Polymerization Techniques	64
2.3.1 Bulk Polymerization.....	64

2.3.2	Solution Polymerization	66
2.3.3	Suspension Polymerization	66
2.3.4	Emulsion Polymerization	67
2.3.5	Solid-State, Gas-Phase, and Plasma Polymerization	69
2.3.6	Polymerization in Supercritical Fluids	71
2.3.7	Polymerization in Ionic Liquids	72
2.4	Polymer Reactivity	74
2.4.1	Chemical Modification	74
2.4.2	Preparation of Polymer Derivatives	76
2.4.3	Click Chemistry	79
2.5	Special Topics in Polymer Synthesis	81
2.5.1	Metathesis	81
2.5.2	Group-Transfer Polymerization	83
2.5.3	Macromers in Polymer Synthesis	84
2.5.4	Genetic Engineering	85
2.5.5	Green Chemistry	86
2.6	Chemical Structure Determination	86
2.6.1	Vibrational Spectroscopy	86
2.6.2	Nuclear Magnetic Resonance Spectroscopy	89
	Suggested Reading	92
	Problems	95
	References	98
3	CONFORMATION, SOLUTIONS, AND MOLECULAR WEIGHT	101
3.1	Polymer Conformation and Chain Dimensions	102
3.2	Thermodynamics of Polymer Solutions	109
3.2.1	The Flory–Huggins Theory	110
3.2.2	Flory–Krigbaum and Modified Flory–Huggins Theories	116
3.2.3	Equation-of-State Theories	117
3.2.4	Phase Equilibria	122
3.2.5	Determination of the Interaction Parameter	125
3.2.6	Predictions of Solubilities	126
3.3	Measurement of Molecular Weight	129
3.3.1	Osmometry	130
3.3.2	Light-Scattering Methods	134
3.3.3	Intrinsic Viscosity Measurements	140
3.3.4	Gel-Permeation Chromatography	143
	Suggested Reading	146
	Problems	146
	References	150

4	SOLID-STATE PROPERTIES	153
4.1	The Amorphous State.....	154
4.1.1	Chain Entanglements and Reptation	154
4.1.2	The Glass Transition	156
4.1.3	Secondary-Relaxation Processes	158
4.2	The Crystalline State	159
4.2.1	Ordering of Polymer Chains.....	159
4.2.2	Crystalline-Melting Temperature	163
4.2.3	Crystallization Kinetics	164
4.2.4	Techniques to Determine Crystallinity.....	165
4.3	Thermal Transitions and Properties	167
4.3.1	Fundamental Thermodynamic Relationships	167
4.3.2	Measurement Techniques.....	172
4.3.3	Structure–Property Relationships.....	177
4.3.4	Effect of Molecular Weight, Composition, and Pressure on T_g ...	179
4.4	Mechanical Properties	183
4.4.1	Mechanisms of Deformation	183
4.4.2	Methods of Testing.....	185
4.5	Solid-State Characterization Methods.....	200
4.5.1	Microscopy	200
4.5.2	Scattering Methods.....	201
	Suggested Reading	202
	Problems.....	203
	References	204
5	VISCOELASTICITY AND RUBBER ELASTICITY	207
5.1	Introduction to Viscoelasticity	208
5.1.1	Dynamic-Mechanical Analysis	208
5.1.2	Mechanical Models of Viscoelastic Behavior.....	221
5.1.3	Viscoelastic Properties of Polymer Solutions and Melts.....	230
5.1.4	Dielectric Analysis	232
5.1.5	Dynamic Calorimetry	239
5.1.6	Time–Temperature Superposition.....	242
5.1.7	Boltzmann Superposition Principle.....	245
5.1.8	Interrelationships between Transient and Dynamic Properties ...	247
5.2	Introduction to Rubber Elasticity	248
5.2.1	Thermodynamics	248
5.2.2	Statistical Theory	252
5.2.3	Phenomenological Model.....	253
5.2.4	Recent Developments.....	254

Suggested Reading	255
Problems	256
References	259
6 POLYMER DEGRADATION AND THE ENVIRONMENT	261
6.1 Polymer Degradation and Stability	262
6.1.1 Thermal Degradation.....	262
6.1.2 Oxidative and UV Stability	267
6.1.3 Chemical and Hydrolytic Stability	269
6.1.4 Effects of Radiation.....	271
6.1.5 Mechanodegradation	272
6.2 Management of Plastics in the Environment.....	272
6.2.1 Recycling.....	273
6.2.2 Incineration.....	274
6.2.3 Biodegradation	275
Suggested Reading	279
References	279
7 ADDITIVES, BLENDS, BLOCK COPOLYMERS, AND COMPOSITES.....	281
7.1 Additives	282
7.1.1 Plasticizers.....	282
7.1.2 Fillers and Reinforcements.....	287
7.1.3 Other Important Additives.....	288
7.2 Polymer Blends and Interpenetrating Networks	293
7.2.1 Polymer Blends	293
7.2.2 Toughened Plastics and Phase-Separated Blends.....	302
7.2.3 Interpenetrating Networks	304
7.3 Block Copolymers.....	306
7.4 Composites.....	310
7.4.1 Mechanical Properties	311
7.4.2 Composite Fabrication	316
7.5 Nanocomposites	318
7.5.1 Montmorillonite Nanocomposites.....	319
7.5.2 Buckyballs, Carbon Nanotubes, Graphene, and POSS	322
Suggested Reading	326
Problems.....	328
References	329

8	BIOPOLYMERS, NATURAL POLYMERS, AND FIBERS	331
8.1	Biopolymers and Other Naturally Occuring Polymers	332
8.1.1	Proteins	332
8.1.2	Polynucleotides	336
8.1.3	Polysaccharides	341
8.1.4	Naturally Occurring Elastomers	344
8.2	Fibers	346
8.2.1	Natural and Synthetic Fibers	346
8.2.2	Cellulosics	349
8.2.3	Non-cellulosics	350
8.2.4	Fiber-Spinning Operations	354
	Suggested Reading	358
	Problems	359
	References	359
9	THERMOPLASTICS, ELASTOMERS, AND THERMOSETS	361
9.1	Commodity Thermoplastics	362
9.1.1	Polyolefins	362
9.1.2	Vinyl Polymers	367
9.1.3	Thermoplastic Polyesters	372
9.2	Elastomers	374
9.2.1	Diene Elastomers	375
9.2.2	Nondiene Elastomers	379
9.2.3	Thermoplastic Elastomers	384
9.3	Thermosets	386
9.3.1	Epoxies	386
9.3.2	Unsaturated Polyesters	387
9.3.3	Formaldehyde Resins	389
	Suggested Reading	393
	Problems	394
	References	395
10	ENGINEERING AND SPECIALTY POLYMERS	397
10.1	Engineering Plastics	399
10.1.1	Polyamides	399
10.1.2	ABS	401
10.1.3	Polycarbonates	402
10.1.4	Modified Poly(phenylene oxide)	404
10.1.5	Acetal	405
10.1.6	Polysulfones	406
10.1.7	Poly(<i>p</i> -phenylene sulfide)	408

10.1.8	Engineering Polyesters	409
10.1.9	Fluoropolymers.....	411
10.2	Specialty Polymers.....	412
10.2.1	Polyimides and Related Specialty Polymers	413
10.2.2	Polyaryletherketones.....	419
10.2.3	Specialty Polyolefins	420
10.2.4	Ionic Polymers.....	421
10.2.5	Inorganic Polymers.....	422
10.2.6	Liquid-Crystalline Polymers.....	424
10.2.7	Conductive Polymers.....	427
10.2.8	High-Performance Fibers.....	429
10.2.9	Dendritic Polymers	430
	Suggested Reading	431
	Problems.....	433
	References	433
11	POLYMER PROCESSING AND RHEOLOGY	435
11.1	Basic Processing Operations	436
11.1.1	Extrusion.....	436
11.1.2	Molding	437
11.1.3	Calendering.....	445
11.1.4	Coating.....	445
11.2	Introduction to Polymer Rheology	446
11.2.1	Non-Newtonian Flow	448
11.2.2	Viscosity of Polymer Solutions and Suspensions.....	452
11.2.3	Constitutive Equations.....	456
11.2.4	Elastic Properties of Polymeric Fluids.....	457
11.2.5	Melt Instabilities	460
11.2.6	Drag Reduction.....	460
11.3	Analysis of Simple Flows	461
11.3.1	Pressure (Poiseuille) Flow	464
11.3.2	Drag Flow	467
11.4	Rheometry	468
11.4.1	Capillary Rheometer	469
11.4.2	Couette Rheometer	473
11.4.3	Cone-and-Plate Rheometer	475
11.4.4	Rheometry of Polymer Solutions and Melts.....	475
11.5	Modeling of Polymer-Processing Operations	476
11.5.1	Extrusion.....	476
11.5.2	Wire Coating.....	482

Appendices	485
11.A.1 Relationships between WLF Parameters and Free Volume	485
11.A.2 Dynamic and Continuity Equations.....	486
Suggested Reading	487
Problems.....	488
References	491
12 POLYMERS FOR ADVANCED TECHNOLOGIES	493
12.1 Membrane Science and Technology	494
12.1.1 Barrier Polymers.....	494
12.1.2 Membrane Separations	495
12.1.3 Mechanisms of Transport	506
12.1.4 Membrane Preparation.....	517
12.2 Biomedical Engineering and Drug Delivery	526
12.2.1 Controlled Drug Delivery	527
12.2.2 Gene Therapy.....	530
12.2.3 Antimicrobial Polymers.....	532
12.2.4 Tissue Engineering	532
12.2.5 Kidney Dialysis and Artificial Organs.....	533
12.3 Applications in Electronics and Energy	533
12.3.1 Electrically Conductive Polymers	533
12.3.2 Polymeric Batteries.....	535
12.3.3 Organic Photovoltaic Polymers	537
12.3.4 Electronic Shielding.....	540
12.3.5 Dielectrics.....	541
12.3.6 Electronic Encapsulation	541
12.4 Photonic Polymers.....	541
12.4.1 Nonlinear Optical Polymers	542
12.4.2 Light-Emitting Diodes.....	543
12.5 Sensor Applications.....	544
Suggested Reading	547
Problems.....	550
References	550
13 CORRELATIONS AND SIMULATIONS IN POLYMER SCIENCE.....	553
13.1 Group-Contribution Methods.....	554
13.1.1 Volumetric Properties.....	554
13.1.2 Glass-Transition Temperature	558
13.1.3 Permeability.....	559
13.1.4 Solubility Parameter	562
13.1.5 Activity Coefficients.....	566

13.2 Topological Indices	574
13.3 Artificial Neural Network	578
13.4 Molecular Simulations	581
13.4.1 Molecular Mechanics Force Fields.....	583
13.4.2 Molecular Dynamics and Monte Carlo Methods.....	588
13.5 Applications of Molecular Simulations.....	591
13.5.1 PVT Simulation	591
13.5.2 Cohesive Energy Density and the Solubility Parameter	593
13.5.3 Glass-Transition Temperature	594
13.5.4 Pair Correlations	595
13.5.5 Time-Correlation Coefficients	597
13.5.6 Scattering Functions	599
13.5.7 Mechanical Properties	600
13.5.8 Sorption Isotherms.....	602
13.5.9 Permeability.....	605
13.5.10 Free Volume.....	610
Suggested Reading	611
Problems.....	612
References	612
A Polymer Abbreviations	617
B Representative Properties of Some Important Commercial Polymers.....	621
C ASTM Standards for Plastics and Rubber	623
D SI Units and Physical Constants	627
E Mathematical Relationships.....	629
F The Major Elements	635
INDEX	637

P R E F A C E

Polymer Science and Technology, Third Edition, provides new and expanded coverage in a number of areas of contemporary interest in polymer science and technology. In particular, Chapter 2 on polymer synthesis provides new coverage of controlled radical polymerization, polymerization in ionic liquids, and the use of click chemistry and green chemistry. Chapter 4, on solid-state properties, includes added coverage on the use of microscopy and scattering methods in solid-state characterization. Chapter 7, on additives, blends, and composites, includes a new section on block copolymers as well as expanded coverage of nanocomposites including the use of buckyballs, carbon nanotubes, graphene, and POSS as nanofillers. Electrospinning has been added to the discussion of fiber-spinning operations in Chapter 8. Coverage of biomedical engineering and drug delivery, solar cells, and sensors has been included in Chapter 12, on polymers for advanced technologies. In addition, an entirely new chapter on correlations and simulation methods in polymer science has been added. This new chapter includes expanded treatment of group-correlation methods to predict polymer properties that has previously appeared in a number of earlier chapters in the second edition. Totally new is the inclusion of topological indices and artificial neural networks to predict properties. For the first time in an introductory polymer textbook, the fundamentals and applications of computational polymer science including the use of molecular dynamics and Monte Carlo methods are presented with a number of examples and exercise problems.

Joel R. Fried
Tallahassee, Florida

ABOUT THE COVER ILLUSTRATION

The cover illustration shows a molecular simulation of a blend of 37 wt% of functionalized C₆₀ fullerene, PCBM, (space-filling representation) in an amorphous cell containing a thiophene copolymer. This system has been reported to provide attractive photovoltaic properties for polymeric photovoltaic cells. Simulations of polymeric systems are described in Chapter 13 of this third edition.

P R E F A C E T O T H E S E C O N D E D I T I O N

*T*he second edition provides new and expanded coverage of important topics in polymer science and engineering and includes additional example calculations, homework problems, and bibliographic references. Additional topics in the treatment of polymer synthesis (Chapter 2) include metallocene catalysis, atom transfer radical and plasma polymerization, the genetic engineering of polymers, and the use of supercritical fluids as a polymerization medium. The new field of dynamic calorimetry (temperature-modulated DSC) has been added to the coverage of polymer viscoelasticity in Chapter 5. Chapter 6 provides expanded coverage of biodegradable polymers while Chapter 7 introduces the important new area of nanocomposites. Chapter 8 has been totally revised to include coverage of biopolymers and naturally occurring polymers including chitin and chitosan, while material on commodity thermoplastics has been moved to Chapter 9. In Chapter 10, new engineering and specialty thermoplastics including dendrimers, hyperbranched polymers, and amorphous Teflon are discussed. Examples of polymer-processing modeling have been expanded to include wire-coating operations in Chapter 11. The topic of drag reduction has been moved from Chapter 12 to the coverage of polymer rheology in Chapter 11, which now also includes an introduction to melt instabilities. The discussion of the electrical and optical applications of engineering polymers has been enhanced and new coverage of barrier polymers has been provided in Chapter 12.

Although the intended audience for this text is advanced undergraduates and graduate students in chemical engineering, the coverage of polymer science funda-

mentals (Chapters 1 through 5) is suitable for a semester course in a materials science or chemistry curriculum. Chapters 6 and 7 discuss more specialized topics such as polymer degradation, recycling, biopolymers, natural polymers, and fibers. Sections from this coverage can be included to supplement the basic coverage provided by the earlier chapters. Chapters 9 and 10 survey the principal categories of polymers—commodity thermoplastics, elastomers, thermosets, and engineering and specialty polymers. Material from these chapters may be included to supplement and reinforce the material presented in the chapters on fundamentals and provides a useful reference source for practicing scientists and engineers in the plastics industry. Polymer engineering principles including rheology and processing operations, introduced in Chapter 11, can be used as the basis of a short course on polymer engineering at the senior undergraduate and graduate level. Chapter 12 describes polymers used in areas of advanced technology including membrane separations, electrolytes for batteries and fuel cells, controlled drug release, nonlinear optical applications, and light-emitting diodes and displays. This coverage may be used as reference material for scientists and engineers and provides a basis for short courses in such areas as membrane science and technology and polymer physics.

Joel R. Fried
Cincinnati, Ohio

P R E F A C E T O T H E F I R S T E D I T I O N

*A*t least dozens of good introductory textbooks on polymer science and engineering are now available. Why then has yet another book been written? The decision was based on my belief that none of the available texts fully address the needs of students in chemical engineering. It is not that chemical engineers are a rare breed, but rather that they have special training in areas of thermodynamics and transport phenomena that is seldom challenged by texts designed primarily for students of chemistry or materials science. This has been a frustration of mine and of many of my students for the past 15 years during which I have taught an introductory course, *Polymer Technology*, to some 350 chemical engineering seniors. In response to this perceived need, I had written nine review articles that appeared in the SPE publication *Plastics Engineering* from 1982 to 1984. These served as a hard copy for my students to supplement their classroom notes but fell short of a complete solution.

In writing this text, it was my objective to first provide the basic building blocks of polymer science and engineering by coverage of fundamental polymer chemistry and materials topics given in Chapters 1 and 7. As a supplement to the traditional coverage of polymer thermodynamics, extensive discussion of phase equilibria, equation-of-state theories, and UNIFAC has been included in Chapter 3. Coverage of rheology, including the use of constitutive equations and the modeling of simple flow geometries, and the fundamentals of polymer processing operations are given in Chapter 11. Finally, I wanted to provide information on the exciting

new materials now available and the emerging areas of technological growth that could motivate a new generation of scientists and engineers. For this reason, engineering and specialty polymers are surveyed in Chapter 10 and important new applications for polymers in separations (membrane separations), electronics (conducting polymer), biotechnology (controlled drug release), and other specialized areas of engineering are given in Chapter 12. In all, this has been an ambitious undertaking and I hope that I have succeeded in at least some of these goals.

Although the intended audience for this text is advanced undergraduates and graduate students in chemical engineering, the coverage of polymer science fundamentals (Chapters 1 through 7) should be suitable for a semester course in a materials science or chemistry curriculum. Chapters 8 through 10, intended as survey chapters of the principal categories of polymers—commodity thermoplastics and fibers, network polymers (elastomers and thermoplastics), and engineering and specialty polymers—may be included to supplement and reinforce the material presented in the chapters on fundamentals and should serve as a useful reference source for the practicing scientist or engineer in the plastics industry.

Joel R. Fried
Cincinnati, Ohio

A C K N O W L E D G M E N T S

*T*his text in its three editions could not have been completed without the help of many colleagues who provided figures and photographs and offered important advice during its preparation. I am particularly indebted to those colleagues who read all or sections of the first edition and offered very helpful advice. These included Professor James E. Mark of the University of Cincinnati, Professor Otto Vogl of the Polytechnic University, Professor Erdogan Kiran of Virginia Polytechnic Institute, Professor Paul Han of the University of Akron, Professor Donald R. Paul of the University of Texas at Austin, and Professor R. P. Danner of Penn State. Appreciation is also extended to many students and colleagues at the University of Cincinnati who have provided important comments over the past few years following the publication of the first edition. These include Professor Michael Greenfield of the University of Rhode Island, Professor Zvi Rigbi of the Technion, Professors U. Sundararaj and Philip Choi of the University of Alberta, Professor Jin Chuk Zjung of Pohang University of Science and Technology, and Professor Carlos Co of the University of Cincinnati. Appreciation is also extended to those who kindly assisted in reviewing portions of the third edition. These include Professors George Odian and Alan Lyons of the College of Staten Island (City University of New York), Dr. Donald Klosterman of the University of Dayton Research Institute, Professor Pengyu Ren of the University of Texas at Austin, and Professors Rufina Alamo, Daniel Hallinan, and Biwu Ma of Florida State University.

I also wish to thank those colleagues who kindly provided some key illustrations and photos. These include Dr. Roger Kambour of General Electric, Professor Bill Koros of the Georgia Institute of Technology, Professor Paul Philips of the University of Tennessee, Dr. Marty Matsuo of Nippon Zeon (Japan), Dr. Robert

Cieslinski of the Dow Chemical Company, Dr. Richard Baker of Membrane Technology and Research, Inc., Dr. Mostafa Aboulfaraj of Pechiney Centre de Recherches de Voreppe (France), Professor Morton Denn of the City College of New York, Professor David Tirrell of the California Institute of Technology, Dr. Graeme Moad of CSIRO (Australia), Craig Hawker of the University of California, Santa Barbara, and Professor Rufina Alamo of Florida State University.

Joel R. Fried
Tallahassee, Florida

ABOUT THE AUTHOR

Dr. Joel R. Fried is professor and chair of the department of chemical and biomedical engineering at Florida State University. Previously, he was professor and the Wright Brothers Endowed Chair in Nanomaterials at the University of Dayton. He is also professor emeritus of chemical engineering and a fellow of the graduate school at the University of Cincinnati, where he directed the Polymer Research Center and served as head of the Department of Chemical Engineering over a career of 32 years. During this time he has advised more than sixty graduate and postdoctoral students, many of whom are currently in academic positions or have prominent positions in industry. Dr. Fried holds B.S. degrees in biology and chemical engineering, and an M.E. degree in chemical engineering from Rensselaer Polytechnic Institute. He also holds M.S. and Ph.D. degrees in polymer science and engineering from the University of Massachusetts, Amherst. Prior to his academic career, Dr. Fried was a senior engineer at the Monsanto Corporate R&D Center in St. Louis and an associate staff member of the GE Corporate R&D Center near Schenectady, New York. At Monsanto, he was a member of a fundamental research group developing hollow fiber membranes for industrial gas separations.



Dr. Fried is an instructor for the short course on Polymer Science and Technology at the National Meetings of the American Chemical Society and has been a course instructor on extrusion for the Plastics Institute of America. He is the author of more than one hundred and fifty publications, including many book chapters and monographs. Dr. Fried has served as editor of *Polymer Contents* and associate editor of *Computational and Theoretical Polymer Science*, has served on the editorial boards of *Polymer* and *Polymer Engineering*, and is a frequent consultant to industry. Current research interests focus on experimental studies and simulations of ion and small molecule transport through polymeric, biological, and biomimetic membranes for separations, energy, and sensor applications.

This page intentionally left blank

Introduction to Polymer Science

*T*he word *polymer* is derived from the classical Greek words *poly* meaning “many” and *meros* meaning “parts.” Simply stated, a polymer is a long-chain molecule that is composed of a large number of *repeating units* of identical structure. Certain polymers, such as proteins, cellulose, and silk, are found in nature, while many others, including polystyrene, polyethylene, and nylon, are produced only by synthetic routes. In some cases, naturally occurring polymers can also be produced synthetically. An important example is natural (Hevea) rubber, known as polyisoprene in its synthetic form.

Polymers that are capable of high extension under ambient conditions find important applications as elastomers. In addition to natural rubber, there are several important synthetic elastomers including nitrile and butyl rubber. Other polymers may have characteristics that enable their fabrication into long fibers suitable for textile applications. The synthetic fibers, principally nylon and polyester, are good substitutes for naturally occurring fibers such as cotton, wool, and silk.

In contrast to the usage of the word *polymer*, those commercial materials other than elastomers and fibers that are derived from synthetic polymers are called *plastics*. A typical commercial plastic resin may contain two or more polymers in addition to various additives and fillers. These are added to improve a particular property such as processability, thermal or environmental stability, or mechanical properties.

The birth of polymer science may be traced back to the mid-nineteenth century. In the 1830s, Charles Goodyear developed the vulcanization process that transformed the sticky latex of natural rubber into a useful elastomer for tire use. In 1847, Christian F. Schönbein reacted cellulose with nitric acid to produce cellulose nitrate. This was used in the 1860s as the first man-made thermoplastic, celluloid. In 1907, Leo Hendrik Baekeland [1] produced Bakelite (phenol–formaldehyde resin). Glyptal (unsaturated-polyester resin) was developed as a protective coating resin by General Electric in 1912.

By the 1930s, researchers at DuPont in the United States had produced a variety of new polymers including synthetic rubber and more “exotic” materials such as nylon and Teflon. By 1938, Dow had produced polystyrene in commercial scale for the first time and, in 1939, polyethylene (low-density) was made by scientists at ICI in England. Efforts to develop new polymeric materials, particularly synthetic rubber, were intensified during World War II when many naturally occurring materials such as Hevea rubber were in short supply. In the 1950s, Karl Ziegler and Giulio Natta independently developed a family of stereospecific transition-metal catalysts that made possible the commercialization of polypropylene as a major commodity plastic. The 1960s and 1970s witnessed the development of a number of high-performance engineering plastics polymers that could compete favorably with more traditional materials, such as metals, for automotive and aerospace applications. These included polycarbonate, poly(phenylene oxide), polysulfones, polyimides, aromatic polyamides such as Kevlar, and other high-temperature rigid-chain polymers. More recently, specialty polymers with electrically conducting, photoconducting, and liquid-crystalline properties have appeared for a variety of applications.

Today, polymeric materials are used in nearly all areas of daily life and their production and fabrication are major worldwide industries. The annual U.S. production of plastics and synthetic fibers in 2012 and the average annual change in production over the decade from 2002 to 2012 are given in Table 1-1. In 2012, the total U.S. production of synthetic fibers (principally non-cellulosic) and plastics was 2.81 and 34.1 million metric tons, respectively. Among plastics, the largest shares of the total production in 2012 were the polyethylenes, followed by polypropylene, poly(vinyl chloride) (PVC), and polystyrene. Although not specifically listed by the data given in Table 1-1, thermosetting resins (principally phenolic, urea, and melamine resins) typically represent around 10% of the total plastics production while

synthetic rubbers, such as styrene–butadiene rubber (SBR) and polybutadiene, represent only about 6% of the total production in recent years.

Table 1-1 U.S. Production of Major Plastics and Synthetic Fibers in 2012^a

	Thousands of Metric Tons ^b	Annual Change (%), 2002–12
PLASTICS		
Polyethylene		
Low-density	3123	-1.5
Linear low-density	8098	1.7
High-density	8046	1.1
Polypropylene	7405	-0.4
Polystyrene	2473	-2.0
PVC & copolymers	6944	0.0
SYNTHETIC FIBERS		
Non-cellulosic		
Nylon	562	-6.6
Olefin	1021	-3.1
Polyester	1203	-2.2
Cellulosic		
Acetate & rayon	27	-10.3

^aData reported in *Chemical and Engineering News*, July 1, 2013, p. 44.

^bConversion: 2,206.6 lbs per metric ton.

1.1 Classification of Polymers

Thousands of different polymers have been synthesized and more will be produced in the future. Conveniently, all polymers can be assigned to one of two groups based upon their processing characteristics or the type of polymerization mechanism. A more specific classification can be made on the basis of polymer structure. Such groupings are useful because they facilitate the discussion of properties.

1.1.1 Thermoplastics and Thermosets

All polymers can be divided into two major groups based on their thermal processing behavior. Those polymers that can be heat-softened in order to process into a desired form are called *thermoplastics*. Waste thermoplastics can be recovered and refabricated by application of heat and pressure. Polystyrene is an important example of a commercial thermoplastic. Other major examples are the polyolefins (e.g., polyethylene and polypropylene) and poly(vinyl chloride). In comparison, *thermosets* are polymers whose individual chains have been chemically linked by covalent bonds during polymerization or by subsequent chemical or thermal treatment during fabrication. Once formed, these crosslinked networks resist heat soft-

ening, mechanical deformation, and solvent attack, but cannot be thermally processed. Such properties make thermosets suitable materials for composites, coatings, and adhesive applications. Principal examples of thermosets include epoxy, phenol–formaldehyde resins, and unsaturated polyesters that are used in the manufacture of glass-reinforced composites such as Fiberglas (see Section 7.4).

1.1.2 Classification Based upon the Mechanism of Polymerization

In addition to classifying polymers on the basis of their processing characteristics, polymers may also be classified according to their mechanism of polymerization. An early scheme classifies polymers as either *addition* or *condensation*—a scheme attributed to Wallace Carothers [2], a pioneer of the polymer industry working at DuPont from 1928 until his untimely death in 1937. Polystyrene, which is polymerized by a sequential addition of styrene monomers (see Figure 1-1), is an example of an addition polymer. Most important addition polymers are polymerized from olefins and vinyl-based monomers. A few other polymers that are traditionally recognized as belonging to the addition class are polymerized not by addition to an ethylene double bond but through a ring-opening polymerization of a sterically strained cyclic monomer. An example is the ring-opening polymerization of trioxane to form polyoxymethylene (an engineering thermoplastic), which is illustrated in Figure 1-2. Table 1-2 lists the chemical structure of the repeating units and the commonly used nomenclature of some of the most important addition-type polymers derived from substituted ethylene.

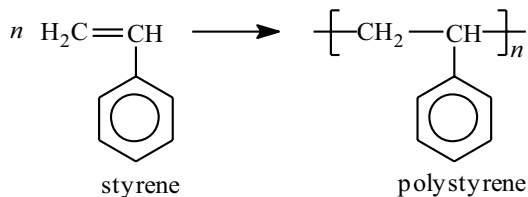


Figure 1-1 Polymerization of styrene.

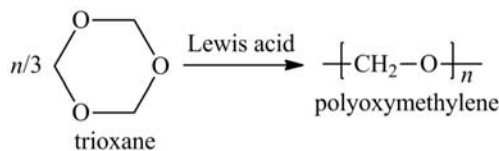
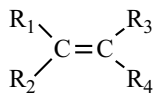


Figure 1-2 Ring-opening polymerization of trioxane.

Table 1-2 Examples of Some Important Addition Polymers Derived from Ethylene



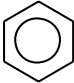
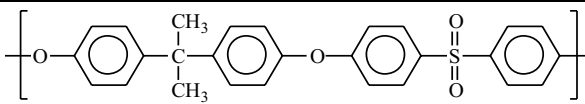
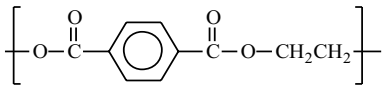
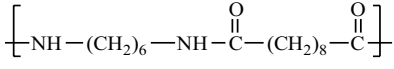
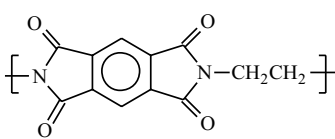
Polymer	R ₁	R ₂	R ₃	R ₄	Repeating Unit
Polyethylene	H	H	H	H	$[-CH_2-CH_2-]$
Polypropylene	H	H	H	CH ₃	$[-CH_2-\underset{\text{CH}_3}{\text{CH}}-]$
Poly(vinyl chloride)	H	H	H	Cl	$[-CH_2-\underset{\text{Cl}}{\text{CH}}-]$
Polyacrylonitrile	H	H	H	C≡N	$[-CH_2-\underset{\text{C}\equiv\text{N}}{\text{CH}}-]$
Poly(vinyl acetate)	H	H	H	$\begin{array}{c} \\ \text{O} \\ \\ \text{C}=\text{O} \\ \\ \text{CH}_3 \end{array}$	$[-CH_2-\underset{\begin{array}{c} \\ \text{O} \\ \\ \text{C}=\text{O} \\ \\ \text{CH}_3 \end{array}}{\text{CH}}-]$
Polystyrene	H	H	H		$[-CH_2-\underset{\text{C}_6\text{H}_5}{\text{CH}}-]$
Poly(methyl methacrylate)	H	H	CH ₃	$\begin{array}{c} \\ \text{C}=\text{O} \\ \\ \text{O} \\ \\ \text{CH}_3 \end{array}$	$[-CH_2-\underset{\begin{array}{c} \text{CH}_3 \\ \\ \text{C} \\ \\ \text{C}=\text{O} \\ \\ \text{O} \\ \\ \text{CH}_3 \end{array}}{\text{C}}-]$
Poly(vinylidene chloride)	H	H	Cl	Cl	$[-CH_2-\underset{\text{Cl}}{\overset{\text{Cl}}{\text{C}}}-]$

Table 1-3 Examples of Some Condensation Thermoplastics

Polymer	Repeating Unit
Polysulfone	
Poly(ethylene terephthalate)	
Poly(hexamethylene sebacamide) (nylon-6,10)	
Poly(ethylene pyromellitimide)	

More recently, another classification scheme based on polymerization kinetics has been adopted over the more traditional addition and condensation categories. According to this scheme, all polymerization mechanisms are classified as either *step* growth or *chain* growth. Most condensation polymers are step growth, while most addition polymers are chain growth; however, a number of important exceptions exist, as will be discussed in Chapter 2. During chain-growth polymerization, high-molecular-weight polymer is formed early during the polymerization, and the polymerization yield, or the percent of monomer converted to polymer, gradually increases with time. In step-growth polymerization, high-molecular-weight polymer is formed only near the end of the polymerization (i.e., at high monomer conversion, typically >98%). Details of the mechanisms for chain-growth and step-growth polymerizations are discussed in Chapter 2.

1.1.3 Classification Based upon Polymer Structure

In addition to classification based upon processing and polymerization characteristics, polymers may also be grouped based upon the chemical structure of their backbones. For example, polymers having all carbon atoms along their backbone are important examples of *homochain* polymers. They may be further classified depending upon whether there are single or double bonds along their backbone. Carbon-chain polymers with only single bonds along the backbone are called *polyalkylenes* (or polyalkylidenes). Examples of polyalkylenes include polystyrene, the polyolefins (e.g., polyethylene and polypropylene), and poly(vinyl chloride). Carbon-chain polymers with double bonds along the chain such as the diene

elastomers—polyisoprene and polybutadiene—are called *polyalkenylenes*. Another example of a polyalkenylene is polyacetylene, an electrically conducting polymer (see Section 10.2.7).

Heterochain polymers that contain more than one atom type in their backbone are grouped according to the types of atoms and chemical groups (e.g., carbonyl, amide, or ester) located along the backbone. The most important classes of organic heterochain polymers are listed in Table 1-4. Another important class of heterochain polymers includes polysiloxanes. These have a -Si-O- backbone with methyl or other substituent groups attached to silicon.

Table 1-4 Backbone Structures of Some Important Organic Heterochain Polymers

Polymer Classification	Backbone Group
Carbon–Oxygen Polymers	
Polyethers	—C—O—
Polyesters of carboxylic acids	$\begin{array}{c} \text{O} \\ \\ \text{—C—O—} \end{array}$
Polyanhydrides of carboxylic acids	$\begin{array}{c} \text{O} \quad \quad \text{O} \\ \quad \quad \\ \text{—C—O—C—} \end{array}$
Polycarbonates	$\begin{array}{c} \text{O} \\ \\ \text{—O—C—O—} \end{array}$
Carbon–Sulfur Polymers	
Polythioethers	—S—C—
Polysulfones	$\begin{array}{c} \text{O} \\ \\ \text{—S—C—} \\ \\ \text{O} \end{array}$
Carbon–Nitrogen Polymers	
Polyamines	—C—N—
Polyimines	—C=N—
Polyamides	$\begin{array}{c} \text{O} \\ \\ \text{—C—N—} \end{array}$
Polyureas	$\begin{array}{c} \text{O} \\ \\ \text{—N—C—N—} \end{array}$

1.2 Polymer Structure

The properties of polymers are strongly influenced by details of the chain structure. These details include the overall chemical composition and the sequence of mono-

mer units in the case of copolymers, the stereochemistry or tacticity of the chain, and the geometric isomerization in the case of diene-type polymers for which several synthesis routes may be possible.

1.2.1 Copolymers

Often, it is possible to obtain polymers with new and desirable properties by linking two or three different monomers or repeating units during the polymerization. Polymers with two different repeating units in their chains are called *copolymers*. When there are three chemically different repeating units, the resulting polymer is termed a *terpolymer*. Commercially, the most important copolymers are derived from vinyl monomers such as styrene, ethylene, acrylonitrile, and vinyl chloride.

The exact sequence of monomer units along the chain can vary widely depending upon the relative reactivities of each monomer during the copolymerization process. At the extremes, monomer placement may be totally random or may be perfectly alternating, as illustrated in Figure 1-4. The actual sequence of monomer units is determined by the relative reactivities of the monomers as will be described for free-radical copolymerization in Section 2.2.1. Under special circumstances, it is possible to prepare copolymers that contain a long block of one monomer (A) followed by a block of the other monomer (B). These are called AB-block copolymers. ABA-triblock copolymers have a central B block joined by A blocks at both ends. A commercially important ABA-triblock copolymer is polystyrene-*block*-polybutadiene-*block*-polystyrene or SBS, a thermoplastic elastomer (see Section 9.2.3). In addition to these copolymer structures, *graft* copolymers can be prepared by polymerizing a monomer in the presence of a fully formed polymer of another monomer. Graft copolymers are important as elastomers (e.g., SBR) and high-impact polymers (e.g., high-impact polystyrene and acrylonitrile-butadiene-styrene or ABS resin).

1.2.2 Tacticity

In addition to the type, number, and sequential arrangement of monomers along the chain, the *spatial* arrangement of substituent groups is also important in determining properties. The possible steric configurations of an asymmetric vinyl-polymer chain can be best represented by drawing the chain in its extended-chain or planar zigzag conformation, as illustrated in Figure 1-5. A *conformation* describes the *geometrical* arrangement of atoms in the polymer chain while *configuration* denotes the *stereochemical* arrangement of atoms. Unlike the conformation, the configuration of a polymer chain cannot be altered without breaking chemical bonds. For long, flexible polymer chains, the total number of conformations is nearly infinite. The ex-

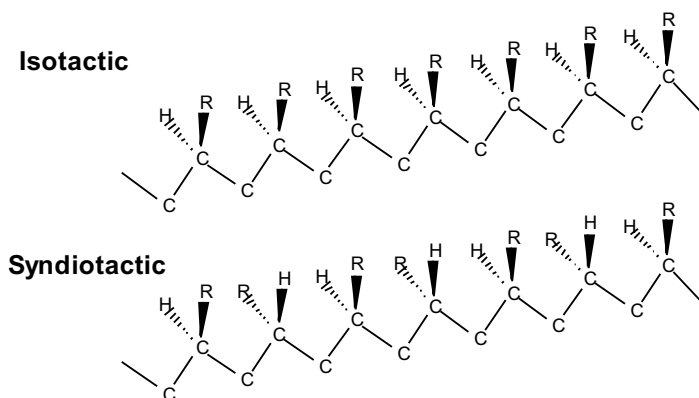


Figure 1-5 Two forms of stereochemical configuration of an extended-chain vinyl polymer having a substituent group R other than hydrogen.

In general, tactic polymers (i.e., isotactic or syndiotactic) are partially crystalline, while atactic polymers are *amorphous* indicating the absence of all crystalline order. In addition to crystallinity, other polymer properties, such as thermal and mechanical behavior, can be significantly affected by the tacticity of the polymer as later examples will show. Whether a specific polymer will be atactic, isotactic, or syndiotactic depends upon the specific conditions of the polymerization, such as the temperature and choice of solvent, as will be discussed in Chapter 2. Commercial polypropylene is an important example of an isotactic polymer. Atactic and syndiotactic forms of this polymer can also be prepared by controlling the polymerization conditions. Atactic polypropylene is an amorphous, tacky polymer with no commercial importance. Commercial poly(vinyl chloride) (PVC) is an example of a polymer with imperfect tactic structure. Although the overall structure of commercial-grade PVC can be reasonably characterized as atactic, there are populations of repeating units whose sequences are highly syndiotactic and that impart a small degree of crystallinity to the commercial resin. Space-filling (CPK) models of a short PVC chain having eight repeating units with all isotactic and all syndiotactic placements of the chlorine atoms are shown in Figure 1-6. Using special polymerization methods, PVC with very high syndiotactic or isotactic content can be made (see Section 9.1.2); however, these crystalline stereoisomers of PVC offer no important advantage compared to the commercial plastic. In the case of polystyrene, syndiotactic polystyrene has been obtained by metallocene polymerization (see Section 2.2.3) and is being studied as an alternative to the atactic “crystal grade” plastic for some applications (see Section 9.1.2).

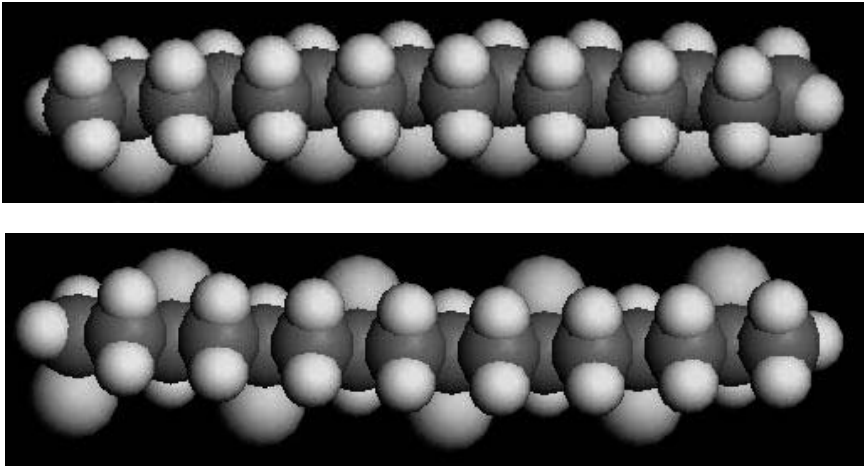


Figure 1-6 Views of computer-generated chains of eight repeating units (octamer) of vinyl chloride with *isotactic* (top) and *syndiotactic* (bottom) structures are shown. These views are looking down on the chain with the chlorine atoms (large spheres) sitting at the base of each chain. Small light gray spheres represent hydrogen atoms while larger dark gray spheres identify the carbon atoms.

1.2.3 Geometric Isomerism

When there are unsaturated sites along a polymer chain, several different isomeric forms are possible. As illustrated by Figure 1-7, 1,3-butadiene (structure A) can be polymerized to give 1,2-poly(1,3-butadiene) (B) or either of two *geometric isomers* of 1,4-poly(1,3-butadiene) (C and D). The numbers preceding the *poly* prefix designate the first and last carbon atoms of the backbone repeating unit. 1,2-poly(1,3-butadiene) has a vinyl-type structure, where the substituent group (ethene) contains an unsaturated site; therefore, this geometric isomer can be atactic, syndiotactic, or isotactic. In the case of the commercially more important 1,4-poly(1,3-butadiene), all four carbons in the repeating unit lie along the chain. Carbons 1 and 4 can lie either on the same side of the central double bond (i.e., *cis*-configuration, C) or on the opposite side (i.e., *trans*-configuration, D). The structure of polybutadiene used in SBR rubber (i.e., a copolymer of styrene and butadiene) is principally the *trans*-1,4 isomer with some *cis*-1,4- and 1,2-poly(1,3-butadiene) content.

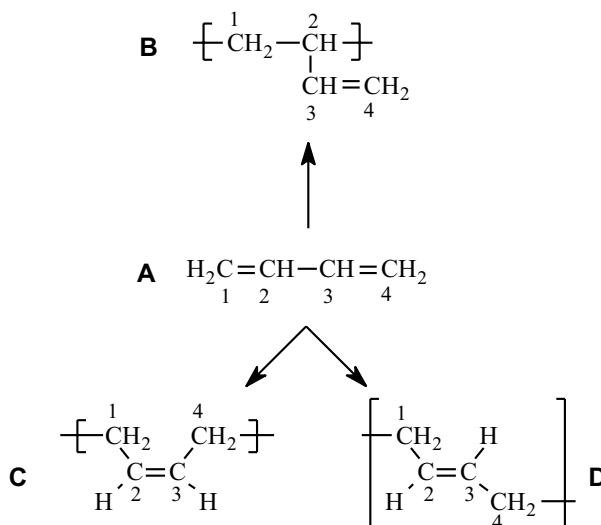


Figure 1-7 Alternative pathways for the polymerization of 1,3-butadiene (A) to give 1,2-poly(1,3-butadiene) (B), *cis*-1,4-poly(1,3-butadiene) (C), or *trans*-1,4-poly(1,3-butadiene) (D).

1.2.4 Nomenclature

As the preceding examples illustrate, a very large number of different polymer structures are possible. In order to identify these as unambiguously as possible, it is important to have a robust nomenclature system. As is already evident, simple vinyl polymers are designated by attaching the prefix *poly* to the monomer name (e.g., polystyrene, polyethylene, and polypropylene); however, when the monomer name consists of more than one word or is preceded by a letter or number, the monomer is enclosed by parentheses preceded by the prefix *poly*. For example, the polymer obtained from the polymerization of 4-chlorostyrene is poly(4-chlorostyrene) and that from vinyl acetate is poly(vinyl acetate). Tacticity may be noted by prefixing the letter *i* (isotactic) or *s* (syndiotactic) before *poly* as in *i*-polystyrene. Geometric and structural isomers may be indicated by using the appropriate prefixes, *cis* or *trans* and 1,2- or 1,4-, before *poly*, as in *trans*-1,4-poly(1,3-butadiene).

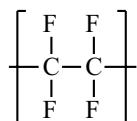
Nomenclature rules for non-vinyl polymers such as condensation polymers are generally more complicated than for vinyl monomers. These polymers are usually named according to the initial monomer or the functional group of the repeating unit. For example, the most important commercial nylon, commonly called nylon-6,6 (66 or 6/6), is more descriptively called poly(hexamethylene adipamide) denoting the polyamidation of hexamethylenediamine (alternatively called 1,6-hexane

diamine) with adipic acid (see Figure 1-3A). Similarly, the aliphatic nylon obtained by the polyamidation of hexamethylenediamine with a 10-carbon dicarboxylic acid, sebacic acid, is nylon-6,10 or poly(hexamethylene sebacamide) (see structure shown in Table 1-3).

In some cases, “common” names are used almost exclusively in place of the more chemically correct nomenclature. For example, the polycondensation of phosgene and bisphenol-A—the common name for 2,2-bis(4-hydroxyphenyl)propane—produces the engineering thermoplastic, polycarbonate (Figure 1-3B). Often, the prefix bisphenol-A is placed before polycarbonate to distinguish it from other polycarbonates that can be polymerized by using bisphenol monomers other than bisphenol-A, such as tetramethylbisphenol-A.

For many years, the International Union of Pure and Applied Chemistry (IUPAC) and the American Chemical Society (ACS) have developed a detailed, structure-based nomenclature for polymers. In addition, an industrial standard (ASTM D-4000) for specifying specific commercial grades of reinforced and non-reinforced plastics has been offered by the American Society for Testing and Materials (ASTM).

The IUPAC structure-based rules for naming organic, inorganic, and coordination polymers have been compiled in several publications [3–8]. Although such nomenclature provides an unambiguous method for identifying the large number of known polymers (more than 60,000 polymers are listed in the Chemical Abstracts Service (CAS) Chemical Registry System, semi-systematic or trivial names and sometimes even principal trade names (much to the displeasure of the manufacturer) continue to be used in place of the sometimes unwieldy IUPAC names. As examples, the IUPAC name for polystyrene is poly(1-phenylethylene) and that for polytetrafluoroethylene



is poly(difluoromethylene)—a polymer more typically recognized by its trademark, Teflon. The IUPAC name for the polycarbonate of bisphenol-A mentioned earlier is poly(oxycarbonyloxy-1,4-phenyleneisopropylidene-1,4-phenylene).

For convenience, several societies have developed a very useful set of two-, three-, and four-letter abbreviations for the names of many common thermoplastics, thermosets, fibers, elastomers, and additives. Sometimes, abbreviations adopted by different societies for the same polymer may vary, but there is widespread agreement on the abbreviations for a large number of important polymers. These abbreviations are convenient and widely used. As examples, PS is generally recognized as the abbreviation for polystyrene, PVC for poly(vinyl chloride), PMMA for poly(methyl methacrylate), PTFE for polytetrafluoroethylene, and PC for bis-

phenol-A polycarbonate. A listing of commonly accepted abbreviations is given in Appendix A at the end of this book.

Following IUPAC recommendations, copolymers are named by incorporating an italicized connective term between the names of monomers contained within parentheses or brackets or between two or more polymer names. The connective term designates the type of copolymer as indicated for six important classes of copolymers in Table 1-5.

Table 1-5 Scheme for Naming Copolymers

Type	Connective	Example
Unspecified	<i>-co-</i>	Poly[styrene- <i>co</i> -(methyl methacrylate)]
Statistical ^a	<i>-stat-</i>	Poly(styrene- <i>stat</i> -butadiene)
Random	<i>-ran-</i>	Poly[ethylene- <i>ran</i> -(vinyl acetate)]
Alternating	<i>-alt-</i>	Poly[styrene- <i>alt</i> -(maleic anhydride)]
Block	<i>-block-</i>	Polystyrene- <i>block</i> -polybutadiene
Graft	<i>-graft-</i>	Polybutadiene- <i>graft</i> -polystyrene

^a A statistical polymer is one in which the sequential distribution of the monomeric units obeys statistical laws. In the case of a random copolymer, the probability of finding a given monomeric unit at any site in the chain is independent of the neighboring units in that position.

1.3 Molecular Weight

1.3.1 Molecular-Weight Distribution

A typical synthetic polymer sample contains chains with a wide distribution of chain lengths. This distribution is seldom symmetric and contains some molecules of very high molecular weight. A representative distribution is illustrated in Figure 1-8. The exact breadth of the molecular-weight distribution depends upon the specific conditions of polymerization, as will be described in Chapter 2. For example, the polymerization of some olefins can result in molecular-weight distributions that are extremely broad. In other polymerizations, polymers with very narrow molecular-weight distributions can be obtained. As will be shown in subsequent chapters, many polymer properties, such as melt viscosity, are dependent on molecular weight and molecular-weight distribution. Therefore, it is useful to define molecular-weight averages associated with a given molecular-weight distribution as detailed in this section.

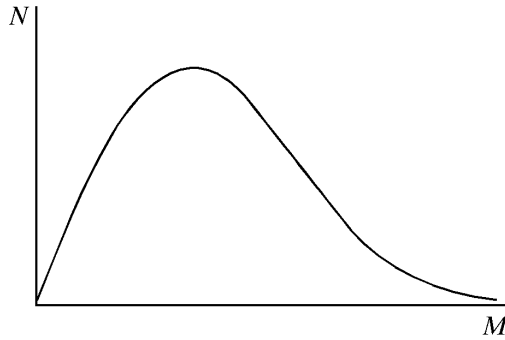


Figure 1-8 A representation of a continuous distribution of molecular weights shown as a plot of the number of moles of chains, N , having molecular weight M , against M .

1.3.2 Molecular-Weight Averages

For a discrete distribution of molecular weights, an average molecular weight, \bar{M} , may be defined as

$$\bar{M} = \frac{\sum_i N_i M_i^\alpha}{\sum_i N_i M_i^{\alpha-1}} \quad (1.1)$$

where N_i indicates the number of moles of molecules having a molecular weight of M_i and the parameter α is a weighting factor that defines a particular average of the molecular-weight distribution. The weight, W_i , of molecules with molecular weight M_i is then

$$W_i = N_i M_i. \quad (1.2)$$

Molecular weights that are important in determining polymer properties are the number-average, \bar{M}_n ($\alpha = 1$), the weight-average, \bar{M}_w ($\alpha = 2$), and the z -average, \bar{M}_z ($\alpha = 3$), molecular weights.

Since the molecular-weight distribution of commercial polymers is normally a continuous function, molecular-weight averages can be determined by integration if the appropriate mathematical form of the molecular-weight distribution (i.e., N as a function of M as illustrated in Figure 1-8) is known or can be approximated. Such mathematical forms include theoretical distribution functions derived on the basis of a statistical consideration of an idealized polymerization, such as the Flory, Schultz, Tung, and Pearson distributions [9] (see Example 1.1 and Problem 1.3) and standard probability functions, such as the Poisson and logarithmic-normal distributions.

It follows from eq. (1.1) that the *number-average molecular weight* for a discrete distribution of molecular weights is given as

$$\bar{M}_n = \frac{\sum_{i=1}^N N_i M_i}{\sum_{i=1}^N N_i} = \frac{\sum_{i=1}^N W_i}{\sum_{i=1}^N (W_i/M_i)} \quad (1.3)$$

where N is the total number of molecular-weight species in the distribution. The expression for the number-average molecular weight of a continuous distribution function is

$$\bar{M}_n = \frac{\int_0^\infty NM dM}{\int_0^\infty N dM}. \quad (1.4)$$

The respective relationships for the *weight-average molecular weight* of a discrete and a continuous distribution are given by

$$\bar{M}_w = \frac{\sum_{i=1}^N N_i M_i^2}{\sum_{i=1}^N N_i M_i} = \frac{\sum_{i=1}^N W_i M_i}{\sum_{i=1}^N W_i} \quad (1.5)$$

and

$$\bar{M}_w = \frac{\int_0^\infty NM^2 dM}{\int_0^\infty NM dM}. \quad (1.6)$$

In the case of high-molecular-weight polymers, the number-average molecular weight is directly determined by membrane osmometry, while the weight-average molecular weight is determined by light-scattering and other scattering techniques as described in Chapter 3. As mentioned earlier, a higher moment of the molecular-weight distribution is the z -average molecular weight (\bar{M}_z) where $\alpha = 3$. As discussed later in Chapter 3 (Section 3.3.3), a viscosity-average molecular weight, \bar{M}_v , can be obtained from dilute-solution viscometry. The viscosity-average molecular weight falls between \bar{M}_n and \bar{M}_w depending upon whether the solvent is a good or poor solvent for the polymer. In the case of a good solvent, $\bar{M}_v = \bar{M}_w$.

A measure of the breadth of the molecular-weight distribution is given by the ratios of molecular-weight averages. For this purpose, the most commonly used ratio is \bar{M}_w/\bar{M}_n , called the *polydispersity index* or PDI [9]. Recent IUPAC recommendations suggest the use of the term *molar-mass dispersity*, D_M , for this ratio

[10]. The PDIs of commercial polymers vary widely. For example, commercial grades of polystyrene with a \bar{M}_n of over 100,000 have polydispersity indices between 2 and 5, while polyethylene synthesized in the presence of a stereospecific catalyst may have a PDI as high as 30.* In contrast, the PDI of some vinyl polymers prepared by “living” polymerization (see Chapter 2) can be as low as 1.06. Such polymers with nearly *monodisperse* molecular-weight distributions are useful as molecular-weight standards for the determination of molecular weights and molecular-weight distributions of commercial polymers (see Section 3.3.4).

Example 1.1

A polydisperse sample of polystyrene is prepared by mixing three *monodisperse* samples in the following proportions:

1 g	10,000 molecular weight
2 g	50,000 molecular weight
2 g	100,000 molecular weight

Using this information, calculate the number-average molecular weight, weight-average molecular weight, and PDI of the mixture.

Solution

Using eqs. (1.3) and (1.5), we obtain the following:

$$\bar{M}_n = \frac{\sum_{i=1}^3 N_i M_i}{\sum_{i=1}^3 N_i} = \frac{\sum_{i=1}^3 W_i}{\sum_{i=1}^3 (W_i / M_i)} = \frac{1 + 2 + 2}{\frac{1}{10,000} + \frac{2}{50,000} + \frac{2}{100,000}} = 31,250$$

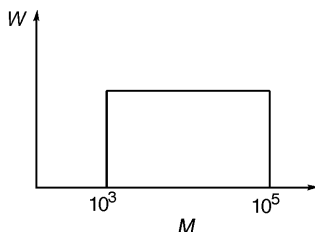
$$\bar{M}_w = \frac{\sum_{i=1}^3 N_i M_i^2}{\sum_{i=1}^3 N_i M_i} = \frac{\sum_{i=1}^3 W_i M_i}{\sum_{i=1}^3 W_i} = \frac{10,000 + 2(50,000) + 2(100,000)}{5} = 62,000$$

$$\text{PDI} = \frac{\bar{M}_w}{\bar{M}_n} = \frac{62,000}{31,250} = 1.98$$

* New metallocene-catalyzed polymerizations can produce polyolefins and other polymers with very controlled structures and narrow-molecular-weight distributions (see Section 2.2.3).

Example 1.2

A polymer is fractionated and is found to have the continuous molecular-weight distribution shown below as a plot of the weight, W , of molecules having molecular weight, M , versus M . Given this molecular-weight distribution, calculate \bar{M}_n and \bar{M}_w .



Solution

Using eqs. (1.4) and (1.6), we obtain the following:

$$\bar{M}_n = \frac{\int_{10^3}^{10^5} dM}{\int_{10^3}^{10^5} (1/M) dM} = \frac{10^5 - 10^3}{\ln(10^5/10^3)} = 21,498$$

$$\bar{M}_w = \frac{\int_{10^3}^{10^5} M dM}{\int_{10^3}^{10^5} dM} = \frac{(M^2/2)_{10^3}^{10^5}}{9.9 \times 10^4} = 50,500$$

Example 1.3

The single-parameter Flory distribution is given as

$$W(X) = X (\ln p)^2 p^X$$

where X is the degree of polymerization and p is the fractional monomer conversion in a step-growth polymerization. Using this equation, obtain expressions for the number-average and weight-average *degrees of polymerization** in terms of X and p .†

Solution

Using the following geometric series:

* Note that $\bar{M}_n = M_0 \bar{X}_n$ and $\bar{M}_w = M_0 \bar{X}_w$ where M_0 is the molecular weight of one repeat unit.

† For a comprehensive treatment of molecular-weight distributions, see Chapter VIII in Paul J. Flory's *Principles of Polymer Chemistry*.

$$\sum_{X=1}^{\infty} p^{X-1} = 1 + p + p^2 + p^3 + \dots = \frac{1}{1-p} \quad (-1 < p < 1)$$

$$A = \sum_{X=1}^{\infty} Xp^{X-1} = 1 + 2p + 3p^2 + \dots = \frac{1}{1-p}$$

$$B = \sum_{X=1}^{\infty} X^2 p^{X-1} = 1 + 2^2 p + 3^2 p^2 + \dots$$

Since it can be shown that $B(1-p) = A(1+p)$, it follows that

$$B = \frac{1+p}{1-p}, \text{ and then}$$

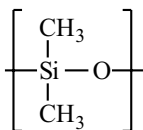
$$\bar{X}_n = \frac{\sum_{X=1}^{\infty} W(X)}{\sum_{X=1}^{\infty} W(X)/X} = \frac{(\ln p)^2 p \sum_{X=1}^{\infty} Xp^{X-1}}{(\ln p)^2 p \sum_{X=1}^{\infty} p^{X-1}} = \frac{\sum_{X=1}^{\infty} Xp^{X-1}}{\sum_{X=1}^{\infty} p^{X-1}} = \frac{1/(1-p)^2}{1/(1-p)} = \frac{1}{1-p}$$

$$\bar{X}_w = \frac{\sum_{X=1}^{\infty} XW(X)}{\sum_{X=1}^{\infty} W(X)} = \frac{(\ln p)^2 p \sum_{X=1}^{\infty} X^2 p^{X-1}}{(\ln p)^2 p \sum_{X=1}^{\infty} Xp^{X-1}} = \frac{\sum_{X=1}^{\infty} X^2 p^{X-1}}{\sum_{X=1}^{\infty} Xp^{X-1}} = \frac{(1+p)/(1-p)^3}{1/(1-p)^2} = \frac{1+p}{1-p}$$

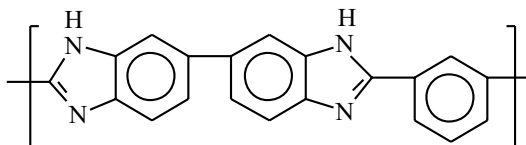
1.4 Chemical Structure and Thermal Transitions

As the previous discussion has shown, many important synthetic polymers such as polystyrene and poly(methyl methacrylate) consist of long, flexible chains of very high molecular weight. In many cases, individual chains are randomly coiled and intertwined with no molecular order or structure. Such a physical state is termed *amorphous*. Commercial-grade (atactic) polystyrene and poly(methyl methacrylate) are examples of polymers that are amorphous in the solid state. Below a certain temperature called the glass-transition temperature (T_g), long-range, cooperative motions of individual chains cannot occur; however, short-range motions involving several contiguous groups along the chain backbone or substituent group are possible. Such motions are called *secondary-relaxation* processes and can occur at tem-

peratures as low as 70 K. By comparison, glass-transition temperatures vary from 150 K for polymers with very flexible chains such as polydimethylsiloxane

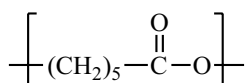


to well over 600 K for those with highly rigid aromatic backbones such as the high-modulus fiber poly[2,2'-(*m*-phenylene)-5,5'-bibenzimidazole] (PBI) (see Section 10.2.1)

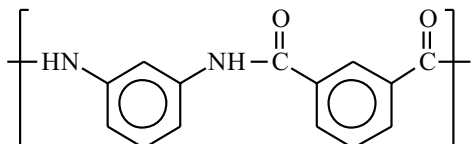


with a T_g reported in the range from 700 to 773 K.

Polymer chains with very regular structures, such as linear polyethylene and isotactic polypropylene, can be arranged in highly regular structures called crystallites. Each crystallite consists of rows of folded chains. Since sufficient thermal energy is needed to provide the necessary molecular mobility for the chain-folding process, crystallization can occur only at temperatures above T_g . If the temperature is too high, chain folds become unstable and high thermal energy disorders the crystallites—a crystalline–amorphous transition then occurs. The temperature that marks this transition is called the *crystalline-melting temperature* or T_m . Crystalline melting temperatures can vary from 334 K for simple, flexible-chain polyesters such as polycaprolactone



to over 675 K for aromatic polyamides such as poly(*m*-phenylene isophthalamide) (Nomex)



As an approximate rule of thumb, T_g is one-half to two-thirds of T_m expressed in absolute temperature (Kelvins). The glass-transition and crystalline-melting temperatures can be determined by a wide range of techniques including measurement of

volume (dilatometry), specific heat (calorimetry), and mechanical properties, particularly modulus (e.g., dynamic mechanical analysis), as discussed in Chapter 4.

SUGGESTED READING

- Furukawa, F., *Inventing Polymer Science: Staudinger, Carothers, and the Emergence of Macromolecular Chemistry*. 1998, Philadelphia: University of Pennsylvania Press.
- Harris, F. W., *Introduction to Polymer Chemistry*. *Journal of Chemical Engineering*, 1981. **58**: p. 837.
- Hermes, M. E., *Enough for One Lifetime: Wallace Carothers, Inventor of Nylon*. 1996, Washington, DC, and Philadelphia: American Chemical Society and Chemical Heritage Foundation.
- Mandelkern, L., *An Introduction to Macromolecules*. 1983, New York: Springer-Verlag.
- Mark, H. F., *Polymer Chemistry: The Past 100 Years*. *Chemical Engineering News*, April 6, 1976, p. 176.
- Morawetz, H., *Polymers: The Origins and Growth of a Science*. 1985, New York: John Wiley & Sons.
- Ober, C. K., S. Z. D. Cheng, P. T. Hammond, M. Muthukumar, E. Reichmanic, K. L. Wooley, and T. P. Lodge, *Research in Macromolecular Science: Challenges and Opportunities for the Next Decade*. *Macromolecules*, 2009. **42**(2): p. 465.
- Rogošič, M., H. J. Mencer, and Z. Gomzi, *Polydispersity Index and Molecular Weight Distributions of Polymers*. *European Polymer Journal*, 1996. **31**(11): p. 1337.
- Schnöll-Bitai, I., *A Comparative Study of the Properties of Different Distribution Curves*. *Macromolecular Chemistry and Physics*, 2002. **203**: p. 1754.
- Seymour, R. B., *Polymer Science Before and After 1899: Notable Developments During the Lifetime of Maurits Dekker*. *Journal of Macromolecular Science—Chemistry*, 1989. **A26**(8): p. 1023.
- Seymour, R. B., and C. E. Carraher, *Giant Molecules*. 1990, New York: John Wiley & Sons.
- Stepito, R., K. Horie, T. Kitayama, and A. Abe, *Mission and Challenges of Polymer Science and Technology*. *Pure and Applied Chemistry*, 2003. **75**(10): p. 1359.
- Tonelli, A. E., and M. Srinivasarao, *Polymers from the Inside Out*. 2001, New York: John Wiley & Sons.
- Ward, T. C., *Molecular Weight Distributions in Synthetic Polymers*. *Journal of Chemical Education*. 1981. **58**(11): p. 867.

PROBLEMS

1.1 A polymer sample combines five different molecular-weight fractions of equal weight. The molecular weights of these fractions increase from 20,000 to 100,000 in increments of

20,000. Calculate \bar{M}_n , \bar{M}_w , and \bar{M}_z . Based upon these results, comment on whether this sample has a broad or narrow molecular-weight distribution compared to typical commercial polymer samples.

1.2 A 50-g polymer sample was fractionated into six samples of different weights given in the table below. The viscosity-average molecular weight, \bar{M}_v , of each was determined and is included in the table. Estimate the number-average and weight-average molecular weights of the original sample. For these calculations, assume that the molecular-weight distribution of each fraction is extremely narrow and can be considered to be *monodisperse*. Would you classify the molecular-weight distribution of the original sample as narrow or broad?

Fraction	Weight (g)	\bar{M}_v
1	1.0	1500
2	5.0	35,000
3	21.0	75,000
4	15.0	150,000
5	6.5	400,000
6	1.5	850,000

1.3 The Schultz–Zimm [11] molecular-weight-distribution function can be written as

$$W(M) = \frac{a^{b+1}}{\Gamma(b+1)} M^b \exp(-aM)$$

where a and b are adjustable parameters (b is a positive real number) and Γ is the gamma function (see Appendix E) that is used to normalize the weight fraction.

(a) Using this relationship, obtain expressions for \bar{M}_n and \bar{M}_w in terms of a and b and an expression for M_{\max} , the molecular weight at the peak of the $W(M)$ curve, in terms of \bar{M}_n .

(b) Derive an expression for M_{\max} , the molecular weight at the peak of the $W(M)$ curve, in terms of \bar{M}_n .

(c) Show how the value of b affects the molecular-weight distribution by graphing $W(M)$ versus M on the same plot for $b = 0.1, 1,$ and 10 given that $\bar{M}_n = 10,000$ for the three distributions.

Hint: $\int_0^\infty x^n \exp(-ax) dx = \Gamma(n+1)/a^{n+1} = n!/a^{n+1}$ (if n is a positive integer).

1.4 The following requested calculations refer to Examples 1.1, 1.2, and 1.3 in the text:

(a) Calculate the z -average molecular weight, \bar{M}_z , of the discrete molecular weight distribution described in Example 1.1.

(b) Calculate the z -average molecular weight, \bar{M}_z , of the continuous molecular-weight distribution shown in Example 1.2.

(c) Obtain an expression for the z -average degree of polymerization, \bar{X}_z , for the Flory distribution described in Example 1.3.

REFERENCES

1. Baekeland, L. H., *The Synthesis, Constitution, and Uses of Bakelite*. Journal of Industrial and Engineering Chemistry, 1909. **1**: p. 149–161.
2. Carothers, W. H., *Polymerization*. Chemical Reviews, 1931. **8**: p. 353–426.
3. Platé, N. A., and I. M. Papisov, *A Classification of Linear Single-Strand Polymers*. Pure and Applied Chemistry, 1989. **61**(2): p. 243–254.
4. Metanomski, W. V., *Compendium of Macromolecular Nomenclature*. 1991, Oxford: Blackwell Scientific Publications.
5. Mita, I., R. F. T. Stepto, and U. W. Suter, *Basic Classification and Definitions of Polymerization Reactors*. Pure and Applied Chemistry, 1994. **66**(12): p. 2483–2486.
6. Hatada, K., et al., *Definitions of Terms Relating to Degradation, Aging, and Related Chemical Transformations of Polymers*. Pure and Applied Chemistry, 1996. **68**(12): p. 2313–2323.
7. Jenkins, A. D., et al., *Glossary of Basic Terms in Polymer Science*. Pure and Applied Chemistry, 1996. **68**(12): p. 2287–2311.
8. Kahovec, J., et al., *Source-Based Nomenclature for Non-Linear Macromolecules and Macromolecular Assemblies*. Pure and Applied Chemistry, 1997. **69**(12): p. 2511–2521.
9. Rogošič, M., H. J. Mencer, and Z. Gomzi, *Polydispersity Index and Molecular Weight Distributions of Polymers*. European Polymer Journal, 1996. **32**(11): p. 1337–1344.
10. Stepto, R. F. T., *Dispersity in Polymer Science (IUPAC Recommendation 2009)*. Pure and Applied Chemistry, 2009. **81**(2): p. 351–353.
11. Zimm, B. H., *The Scattering of Light and the Radial Distribution Function of High Polymer Solutions*. Journal of Chemical Physics, 1948. **16**: p. 1093–1099.

Polymer Synthesis

As discussed in Chapter 1, a useful classification of all polymers is based upon the kinetics of the polymerization. According to this classification scheme, a *step-growth* polymerization is defined as one that involves a *random* reaction between two molecules that may be any combination of monomer, oligomer, or longer-chain molecule. High-molecular-weight polymer is formed only near the end of the polymerization when most of the monomer has been depleted. In *chain-growth* polymerization, the only chain-extension reaction is that of attachment of a monomer to an “active” chain. The active end may be a free radical or an ionic site (i.e., anion or cation). In contrast to step-growth polymerization, high-molecular-weight polymer is formed in the early stages of a chain-growth polymerization.

2.1 Step-Growth Polymerization

The major classifications of step-growth polymers are given in Table 2-1. Of these, the most important in terms of the size of the commercial market are the aliphatic polyamides or nylons (e.g., nylon-6, nylon-6,6, and nylon-6,10) and polyesters (e.g., poly(ethylene terephthalate)). Specialty or engineering-grade step-growth polymers include polycarbonate (e.g., Lexan), aromatic polyamides (e.g., Nomex and Kevlar), polyimides (e.g., Kapton), polysulfones (e.g., Udel), polyurethanes, and poly(2,6-dimethyl-1,4-phenylene oxide) (PPO), as discussed in Chapter 10.

Table 2-1 Classification of Step-Growth Polymers

Classification	Monomer 1	Monomer 2
<i>Condensation</i>		
Polyamide	Dicarboxylic acid	Diamine
Polycarbonate	Bisphenol	Phosgene
Polyester	Dicarboxylic acid	Diol or polyol
Polyimide	Tetracarboxylic acid	Diamine
Polysiloxane	Dichlorosilane	Water
Polysulfone	Bisphenol	Dichlorophenylsulfone
<i>Non-condensation</i>		
Polyurethane	Diisocyanate	Diol or polyol
Poly(phenylene oxide)	2,6-Disubstituted phenol	Oxygen

Several examples of commercially important step-growth polymerizations are illustrated in Figure 2-1. Most step-growth polymerizations involve a classical condensation reaction such as esterification (Figure 2-1A), ester interchange (Figure 2-1B), or amidation (Figure 2-1C). Note that two routes exist for the preparation of the aromatic polyester, poly(ethylene terephthalate) (PET)—polyesterification of terephthalic acid and ethylene glycol (Figure 2-1A) and an ester-interchange reaction involving dimethyl terephthalate and ethylene glycol (Figure 2-1B). These polymerizations and the preparation of the aliphatic polyamide, poly(hexamethylene adipamide) or nylon-6,6 (Figure 2-1C), are examples of A~A/B~B step-growth condensation polymerizations. Each of the two monomers is bifunctional and contains the same functionality at each end (i.e., A or B functional group). For example, PET may be formed by the polycondensation of a dicarboxylic acid (terephthalic acid) and a diol (ethylene glycol) (Figure 2-1A). Alternatively, an aliphatic polyester, poly(ω -hydroxycaproic acid), can be formed by the *self-condensation* of ω -hydroxycaproic acid (Figure 2-1D). Since the functional end groups of this acid are different (i.e., a carboxylic acid and a hydroxyl group at opposite ends), this polyesterification is an example of an A~B step-growth polycondensation.

pared by the ionic *addition* of a diol (1,4-butanediol) to a diisocyanate (1,6-hexane diisocyanate). Note that, unlike a condensation polymerization, a small molecule is not liberated as a by-product of this polymerization. Shown in Figure 2-2B is the polymerization of a high-temperature thermoplastic, poly(2,6-dimethyl-1,4-phenylene oxide), by the oxidative-coupling polymerization of 2,6-xyleneol. The mechanism of this polymerization is *free radical*, but the kinetics of this and the previous polymerization are distinctly step growth, which means that high-molecular-weight polymer is obtained only at the end of the polymerization. Normally, the kinetics of a free-radical polymerization is chain growth, as will be described in Section 2.2.1.

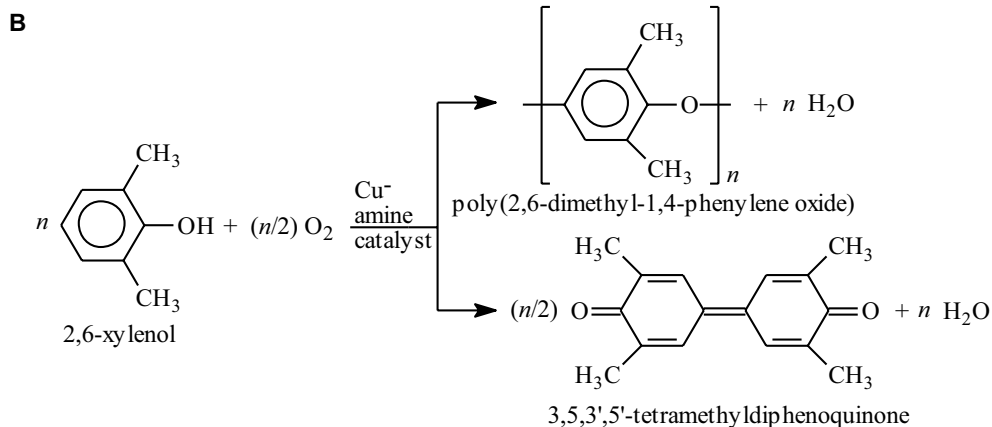
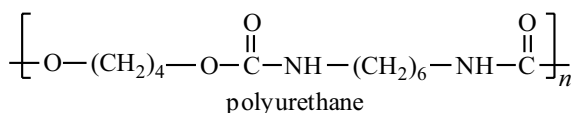
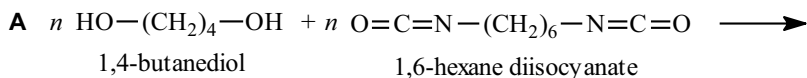


Figure 2-2 Two non-condensation step-growth polymerizations. **A.** Addition polymerization of a polyurethane. **B.** Oxidative-coupling polymerization of 2,6-xyleneol to yield a high-molecular-weight polymer or a low-molecular-weight quinone as a by-product.

2.1.1 Molecular Weight in a Step-Growth Polymerization

Polymer molecular weight in a step-growth polymerization is determined by the fractional conversion, p , of the monomer during this polymerization. One way to

express molecular weight is through the *degree of polymerization*, which normally represents the number of repeating units in the polymer chain. Since any polymerization mechanism yields a distribution of molecular weights, it is useful to define an average degree of polymerization in the same way as average molecular weight was defined earlier (see Section 1.3.2). The average degree of polymerization is designated as \bar{X} or (\overline{DP}) . The most important averages are the number-average (\bar{X}_n) and weight-average (\bar{X}_w) degrees of polymerization. An equation attributed to Carothers [1] relates the number-average degree of polymerization to fractional monomer conversion, p , in a step-growth polymerization as* (see Example 1.3 in Chapter 1)

$$\boxed{\bar{X}_n = \frac{1}{1-p}}. \quad (2.1)$$

The weight-average degree of polymerization is given as

$$\bar{X}_w = \frac{1+p}{1-p}. \quad (2.2)$$

These equations do not apply to interfacial polycondensations or to the step-growth polymerization of monomers having more than two functional groups. Use of eq. (2.1) indicates that, in order to achieve a typical commercial \bar{X}_n of 50, a monomer conversion of 98% ($p = 0.98$) must be obtained; for \bar{X}_n of 100, the monomer conversion must be 99%! This requirement for high conversion necessitates that a nearly exact stoichiometric equivalence of monomers be maintained to obtain high monomer conversion in an A~A/B~B polycondensation. Often, this can be achieved by polymerizing an intermediate low-molecular-weight salt that can be isolated and then further polymerized to higher conversion and, therefore, higher molecular weight. On the other hand, a slight excess of one monomer may be used in a polycondensation reaction to purposely lower molecular weight.

In addition to high conversion, a step-growth polymerization requires high *yield*. High yield means the absence of any side reactions that could deactivate the polymerization process. For example, a carbon-carbon coupling to give a low-molecular-weight quinone derivative is competitive to the carbon-oxygen coupling polymerization of 2,6-xyleneol, as shown in Figure 2-2B. In this case, the yield of

* It follows that the number-average *molecular weight* is given as

$$\bar{M}_n = \bar{X}_n M_o = \frac{M_o}{1-p}$$

where M_o is the molecular weight of the repeating unit.

the high-molecular-weight polymer is determined by the type of catalyst and other polymerization conditions.

High monomer *purity* is also very important in order to obtain high-molecular-weight polymer. In A~A/B~B polycondensation, the incorporation of any monomer that is monofunctional (i.e., having a single A or B group) in the growing polymer chain will terminate the polymerization. An example is the use of a monofunctional amine in place of the diamine in the preparation of nylon-6,6 (see Figure 2-1C). Sometimes, a monofunctional monomer may be added during the polymerization process to control molecular weight. Trifunctional monomers can be used to create crosslinked polymers (i.e., thermosets), as will be discussed in Section 9.3.

In summary, high-molecular-weight polymer can be obtained in a step-growth polymerization only if the following conditions are achieved:

- High monomer conversion
- High monomer purity
- High reaction yield
- Stoichiometric equivalence of functional groups
(in A~A/B~B polymerizations)

2.1.2 Step-Growth Polymerization Kinetics

A step-growth polymerization may be second- or third-order depending on whether it is an A~B or A~A/B~B type and whether a catalyst is involved. The polymerization rate, R_o , may be expressed as the time rate of change of monomer concentration. For a non-catalyzed A~A/B~B polymerization, this polymerization rate, as defined by the rate of *disappearance* of monomer, is second-order in monomer concentration, as given by the expression

$$R_o = -\frac{d[A\sim A]}{dt} = k[A\sim A][B\sim B] \quad (2.3)$$

where k is the polymerization rate constant and the brackets indicate monomer (e.g., A~A or B~B) concentration. Assuming a stoichiometric balance of monomer concentration, eq. (2.3) can be simplified as

$$-\frac{d[A\sim A]}{dt} = k[A\sim A]^2. \quad (2.4)$$

Integration of eq. (2.4) then gives the relation

$$\frac{1}{[A\sim A]} - \frac{1}{[A\sim A]_0} = kt \quad (2.5)$$

where $[A\sim A]_0$ represents the *initial* monomer concentration (i.e., at $t = 0$). The non-polymerized monomer concentration at any time t is related to the fractional conversion and initial monomer concentration by

$$[A\sim A] = (1 - p)[A\sim A]_0. \quad (2.6)$$

Rearrangement of eq. (2.6) for $(1-p)$ and subsequent substitution into the Carothers equation (eq. (2.1)) gives

$$\bar{X}_n = \frac{[A\sim A]_0}{[A\sim A]} \quad (2.7)$$

or

$$[A\sim A] = \frac{[A\sim A]_0}{\bar{X}_n}. \quad (2.8)$$

Substitution of eq. (2.8) into eq. (2.5) and subsequent rearrangement gives the final result

$$\bar{X}_n = [A\sim A]_0 kt + 1. \quad (2.9)$$

Equation (2.9) indicates that the number-average degree of polymerization is a linear function of time in this second-order step-growth reaction.

2.2 Chain-Growth Polymerization

Chain-growth polymerizations require the presence of an initiating molecule that can react with a monomer molecule at the start of the polymerization. The initiating species may be a radical, anion, or cation, as discussed in the following sections. Free-radical, anionic, and cationic chain-growth polymerizations share three common steps—*initiation*, *propagation*, and *termination*. In the case of the polymerization of vinyl monomers (see Table 1-2, Chapter 1), the polymerization mechanism (i.e., free radical, anionic, or cationic) depends, in part, on the chemical nature of the substituent group (i.e., R_1 , R_2 , R_3 , and R_4 , Table 1-2). In terms of general guidelines, monomers with an *electron-withdrawing* group can polymerize by an anionic pathway, while those with an *electron-donating* group follow a cationic pathway.

Some important vinyl monomers such as methyl methacrylate and styrene can be polymerized by more than one pathway (e.g., free radical and anionic).

2.2.1 Free-Radical Polymerization and Copolymerization

Like other chain-growth polymerizations, a free-radical polymerization has three principal steps:

- Initiation of the active monomer
- Propagation or growth of the active (i.e., free-radical) chain by sequential addition of monomers
- Termination of the active chain to give the final polymer product

These steps and their associated kinetics are described next in general terms for free-radical polymerizations, with the polymerization of styrene used as an example.

The Initiation Step. Initiation in a free-radical polymerization consists of two steps—a *dissociation* of the initiator to form two radical species, followed by addition of a single monomer molecule to the initiating radical (the *association* step). The dissociation of the initiator ($I \sim I$) to form two free-radical initiator species ($I\cdot$) can be represented as



where k_d is the *dissociation rate constant*. The dissociation rate constant follows an Arrhenius dependence on temperature given as

$$k_d = A \exp(-E_a/RT) \quad (2.11)$$

where A in eq. (2.11) is a rate parameter and E_a is the *activation energy* for dissociation. In addition to a strong dependence on temperature, dissociation rate constants for different initiators vary with the nature of the solvent used in solution polymerization, as shown by data given in Table 2-2.

Initiators for free-radical polymerizations include any organic compound with a chemical group capable of homolytic cleavage, such as an azo ($-N=N-$), disulfide ($-S-S-$), or peroxide ($-O-O-$) compound. The labile bond of the initiator can be broken by application of heat or radiation, such as UV or γ -irradiation. An important example of a free-radical initiator is benzoyl peroxide that dissociates into two identical radical species

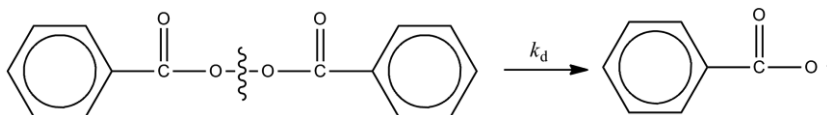
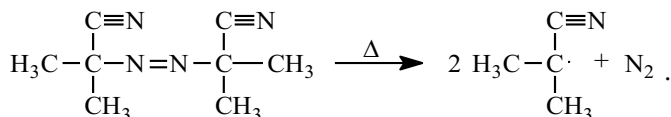


Table 2-2 Dissociation Rate Constants for Some Common Initiators in Solution

Initiator	Solvent	T ($^{\circ}\text{C}$)	k_d (s^{-1})	E_a (kJ mol^{-1})
Benzoyl peroxide	Benzene	30	4.80×10^{-8}	116
		70	1.38×10^{-5}	
	Toluene	30	4.94×10^{-8}	121
		70	1.10×10^{-5}	
AIBN	Benzene	40	5.44×10^{-7}	128
		70	3.17×10^{-5}	
	Toluene	70	4.00×10^{-5}	121

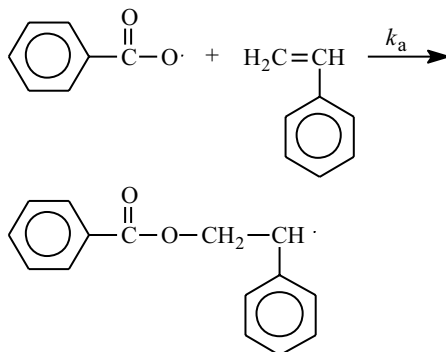
Another important group of free-radical initiators is the family of azo ($\text{R}-\text{N}=\text{N}-\text{R}$) compounds such as 2,2'-azobis(isobutyronitrile) (AIBN), which thermally decomposes into nitrogen gas and two cyanoisopropyl radicals ($\text{R}\cdot$) as



In the second step of initiation (i.e., *association*), a monomer molecule (M) is attached to the initiator radical. This addition step may be represented as



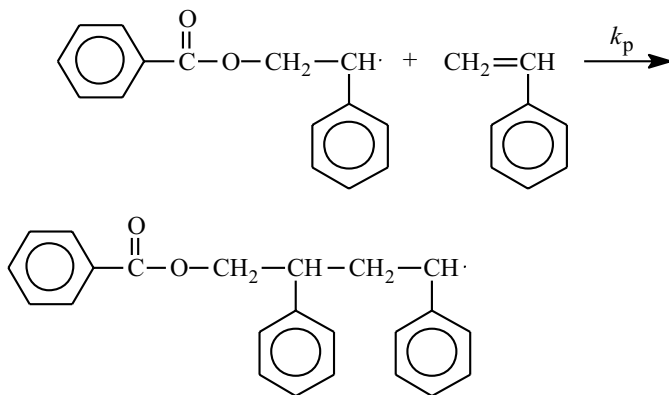
where k_a is the rate constant for monomer association. In the specific case of the polymerization of styrene initiated by benzoyl peroxide, the addition occurs as



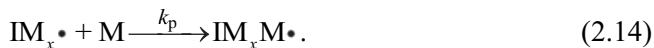
The Propagation Step. In the next step, called *propagation*, additional monomer units are added to the initiated monomer species as



where k_p is the *propagation rate constant*. For styrene addition with benzoyl peroxide initiation, the first propagation step is

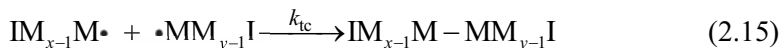


Additional monomers are added sequentially during subsequent propagation steps, as represented by the generalized equation

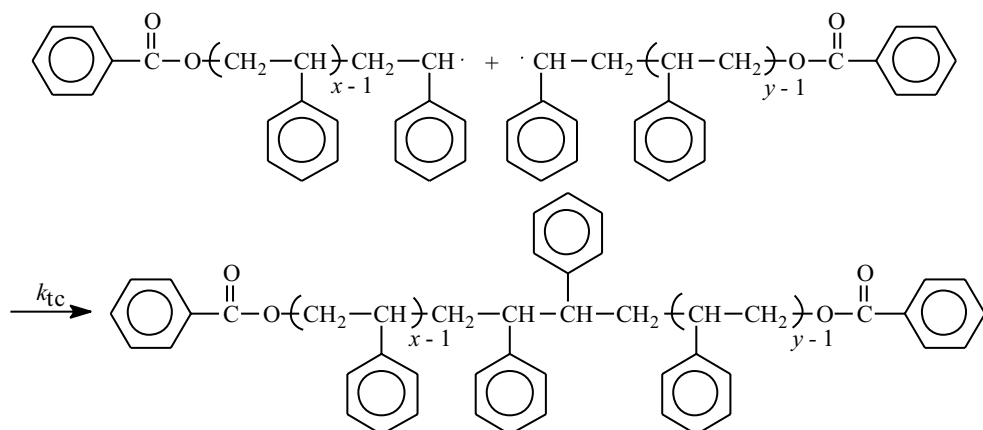


During the propagation step in vinyl polymerization, the energetically preferred placement of monomers is head-to-tail where the carbon atom with the larger substituent groups can be considered the “head.” Head-to-head placement can occur, for example, during termination by combination as discussed in the next section.

Termination. Propagation will continue until an actual termination process occurs. An obvious termination mechanism involves two propagating radical chains having arbitrary degrees of polymerization (x and y) meeting at their free-radical ends. Termination in this manner occurs by *combination* giving one terminated chain of degree of polymerization $x+y$ through the formation of a covalent bond between the two combining radical chains. Termination by combination is illustrated by the following reaction:



where k_{tc} is the termination rate constant. In the example of styrene polymerization, termination by combination gives the following reaction:

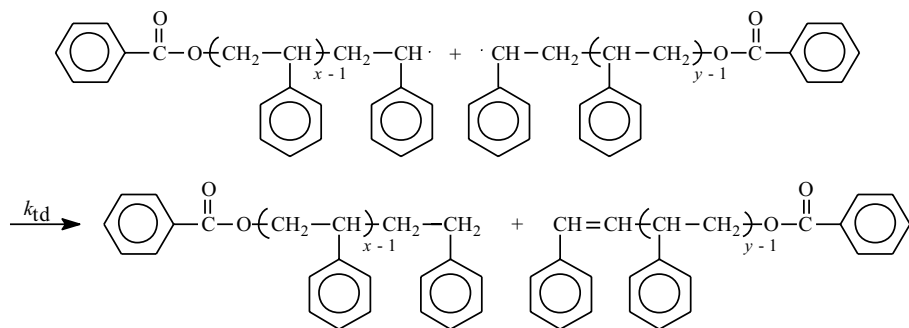


The structure resulting from termination by combination has a single head-to-head placement of styrene units at the combination site.

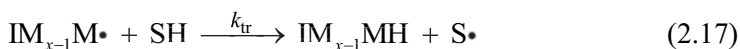
Termination also can occur by a *disproportionation* reaction to give two terminated chains, as illustrated below. In this case, one terminated chain will have an unsaturated carbon group while the other terminated end is fully saturated. In both cases of termination, one end of each polymer chain (i.e., in termination by disproportionation) or both ends of the chain (i.e., in termination by combination) contain the initiating free-radical group of the initiator molecule. In the case of termination by combination, the benzoyl peroxide group caps *both* ends of the chain. This indicates an important difference between an initiator, which becomes part of the terminated chain, and a polymerization *catalyst*, which promotes the polymerization but is fully recovered at the end of the polymerization. Catalysts are used in cationic and coordination polymerizations as discussed in Sections 2.2.2 and 2.2.3. Termination by disproportionation is illustrated by the following reaction (rate constant, k_{td}):



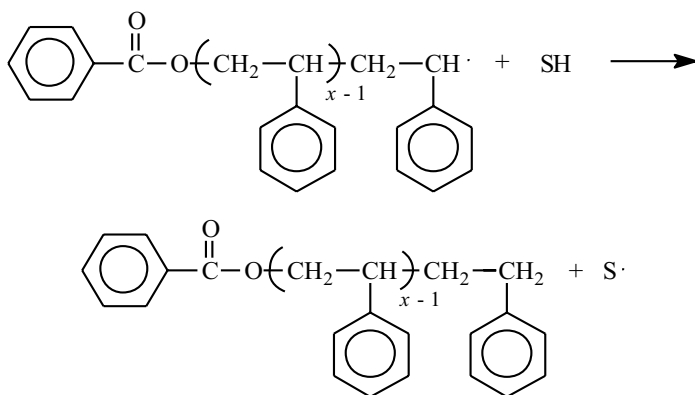
In the example of styrene polymerization, termination by disproportionation gives the following reaction:



In addition to termination by combination and disproportionation, another mechanism of termination is *chain transfer* by hydrogen abstraction from an initiator, monomer, polymer, or solvent molecule. In general terms, this process can be represented as



where k_{tr} is the rate constant for the chain-transfer reaction and SH represents a solvent or any other molecule with an abstractable hydrogen atom. In the specific case of the benzoyl-peroxide-initiated polymerization of styrene, termination by chain transfer occurs as



As illustrated, the radical site is transferred to the chain-transfer agent ($\text{S}\cdot$), which can then sequentially add monomer units to continue the polymerization process. Subsequent termination of the growing chain-transfer radical chain ($\text{SM}_x\cdot$) will result in a terminated chain having one (i.e., termination by disproportionation) or two (i.e., termination by combination) chain-transfer (S) groups at the polymer ends.

Examples of propagation and termination rate constants are given in Table 2-3. Both k_p and k_t show a strong (Arrhenius) dependence upon temperature, as illustrat-

ed by temperature data for styrene. Rate constants can vary by several orders of magnitude depending on monomer type (i.e., vary with the chemical nature of the substituent group in vinyl polymerization).

Table 2-3 Representative Values of Propagation and Termination Rate Constants

Monomer	T (°C)	k_p (L mol ⁻¹ s ⁻¹)	k_t (L mol ⁻¹ s ⁻¹) × 10 ⁻⁶
Styrene	25	44	48
	30	55	51
	60	176	72
Vinyl acetate	25	1012	59
Vinyl chloride	25	3130	2300
Vinylidene chloride	25	6.6	0.175
Acrylonitrile	25	52	5
Ethylene ^a	83	470	1050
Methyl methacrylate	40	513	47

^a Polymerization in benzene.

Free-Radical Polymerization Kinetics. The overall rate of polymerization (R_o) in a free-radical polymerization is simply the rate of chain propagation (R_p), which is obtained from eq. (2.14) as

$$R_o \equiv R_p = k_p [IM_x \cdot][M]. \quad (2.18)$$

This statement makes the assumption that all steps, including the first, in the propagation step have equal reactivity. Compared to step-growth polymerization, the propagation rate for free-radical, chain-growth polymerization is very rapid. A very high-molecular-weight polymer chain can be formed in less than one second although not all chains in the same sample form at the same instant.

One problem with the use of eq. (2.18) to determine the polymerization rate is that the radical concentration, $[IM_x \cdot]$, normally is not known. To overcome this difficulty, the radical concentration can be related to more easily determined concentrations (i.e., monomer and initiator concentrations) by assuming that the total radical population obtains a *steady-state* concentration over most of the polymerization process. Since radicals are formed in the initiation step and consumed in the termination step, the steady-state condition can be expressed as

$$R_i \equiv R_t. \quad (2.19)$$

As described previously, the initiation process involves two distinct steps—initiator dissociation and monomer association. *The overall rate of initiation is controlled by the slower step—the dissociation of the initiator.* The rate of initiation, expressed as the time rate of increase in radical-initiator concentration, is then obtained from the dissociation expression (eq. (2.10)) as

$$R_i = \frac{d[\mathbf{I}\cdot]}{dt} = 2k_d[\mathbf{I}] \quad (2.20)$$

where $[\mathbf{I}]$ represents the initiator ($\mathbf{I-I}$) concentration. The factor of 2 appearing on the RHS of eq. (2.20) indicates that *two* radicals are produced in each dissociation step. In order to obtain an expression for the rate of polymerization, it is necessary to consider only those initiator radicals that add monomer and, therefore, contribute to chain propagation. Some initiator radicals may recombine with other radicals (e.g., initiator and monomer radical groups) or partially decompose into non-initiating products. For these reasons, only some fraction, f , of the original initiator concentration is effective in contributing to the polymerization process. Typical initiator efficiencies fall in the range from 0.3 to 0.8 (e.g., $f \sim 0.6$ for AIBN over a wide range of monomer concentrations). The fraction of effective initiator radicals can then be introduced in the rate expression (eq. (2.20)) to give

$$R_i = \frac{d[\mathbf{I}\cdot]}{dt} = 2fk_d[\mathbf{I}]. \quad (2.21)$$

In a similar fashion, the rate of termination is the time rate of decrease in radical concentration (i.e., the propagating radical chain) resulting from all operative termination steps—combination (eq. (2.15)), dissociation (eq. (2.16)), and/or chain transfer (eq. (2.17)). For the moment, it is convenient to consider only termination by combination and disproportionation and leave termination by chain transfer for later treatment. As an additional simplification, termination by *both* combination and disproportionation can be expressed as



where \mathbf{P} represents the *deactivated* polymer and the termination rate constant, k_t , is the sum of the individual termination rate constants for combination and disproportionation (i.e., $k_t = k_{tc} + k_{td}$). Therefore, the termination rate equation can be written for the reaction given in eq. (2.22) as

$$R_t = -\frac{d[\mathbf{IM}_x\cdot]}{dt} = 2k_t[\mathbf{IM}_x\cdot]^2. \quad (2.23)$$

The factor of 2 arises because two radicals are consumed in each termination step.

Applying the steady-state assumption (eq. (2.19)) by equating eqs. (2.21) and (2.23) gives the expression for the radical concentration as

$$[\mathbf{IM}_x\cdot] = \left(\frac{fk_d}{k_t} \right)^{1/2} [\mathbf{I}]^{1/2}. \quad (2.24)$$

Finally, substitution of eq. (2.24) into the polymerization rate equation (eq. (2.18)) gives the following important result:

$$R_o = k_p \left(\frac{fk_d}{k_t} \right)^{1/2} [I]^{1/2} [M]. \quad (2.25)$$

Equation (2.25) shows that the polymerization rate in free-radical polymerization is proportional to monomer concentration and to the square root of initiator concentration.*

The number-average degree of polymerization at any time can be obtained as the ratio of the rate of propagation to the rate of termination†

$$\bar{X}_n = \frac{R_p}{R_t} \quad (2.26)$$

which at steady state is given (from eqs. (2.18), (2.23), and (2.24)) as

* It is important to recognize that eq. (2.25) gives the polymerization rate at some arbitrary time t when the initiator and monomer concentrations at that time are $[I]$ and $[M]$. These concentrations differ from their initial concentrations, $[I]_o$ and $[M]_o$, which are known at the beginning of the polymerization. The relationships between $[I]$ and $[I]_o$ and between $[M]$ and $[M]_o$ are obtained from their corresponding rate equations. For example, the initiator concentration is obtained from the rate of dissociation obtained from eq. (2.10) as

$$-\frac{d[I]}{dt} = k_d[I].$$

Rearrangement and integration of the above equation from $t = 0$ to a time t gives

$$[I] = [I]_o \exp(-k_d t).$$

Similarly, monomer concentration is obtained from the propagation step (eq. (2.14)) as

$$-\frac{d[M]}{dt} = k_p [IM_x^\bullet] [M]$$

which upon integration gives

$$[M] = [M]_o \exp(-k_p [IM_x^\bullet] t)$$

where $[IM_x^\bullet]$ can be obtained from $[I]$ by means of eq. (2.24).

† A *kinetic chain length*, ν , is defined as the average number of steps of growth per effective radical expressed as the ratio of the propagation and initiation rates ($\nu = R_p/R_i$).

$$\bar{X}_n = \frac{k_p [M]}{2(k_t f k_d [I])^{1/2}}. \quad (2.27)$$

In the preceding derivations, we have considered only termination by combination and disproportionation. If termination by chain transfer also occurs, the degree of polymerization (eq. (2.26)) must be modified to include this contribution to the termination rate. As the chain-transfer process increases the overall rate of termination, it is clear from eq. (2.26) that the degree of polymerization, therefore, should decrease. We can write the number-average degree of polymerization in the case of termination by all three termination mechanisms as

$$\bar{X}_n = \frac{R_p}{R_{tc} + R_{td} + R_{tr}} \quad (2.28)$$

where R_{tr} is the rate of termination by chain transfer obtained from eq. (2.17) as

$$R_{tr} = k_{tr} [IM_x \cdot] [SH]. \quad (2.29)$$

Rearrangement of eq. (2.28), followed by substitution of the rate equation for R_{tr} (eq. (2.29)) and that for R_p (eq. (2.18)), gives

$$\frac{1}{\bar{X}_n} = \frac{1}{(\bar{X}_n)_o} + C \left(\frac{[SH]}{[M]} \right) \quad (2.30)$$

where $(\bar{X}_n)_o$ is the number-average degree of polymerization in the *absence* of chain transfer (i.e., eq. (2.26)) and C is the *chain-transfer coefficient* given as

$$C = \frac{k_{tr}}{k_p}. \quad (2.31)$$

Representative values of chain-transfer constants for several common monomers and chain-transfer agents (i.e., initiator, monomer, polymer, solvent, or additive) are given in Table 2-4. As indicated by the form of eq. (2.30), molecular weight will decrease with an increase in the concentration of the chain-transfer agent (SH).

Table 2-4 Representative Values of Chain-Transfer Constants

Monomer	Chain-Transfer Agent	T ($^{\circ}\text{C}$)	$C \times 10^4$
Styrene	Styrene	25	0.279
		50	0.35–0.78
	Polystyrene	50	1.9–16.6
	Benzoyl peroxide	50	0.13
	Toluene	60	0.125
Methyl methacrylate	Methyl methacrylate	30	0.117
		70	0.2
	Poly(methyl methacrylate)	50	0.22–1000
	Benzoyl peroxide	50	0.01
	Toluene	40	0.170

Thermodynamics of Free-Radical Polymerization. As illustrated in Figure 2-3, most chain-growth polymerization become reversible at a given temperature called the *ceiling temperature*, T_c , which depends upon monomer concentration as discussed below.

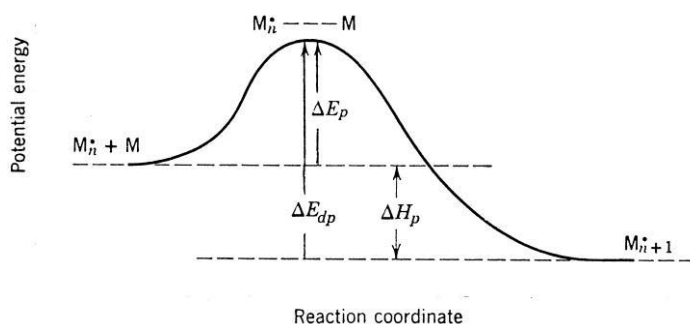
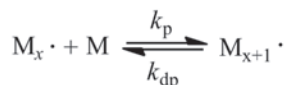


Figure 2-3 Reaction coordinate representation of polymerization and depolymerization. Adapted from R. W. Lenz, *Organic Chemistry of Synthetic High Polymers*, 1967. New York: Interscience Publishers (John Wiley & Sons). Diagram 11-53, p. 326.

The reversible polymerization can be written as



where k_p and k_{dp} are the rate constants for polymerization (or propagation) and depolymerization, respectively. The chemical equilibrium constant, K , is then given as

$$K = \frac{k_p}{k_{dp}} = \frac{[M_{x+1} \cdot]}{[M_x \cdot][M]} \approx \frac{1}{[M]}. \quad (2.32)$$

From the first and second laws of thermodynamics for a reversible process and using eq. (2.32), the standard-state Gibbs free energy of polymerization at the ceiling temperature, T_c , where the rates of polymerization and depolymerization are equal, can be written as

$$\Delta G_p^\circ = 0 = \Delta H_p^\circ + T_c \Delta S_p^\circ = -RT_c \ln K = RT_c \ln [M]_c \quad (2.33)$$

where the standard state of the monomer is taken to be pure monomer or a 1 M solution at 25°C. The standard state for the polymer is the solid polymer at 25°C. The entropy change, resulting from the loss in translational entropy of the monomer due to polymerization, is relatively insensitive to monomer type. The *heat of polymerization*, ΔH_p , is defined as

$$\Delta H_p = E_{dp} - E_p \quad (2.34)$$

where E_{dp} and E_p are the activation energies for depolymerization* and propagation,† respectively. Rearranging eq. (2.33) gives an expression for the ceiling temperature as

$$T_c = \frac{\Delta H_p^\circ}{\Delta S_p^\circ + R \ln [M]_c}. \quad (2.35)$$

Alternatively, rearrangement of eq. (2.35) gives an expression for monomer concentration as a function of temperature in the form

$$\ln [M]_c = \frac{\Delta H_p^\circ}{RT_c} - \frac{\Delta S_p^\circ}{R} \quad (2.36)$$

where $\Delta H_p^\circ \approx \Delta H_p$ since the enthalpy change is independent of the monomer concentration. Values of ΔH_p° and T_c (for pure monomer, $[M] = 1$) for some common monomers are given in Table 2-5.

* $k_{dp} = A_{dp} \exp(-E_{dp}/RT)$.

† $k_p = A_p \exp(-E_p/RT)$.

Table 2-5 Representative Heats of Polymerization and Ceiling Temperatures

Monomer	ΔH_p (kJ mol ⁻¹)	T_c (°C)
α -Methylstyrene	-35	61
Methyl methacrylate	-55	220
Propylene	-69	300
Styrene	-69	310
Ethylene	-94	400
Tetrafluoroethylene	-192	580

Free-Radical Copolymerization. As illustrated in Figure 2-4, four separate propagation steps are possible in a free-radical copolymerization. Each propagation step has its own rate constant k_{ij} , where the first subscript, i , identifies the monomer at the end of the propagating chain (i.e., $\sim\sim\sim M_i \cdot$) prior to addition of monomer j . The rates of disappearance of comonomers M_1 and M_2 can be obtained by considering the individual steps by which M_1 (see propagation steps A and C) and M_2 (see propagation steps B and D) are consumed. The rate equations are, therefore, given as

$$\frac{-d[M_1]}{dt} = k_{11} [\sim\sim\sim M_1 \cdot][M_1] + k_{21} [\sim\sim\sim M_2 \cdot][M_1] \quad (2.37)$$

and

$$\frac{-d[M_2]}{dt} = k_{12} [\sim\sim\sim M_1 \cdot][M_2] + k_{22} [\sim\sim\sim M_2 \cdot][M_2]. \quad (2.38)$$

In the case of a terpolymerization (three monomers), the number of propagation steps would increase from four to nine and *three* separate rate equations would be needed.

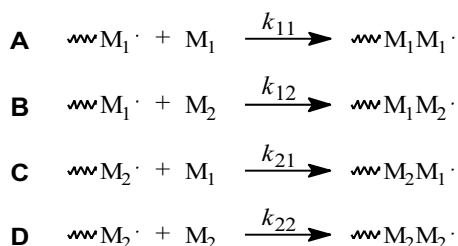


Figure 2-4 The four propagation steps that can occur during a free-radical copolymerization.

During a copolymerization it is important to be able to predict how copolymer composition varies as a function of comonomer reactivity and concentration at any

time. The approach used relies on the realization that a monomer consumed during the copolymerization becomes incorporated into the copolymer structure and, therefore, any relative change in the composition of the comonomer mixture reflects the composition of the copolymer formed at that instance of time. The relative change in the comonomer composition is given by the *instantaneous copolymerization equation* obtained by dividing eq. (2.37) by eq. (2.38) in the form

$$\frac{d[M_1]}{d[M_2]} = \frac{[M_1]}{[M_2]} \frac{k_{11} [\text{---}M_1\cdot] + k_{21} [\text{---}M_2\cdot]}{k_{12} [\text{---}M_1\cdot] + k_{22} [\text{---}M_2\cdot]} \quad (2.39)$$

Equation (2.39) can be expressed in a more concise form by use of monomer *reactivity ratios*. Reactivity ratios for monomers 1 and 2 are defined by

$$r_1 = \frac{k_{11}}{k_{12}} \quad (2.40)$$

and

$$r_2 = \frac{k_{22}}{k_{21}} \quad (2.41)$$

These expressions indicate that the reactivity ratio for monomer 1, r_1 , is simply the ratio of the propagation rate constants for the addition of M_1 (i.e., homopolymerization) and addition of M_2 (i.e., copolymerization) to a propagating radical chain with monomer 1 at the radical end ($\text{---}M_1\cdot$). Similarly, the reactivity ratio for monomer 2 is the ratio of the propagation rate constants for the addition of M_2 (i.e., homopolymerization) and addition of M_1 (i.e., copolymerization) to a propagating radical chain with monomer 2 at the radical end ($\text{---}M_2\cdot$). The definitions of reactivity ratios (eqs. (2.40) and (2.41)) indicate that when both reactivity ratios equal unity, there is no preferential monomer incorporation into the propagating chain (i.e., $k_{11} = k_{12}$ and $k_{22} = k_{21}$). This means that the monomer sequence in the resulting copolymer is completely *random*. An example of a nearly random or “ideal” copolymerization is that of styrene and 4-chlorostyrene (see Problem 2.4). When both reactivity ratios are zero (i.e., $k_{11} = k_{22} = 0$), the monomer sequence will be *alternating*, as approached by the copolymerization of styrene and maleic anhydride. If both reactivity ratios are small but not exactly zero, the comonomer sequence will not be completely alternating but will have segments of alternating sequences. Examples include the commercially important copolymers of styrene and acrylonitrile. On the other hand, when *both* reactivity ratios are very much larger than unity (i.e., $k_{ii} \gg k_{ij}$), only a block copolymer or a mixture of the two homopolymers will form.

Reactivity ratios have been determined for many important combinations of monomers and have been tabulated in several reference sources, such as the *Polymer Handbook* [2]. Some representative values are given in Table 2-6. Reactivity ratios for less common monomer pairs can be calculated by means of the Q - e scheme proposed by Alfrey and Price [3] in 1946. In this approach, the propagation rate constant, k_{ij} , is obtained from the relationship

$$k_{ij} = P_i Q_j \exp(-e_i e_j) \quad (2.42)$$

where P_i is a proportionality constant, Q_j is a measure of the monomer reactivity, and e represents the polarity of the radical $M_1\cdot$ (i.e., e_1) or $M_2\cdot$ (i.e., e_2). It then follows from the definition of the reactivity ratios, eqs. (2.40) and (2.41), that

$$r_1 = \frac{k_{11}}{k_{12}} = \left(\frac{Q_1}{Q_2} \right) \exp[-e_1(e_1 - e_2)] \quad (2.43)$$

and

$$r_2 = \frac{k_{22}}{k_{21}} = \left(\frac{Q_2}{Q_1} \right) \exp[-e_2(e_2 - e_1)]. \quad (2.44)$$

Table 2-6 Reactivity Ratios for Free-Radical Copolymerization

Monomer 1	Monomer 2	r_1	r_2
Ethylene	Vinyl acetate	0.13	1.23
	Carbon monoxide	0.025	0.004
	Propylene	3.2	0.62
	Tetrafluoroethylene	0.575	0.065
	Vinylidene chloride	0.018	0.005
Styrene	Acrylonitrile	0.29	0.02
	Butadiene	0.82	1.38
	<i>p</i> -Divinylbenzene	0.26	1.18
	Methyl acrylate	0.53	0.46
	Maleic anhydride	0.97	0.001
	Methacrylonitrile	0.38	0.42
	Methyl methacrylate	0.585	0.478
	4-Chlorostyrene	0.816	1.062
	Vinyl acetate	60	0.16
	Vinylidene chloride	1.7	0.11
Vinyl chloride	Vinylidene chloride	0.205	3.068
Methyl methacrylate	Methacrylic acid	0.77	1.84
	Maleic anhydride	3.85	0.01

Values of Q and e also have been tabulated [2] for many monomers and can be calculated from quantum chemical calculations [4]. Table 2-7 gives values for some commercially important monomers. Values of Q and e are referenced to styrene, the most common comonomer, for which Q is set to 1.0. In general, the value of a reactivity ratio is independent of the nature of the initiator and solvent in a free-radical copolymerization; however, there is a weak dependence on temperature.

A limitation of the copolymerization equation as written in eq. (2.39) is the use of radical-chain concentrations, which are typically not known. By using the definitions of reactivity ratios and by assuming a steady-state concentration of radicals for either $\cdot M_1$ or $\cdot M_2$ during propagation, the instantaneous copolymerization equation, as first derived by Mayo and Lewis [5], becomes

$$\frac{d[M_1]}{d[M_2]} = \frac{[M_1] \left(r_1 [M_1] + [M_2] \right)}{[M_2] \left([M_1] + r_2 [M_2] \right)}. \quad (2.45)$$

Since the relative rate of monomer disappearance must be equal to the relative rate of monomer incorporation, eq. (2.45) can be used to estimate copolymer composition when the reactivity ratios are known. Conversely, knowledge of monomer concentration and determination of the copolymer composition can be used to obtain experimental values for the reactivity ratios.

Table 2-7 Q-e Values for Free-Radical Copolymerization

Monomer	Q	e
Acrylamide	0.23	0.54
Acrylonitrile	0.48	1.23
Butadiene	1.70	-0.50
4-Chlorostyrene	1.33	-0.64
Ethylene	0.016	0.05
Isobutylene	0.023	-1.20
Isoprene	1.99	-0.55
Maleic anhydride	0.86	3.69
Methacrylic acid	0.98	0.62
Methyl methacrylate	0.78	0.40
N-Vinyl pyrrolidone	0.088	-1.62
Styrene	1.00	-0.80
Vinyl acetate	0.026	-0.88
Vinyl chloride	0.056	0.16
Vinylidene chloride	0.31	0.34

The copolymerization equation (eq. (2.45)) may be expressed in an alternative form that is useful for calculating the instantaneous copolymer composition for a given monomer concentration. For this purpose, the mole fraction of monomer 1 in the monomer mixture is defined as

$$f_1 = \frac{[M_1]}{[M_1] + [M_2]} \quad (2.46)$$

where $f_1 + f_2 = 1$. In a similar fashion, the mole fraction of monomer 1 in the copolymer, F_1 , is given by the relative differential change in monomer concentration as

$$F_1 = \frac{d[M_1]}{d[M_1] + d[M_2]} \quad (2.47)$$

where $F_1 + F_2 = 1$. If the numerator and denominator of eq. (2.47) are each divided by $d[M_2]$, use of eqs. (2.45) and (2.46) gives the following useful relationship:

$$F_1 = \frac{r_1 f_1^2 + f_1 f_2}{r_1 f_1^2 + 2f_1 f_2 + r_2 f_2^2}. \quad (2.48)$$

An illustration of several possible relationships between f_1 and F_1 is given by Figure 2-5. Use of eq. (2.48) indicates that $F_1 = f_1$ when $r_1 = r_2 = 1$. This is the limiting case of *ideal* or random copolymerization illustrated by the dashed line (originating at the origin) in Figure 2-5. Inspection of eq. (2.48) also indicates that $F_1 = 0.5$ when $r_1 = r_2 = 0$. In this case, the copolymer sequence is always *alternating* and is, therefore, *independent of the comonomer concentration of the feed* as indicated by the horizontal broken line in Figure 2-5. An example of a copolymerization that is intermediate between these two extremes of ideal and alternating copolymerization is that of styrene and methyl methacrylate, illustrated by the curve in Figure 2-5. In such copolymerizations that are neither ideal (i.e., random) nor perfectly alternating, the most reactive monomer will be preferentially consumed. This means that the monomer feed composition will change (i.e., drift) with time. If this drift is appreciable, the product copolymer obtained at high monomer conversion will be a heterogeneous mixture of individual copolymers having different compositions. This heterogeneity can lead to undesirable properties such as low mechanical strength due to phase separation in the solid state. To avoid significant drift, copolymerization conversion can be kept low. Unfortunately, low conversion results in high costs for copolymer recovery. In commercial practice, the more rapidly depleted monomer may be continuously added to the copolymerization mixture to maintain a constant feed composition. As shown in Figure 2-5, there is a composition where the copolymerization curve crosses over the ideal copolymerization (i.e., diagonal) line and the copolymer will have the same composition as the monomer feed. This point is termed *azeotropic copolymerization*.

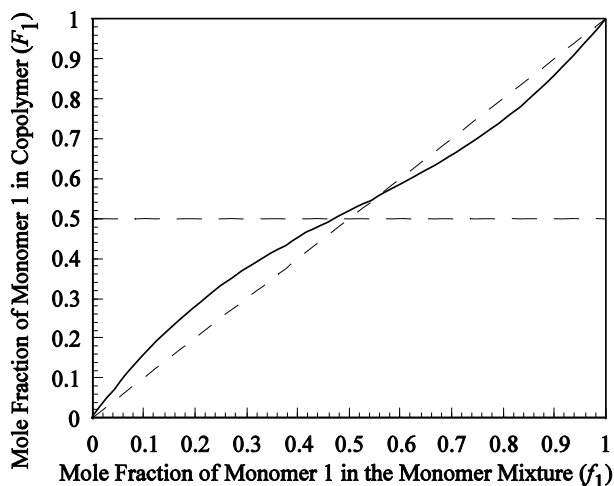


Figure 2-5 Plot of mole fraction of monomer 1 in the copolymer, F_1 , versus mole fraction of monomer 1 in the feed, f_1 , for (---) ideal ($r_1 = r_2 = 1$), (- -) alternating ($r_1 = r_2 = 0$), and (—) partially alternating copolymerization (the copolymerization of styrene and methyl methacrylate, where $r_1 = 0.585$ and $r_2 = 0.478$, respectively).

Example 2.1

Using reactivity ratios of styrene (1) and 4-chlorostyrene (2) calculated from Q - e values given in Table 2-7, determine the instantaneous copolymer composition (i.e., mole fraction of styrene) resulting from the free-radical copolymerization of an equimolar mixture of styrene and 4-chlorostyrene.

Solution

From eq. (2.43), we have

$$r_1 = \left(\frac{1.0}{1.33} \right) \exp[0.80(-0.80 + 0.64)] = 0.752 \exp(-0.128) = 0.662.$$

and from eq. (2.44), we have

$$r_2 = \left(\frac{1.33}{1.0} \right) \exp[0.64(-0.64 + 0.80)] = 1.33 \exp(0.102) = 1.47.$$

These values differ from those given in Table 2-6; however, it is noted that there is typically significant variations in reported reactivity ratios obtained from experiment. For example, the reactivity ratio (r_2) for 4-chlorostyrene in styrene/4-chlorostyrene copolymerization has been reported in the range from 0.76 to 1.76 [2]. Using the Q - e values for r_1 and r_2 , the instantaneous mole fraction of styrene in the copolymer is:

$$F_1 = \frac{r_1 f_1^2 + f_1 f_2}{r_1 f_1^2 + 2 f_1 f_2 + r_2 f_2^2} = \frac{0.662(0.5)^2 + 0.5^2}{0.662(0.5)^2 + 2(0.5)^2 + 1.47(0.5)^2} = \frac{0.166 + 0.25}{0.166 + 0.5 + 0.368}$$

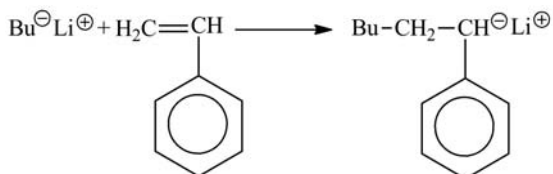
$$= \frac{0.416}{1.03} = 0.404.$$

This result indicates that the copolymer would be expected to be enriched in monomer 2 (i.e., 4-chlorostyrene) as has been observed experimentally.

2.2.2 Ionic Polymerization and Copolymerization

Ionic polymerizations follow the same basic steps as free-radical chain-growth polymerizations (i.e., initiation, propagation, and termination); however, there are some important differences, as will be discussed in the following sections. Either a carbanion (C^\ominus) or carbonium (C^\oplus) ionic site can be formed in the initiation process. Polymerization of vinyl monomers with an electron-withdrawing group can proceed by an anionic pathway, while monomers with an electron-donating group (e.g., methyl) can polymerize by a cationic mechanism.

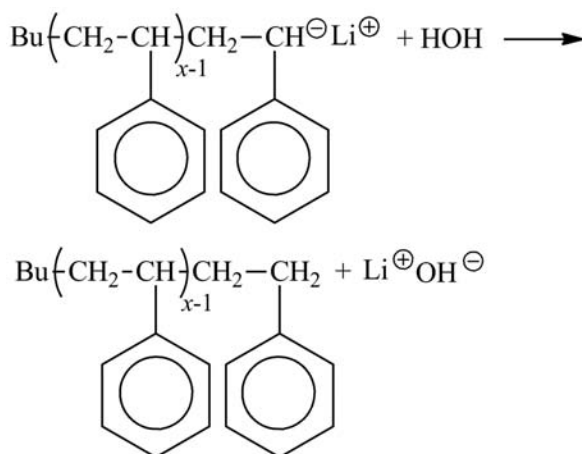
Anionic Polymerization. The initiator in an anionic polymerization may be any strong nucleophile, including Grignard reagents* and other organometallic compounds like *n*-butyl (*n*-C₄H₉) lithium. As an example, the anionic initiation of styrene is illustrated next:



During the initiation process, the addition of the butyl anion to styrene produces a carbanion at the head end in association with the positively charged lithium *counterion*. The chain propagates by insertion of additional styrene monomers between the carbanion and counterion.

If the starting reagents are pure and if the polymerization reactor is purged of all oxygen and traces of water, propagation can proceed indefinitely or until all monomer is consumed. For this reason, anionic polymerization is sometimes called “living” polymerization [6]. In this case, termination occurs only by the deliberate introduction of oxygen, carbon dioxide, methanol, or water as follows:

* The chemical formula of a Grignard reagent can be expressed as RMgX, where R can be an alkyl, aryl, or other organic group and X is a halogen, typically Cl, Br, or I.



Note that the initiating species in this example ($n\text{-C}_4\text{H}_9$) has been incorporated as an end group of the terminated polymer chain. This illustrates the role of butyllithium as an initiator—rather than a catalyst—as was also the case for benzoyl peroxide in the free-radical polymerization of styrene.

In the absence of a termination mechanism, each monomer in an anionic polymerization has an equal probability of attaching to an anionic site. Therefore, the number-average degree of polymerization, \bar{X}_n , is simply equal to the ratio of initial monomer to initiator concentration

$$\bar{X}_n = \frac{[\text{M}]_0}{[\text{I}]_0} \quad (2.49)$$

as illustrated in Example 2.2. The absence of termination during a *living polymerization* leads to a very narrow-molecular-weight distribution with polydispersities (see Section 1.3.2) as low as 1.04.

Example 2.2

Calculate the number-average molecular weight of polystyrene obtained at the completion of an anionic (i.e., “living”) polymerization in which 0.01 g of n -butyllithium and 10 g of styrene monomer are used. The molecular weights of butyllithium and styrene are 64.06 and 104.12, respectively.

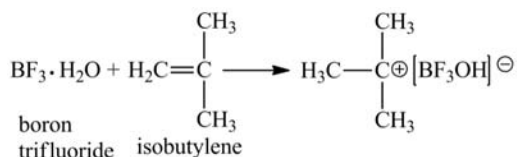
Solution

$$\bar{X}_n = \frac{[\text{M}]_0}{[\text{I}]_0} = \frac{10/104.2}{0.01/64.06} = 615.2$$

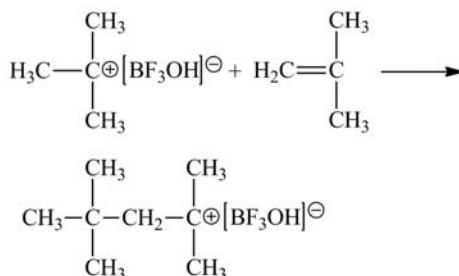
$$\bar{M}_n = \bar{X}_n M_0 = 615.2(104.12) = 64,055$$

As described in the next section, some cationic polymerizations, such as the cationic ring-opening polymerization (CROP) of tetrahydrofuran [7], also can be used to prepare polymers with controlled-molecular-weight and narrow-molecular-weight distribution as discussed in the following section. While polydispersities as high as 20 can result from traditional free-radical polymerization, some radical polymerizations can be controlled to produce narrow-molecular-weight distributions comparable to living polymerizations. This category of controlled/living radical polymerization (CRP) includes nitroxide-mediated polymerization (NMP), atom-transfer radical polymerization (ATRP), and reversible addition-fragmentation chain transfer (RAFT) polymerization discussed later in Section 2.2.4.

Cationic Polymerization. Unlike free-radical and anionic polymerizations, initiation in cationic polymerization employs a “catalyst” that is restored at the end of the polymerization and does not become incorporated into the terminated polymer chain. Any strong Lewis acid* such as boron trifluoride (BF₃) can be used as the catalyst. In this case, a *co-catalyst* (e.g., water) is required as the actual proton source. Cationic initiation is illustrated next for the commercially important example of isobutylene polymerization:



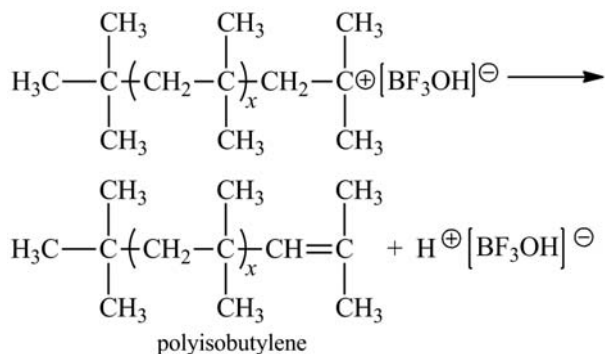
In the above case, proton addition yields a *t*-butyl *carbonium* ion that forms an association with the BF₃•OH counterion or *gegen* ion. The carbonium ion can then add to the double bond of another isobutylene molecule during propagation, as follows:



Unlike the case of free-radical polymerization, termination by combination of two cationic polymer chains cannot occur. In certain cationic polymerizations, a

* A Lewis acid is an *electron acceptor* such as H⁺, BF₃, or AlCl₃.

distinct termination step may not take place (i.e., “living” cationic polymerization); however, *chain transfer* to a monomer, polymer, solvent, or counterion will usually occur. The process of chain transfer to the counterion is



As this termination step shows, the catalyst and co-catalyst are restored at the end of the polymerization.

Cationic polymerizations are usually conducted in solution and often at low temperature, typically -80° to -100°C , which provides satisfactory polymerization rates. The choice of solvent for cationic polymerizations is important because of the role of solvent in controlling the association between cation and counterion. A “tight” association will prevent monomer insertion during propagation. Typically, there is a linear increase in polymer chain length and an exponential increase in polymerization rate as the dielectric strength of the solvent increases.

In 1974, Matyjaszewski and coworkers [7] showed that “living” polymerization could be achieved in a cationic ring-opening polymerization (CROP) of tetrahydrofuran (THF) in carbon tetrachloride using a triflate anion as shown in Figure 2-6. In this case, the triflate anion, CF_3SO_3^- , is a very weak nucleophile and, therefore, serves as a good leaving group. Living CROP has been extended to other heterocyclic monomers to produce polymers and copolymers with narrow-molecular-weight distribution.

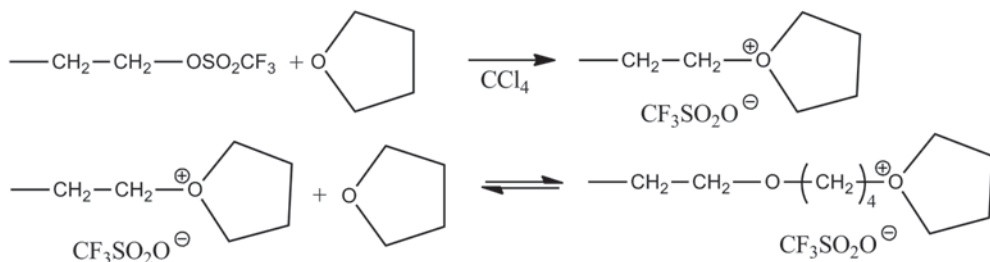
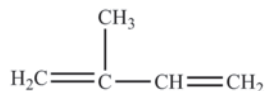


Figure 2-6. Cationic ring-opening polymerization (CROP) of THF in carbon tetrachloride [7].

Ionic Copolymerization. As in the case of free-radical copolymerization, two or more monomers can be copolymerized by an ionic mechanism. For example, the commercial elastomer of polyisobutylene (butyl rubber) is a copolymer obtained by the cationic copolymerization of isobutylene with 0.5% to 2% of isoprene* (structure shown below).



This comonomer, isoprene, provides unsaturated sites for subsequent vulcanization (see Section 9.2.1).

Another important example of an ionic copolymerization is the triblock copolymer SBS, which has a central butadiene block with a styrene block at each end of the chain. This triblock copolymer is an example of a thermoplastic elastomer that is elastic at ambient temperature but can be molded like other thermoplastics at higher temperatures. It can be prepared by adding styrene monomer to an active butadiene chain having anionic sites at both ends (i.e., a butadiene dianion). The dianion is obtained by using an electron-transfer initiator such as sodium naphthalenide prepared by reacting naphthalene with sodium as shown in Figure 2-7A. The naphthalene radical anion can transfer an electron to the monomer (butadiene) to form a monomer radical anion, as illustrated in Figure 2-7B. Two of these radical anions can combine to give a dimer with carbanion sites at opposite ends, as illustrated in Figure 2-7C. The carbanion sites are then available for the addition of more butadiene monomers to obtain a predetermined degree of polymerization. At that point, styrene monomer can be added to form the SBS triblock copolymer.

2.2.3 Coordination Polymerization

One of the earliest and most important groups of thermoplastics includes the polyolefins—polyethylene and polypropylene (see Section 9.1.1). In 1939, a high-pressure, free-radical process was developed at ICI in England to polymerize ethylene. This polymer had a $-\text{CH}_2-\text{CH}_2-$ backbone with some short- and long-chain alkane branches. Crystallinity was moderate and both thermal and mechanical properties were suitable for film and bottle applications. Today, this particular grade of polyethylene is called low-density polyethylene (LDPE) and is among the most important commodity thermoplastics. In contrast, free-radical polymerization of propylene yields an amorphous polymer that is a tacky gum at room temperature

* 2-methyl-1,3-butadiene.

and has no significant commercial use. It was not until 1954, through the work of Giulio Natta [8] in Italy, that a stereochemical process was developed to synthesize *isotactic* polypropylene (*i*-PP). This form of polypropylene had a level of crystallinity comparable to that of LDPE and exhibited good mechanical properties over a wide range of temperatures. A process similar to that used in the production of *i*-PP was developed by Karl Ziegler [9] in Germany to polymerize ethylene at substantially lower temperature and pressure than required to reduce the extent of branching occurring during the free-radical polymerization of ethylene. This polyethylene—high-density polyethylene (HDPE)—had fewer branches and, therefore, could obtain a higher degree of crystallinity than LDPE. For their work in developing these processes, Ziegler and Natta shared the 1963 Nobel Prize in chemistry.

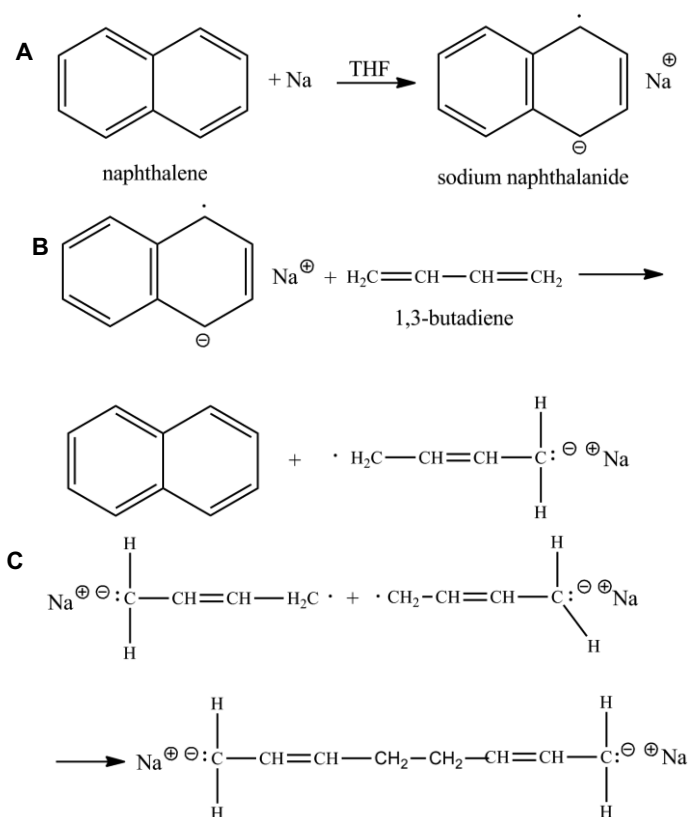


Figure 2-7 Use of sodium naphthalenide in the synthesis of an SBS triblock copolymer. **A.** Formation of sodium naphthalenide from naphthalene and sodium. **B.** Reaction of sodium naphthalenide with butadiene monomer. **C.** Combination of radicals to give a dianion that is available for anionic polymerization at both ends.

The processes used in the polymerization of both *i*-PP and HDPE employ a class of transition-metal catalysts, called Ziegler–Natta (Z–N) catalysts, which utilize a coordination- or insertion-type mechanism during polymerization. In general, a Ziegler–Natta catalyst is a bimetallic coordination complex of a metal cation from groups I–III in the periodic table, such as triethyl aluminum, $\text{Al}(\text{C}_2\text{H}_5)_3$, and a transition metal compound from groups IV–VIII, such as titanium tetrachloride (TiCl_4). As an example, linear (i.e., high-density) polyethylene can be prepared by bubbling ethylene into a suspension of $\text{Al}(\text{C}_2\text{H}_5)_3$ and TiCl_4 in hexane at room temperature. Polypropylene of nearly 90% isotacticity can be prepared by the polymerization of propylene in the presence of titanium trichloride (TiCl_3) and diethylaluminum chloride, $\text{Al}(\text{C}_2\text{H}_5)_2\text{Cl}$, at 50°C . Similar catalyst systems can be used to polymerize other α -olefins such as 1-butene ($\text{H}_2\text{C}=\text{CH}-\text{CH}_2-\text{CH}_3$), geometric isomers of diolefins (e.g., isoprene), and even acetylene ($\text{HC}\equiv\text{CH}$).

Although the exact mechanism of coordination polymerization is still unclear, it is believed that the growing polymer chain is bound to the metal atom of the catalyst and that monomer insertion involves a coordination of the monomer with the metal atom. It is this coordination of the monomer that results in the stereospecificity of the polymerization. A mechanism for the Z–N polymerization of propylene proposed by Cossee [10] is illustrated in Figure 2-8. Coordination polymerizations can be terminated (poisoned) by contact with water, hydrogen, aromatic alcohol, or certain metals such as zinc.

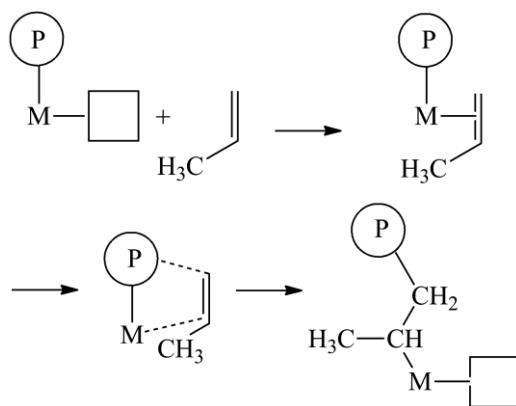


Figure 2-8 Proposed mechanism of monomer insertion during the Ziegler–Natta polymerization of propylene [10]. The small box represents a vacant coordination site on an octahedrally coordinated transition metal ion (M) that can coordinate with the π -bond of propylene. The symbol P represents the growing polypropylene chain.

First-generation heterogeneous Z–N catalysts (e.g., $\text{TiCl}_3/\text{Al}(\text{C}_2\text{H}_5)_2\text{Cl}$) for propylene polymerization achieved high isotacticity (ca. 90%) but low yield (e.g., 5

kg *i*-PP per g of Ti). Second-generation catalysts incorporating a Lewis base improved both catalyst activity and stereospecificity. Unfortunately, a problem with these catalyst systems was contamination of *i*-PP with inactive Ti salts. More recent Z–N catalysts consist of TiCl₄ supported on MgCl₂, a trialkyl aluminum co-catalyst, and one or two Lewis bases as electron donors. These third-generation catalysts achieve up to 98% isotacticity with high catalyst performance (>2400 kg PP/g Ti), which eliminates the need for catalyst removal.

Metallocene Polymerizations. In 1980, Sinn and Kaminsky [11] reported a significant advance in the stereoregular homogeneous polymerization of ethylene, α -olefins including propylene, and several other commercially important monomers including styrene and methyl methacrylate. This new type of coordination polymerization uses metallocene catalysts.* Several different transition metals (typically from group IVb) have been used in the preparation of metallocene catalysts including zirconium (i.e., zirconocene), titanium (i.e., titanocene), and hafnium (i.e., hafnocene). The order of metallocene activity is generally Zr>Hf>Ti. Metallocenes can be used to obtain extremely uniform polymers with narrow-molecular-weight distribution. Ethylene was the first olefin to be polymerized using metallocene catalysts. Metallocenes also can be used to copolymerize ethylene with propylene, butene, hexene, and octene. Compared with Z–N catalysts, metallocenes are more expensive but can be more productive in terms of the amount of polymer produced per quantity of catalyst.

Commercial metallocene polymers, with properties ranging from crystalline to elastomeric, were first produced in 1991 and have been rapidly capturing the polyolefin market. The enhanced properties of some metallocene-catalyzed polymers open new opportunities for traditional commodity thermoplastics. For example, superior optical clarity, low-temperature ductility, and reduced amounts of impurities (e.g., catalyst metal residues) make metallocene polymers suitable for many biomedical applications. Nearly 100% syndiotactic polypropylene (*s*-PP) (see Section 9.1.1) and syndiotactic polystyrene (*s*-PS) (see Section 9.1.2) have been produced for the first time on a commercial scale using metallocene polymerizations.

Metallocene catalysts are used with a co-catalyst, typically methylaluminoxane (MAO), a complex mixture of methylaluminum oxide oligomers (–CH₂AlO–). MAO is formed by the controlled hydrolysis of trimethylaluminum. The catalytic activity of metallocene catalysts is directly proportional to the degree of oligomerization of the aluminoxane. Other Lewis acid co-catalysts like tetraphenylborates can be used to polymerize monomers containing substituent groups, such as methyl methacrylate.

* The term *metallocene* was coined in the early 1950s to describe dicyclopentadienyliron (Cp₂Fe) ferrocene.

The majority of reactors for Ziegler–Natta polymerization reactors are designed for use with heterogeneous catalysis. To utilize existing facilities, metallocenes can be supported on a number of inorganic oxides such as SiO_2 (silica gel), Al_2O_3 , and MgCl_2 with or without MAO. For example, silica-supported metallocenes can be used to obtain linear low-density polyethylene (LLDPE) using the Unipol gas-phase process (see Section 2.3.5).

The most widely used metallocene catalysts consist of two (bent) cyclopentadienyl ligands (Cp_2MX_2), illustrated in Figure 2-9A. Many other metallocene structures are possible including a single cyclopentadienyl ring (Figure 2-9B) used in polymerization of *s*-PS. The cyclopentadienyl ring of a metallocene is singly bonded to the central metal atom by a π -bond. A proposed mechanism of active-site generation due to mixing of a bent metallocene with excess MAO in a solvent is illustrated in Figure 2-10.

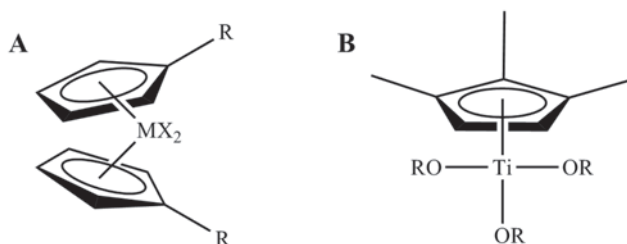


Figure 2-9 **A.** Typical metallocene catalyst for olefin polymerization (e.g., LLDPE, HDPE, *a*-PP, and ethylene–cycloalkene copolymer). The symbol M represents a transition metal (e.g., Ti, Hf, or Zr), R represents hydrogen or an alkyl group, and X represents a halogen (typically Cl or Br). **B.** Single cyclopentadienyl ligand used in the metallocene polymerization of *s*-PS.



Figure 2-10 Proposed mechanism of active-site generation in metallocene polymerization.

2.2.4 Controlled Radical Polymerizations

As discussed earlier in this chapter, living polymerizations are chain-growth reactions for which termination or chain-transfer events do not occur, as in the case of anionic polymerizations and some cationic polymerizations (see Section 2.2.2). In

traditional free-radical polymerization where chain-terminating mechanisms are prevalent, initiation reactions are slow while high-molecular-weight polymers form in the early stages of the polymerization process. This sequence of events results in increasing polydispersity as the polymerization proceeds and molecular weight decreases. Several recent polymerization schemes follow a free-radical mechanism but are able to control molecular weight, molecular-weight distribution, and polymer architecture. These techniques establish a form of dynamic equilibrium between propagating radicals and dormant species. The process may involve a reversible trapping of radicals in a deactivation/activation process or a reversible transfer. These are called controlled “living” radical polymerizations (CRP)* and include the use of special initiators called iniferters [12], nitroxide-mediated polymerization (NMP), atom transfer radical polymerization (ATRP), and reversible addition-fragmentation chain transfer (RAFT) polymerization. Related to the RAFT technique is cobalt-mediated polymerization. Other methods include iodine-transfer polymerization and tellurium-mediated polymerization. A description of frequently used controlled radical polymerization schemes—NMP, ATRP, and RAFT—are discussed in this section in the order of their development.

Nitroxide-Mediated Polymerization. Several polymers, particularly polystyrene, can be prepared with narrow-molecular-weight distribution by a controlled radical polymerization technique called *nitroxide-mediated polymerization* (NMP) [13, 14] developed in the early 1980s. Monomers other than styrene that have been prepared by NMP include acrylonitrile, acrylamides, acrylates, and 1,3-dienes. NMP can also be used to prepare ABA triblock copolymer, to build up highly dense polymer brushes, and to functionalize nanoparticles. The nitroxide-mediated polymerization of styrene [15] is illustrated in Figure 2-11. As illustrated, the polymerization involves activation/deactivation with a reversible combination of propagating radicals (propagation rate constant, k_p) with nitroxide radical species.

* IUPAC has recommended the term *reversible deactivation radical polymerization* (RDRP); however, alternative terms such as *living radical*, *controlled radical*, and *controlled/living radical polymerization* are typically used.

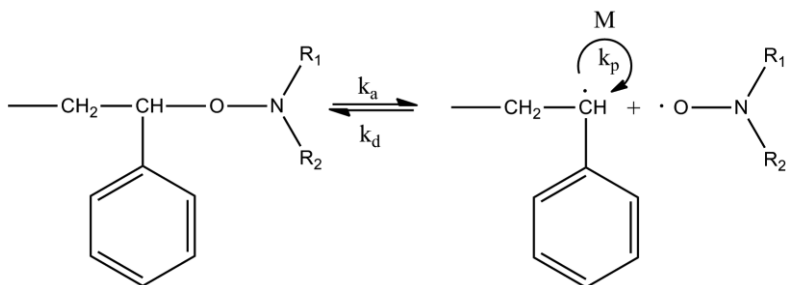


Figure 2-11 Nitroxide-mediated polymerization of styrene. The rate constants k_a and k_d represent activation (forward) and deactivation (backward) processes, respectively.

Early nitroxide-mediated polymerizations used 2,2,6,6-tetramethyl-piperidinyloxy (TEMPO) as the mediating nitroxide. Second-generation nitroxides include 2,2,5-trimethyl-4-phenyl-3-azahexane-3-nitroxide (TIPNO) and *N-tert*-butyl-*N*-(1-diethylphosphono-2,2-dimethyl-propyl) nitroxide (DEPN). Chemical structures of TEMPO, TIPNO, and DEPN are illustrated in Figure 2-12. SG1 exhibits a *higher* activation/deactivation equilibrium constant than TEMPO and is soluble in concentrated solutions of water-soluble monomers such as acrylamide.

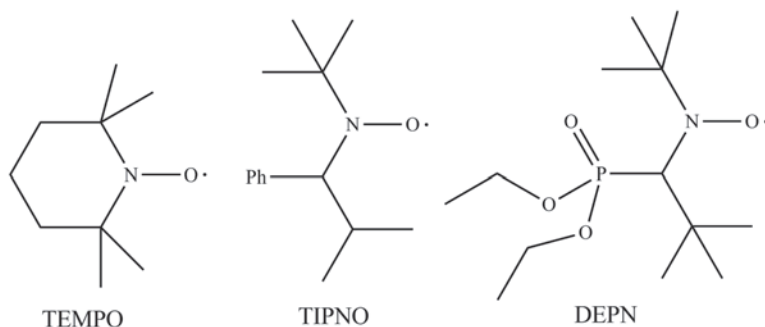


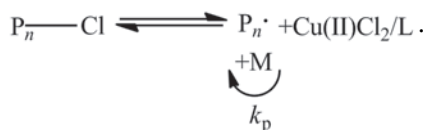
Figure 2-12 Three common mediating nitroxides: TEMPO (2,2,6,6-tetramethyl-piperidinyloxy), TIPNO (2,2,5-trimethyl-4-phenyl-3-azahexane-3-nitroxide), and DEPN (*N-tert*-butyl-*N*-(1-diethylphosphono-2,2-dimethylpropyl)nitroxide).

Atom Transfer Radical Polymerization (ATRP). Atom transfer radical addition, ATRA, is a tool used in the formation of carbon-carbon bonds in organic synthesis. In 1995, Matyjaszewski [16, 17] adopted this approach to the polymerization of styrene and (meth)acrylates. This extension of ATRA to free-radical polymerization is called *atom transfer radical polymerization* or simply ATRP. Polymers with high molecular weight (ca. 10^5) and a low polydispersity ($\bar{M}_w/\bar{M}_n <$

1.3–1.5) can be obtained by ATRP. ATRP can be used to polymerize acrylonitrile and acrylamide and also prepare a variety of block copolymers, star polymers, and hyperbranched polymers.

Typical ingredients of an ATRP include a transition-metal catalyst, M_t^n (Cu or Fe),* complexed by a ligand (L) that serves as a halogen atom transfer promoter, and an organic halide, $R-X$ ($X = \text{Br}, \text{Cl}$), that functions as the free-radical initiator. By using specialized initiators, ATRP can be used to obtain polymers with specific end-functional groups such as vinyl, hydroxyl, and cyano groups [18]. A common example of a transition-metal halide used in ATRP is Cu(I)Cl . Typical ligands include multidentate nitrogen compounds such as 2,2'-bipyridine (bpy), 4,4'-di(5-nonyl)-2,2'-bipyridine (dnbpy), and 1,10-phenanthroline (phen). An early recipe for the ATRP of styrene included the transition-metal catalyst Cu(I)Cl , the ligand bpy, and the free-radical initiator 1-phenylethyl chloride (1-PECl). More recently, ligands with reduced toxicity and cost, such as iminodiacetic acid (IDA), which complexes with Fe(II) and Fe(III) , have been evaluated for ATRP use [19, 20].

As an initial step in ATRP, the transition-metal complex, M_t^n/L , abstracts the halogen atom from the organic halide to form the oxidized species $X-M_t^{n+1}/L$ and the organic radical $R\cdot$. The radical can then sequentially add monomer molecules, M , during the propagation step. The radical is rapidly deactivated by reacting with the oxidized transition-metal halide complex to reform the initial transition-metal complex and halogen-terminated chain, P_n-X , as illustrated below for the Cu(I)Cl redox equilibrium:



The living nature of ATRP is due to the fast equilibration between $P_n\cdot$ and the non-propagating halogen-terminated polymer (P_n-X). For ATRP using copper halide, the equilibrium constant can be written as

$$K_e = \frac{k_{\text{act}}}{k_{\text{deact}}} = \frac{[P_n\cdot][\text{Cu(II)X}_2]}{[P_n-X][\text{Cu(I)X}]} \quad (2.50)$$

A small equilibrium constant is required to maintain a low radical concentration, thereby reducing the potential of termination reactions. The number-average degree of polymerization in ATRP is determined by the ratio of initial monomer to organic halide initiator as

* The superscript n in M_t^n represents the oxidation state of the transition metal.

$$\bar{X}_n = \frac{[M]_0}{[RX]_0} \times \text{monomer conversion.} \quad (2.51)$$

An attractive feature of ATRP is that it combines the advantages of controlled molecular weight and low polydispersity offered by anionic living polymerization (see Section 2.2.2) with the ease of a free-radical polymerization. The requirement of achieving extremely pure polymerization conditions that limit the general applicability of anionic living polymerization is not an issue in ATRP. Ionic solvents (see Section 2.3.7) can solvate the catalyst and, thereby, the polymer may be more easily separated than if an organic solvent was used.

An interesting application of ATRP is the graft copolymerization of cellulose with styrene or methacrylates in an ionic solvent using 2-bromopropionyl bromide to functionalize the hydroxyl groups in cellulose [21] as illustrated in Figure 2-13. This functionalized cellulose can then be used in atom transfer radical copolymerization with styrene or a methacrylate.

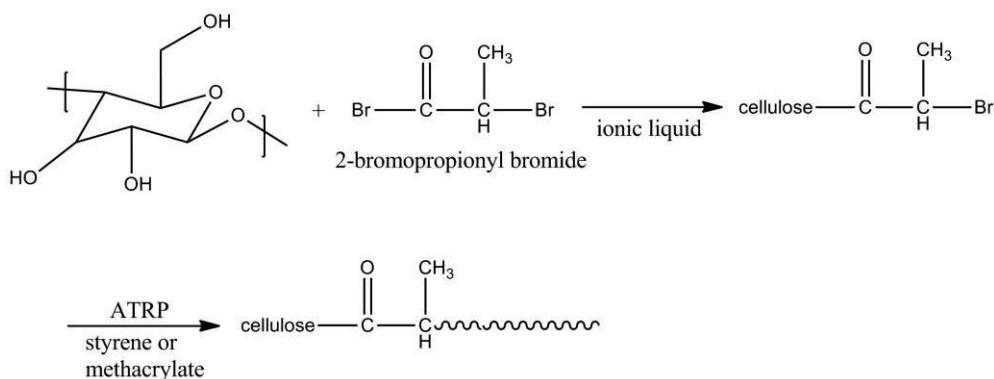
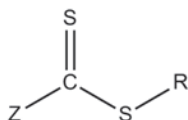


Figure 2-13 Graft copolymerization of cellulose using ATRP chemistry.

RAFT Polymerization. Another example of controlled free-radical polymerization is *reversible addition-fragmentation chain transfer* (RAFT) polymerization developed in the 1990s. RAFT polymerization can be used with a wide variety of monomers to prepare polymers with narrow polydispersity (i.e., <1.1 or <1.2) and block copolymers with controlled composition and structure [14, 22]. In addition to diblock copolymers, gradient copolymers, star polymers, microgels, and polymer brushes have been prepared by RAFT polymerization. RAFT polymerizations can be conducted under a variety of polymerization conditions including solution, emulsion, and suspension. Common chain-transfer or RAFT agents include di- or trithiocarbonyl compounds based on the following structure:



where Z and R represent a variety of organic groups such as methyl and phenyl groups, or a number of linear aliphatic chains. RAFT polymerization involves a reversible addition-fragmentation step whereby transfer of the S=C(Z)S– moiety between active and dormant chains serves to maintain a living polymerization scheme as illustrated in Figure 2-14. As a consequence of RAFT polymerization, the S=C(Z)S– end group is retained in the polymer product.

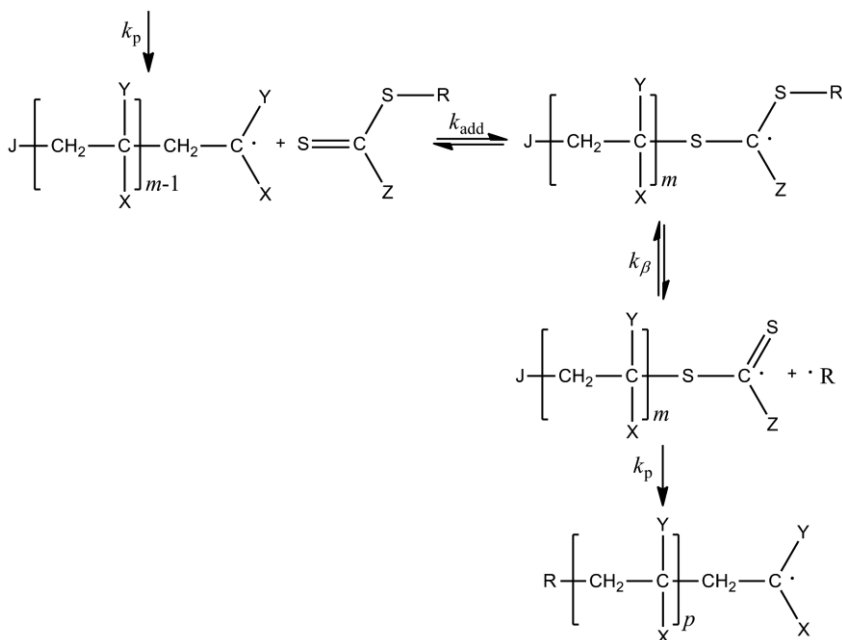
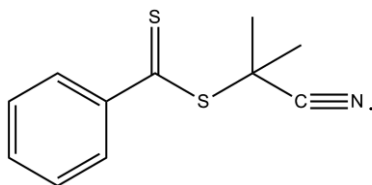


Figure 2-14 Scheme proposed for RAFT polymerization [22]. The symbols J and R represent molecular groups that can initiate free-radical polymerization such as a dithio compound.

Careful selection of the Z and R groups is very important for successful RAFT polymerization. In order to achieve a high transfer constant, an appropriate Z group (e.g., an alkyl or aryl group) should activate the C=S double bond toward radical addition while the R group should be a good free-radical leaving group such as a cumyl or cyanoisopropyl group. The expelled radical ($\text{R}\cdot$) should be effective in re-initiating free-radical polymerization. An example of a RAFT agent is 2-cyano-prop-2-yl dithiobenzoate (CPDB) shown by the following structure:



CPDB has been used in the RAFT polymerization of dimethylaminoethyl methacrylate [23] and triazole [24] monomers. Its reaction with an initiator, usually AIBN, creates the propagating chain. The RAFT process involves a reversible addition-fragmentation sequence in which transfer of the $S=C(Z)S-$ moiety occurs between active and dormant chains. Monomers that have been polymerized using RAFT polymerization include methyl methacrylate, butyl methacrylate, styrene, and acrylic acid. Functional monomers that contain an acid, an acid salt, or a tertiary amino moiety can also be polymerized by RAFT polymerization. The monomer determines which of two RAFT agents should be used. Generally, tertiary cyanoalkyl trithiocarbonate is suitable for (meth)acrylamate, (meth)acrylamide, and styrenic monomer. In the case of the RAFT polymerization of vinyl acetate or *N*-vinylpyrrolidone, *O*-ethyl *S*-cyanomethyl xanthate is an appropriate RAFT agent.

The number-average degree of polymerization for a RAFT polymerization can be estimated from the initial concentration of the RAFT agent, $[R]_0$, as

$$\bar{X}_n \approx \frac{[M]_0 - [M]_t}{[R]_0} \quad (2.52)$$

where $[M]_0 - [M]_t$ represents the amount of monomer *consumed* at time *t*. An example of a molecular-weight calculation in the RAFT polymerization of methyl methacrylate is given next. Polydispersity in RAFT polymerization can be as narrow as 1.4 as illustrated in Figure 2-15 for the polymerization of styrene in conventional (thermal) and RAFT free-radical polymerization.

Example 2.3

Consider the RAFT polymerization of 6.55 M methyl methacrylate (100.12 molecular weight) in benzene using a 1,1'-azobis(1-cyclohexanenitrile) (0.0018 M) initiator and 2.48×10^{-2} M of the RAFT agent *S*-dodecyl *S*-(2-cyano-4-carboxy)but-2-yl trithiocarbonate at 90°C. At a conversion of 92% of the monomer, estimate the number-average molecular weight.

Solution

The number-average degree of polymerization is first calculated as

$$\bar{X}_n \approx \frac{[M]_0 - [M]_t}{[R]_0} = \frac{0.92(6.55) M}{2.48 \times 10^{-2} M} = \frac{6.03}{2.48 \times 10^{-2}} = 243.$$

The number-average molecular weight is then obtained as

$$\bar{M}_n = 243 \times 100.1 = 24,324.$$

This value compares well with the experimental value of 21,800 [25].

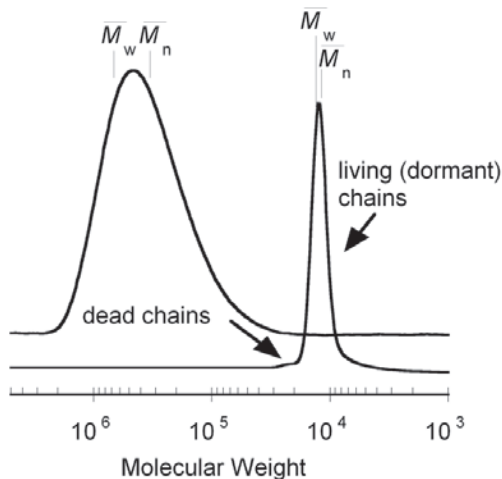


Figure 2-15 Comparison of molecular-weight distributions of polystyrene prepared by thermal polymerization ($\bar{M}_n = 324,000$; $\bar{M}_w/\bar{M}_n = 1.74$) (left) compared to the molecular-weight distribution obtained by RAFT polymerization using cumyl dithiobenzoate ($\bar{M}_n = 14,400$; $\bar{M}_w/\bar{M}_n = 1.04$) (right). Reprinted with permission from G. Moad, R. Rizzardo, and S. H. Thang, *Toward Living Radical Polymerization*. Accounts of Chemical Research, 2008. **41**(9): p. 1123–1143.

2.3 Polymerization Techniques

2.3.1 Bulk Polymerization

The simplest technique, and the one that gives the highest-purity polymer, is bulk polymerization. Only monomer, a monomer-soluble initiator, and perhaps a chain-transfer agent to control molecular weight are used. Advantages of this technique include high yield per reactor volume, easy polymer recovery, and the option of

casting the polymerization mixture into final product form (i.e., cast polymerization). Among the limitations of bulk polymerization are the difficulty of removing residual traces of monomer and the problem of dissipating heat produced during the polymerization. Free-radical polymerizations are highly exothermic (typically 42 to 88 kJ mol⁻¹; see Table 2-5 for some examples), while the thermal conductivity of organic monomers and polymers is low as shown by values given in Table 2-8. An increase in temperature will increase the polymerization rate and, therefore, generate additional heat to dissipate. Heat removal becomes particularly difficult near the end of the polymerization when viscosity is high. This is because high viscosity limits the diffusion of long-chain radicals required for termination. This means that radical concentration will increase and, therefore, the rate of polymerization also will increase, as indicated by eq. (2.18). By comparison, the diffusion of small monomer molecules to the propagation sites is less restricted. This means that the termination rate decreases more rapidly than the propagation rate, and the overall polymerization rate, therefore, increases with accompanying additional heat production. This autoacceleration process has been called the Norrish–Smith [26], Trommsdorff [27], or gel effect. In practice, heat dissipation during bulk polymerization can be improved by providing special baffles for improved heat transfer or by performing the bulk polymerization in separate steps of low to moderate conversion.

Table 2-8 Heat Capacity and Thermal Conductivity at 298 K

Material	C_p (kJ mol ⁻¹ K ⁻¹)	k^a (J m ⁻¹ s ⁻¹ K ⁻¹)
Water	0.075	0.607
Benzene	0.136	0.141
Toluene	0.157	0.131
Styrene	0.182	0.137
Polystyrene	0.127	0.142
Poly(methyl methacrylate)	0.137	0.193
Poly(vinyl chloride)	0.059	0.168

^a k , thermal conductivity.

Bulk-polymerization processes can be used for many free-radical polymerizations and some step-growth (condensation) polymerizations. Important examples of polymers usually polymerized by free-radical bulk polymerization include polystyrene and poly(methyl methacrylate) for which cast polymerization accounts for about half of the total production. Low-density (i.e., high-pressure) polyethylene and some ethylene copolymers are sometimes produced by bulk free-radical polymerizations.

2.3.2 Solution Polymerization

Heat removal during polymerization can be facilitated by conducting the polymerization in an organic solvent or preferably water, which has both cost and handling advantages as well as high thermal conductivity (Table 2-8). The requirements for selection of the solvent are that both the initiator and monomer be soluble in it and that the solvent have acceptable chain-transfer characteristics and suitable melting and boiling points for the conditions of the polymerization and any subsequent solvent-removal step. Solvent choice may be influenced by other factors such as flash point, cost, and toxicity. Examples of suitable organic solvents include aliphatic and aromatic hydrocarbons, esters, ethers, and alcohols. Often, the polymerization can be conducted under conditions of solvent reflux to maximize heat removal. Reactors are usually stainless steel or glass-lined. The obvious disadvantages of solution polymerization are the small yield per reactor volume and the requirement for a separate solvent-recovery step.

Many free-radical and ionic polymerizations are conducted in solution. Important water-soluble polymers that can be synthesized in aqueous solution include poly(acrylic acid), polyacrylamide, poly(vinyl alcohol), and poly(*N*-vinylpyrrolidone). Poly(methyl methacrylate), polystyrene, polybutadiene, poly(vinyl chloride), and poly(vinylidene fluoride) can be polymerized in organic solvents.

2.3.3 Suspension Polymerization

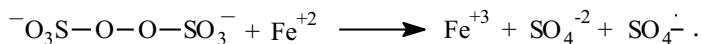
Improved heat transfer can also be obtained by utilizing the high thermal conductivity of water through either suspension or emulsion polymerization. In suspension (“bead” or “pearl”) polymerization, a batch reactor fitted with a mechanical agitator is charged with a water-*insoluble* monomer and initiator. Sometimes, a chain-transfer agent may be added to control molecular weight in a free-radical polymerization. Droplets of monomer containing the initiator and chain-transfer agent are formed. These are typically between 50 and 200 μm in diameter and serve as miniature reactors for the polymerization. Coalescence of these “sticky” droplets is prevented by the addition of a protective colloid, typically poly(vinyl alcohol), and by constant agitation of the polymerization mixture. Near the end of the polymerization, the particles harden and can then be recovered by filtration, which is followed by a final washing step. Although solvent cost and recovery operations are minimal in comparison with solution polymerization, polymer purity is low due to the presence of suspending and other stabilizing additives that are difficult to completely remove. In addition, reactor capital costs are typically higher than for solution polymerization. Polymers commonly produced by free-radical suspension polymerization include styrenic ion-exchange resins (Section 2.4.1), extrusion and injection-

molding grades of poly(vinyl chloride), poly(styrene-*co*-acrylonitrile) (SAN), and extrusion-grade poly(vinylidene chloride-*co*-vinyl chloride).

2.3.4 Emulsion Polymerization

Another technique that utilizes water as a heat-transfer agent is emulsion polymerization. In addition to water and monomer, a typical reactor charge for an emulsion polymerization consists of a *water-soluble* initiator, a chain-transfer agent, and a surfactant such as the sodium salt of a long-chain fatty acid. The (hydrophobic) monomer molecules form large droplets. These are stabilized by the surfactant molecules whose hydrophilic ends point outward and whose hydrophobic (aliphatic) ends point inward toward the monomer droplet, as illustrated in Figure 2-16. The size of monomer droplets depends upon the polymerization temperature and the rate of agitation. Above a certain surfactant concentration, the *critical micelle concentration*, residual surfactant molecules can align to form *micelles*. Depending upon the nature of the surfactant, the micelles are small rod-like or spherical structures (~50 Å in length) that contain between 50 and 100 surfactant molecules. Surfactants prepared from long-chain fatty acids favor the formation of rod-like micelles.

As indicated above, an important difference between suspension and emulsion polymerization is that the initiator used in an emulsion polymerization must be soluble in water. An example of a commonly used water-soluble initiator is the persulfate-ferrous (K_2SO_4) *redox* initiator [28], which yields a radical sulfate anion through the reaction



Near-ambient temperature and a neutral pH typically favor K_2SO_4 -initiated emulsion polymerization.

During the emulsion-polymerization process, monomer molecules that have a small but significant water solubility can migrate from the monomer droplets through the water medium to the center of the micelles. Polymerization is initiated when the water-soluble initiating radical enters a monomer-containing micelle. Due to the very high concentration of micelles, typically 10^{18} per mL, compared to that of the monomer droplets (10^{10} to 10^{11} per mL), the initiator is statistically more likely to enter a micelle than a monomer droplet. As the polymerization proceeds, additional monomer molecules are transferred from the droplets to the growing micelles. At 50% to 80% monomer conversion, the monomer droplets are depleted and the swollen micelles are transformed to relatively large polymer particles, typically between 0.05 and 0.2 μm in diameter. The suspension of polymer particles in water is called a *latex*. The latex is very stable and can be used as is (e.g., latex paints) or the polymer can be recovered by coagulation of the latex with acids or salts.

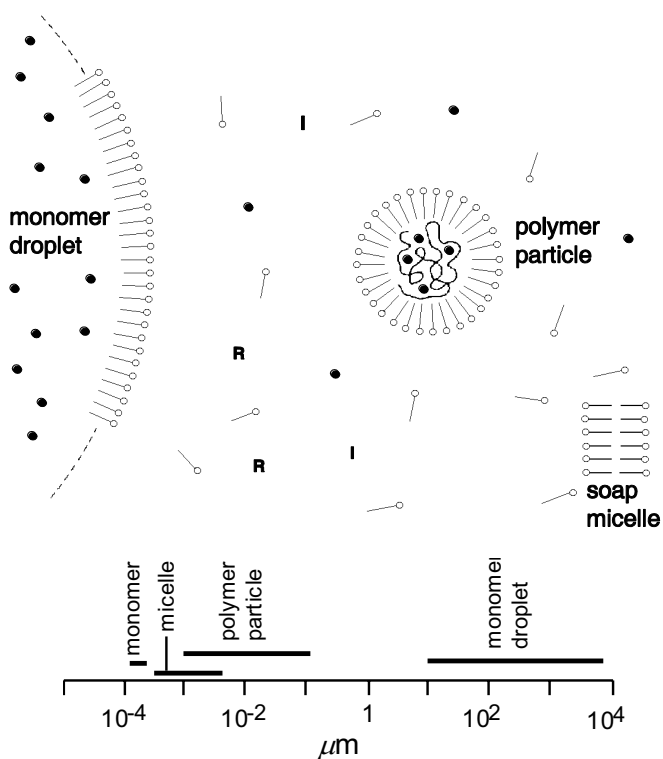


Figure 2-16 Representation of the composition of an emulsion polymerization and relative particle size. Symbols: ●, monomer molecule; I, initiator molecule; and R, primary radical. Adapted from P. Rempp and E. W. Merrill, *Polymer Synthesis*, 1986. Basel: Hüthig & Wepf Verlag, Wiley-VCH. Fig. 12.2, p. 247.

The free-radical kinetics of emulsion polymerization is different from the usual free-radical kinetics of bulk, solution, or suspension polymerization as described in Section 2.2.1. Smith and Ewart [29] have analyzed the kinetics of free-radical emulsion polymerization. They assumed that the monomer-swollen micelles are sufficiently small that, on the average, only *one* propagating chain or *one* terminated chain can exist inside a particle at any time. This means that the radical concentration, $[IM_x\cdot]$, is simply equal to one-half of the particle concentration, N (units of particle number per mL), which in turn is determined by the surfactant and initiator concentrations, among other factors. Therefore, the polymerization rate (see eq. (2.18)) is given as

$$R_o = k_p (N/2)[M] \quad (2.53)$$

where $[M]$ is the concentration of monomer inside the swollen polymer particles. This expression should be compared to the usual steady-state rate expression for free-radical polymerization given by eq. (2.25). While both rates are proportional to monomer concentration, the rate of emulsion polymerization is no longer proportional to the square root of initiator concentration but follows a more complicated dependence on initiator concentration through its dependence on N .

Inverse Emulsion. When the monomer is hydrophilic, emulsion polymerization may proceed through an *inverse emulsion* process. In this case, the monomer (usually in aqueous solution) is dispersed in an organic solvent using a water-in-oil emulsifier. The initiator may be soluble in either the water or oil phase. The final product in an inverse emulsion polymerization is a colloidal dispersion of a water-swollen polymer in the organic phase.

Miniemulsions. Another variation of the emulsion technique is called miniemulsion polymerization [30]. While monomer droplets in traditional emulsion polymerization are relatively large (1–20 μm) compared to monomer-swollen micelles (10–20 nm), droplets in miniemulsions are similar in size to the micelles and, therefore, have comparable probability of being initiated. This is achieved by using long-chain fatty alcohols that increase the capacity of surfactants to stabilize oil-in-water emulsions. The elimination of the need of monomers to diffuse from the monomer droplets through the aqueous medium to the micelles in traditional emulsion polymerizations enables the use of more hydrophobic monomers. Such miniemulsions can be stable for periods of months. Controlled radical polymerizations (Section 2.2.4) can utilize miniemulsion techniques and many unique latex materials can be prepared.

2.3.5 Solid-State, Gas-Phase, and Plasma Polymerization

In addition to the usual methods of polymerization such as bulk and solution, polymers can be prepared in the gas or vapor phase. This is especially the case for the polymerization of olefins such as ethylene. In the Unipol process for PE, which is illustrated in Figure 2-17, gaseous ethylene and solid catalyst (chromium or other complexes) are combined in a continuous fluidized-bed reactor. Since the polymerization is highly exothermic, proper management of heat transfer is critical to prevent agglomeration of the particles and a shutdown of the process. Variations of this process, which accounts for over 50% of the world's licenses for polyethylene production, have been used for the polymerization of propylene and the copolymerization of ethylene and propylene. The Unipol II process is used to produce linear low-density polyethylene (LLDPE) for film application [31].

Solid-State Polymerization. In addition to gas-phase polymerizations, solid-state polymerization is sometimes used to produce some polymers for specialty ap-

plications. For example, some monomers in their crystalline state can be polymerized by heating or by irradiation (visible, X-ray, UV, or γ -radiation) to give extended-chain polymers oriented along crystallographic directions. The result is a polymer single crystal with interesting optical properties. As an example, crystalline polyoxymethylene can be obtained by the γ -irradiation of trioxane or tetraoxane crystals.

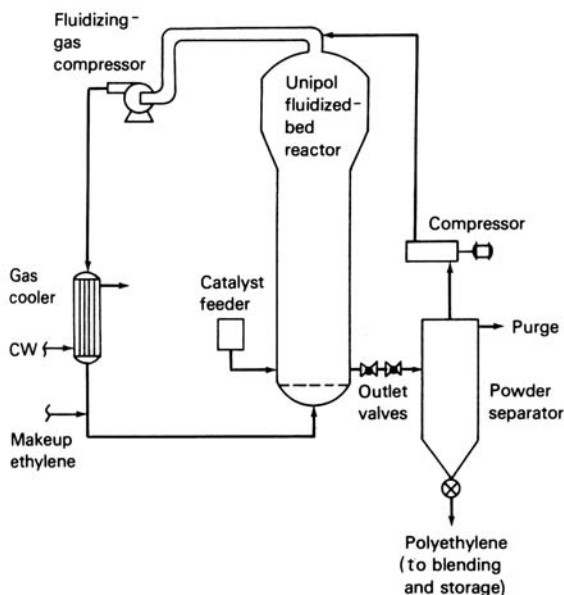


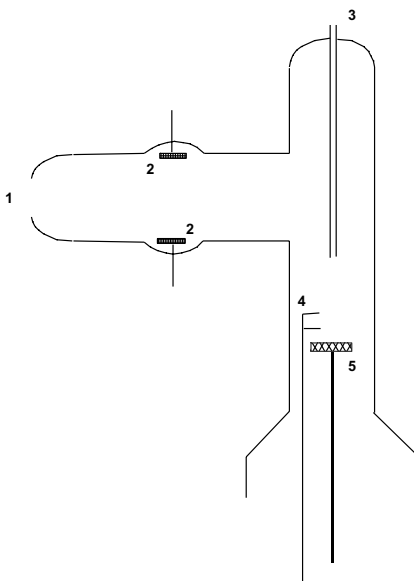
Figure 2-17 Unipol process for the polymerization of ethylene. Adapted from N. F. Brockmeier, in *The Concise Encyclopedia of Polymer Science and Engineering*, J. I. Kroschwitz, ed. Fig. 1, p. 427. Copyright © 1990 by John Wiley & Sons. This material is used by permission of John Wiley & Sons, Inc.

Plasma Polymerization. A wide variety of monomers can also be polymerized in a plasma environment consisting of a low-pressure glow discharge of positively and negatively charged species, electrons, excited and neutral species, and electromagnetic radiation. Plasma polymerization can be used to prepare graft copolymers or to deposit a thin polymer film on a metal or other substrate (e.g., a photoresist on a silicon wafer or a corrosion-resistant coating on a metal). Dense, uniform films of polyfuran and polythiophene can be prepared by plasma polymerization for polymer waveguides. Plasma activation can be used to modify surface properties such as wettability, adhesion, and biocompatibility. For example, catheters can be plasma-modified with heparin to prevent blood clotting. Plasma treat-

ment also can be used to remove contamination from the surface of composite fibers to improve adhesion to the matrix. Plasma-polymerized films can be extremely uniform but are typically strongly crosslinked. For this reason, electron spectroscopy for chemical analysis (ESCA) and static secondary ion mass spectroscopy (SIMS) are the primary methods used to characterize plasma-modified surfaces. These techniques provide significant information about the elemental and chemical composition of the film including the presence of functional groups on the surface.

The preferred method for plasma polymerization is by the injection of an organic precursor into a flowing afterglow reactor as illustrated in Figure 2-18. In this scheme, a large flow of argon gas passes between two aluminum electrodes. The argon is excited by the generation of radio frequency (RF) energy between the electrodes. The RF energy dissociates the gas into electrons, ions, free radicals, and metastable excited species. A flow of an organic precursor is added through a small-diameter tube. The excited species formed in the afterglow where the precursor is introduced reacts with the surface of the substrate.

Figure 2-18 Schematic representation of a flowing afterglow plasma reactor. 1. Argon inlet. 2. Al electrodes. 3. Organic precursor reentrant tube. 4. Langmuir probe used to measure plasma density. 5. Quartz microbalance or substrate. Adapted from P. D. Haaland and S. J. Clarson, *Plasma and Polymers: Synthesis under Extreme Conditions*, Trends in Polymer Science, 1993, vol. 1. Fig. 3, p. 43. Copyright 1993, with permission from Elsevier Science.



2.3.6 Polymerization in Supercritical Fluids

A supercritical fluid (SCF) is defined as one that is above its critical temperature (T_c) and critical pressure (p_c). Supercritical fluids share some of the properties of both gases and liquids such as high diffusivity, low viscosity, and liquid-like densities. Supercritical fluids also show unusual dissolving power (e.g., supercritical water can dissolve oil). Solvent strength can be adjusted through control of pressure,

temperature, or both. Analytical applications include decaffeination of coffee, desulfurization of coal, pulp processing, and chemical extraction. Other potential applications include plastic recycling, fiber spinning, and drug impregnation.

Critical properties of water, carbon dioxide, and several organic compounds are listed in Table 2-9. As shown, critical properties vary widely. For analytical and commercial extraction processes, carbon dioxide is the most commonly used supercritical fluid due to its low critical temperature (31°C) and pressure (73 atm), low cost, low toxicity, and ease of disposal. For example, supercritical CO₂ is used as an alternative to chlorinated solvents for the decaffeination of coffee. By comparison, water has very high critical properties ($T_c = 374^\circ\text{C}$, $p_c = 218$ atm); however, the properties of supercritical water are such that it has received attention as a means to destroy hazardous wastes.

Table 2-9 Critical Properties of Important Supercritical Fluids

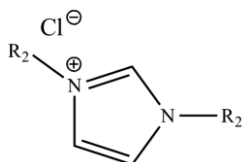
Compound	T_c (°C)	p_c (atm)
Methane	-82.1	45.8
Carbon dioxide	31.0	72.9
Ethane	32.2	48.2
Propane	96.7	41.9
<i>n</i> -Butane	152.0	38.2
Toluene	320.8	41.6
Water	374.1	218.3

Recently, a number of monomers have been polymerized in SCFs. The propagation rate of free-radical polymerization increases with increasing pressure and, therefore, high-molecular-weight polymers can be obtained by using SCFs. Advantages of supercritical fluids include the adjustment of the precipitation threshold and the minimization of swelling of the precipitate. Examples of the use of SCFs include the free-radical polymerization of styrene, vinyl acetate, acrylonitrile, and methyl methacrylate. Initiators consist of typical free-radical initiators including AIBN and *t*-butyl peroxide (see Section 2.2.1). A particular advantage of supercritical fluids lies in the synthesis of fluoropolymers for which supercritical CO₂ can be used in place of chlorofluorocarbons. Supercritical CO₂ also can be used for cationic and ring-opening metathesis reactions (see Section 2.5.1). In addition to fluoropolymers, polymers that have been prepared by polymerization in supercritical fluids include polyimides and poly(methyl methacrylate) (PMMA). Recently, supercritical CO₂ has been used to prepare molecularly imprinted poly(diethylene glycol dimethacrylate) for drug delivery.

2.3.7 Polymerization in Ionic Liquids

Ionic liquids are salts having low melting points, typically <100°C, compared to a melting point of over 800°C for sodium chloride as an example. Low melting tem-

peratures are achieved by selecting anions and cations that disturb a salt's normally highly crystalline nature. Cations are typically nitrogen-containing organic cations while the anion is usually inorganic. As an example, the melting point of imidazolium chloride, a prototypical ionic liquid, is only 80°C. In this case, this low melting temperature is achieved by replacing sodium with the bulky imidazolium cation whose structure is shown below.



The particular combination of cation and anion also affects such properties as viscosity and density. Other than imidazolium, typical cations include tetraalkylammonium, tetraalkylphosphonium, and 1,4-disubstituted pyridinium. Anions include tetrafluoroborate (BF_4^-), hexafluorophosphate (PF_6^-), alkylsulfate, and several other more complicated structures. The preparation of 1-butyl-3-methylimidazolium hexafluorophosphate (bmim) [PF_6^-] is shown in Figure 2-19.

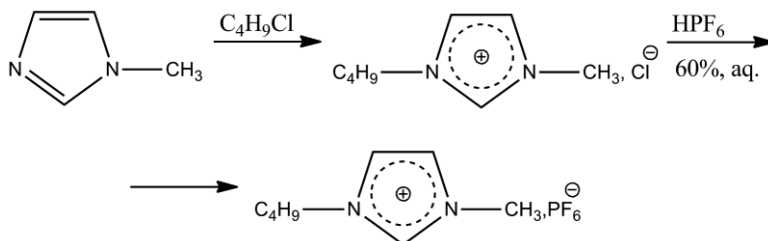


Figure 2-19 Preparation of 1-butyl-3-methylimidazolium hexafluorophosphate [PF_6^-].

The non-volatility of ionic liquids and their special ionic character have suggested that these interesting liquids could have advantages as solvents for polymerizations. In the case of free-radical polymerizations, the ratio of the polymerization rate constant to the termination rate constant is higher than is typical for traditional organic solvents. Ionic liquids can also be used as solvents for ionic polymerizations and many of the newest polymerization techniques including controlled living polymerization such as nitroxide-mediated polymerization (NMP), atom transfer radical polymerization (ATRP), and reverse addition-fragmentation (RAFT) polymerization as discussed in Section 2.2.4.

2.4 Polymer Reactivity

In many cases a polymer can be chemically modified to improve some property, such as biocompatibility, fire retardancy, or adhesion, or to provide specific functional groups for ion-exchange or other applications. For example, bromination is sometimes used to impart fire retardancy to some polymers. As another example, poly(vinyl chloride) can be chlorinated after polymerization to increase its softening temperature or to improve its ability to blend with other polymers. In some cases, important commercial polymers can be produced only by the chemical modification of a precursor polymer. Examples include poly(vinyl alcohol), poly(vinyl butyral), cellulose derivatives such as cellulose acetate and cellulose nitrate, and polyphosphazenes—an interesting group of inorganic polymers. Recently, significant attention has been paid to the use of a select group of highly efficient, low-temperature chemical reactions to prepare new polymers including block copolymers with controlled-molecular-weight and narrow-molecular-weight distribution as well as to modify surfaces and functionalize polymers. This growing area of activity is often called “click chemistry” and is covered in Section 2.4.3.

2.4.1 Chemical Modification

Chloromethylation. Chloromethylation of polystyrene (see Figure 2-20), by reacting with a chloromethyl ether in the presence of a Friedel–Crafts catalyst like aluminum chloride, AlCl_3 , can be used to introduce functionality such as aldehyde or carboxylic acid groups in polystyrene. Aldehydes serve to form a Schiff base with protein amines. In the Merrifield synthesis of proteins [32], crosslinked polystyrene (PS) beads that have been lightly chloromethylated provide the anchoring sites for the sequential addition of amino acids. Highly chloromethylated PS can be quaternized with tertiary amines to yield water-soluble polymers, ionomers, and ion-exchange resins, as described in the following section. Chloromethylated PS also can be reacted with a phosphide to introduce phosphinic ligands for binding metal coordination complexes in the preparation of polymer-bound catalysts.

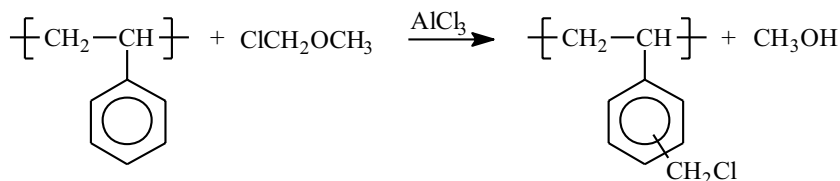


Figure 2-20 Chloromethylation of polystyrene.

Surface Modification. In many cases it may be desirable to modify the surface of a polymer to provide sites for immobilization of enzymes or other biopolymers or to improve the solvent resistance or biocompatibility of a polymer. As mentioned earlier (Section 2.3.5), plasma activation is one approach to modify polymer surfaces. Another method is direct fluorination, oxidation, nitration, and sulfonation. For example, the surface of a hydrocarbon polymer such as polyethylene or polypropylene can be fluorinated by exposure to 5% to 10% fluorine gas diluted in nitrogen for 1 to 15 minutes. The fluorinated surface provides hydrophobicity, oxidation resistance, and solvent resistance for applications such as plastic fuel tanks and rubber gloves.

Ion-Exchange Resins. Another need for chemical modification is the preparation of ion-exchange resins. Cation-exchange resins possess a fixed negative charge and exchange cations such as Ca^{2+} , Na^+ , and H^+ . Anion-exchange resins possess a positive charge on the functional group or are positively charged during the ion-exchange reaction during which anions such as HCO_3^- , SO_4^- , and OH^- are exchanged. Most ion-exchange resins are prepared by suspension polymerization of monomers such as styrene, which can be crosslinked by incorporation of a few percent of a difunctional comonomer such as divinylbenzene. The resulting beads are macroporous and can be used as a column packing. Functionalization can be obtained by different chemical routes, such as sulfonation, phosphonation, phosphination, chloromethylation, amino-methylation, aminolysis, and hydrolysis. For example, a cation-exchange resin can be prepared by sulfonation of a crosslinked polystyrene bead in concentrated sulfuric acid or in a molecular complex of SO_3 with an organic solvent, such as dioxane. Sulfonation primarily occurs at the *para*-position with some *ortho*-substitution. A styrenic anion-exchange resin can be prepared by reacting the benzyl chloride of chloromethylated polystyrene (see Figure 2-20) with a tertiary amine, $\text{N}(\text{CH}_3)_3$. Examples of styrenic ion-exchange resins are illustrated in Figure 2-21.

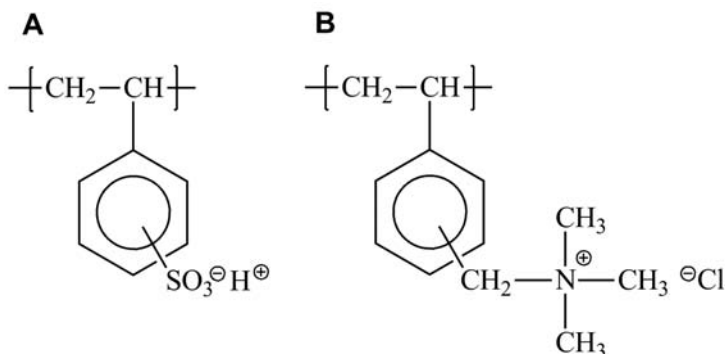


Figure 2-21 Examples of a strongly acidic cation-exchange resin (A) and a strongly basic anion-exchange resin (B) prepared from polystyrene.

2.4.2 Preparation of Polymer Derivatives

Cellulose. Cellulose, which can be obtained from wood pulp and short fibers left from cotton recovery, is one of nature's most abundant biopolymers. A typical chain consists of 2000 to 6000 anhydroglucose units (typical molecular weight of 300,000 to 1,000,000), each of which contains three hydroxyl groups and is linked by an acetal bridge, as illustrated in Figure 2-22. The rigid chain of cellulose is strongly hydrogen-bonded and highly crystalline. For these reasons, cellulose is essentially insoluble and infusible and, as a result, fibers and films can be obtained only by chemically modifying cellulose. Cellulose fiber (rayon) or film (cellophane) can be obtained by the *viscose* process by which cellulose pulp is reacted with carbon disulfide to form cellulose xanthate, soluble in a caustic solution. Cellulose xanthate is then converted back to cellulose by treatment with aqueous sulfuric acid.

Various soluble cellulose derivatives can be obtained by chemical modification of the hydroxyl groups. An important example is cellulose acetate (CA), which is obtained by reacting cellulose with glacial acetic acid in the presence of acetic anhydride and traces of sulfuric acid in refluxing methylene chloride (Figure 2-22). If all the hydroxyl groups are reacted, the polymer is known as cellulose triacetate (CTA), which can be wet-spun into fiber (acetate) from a methylene chloride–alcohol solvent mixture. Partial hydrolysis gives cellulose diacetate in which two of the three hydroxyl groups in each anhydroglucose unit remain acetylated. In commercial grades of cellulose acetate, about 65% to 75% of all available hydroxyl groups remain acetylated. This polymer is amorphous and highly soluble in many solvents including acetone, from which it can be dry-spun (see Section 8.2.4).

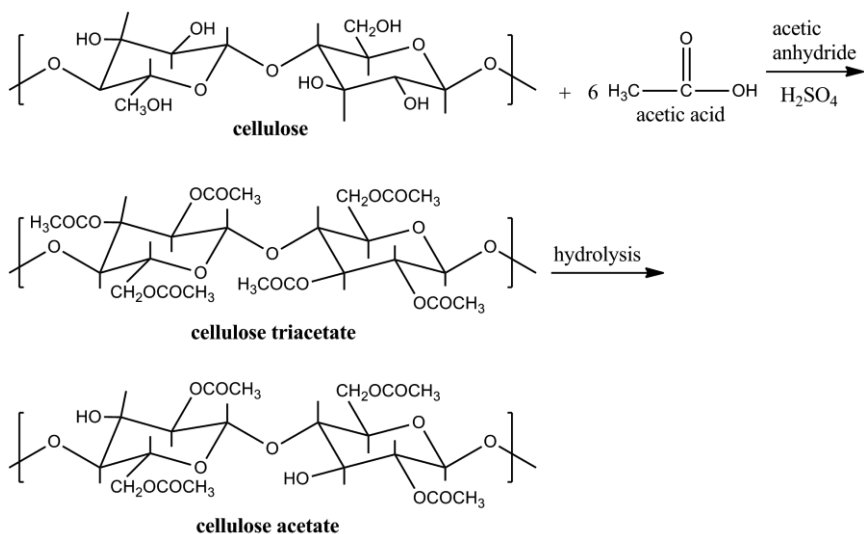
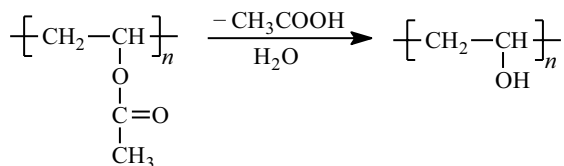


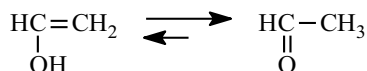
Figure 2-22 Preparation of cellulose acetate from cellulose.

Recently, it has been shown [21] that unmodified cellulose with a DP in the range from 290 to 1200 can dissolve to a concentration of about 20% in the ionic liquid [bmim] [PF₆] (structure shown in Figure 2-19). Ionic liquids also can be used to prepare graft copolymers of cellulose.

Poly(vinyl alcohol) and Poly(vinyl butyral). Poly(vinyl alcohol) (PVAL) is obtained by the direct hydrolysis (or catalyzed alcoholysis) of poly(vinyl acetate) (PVAC) as shown by the following reaction:



Poly(vinyl acetate) is produced by free-radical emulsion or suspension polymerization. It has a low glass-transition temperature (ca. 29°C) and finds some applications as an adhesive. Poly(vinyl alcohol), which is used as a stabilizing agent in emulsion polymerizations and as a thickening and gelling agent, cannot be polymerized directly because its monomer, vinyl alcohol, is isomeric with acetaldehyde as illustrated below.



In this isomerization, the equilibrium is biased toward the ketone structure.

Another important polymer, poly(vinyl butyral) (PVB), which is used as the film between the layers of glass in safety windshields, is obtained by partially reacting PVAL with butyraldehyde, as shown in Figure 2-23. For safety-glass applications, approximately 25% of the repeating units of PVAL are left unreacted to promote adhesion to the glass through interaction of the hydroxyl group with the surface (i.e., silanol) groups of the glass.

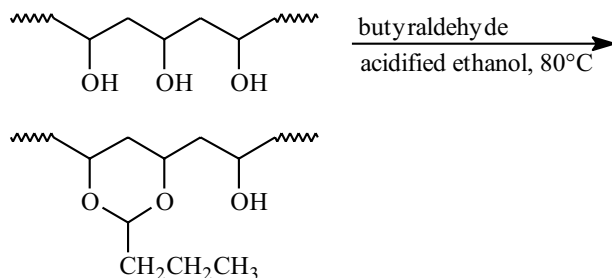
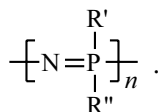


Figure 2-23 Production of poly(vinyl butyral) from a poly(vinyl alcohol) precursor.

Poly(organophosphazenes). Another class of polymers that are obtained by chemical modification of a precursor polymer is the poly(organophosphazenes) [33]. These polymers have an alternating nitrogen–phosphorus backbone, as follows:



A very large number of different substituent groups (R', R'') can be linked to the phosphorus atom. These include alkoxy, aryloxy, amino, alkyl, aryl, or even an inorganic or organometallic unit. Properties vary from elastomeric ($T_g \sim -80^\circ\text{C}$) to microcrystalline. Potential applications of poly(organophosphazenes) include those in which good chemical stability is required including O-rings, gaskets, and fuel lines, and in areas where good biostability and biocompatibility are necessary. Poly(organophosphazenes) also exhibit extremely high permeability for fixed gases and organic liquids and may find use in membrane applications (see Section 12.1).

The precursor polymer for all poly(organophosphazenes) is poly(dichlorophosphazene), which is obtained from the radiation or plasma polymerization of hexachlorocyclotriphosphazene (Section 2.3.5). Poly(dichlorophosphazene) is unstable due to its high susceptibility to hydrolysis; however, the active chlorine sites can be readily substituted by nucleophiles such as alkoxides, aryloxides, and amines to yield chemically and thermally stable derivatives as illustrated in Figure 2-24.

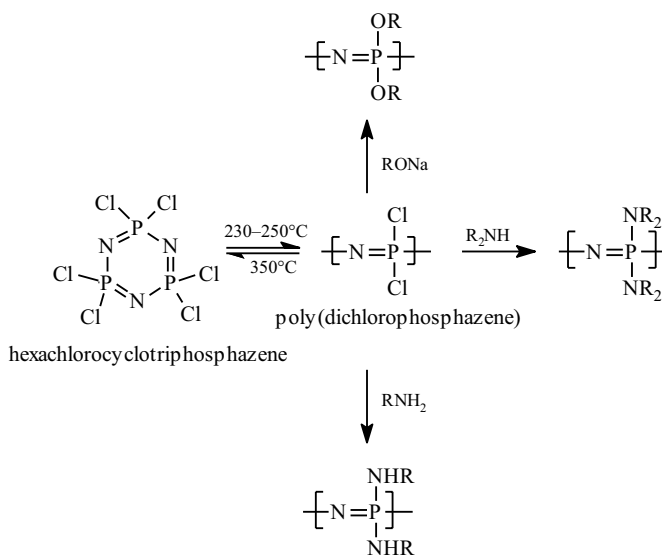


Figure 2-24 Ring-opening polymerization of hexachlorocyclotriphosphazene to poly(dichlorophosphazene) and representative substitution reactions.

2.4.3 Click Chemistry

Click chemistry refers to a class of reactions that are quantitative, highly efficient, rapid, broadly applicable, and tolerant to different functional groups and to the presence of solvent. Click reactions should produce no by-products or side reactions and can be used under mild reaction conditions including low to moderate temperatures (i.e., 25° to 70°C). These reactions can be used to join small modular units and recently have been used in the synthesis of new polymers and postpolymerization side- and end-group functionalization. Important click reactions include the classical Diels–Alder diene + olefin cycloaddition reaction illustrated in Figure 2-25A. Another particularly important click reaction is the copper-catalyzed Huisgen Cu(I) 1,3-dipolar cycloaddition between a terminal alkyne and an azide (Figure 2-25B) to produce a 1,2,3-triazole derivative where R₁ and R₂ designate functional groups. The high reactivity of alkyne–azide click reactions can be used to functionalize the surfaces of fullerenes and carbon nanotubes and resin materials. A third choice for use for click chemistry is the thiol–ene reaction shown in Figure 2-25C. Click reactions can be used to prepare block polymers as shown by the azide–alkyne coupling reaction in Figure 2-25D.

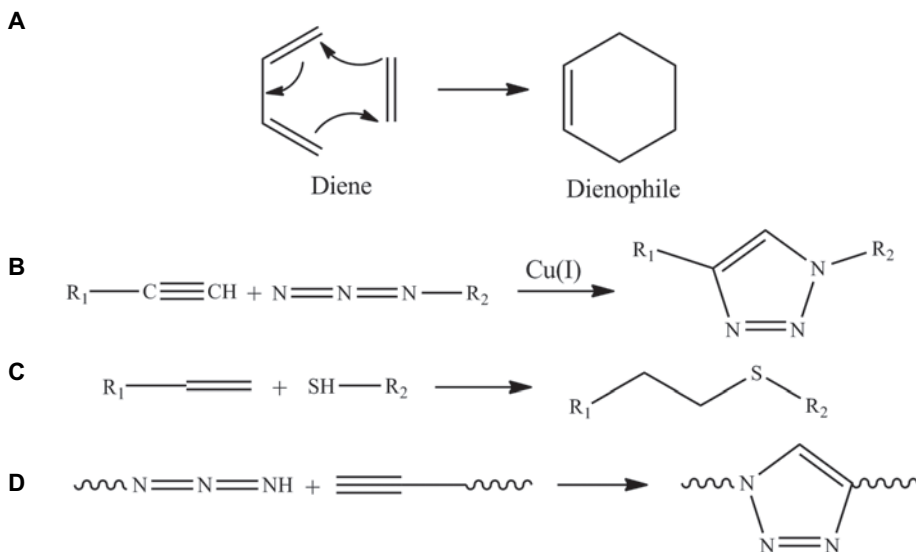
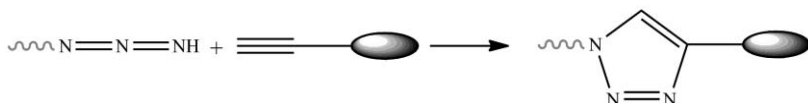


Figure 2-25 Examples of important click chemistry reactions. **A.** Diels–Alder diene + olefin cycloaddition reaction. **B.** Copper-catalyzed Huisgen Cu(I) 1,3-dipolar cycloaddition. **C.** Thiol–ene reaction. **D.** Azide–alkyne coupling reaction.

Branched polymers and dendrimers can also be prepared by click chemistry. In addition, polymers can be functionalized through incorporation of side chains or end groups by means of the azide–alkyne coupling reaction (Figure 2-25D) as illustrated below for the incorporation of end-linked fluorescent tag (oval structure).



Click chemistry has also been used to prepare crosslinked hydrogels as illustrated by the azide–alkyne coupling of poly(ethylene oxide) building blocks as illustrated in Figure 2-26.

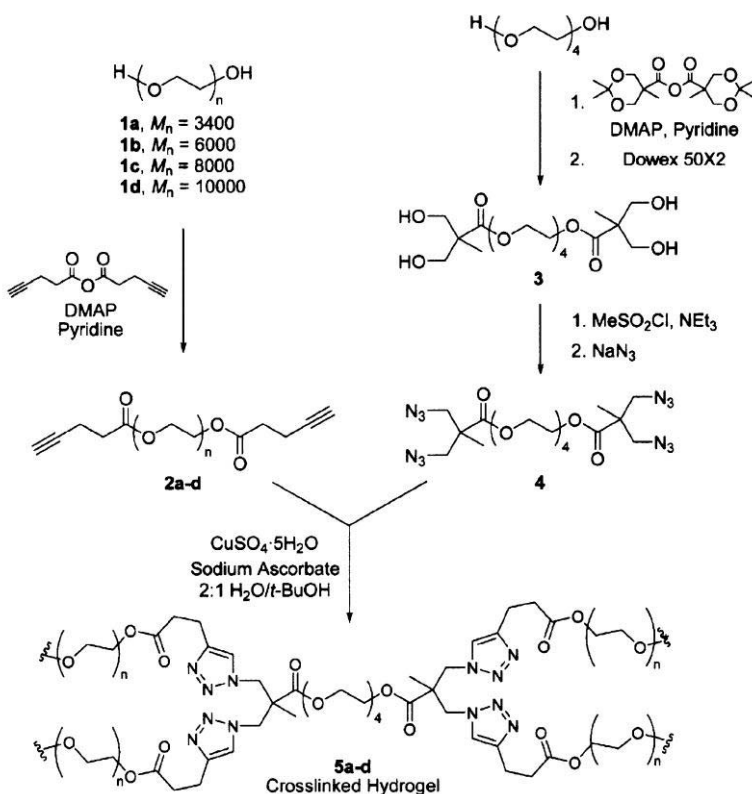


Figure 2-26 Formation of a crosslinked hydrogel through the coupling of azide and acetylene terminated units. Reprinted from M. Malkoch et al., *Synthesis of Well-Defined Hydrogel Networks Using Click Chemistry*. Chemical Communications, 2006, p. 2774–2776.

2.5 Special Topics in Polymer Synthesis

Sections 2.1 and 2.2 described the traditional step-growth and chain-growth polymerization methods that have been developed over the past 75 years and are widely used in today's commercial plastics industry. This coverage also included the important recent development of controlled radical methods to produce polymers and copolymers with controlled composition, defined structure, and narrow-molecular-weight distribution (Section 2.2.4). Several other specialized polymerization approaches of important but perhaps more limited applications have been developed over the years. These include metathesis ring-opening polymerization, first developed in the early 1960s, the use of macromers for the preparation of graft copolymers, group-transfer polymerization, and genetic engineering.

2.5.1 Metathesis

Metathesis reactions include use in small-molecule chemistry such as cross-metathesis and ring-opening and ring-closing metathesis as illustrated in Figure 2-27. Of particular interest here is the use of metathesis reactions in ring-opening metathesis polymerization or ROMP.*

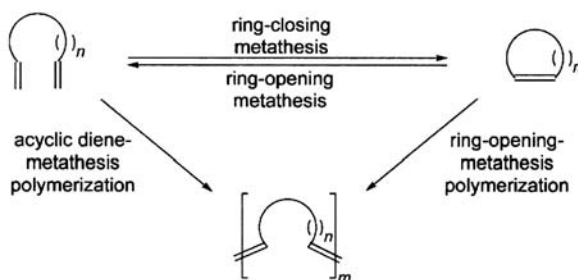


Figure 2-27 Alkene-metathesis reactions. Reproduced from K. C. Nicolaou, P. G. Bulger, and D. Sariah, *Metathesis Reactions in Total Synthesis*. *Angewandte Chemie, International Edition*, 2005. **44**(29): p. 4490–4577.

* For their work with olefin metathesis and its potential for use in green chemistry, Richard R. Shrock, Robert H. Grubbs, and Yves Chauvin received the 2005 Nobel Prize in chemistry.

Cyclic olefins, like cyclobutene and cyclopentene, can undergo a ring-opening polymerization called *metathesis* to yield elastomers (polyalkenamers). Polyalkenamers obtained from the metathesis polymerization of cyclooctene and norbornene (bicyclo[2.2.1]hept-2-ene) are specialty elastomers. Polymerizations proceed with good rates at room temperature. Stereochemistry can be controlled by the choice of catalyst. Typical catalysts for olefin metathesis include Ziegler types such as prepared from the reaction product of tungsten hexachloride with ethanol and ethylaluminum dichloride, $WCl_6/(C_2H_5)_3Al$. Other important examples of catalysts include MoO_3/Al_2O_3 and $TiCl_4/LiAlR_4$. As an illustration, routes in the production of *cis*- and *trans*-isomers of polypentenamer by the metathesis polymerization of cyclopentene are illustrated in Figure 2-28. The unsaturated site of the polypentenamer is available for subsequent functionalization reactions.

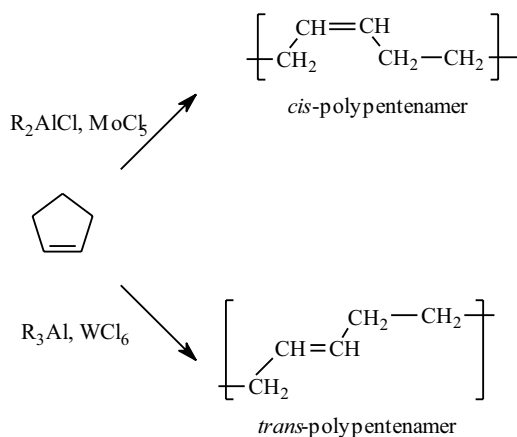


Figure 2-28 Ring-opening metathesis of cyclopentene.

The mechanism of metathesis polymerization is a typical coordination type involving the propagation of a metal-carbene complex via a metallacyclobutane intermediate, as illustrated in Figure 2-29. Metathesis polymerization of highly strained cycloalkanes such as norbornene and cyclobutene proceed much more rapidly than less strained structures such as cyclopentene (Figure 2-28).

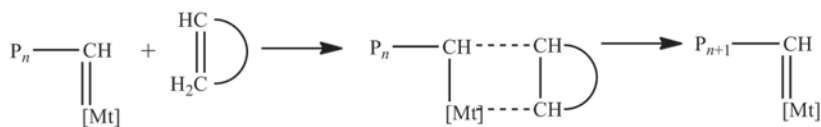


Figure 2-29 A propagation step in the metathesis polymerization of a cycloalkene where P represents a repeat unit, n is the degree of polymerization, and Mt represents a metal complex.

2.5.2 Group-Transfer Polymerization

Group-transfer polymerization (GTP), developed in 1983 by Owen Webster and coworkers at DuPont [34, 35], is the “living” polymerization of α,β -unsaturated esters (principally acrylates and methacrylates), ketones, nitriles, or amides with initiation by silyl ketene acetals. Examples of monomers that can be polymerized in this manner include methyl methacrylate, ethyl acrylate, butyl acrylate, 2-methacryl-oxyethyl acrylate, and methacrylonitrile. Typical initiators are 1-alkoxy-1-(trimethylsiloxy)-2-methyl-1-alkenes such as 1-methoxy-1-(tri-methylsiloxy)-2-methyl-1-propene used in the polymerization of methyl methacrylate. The initiator is activated by nucleophilic catalysts such as soluble fluorides, bifluorides (e.g., tris(dimethylamino)sulfonium bifluoride), azides, and cyanides. Block copolymers such as poly(methyl methacrylate)-*b*-poly(ethyl acrylate) can be prepared by sequential GTP.

During the polymerization, the reactive ketene silyl acetal group is transferred to the head of each new monomer molecule as it adds to the chain, hence the name group-transfer polymerization. As in anionic polymerization, the ratio of monomer to initiator concentration determines the molecular weight. An important example is the GTP of methyl methacrylate shown in Figure 2-30.

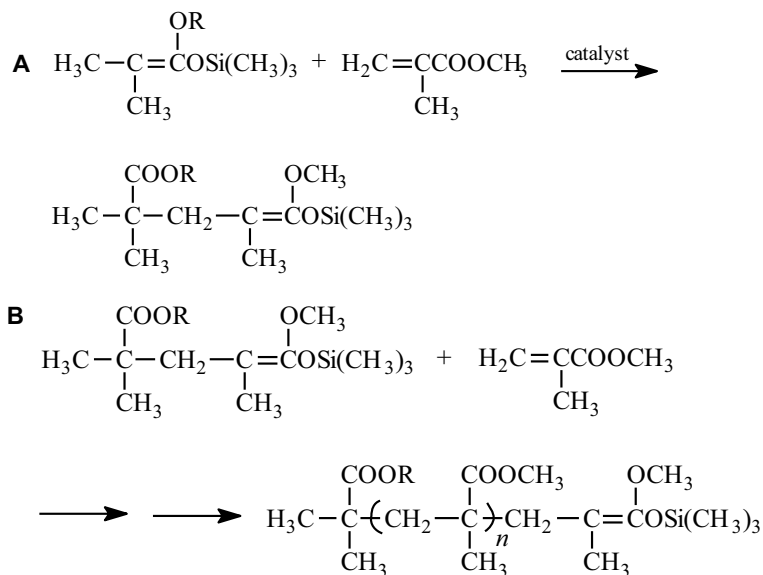


Figure 2-30 Group-transfer polymerization of methyl methacrylate. **A.** Initiation of monomer. **B.** Propagation.

Group-transfer polymerizations are typically conducted in a solution using an organic solvent such as toluene and THF at low temperatures (ca. 0° to 50°C). Active hydrogen compounds like some protonic solvents will stop the polymerization. For this reason, the polymerization environment must be completely free of water. Under these conditions, the polymerization will proceed until all monomer is exhausted as in other “living” polymerizations; however, high-molecular-weight polymers with molecular weights in excess of 100,000 are difficult to achieve unless the monomer, solvent, initiator, and catalyst are extremely pure. The high cost of GTP relative to more traditional free-radical polymerizations and the use of toxic catalysts such as azides and cyanides have limited widespread commercial utilization. Potential applications include high-performance automotive finishes, the fabrication of silicon chips, and coatings for optical fibers.

2.5.3 Macromers in Polymer Synthesis

A macromer or macromonomer is an abbreviation of the term *macromolecular monomer*. As the name suggests, a macromer is a low-molecular-weight oligomer or polymer with a functional group (F) at the chain end. This functional group can further polymerize to yield a higher-molecular-weight polymer. Examples of functional moieties include a vinyl group as well as a variety of difunctional chemical groups such as a dicarboxylic acid, diol, or diamine that can be used in a step-growth (or condensation) polymerization step. One use for macromers is controlled graft copolymerization. In this case, suitable comonomer units containing F_1 functional groups are contained in a prepolymer. A macromer containing complementary F_2 groups then attaches to the available F_1 sites at the comonomer sites and forms branches, as illustrated in Figure 2-31. These graft copolymers can be used as compatibilizers for polymer blends (Section 7.2) and as surface-modifying agents.

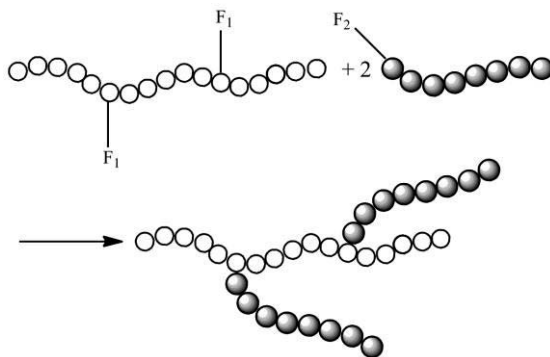


Figure 2-31 Graft polymerization by attachment of two macromers with functional group F_2 to a prepolymer with two complementary functional groups F_1 .

2.5.4 Genetic Engineering

Naturally occurring structural polymers such as collagen, silk, and elastin (see Section 8.1.1) contain repetitious short sequences of amino acids that contribute to their high tensile strength and resilience. Synthetic analogs of these polymers can be obtained by the synthesis of genes and their bacterial expression [36, 37]. Such recombinant DNA methods offer opportunities to prepare polymers with precise control of molecular weight, stereochemistry, and monomer sequence. As illustrated in Figure 2-32, the first step is to encode the desired amino acid sequence into a complementary segment of double-stranded DNA obtained by solid-phase organic synthesis. Next, the synthetic gene is incorporated into a plasmid (a circular portion of a double-stranded DNA) obtained from the bacterium *Escherichia coli*. The recombinant plasmid is then inserted into a strain of *E. coli* that can express the target protein.

Examples of genetically engineered protein-like polymers include elastin analogs capable of temperature- or pH-dependent dimensional changes. For example, poly(valine–proline–glycine–valine–glycine), crosslinked by γ -irradiation, will contract with an increase in temperature. Other examples include adhesive proteins, monodisperse liquid crystalline poly(γ -benzyl-L-glutamate), optically active poly(α ,L-glutamic acid), and other synthetic structural proteins such as spider silk and collagen. Genetic engineering provides an opportunity for molecular design of new materials through substitution of any one of the 20 naturally occurring α -amino acids (see Section 8.1.1) by the corresponding amino acid chemically modified for specific functionality. For example, interesting selenium arrays have been prepared by incorporating selenomethionine in place of methionine [37].

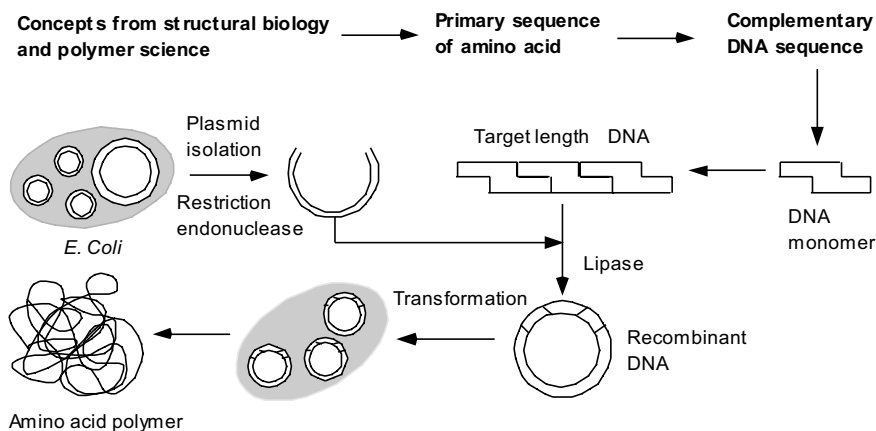


Figure 2-32 Steps in the genetic synthesis of new protein-like polymers. Courtesy of D. Tirrell.

2.5.5 Green Chemistry

The U.S. Environmental Protection Agency defines green chemistry as the “design of chemical products and processes that reduce or eliminate the use or generation of hazardous substances.” Utilizing green chemistry, the risk of a chemical having an adverse impact on the environment is minimized by reducing the potential hazard of monomers, solvents, and catalysts [38]. Falling within the category of green chemistry is the use of genetic engineering to produce polymers from bacterial resources as described in the previous section. An additional application of green chemistry is the use of plant fats and oils for the preparation of monomers and polymers [39]. Plant oils are triglycerides formed by the esterification of esters of glycerol with long-chain fatty acids. An example of the use of plant oils in polymer synthesis is the production of epoxies, polyurethanes, and nylon-11. In some cases, natural or synthetic polymers can be functionalized using enzymes in place of conventional chemical catalysts. An example is the use of mushroom tyrosinase to functionalize chitosan with phenolic groups [40]. Another example is the preparation of telechelic poly(ethylene glycol) by the transesterification of vinyl methacrylate using *Candida antarctica* lipase B [41].

2.6 Chemical Structure Determination

This chapter has described a variety of techniques used to synthesize polymers and copolymers. Once the polymer has been made, several analytical methods are available to confirm that the polymer made is actually the one desired and to identify various specific features of the polymer microstructure, such as comonomer composition and sequence, stereoregularity, branching, crystallinity, orientation, and oxidation sites if thermooxidative degradation has occurred (see Chapter 6). In addition, the presence of various additives, such as stabilizers and lubricating agents, or contaminants that may have been introduced during polymerization or in processing can be readily identified. The most important of these techniques include the common spectroscopic methods such as infrared, nuclear magnetic resonance (NMR), and Raman spectroscopy. Applications of spectroscopic methods to polymer characterization are briefly described in this section. In this, a general understanding of the basic principles of spectroscopy is assumed.

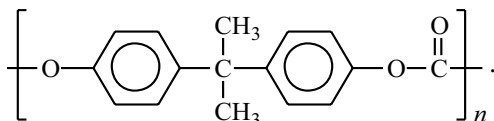
2.6.1 Vibrational Spectroscopy

Perhaps the most widely used method to characterize polymer structure is infrared spectroscopy, particularly Fourier transform infrared (FTIR) spectroscopy [42].

Polymer samples for IR analysis can have a variety of forms including thin film, solution, or a solid pellet containing a mixture of the granulated polymer and an IR-transparent powder such as potassium bromide. Bulk samples can be analyzed by reflection or attenuated total reflectance (ATR).

The IR spectrum of a polymer is unique, and a large number of spectra libraries are available to assist identification [43]. Several atomic groups, such as $-\text{CH}$, $-\text{CO}$, and $-\text{CH}_3$, are readily identified by the presence of a single absorption band. As an example, the $-\text{CH}-$ stretching vibration can be found in the narrow frequency range from 2880 to 2900 cm^{-1} . The exact location of the principal absorption band or bands of other chemical groups depends on the local chemical environment, especially the occurrence of intra- or intermolecular hydrogen bonding. In the case of the carbonyl group, which can easily bond with hydrogen, absorption may occur over the broad range from 1700 to 1900 cm^{-1} . The presence of stereoisomers (i.e., tacticity and geometry isomers) may be identified by the appearance of new absorption frequencies, shifting of absolute frequencies, and band broadening in the infrared spectrum.

A good example of a typical FTIR spectrum is that shown in Figure 2-33 for the engineering thermoplastic, polycarbonate:



The IR spectrum of this polymer is very distinctive. Principal absorption bands include those at 823 cm^{-1} (ring $\text{C}-\text{H}$ bending), 1164 and 1231 cm^{-1} ($\text{C}-\text{O}$ stretching), 1506 cm^{-1} (skeletal ring vibrations), and 1776 ($\text{C}=\text{O}$ stretching).

The locations of IR absorbance peak maxima can also be sensitive to whether the chemical groups lie in crystalline lamellae (see Chapter 4) or in amorphous regions and, therefore, FTIR measurements can be used as a means to determine the degree of crystallinity of a sample. For example, FTIR measurements can be used to follow the development of crystallinity in a sample of poly(vinyl chloride) as a function of heat treatment. Commercial-grade PVC is a polymer of low crystalline order (ca. 7 to 10% crystallinity). When heated above its glass-transition temperature (87°C) and below its crystalline-melting temperature (212°C), the degree of crystallinity can be increased. One way of determining the percent of crystallinity is by density measurements (see Section 4.2.4). Another method is by quantitative measurements of the intensity of certain IR-absorbance peaks.

In the case of PVC, there are two principal overlapping absorbance peaks lying between 550 and 665 cm^{-1} and attributed to $\text{C}-\text{Cl}$ stretching vibrations. One peak that appears to be crystalline sensitive is located at 635 cm^{-1} , while the other is crystalline insensitive and is located at 615 cm^{-1} . The ratio of the amplitude of the 635 - and 615-cm^{-1} peaks can, therefore, be used as a quantitative measure of the

degree of crystallinity. This ratio is plotted as a function of crystallization time in Figure 2-34. As shown, the increase in the absorbance ratio closely follows the percent crystallinity determined from density measurements of the same samples.

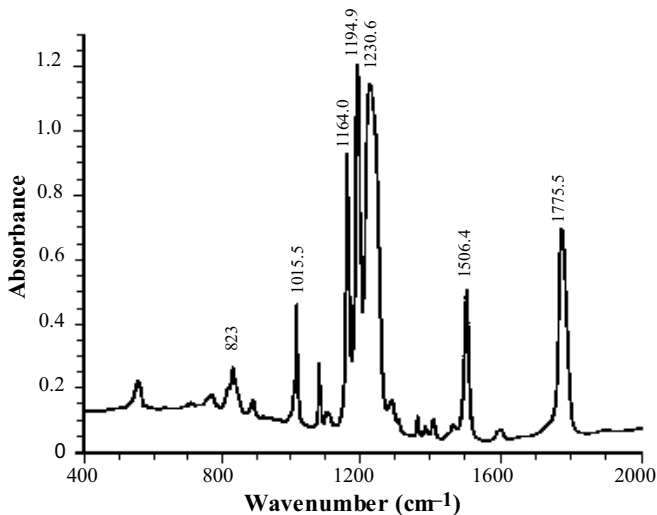


Figure 2-33 FTIR spectrum of a polycarbonate film.

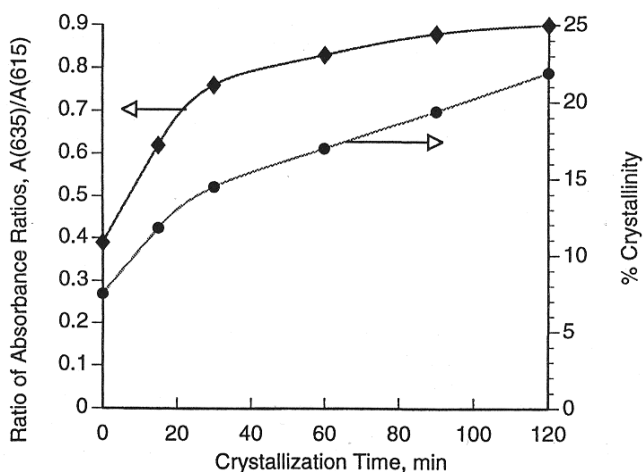


Figure 2-34 Plot of the ratio of the amplitudes of the FTIR absorbance peaks (◆) for poly(vinyl chloride) at 635 and 615 cm⁻¹ as a function of crystallization time at 110° to 115°C [44]. Comparison is made to the percent crystallinity (●) determined from density measurements.

Raman Spectroscopy. A technique related to infrared spectroscopy is Raman scattering, which results from a change in induced dipole moment or polarization of a molecule upon irradiation. In the case of Rayleigh scattering, there is no exchange of energy between the incident light and the molecule and therefore the scattered light has the same frequency, ν_R , as the incident light, ν_0 . In Raman scattering, the molecule returns inelastically to an energy level different from the original state, and therefore the frequency of the scattered light will be different (i.e., $\nu_R = \nu_0 + \Delta\nu$). The strongest bands are those appearing at lower frequencies (i.e., the Stokes bands) and are the ones normally recorded. Perhaps the greatest advantage of Raman scattering in polymer characterization is that no special sample preparation is required, and therefore liquids and solids can be studied nondestructively. For this reason, Raman spectroscopy particularly lends itself to the study of polymer morphology, especially the study of crystalline structure and orientation effects.

2.6.2 Nuclear Magnetic Resonance Spectroscopy

Nuclear magnetic resonance (NMR) spectroscopy is a very powerful technique for polymer characterization that can be used to determine tacticity, branching, structural defects such as the occurrence of head-to-head placement of monomers in vinyl polymers, the sequence of comonomer units in a copolymer chain, and chemical changes such as oxidation states, which can be detected at levels as low as one site per 500 repeat units. Although ^{13}C NMR is commonly used in polymer characterization, NMR measurements employing other NMR-active nuclei such as ^1H , ^{13}C , ^{17}O , and ^{19}F having magnetic moments may have an advantage in the study of some polymers.* For example, ^{29}Si NMR may be used in the characterization of polysiloxanes, ^{19}F NMR for fluoropolymers, ^{15}N NMR for polyamides, and ^{31}P NMR for polyphosphazenes. Two factors that contribute to relative sensitivity and utility of a particular nucleus in NMR spectroscopy are its natural abundance and gyromagnetic ratio (γ). The ^1H isotope with nearly 100% abundance and high gyromagnetic ratio is the most sensitive nucleus for NMR study. A listing of important NMR-active nuclei and their natural abundance is given in Table 2-10.

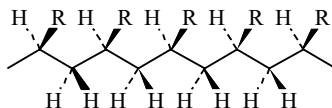
* Any atomic nuclei having a *nonzero* spin quantum number, I , possess a magnetic moment. When placed in a magnetic field, these nuclei occupy $2I + 1$ quantized magnetic energy levels, called Zeeman levels. Transitions (resonance) between energy levels can occur by application of a resonant RF field of frequency ν_0 (equal to the Larmor precession frequency). Resonance for a particular nucleus will occur at slightly different frequencies depending upon its chemical environment (i.e., its chemical bonding and position in the molecule) due to the shielding effect of electron clouds on a nucleus, which reduces the Larmor frequency. These frequency changes are termed *chemical shifts* and are given in reference to tetramethylsilane (TMS) as a standard. The range of chemical shifts is about 100 ppm for ^1H but more than 200 ppm for ^{13}C and other nuclei.

Table 2-10 Nuclei Used in Polymer NMR

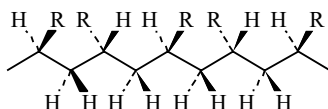
Nuclei	Spin	Natural Abundance (%)	Shift Range (ppm)
^1H	1/2	99.985	15
^2H	1	0.0156	15
^{13}C	1/2	1.108	220
^{14}N	1	9.634	900
^{15}N	1/2	0.365	900
^{17}O	5/2	0.037	800
^{19}F	1/2	100	800
^{29}Si	1/2	4.70	250
^{31}P	1/2	100	700

Two techniques of NMR measurements have been used in polymer studies. Broad-line NMR methods, usually proton relaxation, can be used to determine amorphous content and chain orientation in semicrystalline polymers. High-resolution NMR measurements can be used to obtain information concerning the sequence of repeating units in the chain; this enables the determination of tacticity and comonomer distribution, as described next.

Chemical Structure Determination by NMR Measurements. NMR measurements can provide a very detailed description of the chemical microstructure of a polymer chain, such as branching, head-to-head or head-to-tail addition, comonomer sequence, and tacticity, by measuring chemical shifts that are sensitive to the local environment (electron shielding) of a particular nucleus. For example, NMR measurements can be used to determine the isotactic content of a particular polymer. To understand NMR analysis of tacticity, it is useful to look at the spatial arrangement of several monomer units having an asymmetric substituent group, R. For a sequence of five monomer units, called a pentad, two extreme cases are possible, as discussed in Chapter 1. In an isotactic sequence, all the R groups lie on the same side of the chain as shown below.

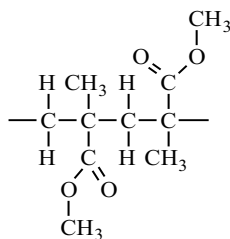


In this case, the four sequential pairs of monomer units (diads) are called meso (m) and, therefore, this particular pentad can be described as mmmm. For four repeating units (quartet), the sequence is represented as mmm and for three repeating units (triad), the sequence is represented as mm. In the case of syndiotactic chain structure, the substituent (R) groups alternate from side to side as shown next.



The sequence is all racemic (r) and the pentad can be described as rrrr. Correspondingly, the quartet is rrr and the triad is rr. The surrounding molecular environment can affect the chemical shift of the proton on a β -methylene (CH_2) group or a proton on the α -carbon substituent group. Whether the resolution can extend to triad, quartet, or pentad sequence identification depends upon the strength of the applied magnetic field.

A good illustration of the use of NMR measurements to determine polymer structure is the use of NMR to study the tacticity of PMMA. Two repeating units (a diad) of an isotactic sample of PMMA are shown below.



If the polymer chain is syndiotactic, the two protons on the β -methylene groups are equivalent and, therefore, there should be a single resonance; however, if the chain is isotactic, the local environments of the two protons are different due to electron-cloud shielding, and four principal resonances (due to spin-spin interactions) result. NMR spectra for predominantly syndiotactic and predominantly isotactic PMMA samples in 10% chlorobenzene at 135°C and observed at high frequency (220 MHz) are shown in Figure 2-35. The major peak intensity is assigned to the rrr quartet of the predominantly syndiotactic sample (Figure 2-35A) and four major peaks are assigned to the mmm quartet of the predominantly isotactic sample (Figure 2-35B).

Solid-State NMR. The spectral line width of solid samples is broad relative to that of liquids (0.2 to 5.0 Hz). This is because the relative immobility of molecules in the solid state results in stronger interactions compared to highly mobile molecules in the liquid state for which intramolecular interactions are averaged out. A technique that allows high-resolution NMR measurements of polymers in the solid state is called magic-angle spinning (MAS) NMR [45]. In this procedure, a cylindrical sample is rotated at high speed (>2 kHz) at an angle of 54.7° relative to the static field. Under these circumstances, line widths decrease to those comparable to solution samples (~ 1 ppm). Solid-state NMR can be used to investigate the segmental mobility of polymer chains, the diffusion of small molecules in polymers, and polymer annealing and aging processes.

Noshey, A., and J. E. McGrath, *Block Copolymers*. 1977, New York: Academic Press.

CLICK CHEMISTRY

Binder, W. H., and R. Sachsenhofer, *Click Chemistry in Polymer Science and Materials Science*. *Macromolecular Rapid Communication*, 2007. **58**: p. 15.

Evans, R. A., *The Rise of Azide-Alkyne 1,3-Dipolar Click Cycloaddition and Its Application to Polymer Science and Surface Modification*. *Austrian Journal of Chemistry*, 2007. **60**: p. 384.

Kolb, H. C., M. G. Finn, and K. B. Sharpless, *Click Chemistry: Diverse Chemical Function from a Few Good Reactions*. *Angewandte Chemie International Edition*, 2001. **40**: p. 2004.

CONTROLLED/LIVING RADICAL POLYMERIZATION

Braunecker, W. A., and K. Matyjaszewski, *Controlled/Living Radical Polymerization: Features, Developments, and Perspectives*. *Progress in Polymer Science*, 2007. **32**: p. 93.

Goto, G., and T. Fukuda, *Kinetics of Living Radical Polymerization*. *Progress in Polymer Science*, 2004. **29**: p. 329.

Hawker, C. J., A. W. Bosman, and E. Harth, *New Polymer Synthesis by Nitroxide Mediated Living Radical Polymerization*. *Chemical Reviews*, 2001. **101**: p. 3661.

Meijs, F. C., L. Moad, E. Rizzardo, and S. H. Thang, *Living Free-Radical Polymerization by Reversible Addition-Fragmentation Chain Transfer: The RAFT Process*. *Macromolecules*, 1998. **31**: p. 5559.

Moade, G., *Toward Living Radical Polymerization*. *Accounts of Chemical Research*, 2008. **41**: p. 1133.

Solomon, D. H., *Genesis of the CSIRO Polymer Groups and the Discovery and Significance of Nitroxide-Mediated Living Radical Polymerization*. *Journal of Polymer Science: Part A*, 2005. **43**: p. 5748.

COORDINATION POLYMERIZATION

Boor, J., *Ziegler-Natta Catalysts and Polymerization*. 1979, New York: Academic Press.

Breslow, D. S., *Metathesis Polymerization*. *Progress in Polymer Science*, 1993. **18**: p. 1141.

Hamielec, A. E., and J. B. P. Soares, *Polymerization Reaction Engineering—Metallocene Catalysts*. *Progress in Polymer Science*, 1996. **21**: p. 651.

Imanishi, Y., and N. Naga, *Recent Developments in Olefin Polymerizations with Transition Metal Catalysts*. *Progress in Polymer Science*, 2001. **26**: p. 1147.

Kaminsky, W., *New Polymers by Metallocene Catalysis*. *Macromolecular Chemistry and Physics*, 1996. **197**: p. 3907.

Kaminsky, W., and M. Arndt, *Metallocenes for Polymer Catalysis*. *Advances in Polymer Science*, 1997. **127**: p. 143.

Kaminsky, W., and R. Steiger, *Polymerization of Olefins with Homogeneous Zirconocene/Alumoxane Catalysts*. *Polyhedron*, 1988. **7**: p. 2375.

Price, C. C., and E. J. Vandenberg, eds., *Coordination Polymerization*. 1983, New York: Plenum.

Qiu, J., B. Charleux, and K. Matyjaszewski, *Controlled/Living Radical Polymerization in Aqueous Media: Homogeneous and Heterogeneous Systems*. *Progress in Polymer Science*, 2001. **26**: p. 2083.

Soga, K., and T. Shiono, *Ziegler–Natta Catalysts for Olefin Polymerizations*. Progress in Polymer Science, 1997. **22**: p. 1503.

Zakharov, V. A., G. D. Bukatov, and Y. I. Yermakov, *On the Mechanism of Olefin Polymerization by Ziegler–Natta Catalysts*. Advances in Polymer Science, 1983. **52/53**: p. 61.

EMULSION POLYMERIZATION

Asua, J. M., *Miniemulsion Polymerization*. Progress in Polymer Science, 2002. **27**: p. 1283.

Chern, C.S., *Emulsion Polymerization Mechanisms and Kinetics*. Progress in Polymer Science, 2006. **31**: p. 443.

Thickett, S. C., and R. Gilbert, *Emulsion Polymerization: State of the Art in Kinetics and Mechanisms*. Polymer, 2007. **48**: p. 6965.

FREE-RADICAL POLYMERIZATION

Bisht, H. S., and A. K. Chatterjee, *Living Free-Radical Polymerization—A Review*. Journal of Macromolecular Science—Polymer Reviews, 2001. **C41**: p. 139.

Haaland, P. D., and S. J. Clarson, *Plasma and Polymers: Synthesis under Extreme Conditions*. Trends in Polymer Science, 1993. **1**: p. 40.

Kiran, E., and V. P. Saraf, *Polymerization of Styrene in Supercritical n-Butane*. Journal of Supercritical Fluids, 1990. **3**: p. 198.

Matyjaszewski, K., and T. P. Davis, *Handbook of Radical Polymers*. 2002, Hoboken: John Wiley & Sons.

O’Neil, G. A., M. B. Wisnudel, and J. M. Torkelson, *A Critical Experimental Examination of the Gel Effect in Free-Radical Polymerization: Do Entanglements Cause Autoacceleration?* Macromolecules, 1996. **29**: p. 7477.

Vogl, O., *Head-to-Head Polymers*. Journal of Polymer Science, Polymer Chemistry Edition, 2000. **38**: p. 4013.

FUNCTIONAL POLYMERS

Akelah, A., and A. Moet, *Functionalized Polymers and Their Applications*. 1990, London: Chapman and Hall.

Klemm, D., T. Heinze, and W. Wagenknecht, *New Approaches to Advanced Polymers by Selective Cellulose Functionalization*. Acta Polymerica, 1997. **48**: p. 277.

IONIC LIQUIDS

Baško, M., T. Biedroń, and P. Kubisa, *Polymer Processes in Ionic Liquids. Cationic Polymerization of Styrene*, Macromolecular Symposium, 2006. **240**: p. 107.

Kubisa, P., *Ionic Liquids in the Synthesis and Modification of Polymers*. Journal of Polymer Science: Part A: Polymer Chemistry, 2005. **43**: p. 4675.

Lu, J., F. Yan, and J. Texter, *Advanced Applications of Ionic Liquids in Polymer Science*. Progress in Polymer Science, 2009. **34**: p. 431.

IONIC POLYMERIZATION

Altares, T., Jr., and E. L. Clark, *Pilot Plant Preparation of Polystyrene of Very Narrow Molecular Weight Distribution*. Industrial and Engineering Chemistry, 1970. **9**: p. 168.

Bywater, S., *Structure and Mechanism in Anionic Polymerization*. Progress in Polymer Science, 1994. **19**: p. 287.

- Kennedy, J. P., *Cationic Polymerization: Past—Present—Future*. Trends in Polymer Science, 1995. **3**: p. 386.
- Kubisa, P., *Ionic Liquids as Solvents for Polymerization Processes—Progress and Challenges*, Progress in Polymer Science, 2009. **34**: p. 1333.
- Sarac, A. S., *Redox Polymers*. Progress in Polymer Science, 1999. **24**: p. 1149.
- Szwarc, M., *Living Polymers and Mechanisms of Anionic Polymerization*. Advances in Polymer Science, 1983. **52/53**: p. 1.

LIVING POLYMERIZATION

- Franta, E., T. Hogen-Esch, M. Van Beylen, and J. Smid, *Fifty Years of Living Polymers*. Journal of Polymer Science: Part A: Polymer Chemistry, 2007. **45**: p. 2576.
- Levy, M., *The Impact of the Concept of “Living Polymer” on Materials Science*. Polymers for Advanced Technology, 2007. **18**: p. 681.

STRUCTURAL CHARACTERIZATION

- Barth, H. G., and J. W. Mays, *Modern Methods of Polymer Characterization*. 1991, New York: John Wiley & Sons.
- Bodor, G., *Structural Investigation of Polymers*. 1991, London: Ellis Horwood.
- Bovey, F. A., *High Resolution NMR of Macromolecules*. 1972, New York: Academic Press.
- Koenig, J. L., *Chemical Microstructure of Polymer Chains*. 1980, New York: John Wiley & Sons.
- Koenig, J. L., “Molecular Spectroscopy,” in *Physical Properties of Polymers*. 2nd ed. J. E. Mark, A. Eisenberg, W. W. Graessley, L. Mandelkern, E. T. Samulski, J. L. Koenig, and G. D. Wignall, eds. 1993, Washington, DC: American Chemical Society, p. 263–312.
- Koenig, J. L., *Spectroscopy of Polymers*. 2nd ed. 1999, Amsterdam: Elsevier.

PROBLEMS

- 2.1** If the half-life time, $t_{1/2}$, of the initiator AIBN in an unknown solvent is 22.6 h at 60°C, calculate its dissociation rate constant, k_d , in units of reciprocal seconds.
- 2.2** Styrene is polymerized by free-radical mechanism in solution. The initial monomer and initiator concentrations are 1 M (molar) and 0.001 M, respectively. At the polymerization temperature of 60°C, the initiator efficiency is 0.30. The rate constants at the polymerization temperature are as follows:

$$k_d = 1.2 \times 10^{-5} \text{ s}^{-1}$$

$$k_p = 176 \text{ M}^{-1} \text{ s}^{-1}$$

$$k_t = 7.2 \times 10^7 \text{ M}^{-1} \text{ s}^{-1}$$

Given this information, determine the following:

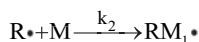
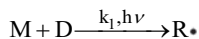
- (a) Rate of initiation at 1 min and at 16.6 h
- (b) Steady-state free-radical concentration at 1 min
- (c) Rate of polymerization at 1 min

(d) Average free-radical lifetime, τ , at 1 min, where τ is defined as the radical concentration divided by the rate of termination

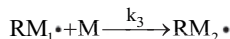
(e) Number-average degree of polymerization at 1 min

2.3 It has been reported that the rate of a batch *photopolymerization* of an aqueous acrylamide solution using a light-sensitive dye is proportional to the square of the monomer concentration, $[M]^2$, and the square root of the absorbed light intensity, $I^{1/2}$. Note that, although this polymerization is free radical, the apparent kinetics appear not to be typical of usual free-radical polymerization for which the rate of polymerization is proportional to the first power of monomer concentration and to the square root of the initiator concentration (eq. (2.25)). The following polymerization mechanism has been proposed to explain the observed kinetics:

Initiation



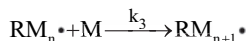
Propagation



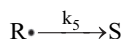
...

...

...



Termination



where

M, monomer

D, dye

P, terminated polymer

S, deactivated initiator

Show that this mechanism appears to be correct by deriving an equation for the rate of propagation in terms of $[M]$, I , and the appropriate rate constants. The following assumptions may be made:

1. Equal reactivity in the propagation steps
2. Steady-state concentration of $R\cdot$ and $RM_n\cdot$

3. $k_2 \ll k_5$

4. The concentration of dye, $[D]$, that has been activated by light and thereby contributes to the first initiation step is proportional to the absorbed light intensity.

2.4 Reactivity ratios for styrene and 4-chlorostyrene are given in Table 2-6.

(a) Using these values, plot the instantaneous copolymer composition of poly(styrene-co-4-chlorostyrene) as a function of comonomer concentration in the copolymerization mixture.

(b) Comment on the expected monomer sequence distribution in the resulting copolymer.

2.5 If the number-average degree of polymerization for polystyrene obtained by the bulk polymerization of styrene at 60°C is 1000, what would be the number-average degree of polymerization if the polymerization were conducted in a 10% solution in toluene (900 g of toluene per 100 g of styrene) under otherwise identical conditions? The molecular weights of styrene and toluene are 104.12 and 92.15, respectively. State any assumptions that are needed.

2.6 Assume that a polyesterification is conducted in the absence of solvent or catalyst and that the monomers are present in stoichiometric ratios. Calculate the time (min) required to obtain a number-average degree of polymerization of 50 given that the initial dicarboxylic acid concentration is 3 mol L⁻¹ and that the polymerization rate constant is 10⁻² L mol⁻¹ s⁻¹.

2.7 Show how the assumption of steady-state free radical concentration, $\overline{M}_1\cdot$ or $\overline{M}_2\cdot$, can be used to obtain the instantaneous copolymerization equation in the form of eq. (2.45) starting with eq. (2.39).

2.8 Show that the ceiling temperature in a free-radical polymerization can be obtained as

$$T_c = \frac{-\Delta H_p}{R \ln(A_p [M] / A_{dp})}$$

2.9 Find the azeotropic composition for the free-radical copolymerization of styrene and acrylonitrile.

2.10 Describe the copolymer composition that would be expected in the free-radical copolymerization of styrene and vinyl acetate.

2.11 Explain why high pressure favors the propagation step in a free-radical polymerization. How would the rate of termination be affected by pressure?

2.12 From data available in Section 2.2.1, calculate the activation energy for propagation for the free-radical polymerization of styrene. Do you expect the activation energy to be dependent upon solvent in a solution polymerization?

2.13 Draw the chemical structures of the two ends of a terminated polystyrene chain obtained by the atom transfer radical polymerization of styrene using 1-phenylethyl chloride (1-PECl) as the initiator, CuCl as the catalyst, and 2,2'-bipyridine as the complexing agent.

2.14 Show that the rate of polymerization in atom transfer radical polymerization is proportional to the equilibrium constant defined in eq. (2.50).

2.15 Show that azeotropic copolymerization occurs when the feed composition is given as

$$f_1 = \frac{1-r_1}{2-r_1-r_2}.$$

2.16 Methyl methacrylate is copolymerized with 2-methylbenzyl methacrylate (M_1) in 1,4-dioxane at 60°C using AIBN as the free-radical initiator.

(a) Draw the repeating unit of poly(2-methylbenzyl methacrylate).

(b) From the data given in the table below, estimate the reactivity ratios of both monomers.

f_1	F_1^a
0.10	0.14
0.25	0.33
0.50	0.52
0.75	0.70
0.90	0.87

^a From ¹H-NMR measurements.

REFERENCES

- Carothers, W. H., *Polymerization*. Chemical Reviews, 1931. **8**(3): p. 353–426.
- Brandrup, J., E. H. Immergut, and E.A. Grulke, eds., *Polymer Handbook*. 4th ed. 1999, New York: John Wiley & Sons.
- Alfrey, T., Jr., and C. C. Price, *Relative Reactivities in Vinyl Copolymerization*. Journal of Polymer Science, 1946. **2**(1): p. 101–106.
- Yu, X., X. Wang, and N. Li, *Prediction of the Q-e Parameters from Radical Structures*. Colloid and Polymer Science, 2010. **288**: p. 951–958.
- Mayo, F. R., and F. M. Lewis, *Copolymerization. I. A Basis for Comparing the Behavior of Monomers in Copolymerization; The Copolymerization of Styrene and Methyl Methacrylate*. Journal of the American Chemical Society, 1944. **66**: p. 1594–1601.

- Szwarc, M., *Electron Transfer Reactions and Living Polymers*. Proceedings of the Royal Society of London. Series A, Mathematical and Physical Science, 1964. **279**(1377): p. 260–290.
- Matyjaszewski, K., P. Kubisa, and S. Penczek, *Ion-Ester Equilibria in the Living Cationic Polymerization of Tetrahydrofuran*. Journal of Polymer Science: Polymer Chemistry Edition, 1974. **12**: p. 1333–1336.
- Natta, G., *Stereospezifische Katalysen und Isotaktische Polymere*. Angewandte Chemie, 1956. **68**(12): p. 393–403.
- Ziegler, K., et al., *Das Mulheimer Normaldruck-Polyethylene-Verfahren*. Angewandte Chemie, 1955. **67**(19,20): p. 541–547.
- Cossee, P., *Ziegler-Natta Catalysis I. Mechanism of Polymerization of α -Olefins with Ziegler-Natta Catalysts*. Journal of Catalysis, 1964. **3**: p. 80–88.
- Sinn, H., and W. Kaminsky, *Ziegler-Natta Catalysts*. Advances in Organometallic Chemistry, 1980. **18**: p. 99–149.
- Otsu, T., *Iniferter Concept and Living Radical Polymerization*. Journal of Polymer Science: Part A: Polymer Chemistry, 2000. **38**: p. 2121–2136.
- Hawker, C. J., A. W. Bosman, and E. Harth, *New Polymer Synthesis by Nitroxide Mediated Living Radical Polymerizations*. Chemical Reviews, 2001. **101**: p. 3661–3688.
- Moad, G., E. Rizzardo, and S. H. Thang, *Toward Living Radical Polymerization*. Accounts of Chemical Research, 2008. **41**(9): p. 1133–1142.
- Bartholome, C., et al., *Nitroxide-Mediated Polymerization of Styrene Initiated from the Surface of Silica Nanoparticles. In Situ Generation and Grafting of Alkoxy Initiators*. Macromolecules, 2005. **38**: p. 1099–1106.
- Wang, J.-S., and K. Matyjaszewski, *Controlled/“Living” Radical Polymerization. Halogen Atom Transfer Radical Polymerization Promoted by a Cu(I)/Cu(II) Redox Process*. Macromolecules, 1995. **28**: p. 7901–7910.
- Wang, J.-S., and K. Matyjaszewski, *Controlled/“Living” Radical Polymerization. Atom Transfer Radical Polymerization in the Presence of Transition-Metal Complexes*. Journal of the American Chemical Society, 1995. **117**: p. 5614–5615.
- Kato, M., et al., *Polymerization of Methyl Methacrylate with the Carbon Tetrachloride/Dichlorotris(triphenylphosphine)ruthenium(II)/Methylaluminum Bis(2,6-di-tert-butylphenoxide) Initiating Systems: Possibility of Living Radical Polymerization*. Macromolecules, 1995. **28**: p. 1721–1723.
- Zhu, S., and D. Yan, *Atom Transfer Radical Polymerization of Styrene and Methyl Methacrylate Catalyzed by $FeCl_2$ /Iminodiacetic Acid*. Journal of Polymer Science: Part A: Polymer Chemistry, 2000. **38**: p. 4308–4314.
- Coessens, V., T. Pintauer, and K. Matyjaszewski, *Functional Polymers by Atom Transfer Radical Polymerization*. Progress in Polymer Science, 2001. **26**: p. 337–377.
- Kubisa, P., *Ionic Liquids as Solvents for Polymerization Processes—Progress and Challenges*. Progress in Polymer Science, 2009. **34**: p. 1333–1347.
- Chiefari, J., et al., *Living Free Radical Polymerization by Reversible Addition-Fragmentation Chain Transfer: The RAFT Process*. Macromolecules, 1998. **31**: p. 5559–5562.
- Sahnoun, M., et al., *Synthesis and Characterization Aspects of Dimethylaminoethyl Methacrylate Reversible Addition Fragmentation Chain Transfer (RAFT) Polymerization*. Journal of Polymer Science: Part A: Polymer Chemistry, 2005. **43**: p. 3551–3565.
- Jin, Y., et al., *Synthesis and Characterizations of 1,2,3-Triazole Containing Polymers via Reversible Addition-Fragmentation Chain Transfer (RAFT) Polymerization*. European Polymer Journal, 2008. **44**: p. 1743–1751.
- Moad, G., E. Rizzardo, and S. H. Thang, *Living Radical Polymerization by the RAFT Process*. Australian Journal of Chemistry, 2005. **58**: p. 379–410.

26. Norrish, R. G. W., and R. R. Smith, *Catalyzed Polymerization of Methyl Methacrylate in the Liquid Phase*. *Nature*, 1942. **150**: p. 336–337.
27. von Trommsdorff, E., H. Kohle, and P. Lagally, *Zur Polymerisation des Methacrylsaure-methylesters*. *Makromolekulare Chemie*, 1947. **1**: p. 169–198.
28. Sarac, A. S., *Redox Polymerization*. *Progress in Polymer Science*, 1999. **24**: p. 1149–1204.
29. Smith, W. V., and R. H. Ewart, *Kinetics of Emulsion Polymerization*. *Journal of Chemical Physics*, 1948. **16**(6): p. 592–599.
30. Asua, J. M., *Miniemulsion Polymerization*. *Progress in Polymer Science*, 2002. **27**: p. 1283–1346.
31. Chiu, D. Y., et al., *Unipol II LLDPE—Gas Phase LLDPE for the Shrink Market*. *Journal of Plastic Film and Sheeting*, 1999. **15**: p. 153–178.
32. Merrifield, R. B., *Solid Phase Peptide Synthesis. I. The Synthesis of a Tetrapeptide*. *Journal of the American Chemical Society*, 1963. **85**: p. 2149–2154.
33. Allcock, H. R., *Polyphosphazenes*. *Journal of Inorganic and Organometallic Polymers*, 1992. **2**(2): p. 197–211.
34. Webster, O. W., et al., *Group-Transfer Polymerization. I. A New Concept for Addition Polymerization with Organosilicon Initiators*. *Journal of the American Chemical Society*, 1983. **105**: p. 5706–5708.
35. Webster, O. W., *The Discovery and Commercialization of Group Transfer Polymerization*. *Journal of Polymer Science: Part A: Polymer Chemistry*, 2000. **38**: p. 2855–2860.
36. Tirrell, D. A., M. J. Fournier, and T. L. Mason, *Genetic Engineering of Polymeric Materials*, *MRS Bulletin*, 1991, p. 23–28.
37. Krejchi, M. T., et al., *Chemical Sequence Control of β -Sheet Assembly in Macromolecular Crystals of Periodic Polypeptides*. *Science*, 1994. **265**: p. 1427–1432.
38. Poliakov, M., et al., *Green Chemistry: Science and Politics of Change*. *Science*, 2002. **297**: p. 807–810.
39. Meier, M. A. R., J. O. Metzger, and U. S. Schubert, *Plant Oil Renewable Resources as Green Alternatives in Polymer Science*. *Chemical Society Review*, 2007. **36**: p. 1788–1802.
40. Puskas, J. E., M. Y. Sen, and J. P. Kasper, *Green Polymer Chemistry: Telechelic Poly(ethylene Glycol)s via Enzymatic Catalysis*. *Journal of Polymer Science: Part A: Polymer Chemistry*, 2008. **46**: p. 3024–3028.
41. Puskas, J. E., M. Y. Sen, and K. S. Seo, *Green Chemistry Using Nature's Catalysts, Enzymes*. *Journal of Polymer Science: Part A: Polymer Chemistry*, 2009. **47**: p. 2959–2976.
42. Koenig, J. L., *Fourier Transform Infrared Spectroscopy of Polymers*. *Advances in Polymer Science*, 1983. **54**: p. 89–154.
43. Hummel, D. O., *Atlas of Polymer and Plastics Analysis*. 1978, Munich: Carl Hanser Verlag.
44. Ballard, R. L., *The Sorption and Transport of Carbon Dioxide and Methane in Plasticized Poly(vinyl chloride)*, PhD Dissertation, Department of Chemical Engineering, University of Cincinnati, 1992.
45. Schaefer, J., E. O. Stejskal, and R. Buchdahl, *High-Resolution Carbon-13 Nuclear Magnetic Resonance Study of Some Solid, Glassy Polymers*. *Macromolecules*, 1975. **8**(3): p. 291–296.

Conformation, Solutions, and Molecular Weight

Solvents are frequently used during the polymerization process (Chapter 2), during fabrication (e.g., film casting, fiber formation, and coatings), and for determining molecular weights and molecular-weight distributions. Interactions between a polymer and solvent influence chain dimensions (i.e., conformations) and, more importantly, determine solvent activities. The measurement of osmotic pressure and scattered-light intensity from dilute polymer solutions—techniques based upon the principles of polymer-solution thermodynamics—are the primary methods used to determine number-average and weight-average molecular weights, respectively. Other solution-property techniques, such as the determination of intrinsic viscosity and gel-permeation chromatography (GPC), are widely used as rapid and convenient methods to determine polymer molecular weight and, in the case of GPC, molecular-weight distributions as described in this chapter.

3.1 POLYMER CONFORMATION AND CHAIN DIMENSIONS

As briefly discussed in Chapter 1, the *configuration* of a polymer chain refers to the stereochemical arrangement of atoms along that chain. Examples include tactic and geometric isomers, which are determined by the mechanism of the polymerization and, therefore, cannot be altered without breaking primary valence bonds. In contrast, polymer chains in solution are free to rotate around individual bonds, and almost a limitless number of *conformations* or chain orientations in three-dimensional space are possible for long, flexible macromolecules.

To describe the conformation of polymer molecules, a highly idealized model of a *random flight* or *freely jointed* and *volumeless* chain is often used as a starting point. Such a hypothetical chain is assigned n freely jointed links having equal length, ℓ . If one end of this hypothetical chain is fixed at the origin of a Cartesian coordinate system, the other end of the chain has some finite probability of being at any other coordinate position, as illustrated by Figure 3-1. One of the many possible conformations, and the simplest, for this idealized chain is the fully extended (i.e., linear) chain where the end-to-end distance, r , is simply

$$r = n\ell. \quad (3.1)$$

Flory [1] was the first to derive an expression for the probability of finding one end of the freely jointed polymer chain in some infinitesimal volume ($dV = dx \cdot dy \cdot dz$) around a particular coordinate point (x, y, z) when one end of the chain is fixed at the origin of a Cartesian coordinate system, as illustrated in Figure 3-1. The probability is given by a *Gaussian distribution* in the form

$$\omega(x, y, z) dx dy dz = \left(\frac{b}{\pi^{1/2}} \right)^3 \exp(-b^2 r^2) dx dy dz \quad (3.2)$$

where $\omega(x, y, z)$ is called the Gaussian distribution function, r is the radius of a spherical shell centered at the origin where

$$r^2 = x^2 + y^2 + z^2, \quad (3.3)$$

and

$$b^2 = \frac{3}{2n\ell^2}. \quad (3.4)$$

Alternatively, the probability that a chain displacement length has a value in the range r to $r+dr$ is given as

$$\omega(r)dr = \left(\frac{b}{\pi^{1/2}}\right)^3 \exp(-b^2 r^2) 4\pi r^2 dr \quad (3.5)$$

where $\omega(r)$ is called the *radial* distribution function. The radial distribution function for a freely jointed polymer chain consisting of 10^4 freely jointed links each of length 2.5 \AA is plotted as a function of the radial distance, r , in Figure 3-2.

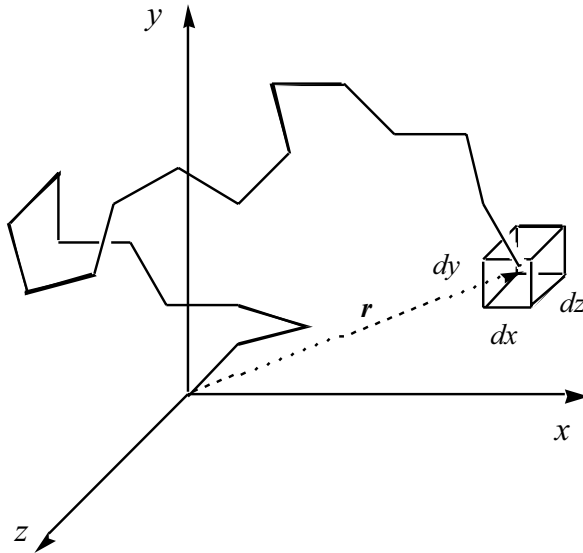


Figure 3-1 Illustration of a random conformation of an idealized freely jointed polymer chain having 20 segments of equal length. The end-to-end distance of this conformation is indicated as r . With one end of the chain fixed at the origin of the Cartesian coordinate system, the probability of finding the other end in some infinitesimal volume element ($dV = dx \cdot dy \cdot dz$) is given by the Gaussian distribution function (eq (3.2)).

The mean-square end-to-end distance is obtained from the second moment of the radial distribution function as

$$\langle r^2 \rangle = \frac{\int_0^\infty r^2 \omega(r) dr}{\int_0^\infty \omega(r) dr} \quad (3.6)$$

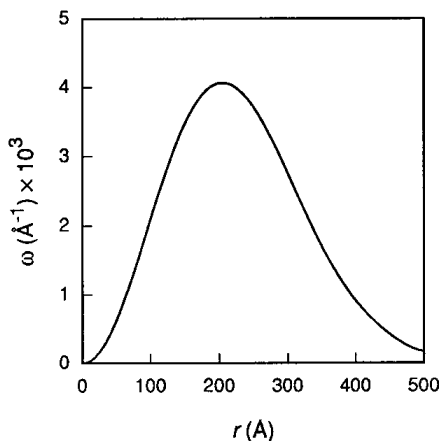


Figure 3-2 The radial distribution function calculated (eq. (3.5)) for a hypothetical polymer chain consisting of 10^4 freely jointed segments of length 2.5 Å.

Substitution of the radial-distribution function (eq. (3.5)) into eq. (3.6) and evaluating the integral gives the mean-square end-to-end distance of the freely jointed and volumeless chain as

$$\langle r^2 \rangle = n\ell^2. \quad (3.7)$$

Alternatively, the *root*-mean-square end-to-end distance, $\langle r^2 \rangle^{1/2}$, of the freely rotating chain is given as

$$\langle r^2 \rangle^{1/2} = n^{1/2}\ell. \quad (3.8)$$

Real polymer chains differ from the above idealized, freely jointed model in the following three significant ways:

- **Valence angles of real bonds are fixed.** For example, the tetrahedrally bonded C–C bond angle is 109.5° . Introducing fixed bond angles results in an expansion of the chain expressed by the mean-square end-to-end distance as (for large n)

$$\langle r^2 \rangle = n\ell \frac{1 - \cos \theta}{1 + \cos \theta} \quad (3.9)$$

where θ is the valence bond angle, as illustrated for an extended chain conformation in Figure 3-3. In the case of tetrahedral valence angles, $\cos \theta \approx -1/3$, and, therefore,

$$\langle r^2 \rangle = 2n\ell^2. \quad (3.10)$$

Comparison of this result with that of eq. (3.7) indicates that restricting the valence angle to 109.5° results in a doubling of the mean-square end-to-end distance compared to the freely rotating model.

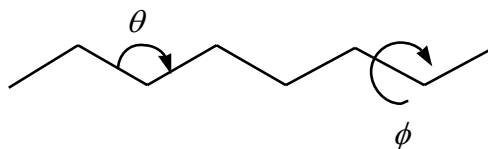


Figure 3-3 Illustration of an extended polymer chain showing the valence bond angle, θ , and bond-rotation angle, ϕ .

• **Rotations of polymer chains may be hindered due to steric interference from bulky substituent groups.** As illustrated by the potential-energy diagram shown in Figure 3-4, overlap of bulky substituent groups on adjacent carbon atoms results in a high-energy, unfavorable conformational state. The result of this steric interference is to further expand chain dimensions over the random-flight model. Equation (3.7) may be further modified to include the effects of both fixed bond angles and hindered rotations as

$$\langle r^2 \rangle = n\ell \frac{1 - \cos \theta}{1 + \cos \theta} \frac{1 + \langle \cos \phi \rangle}{1 - \langle \cos \phi \rangle} \quad (3.11)$$

where $\langle \cos \phi \rangle$ represents the average cosine of the bond-rotation angle, ϕ , identified in Figure 3-3. This second contribution is much more difficult to evaluate but can be obtained by statistical-weighting methods, as discussed by Flory [2].

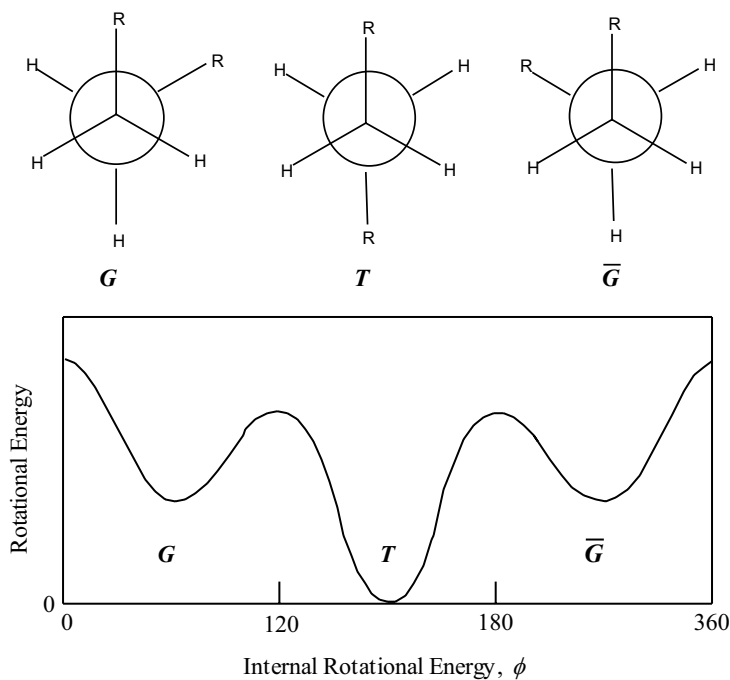


Figure 3-4 Newman projections (top) of three lowest energy projections of two adjacent bond atoms with substituent group R. In the case of a polymer chain, R represents all chain segments before and after the bond in question. The potential-energy diagram (bottom) displays the three lowest energy rotational states—*trans* (*T*) and the two *gauche* forms, *G* and \bar{G} .

• **Real chain bonds have a finite (van der Waals) volume and, therefore, some volume is excluded.** This means that a real bond cannot occupy the same space of any other bond—a condition not imposed in the random-flight model. As in the case of restricted rotation, the effect of excluded volume is to increase the spatial dimensions of the polymer chain over those of the random-flight model.

Beyond the calculation of mean-square end-to-end distances, the conformations of realistic polymer models can be simulated by computer. For example, Figure 3-5 shows the results of a Monte Carlo simulation of the conformation of a small polyethylene chain having 200 skeletal bonds using values of actual bond lengths, bond angles, and the known preference for *trans*-rotational states for this polymer [3].

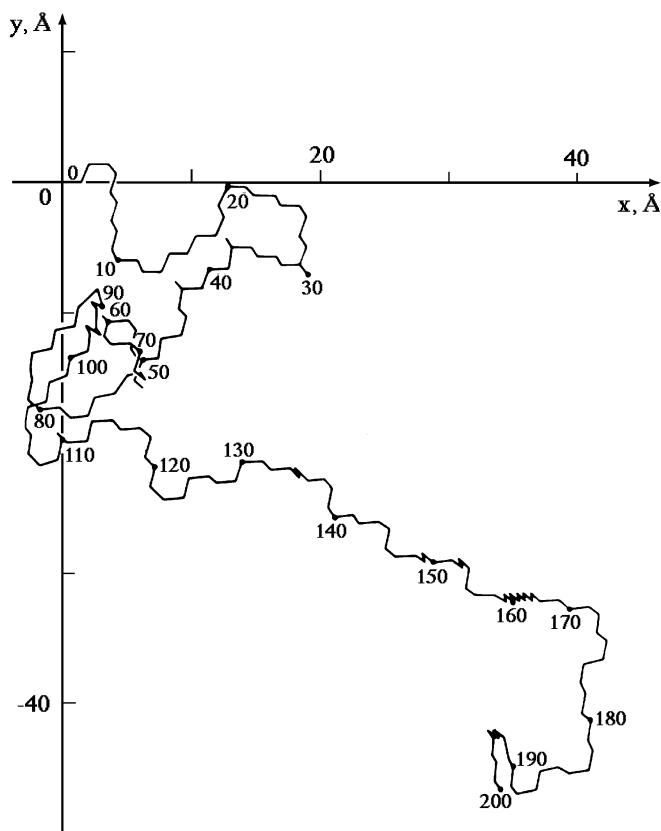


Figure 3-5 A three-dimensional computer simulation of a conformation of a small polyethylene chain (200 bonds) projected on the plane of the graph. Used with permission from the *Journal of Chemical Education*, 1981, **58**(11): p. 898–903. Copyright © 1981, Division of Chemical Education, Inc.

As a convenient way to express the size of a real polymer chain in terms of parameters that can be readily measured, the freely rotating chain model (eq. (3.7)) may be modified to include the effects of fixed bond angles, restricted rotation, and excluded volume on the root-mean-square end-to-end distance in the following way:

$$\langle r^2 \rangle^{1/2} = \alpha (nC_\infty)^{1/2} \ell. \quad (3.12)$$

In this expression, α is called the *chain expansion factor*, which is a measure of the effect of excluded volume, and C_∞ is called the *characteristic ratio*, which contains the contributions from both fixed valence angles and restricted chain rotations. For large polymer chains, typical values of C_∞ range from about 5 to 10 as shown by some representative values in Table 3-1. Another way to represent eq. (3.12) is by use of an *unperturbed* root-mean-square end-to-end distance, $\langle r^2 \rangle_0^{1/2}$, as

$$\langle r^2 \rangle^{1/2} = \alpha \langle r^2 \rangle_0^{1/2}. \quad (3.13)$$

Table 3-1 Examples of Characteristic Ratios [4]

Polymer	C_∞
Polyethylene	6.7
Polystyrene	10.
Polypropylene	5.8
Poly(vinyl alcohol)	8.3
Poly(vinyl acetate)	9.4
Poly(vinyl chloride)	7.6
Poly(methyl methacrylate)	8.2
Poly(ethylene oxide)	4.2
Polycarbonate	2.4

Comparison of eqs. (3.12) and (3.13) indicates that *unperturbed* dimensions are those of a real polymer chain in the absence of excluded-volume effects (i.e., for $\alpha = 1$). By equating eqs. (3.12) and (3.13), the characteristic ratio* is obtained as the ratio of the unperturbed mean-square end-to-end distance to the mean-square end-to-end distance of the freely jointed model (eq. (3.7)):

$$C_\infty = \frac{\langle r^2 \rangle_0}{nl^2}. \quad (3.14)$$

Unperturbed dimensions are realized in the case of a polymer in solution with a thermodynamically poor solvent at a temperature near incipient precipitation. This temperature is called the *theta* (θ) temperature. Experiments using small-angle neutron scattering have indicated that the dimensions of polymer chains in the amorphous solid state are also unperturbed [5]. In solution with a good solvent (i.e.,

* The characteristic ratio can be calculated from a knowledge of actual valence angles, θ , and the statistical weighting of torsional angles, ϕ (see eq. (3.11)), as

$$C_\infty = \frac{1 - \cos \theta}{1 + \cos \theta} \frac{1 + \langle \cos \phi \rangle}{1 - \langle \cos \phi \rangle}.$$

$\alpha > 1$), where polymer–solvent interactions are stronger than polymer–polymer or solvent–solvent interactions, dimensions of the polymer chain are expanded over those in the unperturbed state ($\alpha = 1$).

3.2 THERMODYNAMICS OF POLYMER SOLUTIONS

It was recognized in the 1940s that the thermodynamics of polymeric systems needs to be treated in a special way. In 1942, Gee and Treloar [6] reported that even dilute polymer solutions deviated strongly from ideal-solution behavior. In these early experiments, a high-molecular-weight rubber was equilibrated with benzene vapor in a closed system and the partial pressure of the benzene (the solvent), p_1 , was measured. The solvent activity, a_1 , was calculated as the ratio of p_1 to the saturated vapor pressure of pure benzene, p_1° , at the system temperature as*

$$a_1 = \frac{p_1}{p_1^\circ}. \quad (3.15)$$

Experimental benzene activity is plotted as a function of the *volume fraction* of rubber, ϕ_2 , in Figure 3-6. These data are compared with predictions of *Raoult's law* for an ideal solution given as

$$p_1 = x_1 p_1^\circ \quad (3.16)$$

where x_1 is the mole fraction of the solvent. Substitution of eq. (3.16) into eq. (3.15) yields the result that $a_1 \equiv x_1$ for an ideal solution. As the experimental data (Figure

* By definition, the activity of the i th component in a mixture is defined as

$$a_i = \frac{\hat{f}_i}{f_i^\circ}$$

where \hat{f}_i is the fugacity of that component in the mixture and f_i° is the standard-state fugacity, usually the fugacity of the pure liquid component at the system temperature. In the limit of low pressure at which the vapor mixture becomes ideal, the two fugacities may be replaced by the corresponding pressure terms (i.e., $\hat{f}_i = p_i = x_i p$ and $f_i^\circ = p_i^\circ$). If the vapor phase is nonideal, the solvent activity can be obtained from the relationship

$$a_1 = \frac{p_1}{p_1^\circ} \exp \left[-\frac{B}{RT} (p_1^\circ - p_1) \right]$$

where B is the second virial coefficient of the pure vapor at the system temperature.

3-6) show, polymer-solution behavior follows a strong *negative* deviation from Raoult's ideal-solution law.

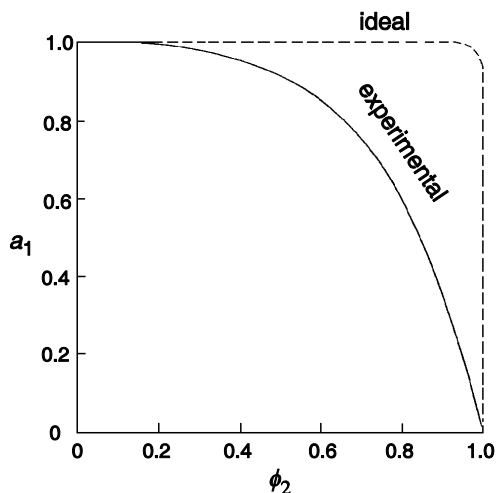


Figure 3-6 Plot of benzene activity, a_1 , versus volume fraction of rubber, ϕ_2 . Dashed line represents ideal-solution behavior. Reprinted from Paul J. Flory, *Principles of Polymer Chemistry*. Fig. 108, p. 496. Copyright © 1953 Cornell University and copyright © 1981 Paul J. Flory. Used by permission of the publisher, Cornell University Press.

3.2.1 The Flory–Huggins Theory

In the early 1940s, Paul Flory [7, 8] and Maurice Huggins [9, 10], working independently, developed a theory based upon a simple lattice model that could be used to understand the nonideal nature of polymer solutions. An excellent review of the development of the lattice model has been given by Flory [11]. In the *Flory–Huggins model*, the lattice sites, or holes, are chosen to be the size of the solvent molecule. As the simplest example, consider the mixing of a low-molecular-weight solvent (component 1) with a low-molecular-weight solute (component 2). The solute molecule is assumed to have the same size as a solvent molecule, and therefore only one solute or one solvent molecule can occupy a single lattice site at a given time. The lattice model for this case is illustrated in Figure 3-7.

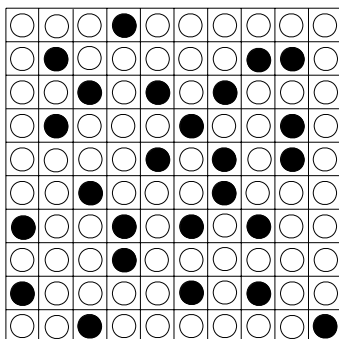


Figure 3-7 Representation of two-dimensional Flory–Huggins lattice containing solvent molecules (○) and a low-molecular-weight solute (●).

The increase in entropy due to mixing of a solvent and solute, ΔS_m , may be obtained from the *Boltzmann relation*

$$\Delta S_m = k \ln \Omega \quad (3.17)$$

where k is Boltzmann's constant ($1.38 \times 10^{-23} \text{ J K}^{-1}$) and Ω gives the total number of ways of arranging n_1 indistinguishable solvent molecules and indistinguishable n_2 solute molecules, where $N = n_1 + n_2$ is the total number of lattice sites. The probability function is given as

$$\Omega = \frac{N!}{n_1! n_2!} \quad (3.18)$$

Using the Stirling approximation

$$\ln n! = n \ln n - n \quad (3.19)$$

leads to the expression for the entropy of mixing *per molecule* as

$$\Delta S_m = -k(n_1 \ln x_1 + n_2 \ln x_2). \quad (3.20)$$

Alternatively, the *molar* entropy of mixing can be written as

$$\Delta S_m = -R(x_1 \ln x_1 + x_2 \ln x_2) \quad (3.21)$$

where R is the ideal gas constant* and x_1 is the mole fraction of the solvent given as

* $R = N_A k$ where N_A is Avogadro's number.

$$x_1 = \frac{n_1}{n_1 + n_2}. \quad (3.22)$$

Equation (3.21) is the well-known relation for the entropy change due to mixing of an *ideal* mixture, which can also be obtained from classical thermodynamics of an ideal solution following the Lewis–Randall law.* Equation (3.20) can be written for a multicomponent system having N components as

$$\Delta S_m^{\text{id}} = -R \sum_{i=1}^N x_i \ln x_i. \quad (3.23)$$

* The relationship between the partial-molar Gibbs free energy and fugacity is given as

$$d\bar{G}_i \equiv d\mu_i = RT d \ln \hat{f}_i.$$

Integration from the standard state to some arbitrary state gives

$$\bar{G}_i - G_i^\circ \equiv \overline{\Delta G}_i = RT \ln \frac{\hat{f}_i}{f_i^\circ}$$

where \hat{f}_i is the fugacity of component i in a mixture and f_i° is the standard-state fugacity. Substitution of the Lewis–Randall law

$$\hat{f}_i^{\text{id}} = x_i f_i^\circ$$

gives

$$\overline{\Delta G}_i^{\text{id}} = RT \ln x_i.$$

Since the thermodynamic properties of a solution are the sum of the product of the mole fraction and the partial-molar property of each of m components in the mixture, it follows that the molar change in Gibbs free energy of an ideal solution is then expressed as

$$\Delta G^{\text{id}} = \sum_{i=1}^m x_i \left(\overline{\Delta G}_i^{\text{id}} \right) = RT \sum_{i=1}^m x_i \ln x_i.$$

Since

$$\overline{\Delta G}_i^{\text{id}} = \overline{\Delta H}_i^{\text{id}} - T \overline{\Delta S}_i^{\text{id}}$$

and $\overline{\Delta H}_i^{\text{id}} = 0$ for an ideal solution, we have

$$\overline{\Delta S}_i^{\text{id}} = -\frac{1}{T} \overline{\Delta G}_i^{\text{id}} = -R \ln x_i$$

and

$$\Delta S^{\text{id}} = \sum_{i=1}^m x_i \left(\overline{\Delta S}_i^{\text{id}} \right) = -R \sum_{i=1}^m x_i \ln x_i.$$

The entropy of mixing a low-molecular-weight solvent with a *high*-molecular-weight *polymer* is smaller than given by eq. (3.20) for a low-molecular-weight mixture. This is due to the loss in conformational entropy resulting from the linkage of individual repeating units along a polymer chain compared to the less ordered case of unassociated low-molecular-weight solute molecules dispersed in a low-molecular-weight solvent. In the development of an expression for ΔS_m for a high-molecular-weight polymer in a solvent, the lattice is established by dividing the polymer chain into r segments, each the size of a solvent molecule, where r is the ratio of polymer volume to solvent volume (i.e., a lattice site). For n_2 polymer molecules, the total number of lattice sites is then $N = n_1 + rn_2$. A lattice containing low-molecular-weight solvent molecules and a single polymer chain is illustrated in Figure 3-8.

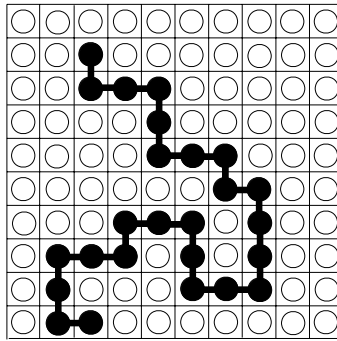


Figure 3-8 Lattice model for a polymer chain in solution. Symbols represent solvent molecules (o) and polymer-chain segments (•).

The expression for the entropy change due to mixing obtained by Flory and Huggins is given as

$$\Delta S_m = -k(n_1 \ln \phi_1 + n_2 \ln \phi_2) \quad (3.24)$$

where ϕ_1 and ϕ_2 are the lattice *volume* fractions of solute (component 1) or polymer (component 2), respectively. These are given as

$$\phi_1 = \frac{n_1}{n_1 + rn_2} \quad (3.25)$$

and

$$\phi_2 = \frac{rn_2}{n_1 + rn_2} . \quad (3.26)$$

For a polydisperse polymer, eq. (3.24) can be modified as

$$\Delta S_m = -k \left(n_1 \ln \phi_1 + \sum_{i=2}^N n_i \ln \phi_i \right) \quad (3.27)$$

where the summation is over all polymer chains (N) in the molecular-weight distribution. For simplicity, the most commonly used form of the entropy expression, eq. (3.24), will be used in further discussion. Equation (3.24) provides the entropy term in the expression for the Gibbs free energy of mixing, ΔG_m , of a polymer solution given as

$$\Delta G_m = \Delta H_m - T \Delta S_m. \quad (3.28)$$

Once an expression for the enthalpy of mixing, ΔH_m , is known, expressions for the chemical potential and activity of the solvent can be obtained as

$$\Delta \mu_1 = \mu_1 - \mu_1^0 = \overline{\Delta G_m} = \left(\frac{\partial \Delta G_m}{\partial n_1} \right)_{T,p} \quad (3.29)$$

where $\overline{\Delta G_m}$ is the partial-molar Gibbs free energy of mixing and the activity is related to the chemical potential as

$$\ln a_1 = \frac{\Delta \mu_1}{kT}. \quad (3.30)$$

For an *ideal* solution, $\Delta H_m = 0$. Solutions for which $\Delta H_m \neq 0$ but for which ΔS_m is given by eq. (3.20) are termed *regular* solutions and are the subject of most thermodynamic models for polymer mixtures. The expression that Flory and Huggins gave for the enthalpy of mixing is

$$\Delta H_m = z n_1 r_1 \phi_2 \Delta \omega_{12} \quad (3.31)$$

where z is the lattice coordination number or number of cells that are first neighbors to a given cell, r_1 represents the number of "segments" in a solvent molecule for consideration of the most general case, and $\Delta \omega_{12}$ is the change in internal energy for formation of an unlike molecular pair (solvent-polymer or 1-2) contacts given by the *mean-field expression* as

$$\Delta \omega_{12} = \omega_{12} - \frac{1}{2} (\omega_{11} + \omega_{22}) \quad (3.32)$$

where ω_{ij} is the energy of i - j contacts. It is clear from eqs. (3.31) and (3.32) that an ideal solution ($\Delta H_m = 0$) is one for which the energies of 1-1, 1-2, and 2-2 molecular interactions are equal.

Since z and ω_{12} have the character of empirical parameters, it is useful to define a single energy parameter called the Flory *interaction parameter*, χ_{12} , given as

$$\chi_{12} = \frac{zr_1\Delta\omega_{12}}{kT}. \quad (3.33)$$

The interaction parameter is a dimensionless quantity that characterizes the interaction energy per solvent molecule (having r_1 segments) divided by kT . As eq. (3.33) indicates, χ_{12} is inversely related to temperature but is independent of concentration in the Flory–Huggins model.

The expression for the enthalpy of mixing may then be written by combining eqs. (3.31) and (3.33) as

$$\Delta H_m = kT \chi_{12} n_1 \phi_2. \quad (3.34)$$

Combining the expression for the entropy (eq. (3.24)) and enthalpy (eq. (3.34)) of mixing gives the well-known Flory–Huggins expression for the Gibbs free energy of mixing

$$\boxed{\Delta G_m = kT (n_1 \ln \phi_1 + n_2 \ln \phi_2 + \chi_{12} n_1 \phi_2)}. \quad (3.35)$$

From this relationship, the activity of the solvent (eq. (3.30)) can be obtained from eq. (3.35) as

$$\ln a_1 = \ln(1 - \phi_2) + \left(1 - \frac{1}{r}\right) \phi_2 + \chi_{12} \phi_2^2. \quad (3.36)$$

In the case of high-molecular-weight polymers for which the number of solvent-equivalent segments, r^* , is large, the $1/r$ term within parentheses on the RHS of eq. (3.36) can be neglected to give

$$\boxed{\ln a_1 = \ln(1 - \phi_2) + \phi_2 + \chi_{12} \phi_2^2}. \quad (3.37)$$

The Flory–Huggins equation is still widely used and has been largely successful in describing the thermodynamics of polymer solutions; however, there are a number of important limitations of the original expression that should be emphasized. The most important are the following:

* For a polymer sample containing a distribution of molecular weights, r may be taken to be the number-average degree of polymerization, \bar{X}_n .

- Solutions are sufficiently concentrated that they have uniform segment density.
- There is no volume change of mixing (whereas favorable interactions between polymer and solvent molecules should result in a *negative* volume change).
- There are no energetically preferred arrangements of polymer segments and solvent molecules in the lattice.
- The Flory interaction parameter, χ_{12} , is independent of composition.

There have been a number of subsequent developments to extend the applicability of the original Flory–Huggins theory and to improve agreement between theoretical and experimental results. For example, Flory and Krigbaum [12] have developed a thermodynamic theory for dilute polymer solutions, which was described in Flory’s original text [1]. Koningsveld [13] and others have improved the agreement of the original Flory–Huggins theory with experimental data by an empirical modification of χ_{12} to include a composition dependence and to account for polydispersity. Both of these approaches are presented briefly in the following section. More recent approaches employ equation-of-state theories such as those developed by Flory [11] and others for which a volume change of mixing can be incorporated. These are developed later in Section 3.2.3.

3.2.2 Flory–Krigbaum and Modified Flory–Huggins Theories

Flory–Krigbaum Theory. Flory and Krigbaum [12] have provided a model to describe the thermodynamics of a dilute polymer solution. In contrast to the case of a semidilute solution addressed by the Flory–Huggins theory, segmental density can no longer be considered to be uniform. In their development, Flory and Krigbaum viewed the dilute solution as a dispersion of clouds consisting of polymer segments surrounded by regions of pure solvent. For a dilute solution, the expression for solvent activity was given as

$$\ln a_1 = (\kappa_1 - \psi_1) \phi_2^2 \quad (3.38)$$

where κ_1 and ψ_1 are heat and entropy parameters,* respectively. Flory and Krigbaum defined an “ideal” or *theta* (θ) temperature as

* $\overline{\Delta H}_1 = RT\kappa_1\phi_2^2$; $\overline{\Delta S}_1 = R\psi_1\phi_2^2$.

$$\theta = \frac{\kappa_1 T}{\psi_1} \quad (3.39)$$

from which eq. (3.38) can be written as

$$\ln a_1 = -\psi_1 \left(1 - \frac{\theta}{T} \right) \phi_2^2. \quad (3.40)$$

It follows from eq. (3.40) that solvent activity approaches unity as temperature approaches the θ temperature. At the θ temperature, the dimensions of a polymer chain collapse to unperturbed dimensions (i.e., in the absence of excluded-volume effects), as described in Section 3.1.

Modified Flory–Huggins. In the original lattice theory, χ_{12} was given an inverse dependence upon temperature (eq. (3.33)) but there was no provision for a concentration dependence, which experimental studies have shown to be important. Koningsveld [13] and others have introduced an empirical dependence to improve the agreement with experimental data by casting the Flory–Huggins expression in the general form

$$\Delta G_m = RT(\phi_1 \ln \phi_1 + \phi_2 \ln \phi_2 + g\phi_1\phi_2). \quad (3.41)$$

In eq. (3.41), g is an interaction energy term for which the concentration dependence can be given as a power series in ϕ_2 as

$$g = g_0 + g_1\phi_2 + g_2\phi_2^2 + \dots \quad (3.42)$$

where each g term, g_k ($k = 0, 1, 2, \dots$), has a temperature dependence that can be expressed in the form

$$g_k = g_{k,1} + \frac{g_{k,2}}{T}. \quad (3.43)$$

3.2.3 Equation-of-State Theories

Although the Flory–Huggins theory is still useful as a starting point for describing polymer thermodynamics, there are a number of weaknesses. For example, the simple lattice model does not accommodate a volume change of mixing, which can be significant in the case of a thermodynamically good solution. Such an inability to incorporate a volume change of mixing can lead to particular weakness in the prediction of phase equilibrium. Substantial improvement in the theoretical treatment of polymer thermodynamics has been obtained by adopting a statistical-thermodynamics approach based upon an equation of state (EOS) as first proposed by

Flory [14]. Other successful EOS theories have been proposed by Sanchez [15] and by Simha [16]. For the purpose of providing an introduction to the use of EOS theories in the treatment of polymer thermodynamics, only the Flory EOS theory, which was the first and is still widely used, is described in this section.

Flory Equation of State. Thermodynamic variables in statistical thermodynamics are obtained from a suitable partition function, which can be a simple or complex function depending upon the size and physical state of the molecule being considered. The simplest partition functions are obtained for monatomic and diatomic gases such as helium and nitrogen. The partition function chosen by Flory for the polymer was obtained from contributions by internal (i.e., intramolecular chemical-bond forces) and external (i.e., intermolecular forces) degrees of freedom. The internal contribution is dependent upon temperature, while the external contribution is dependent upon both temperature and volume. The Flory partition function can be given in reduced form as [11]

$$Z = Z_{\text{comb}} (g\nu^*)^{rnc} (\tilde{\nu}^{1/3} - 1)^{3rnc} \exp(rnc / \tilde{\nu}\tilde{T}). \quad (3.44)$$

Here, Z_{comb} is a combinatory factor, g is an inconsequential geometric factor, ν^* is a characteristic (specific) volume per segment (usually called the hard-core or closed-packed volume), $\tilde{\nu}$ is a reduced volume per segment defined in terms of the characteristic volume, r is the mean number of segments per molecule, n is the number of molecules (or mers), c is the mean number of external degrees of freedom per segment, $*$ and \tilde{T} is a reduced temperature as defined later. The exponential term in eq. (3.44) is related to the configurational or mean potential energy (in van der Waals form), which is inversely proportional to volume.

Statistical thermodynamics provides the following equation to obtain an EOS from the partition function:

$$p = kT \left(\frac{\partial \ln Z}{\partial V} \right)_T. \quad (3.45)$$

The resulting EOS obtained from the partition function given by eq. (3.44) can be expressed in reduced form as

$$\frac{\tilde{p}\tilde{\nu}}{\tilde{T}} = \frac{\tilde{\nu}^{1/3}}{\tilde{\nu}^{1/3} - 1} - \frac{1}{\tilde{T}\tilde{\nu}} \quad (3.46)$$

* The total number of degrees of freedom in the system is $3rnc$.

where \tilde{p} is the reduced pressure. The reduced parameters are defined in terms of the characteristic parameters (three EOS parameters, v^* , T^* , and p^* , for each of the pure components) as

$$\tilde{v} = \frac{v}{v^*}, \quad (3.47)$$

$$\tilde{T} = \frac{T}{T^*} = \frac{2v^*cRT}{s\eta}, \quad (3.48)$$

and

$$\tilde{p} = \frac{p}{p^*} = \frac{2pv^{*2}}{s\eta}, \quad (3.49)$$

where c represents the mean number of external degrees of freedom per segment, s is the number of contact sites per segment, and η is an energy parameter characterizing a pair of sites in contact. The characteristic parameters can be obtained from experimental PVT data.* Representative values for Flory EOS parameters evaluated

* Differentiation of the EOS (eq. (3.46)) with respect to temperature at constant pressure yields at zero pressure the characteristic hard-core volume as

$$v^* = v \left[\frac{3 + 3\alpha T}{3 + 4\alpha T} \right]^3.$$

Differentiation of the EOS with respect to temperature at constant volume yields at zero pressure the characteristic pressure

$$p^* = \gamma T \tilde{v}^2 = (\alpha / \beta) \tilde{T}^2$$

where α is the *thermal-expansion coefficient*

$$\alpha = \frac{1}{V} \left(\frac{\partial V}{\partial T} \right)_p,$$

β is the *compressibility coefficient*

$$\beta = -\frac{1}{V} \left(\frac{\partial V}{\partial p} \right)_T,$$

and γ is the *thermal-pressure coefficient*

$$\gamma = \left(\frac{\partial p}{\partial T} \right)_v.$$

Finally, the characteristic temperature is obtained from the EOS by letting $\tilde{p} = 0$:

at 25°C for four low-molecular-weight organic compounds and for four polymers are given in Table 3-2. In general, v^* and T^* increase with increasing temperature while p^* decreases.

Table 3-2 Flory Equation-of-State Parameters at 25°C

Polymer	v^* (cm ³ g ⁻¹)	T^* (K)	p^* (J cm ⁻³)
Benzene	0.8860	4709	628
Cyclohexane	1.0012	4721	530
Methyl ethyl ketone	0.9561	4555	582
Toluene	0.9275	5197	547
Natural rubber	0.9432	6775	519
Polydimethylsiloxane	0.8395	5530	241
Polyisobutylene	0.9493	7580	448
Polystyrene	0.8098	7420	547

Adaptation of the Flory EOS to *mixtures* is based upon the following two premises:

1. Core volumes of the solution components are additive. For example, the hard-core volume of a binary mixture is given as

$$v^* = \frac{n_1 v_1^* + n_2 v_2^*}{n_1 + n_2} \quad (3.50)$$

2. The intermolecular energy depends on the *surface* area of contact between molecules and/or segments.

Since a segment is an arbitrary unit, the segment size can be chosen such that $v_1^* = v_2^* = v^*$. This gives the following mixing rules for the binary mixture:

$$\frac{1}{r} = \frac{\phi_1}{r_1} + \frac{\phi_2}{r_2} \quad (3.51)$$

where ϕ_1 and ϕ_2 are *segment* (or *core-volume*) *fractions*:

$$\phi_1 = 1 - \phi_2 = \frac{n_1 v_1^*}{n_1 v_1^* + n_2 v_2^*} \quad (3.52)$$

The *number of contact sites*, s , for the mixture is given as

$$T^* = \frac{T \bar{v}^{4/3}}{\bar{v}^{1/3} - 1}$$

$$s = \phi_1 s_1 + \phi_2 s_2 \quad (3.53)$$

where s_i is the *surface area* of a segment of component i . In a similar manner, the mean number of external degrees of freedom for the mixture can be written as

$$c = \phi_1 c_1 + \phi_2 c_2. \quad (3.54)$$

The *site fraction* is defined as

$$\theta_2 = 1 - \theta_1 = \frac{\phi_2 s_2}{s}. \quad (3.55)$$

The *characteristic pressure* for the mixture is given as

$$p^* = \phi_1 p_1^* + \phi_2 p_2^* = \phi_1 \theta_2 X_{12} \quad (3.56)$$

where X_{12} is called the *exchange interaction parameter*, defined as

$$X_{12} = \frac{s_1 (\eta_{11} + \eta_{22} - 2\eta_{12})}{2v^{*2}} = \frac{s_1 \Delta\eta}{2v^{*2}} \quad (3.57)$$

where the η_{ij} terms are energy parameters for the i - j segment pairs and $\Delta\eta = \eta_{11} + \eta_{22} - 2\eta_{12}$. The exchange interaction parameter is analogous to $\Delta\omega_{12}$ in the Flory–Huggins theory (i.e., eq. (3.32)) but has the dimensions of energy density. Finally, the *characteristic temperature* for the mixture is given as

$$T^* = \frac{\phi_1 p_1^* + \phi_2 p_2^* - \phi_1 \theta_2 X_{12}}{\frac{\phi_1 p_1^*}{T_1^*} + \frac{\phi_2 p_2^*}{T_2^*}}. \quad (3.58)$$

The EOS of the mixture is given in the same form as that of the pure component (eq. (3.46)) except that the reduced parameters refer to those of the mixture. The reduced volume of the mixture, \tilde{v} , may be obtained from the EOS with \tilde{p} set to zero for low pressures and \tilde{T} defined by use of the characteristic temperature given by eq. (3.58) for the mixture. Subsequently, other important quantities can be calculated such as the molar enthalpy of mixing as

$$\Delta H_m = \frac{\theta_2 x_1 v_1^* X_{12}}{\tilde{v}} + x_1 v_1^* p_1^* \left(\frac{1}{\tilde{v}_1} - \frac{1}{\tilde{v}} \right) + x_2 v_2^* p_2^* \left(\frac{1}{\tilde{v}_2} - \frac{1}{\tilde{v}} \right) \quad (3.59)$$

where

$$x_1 = \frac{n_1}{n_1 + n_2}. \quad (3.60)$$

An important relationship is the Flory EOS expression for $\Delta\mu_1$ given as

$$\Delta\mu_1 = RT \left[\ln \phi_1 + \left(1 - \frac{v_1^*}{v_2^*} \right) \phi_2 \right] + \frac{\theta_2^2 v_1^* X_{12}}{\tilde{v}} + v_1^* p_1^* \left[3\tilde{T}_1 \ln \left(\frac{\tilde{v}_1^{1/3} - 1}{\tilde{v}^{1/3} - 1} \right) + \frac{1}{\tilde{v}_1} - \frac{1}{\tilde{v}} \right]. \quad (3.61)$$

Alternatively, eq. (3.61) has been given in the form

$$\Delta\mu_1 = RT \left(\ln \phi_1 + \frac{1-r_1}{r_2} \phi_2 \right) + p_1^* v_1^* \left[3\tilde{T}_1 \ln \left(\frac{\tilde{v}_1^{1/3} - 1}{\tilde{v}^{1/3} - 1} \right) + \tilde{v}_1^{-1} - \tilde{v}^{-1} + \tilde{p}_1 (\tilde{v} - \tilde{v}_1) \right] + (X_{12} - TQ_{12}\tilde{v})v_1^* \frac{\theta_2^2}{\tilde{v}}. \quad (3.62)$$

A principal difference between eqs. (3.61) and (3.62) is the appearance of Q_{12} in the last term of eq. (3.62). This parameter is called the *non-combinational entropy correction* and generally is used as an adjustable parameter. Comparison of the standard Flory–Huggins relationship (eq. (3.36), where $\Delta\mu_1 = RT \ln a_1$ and $\phi_1 = 1 - \phi_2$) with the Flory EOS (eq. (3.61)) shows that the first term within brackets in eq. (3.61) is simply a combinatorial term. Despite its cumbersome form, the Flory EOS theory provides substantial improvement over the earlier lattice theory. For example, the theory reasonably predicts an excess volume of mixing as

$$\frac{V^E}{V} = \frac{v^E}{\tilde{v}} = 1 - \frac{\phi_1 \tilde{v}_1 + \phi_2 \tilde{v}_2}{\tilde{v}}. \quad (3.63)$$

Furthermore, it is capable of modeling the complete range of the observed phase behavior of polymer solutions, as discussed in the next section.

3.2.4 Phase Equilibria

Whether or not a polymer and solvent are mutually soluble, or *miscible*, is governed by the sign of the Gibbs free energy of mixing, ΔG_m , which is related to the enthalpy and entropy of mixing by eq. (3.28). Three different dependencies of ΔG_m on solution composition (i.e., volume fraction of polymer) at constant temperature are illustrated in Figure 3-9. If ΔG_m is positive over the entire composition range, as illustrated by curve I, the polymer and solvent are totally immiscible over the complete composition range and will coexist at equilibrium as two distinct phases. Two other possibilities are those of partial and total miscibility, as illustrated by curves II and III, respectively. For total miscibility, it is *necessary* that

$$\Delta G_m < 0 \quad (3.64)$$

and that the second derivative of ΔG_m with respect to the volume fraction of solvent (component 1) or polymer (component 2) be greater than zero over the entire composition range as formally expressed by

$$\left(\frac{\partial^2 \Delta G_m}{\partial \phi_2^2} \right)_{p,T} > 0. \quad (3.65)$$

Both conditions for miscibility are satisfied by curve III but not curve II, which exhibits two minima in ΔG_m , and therefore the derivative criterion expressed by eq. (3.65) is not satisfied at all points along the ΔG_m -composition curve. A solution that exhibits such minima will phase-separate at equilibrium into two phases containing different compositions of both components. The compositions of the two phases are given by the points of common tangent as illustrated in Figure 3-9, where the composition of the solvent-rich phase is identified as ϕ_2^A and that of the polymer-rich phase as ϕ_2^B .

Phase equilibrium is strongly affected by solution temperature. In fact, any of three types of phase behavior illustrated in Figure 3-9 may result from a change in the temperature (or pressure) of the system. Our usual experience with solutions of low-molecular-weight compounds is that solubility increases with an increase in temperature, as illustrated by the phase diagram shown in Figure 3-10. In this example, the solution is homogeneous (i.e., the two components are totally miscible) at temperatures above the point identified as UCST, which stands for the *upper critical solution temperature* as described below. At lower temperatures (i.e., below the UCST), phase separation may occur depending upon the overall composition of the mixture. At a given temperature below the UCST (e.g., T_1), compositions lying *outside* the curves are those constituting a homogeneous phase, while those lying *inside* the curves are thermodynamically unstable and, therefore, the solution will phase-separate at equilibrium. The compositions of the two phases, identified as phases A and B, are given by points lying along the curve called the *binodal*. The binodal is the locus of points that satisfy the conditions for thermodynamic equilibrium of a binary mixture given as

$$\mu_1^A = \mu_1^B \quad (3.66)$$

and

$$\mu_2^A = \mu_2^B. \quad (3.67)$$

As the chemical potential is given by the derivative of the Gibbs free energy with respect to composition (eq. (3.29)), the chemical potentials are obtained graphically from the intercepts of the common tangent drawn to curve II with the free energy axes as illustrated in Figure 3-9.

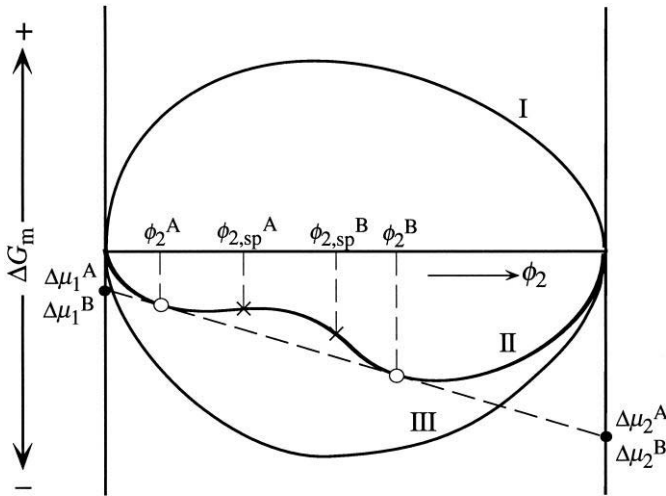


Figure 3-9 Dependence of the Gibbs free energy of mixing, ΔG_m , of a binary mixture on volume fraction of polymer, ϕ_2 , at constant pressure and temperature. I. Total immiscibility. II. Partial miscibility. III. Total miscibility. In the case of partial miscibility (curve II), the mixture will separate into two phases whose compositions (\circ) are marked by the volume-fraction coordinates, ϕ_2^A and ϕ_2^B , corresponding to points of common tangent to the free-energy curve. Spinodal points, compositions $\phi_{2,sp}^A$ and $\phi_{2,sp}^B$, occur at the points of inflection (\times).

Between the binodal and the unstable region lies the *metastable* region, which is bounded by the *spinodal*. In the metastable region, the system can resist small concentration fluctuations but will eventually equilibrate to the stable two-phase state given by the binodal. Points lying along the spinodal correspond to the points of inflection identified in curve II of the free-energy diagram (Figure 3-9) and satisfy the relationship

$$\left(\frac{\partial^2 \Delta G_m}{\partial \phi_2^2} \right)_{p,T} = 0. \quad (3.68)$$

The binodal and spinodal coincide at the *critical point*, which satisfies the following equality for the third derivative of the Gibbs free energy with respect to composition:

$$\left(\frac{\partial^3 \Delta G_m}{\partial \phi_2^3} \right)_{p,T} = 0. \quad (3.69)$$

In the case of the upper critical solution temperature (UCST), the critical point lies at the top of the phase diagram as shown in Figure 3-10.

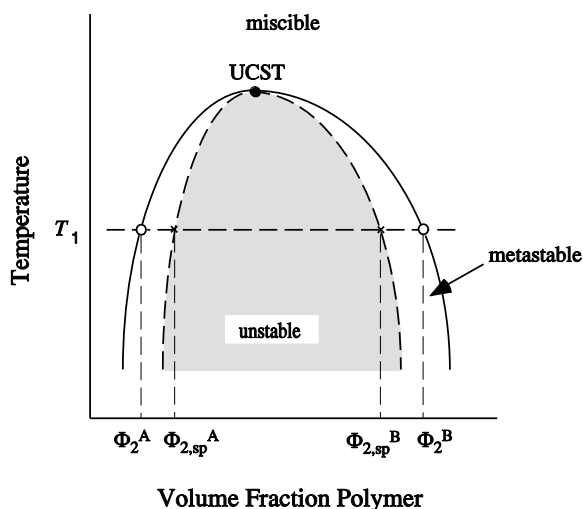


Figure 3-10 Representative phase diagrams for a polymer solution showing an upper critical solution temperature (UCST) (\circ), spinodal curve (---), and binodal curve (—).

Although the UCST behavior of dilute polymer solutions had been observed for many years, it was not until 1961 that phase separation of polymer solutions was first reported to occur with an *increase* in temperature [17]. In this case, the binodal and spinodal curves coincide at a temperature and composition called the *lower critical solution temperature* or LCST. One serious limitation of the Flory–Huggins theory (Section 3.2.1) is that it fails to predict LCST behavior. The more recent equation-of-state theories (Section 3.2.3) are much more successful in predicting the entire range of phase behavior, as will be discussed in Section 7.2.

3.2.5 Determination of the Interaction Parameter

Experimentally, χ_{12} as well as the exchange interaction parameter, X_{12} , in the Flory EOS theory can be determined by a variety of techniques, including several scattering methods as discussed in the next section and from the melting-point depression of semicrystalline polymers (see Section 4.2.2). A commonly used method to determine polymer–solvent as well as polymer–polymer interaction parameters (Chapter 7) has been inverse gas chromatography or IGC [18] as described in the following section.

Inverse Gas Chromatography. The term *inverse* is used to indicate that the substance being characterized constitutes the stationary phase (i.e., the bed packing) rather than the mobile phase, as is the case in traditional gas chromatography. The stationary phase is prepared by coating a thin layer of a polymer or polymer blend from a dilute solution onto a commercial packing material in the form of small beads. A fluidized bed is sometimes used in the coating process. The coated packing is vacuum-dried to remove all residual solvent and then packed into a GC column that is heated to approximately 50°C above the glass-transition temperature (T_g). A solvent probe is then injected into the carrier gas (He or H₂), and the time for the probe to be eluted from the column is measured. During its passage, the probe is free to be sorbed into the liquid polymer coating of the packed bed. The extent of solubility (i.e., activity) is directly related to the retention time from which a *specific retention volume*, V_g , can be calculated. From this value, the infinite-dilution volume-fraction activity coefficient is then obtained as [19]

$$\ln \gamma_1^\infty = \ln \left(\frac{a_1}{\phi_1} \right)^\infty = \lim_{\phi_1 \rightarrow 0} \left(\frac{a_1}{\phi_1} \right) = \ln \left(\frac{273.16Rv_2}{V_g p_1^\circ} \right) - \frac{p_1^\circ (B_{11} - V_1)}{RT} \quad (3.70)$$

where ϕ_1 is the volume fraction of solvent (probe), p_1° is the vapor pressure of the probe (solvent) in the carrier gas, v_2 is the specific volume of the polymer, V_1 is the molar volume of the probe, and B_{11} is the second virial coefficient of the pure probe vapor at the measurement temperature. From the measurement of γ_1^∞ at different temperatures, the heat of mixing can be determined as

$$\Delta H_m = R \left[\frac{\partial \ln \gamma_1^\infty}{\partial (1/T)} \right]. \quad (3.71)$$

From eq. (3.70) and the Flory–Huggins equation (eq. (3.37)), it is easily shown that the Flory interaction parameter is obtained directly as

$$\chi_{12} = \ln \left(\frac{273.16Rv_2}{V_g p_1^\circ V_1} \right) - \frac{p_1^\circ (B_{11} - V_1)}{RT} - 1. \quad (3.72)$$

In a similar manner, the interaction energy, X_{12} , in the Flory equation of state also can be obtained (see Problem 3.11).

3.2.6 Predictions of Solubilities

Solubility Parameters. As discussed in the previous section, there are a number of experimental methods by which approximate values of χ_{12} can be obtained; howev-

er, there is no theory by which values of χ_{12} can be *predicted* at the present time. One approach that can be used to estimate χ_{12} and predict solubility is based upon the concept of the *solubility parameter*, δ , which was originally developed to guide solvent selection in the paint and coatings industry. The solubility parameter is related to the cohesive energy density, E^{coh} , or the molar energy of vaporization of a pure liquid, ΔE^{v} , as

$$\delta_i = \sqrt{E_i^{\text{coh}}} = \sqrt{\frac{\Delta E_i^{\text{v}}}{V_i}} \quad (3.73)$$

where ΔE^{v} is defined as the energy change upon isothermal vaporization of the saturated liquid to the ideal gas state at infinite dilution* and V_i is the molar volume of the liquid. Units of δ are $(\text{cal cm}^{-3})^{1/2}$ or $(\text{MPa})^{1/2}$.† Equation (3.73) can be used to calculate the solubility parameter of a pure solvent given values of ΔE^{v} and V_i . Since it is not reasonable to talk about an energy of vaporization for solid polymers, the solubility parameter of a polymer has to be determined indirectly or calculated by group-contribution methods. Experimentally, the solubility parameter of a polymer can be estimated by comparing the swelling of a crosslinked polymer sample immersed in different solvents. The solubility parameter of the polymer is taken to be that of the solvent resulting in maximum swelling. Alternatively, the solubility parameter can be estimated by use of group-contribution methods as discussed in Section 13.1.4. An additional approach that can be used to calculate δ is based upon knowledge of the equation of state, $V(p, T)$, for the polymer [20]

$$\delta \cong \sqrt{\frac{T\alpha}{\beta}} \quad (3.74)$$

where α is the (isobaric) thermal-expansion coefficient,

$$\alpha = \left(\frac{1}{V}\right) \left(\frac{\partial V}{\partial T}\right)_p, \quad (3.75)$$

and β is the (isothermal) compressibility coefficient,‡

* The energy of vaporization is approximately related to the enthalpy of vaporization as

$$\Delta E_i^{\text{v}} = \Delta H_i^{\text{v}} - RT.$$

† $1 (\text{cal cm}^{-3})^{1/2} = 2.045 (\text{MPa})^{1/2}$.

‡ Since volume *decreases* with increasing pressure, the negative sign in eq. (3.76) provides a positive value for β .

$$\beta = -\left(\frac{1}{V}\right)\left(\frac{\partial V}{\partial P}\right)_T. \quad (3.76)$$

Equations of state are now available for most commercial polymers [21, 22].

From values of the solubility parameters for the solvent and polymer, the heat of mixing can be estimated by the Scatchard [23]–Hildebrand [24] equation as

$$\Delta H_m = V(\delta_1 - \delta_2)^2 \phi_1 \phi_2 \quad (3.77)$$

where V is the volume of the mixture. Making use of eq. (3.34), the interaction parameter can be estimated from this value of ΔH_m as*

$$\chi_{12} \cong \frac{V_1}{RT}(\delta_1 - \delta_2)^2 \quad (3.78)$$

where V_1 is the molar volume of component 1. As the form of eq. (3.77) indicates, the solubility parameter approach can be used to estimate the heat of mixing when $\Delta H_m \geq 0$ but not when $\Delta H_m < 0$ (i.e., for exothermic heat of mixing).

The matching of polymer and solvent solubility parameters to minimize ΔH_m is a useful approach for solvent selection in many cases but often fails when specific interactions such as hydrogen bonding occur. To improve the prediction, two- and three-dimensional solubility parameters, which give individual contributions for dispersive (i.e., van der Waals), polar, and hydrogen-bonding interactions, are sometimes used. In the case of the three-dimensional model proposed by Hansen [25], the overall solubility parameter can be obtained as

$$\delta = \sqrt{\delta_d^2 + \delta_p^2 + \delta_h^2} \quad (3.79)$$

where δ_d , δ_p , and δ_h are the dispersive, polar, and hydrogen-bonding solubility parameters, respectively. Values of δ calculated from eq. (3.79) for common solvents and polymers are given in Table 3-3.

* Sometimes, the Flory interaction parameter is considered to have both an enthalpic component, χ_H , and entropic (or residual) component, χ_S . In this case, we can write

$$\chi_{12} = \chi_S + \chi_H = \chi_S + \frac{V_1}{RT}(\delta_1 - \delta_2)^2 \approx 0.34 + \frac{V_1}{RT}(\delta_1 - \delta_2)^2.$$

Table 3-3 Solubility Parameters of Some Common Solvents and Polymers

	Solubility Parameter, δ^a	
	(MPa) ^{1/2}	(cal cm ⁻³) ^{1/2}
Solvents		
<i>n</i> -Hexane	14.9	7.28
Carbon tetrachloride	17.8	8.70
Toluene	18.2	8.90
Benzene	18.6	9.09
Chloroform	19.0	9.29
Tetrahydrofuran	19.4	9.48
Chlorobenzene	19.6	9.58
Methylene chloride	20.3	9.92
1,4-Dioxane	20.5	10.0
<i>N</i> -Methyl-2-pyrrolidone	22.9	11.2
Dimethylformamide	24.8	12.1
Methanol	29.7	14.5
Water	47.9	23.4
Polymers		
Polyisobutylene	15.5	7.58
Polysulfone	20.3	9.92
Poly(vinyl chloride)	21.5	10.5
Polystyrene	22.5	11.0
Poly(methyl methacrylate)	22.7	11.1
Cellulose acetate	25.1	12.3
Polyacrylonitrile	25.3	12.4
Poly(vinyl acetate)	25.7	12.7

^a Calculated from Hansen solubility parameters using eq. (3.79) at 25°C; conversion: 1 MPa^{1/2} = 0.489 (cal cm⁻³)^{1/2}.

3.3 MEASUREMENT OF MOLECULAR WEIGHT

As discussed in Section 1.3, commercial polymers have broad distributions of molecular weights, and it is, therefore, necessary to report an average molecular weight when characterizing a sample. There are three important molecular-weight averages—number-average (\bar{M}_n), weight-average (\bar{M}_w), and *z*-average (\bar{M}_z). Absolute values of \bar{M}_n , \bar{M}_w , and \bar{M}_z can be obtained by the *primary* characterization methods of osmometry, scattering, and sedimentation, respectively. In addition to these accurate but time-consuming techniques, there are a number of *secondary* methods by which average molecular weights can be determined provided that polymer samples with narrow molecular-weight distributions are available for reference and calibration. The most important of these secondary methods is gel-permeation chromatography (GPC), sometimes called size-exclusion chromatography (SEC). This

method is capable of determining the entire molecular-weight distribution of a polymer sample from which all molecular-weight averages can be determined. Another widely used secondary method is the determination of intrinsic viscosity from which the viscosity-average molecular weight can be determined. The viscosity-average molecular weight (\bar{M}_v) normally lies between \bar{M}_n and \bar{M}_w . The principles behind both primary and secondary methods for molecular-weight determination are discussed next.

3.3.1 Osmometry

Membrane Osmometry. The osmotic pressure, Π , of a polymer solution may be obtained from the chemical potential, $\Delta\mu_1$, or equivalently from the activity, a_1 , of the solvent through the basic relationship

$$\Delta\mu_1 = RT \ln a_1 = -\Pi V_1 \quad (3.80)$$

where V_1 is the molar volume of the solvent. Substitution of the Flory–Huggins expression for solvent activity (eq. (3.37)) into eq. (3.80) and subsequent rearrangement give

$$\Pi = -\frac{RT}{V_1} \left[\ln(1 - \phi_2) + \phi_2 + \chi_{12} \phi_2^2 \right]. \quad (3.81)$$

Simplification of this relation can be achieved by expansion of the logarithmic term in a Taylor series (see Appendix E) and the substitution of polymer concentration, c , for volume fraction, ϕ_2 , through the relationship

$$\phi_2 = cv \quad (3.82)$$

where v is the specific volume of the polymer. Substitution and rearrangement give the expression

$$\frac{\Pi}{c} = \frac{RT}{M} \left[1 + \left(\frac{Mv^2}{V_1} \right) \left(\frac{1}{2} - \chi_{12} \right) c + \frac{1}{3} \left(\frac{Mv^3}{V_1} \right) c^2 + \dots \right]. \quad (3.83)$$

The classical van't Hoff equation for the osmotic pressure of an ideal solution

$$\frac{\Pi}{c} = \frac{RT}{M} \quad (3.84)$$

may be seen as a special or limiting case of eq. (3.83) obtained when $\chi_{12} = 1/2$ and second- and higher-order terms in c can be neglected (i.e., for dilute solution). For high-molecular-weight, polydisperse polymers, the appropriate molecular weight to

use in eq. (3.83) is the number-average molecular weight, \bar{M}_n . Equation (3.83) can then be rearranged to give the widely used relation

$$\Pi = RTc \left(\frac{1}{\bar{M}_n} + A_2c + A_3c^2 + \dots \right) \quad (3.85)$$

where A_2 and A_3 are the second and third virial coefficients, respectively. Comparison of eqs. (3.83) and (3.85) reveals the following two relations for the virial coefficients:

$$A_2 = \frac{v^2}{V_1} \left(\frac{1}{2} - \chi_{12} \right) \quad (3.86)$$

$$A_3 = \frac{1}{3} \left(\frac{v^3}{V_1} \right). \quad (3.87)$$

In the limit of dilute solution (typically less than 1 g dL⁻¹), terms containing second- and higher-order powers of c can be neglected, and therefore a plot of Π/RTc versus c yields a straight line with an intercept, $1/\bar{M}_n$, and slope, A_2 . In Figure 3-11, plots of osmotic data for different molecular-weight fractions of polyisobutylene in a good (cyclohexane) and poor (benzene) solvent are compared.

As shown by the relation between A_2 and χ_{12} given by eq. (3.86), the second virial coefficient is a convenient measure of the *quality* of polymer-solvent interactions. In good solvents in which the polymer chains are expanded (i.e., $\alpha > 1$, eq. (3.13)), A_2 is large and, therefore, χ_{12} is small (e.g., < 0.5). At θ conditions (i.e., $\alpha = 1$), $A_2 = 0$ and $\chi_{12} = 0.5$.

Experimental procedures to determine osmotic pressure are relatively simple although often very time-consuming. A basic osmometer design is illustrated in Figure 3-12. In operation, pure solvent and a dilute solution of the polymer in the same solvent are placed on opposite sides of a semipermeable membrane, typically prepared from cellulose or a cellulose derivative. Regenerated cellulose is an especially good membrane polymer because it is insoluble in most organic solvents. Normally, the membrane is first preconditioned in the solvent used in the measurements. An ideal membrane will allow the solvent to pass through the membrane but will retain the polymer molecules in solution. The resulting difference in chemical potential between solvent and the polymer solution causes solvent to pass through the membrane and raise the liquid head of the solution reservoir. The osmotic pressure is calculated from the height, h , of the equilibrium head representing the difference between the height of solvent in the solvent capillary and the height of solution in the opposite capillary at equilibrium as

$$\Pi = \rho gh. \quad (3.88)$$

where ρ is the solvent density and g is the gravitational acceleration (9.8066 m s^{-2}).

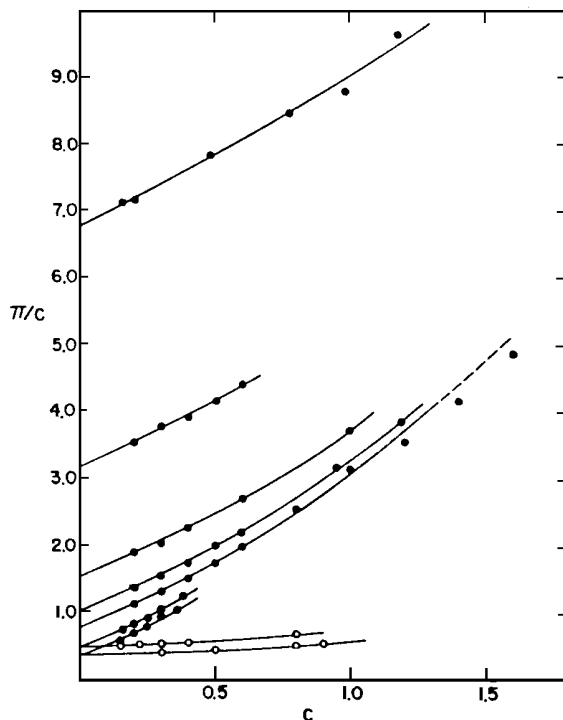


Figure 3-11 Plot of Π/c versus c (g cm^{-3}) for polyisobutylene fractions (molecular weights ranging from 38,000 and 720,000) in benzene (\circ) and in cyclohexane (\bullet). Adapted with permission from W. R. Krigbaum and P. J. Flory, *Statistical Mechanics of Dilute Polymer Solutions. IV. Variation of the Osmotic Second Coefficient with Molecular Weight*. Journal of the American Chemical Society, 1953. **75**(8): p. 1775–1784.

One intrinsic problem with membrane osmometry is the performance of the membrane. No membrane is completely impervious to the passage of small molecules, and any migration of smaller polymer molecules across the membrane during measurement will not contribute to the osmotic pressure and, therefore, an artificially high value of \bar{M}_n will be obtained. For this reason, membrane osmometry is accurate only for polymer samples with molecular weights above about 20,000. The upper limit for molecular weight is approximately 500,000 due to inaccuracy in measuring small osmotic pressures. For the characterization of low-molecular-weight (i.e., $<20,000$) oligomers and polymers, an alternative technique called vapor-pressure osmometry (VPO) is preferred, particularly when molecular weight is less than about 10,000. The basic principles of this technique are described next.

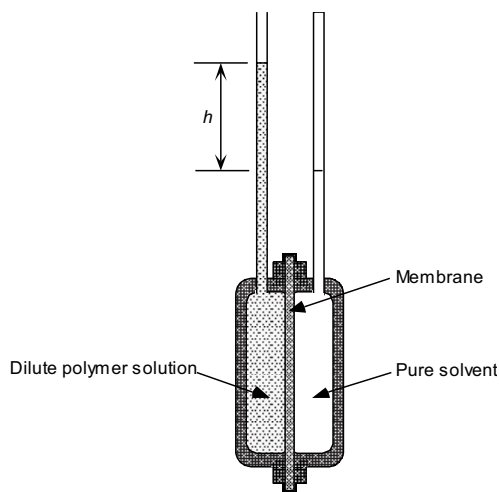


Figure 3-12 Schematic of a simple membrane osmometer.

Vapor-Pressure Osmometry. When a polymer is added to a solvent, the vapor pressure of the solvent will be lowered due to the decrease in solvent activity. The relation between the difference in vapor pressure between solvent and solution, $\Delta p (= p_1 - p_1^\circ)$, and the number-average molecular weight, \bar{M}_n , of the polymer is given as

$$\lim_{c \rightarrow 0} \left(\frac{\Delta p}{c} \right) = - \frac{p_1^\circ V_1^\circ}{\bar{M}_n} \quad (3.89)$$

where p_1° and V_1° are, respectively, the vapor pressure and molar volume of the pure solvent. Due to the inverse dependence of Δp on \bar{M}_n given by eq. (3.89), the effect of even a low-molecular-weight polymer on the lowering of vapor pressure will be very small and, therefore, direct measurement of the vapor pressure is a very imprecise method of molecular-weight determination. For this reason, an indirect approach, based upon thermoelectric measurements, is used in commercial instrumentation as described below.

As shown by Figure 3-13, a commercial vapor-pressure osmometer uses two matched thermistors that are placed in a closed, constant-temperature ($\pm 0.001^\circ\text{C}$) chamber containing saturated solvent vapor. A drop of solvent is placed by syringe on one thermistor and a drop of dilute polymer solution on the other. As a result of condensation of solvent vapor onto the solution, the temperature of the solution thermistor increases until the vapor pressure of the solution equals that of the solvent. The difference in temperature between the two thermistors is recorded in terms of a difference in resistance (ΔR), which is calibrated by use of a standard

low-molecular-weight sample. Extrapolation of $\Delta R/c$ over a range of dilute-solution concentrations to zero concentration yields \bar{M}_n through

$$\left(\frac{\Delta R}{c} \right)_{c \rightarrow 0} = \frac{K_{\text{VPO}}}{\bar{M}_n} \quad (3.90)$$

where K_{VPO} is the calibration constant obtained by measuring ΔR for a low-molecular-weight standard whose molecular weight is precisely known. As in membrane osmometry, the slope of the plot of $\Delta R/c$ versus c is related to the second virial coefficient. Criteria for the selection of calibrants for VPO include high purity (>99.9%) and low vapor pressure (<0.1% of p_1°). Examples of calibrant include mannitol and sucrose for aqueous solution measurements and pentaerythritol tetrastearate, and low-polydispersity, low-molecular-weight polystyrene and polyisobutylene standards for organic-solution determinations. Since calibration by a low-molecular-weight standard is required to obtain K_{VPO} , VPO is considered a secondary method of molecular-weight determination, in contrast to membrane osmometry for which no calibration is required.

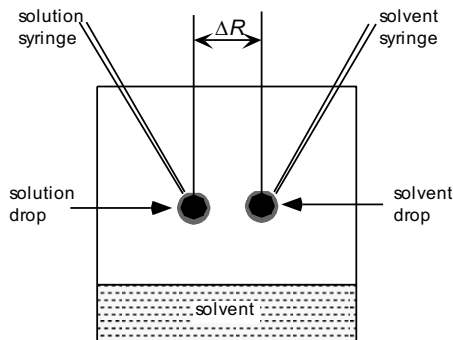


Figure 3-13 Illustration of basic instrumentation for vapor-pressure osmometry.

3.3.2 Light-Scattering Methods

The weight-average molecular weight can be obtained directly only from scattering measurements. The most commonly used technique is light scattering from dilute polymer solution. It is also possible to determine \bar{M}_w by small-angle neutron scattering of specially prepared solid samples. Although this technique has great current importance in polymer research, it is not routinely used for molecular-weight determination because of the difficulty and expense of sample preparation and the

specialized facilities required. The basic principles of light-scattering measurements of dilute polymer solutions are described next.

The fundamental relationship for light scattering is given as*

$$\frac{Kc}{R(\theta)} = \frac{1}{\bar{M}_w P(\theta)} + 2A_2c + \dots \quad (3.91)$$

In this equation, K is a function of the refractive index, n_o , of the pure solvent, the specific refractive increment, dn/dc , of the dilute polymer solution, and the wavelength, λ , of the incident light according to the relationship

$$K = \frac{2\pi^2 n_o^2}{N_A \lambda^4} \left(\frac{dn}{dc} \right)^2 \quad (3.92)$$

where N_A is Avogadro's number (6.023×10^{23} molecules mol⁻¹). The specific refractive increment is the change in refraction index, n , of dilute polymer solutions with increasing polymer concentration. The term $R(\theta)$ appearing in eq. (3.91) is called the *Rayleigh ratio* defined as

$$R(\theta) = \frac{i(\theta)r^2}{I_o V} \quad (3.93)$$

In this equation, I_o is the intensity of the incident light beam and $i(\theta)$ is the intensity of the *scattered* light measured at a distance of r from the scattering volume, V , and at an angle θ with respect to the incident beam. The parameter $P(\theta)$ appearing in eq. (3.91) is called the *particle-scattering function*, which incorporates the effect of chain size and conformation on the angular dependence of scattered light intensity, as illustrated in Figure 3-15. Spherical particles having dimensions smaller than the wavelength of light act as independent scattering centers generating a symmetrical envelope of scattered light intensity. In the case of small particles, $P(\theta)$ is unity, but in the case of polymer chains whose dimensions are $> \lambda/20$, scattering may occur from different points along the same chain and $P(\theta) < 1$. For this reason, diminution of scattered light intensity can occur due to interference, and the scattering envelope is no longer spherically symmetrical, as seen in Figure 3-14. In this case, the angular dependence of scattered light intensity is given by the particle-scattering func-

* It can be shown from the thermodynamic theory of fluctuations that the relationship between scattered light intensity and chemical potential is given as

$$R(\theta) = \frac{KcRTV_1(1 + \cos^2 \theta)}{-\partial\mu/\partial c} = \frac{KcRTV_1(1 + \cos^2 \theta)}{\partial\Pi/\partial c}$$

tion, which, for a *monodisperse* system of randomly coiling molecules in dilute solution, is given by the expression

$$P(\theta) = \frac{2}{v^2} [e^{-v} - (1-v)] \quad (3.94)$$

where

$$v = 16 \left(\frac{\pi n}{\lambda} \right)^2 \langle s^2 \rangle \sin^2 \left(\frac{\theta}{2} \right) \quad (3.95)$$

and $\langle s^2 \rangle$ is called the mean-square radius of gyration. For linear-chain polymers, $\langle s^2 \rangle$ is related to the mean-square end-to-end distance as

$$\langle s^2 \rangle = \frac{\langle r^2 \rangle}{6}. \quad (3.96)$$

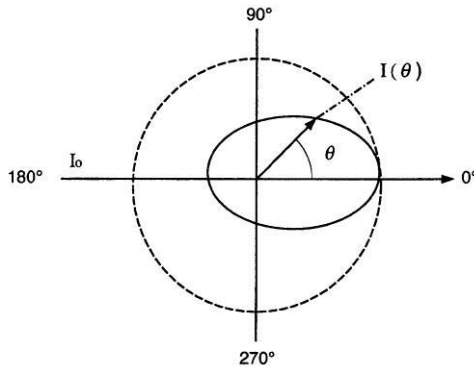


Figure 3-14 Intensity distribution of light scattering at various angles for a small particle (dashed circle) and a large polymer molecule (solid ellipse).

Basic instrumentation for light-scattering measurements is illustrated in Figure 3-15. Light from a high-intensity mercury lamp is polarized and filtered before passing through a glass cell that contains a filtered, dilute polymer solution. Scattered light intensity at an angle θ is recorded as a signal from a movable high-voltage photomultiplier tube.

To determine \bar{M}_w from eq. (3.91), it is necessary to know the value of $P(\theta)$ at each angle for which $R(\theta)$ has been measured. When the molecular-weight distribution of a polymer is polydisperse, as it usually is, $P(\theta)$ is not precisely given by eq. (3.94), but by a summation of similar equations for polymer chains of different sizes weighted by the amount of variously sized chains present in the polymer sample.

Since this information is generally not known, it is customary to treat the data in a way that does not require explicit knowledge of $P(\theta)$. In practice, two approaches can be used. These are called the *Zimm* and *dissymmetry* methods, which are discussed in the following sections.

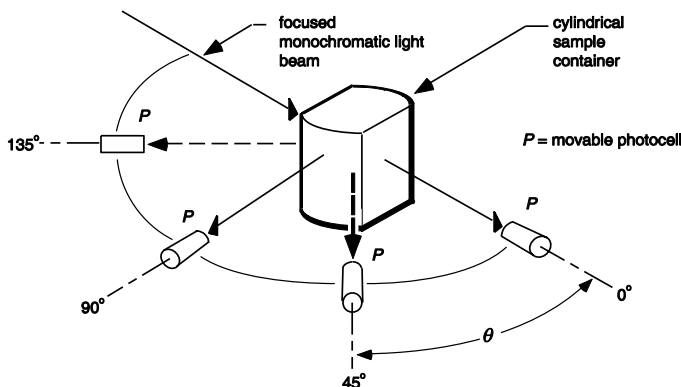


Figure 3-15 Conventional light-scattering instrumentation. From F. Rodriguez, *Principles of Polymer Systems*. 2003. Reproduced with permission of Routledge Publishing, Inc., in book format via Copyright Clearance Center.

Zimm Method. The most rigorous approach to determine \bar{M}_w from light-scattering data is a *Zimm plot*. This procedure has the advantage that chain conformation need not be known in advance; however, Zimm plots require tedious measurements of scattered light intensity at many more angles than are needed by the dissymmetry technique. A double extrapolation to both zero concentration *and* zero angle is used to obtain information concerning molecular weight, second-virial coefficient, and chain dimensions, as discussed next.

In the limit of small angles where $P(\theta)$ approaches unity, it can be shown by means of a series expansion of $1/P(\theta)$ that eq. (3.91) becomes*

$$\frac{Kc}{R(\theta)} = \frac{1}{\bar{M}_w} \left[1 + \frac{16}{3} \left(\frac{\pi n}{\lambda} \right)^2 \langle s^2 \rangle \left(\frac{\theta}{2} \right) \right] + 2A_2c. \quad (3.97)$$

* The Rayleigh ratio used in the scattering of dilute polymer solutions is the excess or reduced Rayleigh ratio,

$$\Delta R_\theta = R_\theta(\text{solution}) - R_\theta(\text{solvent}).$$

As illustrated in Figure 3-16, light-scattering data are plotted in the form of $Kc/R(\theta)$ versus $\sin^2(\theta/2) + kc$ for different angles and concentrations (where k is an arbitrary constant added to provide spacing between curves). A *double* extrapolation to $\theta = 0^\circ$ and $c = 0$, for which the second and third terms on the right of eq. (3.97) become zero, yields \bar{M}_w as the reciprocal of the intercept. As inspection of eq. (3.97) indicates, A_2 is then obtained as one-half of the slope of the extrapolated line at $\theta = 0$; the mean-square radius of gyration is obtained from the initial slope of the extrapolated line at $c = 0$ as

$$\langle s^2 \rangle = \frac{3\bar{M}_w}{16} \left(\frac{\lambda}{\pi n} \right)^2 \times \text{slope (at } c = 0). \quad (3.98)$$

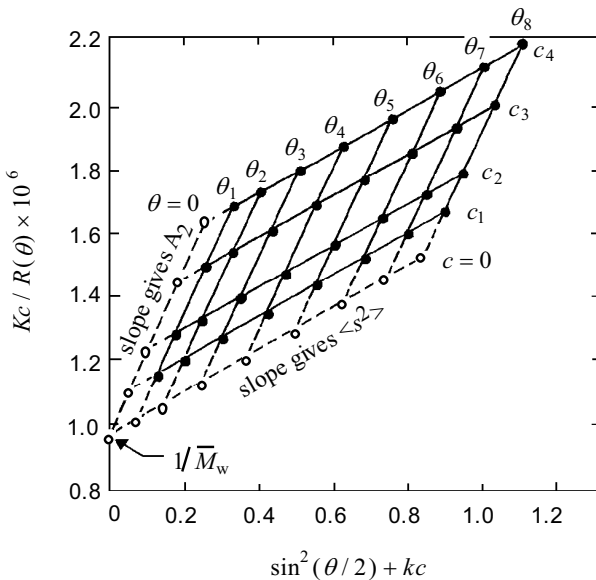


Figure 3-16 Idealized Zimm plot of light-scattering data (•) taken at different angles (θ) and solution concentrations (c). Double extrapolations to zero concentration and zero scattering angle are represented by broken lines.

One obvious difficulty with the Zimm method is that a large number of time-consuming measurements is required; however, the method provides a great deal of information— \bar{M}_w , A_2 , and $\langle s^2 \rangle$. The number of experiments is greatly reduced by using the dissymmetry method; however, chain dimensions are less certain, as discussed next.

Dissymmetry Method. Molecular-weight determination by the *dissymmetry* method requires measurement of the scattered intensity at three angles—typically

45°, 90°, and 135° (see Figure 3-14)—and at several different (dilute) polymer concentrations. A dissymmetry ratio, z , is defined as

$$z = \frac{i(45^\circ)}{i(135^\circ)}. \quad (3.99)$$

Since z is normally concentration-dependent, a value at zero concentration is determined by plotting $(z - 1)^{-1}$ versus concentration. This value can then be used to obtain $P(90^\circ)$ and also $\langle r^2 \rangle^{1/2}$ from published values if the conformational state (e.g., rods, disks, spheres, or random coils) of the polymer in solution is known. In the absence of information to the contrary, a random-coil conformation, typical of flexible-chain polymers, is assumed. Once $P(90^\circ)$ is known, \bar{M}_w can be obtained from the intercept and A_2 obtained from the slope of a plot of $Kc/R(90^\circ)$ versus concentration extrapolated to zero concentration.

Low-Angle Laser Light Scattering (LALLS). In recent years, helium–neon (He–Ne) lasers ($\lambda = 6328 \text{ \AA}$) have replaced conventional light sources in some commercial light-scattering instruments. The high intensity of these light sources permits scattering measurements at much smaller angles (2° to 10°) than is possible with conventional light sources and for smaller samples at lower concentrations. Since at low angles the particle-scattering function, $P(\theta)$, approaches unity, eq. (3.91) reduces to the classical *Debye equation* for scattering by small spherical particles as

$$\boxed{\frac{Kc}{R(\theta)} = \frac{1}{\bar{M}_w} + 2A_2c}. \quad (3.100)$$

Therefore, a plot of $Kc/R(\theta)$ versus c at a single angle gives \bar{M}_w as the inverse of the intercept and A_2 as one-half of the slope.

A representative LALLS plot of $Kc/R(\theta)$ versus c is shown for cellulose acetate (CA) in acetone at 25°C in Figure 3-17. From the intercept, a value of 150,000 is obtained for \bar{M}_w of the CA sample; the second virial coefficient, A_2 , is obtained from the slope as $7.53 \times 10^{-3} \text{ mL mol g}^{-2}$. One limitation of the LALLS method is that chain dimensions cannot be obtained since scattering is measured only at a single angle.

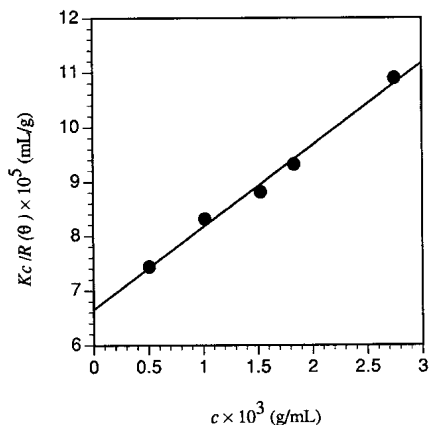


Figure 3-17. Plot of low-angle laser light-scattering data for cellulose acetate in acetone [26].

3.3.3 Intrinsic Viscosity Measurements

A method widely used for routine molecular-weight determination is based upon the determination of the intrinsic viscosity, $[\eta]$, of a polymer in solution through measurements of solution viscosity. Molecular weight is related to $[\eta]$ by the *Mark–Houwink–Sakurada equation* given as

$$[\eta] = K\bar{M}_v^a \quad (3.101)$$

where \bar{M}_v is the viscosity-average molecular weight defined for a discrete distribution of molecular weights (see Section 1.3) as

$$\bar{M}_v = \left[\frac{\sum_{i=1}^N N_i M_i^{1+a}}{\sum_{i=1}^N N_i M_i} \right]^{1/a} \quad (3.102)$$

Both K and a are empirical (Mark–Houwink) constants that are specific for a given polymer, solvent, and temperature. The exponent a normally lies between the values of 0.5 for a θ solvent and 1.0 for a thermodynamically good solvent. Extensive tables of Mark–Houwink parameters for most commercially important polymers are available [21]. Some typical values for representative polymers are given in Table 3-4. The value of \bar{M}_v normally lies between the values of \bar{M}_n and \bar{M}_w obtained by osmometry and light-scattering measurements, respectively. As indicated by eq. (3.102), $\bar{M}_v \equiv \bar{M}_w$ in the case of a thermodynamically good solvent when $a = 1$. The relationship between molecular weights for the *most probable distribution* given by Flory [1] is given by the expression

$$\bar{M}_n : \bar{M}_v : \bar{M}_w :: 1 : [(1+a)\Gamma(1+a)]^{1/a} : 2$$

where Γ is the gamma function (see Appendix E).

Table 3-4 Mark-Houwink Parameters, K and a , for Some Polymers at 25°C^a

Polymer	Solvent	$K \times 10^3$ (mL g ⁻¹)	a
Cellulose acetate ^b	Tetrahydrofuran	51.3	0.69
Polycarbonate	Tetrahydrofuran	38.9	0.70
Polydimethylsiloxane	Toluene	2.4	0.84
Poly(2,6-dimethyl-1,4-phenylene oxide)	Toluene	28.5	0.68
Poly(methyl methacrylate)	Benzene	5.5	0.76
Polystyrene	Tetrahydrofuran	14	0.70
	Toluene	7.5	0.75
	Benzene	9.2	0.74
Poly(vinyl acetate)	Butanone	42.0	0.62
Poly(vinyl chloride)	Tetrahydrofuran	16.3	0.77

^a Values obtained from light-scattering data.

^b 55.5 wt% acetal content.

Intrinsic viscosity is implicitly expressed by the Huggins equation [27]

$$\frac{\eta_i}{c} = [\eta] + k_H [\eta]^2 c \quad (3.103)$$

where k_H is a dimensionless parameter (the Huggins coefficient) whose value depends upon temperature as well as the specific polymer/solvent combination. The parameter η_i is called the *relative viscosity increment*, which is defined as

$$\eta_i = \frac{\eta - \eta_s}{\eta_s} \quad (3.104)$$

where η and η_s are the viscosities of the dilute polymer solution and pure solvent, respectively. The ratio η_i/c is commonly called the reduced viscosity, η_{red} , or viscosity number according to recommended IUPAC* nomenclature.

As indicated by the form of eq. (3.103), $[\eta]$ can be obtained from the intercept of a plot of reduced viscosity versus c as shown for cellulose acetate in acetone at 25°C in Figure 3-18. In actual practice, reduced viscosity is obtained at different concentrations not by direct measurement of solution and solvent viscosities but by

* International Union of Pure and Applied Chemistry.

measurement of the time required for a dilute solution (t) and pure solvent (t_s) to fall from one fiducial mark to another in a small glass capillary. If these efflux times are sufficiently long (e.g., >100 s), the relative viscosity increment can be obtained as

$$\eta_i = \frac{t - t_s}{t_s}. \quad (3.105)$$

Efflux times may be noted visually or more precisely by means of commercially available photocell devices.

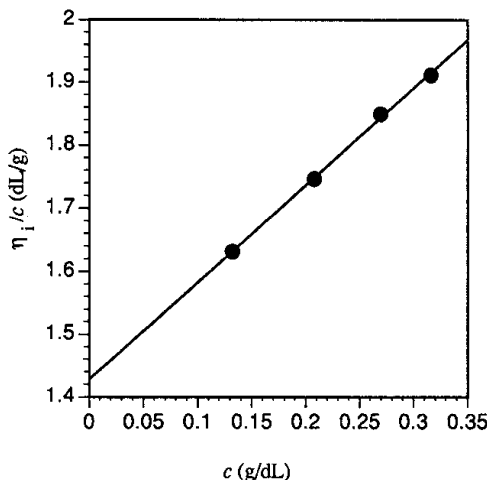


Figure 3-18 Plot of reduced viscosity of a cellulose acetate (intrinsic viscosity of 1.43 dL g^{-1}) in acetone at 25°C [26].

Capillary viscometers may be either Ostwald–Fenske or Ubbelohde types as illustrated in Figure 3-19. The latter have the advantage that different solution concentrations can be made directly in the viscometer by successive dilutions with pure solvent. During measurement, the viscometer is immersed in a constant-temperature bath controlled to within 0.02°C of the set temperature, typically 25° or 30°C .

In addition to determination of molecular weight, measurement of intrinsic viscosity can also be used to estimate chain dimensions in solution. The mean-square end-to-end distance is related to intrinsic viscosity through the relationship [27]

$$\langle r^2 \rangle = \left(\frac{M[\eta]}{\Phi} \right)^{2/3} \quad (3.106)$$

where Φ is considered to be a universal constant ($\Phi \approx 2.1 \pm 0.2 \times 10^{21} \text{ dL mol}^{-1} \text{ cm}^{-3}$) known as the *Flory constant*.

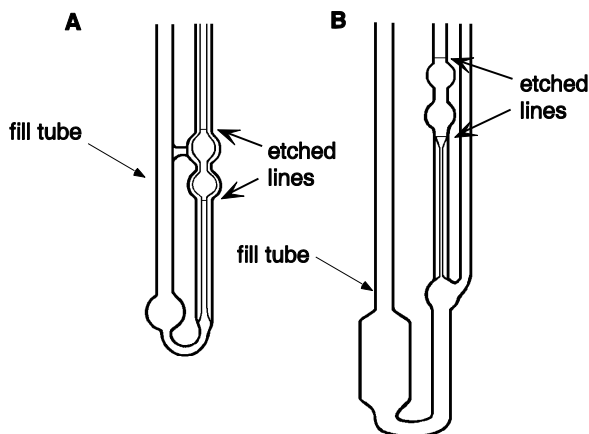


Figure 3-19 Ostwald–Fenske (A) and Ubbelohde (B) capillary viscometers.

3.3.4 Gel-Permeation Chromatography

One of the most widely used methods for the routine determination of molecular weight and molecular-weight distribution is gel-permeation chromatography (GPC), which employs the principle of size-exclusion chromatography (sometimes referred to as SEC) to separate samples of polydisperse polymers into fractions of narrower-molecular-weight distribution. Basic instrumentation for GPC analysis is shown in Figure 3-20. Several small-diameter columns, typically 30 to 50 cm in length, are packed with small, highly porous beads. These are usually fabricated from polystyrene (crosslinked with a small fraction of divinylbenzene as a comonomer) or the packing may be porous glass beads that are usually modified with an ether or diol linkage. Pore diameters of the beads may range from 10 to 10^7 \AA , which approximate the dimensions of polymer molecules in solution. During GPC operation, pure prefiltered solvent is continuously pumped through the columns at a constant flow rate, usually 1 to 2 mL min^{-1} . Then, a small amount (1 to 5 mL) of a dilute polymer solution ($<0.2 \text{ g dL}^{-1}$) is injected by syringe into the solvent stream and carried through the columns. Polymer molecules can then diffuse from this mobile phase into the stationary phase composed of solvent molecules occupying the pore volumes. The smallest polymer molecules are able to penetrate deeply into the interior of the bead pores, but the largest molecules may be completely excluded by the

smaller pores or only partially penetrate the larger ones. As pure solvent elutes the columns after injection, the largest polymer molecules pass through and finally out of the packed columns. These are followed by the next-largest molecules, then the next-largest, and so on, until all the polymer molecules have been eluted out of the column in descending order of molecular weight. Total sample elution in high-resolution columns may require several hours.

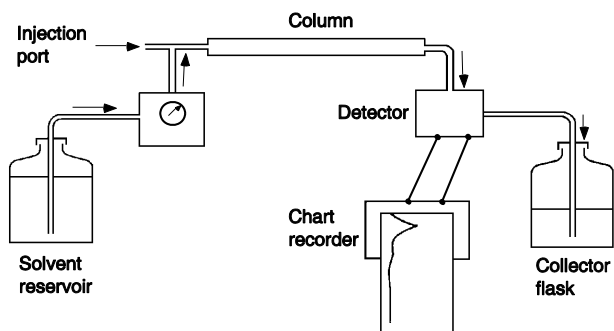


Figure 3-20 Gel-permeation chromatography (GPC). Harry Allcock and Frederick W. Lampe, *Contemporary Polymer Chemistry*. 2nd ed., © 1990, p. 396. Reprinted by permission of Prentice Hall, Englewood Cliffs, NJ.

The concentration of polymer molecules in each eluting fraction can be monitored by means of a polymer-sensitive detector, such as an infrared or ultraviolet device. Usually, the detector is a differential refractometer, which can detect small differences in refractive index between pure solvent and polymer solution. A signal from the detector is recorded as a function of time, which for a fixed flow rate is directly proportional to the elution volume, V_r . A representative GPC chromatogram for a commercial polystyrene sample is shown in Figure 3-21.

For a given polymer, solvent, temperature, pumping rate, and column packing and size, V_r is related to molecular weight. The form of this relation can be found only by comparing elution volumes with those of known molecular weight and narrow-molecular-weight distribution, under identical conditions. Usually, only polymer standards of polystyrene and a few other polymers such as poly(methyl methacrylate) that can be prepared by anionic “living” polymerization (see Section 2.2.2) are available commercially for this purpose. Such standards are available with molecular weights ranging from about 500 to over 2 million with polydispersities as low as 1.06. Since different polymer molecules in the same solvent can have different dimensions, care must be exercised when using polystyrene standards to calibrate elution volumes of other polymers for which standards are not available. The most exact although demanding procedure is to use a universal calibration curve, as illustrated in Figure 3-22.

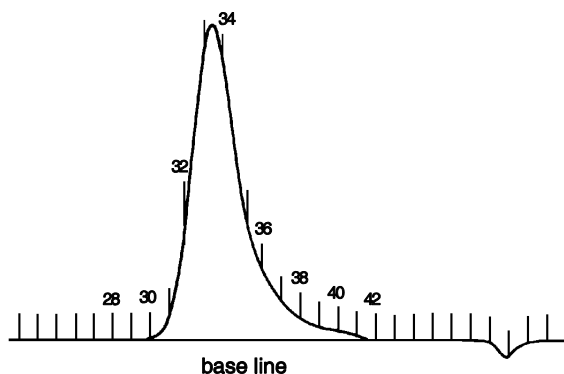


Figure 3-21 GPC chromatogram of polystyrene in tetrahydrofuran at 2.0 mL min^{-1} . Vertical marks represent elution counts. The negative peak at high counts may be due to low-molecular-weight impurities, such as stabilizer, water, or dissolved air. Adapted from L. H. Sperling, *Introduction to Physical Polymer Science*. Fig. 319, p. 88. Copyright © 1986 John Wiley & Sons. Used by permission of John Wiley & Sons, Inc.

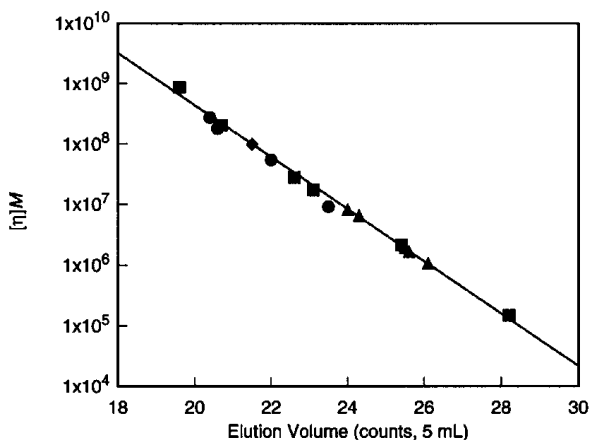


Figure 3-22 Universal GPC calibration curve showing data points for polystyrene (■), poly(vinyl chloride) (▲), polybutadiene (◆), and poly(methyl methacrylate) (●) standards in tetrahydrofuran. Line represents best fit of data [28].

The universal calibration approach is based on the fact that the product $[\eta]M$ is proportional to the hydrodynamic volume of a polymer molecule in solution (see eq (3.106)). This hydrodynamic volume is the effective molecular volume as seen by the pore sites. Universal calibration can be used if the Mark–Houwink constants

(see eq. (3.101)) are known for both the standard and unknown polymer samples in the same solvent and at the same temperature. In the calculation of molecular-weight averages, the signal strength (i.e., peak height in Figure 3-21) is proportional to W_i (eq (1.2)). Once a proper calibration curve is available to relate V_r to the molecular weight (M_i) of the calibration standard, direct calculation of all molecular weights— M_n , M_w , M_z , and even M_{z+1} —is possible, typically by commercially available software. Online coupling of GPC with low-angle light-scattering instrumentation (Section 3.3.2) has enabled rapid online computation of molecular weight without the need for separation calibration of the elution curve.

SUGGESTED READING

- Al-Saigh, Z. Y., *Recent Advances in the Characterization of Polymers and Polymer Blends Using the Inverse Gas Chromatography Method*. Polymer News, 1994. **19**: p. 269.
- Barth, H. G., B. E. Boyes, and C. Jackson, *Size Exclusion Chromatography*. Analytical Chemistry, 1996. **68**: p. 445R.
- Barth, H. G., and J. W. Mays, *Modern Methods of Polymer Characterization*. 1991, New York: John Wiley & Sons.
- Cantow, M. J. R., ed., *Polymer Fractionation*. 1967, New York: Academic Press.
- Danner, R. P., and M. S. High, *Handbook of Polymer Solution Thermodynamics*. 1993, New York: American Institute of Chemical Engineers.
- Einaga, Y., *Thermodynamics of Polymer Solutions and Mixtures*. Progress in Polymer Science, 1994. **19**: p. 1.
- Evans, J., *Gel Permeation Chromatography: A Guide to Data Interpretation*. Polymer Engineering and Science, 1973. **13**: p. 401.
- Forsman, W. C., ed., *Polymers in Solution: Theoretical Considerations and Newer Methods of Characterization*. 1986, New York: Plenum.
- Hansen, C., *Hansen Solubility Parameters: A User's Handbook*. 1999, Boca Raton: CRC Press.
- Hunt, B. J., and S. R. Holding, eds., *Size Exclusion Chromatography*. 1989, New York: Chapman and Hall.
- Morawetz, H., *Macromolecules in Solution*. 1975, New York: John Wiley & Sons.
- Ward, T. C., *Molecular Weight and Molecular Weight Distributions in Synthetic Polymers*. Journal of Chemical Education, 1981. **58**: p. 867.
- Yau, W. W., J. J. Kirkland, and D. D. Bly, *Modern Size-Exclusion Chromatography*. 1979, New York: John Wiley & Sons.

PROBLEMS

3.1 Polyisobutylene (PIB) is equilibrated in propane vapor at 35°C. At this temperature, the saturated vapor pressure (p_1^0) of propane is 9050 mm Hg and its density is 0.490 g cm⁻³. Polyisobutylene has a molecular weight of approximately 1 million and a density of 0.915 g

cm^{-3} . The concentration of propane, c , sorbed by PIB at different partial pressures of propane (p_1) is given in the following table. Using this information, determine an average value of the Flory interaction parameter, χ_{12} , for the PIB–propane system.

p_1 (mm Hg)	c (g propane/g PIB)
496	0.0061
941	0.0116
1446	0.0185
1452	0.0183

3.2 The following osmotic pressure data are available for a polymer in solution:

c (g dL^{-1})	h (cm of solvent)
0.32	0.70
0.66	1.82
1.00	3.10
1.40	5.44
1.90	9.30

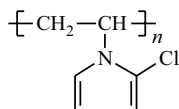
Given this information and assuming that the temperature is 25°C and that the solvent density is 0.85 g cm^{-3} , provide the following:

- (a) A plot of Π/RTc versus concentration, c .
 (b) The polymer molecular weight and the second virial coefficient, A_2 .

3.3 (a) What is the osmotic pressure (units of atm) of a 0.5 wt% solution of poly(methyl methacrylate) ($\bar{M}_n = 100,000$) in acetonitrile (density, 0.7857 g cm^{-3}) at 45°C for which $[\eta] = 4.8 \times 10^{-3} \text{ M}^{0.5}$?

- (b) What is the osmotic head in units of cm?
 (c) Estimate the Flory interaction parameter for polysulfone in methylene chloride.
 (d) Based upon your answer above, would you expect methylene chloride to be a good or poor solvent for polysulfone?

3.4 The osmotic pressure of two samples, A and B, of poly(vinyl pyridinium chloride)



were measured in different solvents. The following data were obtained:

Osmotic Pressure Data in Distilled Water		
Sample	c (g mL ⁻¹)	Π (atm $\times 10^3$)
A	0.002	29
A	0.005	50
B	0.002	31
B	0.005	52

Osmotic Pressure Data in 0.01 <i>N</i> Aqueous NaCl		
Sample	c (g mL ⁻¹)	Π (atm $\times 10^3$)
A	0.002	5
A	0.005	13
B	0.002	2
B	0.005	5.5

Discuss these results and account for any features that you consider anomalous.

3.5 The following viscosity data were obtained for solutions of polystyrene (PS) in toluene at 30°C:

c (g dL ⁻¹)	t (s)
0	65.8
0.54	101.2
1.08	144.3
1.62	194.6
2.16	257.0

Using this information:

- Plot the reduced viscosity as a function of concentration.
- Determine the intrinsic viscosity and the value of the Huggins constant, k_H .
- Calculate the molecular weight of PS using Mark–Houwink parameters of $a = 0.725$ and $K = 1.1 \times 10^{-4}$ dL g⁻¹.

3.6 Given that the molecular weight of a polystyrene (PS) repeating unit is 104 and that the carbon–carbon distance is 1.54 Å, calculate the following:

- The mean-square end-to-end distance for a PS molecule of 1 million molecular weight assuming that the molecule behaves as a freely rotating, freely jointed, volumeless chain. Assume that each link is equivalent to a single repeating unit of PS.
- The unperturbed root-mean-square end-to-end distance, $\langle r^2 \rangle_0^{1/2}$, given the relationship for intrinsic viscosity, $[\eta]$, of PS in a θ solvent at 35°C as

$$[\eta] = 8 \times 10^{-4} M^{0.5}$$

where $[\eta]$ is in units of dL g⁻¹.

- The characteristic ratio, C_N , for PS.

3.7 The use of universal calibration curves in GPC is based upon the principle that the product $[\eta]M$, the hydrodynamic volume, is the same for all polymers at equal elution volumes. If the retention volume for a monodisperse polystyrene (PS) sample of 50,000 molecular weight is 100 mL in toluene at 25°C, what is the molecular weight of a fraction of poly(methyl methacrylate) (PMMA) at the same elution volume in toluene at 25°C? The Mark–Houwink parameters, K and a , for PS are given as $7.54 \times 10^{-3} \text{ mL g}^{-1}$ and 0.783, respectively; the corresponding values for PMMA are $8.12 \times 10^{-3} \text{ mL g}^{-1}$ and 0.71.

3.8 Show that the most probable end-to-end distance of a freely jointed polymer chain is given as $(2nl^2/3)^{1/2}$.

3.9 The (reduced or excess) Rayleigh ratio (R_θ) of cellulose acetate (CA) in dioxane was determined as a function of concentration by low-angle laser light-scattering measurements. Data are given in the following table. If the refractive index (n_0) of dioxane is 1.4199, the refractive-index increment (dn/dc) for CA in dioxane is $6.297 \times 10^{-2} \text{ cm}^3 \text{ g}^{-1}$, and the wavelength (λ) of the light is 6328 Å, calculate the weight-average molecular weight of CA and the second virial coefficient (A_2).

$c \times 10^3$ (g mL ⁻¹)	$R(\theta) \times 10^5$ (cm ⁻¹)
0.5034	0.239
1.0068	0.440
1.5102	0.606
2.0136	0.790
2.517	0.902

3.10 Chromosorb P was coated with a dilute solution of polystyrene in chloroform, thoroughly dried, and packed into a GC column. The column was then heated in a GC oven and maintained at different temperatures over a range from 200° to 270°C under a helium purge. At each temperature, a small amount of toluene was injected and the time for the solute to elute the column was recorded and compared to that for air. From this information, the specific retention volume was calculated as given in the table below. Using these data, plot the apparent Flory interaction parameter as a function of temperature.

T (°C)	V_g (mL/g-coating)
200	6.55
210	5.58
220	4.66
230	4.07
240	3.38
250	2.87
260	2.88
270	2.38

3.11 (a) Derive eq. (3.72) and then (b) develop an expression that can be used to obtain the exchange interaction parameter, X_{12} , appearing in the Flory equation of state from inverse gas chromatography measurements.

3.12 Derive the expression for osmotic pressure given by eq. (3.83).

3.13 Show how eq. (3.78) for the relation between the Flory–Huggins interaction parameter and the solubility parameters of polymer and solvent was derived.

REFERENCES

1. Flory, P. J., *Principles of Polymer Chemistry*. 1953, Ithaca: Cornell University Press.
2. Flory, P. J., *Statistical Mechanics of Chain Molecules*. 1989, New York: Oxford University Press.
3. Mark, J. E., *Rubber Elasticity*. *Journal of Chemical Engineering*, 1981. **58**(11): p. 898–903.
4. Wool, R. P., *Polymer Entanglements*. *Macromolecules*, 1993. **26**: p. 1564–1569.
5. Flory, P. J., *Conformations of Macromolecules in Condensed Phases*. *Pure and Applied Chemistry*, 1984. **56**(3): p. 305–312.
6. Gee, G., and L. R. G. Treloar, *The Interaction between Rubber and Liquids. 1. A Thermodynamical Study of the System Rubber–Benzene*. *Transactions of the Faraday Society*, 1942. **38**: p. 147–165.
7. Flory, P. J., *Thermodynamics of High Polymer Solutions*. *Journal of Chemical Physics*, 1941. **9**: p. 660–661.
8. Flory, P. J., *Thermodynamics of High Polymer Solutions*. *Journal of Chemical Physics*, 1942. **10**: p. 51–61.
9. Huggins, M. L., *Solutions of Long Chain Compounds*. *Journal of Chemical Physics*, 1941. **9**: p. 440.
10. Huggins, M. L., *Theory of Solutions of High Polymers*. *Journal of the American Chemical Society*, 1942. **64**: p. 1712–1719.
11. Flory, P. J., *Thermodynamics of Polymer Solutions*. *Discussions of the Faraday Society*, 1970. **49**: p. 7–29.
12. Flory, P. J., and W. R. Krigbaum, *Statistical Mechanics of Dilute Polymer Solutions. II*. *Journal of Chemical Physics*, 1950. **18**(8): p. 1086–1094.
13. Koningsveld, R., L. A. Kleintjens, and H. M. Schoffeleers, *Thermodynamic Aspects of Polymer Compatibility*. *Pure and Applied Chemistry*, 1974. **39**: p. 1–31.
14. Flory, P. J., *Statistical Thermodynamics of Liquid Mixtures*. *Journal of the American Chemical Society*, 1965. **87**: p. 1833–1838.
15. Sanchez, I. C., and R. H. Lacombe, *Statistical Thermodynamics of Polymer Solutions*. *Macromolecules*, 1978. **11**: p. 1145–1156.
16. Jain, R. K., and R. Simha, *On the Statistical Thermodynamics of Multicomponent Fluids: Equation of State*. *Macromolecules*, 1980. **13**: p. 1501–1508.
17. Freeman, P. I., and J. S. Rowlinson, *Lower Critical Points in Polymer Solutions*. *Polymer*, 1961. **1**: p. 20–26

18. Lipson, J. E. G., and J. E. Guillet, *Study of Structure and Interactions in Polymers by Inverse Gas Chromatography*, in *Developments in Polymer Characterisation*, J. V. Dawkins, ed. 1982, London: Applied Science Publishers, p. 33–74.
19. Everett, D. H., *Effect of Gas Imperfection on G.L.C. Measurements: A Refined Method for Determining Activity Coefficients and Second Virial Coefficients*. Transactions of the Faraday Society, 1965. **61**: p. 1637–1645.
20. Biros, J., L. Zeman, and D. Patterson, *Prediction of the χ Parameter by the Solubility Parameter and Corresponding States Theory*. *Macromolecules*, 1971. **4**: p. 30–35.
21. Brandrup, J., E. H. Immergut, and E. A. Grulke, eds., *Polymer Handbook*. 4th ed. 1999, New York: John Wiley & Sons.
22. Zoller, P., and D. J. Walsh, *Standard Pressure-Volume-Temperature Data for Polymers*. 1995, Lancaster: Technomic.
23. Scatchard, G., *Equilibria in Non-electrolyte Solutions in Relation to the Vapor Pressures and Densities of the Components*. *Chemical Reviews*, 1931. **8**: p. 321–333.
24. Hildebrand, J. H., and R. L. Scott, *The Solubility of Non-electrolytes*. 1959, New York: Reinhold.
25. Hansen, C. M., *The Three Dimensional Solubility Parameter—Key to Paint Component Affinities: I. Solvents, Plasticizers, Polymers, and Resins*. *Journal of Paint Technology*, 1967. **39**: p. 104–117.
26. Wang, C.-S., *The Effect of Solvent Quality on the Viscoelastic Properties of Concentrated Cellulose Acetate Solutions*, PhD Dissertation, Chemical Engineering, University of Cincinnati, 1983.
27. Flory, P. J., and T. G. Fox, *Molecular Configuration and Thermodynamic Parameters from Intrinsic Viscosities*. *Journal of Polymer Science*, 1950. **5**: p. 745–747.
28. Grubisic, Z., P. Rempp, and H. Benoit, *A Universal Calibration for Gel Permeation Chromatography*. *Journal of Polymer Science, Polymer Letters Edition*, 1967. **5**: p. 753–759.

This page intentionally left blank

Solid-State Properties

Some commercial polymers, particularly polyolefins, are highly crystalline materials with well-defined morphology consisting of chain-folded lamella joined in supramolecular structures called spherulites. Although single crystals of some polymers such as polyethylene can be grown under laboratory conditions, no bulk polymer is completely crystalline. In the case of semicrystalline polymers, regular crystalline units are linked by unoriented, random-conformation chains that constitute amorphous regions. Other polymers may have very low crystallinity characterized by poorly defined crystalline microstructure in an amorphous matrix. An important example of commercial polymer with low crystallinity is poly(vinyl chloride). Many other polymers, such as atactic polystyrene and poly(methyl methacrylate), are totally amorphous. In all cases, morphological aspects such as the presence of crystalline structure have a significant influence on the physical, thermal, and mechanical properties of the polymer. Issues concerning polymer-chain microstructure and the relationship between morphology, bulk properties, and chain conformation

and interchain effects are addressed in this chapter as are methods by which bulk properties can be measured.

4.1 The Amorphous State

Completely amorphous polymers like atactic polystyrene exist as long, randomly coiled, interpenetrating chains that are capable of forming stable, flow-restricting *entanglements* at sufficiently high molecular weight. In the amorphous solid state, chains assume their unperturbed dimensions as they do in solution under θ conditions (see Section 3.1). In the melt, thermal energy is sufficiently high for long segments of each polymer chain to move in random micro-Brownian motions. As the melt is cooled, a temperature is reached at which all long-range segmental motions cease. This characteristic temperature is called the *glass-transition temperature*, or T_g , and varies widely with polymer structure. In the glassy state, at temperatures below T_g , the only molecular motions that can occur are short-range motions of several contiguous chain segments and motions of substituent groups. These processes are called *secondary* relaxations. The concepts of chain entanglements, the glass transition, and secondary-relaxation processes are developed in the following sections.

4.1.1 Chain Entanglements and Reptation

As illustrated by Figure 4-1, polymer chains that are sufficiently long can form stable, flow-restricting entanglements. A good analogy can be made to a bowl of spaghetti. When the individual strands of spaghetti are long, it is very difficult to separate one from the others with a fork; however, when the strands are short, they can be removed easily. Entanglements have significant importance in relation to viscoelastic properties (see Chapter 5), melt viscosity (see Chapter 11), and mechanical properties such as stress relaxation, creep, and craze formation, as will be discussed in this chapter.

Critical Molecular Weight. The minimum polymer chain length or *critical molecular weight*, M_c , for the formation of stable entanglements depends upon the flexibility of a polymer chain and may be directly related to the characteristic ratio, a measure of intramolecular steric hindrance (see Section 3.1) [1]. Relatively flexible polymer chains, such as polystyrene, have a high M_c , while more rigid-chain polymers, such as those with aromatic backbones (e.g., polycarbonate), have a lower M_c . A related parameter is the *molecular weight between entanglements* or M_e . Representative values of M_c and M_e are given in Table 4-1. As a rough rule of thumb, $M_c \approx 2M_e$. Typically, the molecular weight of most commercial polymers

is significantly greater than M_c in order to achieve maximum thermal and mechanical properties. For example, the molecular weight of commercial polystyrene typically falls in the range of 100,000 to 400,000, while M_c is only about 31,200 as given in Table 4-1.

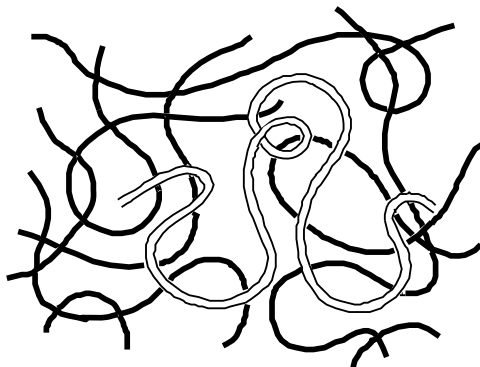


Figure 4-1 Representation of a polymer chain intertwined in a network of entangled chains. Reprinted from Pierre-Gilles de Gennes, *Scaling Concepts in Polymer Physics*. Fig. 11.1, p. 55. Copyright © 1979 by Cornell University. Used by permission of the publisher, Cornell University Press.

Table 4-1 Entanglement Molecular Weights for Linear Polymers^a

Polymer	M_c	M_e
Polycarbonate	4800 ^b	2490 ^c
<i>cis</i> -Polyisoprene	10,000	5800
Polyisobutylene	15,200	8900
Polydimethylsiloxane	24,400	8100
Poly(vinyl acetate)	24,500	12,000
Poly(methyl methacrylate)	27,500	5900
Poly(α -methylstyrene)	28,000	13,500
Polystyrene	31,200	18,100

^a From ref. [2] unless otherwise indicated.

^b From ref. [1].

^c From ref. [3].

Reptation. If individual chains are entangled in the solid state, the question arises as to how long-range movement of chains can occur as the polymer is heated through its T_g and passes from the solid to the melt state. A reasonable explanation has been provided on the basis of the theory of reptation, as originally developed by

Nobel laureate* Pierre-Gilles de Gennes [4] for fixed networks such as a polymer gel and later extended to include melts [5] and concentrated polymer solutions. In the melt state, individual polymer chains can move by local Brownian motion restricted by the topological constraint of neighboring chains. Movement can be visualized as snakelike motion (i.e., reptation) of the chain within a virtual tube, which is defined by the locus of its entanglements with neighboring molecules as illustrated in the top view of Figure 4-2. The theory of reptation has been largely successful in developing a qualitative and quantitative molecular theory for the dynamics and viscoelastic properties of entangled polymers.

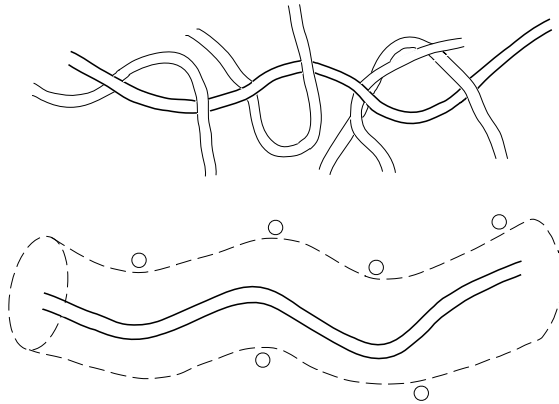


Figure 4-2 Reptation model of a polymer chain constrained in entangled network. A particular chain can be viewed as constrained to move within a virtual tube defined by neighboring entanglement sites. Circles pictured in the lower view represent cross sections of chains constituting the tube constraints. Adapted from J. Klein, *Evidence for Reptation in an Entangled Melt*, *Nature*, 1978. **271**(5641): p. 143, with permission of the Nature Publishing Group.

4.1.2 The Glass Transition

As mentioned earlier, the temperature that marks the transition from the amorphous solid state to the melt state is called the glass-transition temperature or T_g . Several phenomenological models have been used to provide an understanding of the glass transition. One is that the glass transition marks an *isoviscous* state. This means that, as a polymer is cooled from its melt state, viscosity increases rapidly to a common

* 1991 Nobel Prize in physics.

(maximum) value, ca. 10^{12} Pa-s (10^{13} poise) at T_g , for all glassy materials—both low-molecular-weight and polymeric [6].

A second view is that the glass transition represents a state of *isofree volume*. Free volume, V_f , is defined as the difference between the actual volume (or specific volume), V , of the polymer at a given temperature and its corresponding equilibrium volume at absolute zero, V_o ,

$$\boxed{V_f = V - V_o}. \quad (4.1)$$

The volume at absolute zero can be approximated by the sum of the van der Waals volumes of each chain segment, which can be easily obtained by group-contribution methods [7]. The concept of free volume has significant importance for a number of other related subjects in polymer science, including time-temperature superposition of viscoelastic properties (Chapter 5), melt viscosity (Chapter 11), and permeability (Chapter 12).

A third view of the glass transition is that it represents an *isoentropic* state. This is the foundation of the important Gibbs–DiMarzio theory [8]. Gibbs and DiMarzio have suggested that there is a temperature, T_2 , at which the conformational entropy, S_c (a measure of the total number of ways of arranging a polymer molecule or collection of chains), goes to zero. It can be shown (see Section 5.1.6) that this equilibrium-state temperature lies approximately 52°C below the experimentally measured T_g , which depends upon the *rate* at which the polymer sample is heated or cooled during measurement. As discussed in Chapter 3, polymeric chains can exist in a large number of possible spatial conformations in solution or in the melt state. Each of these conformations corresponds to a different energy state. As the melt is cooled, fewer high-energy conformations are accessible. If the melt is cooled at an infinitely slow rate to ensure the attainment of equilibrium, eventually a temperature will be reached (i.e., T_2) at which only the *lowest-energy* conformation is available. At this point, the conformational entropy will be zero.

The glass-transition temperature of amorphous polymers can vary widely with the chemical structure of the polymer chain. As illustrated by representative values of T_g for several important polymers given in Table 4-2, T_g can vary over a range of 300°C or more. In general, polymers with flexible backbones and small substituent groups (e.g., polyethylene and polydimethylsiloxane) have low T_g , while those with rigid backbones, such as polymers containing main-chain aromatic groups (e.g., polysulfone), have high T_g . A more detailed discussion of structure-property relationships for the thermal transitions of polymers is given in Section 4.3.3.

Table 4-2 Glass-Transition Temperatures of Some Amorphous Polymers

Polymer	T_g (°C)
Polydimethylsiloxane	-123
Poly(vinyl acetate)	28
Polystyrene	100
Poly(methyl methacrylate)	105
Polycarbonate	150
Polysulfone	190
Poly(2,6-dimethyl-1,4-phenylene oxide)	220

4.1.3 Secondary-Relaxation Processes

As previously discussed, secondary-relaxation processes are small-scale molecular motions that can occur in the amorphous glassy state. These can involve limited motions of the main-chain or rotations, vibrations, or flips of substituent groups. An example of a main-chain secondary relaxation that has been proposed is the Schatzki *crankshaft* rotation model illustrated in Figure 4-3. According to this model, five contiguous bonds join in rotation around the main chain consisting of C–C bonds. A simpler crankshaft model proposed by Boyer involves the rotation of three contiguous bonds. Such limited, or non-cooperative, motions may occur at very low temperatures (e.g., ca. -120°C). A discussion of possible molecular motions attributed to the γ -relaxation of polyethylene has been discussed by Boyd and Breitling on the basis of conformational energy calculations [9]. Compilations of major secondary group assignments are given in a variety of sources [10].

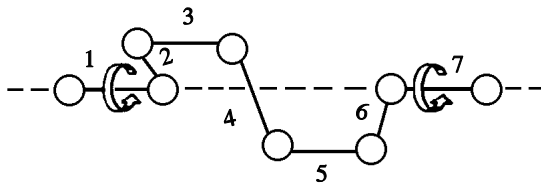


Figure 4-3 Schatzki model of crankshaft motion of a carbon–carbon backbone. The dashed line represents the virtual axis around which bonds 2–6 rotate.

Other examples of main-chain secondary relaxations include rotations of aromatic rings in the backbone of some high-temperature polymers, such as polysulfone and polycarbonate. In addition to these main-chain secondary-relaxation motions, *substituent* groups can rotate or wag at extremely low temperatures in the glassy state. For example, the phenyl ring of polystyrene rotates or wags at 70 K. All these motions can occur in the glassy state, below T_g , as a precursor to the onset

of long-range, main-chain cooperative motions that mark the glass transition. The magnitude and temperature assignment of secondary-relaxation processes can have significant influence on glassy-state properties. For example, the presence of main-chain secondary-relaxation processes has been correlated with impact strength and even with the gas permeability (see Chapter 12) of amorphous polymers.

4.2 The Crystalline State

4.2.1 Ordering of Polymer Chains

Under favorable conditions, some polymers cooled from the melt can organize into regular crystalline structures. Such crystalline polymers have less perfect organization than crystals of low-molecular-weight compounds or low-molecular-weight polymers crystallized from the solution. The basic units of crystalline polymer morphology include crystalline *lamellae* consisting of arrays of folded chains. Reentry of each chain in the folded structure can be adjacent or non-adjacent as illustrated by Figure 4-4. Non-adjacent reentry of chains is illustrated in Figure 4-4A. A chain participating in adjacent reentry can form a tight (or regular) loop (Figure 4-4B) or form a loose (irregular) loop (Figure 4-4C). The thickness of a typical crystallite may be only 100 to 200 Å (10 to 20 nm), indicating that only a portion of the complete chain (e.g., 40 to 80 repeating units in the case of polyethylene) is involved in each fold.

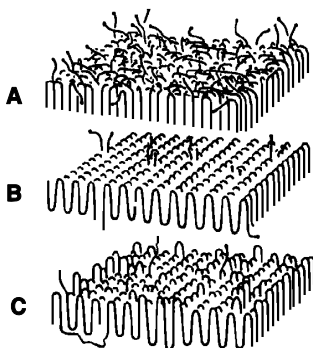


Figure 4-4 Three idealized models for chain folding in polymer crystallites. **A.** Non-adjacent reentry. **B.** Regular adjacent reentry. **C.** Irregular adjacent reentry. Reprinted from J. R. Fried, *Polymer Technology—Part 1: The Polymers of Commercial Plastics*, Plastics Engineering, June 1982. Fig. 7, 38(7), p. 52. Reproduced with permission of Wiley, Inc.

As mentioned earlier, high thermal energy favors a large number of conformations in the melt. As the melt is cooled, the lower-energy conformations are favored, and chains are free to organize into lamellar structure. For many polymers, the lowest-energy conformation is the extended chain or planar zigzag conformation. Such polymers include polyethylene, syndiotactic vinyl polymers, and polymers capable of hydrogen bonding between chains, such as poly(vinyl alcohol) and nylons. In cases of polymers with larger substituent groups, such as the methyl group in polypropylene, for most isotactic polymers, and for polymers of some 1,1-disubstituted ethylenes like polyisobutylene, the lowest-energy conformation is a helix of some preferred geometry [11]. In the case of polypropylene, three repeat units form a single turn in the helix (i.e., 3_1 or $3/1$ helix). In the case of polyoxyethylene, there are seven repeat units per two turns (i.e., 7_2 or $7/2$ helix). A discussion of the concept of chain conformation and dimension was given in Chapter 3.

For some polymers crystallized from the melt or from concentrated solution, crystallites can organize into larger spherical structures called *spherulites*, as illustrated in Figure 4-5. Each spherulite contains arrays of lamellar crystallites that are typically oriented with the chain axis perpendicular to the radial (growth) direction of the spherulite. In a few cases, such as occurs in the crystallization of polypropylene, chain folding will occur with the chain oriented along the radial direction. The anisotropic morphology of a spherulite results in the appearance of a characteristic extinction cross, or Maltese cross, when viewed under polarized light. During the early stages of crystallization, these supramolecular structures are spherical, but as the level of crystallinity increases, the growing spherulites will eventually meet. Impingement ceases primary crystalline growth and the spherical boundaries are lost.

Since no polymer is completely crystalline, even the most crystalline polymers like high-density polyethylene have lattice defect regions that contain unordered, amorphous material. Semicrystalline polymers may exhibit, therefore, both a T_g corresponding to long-range segmental motions in the amorphous regions and a *crystalline-melting temperature*, or T_m , at which crystallites are destroyed and an amorphous, disordered melt is formed. For many polymers, T_g is approximately one-half to two-thirds of T_m (expressed in Kelvins). Representative values of T_g and T_m for some semicrystalline polymers are given in Table 4-3.

The chemical structure of a polymer determines whether it will be crystalline or amorphous in the solid state. In general, symmetrical chain structures, which allow close packing of polymer molecules into crystalline lamellae and specific interactions between chains that favor molecular orientation, favor crystallinity. For example, linear polyethylene and polytetrafluoroethylene, which have symmetrically substituted repeating units, are highly crystalline. Atactic poly(vinyl chloride) (PVC) with its asymmetrically placed chlorine is highly amorphous. When two chlorine atoms are symmetrically located on the same carbon atom, as they are in poly(vinylidene chloride), crystallinity is again favored.

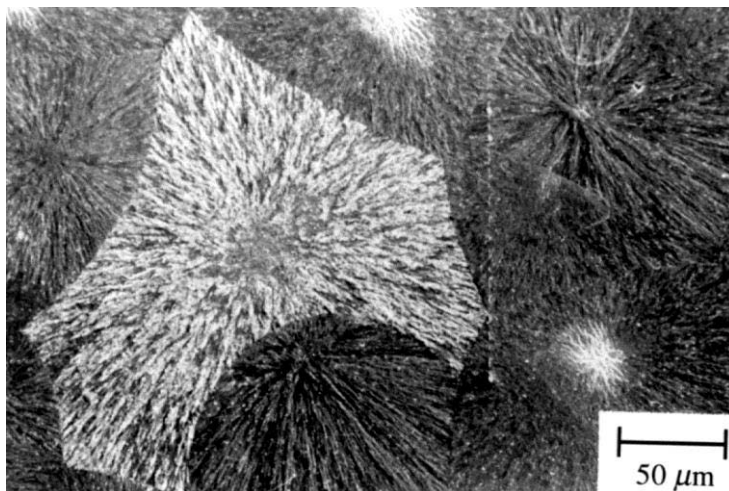


Figure 4-5 Scanning electron micrograph showing the spherulitic structure of polypropylene. The sample was cut using a carborundum-impregnated wire, polished with very fine ($0.1\text{-}\mu\text{m}$) alumina powder, and finally etched using a permanganic acid solution that acts on the amorphous regions of the spherulites to reveal the structure of the lamellae. Polypropylene exists in a number of crystalline forms including a monoclinic α -form (dark areas) and a hexagonal β -form (light areas). The radial structure of the spherulites and impingement of neighboring spherulites are clearly evident in this electron micrograph. Courtesy of M. Aboulfaraj, Pechiney Centre de Recherches de Voreppe, France.

Table 4-3 Thermal Transitions of Some Semicrystalline Polymers

Polymer	T_g ($^{\circ}\text{C}$)	T_m ($^{\circ}\text{C}$)
Polycaprolactone	-60	61
Polyethylene (high-density)	-120	135
Poly(vinylidene fluoride)	-45	172
Polyoxymethylene	-85	195
Poly(vinyl alcohol)	85	258
Poly(hexamethylene adipamide) (nylon-6,6)	49	265
Poly(ethylene terephthalate)	69	265

Although atactic PVC is amorphous, atactic poly(vinyl alcohol) is partly crystalline because of the occurrence of specific interchain interactions (i.e., hydrogen bonding). Specific interactions are particularly important in enhancing crystallinity in the case of nylons, for which hydrogen bonds can form between an amide carbonyl group on one chain and the hydrogen atom of an amide group on an adjacent chain. Such bonding is illustrated in Figure 4-6 for nylon-6,6, poly(hexamethylene

adipamide). The T_m of nylon-6,6 is 265°C compared to 135°C for polyethylene, which, due to the absence of polar groups, is incapable of participating in interchain interactions.

Both tacticity and geometric isomerism (i.e., a *trans* configuration) favor crystallinity. For example, *cis*-polyisoprene is amorphous, while more easily packed *trans*-polyisoprene is crystalline. Although *cis*-1,4-poly(1,3-butadiene) is partly crystalline, its crystalline form is less stable than the preferred *trans* configuration, as indicated by its lower T_m (2°C) compared to *trans*-1,4-poly(1,3-butadiene) (145°C). In general, tactic polymers with their more stereoregular chain structure are more likely to be crystalline than their atactic counterparts. For example, isotactic polystyrene is crystalline, while commercial-grade atactic polystyrene is amorphous. Commercial-grade suspension-polymerized PVC has a portion of its repeating units in syndiotactic placement and, therefore, has some crystallinity (about 11%). By lowering the temperature of PVC polymerization, syndiotactic placement is favored and the crystalline content will be increased.

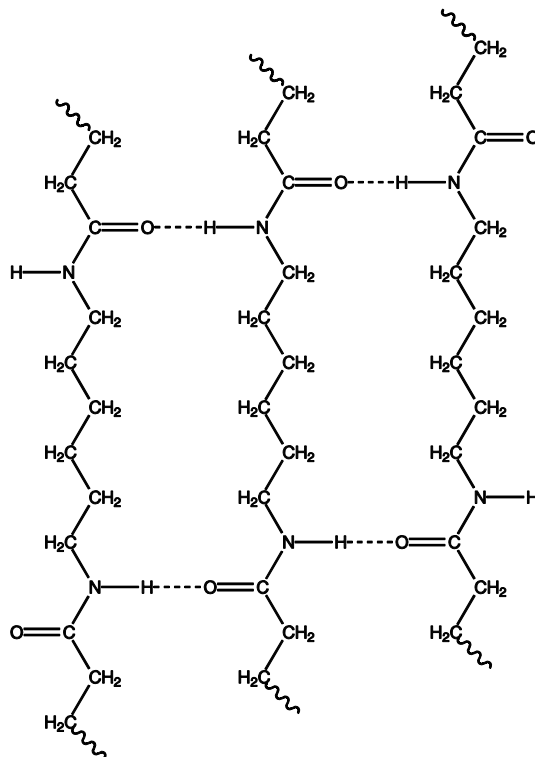


Figure 4-6 Representation of hydrogen bonding between the amide groups in nylon-6,6.

4.2.2 Crystalline-Melting Temperature

From the first law of thermodynamics, the free energy of fusion per repeating unit of the polymer, ΔG_u , can be expressed as

$$\Delta G_u = \Delta H_u - T\Delta S_u \quad (4.2)$$

where ΔH_u and ΔS_u are the enthalpy and entropy of fusion per repeating unit, respectively. At the *equilibrium* melting temperature ($T = T_m^o$), $\Delta G_u = 0$ and, therefore,

$$T_m^o = \frac{\Delta H_u}{\Delta S_u} \quad (4.3)$$

Some representative values of T_m^o , ΔH_u , and ΔS_u are given in Table 4-4.

Table 4-4 Thermodynamic Parameters for Some Semicrystalline and Crystalline Polymers

Polymer	T_m^o (°C)	ΔH_u (cal mol ⁻¹)	ΔS_u (cal K ⁻¹ mol ⁻¹)
Polyethylene	146	960	2.3
Polyoxymethylene	180	590	3.5
Polypropylene	200	1386	2.9
Poly(ethylene terephthalate)	280	6431	11.6
Polycarbonate ^a	335	6348	10.4

^a Solvent-induced crystallization.

In general, the observed crystalline-melting temperature, T_m , is always lower than the equilibrium value, T_m^o . A number of factors can contribute to this melting-point depression. One is due to the kinetic effect of a finite heating or cooling rate. Another is due to crystallite size, which can be influenced by conditions of the crystallization process or by the presence of impurities. The surface free energy increases with decreasing crystallite size and, therefore, T_m decreases with decreasing size. In addition, the presence of a diluent such as residual solvent or plasticizer can reduce T_m on the basis of thermodynamic considerations. Using the Flory–Huggins theory (see Section 3.2.1), the approximate relation for the melting-point depression of a high-molecular-weight polymer by a diluent is

$$\frac{1}{T_m} - \frac{1}{T_m^o} = \left(\frac{R}{\Delta H_u} \right) \left(\frac{V_u}{V_1} \right) (\phi_1 - \chi_{12}\phi_1^2) \quad (4.4)$$

where R is the ideal gas constant, V_u is molar volume per repeating unit of polymer, V_1 is the molar volume of the diluent, ϕ_1 is the volume fraction of the diluent, and

χ_{12} is the Flory interaction parameter between the diluent (component 1) and polymer (component 2). Equation (4.4) indicates that melting-point depression is one way to determine the interaction parameter of a crystallizable polymer in a homogeneous mixture with a solvent, a plasticizer, or a second polymer. Since the presence of a diluent can also decrease T_m by reducing crystallite size, care must be exercised in separating out crystalline size effects from thermodynamic effects [12].

4.2.3 Crystallization Kinetics

For a given polymer, the extent of crystallization attained during melt processing depends upon the rate of crystallization and the time during which melt temperatures are maintained. Above T_m , some polymers that have low rates of crystallization, such as poly(ethylene terephthalate), polycaprolactone, and nylon-6,6, can be quenched rapidly enough to achieve an amorphous state. Other polymers having much higher rates of crystallization, such as polyethylene, cannot be quenched quickly enough to prevent crystallization. For a given polymer, the rate of crystallization depends upon the crystallization temperature, as illustrated by Figure 4-7, which shows the effect of temperature on the rate of spherulite growth in poly(ethylene terephthalate) (PET).

At T_m , the crystalline lamellae are destroyed as fast as they are formed from the melt and, therefore, the net rate of crystallization is zero. Since the large-scale segmental mobility required for chain folding ceases at T_g , the crystallization rate is again zero. At some intermediate temperature, T_{max} , an optimum balance is reached between chain mobility and lamellae growth. The temperature at which the crystallization rate reaches a maximum is independent of molecular weight; however, the maximum crystallization rate decreases as the molecular weight increases.

The rate of crystallization can be followed by a variety of techniques, such as dilatometric measurement of volume changes, infrared spectroscopy, and optical-microscopic measurement of the growth of spherulite radii with time (e.g., Figure 4-7). During the crystallization process, the fractional crystallinity, ϕ , at time t may be approximated by the *Avrami* equation [13, 14]

$$\phi = 1 - \exp(-kt^n) \quad (4.5)$$

where k is a temperature-dependent growth-rate parameter and n is a temperature-independent nucleation index. Typically, n varies between 1 and 4 depending on the nature of nucleation and growth processes. For example, in the case of sporadically nucleating spherulites, as may result during quiescent melt crystallization near T_m , the nucleation index is approximately 4. The fractional crystallinity of a polymer can be determined by a variety of techniques, including infrared spectroscopy as discussed in Section 2.6.1, density and X-ray diffraction measurements as described

in the next section of this chapter, and by calorimetric methods, which will be described in Section 4.3.2.

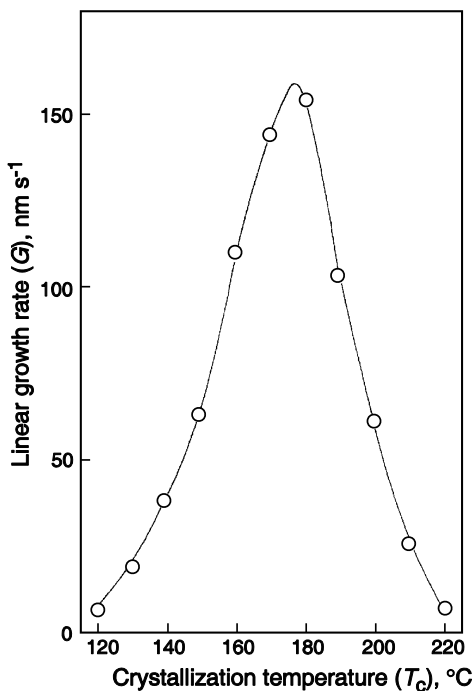


Figure 4-7 Plot of linear growth rate of spherulites in poly(ethylene terephthalate) (PET) as a function of temperature and at a pressure of 1 bar [15]. The maximum growth rate is observed near 178°C. Values of T_g and T_m for PET are approximately 69° and 265°C, respectively.

4.2.4 Techniques to Determine Crystallinity

Density Measurements. Densities can be easily measured at some standard temperature (e.g., 23°C) by means of a calibrated density-gradient column (ASTM* D 792). Once the density (ρ) of the semicrystalline sample has been measured, the fractional crystallinity, ϕ , can be determined as

* See Appendix C for a listing of other important standards.

$$\phi = \frac{\rho - \rho_a}{\rho_c - \rho_a} \quad (4.6)$$

if the densities of a totally amorphous (ρ_a) and totally crystalline sample (ρ_c) are known or can be estimated. Generally, values of amorphous densities are available only for semicrystalline polymers with low crystallization rates that enable rapid quenching from the melt to a totally amorphous state. The crystalline densities of polymers can be obtained from density measurements of single crystals or crystalline low-molecular-weight analogs or may be determined from X-ray determination of crystal densities. Densities for some semicrystalline polymers are given in Table 4-5.

Table 4-5 Amorphous and Crystalline Densities

Polymer	ρ_a (g cm ⁻³)	ρ_c (g cm ⁻³)
Nylon-6	1.09	1.12–1.14
Nylon-6,6	1.09	1.13–1.145
Poly(aryl ether ether ketone) (PEEK)	1.263	1.400
Poly(butylene terephthalate)	1.280	1.396
Poly(ethylene terephthalate)	1.335	1.515
Poly(vinyl chloride)	1.385	1.44–1.53
Polycarbonate	1.196	1.316
Poly(<i>p</i> -phenylene sulfide)	1.32	1.43
Poly(2,6-dimethyl-1,4-phenylene oxide)	1.06	1.31

X-Ray Diffraction. X-ray diffraction is a widely used technique of polymer characterization that can provide information concerning both the crystalline and amorphous states. X-rays are high-energy photons having short wavelengths ($\lambda \approx 0.5$ to 2.5 \AA) that interact with electrons. When an X-ray beam is focused on a material, some electrons will be absorbed, some will be transmitted unmodified, while others will be scattered due to interaction with electrons. This interaction results in a scattering pattern that is a function of the scattering angle, usually designated as 2θ for convenience. The scattering pattern provides information on the electron-density distribution and, therefore, the positions of atoms in a polymer. The relationship between the intensity of an (unpolarized) X-ray beam, I_0 , the scattered intensity, I , and the scattering angle is given by the *Thomson formula*:

$$I = I_0 \frac{K}{r^2} \frac{1 + \cos^2 2\theta}{2} \quad (4.7)$$

In eq. (4.7), r is the distance between the electron and the detector at which the scattered-beam intensity is measured and K is a constant given as

$$K = \frac{e^4}{m^2 c^4} \quad (4.8)$$

where e ($\approx 1.6022 \times 10^{-19}$ C) and m ($\approx 9.1095 \times 10^{-31}$ kg) are the charge and mass of an electron, respectively, and c is the speed of light ($\approx 3.00 \times 10^8$ m s $^{-1}$).

Terms often used in X-ray scattering are wide-angle X-ray scattering (WAXS) and small-angle X-ray scattering (SAXS). WAXS is used for the investigation of small-scale structures (<10 Å) while SAXS is used to study large-scale morphological features (10 to 10^4 Å). The need to measure the scattered-beam intensity at very small angles (e.g., 0.022° to 2.2°) in relation to the transmitted electron beam in the case of SAXS requires collimators for sharply focusing the incident beam and more specialized detectors than are required for WAXS.

WAXS is used for the determination of fractional crystallinity as well as crystalline dimensions [16]. An example of a WAXS diffraction pattern of a highly crystalline polymer is shown in Figure 4-8. In this case, there is an appearance of several large, narrow peaks positioned upon a broad background pattern. The background pattern is due to scattering from amorphous regions (the amorphous halo), while the peaks, called *Bragg peaks*, represent scattering from well-defined crystalline regions having regular spacing. In many cases, the fractional crystallinity can be estimated by comparing the intensity or height of the amorphous halo (I_{am}) of the crystalline sample with the intensity (I_{am}^0) of a totally amorphous polymer as sometimes can be obtained by rapid quenching from the melt as

$$w_c = 1 - \frac{I_{\text{am}}}{I_{\text{am}}^0} \quad (4.9)$$

where w_c is the *weight* fraction of the crystalline phase.

4.3 Thermal Transitions and Properties

4.3.1 Fundamental Thermodynamic Relationships

Many of the commonly used techniques to determine T_g and T_m can be understood on the basis of the thermodynamic definition of a phase transition originally proposed by Paul Ehrenfest [17] in 1933. A *first-order transition* is defined as one for which a discontinuity occurs in the first derivative of the Gibbs free energy (G). According to the first law of thermodynamics for a reversible, closed system, the

Gibbs free energy can be expressed in differential form as a function of temperature and pressure, $G(T, p)$, as

$$dG = -SdT + Vdp \quad (4.10)$$

where S is entropy and V is the system volume.

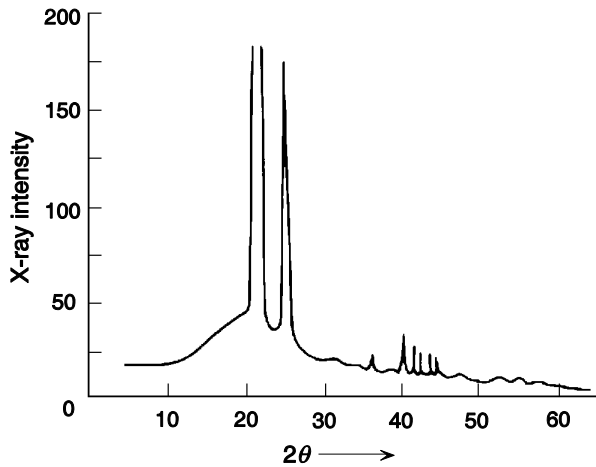


Figure 4-8 X-ray diffraction pattern (WAXS) of high-density polyethylene showing the superposition of crystalline Bragg diffraction peaks on an amorphous background. Adapted from R.-J. Roe, in *The Concise Encyclopedia of Polymer Science and Engineering*, J. I. Kroschwitz, ed. Copyright © 1990 by John Wiley & Sons. This material is used by permission of John Wiley & Sons, Inc.

The free energy may be differentiated with respect to temperature (at constant pressure) as

$$\left(\frac{\partial G}{\partial T}\right)_p = -S \quad (4.11)$$

and with respect to pressure (at constant temperature) as

$$\left(\frac{\partial G}{\partial p}\right)_T = V. \quad (4.12)$$

In terms of describing transitions in polymer systems, the most useful of the preceding relationships is the first derivative with respect to p (eq. (4.12)), which indicates that a *first-order transition should occur as a discontinuity in volume*, as illustrated

in Figure 4-9. Volume is easily measured as a function of temperature by a technique called *dilatometry*, which is described in the next section. The dependence of volume on temperature in the region about the crystalline-melting temperature approximates such a transition (see Figure 4-12).

Second-Order Transitions. The glass transition approximates an Ehrenfest *second-order transition*. This means that a discontinuity should be observed in the *second derivatives* of the Gibbs free energy. Three possible second derivatives can be used to provide a basis for the experimental measurement of T_g . From eqs. (4.11) and (4.12), the corresponding second derivatives are

$$-\left(\frac{\partial^2 G}{\partial T^2}\right)_p = \left(\frac{\partial S}{\partial T}\right)_p, \quad (4.13)$$

$$\left(\frac{\partial^2 G}{\partial p^2}\right)_T = \left(\frac{\partial V}{\partial p}\right)_T, \quad (4.14)$$

and

$$\left[\frac{\partial}{\partial T}\left(\frac{\partial G}{\partial p}\right)_T\right]_p = \left(\frac{\partial V}{\partial T}\right)_p. \quad (4.15)$$

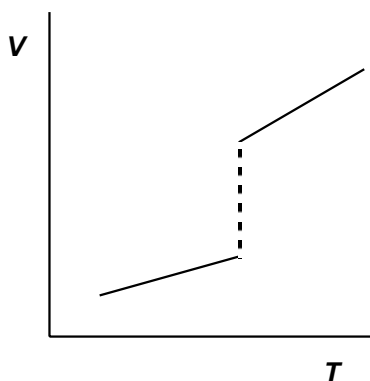


Figure 4-9 Thermodynamic first-order transition in volume at constant pressure.

Since entropy is not an experimentally measurable quantity, eq. (4.13) may be recast into a more useful form in terms of the specific heat at constant pressure, C_p , which is defined as

$$C_p = \left(\frac{\partial H}{\partial T} \right)_p. \quad (4.16)$$

From the first law of thermodynamics, a relation between C_p and entropy can be obtained as*

$$C_p = T \left(\frac{\partial S}{\partial T} \right)_p. \quad (4.17)$$

Substitution of eq. (4.17) into eq. (4.13) indicates that a *second-order transition should occur as a discontinuity in specific heat*, as illustrated in Figure 4-10. Specific heat is easily measured by calorimetric techniques such as differential scanning calorimetry, as described in the next section.

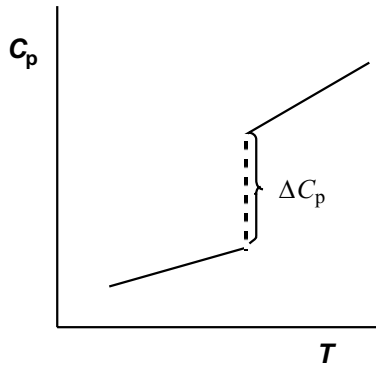


Figure 4-10 Thermodynamic second-order transition in specific heat at constant pressure.

The other two second derivatives indicate that second-order transitions should occur as discontinuities in the slope of volume as a function of pressure (eq. (4.14)) or volume as a function of temperature (eq. (4.15)). These slopes define two useful parameters—the isothermal *compressibility* coefficient, β , and the (isobaric) *thermal-expansion* coefficient, α . As defined earlier, (eqs. (3.73) and (3.74)), these are

* The first law of thermodynamics for a reversible, closed system may be written as

$$dH = TdS + Vdp$$

for which a Legendre transformation gives

$$\left(\frac{\partial H}{\partial T} \right)_p = T \left(\frac{\partial S}{\partial T} \right)_p.$$

$$\beta = -\left(\frac{1}{V}\right)\left(\frac{\partial V}{\partial p}\right)_T \quad (4.18)$$

and

$$\alpha = \left(\frac{1}{V}\right)\left(\frac{\partial V}{\partial T}\right)_p. \quad (4.19)$$

This means that a discontinuity in a plot of α or β versus temperature, or alternatively a change in slope of a plot of volume versus temperature (at constant pressure) or a plot of volume versus pressure (at constant temperature), marks the occurrence of a second-order transition as illustrated in Figures 4-11A and 4-11B, respectively. Both coefficients may be obtained by dilatometric measurements, although the constant-pressure experiment is the easier and, therefore, more commonly used.

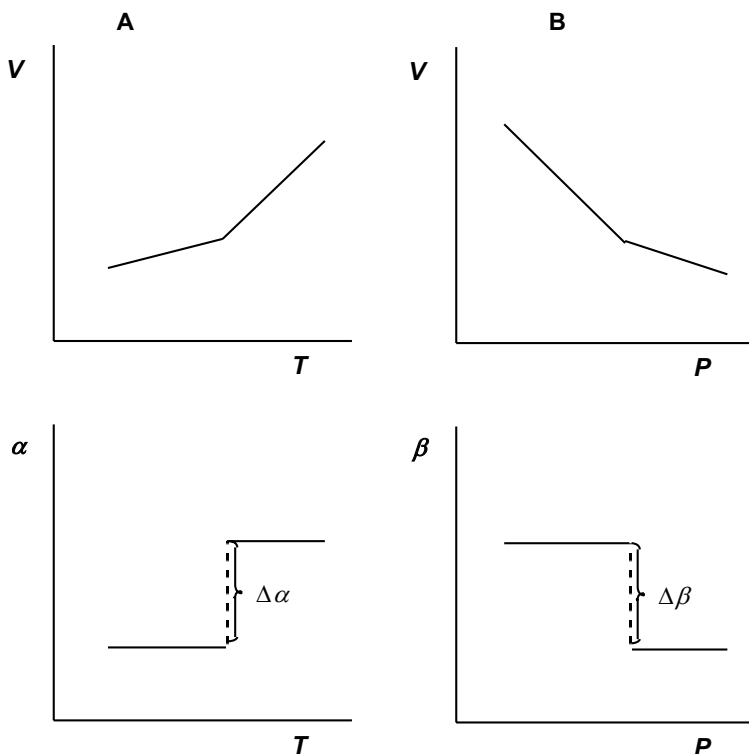


Figure 4-11 **A.** Thermodynamic second-order transition in volume as a function of temperature at constant pressure. **B.** Thermodynamic second-order transition in volume as a function of pressure at constant temperature.

The magnitudes of the discontinuities in C_p , α , and β at the second-order transition may be expressed as

$$\Delta C_p = C_{p,2} - C_{p,1}, \quad (4.20)$$

$$\Delta\alpha = \alpha_2 - \alpha_1, \quad (4.21)$$

and

$$\Delta\beta = \beta_2 - \beta_1 \quad (4.22)$$

where the subscripts, 1 and 2, represent values at temperatures below and above the transition, respectively. These discontinuities are indicated in Figures 4-10 and 4-11.

As illustrated in the next section, the glass transition is not a *true* thermodynamic transition but, rather, it is considered to be a *pseudo*-second-order transition that is influenced by the kinetics of glass formation (i.e., the rate of heating or cooling). Both volume and specific-heat data for polymers closely approximate second-order transition behavior; however, the discontinuities or changes in slope are more gradual and are affected by the heating rate.

4.3.2 Measurement Techniques

A wide variety of experimental methods can be used to determine the glass-transition and crystalline-melting temperatures in polymers. For example, thermal transitions may be detected by changes in refractive index, NMR line width, and birefringence as a function of temperature; however, the most commonly used techniques are dilatometry and, especially, differential scanning calorimetry (DSC), which are described in this section. Another important method of detecting thermal transitions is by recording the response to a cyclical strain (dynamic-mechanical analysis) or electric voltage (dielectric spectroscopy), as will be discussed in Chapter 5. An additional advantage of dynamic-mechanical and dielectric measurements is the ability to detect low-temperature secondary relaxations. By contrast, dilatometric or calorimetric methods are insensitive to the occurrence of secondary-relaxation processes. The glass and melt transitions can also be detected by measurement of modulus as a function of temperature in tensile, stress relaxation, and other mechanical tests, as will be discussed in Section 4.4.2.

Dilatometry. One of the earliest methods used to determine thermal transitions is dilatometry. In this procedure, a small sample of polymer is sealed in a glass bulb to which a precision-bored, calibrated glass capillary is attached. Mercury, whose coefficient of thermal expansion is accurately known, is used to fill the bulb and part of the capillary. The dilatometer is then immersed in a controlled-

temperature bath and the height of the mercury in the capillary is recorded at different temperatures. Heating rate is normally kept very small (1° to 2° min^{-1}) to ensure thermal equilibrium, especially near T_g . From this information, the specific volume of the polymer sample can be obtained as a function of temperature. As illustrated in Figure 4-12, the glass-transition temperature is determined as the temperature at which the volume-temperature curve changes slope (i.e., a discontinuity in α), while at the crystalline-melting temperature (a first-order transition temperature) there is a discontinuity, or step change, in specific volume. Some representative dilatometric data for T_g and thermal-expansion coefficients are given in Table 4-6.

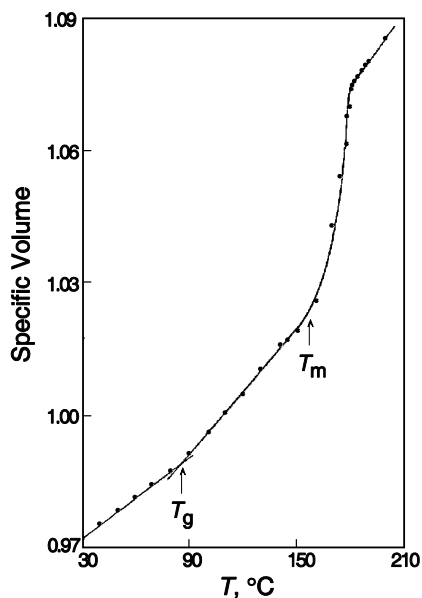


Figure 4-12 Dilatometric data of specific volume of a semicrystalline polymer, poly(*N,N'*-sebacoyl piperazine), plotted against temperature [18]. Results indicate a glass transition near 90°C and a crystalline-melting transition above 160°C .

Table 4-6 Dilatometric Data for Some Representative Polymers [19]

Polymer	T_g (K)	$\alpha' \times 10^4$ (K^{-1})	$\Delta\alpha \times 10^4$ (K^{-1})
Polydimethylsiloxane	150	8.12–12	5.4–9.3
Poly(vinyl acetate)	302	5.98	3.9
Poly(vinyl chloride)	355	5.2	3.1
Polystyrene	373	5.5	3.0
Poly(methyl methacrylate)	378	4.6–5.0	2.45–3.05

As an approximation, the change in thermal-expansion coefficient going from the liquid (i.e., $T > T_g$) to the glassy state (i.e., $T < T_g$),

$$\Delta\alpha = \alpha^{\ell} - \alpha^g, \quad (4.23)$$

is sometimes taken to be $4.8 \times 10^{-4} \text{ K}^{-1}$; however, extensive data have shown that $\Delta\alpha$ increases with decreasing temperature, as the data given in Table 4-6 serve to illustrate. As a better approximation, Simha and Boyer [19] have suggested that

$$\Delta\alpha \approx \frac{0.113}{T_g} \quad (4.24)$$

where T_g is in Kelvins.

Calorimetry. One of the most widely used techniques to measure T_g and T_m is differential scanning calorimetry (DSC). This method uses individual heaters to maintain identical temperatures for two small platinum holders—one contains a small (10 to 30 mg) polymer sample mechanically sealed in a small aluminum pan and the other contains an empty (reference) pan, as illustrated in Figure 4-13. Temperatures are measured by use of identical platinum-resistance thermistors. The differential power needed to maintain both the reference and sample pans at equal temperatures during a programmed heating cycle (range of 0.3125° to $320^\circ\text{C min}^{-1}$) is then recorded as a function of temperature.

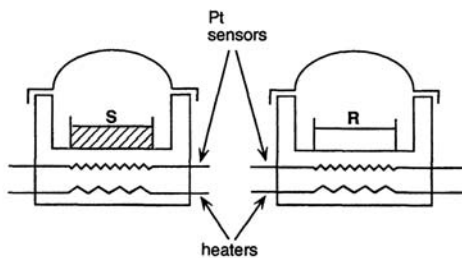


Figure 4-13 Schematic representation of a typical DSC sample cell showing the sample (S) and reference (R) pans, as well as the heating and temperature sensing elements.

In place of differential power, values of specific heat, C_p , may be obtained from the recorded heat-flow rate by calibration with a pure compound such as sapphire for which C_p is known precisely at different temperatures from calorimetry measurements. As illustrated in Figure 4-14, a discontinuity in C_p (i.e., $\Delta C_p = C_p^{\ell} - C_p^g$), characteristic of a second-order transition (see the preceding discussion), is observed at the polymer T_g , which is often identified as the temperature at the midpoint of the step change in C_p (i.e., at $\Delta C_p / 2$). For many amorphous

polymers, T_g (K) and ΔC_p ($\text{J g}^{-1} \text{K}^{-1}$) are related by the approximate relationship [19] that $\Delta C_p \times T_g \approx 115 \text{ J g}^{-1}$ (27.5 cal g^{-1}).

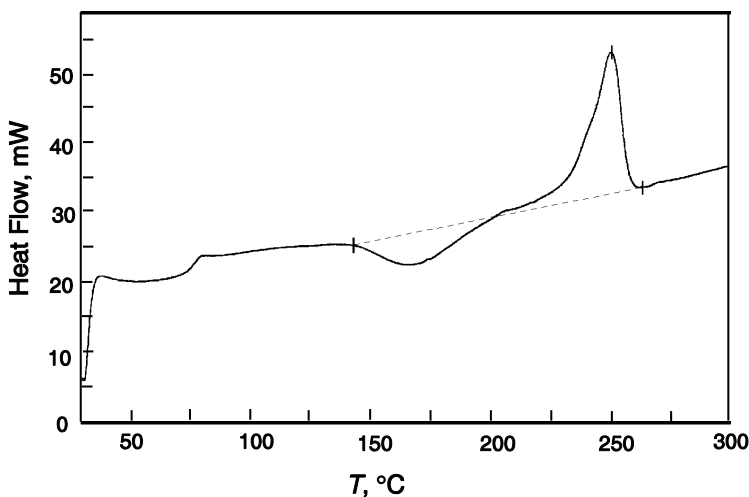


Figure 4-14 DSC thermogram of poly(ethylene terephthalate) crystallized at 200°C for 90 s showing a glass transition near 75°C, an excess crystallization peak above 143°C, and a crystalline-melting endotherm with a peak maximum near 250°C.

During heating of a semicrystalline polymer, additional crystallization may occur at temperatures between T_g and T_m , as illustrated by the crystallization exotherm of poly(ethylene terephthalate) shown in Figure 4-14. At T_m , which may be defined as the extrapolated temperature of the initial slope of the melt endotherm, the crystallites begin to melt over a wide range of temperatures. The breadth of the endotherm is much larger than is typically observed for pure low-molecular-weight compounds as a consequence of the lower order of perfection of polymer crystallites. By calibration with a low-molecular-weight standard such as benzoic acid, the heat of fusion (ΔQ) of a semicrystalline polymer can be determined from measurement of the area under the melt endotherm recorded by DSC. The heat of fusion of the same polymer at 100% crystallinity (ΔH_f) can be estimated from a comparison of the heats of fusion of a homologous series of low-molecular-weight crystals, or from measurement of the melting-point depression of the semicrystalline polymer by diluents (see eq. (4.4)). With this information, the fractional crystallinity (ϕ) of the polymer sample can be obtained by the equation

$$\phi = \frac{\Delta Q}{\Delta H_f} . \quad (4.25)$$

In the case of some polymers, such as isotactic polystyrene with high crystalline order, it is also possible to estimate ϕ from measurement of the specific-heat increment of the semicrystalline polymer at T_g and that of the same polymer in the amorphous state, $(\Delta C_p)_{am}$, obtained by rapid thermal quenching from above T_m , where

$$\phi = 1 - \frac{\Delta C_p}{(\Delta C_p)_{am}}. \quad (4.26)$$

Fractional crystallinity of polymers with low rates of crystallization, such as is the case for polycaprolactone, can be obtained in this manner. For many polymers with low crystalline order, eq. (4.26) will significantly overestimate ϕ because the specific-heat increment of the amorphous phase of the semicrystalline state may be depressed by the presence of small disorganized crystallites that are dispersed in the amorphous matrix.

There have been a number of recent variations of DSC that have broadened its capability of studying thermal events. One is *fast scanning calorimetry* (FSC) that provides scan rates of $750^\circ\text{C min}^{-1}$. These high rates allow the study of kinetics of extremely fast processes. Another variation is *temperature-modulated DSC* (TMDSC). The principle behind TMDSC is the superimposition of a periodic modulation of temperature upon a constant heating (or cooling). TMDSC enables the separation of thermal events such as the glass transition from enthalpy relaxation and crystallization as will be described in the following chapter (see Section 5.1.5).

Heat-Distortion Temperature. An alternative, and more applications-oriented, measure of T_g or T_m is called the *heat-distortion* (or heat-deflection) *temperature* (HDT). The HDT is defined by ASTM Standard D 648* as the temperature at which a sample bar of standard dimensions (e.g., $127 \times 13 \times 3$ mm) deflects by 0.25 mm (0.01 in.) under a standard flexural load of 455 kPa (66 psi)[†] placed at its center. The sample is heated in an immersion bath at a rate of 2°C min^{-1} . In the case of an amorphous polymer, HDT is slightly (10° to 20°C) lower than the T_g as determined by thermal techniques, while in the case of semicrystalline polymers, HDT is more closely identified with T_m , as shown by the values given in Table 4-7. Heat-deflection temperature is, therefore, a useful indicator of the temperature limit above which polymers (or commercial grades of plastics) cannot be used for structural (load-supporting) applications. It is widely used to report the thermal properties of different grades of commercial plastics, including reinforced or filled resins.

* Specification for *tensile* heat-distortion temperature for plastic sheet (0.025 to 1.5 mm in thickness) is given by ASTM D 1637.

[†] A load of 1820 kPa (264 psi) may be specified for a thicker sample.

A listing of other important ASTM standards is given in Appendix C at the end of this text.

Table 4-7 Thermal-Transition Temperatures

Polymer	HDT ^a (°C)	T_g (°C)	T_m (°C)
Polyethylene	29 to 126	-120 to -125	137
Polypropylene	40 to 152	-10 to -18	176
Nylon-6,6	62 to 261	49	265
Poly(vinyl chloride)	60 to 76	87	Low crystallinity
Polycarbonate	39 to 148	150	Amorphous
Polystyrene	63 to 112	100	Amorphous
Polysulfone	146 to 273	190	Amorphous

^a At 1.82 MPa (264 psi); HDT range indicates values reported for all commercial grades that can include filled and other additives.

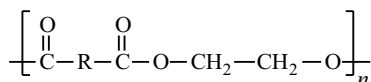
4.3.3 Structure–Property Relationships

As suggested by data given in Tables 4-2 and 4-3, both T_g and T_m are strongly influenced by the chemical structure of the repeating unit. In general, both T_g and T_m increase with decreasing flexibility of the polymer chain. Flexibility decreases with increasing aromatic composition of the main chain or by incorporation of bulky substituent groups or non-rotational groups in the main chain. This is illustrated by the relation of T_m to repeating-unit structure for an analogous series of polyesters in Table 4-8. Replacement of the aliphatic sequence $(CH_2)_4$ of compound A with an aromatic ring (compound B) increases T_m by 220°C. Replacement by two coupled aromatic rings (compound C) further increases T_m by 85°C, but incorporation of a flexible $-CH_2-CH_2-$ group between aromatic rings lowers T_m by 135°C (compound D). By contrast, incorporation of a non-rotational, unsaturated linkage between aromatic rings (compound E) results in the highest T_m .

Chain flexibility is particularly important in determining T_g . Flexible chains, as may be obtained by incorporating an oxygen atom into the main chain (e.g., polydimethylsiloxane), are capable of large-scale molecular motions at very low temperatures and, therefore, have low T_g . Bulky substituent groups hinder chain rotation and therefore raise T_g as shown by structure– T_g comparisons for several vinyl polymers in Table 4-9. For comparably sized substituent groups, increasing polarity, which may enhance intermolecular interactions, can elevate T_g . This is illustrated by T_g data for the vinyl polymers—atactic polypropylene ($T_g = -20^\circ\text{C}$), poly(vinyl chloride) ($T_g = 89^\circ\text{C}$), and polyacrylonitrile ($T_g = 100^\circ\text{C}$)—given in Table 4-9. As illustrated in Table 4-10, increasing flexibility of the side group can lower T_g , as is evident by comparison of the chemical structures of poly(methyl methacrylate), poly(ethyl methacrylate), and poly(propyl methacrylate). Syndiotac-

ticity increases T_g as illustrated by data for poly(methyl methacrylate) (PMMA) prepared with different tacticities: *i*-PMMA ($T_g = 45^\circ\text{C}$), *a*-PMMA ($T_g = 105^\circ\text{C}$), and *s*-PMMA ($T_g = 115^\circ\text{C}$). *Trans* geometric isomers have higher T_g than *cis* isomers, as for example in the case of *cis*-polybutadiene ($T_g = -108^\circ\text{C}$) compared to *trans*-polybutadiene ($T_g = -18^\circ\text{C}$) or in the case of *cis*-polyisoprene ($T_g = -73^\circ\text{C}$) compared to *trans*-polyisoprene ($T_g = -53^\circ\text{C}$).

Table 4-8 Effect of Backbone Structure of the Crystalline-Melting Temperature of Polyesters Derived from Ethylene Glycol (HOCH₂CH₂OH)




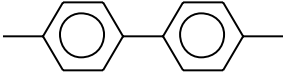
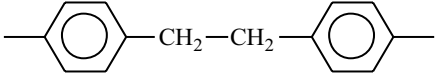
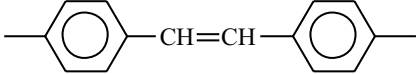
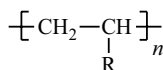
Compound	Main-Chain Unit, R	T_m ($^\circ\text{C}$)
A	—(CH ₂) ₄ —	50
B		270
C		355
D		220
E		420

Table 4-9 Glass-Transition Temperatures of Selected Vinyl Polymers



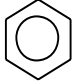
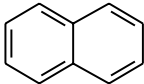
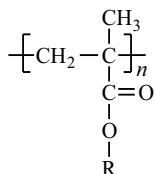
Polymer	Substituent Group, R	T_g ($^\circ\text{C}$)
Polyethylene	H	-125
Polypropylene (atactic)	CH ₃	-20
Poly(vinyl chloride)	Cl	89
Polyacrylonitrile	C≡N	100
Polystyrene		100
Poly(α -vinyl naphthalene)		135

Table 4-10 Effect of Increasing Size of the Substituent Groups on the Glass-Transition Temperature of Polymethacrylates

Polymethacrylate	Substituent Group, R	T_g (°C)
Poly(methyl methacrylate)	CH ₃	105
Poly(ethyl methacrylate)	CH ₂ CH ₃	65
Poly(propyl methacrylate)	CH ₂ CH ₂ CH ₃	35

4.3.4 Effect of Molecular Weight, Composition, and Pressure on T_g

Molecular-Weight Dependence. The glass-transition temperature increases with molecular weight at low molecular weight but reaches a point at moderate molecular weight where further increase in molecular weight has very little effect on T_g . This is an example of a *limiting-property relationship*. The crystalline-melting temperature, T_m , follows a similar dependence on molecular weight. The particular molecular-weight average most relevant to T_g is the number-average, \bar{M}_n (see Section 1.3.2). This dependence can be rationalized on the basis of the free-volume theory of the glass transition. Since larger free volume is associated with the ends of long polymer chains than with other chain segments, free volume increases with an increasing *number* of chain ends (i.e., decreasing molecular weight).

The form of dependence of T_g on molecular weight is approximated by the Fox–Flory eq. [20]

$$T_g = T_g^\infty - \frac{K}{\bar{M}_n} \quad (4.27)$$

where T_g^∞ is the limiting value of T_g at high molecular weight (obtained from the intercept of a plot of T_g versus reciprocal number-average molecular weight) and K is a constant for a given polymer. Equation (4.27) has been found to give a good fit of experimental data for many polymers; however, there is evidence that K may not be constant for molecular weights below about 10,000 [21]. Representative values of the Fox–Flory parameters, T_g^∞ and K , for some well-characterized polymers are given in Table 4-11.

Table 4-11 Fox–Flory Parameters

Polymer	T_g^∞ (K)	K (K)
Polydimethylsiloxane	148	5.9×10^3
Poly(vinyl chloride)	351	8.1×10^4
Polystyrene	373	1.2×10^5
Poly(methyl methacrylate)	387	2.1×10^5
Poly(α -methylstyrene)	446	3.6×10^5

Composition Dependence. When a second component, either a low-molecular-weight additive or a second polymer, is blended to form a *homogeneous* mixture, the T_g of the mixture will depend upon the amount of each component and upon the T_g of the second component. The form of the T_g –composition dependence may be approximated by several theoretical or semiempirical models.

An approximate relationship between the T_g of a miscible mixture and composition is given by the simple *rule of mixtures*, which for a binary mixture is given as

$$T_g = W_1 T_{g,1} + W_2 T_{g,2} \quad (4.28)$$

where W_1 is the weight fraction and $T_{g,i}$ (in Kelvins) is the glass-transition temperature of the i th component (i.e., component 1 or 2 in a binary mixture). For a multi-component mixture, we can write

$$T_g = \sum_{i=1}^N W_i T_{g,i} \quad (4.29)$$

The simple rule of mixtures is a good approximation for blends of two or more polymers but overestimates the T_g of polymers plasticized with a low-molecular-weight organic compound such as an ester or phthalate (see Section 7.1.1).

Improved predictive capability is available through a number of other empirical or theoretical relationships. One of the earliest theoretical expressions is the *Kelley–Bueche equation* [22], which is derived from the isofree volume model of the glass transition. At constant pressure and at a temperature, T , above the glass transition, the fractional free volume, f , is given as

$$f = f_g + \alpha_{f,1} (T - T_{g,1}) \phi_1 + \alpha_{f,2} (T - T_{g,2}) \phi_2 \quad (4.30)$$

where f_g is the fractional free volume at T_g ($f_g \approx 0.025$), α_f is the (isobaric) thermal-expansion coefficient (eq. (4.19)) of the *free volume* of the melt, and ϕ is the volume fraction of the diluent (1) or polymer (2), where $\phi_1 + \phi_2 = 1$. Since the thermal

expansion coefficient of free volume was not a parameter available at the time,* the assumption was made that it was the same as that of the bulk melt state, α , which can be determined by dilatometry (Section 4.3.2) or estimated with good confidence (e.g., eq. (4.24)). By equating T with the T_g of the mixture (whereby $f = f_g$), eq. (4.29) reduces to

$$\alpha_1(T_g - T_{g,1})\phi_1 + \alpha_2(T_g - T_{g,2})\phi_2 = 0 \quad (4.31)$$

which upon rearrangement gives the frequently used Kelley–Bueche expression

$$T_g = \frac{\alpha_1(1 - \phi_2)T_{g,1} + \alpha_2\phi_2T_{g,2}}{\alpha_1(1 - \phi_2) + \alpha_2\phi_2}. \quad (4.32)$$

A more recent relation [23] is based upon a classical thermodynamic treatment of the glass-transition temperature at which the entropies of the glass and liquid phases are equal. The resulting equation for a binary system is given as

$$\ln\left(\frac{T_g}{T_{g,1}}\right) = \frac{W_2\Delta C_{p,2} \ln(T_{g,2}/T_{g,1})}{W_1\Delta C_{p,1} + W_2\Delta C_{p,2}} \quad (4.33)$$

where ΔC_p is the change in specific heat at T_g (see eq. (4.20)). Assuming that the product $T_g\Delta C_p$ is constant for all polymers [24], eq. (4.32) reduces to the simpler form [23]

$$\ln\left(\frac{T_g}{T_{g,1}}\right) = \frac{W_2 \ln(T_{g,2}/T_{g,1})}{W_1(T_{g,2}/T_{g,1}) + W_2}. \quad (4.34)$$

If the $T_{g,s}$ of the polymer and diluent are not too different, a truncated Taylor series expansion of the log terms and rearrangement give the commonly used *inverse rule of mixtures*

$$\boxed{\frac{1}{T_g} = \frac{W_1}{T_{g,1}} + \frac{W_2}{T_{g,2}}} \quad (4.35)$$

which is known as the *Fox equation* when applied to T_g . The Fox equation has been considered to be an empirical relation; however, the preceding derivation shows that it may be viewed as representing a limiting case of the more general theoretical re-

* It is now possible to determine the thermal expansion coefficient of free volume by use of positron annihilation lifetime spectroscopy.

lationship. Another commonly used empirical relation that can be derived from eq. (4.32) is the *logarithmic rule of mixtures* given as

$$\boxed{\ln T_g = W_1 \ln T_{g,1} + W_2 \ln T_{g,2}}. \quad (4.36)$$

Pressure Dependence. Compared to effects of molecular weight and plasticization, T_g is relatively insensitive to pressure. The glass-transition temperature will increase with increasing pressure at a rate of approximately 25 K per kbar of pressure. The pressure dependence can be estimated from the compressibility and thermal expansion coefficients as

$$\frac{dT_g}{dp} = \frac{\Delta\beta}{\Delta\alpha}. \quad (4.37)$$

Effect of Heating Rate. The T_g has a small dependence on the heating or cooling rates in DSC and other methods of thermal characterization. Samples that are slowly heated through the glass transition exhibit a lower T_g than those that are rapidly heated due to the non-equilibrium state of the glass (see Section 4.1.2). The relationship between T_g (K) and the heating rate, q (K min^{-1}), is given in the form [25, 26]

$$T_g = a + b \ln q \quad (4.38)$$

where a and b are polymer-specific parameters (e.g., $a = 372.5$ K and $b = 4.02$ K for PS; $a = 383$ K and $b = 4.23$ K for PMMA).

Effect of Crosslinks. As a result of the restriction of long-range segmental motion, crosslinking elevates T_g . The form of the relationship between T_g and crosslink density is often given by the Fox–Loshaek equation [27]

$$T_g^c = T_g^o + k_c \rho_c \quad (4.39)$$

where T_g^c is the glass-transition temperature of the crosslinked polymer, T_g^o is the glass-transition temperature of the uncrosslinked polymer, k_c is a polymer-specific constant, and ρ_c represents the number of crosslinks per gram.

4.4 Mechanical Properties

4.4.1 Mechanisms of Deformation

At low strain (i.e., <1%), the deformation of most polymers is elastic, meaning that the deformation is homogeneous and full recovery can occur over a finite time. At higher strains, the deformation of glassy polymers occurs by either *crazing*, characteristic of brittle polymers, or by a process called *shear banding*, which is the dominant mechanism for ductile polymers. Such deformations are not reversible unless the polymer is heated above its glass-transition temperature.

Crazing. The term *crazing* owes its origin to the Middle English word *crasen*, which means “to break.” It was originally applied to describe a network of fine cracks appearing on the surface of ceramics and glasses. When some polymers such as polystyrene are deformed to a certain level, the critical strain (ϵ_c), what appear to be small cracks develop in a direction *perpendicular* to the principal direction of deformation. Some typical values of critical strains are given in Table 4-12. These crazes reflect light and result in visual cloudiness or whitening of the sample. Crazes developed in a polycarbonate tensile bar are shown in Figure 4-15.

Table 4-12 Critical Strains for Craze Initiation in Glassy Polymers

Polymer	Critical Strain (%)
Polystyrene	0.35
Styrene-acrylonitrile copolymer (SAN)	0.49
Poly(methyl methacrylate)	0.8–1.30
Poly(2,6-dimethyl-1,4-phenylene oxide)	1.5
Polycarbonate	1.8
Polysulfone	2.5

A craze is a unique morphological feature of polymers and is morphologically different from a true crack. A craze, which can be nanometers to a few micrometers in thickness, consists of polymer microfibrils (0.6 to 30 nm in diameter) stretched in the direction of tensile deformation. The microfibrils are surrounded by void space, which can represent as much as 90% of the total volume of the craze. This anisotropic morphology of a craze results in the scattering of light. An electron micrograph of typical craze structures is shown in Figure 4-16.

The time for the initiation of a craze depends upon many factors, including the magnitude of the applied stress, temperature, and the presence of low-molecular-weight liquids, which may act to promote craze development (see Section 6.1.3). Although the reasons for craze initiation are still uncertain and several different theories have been proposed, it is recognized that crazes constitute the defects from

which brittle cracks initiate. Mechanical fracture of a sample that has begun crazing is initiated by the breakdown of the fibrillar microstructure to form additional voids that grow slowly until some critical size has been reached. Beyond this point, the craze will rapidly propagate as a crack. As the crack propagates, crazes are formed at the crack tip and act to retard its advance.

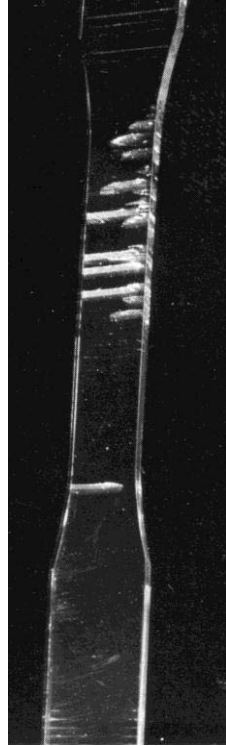


Figure 4-15 Visual view of crazes developed perpendicular to the tensile direction in a polycarbonate dogbone. Courtesy of R. P. Kambour.

Shear Banding. While some polymers such as polystyrene will readily craze when strained in tension, crazes may not develop in other polymers such as polycarbonate under identical conditions. Instead, these polymers will form regions of localized shear deformation. These regions are called shear bands, which develop at angles of 45° to the stretch direction. Other polymers such as SAN can exhibit both modes of deformation. In general, shear-band formation is a dominant mode of deformation during tensile yielding of ductile polymers.

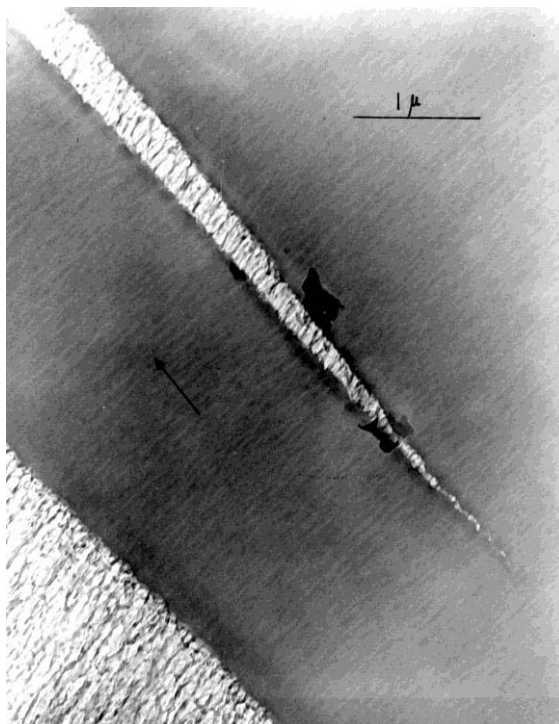


Figure 4-16 Scanning electron micrograph of craze structures in poly(2,6-dimethyl-1,4-phenylene oxide) [28]. The craze structure was preserved prior to microtoming by infusion of liquid sulfur. Courtesy of R. P. Kambour.

4.4.2 Methods of Testing

As the HDT indicates the temperature limits within which a plastic may be used, a variety of methods are used to determine mechanical performance under a variety of loading conditions. These may be classified as static (i.e., tensile and shear), transient (i.e., creep and stress relaxation), impact (Izod and Charpy), and cyclic (i.e., fatigue tests). Static tests are used to measure the force response when a sample is strained, compressed, or sheared at a constant rate. These provide a means to characterize the mechanical properties of a polymer in terms of modulus, strength, and elongation to failure. Transient tests measure the time response of the force (or stress) on a polymer sample when it is rapidly stretched to a given length (*stress relaxation*) or the time response of strain when a load (stress) is rapidly applied (*creep*). Impact tests measure the energy required for a sample to fail under different loading histories, while fatigue tests determine the number of cycles of applied stress required for failure.

Static Testing. Static tests refer to those for which the deformation rate is steady in time. While tensile, compressive, or shear modes may be employed, tensile testing is the most common. In a typical tensile test, a polymer sample, in the form of a dogbone (e.g., Figure 4-17), is clamped at one end and pulled at a constant rate of elongation at the other clamped end.* The thinner portion of the tensile specimen encourages the sample to fail at the center of the bar, where the stress is the highest, and not at the grip sites, where stress concentration may otherwise result in premature failure.

As indicated in Figure 4-17, the initial length of a central section contained within the narrow region of the tensile specimen is called the initial *gauge length*, L_0 . During deformation, force, F , is measured as a function of elongation at the fixed end by means of a transducer. Usually, the tensile response is plotted as *engineering* (nominal) *stress*, σ , versus *engineering* (nominal) *strain*, ε , where

$$\sigma = \frac{F}{A_0} \quad (4.40)$$

and

$$\varepsilon = \frac{\Delta L}{L_0}. \quad (4.41)$$

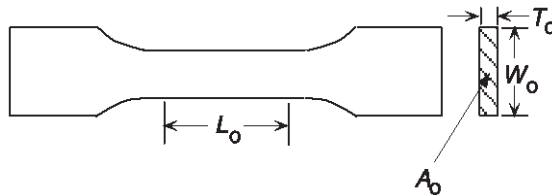


Figure 4-17 Illustration of a typical tensile-dogbone sample. The overall length of the specimens may vary from 63.5 to 246 mm. During tensile measurement, the sample is gripped at the wide ends. Specimen parameters include L_0 , gauge length (distance between test marks or extensometer span, ca. 50 mm); W_0 , initial width (19 or 29 mm); T_0 , initial thickness (4 to 14 mm); and A_0 , initial cross-sectional area.

In eq. (4.40), A_0 is the original (undeformed) cross-sectional area of the gauge region and ΔL in eq. (4.41) is the change in sample gauge length ($L - L_0$) due to the deformation.

* Conditions and sample dimensions for tensile tests are specified by ASTM D 638, "Tensile Properties of Plastics." For specimens of thickness up to 3.2 mm (1/8 in.), conditions and sample dimensions are given by ASTM D 1708, "Tensile Properties of Plastics by Use of Microtensile Specimens."

mation. Sample length can be determined from instrumental settings of the mechanical-testing instrument or by an extensometer, which is a strain gage that is attached to the gage-length region of the tensile specimen.

Alternatively, the stress-strain response of a sample may be reported in terms of true stress and true strain. The *true stress* is defined as the ratio of measured force to the *actual* cross-sectional area, A , at a given elongation

$$\sigma^T = \frac{F}{A}. \quad (4.42)$$

Since the actual cross-sectional area decreases as the sample is elongated, the true stress will always be larger than the engineering stress. Assuming that the volume of the sample remains constant during deformation, it can be shown (see Problem 4-1) that the true stress is simply related to the engineering stress as

$$\sigma^T = \sigma \frac{L}{L_0}. \quad (4.43)$$

The *true strain*, ε^T , is defined as

$$\varepsilon^T = \int_{L_0}^L \left(\frac{1}{\ell} \right) d\ell = \ln \left(\frac{L}{L_0} \right). \quad (4.44)$$

With the exception of elastomers, the assumption of a constant volume during deformation is not strictly correct, because the volume of glassy polymers increases, or dilates, during extension. This change in volume, ΔV , at a given strain may be calculated from the relation

$$\Delta V = V - V_0 = (1 - 2\nu)\varepsilon V_0 \quad (4.45)$$

where V_0 is the initial (unstrained) volume, ε is *true strain*, and ν is called *Poisson's ratio*, which is defined as the ratio of *true strain* in the transverse direction, ε_T , to the *true strain* in the longitudinal direction, ε_L , and is calculated as

$$\nu = -\frac{\varepsilon_T}{\varepsilon_L} = \frac{1}{2} \left[1 - \frac{1}{V} \left(\frac{\partial V}{\partial \varepsilon} \right) \right]. \quad (4.46)$$

For the majority of glassy polymers, $\nu \approx 0.4$, as shown by data for polystyrene, poly(methyl methacrylate), and poly(vinyl chloride) in Table 4-13. For completely incompressible materials, for which the term $(\partial V/\partial \varepsilon)$ within brackets in eq. (4.46) is zero, ν obtains its maximum value of 0.5 as approached by natural rubber and low-density polyethylene ($\nu = 0.49$).

Hooke's law for an ideal elastic solid provides a relationship between stress and strain for tensile deformation as

$$\boxed{\sigma = E\varepsilon} \quad (4.47)$$

where the proportionality factor, E , is called the tensile (or Young's) modulus. Conversely, the strain and stress are related by the tensile *compliance*, D , defined by

$$\varepsilon = D\sigma. \quad (4.48)$$

For tensile deformation, the compliance is therefore the reciprocal of the modulus

$$D = \frac{1}{E}. \quad (4.49)$$

Table 4-13 Poisson's Ratio of Some Common Polymers

Polymer	Poisson's Ratio
Natural rubber	0.49
Polycarbonate	0.40 ^a
Polyethylene (LD)	0.49
Poly(ethylene terephthalate)	0.43 ^a
Poly(methyl methacrylate)	0.37 ^a
Polystyrene	0.35 ^a
Poly(vinyl chloride)	0.39 ^a

^a From Seitz [29].

As shown by the representative stress-strain plot for a typical brittle polymer in Figure 4-18, only the initial portion of the plot follows Hookean behavior. The point at which stress begins to deviate from a linear stress-strain relation is called the *proportional limit*. This normally occurs before 1% strain. Therefore, to designate a value for the modulus, a convenient procedural definition must be adopted. Consequently, the initial slope of the stress-strain curve is called the *initial modulus*. Alternatively, a line may be drawn from the origin to some convenient point along the stress-strain curve, for example, at 1% strain. This line defines a secant and the slope defines the *secant modulus*, the 1% secant modulus in this case. The modulus, or the compliance, is a *material property* that is a function of both temperature and the time scale of the deformation.

Figure 4-19 shows a representative plot of modulus versus temperature. At temperatures below T_g , all glassy materials, polymeric as well as low-molecular-weight substances, have approximately the same value of modulus (ca. 10^9 Pa or 1 GPa). At first, this modulus slowly decreases with increasing temperature and then rapidly decreases in the region of T_g . For low-molecular-weight materials, modulus continues to fall rapidly with increasing temperature. For high-molecular-weight amorphous polymers, modulus drops to a secondary plateau region (approximately

10^6 Pa or 1 MPa) called the *rubbery plateau*. With further increase in temperature, the modulus again rapidly drops. This point marks the *viscous flow* region. Polymers are typically melt-processed in this temperature range in which the viscosity is also low

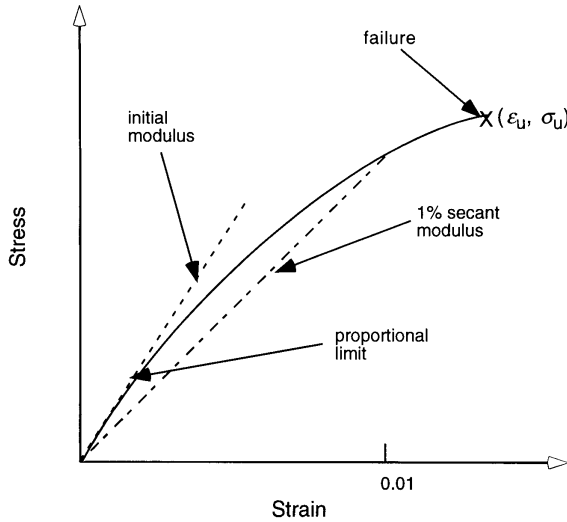


Figure 4-18 Idealized stress-strain curve for a polymer undergoing brittle failure.

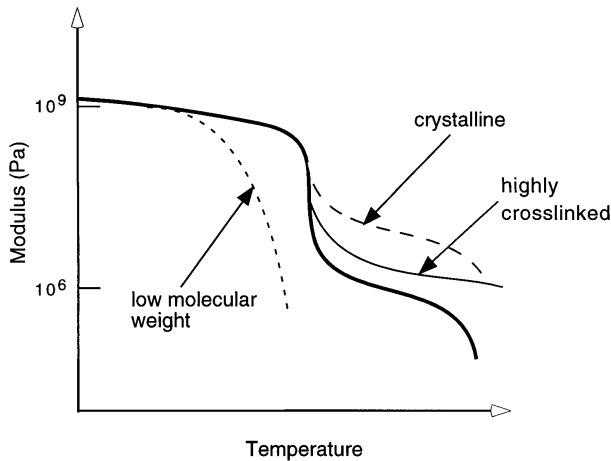


Figure 4-19 Plot of modulus versus temperature for high-molecular-weight amorphous polymers with variations for low-molecular-weight ($M < M_c$), crosslinked, and semicrystalline polymers.

The appearance of a rubbery plateau for high-molecular-weight polymers is the result of the formation of entanglements as described in Section 4.1.1. Entanglements prevent slippage at temperatures immediately above T_g and, therefore, modulus remains relatively high. Above T_g , the entanglements are easily disassociated due to high kinetic energy and the modulus drops. The rubbery plateau modulus, E_p , is inversely proportional to the molecular weight between entanglements, M_e (see Section 4.1.1), as

$$E_p \propto \frac{\rho RT}{M_e} \quad (4.50)$$

where ρ is density.

The temperature behavior of the modulus of semicrystalline polymers is qualitatively similar to that of high-molecular-weight amorphous polymers except that the modulus is typically higher in the secondary plateau (see Figure 4-19) due to the reinforcing effect of crystallites dispersed in an amorphous rubbery phase at temperatures above T_g but below T_m . At T_m , the crystallites melt and the modulus drops in the viscous-flow region.

In addition to tensile deformation, samples may be *compressed* (ASTM D 695) or *sheared*. In the case of compression, the sample is typically prepared in the form of a disk. The measured parameters are the bulk modulus, K , and compliance, B . A simple shear deformation of a solid is illustrated in Figure 4-20. The engineering *shear stress*, τ , is defined as

$$\tau = \frac{F}{A_o} \quad (4.51)$$

where A_o is the area of the *surface* on which the shear force acts. The shear strain, γ , is given by the angle of deformation, θ , as

$$\gamma = \tan \theta = \frac{\Delta X}{C} \quad (4.52)$$

Hooke's law for shear deformation is given as

$$\tau = G\gamma \quad (4.53)$$

where G is the shear modulus, while the shear compliance is normally designated as J ($\equiv 1/G$).

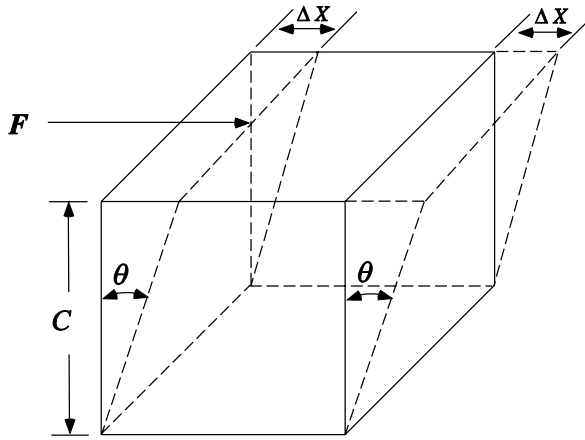


Figure 4-20 Illustration of the shear deformation of a solid with the shear force (F) acting on the top surface of the cube.

Moduli obtained in different deformation modes (tensile, compression, and shear) may be interrelated through Poisson's ratio, ν . For *isotropic* materials, the following relationships hold:

$$E = 2(1 + \nu)G, \quad (4.54)$$

$$J = 2(1 + \nu)D, \quad (4.55)$$

and

$$K = \frac{E}{3(1 - 2\nu)}. \quad (4.56)$$

In the limit of incompressibility (i.e., $\nu = 0.5$), eqs. (4.54), (4.55), and (4.56) reduce to

$$E = 3G, \quad (4.57)$$

$$J = 3D, \quad (4.58)$$

and

$$K \rightarrow \infty, \quad (4.59)$$

respectively. The limiting behavior for bulk modulus expressed by eq. (4.59) simply means that *incompressible* materials cannot be compressed.

Polymers exhibit a wide range of mechanical behavior depending upon temperature and rate of deformation. Typical stress-strain curves covering this range of

behavior are illustrated in Figure 4-21. At normal use temperatures, brittle polymers (e.g., polystyrene) exhibit a rapid increase in stress with increasing strain (i.e., high modulus) up to the point of sample failure (curve 1). The stress at failure is called the *ultimate stress* (σ_u) or stress-at-break (σ_b). Unlike modulus, ultimate stress, resulting from large and irreversible deformation, is a *sample* rather than material property and is strongly influenced by sample defects and processing history. For this reason, a sufficiently large number of samples must be evaluated and their values averaged in order to get a statistically meaningful value.

Ductile polymers, including many engineering thermoplastics, polyamides, and toughened (rubber-modified) plastics, exhibit stress-strain behavior represented by curves 2 and 3 in Figure 4-21. As shown, the stress reaches a maximum value, which is called its *yield stress*, σ_y , at a certain strain, ϵ_y . As strain is further increased, stress at first decreases. This process is called *strain softening*, which usually occurs at strains between 5% and 50%. A minimum in stress reached during strain softening is called the *draw stress*. At this point, the sample may either fail (curve 2) or experience *orientation hardening* (curve 3) prior to failure. During orientation hardening, polymer chains are stretched locally in the tensile direction. Chain extension causes a resistance to further deformation; stress is, therefore, observed to increase. Accompanying the molecular processes that are occurring during orientation are macroscopic changes in the shape of the tensile specimen. Above the yield point, a portion of the tensile dogbone begins to locally decrease in width or *neck* within the gage region. If orientation hardening occurs before sample failure, the neck is said to stabilize. This means that no further reduction in a cross-sectional area occurs and the neck propagates along the length of the gage region until the sample finally breaks. This process of neck propagation is called *cold drawing*.

The initial slope of the stress-strain plot for ductile polymers (curves 2 and 3 in Figure 4-21) is smaller than that observed for polymers that fail in a brittle mode (curve 1). In other words, the modulus of ductile polymers is lower. On the other hand, the energy required to deform the sample to the point of failure is much higher for ductile polymers, as indicated by comparison of the areas under the stress-strain curves for a brittle (curve 1) and for a ductile polymer (curve 3). This means that ductile polymers are able to absorb more energy upon impact.

Rubbery polymers follow stress-strain behavior similar to that of curve 4. Modulus is low, but ultimate extension can be very high, on the order of several hundred percent. Before failure, the rubber may experience an increase in stress as a consequence of strain-induced crystallization caused by molecular orientation in the stretch direction, as discussed in Chapter 5.

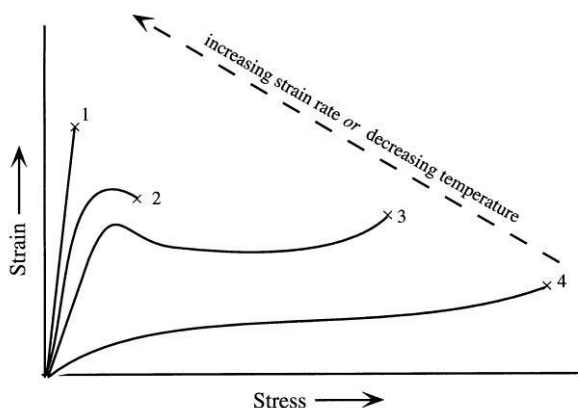


Figure 4-21 Typical stress-strain curves for samples exhibiting brittle failure (curve 1), ductile failure with neck formation (curve 2), ductile failure with cold drawing and orientational hardening (curve 3), and rubbery behavior with evidence of strain-induced crystallization (curve 4). Point of failure is indicated by the symbol \times .

Typical values of modulus, yield strength (stress-at-yield), ultimate strength (stress-at-break), and elongation-to-break for a variety of important thermoplastics are given in Table 4-14. The exact nature of the tensile response of a polymeric material depends upon the chemical structure of the polymer, conditions of sample preparation, molecular weight, molecular-weight distribution, crystallinity, and the extent of any crosslinking or branching. The mechanical response also depends in a very significant way on temperature and the rate of deformation. As illustrated by Figure 4-21, any amorphous polymer can exhibit the entire range of tensile behavior, from brittle to rubbery response, by increasing the testing temperature from room temperature to above the T_g of the polymer or (to a lesser extent) by decreasing the rate of deformation.*

The combined effect of temperature and strain rate on the stress-strain curve of an elastomer can be represented by a *failure envelope*, as shown in Figure 4-22. The ordinate is nominal stress-to-break normalized to an arbitrary reference temperature. All values of ultimate strength obtained over a wide range of temperatures and strain rates comprise points on the outer failure envelope (heavy curve). The curves originating at the origin are selected stress-strain curves at different temperatures and strain rates. As the failure envelope shows, either increasing the strain rate or

* It should be noted that polymers that appear brittle in tensile tests can appear to yield when tested in compression at the same temperature.

decreasing the testing temperature causes the ultimate strength of the sample to decrease.

Table 4-14 Mechanical Properties of Representative Polymers

Polymer	Elastic Modulus (GPa) ^a	Yield Strength (MPa)	Ultimate Strength (MPa)	Elongation to Break (%)
Polycarbonate	2.4	55-69	55-69	60-120
Polyethylene (low-density)	0.14-0.28	6.9-14	10-17	400-700
Poly(methyl methacrylate)	2.4-2.8	48-62	48-69	2-10
Polypropylene	1.0-1.6	23	24-38	200-600
Polystyrene	2.8-3.5	—	38-55	1-2.5
Polytetrafluoroethylene	0.41	10-14	14-28	100-350
Poly(vinyl chloride) (rigid)	2.1-4.1	55-69	41-76	5-60

^a To convert GPa to psi, multiply by 1.45×10^5 ; to convert MPa to psi, multiply by 145.

Transient Testing. As mentioned earlier, two types of transient mechanical tests are creep and stress-relaxation measurements, which can be used to characterize the dimensional stability of a material. A creep test measures the elongation of a specimen subjected to a rapid application of a constant load, σ_0 , at constant temperature. By contrast, a stress-relaxation test records the stress required to hold a specimen at a fixed elongation, ϵ_0 , at constant temperature.

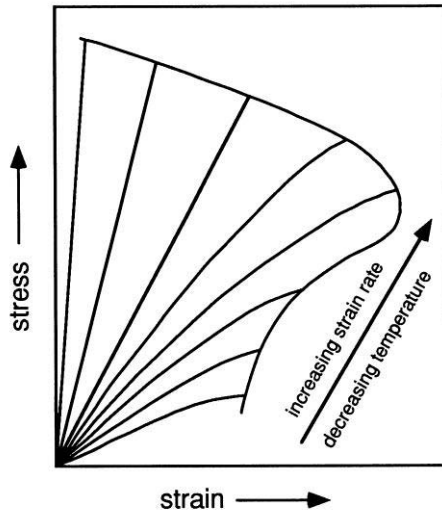


Figure 4-22 Effect of temperature and strain rate on the stress-strain curve.

Creep tests can be made in shear, torsion, flexure, or compression modes, as well as in tension. Results of these tests are particularly important for selecting a polymer that must sustain loads for long periods. Usually, the parameter of interest is the tensile *compliance*, D , which is the ratio of strain to stress. While the stress, σ_0 , is held constant during a creep test, the strain depends upon the time during which the load has been applied and, therefore, the compliance also becomes a function of time as

$$D(t) = \frac{\varepsilon(t)}{\sigma_0}. \quad (4.60)$$

The response of different materials—ideal elastic, ideal viscous, and viscoelastic—to a step change in stress (or load) is illustrated in Figure 4-23. For an ideal (Hookean) elastic material, the resulting strain is instantaneous and constant during the duration of the applied stress. When the load is removed at $t = t'$, the strain instantaneously drops to zero (Figure 4-23A). This follows from Hooke's law applied to the case of a constant stress:

$$\varepsilon = D\sigma_0 = \varepsilon_0. \quad (4.61)$$

In the case of an ideal (Newtonian) viscous fluid, the strain response is obtained by integration of Newton's law of viscosity ($\sigma = \eta\dot{\varepsilon}$) arranged as

$$\varepsilon = \int_0^{t'} (\sigma_0/\eta) dt = (\sigma_0/\eta)t. \quad (4.62)$$

Here, the strain increases linearly with increasing time until the load is removed at $t = t'$, at which time the strain remains constant ($\sigma_0 t'/\eta$) in time (Figure 4-23B) unless an additional load is applied. The deformation is said to be permanent since no elastic recovery is possible.

In the case of a viscoelastic material, recovery can occur due to the elastic contribution of the material. For viscoelastic materials, the strain response will have some of the character of both elastic and viscous materials, as shown in Figure 4-23C. The initial portion of the strain recovery is elastic (i.e., instantaneous) while full recovery is delayed to longer times due to the viscous contribution. The actual viscoelastic response can be reasonably modeled by analyzing the strain response of series or parallel combinations of ideal elastic springs and ideal viscous dashpots (shock absorbers) as discussed in Section 5.1.2.

Instrumentation for creep testing can be a simple laboratory setup whereby a plastic film or bar is clamped at one end to a rigid support (normally enclosed in a temperature-controlled chamber) and a weight is added to the opposite end. The deformation of the loaded specimen is then measured by following the relative movement of two marks, inscribed on the sample, by means of a cathetometer, or traveling microscope.

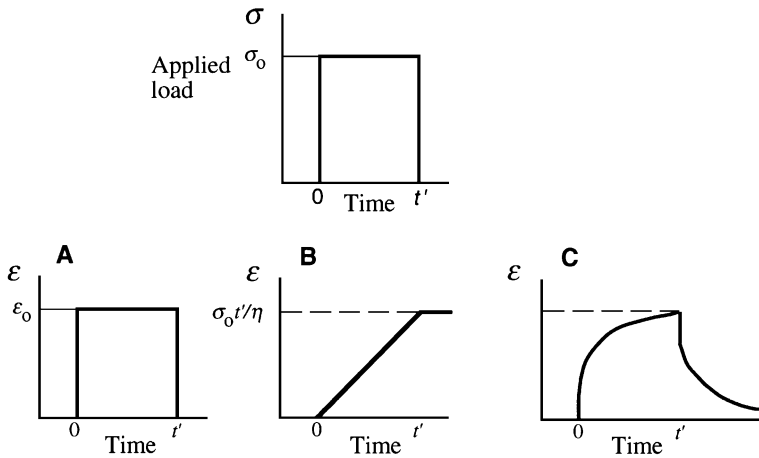


Figure 4-23 Response of different idealized materials to an instantaneous application of a stress at $t = 0$. **A.** Elastic. **B.** Viscous. **C.** Viscoelastic.

Typical creep curves of a low- T_g polymer measured over four decades of time and at several temperatures are shown in Figure 4-24A. As illustrated, creep compliance increases with increasing temperature. This means that the sample softens as temperature is increased, as experience would suggest. As discussed later in Chapter 5 (Section 5.1.6), individual creep curves obtained at different temperatures over short time periods (Figure 4-24A) can be shifted horizontally to yield a master curve at a given temperature and cover a wider range of temperatures. Such a creep master curve showing three regions of viscoelastic behavior is illustrated in Figure 4-24B.

Stress-relaxation experiments can be conveniently performed with the same commercial instruments used in tensile tests. Since deformation must be as close as possible to being instantaneous, the preferred instrumentation is hydraulically driven, rather than screw-driven, tensile testing machines. A rapid extension is applied to the sample and the stress on the sample is measured as a function of time by means of a force transducer. In a stress-relaxation experiment, stress is a function of time and, therefore, the stress-relaxation modulus, E_r ,

$$E_r(t) = \frac{\sigma(t)}{\epsilon_0} \quad (4.63)$$

is also time dependent. Typical stress-relaxation curves are shown in Figure 4-25.

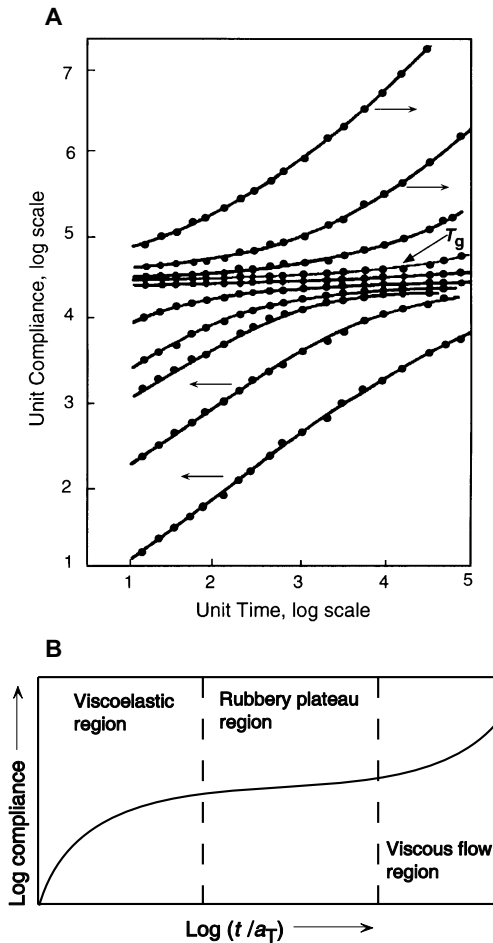


Figure 4-24 A. Plots of creep compliance as a function of time at different temperatures. Arrows show direction of the horizontal shift of data to obtain a master curve at a reference temperature taken as the T_g of the polymer. B. Creep master curve obtained by time-temperature superposition.

The measurement of a full range of stress-relaxation (or creep-compliance) behavior at a given temperature can take years. Fortunately, it is possible to shift data taken over shorter time periods but at different temperatures to construct a master curve covering a longer time scale at some reference temperature. The principle that allows horizontal shifting of data is called *time-temperature superposition*, which is discussed in Section 5.1.6. The result of this shifting of data over a limited time span to form a master curve was shown for creep compliance in Figure 4-24 and is shown for stress-relaxation modulus in Figure 4-25.

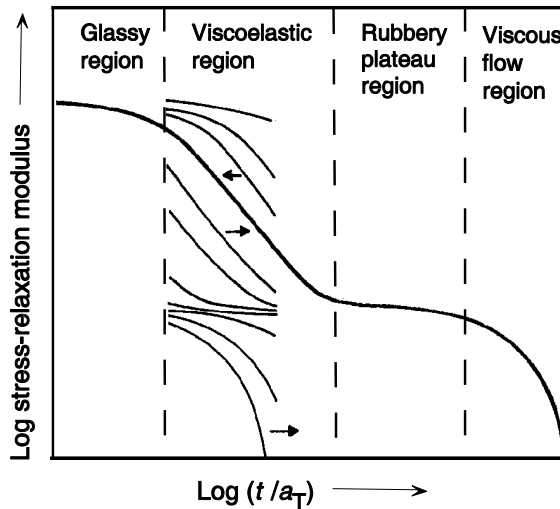


Figure 4-25 Stress-relaxation modulus as a function of time. Arrows show directions of shift to obtain a master curve at reference temperature.

Impact Testing. Impact tests measure the energy expended up to failure under conditions of rapid loading. There are a number of different types of impact tests. These include the widely used Izod and Charpy tests in which a hammer-like weight strikes a specimen and the energy-to-break is determined from the loss in the kinetic energy of the hammer. Other variations include the falling ball or dart test, whereby the energy-to-break is determined from the weight of the ball and the height from which it is dropped. Values of impact strength may also be calculated from the area under the stress-strain curve in high-speed tensile tests. Instrumented impact testing provides a complete report of the load applied to the specimen during the entire impact event and yields information on deformation and fracture processes [30].

Information obtained from impact tests may be used to determine whether a given plastic has sufficient energy-absorbing properties to be useful for a particular application, such as plastics for beverage bottles or window replacement. In such cases, it is important that the material be tested at temperatures and impact conditions close to those of actual use because impact strength will decrease with decreasing temperature and with increasing rate of deformation. The presence of defects that act as stress concentrators will also reduce impact strength. In order to standardize impact results or to study the effect of cracks and other defects on impact properties, samples with inscribed notches of specified dimensions are often used. Typical values of notched-Izod impact strengths for several important polymers are given in Table 4-15. Brittle polymers, such as polystyrene, have very low

impact strengths, while many engineering thermoplastics (e.g., polycarbonate) are very impact resistant.

Table 4-15 Values of Notched-Izod Impact Strength for Some Representative Thermoplastics

Polymer	Impact Strength ^a (J m ⁻¹)
Polystyrene	13–21
Poly(vinyl chloride)	21–160
Polypropylene	27–107
Polystyrene (high-impact)	27–427
Polyethylene (high-density)	27–1068
ABS	53–534
Polysulfone	69–267
Polycarbonate	641–961
Polyethylene (low-density)	854

^a To convert J m⁻¹ to ft-lbf in.⁻¹, divide by 53.38.

Generally, amorphous polymers with large bulky substituent groups and non-linear backbones are brittle. Unoriented crystalline structure also contributes to brittleness in polymers whose T_g is above the testing temperature. Some correlation may exist between the presence of pronounced low-temperature secondary relaxations corresponding to small-scale motions of the chain backbone and the impact properties of many ductile polymers. Brittle polymers can be made to be more impact resistant by dispersing small (<0.1- μ m-diameter) rubber particles within the polymer matrix, as in the case of high-impact polystyrene (HIPS) and ABS resins (see Section 7.2.2). Good adhesion between the rubbery inclusions and brittle matrix polymers is important for high impact resistance and is typically achieved by grafting the rubber and matrix (glassy) polymers.

Fatigue Testing. Fatigue tests are used to determine the number of cycles (N) of applied strain at a given level of stress that a sample can sustain before complete failure. This number of cycles to failure is called the *fatigue life*. The *endurance limit* is the maximum value of applied stress for which failure will not occur regardless of how many cycles the stress is applied. Typically, the value of stress leading to failure at a given N is 20% to 40% of the static tensile strength. The fatigue life decreases with increasing frequency of oscillation and as temperature is decreased. Information obtained by means of fatigue tests is extremely important in evaluating engineering and composite materials considered for load-bearing applications or when frequent periodic stress loading may be encountered, as for example in a plastic hinge joint. A representative fatigue curve is illustrated in Figure 4-26.

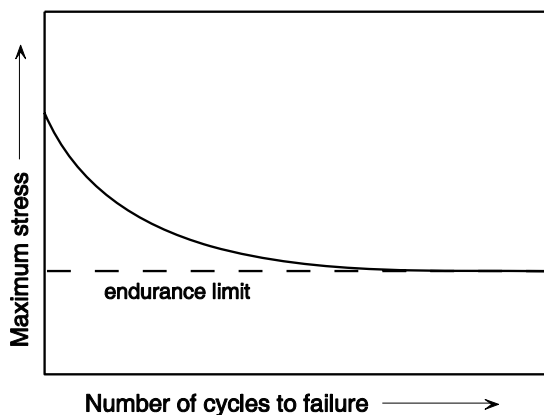


Figure 4-26 Representative fatigue curve.

4.5 Solid-State Characterization Methods

4.5.1 Microscopy

All types of microscopy, including optical and electron microscopy, have been used to investigate the morphology of polymeric materials. These include crystalline polymers, block copolymers, polymer blends, fibers, and composites. In this chapter, Figure 4-5 showed crystalline spherulites of polypropylene as seen by scanning electron microscopy (SEM). A scanning electron micrograph of the craze structures of poly(2,6-dimethyl phenylene oxide) was shown in Figure 4-16. Other illustrations appear in several chapters in this text.

Polymer surface morphology can be characterized at high magnification and resolution by traditional methods of electron microscopy such as SEM and transmission electron microscopy (TEM). During the 1980s, two related methods—scanning tunneling microscopy (STM) and atomic force microscopy (AFM) [31]—were introduced. This new class of microscopy, especially AFM, offered superior resolution with few of the specialized sample preparations such as microtomy, etching, staining, or gold coating that are required for SEM and TEM studies. AFM can be used to investigate polymer crystallinity [32, 33] and for characterizing the surface morphology of polymer films, fibers, coatings, and injection-molded parts at high magnification and resolution up to 0.1 nm. AFM is used particularly for characterizing multiphase polymer systems. As illustrated in Figure 4-27A, both AFM and STM employ a very sharp tip to probe and map the morphology of the surface; however, both the tip and polymer surface need to be conductive for STM measurements, which limits its applicability to polymers. The tip in AFM is typically

silicon (or silicon nitride) with a $\sim 10\text{--}20\text{-nm}$ apex diameter mounted on a rectangular silicon cantilever. Tip–surface interactions can occur by van der Waals, electrical, or magnetic forces [34] that are measured by deflection of the cantilever. An atomic force micrograph showing the detailed lamellae structure of a propylene–ethylene copolymer is shown in Figure 4-27B.

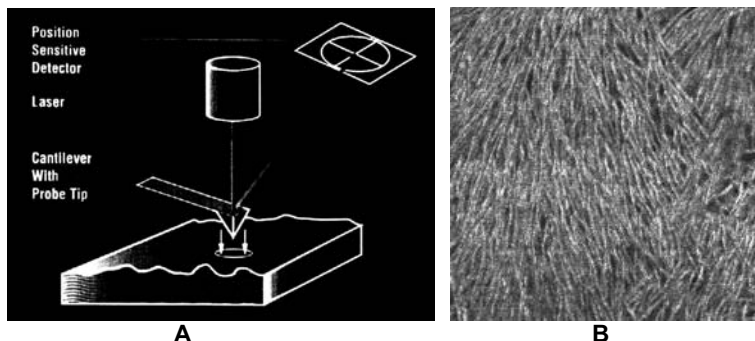


Figure 4-27 **A.** Basic design of an atomic force microscope [33]. Annual Review of Materials Science by Annual Reviews. Reproduced with permission of Annual Reviews in the format. Reproduced in a book via Copyright Clearance Center. **B.** AFM phase image showing radial orientation of crystalline lamellae in a film of a propylene–ethylene random copolymer (15 mole % ethylene) crystallized at 45°C. Courtesy of R. Alamo.

4.5.2 Scattering Methods

A variety of scattering methods have been used for polymer characterization. Light scattering of dilute polymer solutions to determine weight-average molecular weight and chain conformations was discussed in Section 3.3.2. As covered in Section 4.2.4, wide-angle X-ray scattering (WAXS) can be used to determine the fractional crystallinity of semicrystalline polymers and to determine the Bragg spacing [16]. Polymers also can be characterized by small-angle neutron, X-ray, and light scattering [35]. In the case of light scattering, scattering contrast depends upon the difference between the refractive indices of the polymer and its surroundings. Light scattering is useful when the characteristic dimension (D) of the scatterer is greater than $\lambda/4\pi$ where λ is the wavelength of light. Neutron scattering can provide information about both the structure and dynamics of a polymer system. Thermal neutrons have wavelengths in the 2–25 Å range. Examples where small-angle neutron scattering (SANS) has been used to study structure include polymer solutions, blends, gels, nanomaterials, membranes, micelles, and grafted and branched polymers [36].

SUGGESTED READING

ENTANGLEMENTS

de Gennes, P.-G., *Entangled Polymer*. Physics Today, June 1983, p. 33.

Porter, R. S., and J. F. Johnson, *The Entanglement Concept in Polymer Systems*. Chemical Reviews, 1966. **66**: p. 1.

Porter, R. S., W. J. MacKnight, and J. F. Johnson, *Viscous and Elastic Behavior Attributed to Polymer Entanglements*. Rubber Chemistry and Technology, 1967. **40**: p. 1.

THE GLASSY STATE

Eisenberg, A., *The Glassy State and the Glass Transition*, in *Physical Properties of Polymers*. 2nd ed. J. E. Mark, A. Eisenberg, W. W. Graessley, L. Mandelkern, E. T. Samulski, J. L. Koenig, and G. D. Wignall, eds. 1993, Washington, DC: American Chemical Society, p. 61.

Goldstein, M. and R. Simha, eds., *The Glass Transition and the Nature of the Glassy State*. Annals of the New York Academy of Sciences, 1976. **279**: p. 68.

Haward, R. N., ed., *The Physics of Glassy Polymers*. 1973, New York: John Wiley & Sons.

Hutchinson, J., *Physical Aging of Polymers*. Progress in Polymer Science, 1995. **20**: p. 703.

CRYSTALLINITY

Long, Y., R. A. Shanks, and Z. H. Stachurski, *Kinetics of Polymer Crystallisation*. Progress in Polymer Science, 1995. **20**: p. 651.

Mandelkern, L., *The Crystallization of Flexible Polymer Molecules*. Chemical Reviews, 1956. **56**: p. 903.

Mandelkern, L., *The Crystalline State*, in *Physical Properties of Polymers*. 2nd ed. J. E. Mark, A. Eisenberg, W. W. Graessley, L. Mandelkern, E. T. Samulski, J. L. Koenig, and G. D. Wignall, eds. 1993, Washington, DC: American Chemical Society, 1993, p. 145–200.

Philips, P. J., *Polymer Crystals*. Reports on Progress in Physics, 1990. **53**: p. 549.

Samuels, R. J., *Structured Polymer Properties*. 1974, New York: John Wiley & Sons.

Sanchez, I. C., *Modern Theories of Polymer Crystallization*. Journal of Macromolecular Science—Reviews in Macromolecular Chemistry, 1974. **C10**: p. 113.

Sanchez, I. C., and E. A. DiMarzio, *Dilute Solution Theory of Polymer Crystal Growth: A Kinetic Theory of Chain Folding*. Journal of Chemical Physics, 1971. **55**: p. 893.

Sanchez, I. C., and R. K. Eby, *Crystallization of Random Copolymers*. Journal of Research National Bureau of Standards, 1973. **77A**: p. 353.

Schultz, J. M., *Polymer Crystallization*. 2001, Washington DC: American Chemical Society.

MECHANICAL PROPERTIES

Aklonis, J. J., *Mechanical Properties of Polymers*. Journal of Chemical Education, 1981. **58**: p. 892.

Boyd, R. H., *The Conformational Analysis of Crankshaft Motions in Polyethylene*. Macromolecules, 1974. **7**: p. 855.

- Hutchinson, J. H., *Physical Aging of Polymers*. Progress in Polymer Science, 1995. **20**: p. 703.
- Nielsen, L. E., *Cross-Linking Effect on Physical Properties of Polymers*. Journal of Macromolecular Science—Review in Macromolecular Chemistry, 1969. **C3**: p. 69.
- Savadori, A., *Impact Testing of Plastics: Present Knowledge*. Polymer Testing, 1985. **5**: p. 209.
- Stachurski, Z. H., *Deformation Mechanisms and Yield Strength in Amorphous Polymers*. Progress in Polymer Science, 1997. **22**: p. 407.
- Ward, I. M., and D. W. Hadley, *An Introduction to the Mechanical Properties of Solid Polymers*. Chichester: John Wiley & Sons, 1993.

CHARACTERIZATION METHODS

- Bershtein, V. A., and V. M. Egorov, *Differential Scanning Calorimetry of Polymers*. Chichester: Ellis Horwood, 1994.
- Roe, R.-J., *Methods of X-Ray and Neutron Scattering in Polymer Science*. New York: Oxford University Press, 2000.
- Sawyer, L. C., and D. T. Grubb, *Polymer Microscopy*. 1987, London: Chapman and Hall.
- Stein, R. S., and M. Srinivasarao, *Fifty Years of Light Scattering: A Perspective*. Journal of Polymer Science: Part B: Polymer Physics, 1993. **31**: p. 2003.
- Turi, E. A., ed., *Thermal Characterization of Polymeric Materials*. 1981, New York: Academic Press.
- Wunderlich, B., *Thermal Analysis of Macromolecules*. Journal of Thermal Analysis, 1996. **46**: p. 643.
- Zoller, P., and D. Walsh, *Standard Pressure–Volume–Temperature Data for Polymers*. 1995, Lancaster, PA: Technomic.

PROBLEMS

- 4.1** Show that $\sigma^T = \sigma(1 + \varepsilon)$ for an incompressible material.
- 4.2** A tensile strip of polystyrene that is 10 cm in length, 5 cm in width, and 2 cm in thickness is stretched to a length of 10.5 cm. Assuming that the sample is isotropic and deforms uniformly, calculate the resulting width and the percent volume change after deformation.
- 4.3** A polymer has a crystalline growth parameter (n) of 2 and a rate constant (k) of 10^{-2} s^{-2} at 100°C . The polymer is melted and then quenched to 100°C and allowed to crystallize isothermally. After 10 s, what is the percent crystallinity of the sample?
- 4.4** What is the percent volume change that is expected at 100% elongation of natural rubber, assuming that no crystallization occurs during deformation?
- 4.5** Give your best estimate for the weight fraction of plasticizer required to lower the T_g of poly(vinyl chloride) (PVC) to 30°C . Assume that the T_g of PVC is 356 K and that of the plasticizer is 188 K. No other information is available.

4.6 Show that the inverse rule of mixtures given by eq. (4.35) can be obtained from the generalized relationship given by eq. (4.33) when $T_{g,1} \approx T_{g,2}$.

4.7 Polytetrafluoroethylene has been reported to exhibit a negative Poisson ratio. Explain why this polymer exhibits this unusual behavior.

4.8 A sample of poly(ethylene terephthalate) is reported to be 20% crystalline.

(a) What is the expected density of this sample?

(b) What is the expected specific heat increment of this semicrystalline sample?

(c) What is the expected heat of fusion of this sample?

4.9 Twenty wt% of a styrene oligomer having a number-average degree of polymerization of 7 is mixed with a commercial polystyrene sample having a number-average molecular weight of 100,000.

(a) What is the T_g (K) of the styrene oligomer?

(b) What is the T_g (K) of the polystyrene mixture?

4.10 The 1% secant modulus of a polystyrene sample is 3 GPa.

(a) What is the nominal stress (MPa) of this sample at a nominal strain of 0.01?

(b) What is the true stress (MPa) of this sample at a nominal strain of 0.01?

(c) What is the percent change in volume of this sample at the nominal strain of 0.01?

4.11 If the Young's modulus of a sample of polystyrene is determined to be 3 GPa at room temperature, calculate its shear modulus.

4.12 Isotactic poly(methyl methacrylate) has a much lower T_g than the corresponding syndiotactic polymer. How can isotactic and syndiotactic PMMA be polymerized? Explain why the isotactic polymer has the lower T_g .

REFERENCES

1. Wool, R. P., *Polymer Entanglements*. Macromolecules, 1993. **26**: p. 1564–1569.
2. Graessley, W. W., *The Entanglement Concept in Polymer Rheology*. Advances in Polymer Science, 1974. **16**: p. 1–179.
3. Heymans, N., *Diffuse versus Point Entanglements—Homopolymers and Blends*. Journal of Materials Science, 1986. **21**: p. 1919–1926.
4. de Gennes, P. G., *Reptation of a Polymer Chain in the Presence of Fixed Obstacles*. Journal of Chemical Physics, 1971. **55**(2): p. 572–579.
5. Klein, J., *Evidence for Reptation in an Entangled Melt*. Nature, 1978. **271**(5641): p. 143–145.

6. Cohen, M. H., and D. Turnbull, *Molecular Transport in Liquids and Glasses*. Journal of Chemical Physics, 1959. **31**(5): p. 1164–1169.
7. van Krevelen, D. W., *Properties of Polymers*. 3rd ed. 1990, Amsterdam: Elsevier.
8. Gibbs, J. H., and E. A. DiMarzio, *Nature of the Glass Transition and the Glassy State*. Journal of Chemical Physics, 1958. **28**(3): p. 373–383.
9. Boyd, R. H., and S. M. Breitling, *The Conformational Analysis of Crankshaft Motions in Polyethylene*. Macromolecules, 1974. **7**(6): p. 855–862.
10. Fried, J. R., *Sub- T_g Transitions*, in *Physical Properties of Polymers Handbook*, J. E. Mark, ed. 2007, New York: Springer, p. 217–232.
11. Tanaka, T., Y. Chatani, and H. Tadokoro, *Crystal Structure of Polyisobutylene*. Journal of Polymer Science: Polymer Physics Edition, 1974. **12**: p. 515–531.
12. Stein, R. S., *A Comment on “Incompatible Blends: Thermal Effects in a Model System”*. Journal of Polymer Science: Polymer Physics Edition, 1981. **19**: p. 1281.
13. Avrami, M., *Kinetics of Phase Change. I. General Theory*. Journal of Chemical Physics, 1939. **7**: p. 1103–1112.
14. Avrami, M., *Kinetics of Phase Change. II. Transformation-Time Relations for Random Distribution of Nuclei*. Journal of Chemical Physics, 1940. **8**: p. 212–224.
15. Phillips, P. J., and H. T. Tseng, *Influence of Pressure on Crystallization in Poly(ethylene terephthalate)*. Macromolecules, 1989. **22**: p. 1649–1655.
16. Mo, Z., and H. Zhang, *The Degree of Crystallinity in Polymers by Wide-Angle X-Ray Diffraction (WAXD)*. Journal of Macromolecular Science—Reviews in Macromolecular Chemistry and Physics, 1995. **35**: p. 555–580.
17. Ehrenfest, P., Leiden Comm. Suppl., 1933. **76b**.
18. Flory, P. J., L. Mandelkern, and H. K. Hall, *Crystallization in High Polymers. VII. Heat of Fusion of Poly(N,N-sebacoylpiperazine) and Its Interaction with Diluents*. Journal of the American Chemical Society, 1951. **73**: p. 2532–2538.
19. Simha, R., and R. F. Boyer *On a General Relation Involving the Glass Temperature and Coefficients of Expansion of Polymers*. Journal of Chemical Physics, 1962. **37**(5): p. 1003–1007.
20. Fox, T. G., and P. J. Flory, *Second-Order Transition Temperatures and Related Properties of Polystyrene. I. Influence of Molecular Weight*. Journal of Applied Physics, 1950. **21**: p. 581–591.
21. Boyer, R. F., *Variation of Polymer Glass Transition Temperatures with Molecular Weight*. Macromolecules, 1974. **7**(1): p. 142–143.
22. Kelley, F. N., and F. Bueche, *Viscosity and Glass Temperature Relations for Polymer-Diluent Systems*. Journal of Polymer Science, 1961. **50**: p. 549–556.
23. Couchman, P. R., and F. E. Karasz, *A Classical Thermodynamic Discussion of the Effect of Composition on Glass-Transition Temperatures*. Macromolecules, 1978. **11**(1): p. 117–119.
24. Fried, J. R., and S.-Y. Lai, *Experimental Assessment of the Thermodynamic Theory of the Composition Variation of T_g : PVC Systems*. Journal of Applied Polymer Science, 1982. **27**: p. 2869–2883.
25. Judovits, L. H., et al., *The Heat Capacity of Solid and Liquid Polystyrene, p-Substituted Polystyrenes, and Crosslinked Polystyrenes*. Journal of Polymer Science: Part B: Polymer Physics, 1986. **24**: p. 2725–2741.
26. Moynihan, C. T., et al., *Dependence of the Glass Transition Temperature on Heating and Cooling Rate*. Journal of Physical Chemistry, 1974. **78**: p. 2673–2677.
27. Fox, T. G., and S. Loshaek, *Influence of Molecular Weight and Degree of Crosslinking on the Specific Volume and Glass Temperature of Polymers*. Journal of Polymer Science, 1955. **15**: p. 371–390.

28. Kambour, R. P., and A. S. Holik, *Electron Microscopy of Crazes in Glassy Polymers: Use of Reinforcing Impregnants during Microtomy*. *Journal of Polymer Science: Part A-2*, 1969. **7**: p. 1393–1403.
29. Seitz, J. T., *The Estimation of Mechanical Properties of Polymers from Molecular Structure*. *Journal of Applied Polymer Science*, 1993. 1331-1351.
30. Radon, J. C., *Application of Instrumented Impact Test in Polymer Testing*. *Journal of Applied Polymer Science*, 1978. **22**: p. 1569-1581.
31. Binnig, G., C. F. Quate, and C. Gerber, *Atomic Force Microscope*. *Physical Review Letters*, 1986. **56**(9): p. 930-933.
32. Hobbs, J. K., O. E. Farrance, and L. Kailas, *How Atomic Force Microscopy Has Contributed to Our Understanding of Polymer Crystallization*. *Polymer*, 2009. **50**: p. 4281-4292.
33. Magonov, S. N., and D. H. Reneker, *Characterization of Polymer Surfaces with Atomic Force Microscopy*. *Annual Review of Materials Science*, 1997. **27**: p. 175-222.
34. Meyer, E., *Atomic Force Microscopy*. *Progress in Surface Science*, 1992. **41**: p. 3-49.
35. Higgins, J. S., and R. S. Stein, *Recent Developments in Polymer Applications of Small-Angle Neutron, X-ray and Light Scattering*. *Journal of Applied Crystallography*, 1978. **11**: p. 346-375.
36. Hammouda, B., *SANS from Polymers—Review of the Recent Literature*. *Journal of Macromolecular Science—Polymer Reviews*, 2010. **C50**: p. 14–29.

Viscoelasticity and Rubber Elasticity

At the extremes, a polymer may exhibit mechanical behavior characteristic of either an elastic solid or a viscous liquid. The actual response depends upon temperature, in relation to the glass-transition temperature (T_g) of the polymer, and upon the time scale of the deformation. Under usual circumstances, the mechanical response of polymeric materials will be intermediate between that of an ideal elastic or viscous liquid. In other words, polymers are *viscoelastic*. This behavior is readily illustrated by Silly Putty, which is a silicone rubber having a low T_g . If rolled up into a ball and dropped to the floor, it will bounce with the resilience of a rubber ball. This is a manifestation of elastic behavior resulting from rapid deformation. If left on a desk for several days, the ball will flatten—it will flow like a viscous liquid over a long time. If pulled at a moderate rate of strain, the ball will elongate with high extension and eventually fail. This chapter seeks to develop the fundamental concepts of polymer viscoelasticity and rubber elasticity and to describe the basic experimental methods used to study these properties.

5.1 Introduction to Viscoelasticity

Viscoelastic behavior may be characterized by a variety of techniques that record the time-dependent response of a polymeric solid, melt, or solution to a periodic perturbation such as the application of a sinusoidal strain or an electrical voltage. The most commonly used method to measure viscoelastic properties as a function of temperature and time (frequency) is dynamic-mechanical analysis, which records the stress response to an application of a sinusoidal strain. In comparison, dielectric methods record the temperature and frequency dependence of the dielectric constant to an oscillatory voltage applied to a sample pressed between two electrodes. The basic principles of dynamic-mechanical and dielectric analysis and the experimental methods used to measure dynamic-mechanical and dielectric properties of polymers are presented in the following sections.

5.1.1 Dynamic-Mechanical Analysis

In dynamic testing, the stress is measured as a function of strain that is some periodic function of time, usually a sine wave. Unlike fatigue tests (see Section 4.4.2), dynamic-mechanical properties are measured at low strain such that deformation is not permanent. Commercial dynamic-testing instruments are available for operation in several modes of deformation (e.g., tensile, torsion, compression, flexure, and shear) and over several decades of frequencies. The principles of dynamic-mechanical analysis are described next.

Theory. For a tensile strain that is a sinusoidal function of time, t , the strain function may be expressed as

$$\varepsilon = \varepsilon^\circ \sin(\omega t). \quad (5.1)$$

In this expression, ε° is the amplitude of the applied strain and ω is the angular frequency of oscillation (units of radians per second). The *angular* frequency is related to frequency, f , measured in cycles per second (Hz), as $\omega = 2\pi f$. The usual range of frequencies for dynamic-mechanical experiments is 0.1 to 110 Hz (0.628 to 691 rad s⁻¹).

The stress resulting from the applied sinusoidal strain will also be a sinusoidal function, which may be written in the most general form as

$$\sigma = \sigma^\circ \sin(\omega t + \delta) \quad (5.2)$$

where σ° is the amplitude of the stress response and δ is the *phase angle* between the stress and the strain, as illustrated by Figure 5-1. The phase angle is a measure of the viscous response of the material to dynamic strain as discussed later.

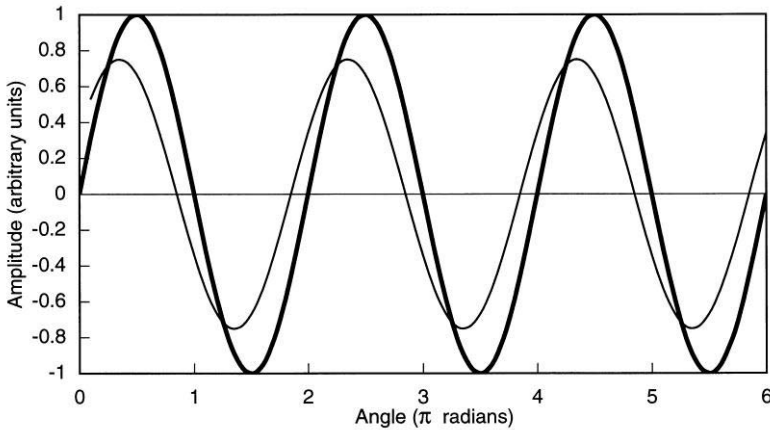


Figure 5-1 Representation of an arbitrary strain function (thick line) and resulting stress response (thin line) of a viscoelastic material. In this example, the stress is out of phase with the strain by 45° (i.e., $\delta = \pi/4$ radians), and its amplitude is arbitrarily set at 75% of the strain amplitude (i.e., $\sigma/\varepsilon^\circ = 0.75$).

In the case of an ideal elastic solid, the stress is always in phase with strain (i.e., $\delta = 0$ in eq. (5.2)). This can be shown from substitution of eq. (5.1) into Hooke's law (eq. 4.46)

$$\sigma = E\varepsilon = E\varepsilon^\circ \sin(\omega t) = \sigma^\circ \sin(\omega t) \quad (5.3)$$

where σ° is the magnitude (i.e., $\sigma^\circ = E\varepsilon^\circ$) of the resulting stress function.

In contrast, the stress of an ideal viscous fluid is always 90° out of phase (i.e., $\delta = \pi/2$) with the strain. This can be shown to result from Newton's law of viscosity, given as

$$\sigma = \eta \left(\frac{d\varepsilon}{dt} \right). \quad (5.4)$$

The derivative of ε , given by eq. (5.1), with respect to time is

$$\frac{d\varepsilon}{dt} = \omega\varepsilon^\circ \cos(\omega t). \quad (5.5)$$

Substitution of this expression into eq. (5.4), and noting that the cosine function is 90° out of phase with the sine function, gives

$$\sigma = \eta\omega\varepsilon^\circ \cos(\omega t) = \sigma^\circ \sin\left(\omega t + \frac{\pi}{2}\right) \quad (5.6)$$

where

$$\sigma^{\circ} = \eta\omega\varepsilon^{\circ}. \quad (5.7)$$

At temperatures below T_g , polymeric materials behave more as Hookean solids at small deformations, but at higher temperatures (i.e., in the vicinity of T_g) their behavior is distinctly viscoelastic. Over these temperatures, δ will have a (temperature-dependent) value between 0° (totally elastic) and 90° (totally viscous).

An alternative, and perhaps more useful, approach to discussing the dynamic response of a viscoelastic material to an applied cyclical strain is by use of complex number notation by which a complex strain, ε^* , can be represented as

$$\varepsilon^* = \varepsilon^{\circ} \exp(i\omega t) \quad (5.8)$$

where $i = \sqrt{-1}$. Following the form of eq. (5.2), the resulting complex stress, σ^* , can be written as

$$\sigma^* = \sigma^{\circ} \exp[i(\omega t + \delta)]. \quad (5.9)$$

It follows from Hooke's law that a *complex modulus*, E^* , can be defined as the ratio of complex stress to complex strain as

$$E^* = \frac{\sigma^*}{\varepsilon^*} = \left(\frac{\sigma^{\circ}}{\varepsilon^{\circ}} \right) \exp(i\delta). \quad (5.10)$$

This complex modulus can be resolved into two components—one that is in phase (i.e., E') and one that is out of phase (i.e., E'') with the applied strain. Substitution of *Euler's identity*

$$\exp(i\delta) = \cos \delta + i \sin \delta \quad (5.11)$$

into eq. (5.10) gives

$$E^* = \left(\frac{\sigma^{\circ}}{\varepsilon^{\circ}} \right) \cos \delta + i \left(\frac{\sigma^{\circ}}{\varepsilon^{\circ}} \right) \sin \delta. \quad (5.12)$$

Equation (5.12) may be written in the form given as

$$\boxed{E^* = E' + iE''} \quad (5.13)$$

where E' is called the (tensile) *storage modulus* given as

$$E' = \left(\frac{\sigma^{\circ}}{\varepsilon^{\circ}} \right) \cos \delta \quad (5.14)$$

and E'' is the (tensile) *loss modulus*:

$$E'' = \left(\frac{\sigma^0}{\varepsilon^0} \right) \sin \delta. \quad (5.15)$$

The ratio of loss and storage moduli defines another useful parameter in dynamic-mechanical analysis called $\tan \delta$ where

$$\tan \delta = \frac{\sin \delta}{\cos \delta} = \frac{E''}{E'}. \quad (5.16)$$

As in static testing (see Section 4.4.2) where the tensile modulus is the inverse of the compliance, the dynamic tensile modulus is inversely related to the dynamic tensile compliance, D^* , as

$$D^* = \frac{1}{E^*} = \frac{\varepsilon^*}{\sigma^*} = \frac{\varepsilon^0 \exp(i\omega t)}{\sigma^0 \exp[i(\omega t + \delta)]} = \left(\frac{\varepsilon^0}{\sigma^0} \right) \exp(-i\delta). \quad (5.17)$$

Substitution of Euler's identity in the form of $\exp(-i\delta) = \cos \delta - i \sin \delta$ into eq. (5.17) gives

$$D^* = \left(\frac{\varepsilon^0}{\sigma^0} \right) \cos \delta - i \left(\frac{\varepsilon^0}{\sigma^0} \right) \sin \delta. \quad (5.18)$$

Equation (5.18) may be written in the form

$$D^* = D' - iD'' \quad (5.19)$$

where D' is called the *storage compliance*,

$$D' = \left(\frac{\varepsilon^0}{\sigma^0} \right) \cos \delta, \quad (5.20)$$

and D'' is the (tensile) *loss compliance*,

$$D'' = \left(\frac{\varepsilon^0}{\sigma^0} \right) \sin \delta. \quad (5.21)$$

The negative sign of the second term (i.e., $-iD''$) in the RHS of eq. (5.19) contrasts with the corresponding positive term (i.e., $+iE''$) in eq. (5.13). As in the case of dynamic modulus (eq. (5.16)), $\tan \delta$ is related to the components of the complex dynamic compliance as

$$\tan \delta = \frac{D''}{D'}. \quad (5.22)$$

It is possible to obtain values of dynamic storage and loss moduli from corresponding values of compliance, and vice versa, by manipulation of their complex conjugates. The complex conjugate of the dynamic modulus (eq. (5.13)) is

$$\overline{E^*} = E' - iE''. \quad (5.23)$$

The *magnitude* of the dynamic modulus, $|E^*|$, is obtained from its complex conjugate as

$$E^* \times \overline{E^*} = |E^*|^2 = (E')^2 + (E'')^2. \quad (5.24)$$

Then (from eqs. (5.17), (5.23), and (5.24)), we can write

$$D^* = \frac{1}{E^*} = \frac{\overline{E^*}}{(E')^2 + (E'')^2} = \frac{E'}{(E')^2 + (E'')^2} - i \left[\frac{E''}{(E')^2 + (E'')^2} \right]. \quad (5.25)$$

Comparison of the form of eq. (5.25) with the expression for D^* (eq. (5.19)) gives the interrelationships between the components of dynamic modulus and dynamic compliance:

$$D' = \frac{E'}{(E')^2 + (E'')^2} \quad (5.26)$$

and

$$D'' = \frac{E''}{(E')^2 + (E'')^2}. \quad (5.27)$$

Similar relationships may be written for E' and E'' as functions of D' and D'' .

Work in Dynamic Deformation. As is the case for other forms of mechanical deformation, work is expended during dynamic-mechanical testing. The amount of work, or power, consumed depends upon the viscoelastic properties of the polymer. The work *per unit of sample volume*, W , may be expressed in terms of stress and strain as

$$W = \int \left(\frac{f}{V} \right) d\ell = \int \left(\frac{f}{A} \right) \frac{d\ell}{\ell} = \int \sigma d\varepsilon \quad (5.28)$$

where f is the force, $d\ell$ is the differential extension of the sample, and V is the sample volume. Per cycle (i.e., 2π radians) of oscillation, the *dynamic* work (now given per unit volume and cycle) is then obtained as

$$W = \int_0^{2\pi} \sigma^* d\varepsilon^* \quad (5.29)$$

Substitution of the appropriate expressions for σ^* (from eq. (5.2)) and $d\varepsilon^*$ (from eq. (5.5)) and integration of eq. (5.29) gives the work per cycle per unit volume for dynamic oscillation of a viscoelastic solid (see Problem 5.2) as

$$W = \pi \sigma^0 \varepsilon^0 \sin \delta \quad (5.30)$$

Rearrangement of eq. (5.15) gives

$$\sin \delta = \left(\frac{\varepsilon^0}{\sigma^0} \right) E''$$

which can be substituted into eq. (5.30) to obtain

$$W = \pi (\varepsilon^0)^2 E'' \quad (5.31)$$

From a consideration of the $\sin \delta$ contribution to W in eq. (5.30), it is obvious that the work of oscillation for an ideal elastic solid (i.e., $\delta = 0$ and $\sin \delta = 0$) is zero, while the maximum work is expended during deformation of an ideal viscous material (i.e., $\delta = \pi/2$, $\sin \delta = 1$, and $W = \pi \sigma^0 \varepsilon^0$). The *power* consumed per unit volume is then obtained by multiplying the work per cycle (per unit volume) given by eq. (5.30) or (5.31) by the number of cycles per unit time (i.e., $f = \omega / 2\pi$) as

$$P = \left(\frac{\omega}{2} \right) \sigma^0 \varepsilon^0 \sin \delta = \left(\frac{\omega}{2} \right) (\varepsilon^0)^2 E'' \quad (5.32)$$

Experimental Techniques. The usual way to report the viscoelastic response of a polymer is by means of a semilog plot of storage modulus and loss modulus (or $\tan \delta$) as a function of temperature at one or more frequencies. The temperature range may be very broad—often extending from liquid-nitrogen temperatures (ca. -150°C) to temperatures in the range of T_g that can be 200°C or more. The dynamic storage modulus behaves much like the tensile (or shear) modulus as a function of temperature (see Figure 4-19). Maxima in loss modulus, or $\tan \delta$, occur both at T_g and at low temperatures, where small-scale molecular motions can occur (i.e., secondary relaxations). In the case of semicrystalline polymers, an additional peak in $\tan \delta$ corresponding to T_m will occur above T_g . Traditionally, the highest-temperature peak is designated the α relaxation (i.e., the glass transition in amor-

phous polymers and the crystalline-melting transition in semicrystalline polymers), the next highest is the β relaxation, then the γ relaxation, and so on.

A number of different instruments have been used to obtain dynamic-mechanical data. The earliest designs used a *free-vibration* approach (torsion pendulum and torsional braid) in which a polymer sample in the form of a bar or cylinder is set to oscillate and the damping of the oscillation is recorded as a function of time at constant temperature. More recent instrumentation employs *forced oscillation* whereby a sinusoidal strain (tensile, flexure, compression, shear, or torsional) is applied and the stress response is recorded as a function of temperature at different frequencies. These techniques are described in the following sections.

Free-Vibration Methods. The simplest and earliest dynamic-mechanical technique, the *torsion pendulum*, is a free-vibration technique [1]. In this experiment, a polymer film is rigidly clamped at one end, while the other end is attached to an inertia disk that is free to oscillate. Once the disk is set in oscillation, the viscous response of the polymer sample causes the amplitude of the oscillation to decay, as illustrated in Figure 5-2. The time required for one complete oscillation is called the *period* of oscillation (P).

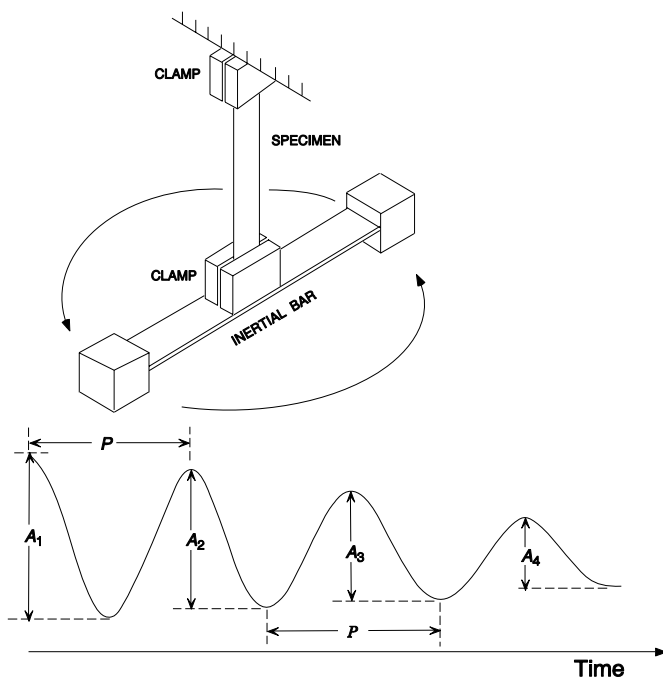


Figure 5-2 Torsion-pendulum apparatus (top) and a plot of amplitude of oscillation (bottom). Adapted from L. Nielsen, *Dynamic Mechanical Properties of High Polymers*. SPE Journal, 1960.16: p. 525–532.

The value of $\tan \delta$ can be determined from the ratio of amplitudes (A) of any two consecutive peaks as

$$\Delta = \pi \tan \delta = \ln \frac{A_1}{A_2}. \quad (5.33)$$

where δ is called the *log decrement*. Frequencies of disk oscillation may range from 0.01 to 50 Hz as determined by sample characteristics. Usually, frequency is approximately 1 Hz and will vary slightly with temperature over the course of the experiment.

Since the mode of deformation is actually torsion, it is usual to represent the response in terms of dynamic *shear* moduli, G' and G'' (where $G^* = G' + iG''$). The shear *storage* modulus, G' , is obtained from the sample geometry (F_s), moment of inertia (I), and period of oscillation (P) as

$$G' = F_s I \left(\frac{1}{P^2} \right). \quad (5.34)$$

The relationships from which the geometry factor may be calculated depend upon whether the sample is cylindrical or rectangular [2]. For a rectangular sample, the geometry parameter is given as

$$F_s = \frac{64\pi^2 L}{uWt^3} \quad (5.35)$$

where L is the sample length, W is width, t is thickness, and u is a shape factor that depends upon the (aspect) ratio of the samples (W/t). Once G' and $\log \Delta$ have been measured, the shear loss modulus, G'' can be calculated as

$$G'' = G' \tan \delta = \frac{G' \Delta}{\pi}. \quad (5.36)$$

As an example of dynamic-mechanical data, values of the storage modulus and log decrement obtained by early torsion-pendulum measurements [1] of poly(methyl methacrylate) (PMMA) are plotted against temperature in Figure 5-3. The data indicate an α relaxation corresponding to T_g (i.e., maximum in $\log \Delta$ and sharp decrease in the value of G') near 130°C and a (β) secondary-relaxation peak (see Section 4.1.3) near 40°C. A small drop in G' accompanies the broad maximum in $\log \Delta$ at the β relaxation. The β relaxation was attributed in this study to the motion of the large ($-\text{COOCH}_3$) pendant group of PMMA whose structure is as follows:

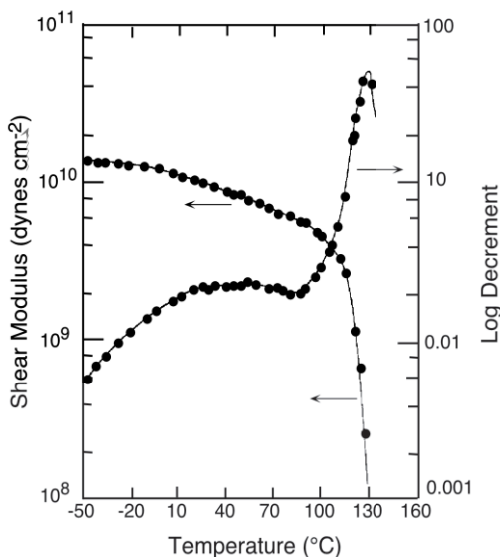
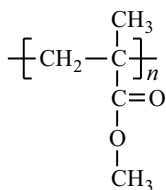


Figure 5-3 Values of the shear modulus (G') and log decrement (Δ) of poly(methyl methacrylate) plotted as a function of temperature. Data were obtained by torsion-pendulum measurements [1].

The torsion pendulum is still actively used today and is available commercially as a fully automated instrument. A schematic diagram of a modern torsion-pendulum apparatus is shown in Figure 5-4. Temperature can be controlled to within $\pm 0.05^\circ\text{C}$ isothermally from 25° to 400°C or may be ramped up or down at rates of 0.1°C h^{-1} to 5°C min^{-1} from -180° to 400°C . The frequency and damping are optically tracked for data acquisition. As shown in Figure 5-4, a light beam passes through a pair of polarizers housed in the optical cage. The upper polarizer oscillates with the specimen, and the intensity of light measured by means of a non-drag optical transducer is a linear function of the angular displacement of the pendulum.

An important variation of the torsion-pendulum technique is called *torsional-braid analysis* (TBA) [3]. Instrumentation is the same as used for torsion-pendulum analysis of films, rods, or bars; however, the TBA sample is *supported* on a braid, typically made from glass fibers. The braid is coated with a dilute solution of the

sample and dried in a vacuum to remove all solvent. Although the quantitative values of dynamic moduli of this composite geometry are *not* the same as the unsupported polymer, the *qualitative* dependence of $\tan\delta$ on temperature is a good representation of the actual polymer response. The advantage of this technique is that the support provided by the braid enables the dynamic-mechanical characterization of low-molecular-weight and *liquid* samples as well as high-molecular-weight polymer samples near and above T_g , where softening would preclude the use of unsupported-sample techniques. For example, the cure of an epoxy resin can be followed by recording the increase in G' with time at a fixed temperature.

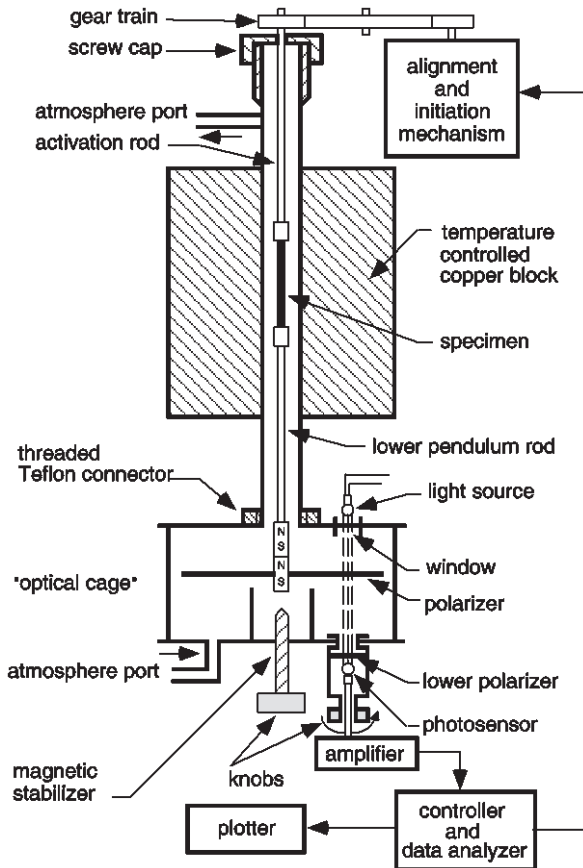


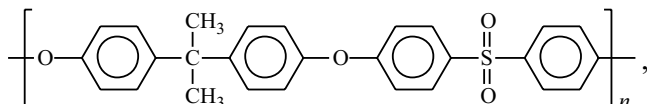
Figure 5-4 Schematic diagram of a commercial torsion-pendulum apparatus. Courtesy of J. K. Gillham.

As an illustration of TBA data, the loss modulus of PMMA samples [4] with different tacticity is plotted against temperature in Figure 5-5. Results indicate that

the lowest T_g (determined as the temperature at the maximum of the high-temperature α peak) is observed for isotactic PMMA, i -PMMA, ($T_g = 334$ K), while the T_g s of atactic PMMA (a -PMMA) and syndiotactic PMMA (s -PMMA) are higher and nearly equal (i.e., 384 K for a -PMMA and 399 K for s -PMMA). These values compare favorably with T_g s determined by calorimetric measurements of i -PMMA (318 K), a -PMMA (378 K), and s -PMMA (388 K) [5]. In contrast, the temperatures corresponding to the β peaks are nearly invariant, but the magnitude of the β peak decreases with increasing isotactic content. The decrease in the intensity of the β peak for the isotactic form of PMMA is believed to be due to the immobilization of the ester substituent groups in the (5/1) helical conformation* of this crystalline isomer.

Forced-Vibration Methods. Today, the most frequently used commercial instruments utilize a *forced*- (rather than free-) vibration method by which a dynamic tensile, compressive, torsional, or flexural strain is applied to the sample, which is cut or molded in the form of a thin film or bar. One important advantage of the forced-vibration mode is that frequency can be controlled precisely over a wider range (0.001 to 100 rad s^{-1}) than is possible for free-vibration methods. As discussed next, comparison of dynamic-mechanical spectra obtained at several frequencies provides useful additional information on the viscoelastic properties of the polymer. Section 5.1.4 outlines the principles of dielectric spectroscopy, which provides viscoelastic information over a much wider range of frequencies (up to 10^{10} Hz).

A representative dynamic-mechanical spectrum of an engineering thermoplastic, polysulfone, whose chemical structure is



is shown in Figure 5-6. In this example, the dynamic-mechanical data were obtained by forced-vibration instrumentation at 10 rad s^{-1} (ca. 1.6 Hz) in the tensile mode [6]. In addition to the glass transition (α peak), which occurs near 481 K (188°C), there is a major secondary-relaxation process (the γ peak) showing a broad maximum located near 166 K (-107°C). It is believed that this low-temperature transition reflects short-range mobility of the main chain including flips of phenylene rings and possibly coupled rotations of methyl groups. There is also a suggestion of a small, very broad transition (β peak) at intermediate temperatures near 340 K. This peak appears to be sensitive to the thermal history of the sample and is believed to be asso-

* The first number identifying the conformational form of a helix indicates the number of repeating units participating in a given number of turns of the helix. In the case of a 5/1 (or 5_1) helix, five repeating units form one complete turn of the helix.

ciated with limited segmental motions appearing as a precursor to the longer-range motions occurring at the glass transition.

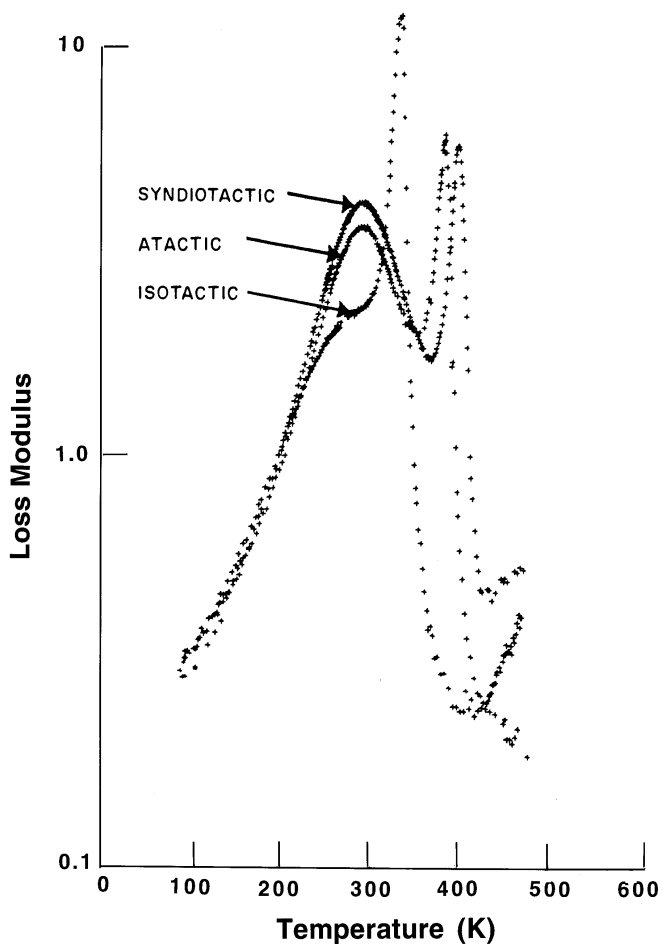


Figure 5-5 Loss-modulus data for PMMA samples with different tacticities as obtained by torsion-braid analysis at a heating rate of $2^{\circ}\text{C min}^{-1}$. From J. K. Gillham, S. J. Stadnicki, and Y. Hazony, *Journal of Applied Polymer Science*, 1977, 21: p. 401. Copyright © 1977 John Wiley & Sons. Reprinted by permission of John Wiley & Sons, Inc.

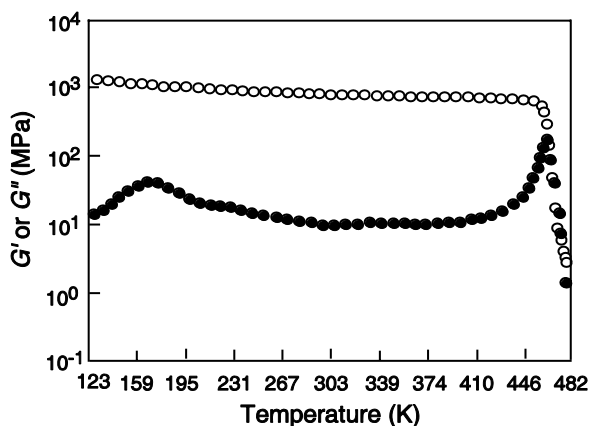


Figure 5-6 Dynamic-mechanical spectrum of polysulfone obtained in forced torsion at 10 rad s^{-1} ($\sim 1.6 \text{ Hz}$) [6]. Data points indicate (O) shear storage-modulus (G') and (●) shear loss modulus (G''). A low-temperature, secondary-relaxation (γ) peak with a broad maximum near 166 K (-107°C) appears in the loss-modulus plot. The glass transition (i.e., α peak) occurs at 481 K (188°C).

Activation Energies. Energies required for main-chain and side-group motions can be obtained by determining the effect of frequency on the maximum temperatures of the loss, or $\tan \delta$, peaks. The ability to vary oscillation frequency makes forced-vibration techniques the choice for these studies. The temperature at the peak maxima, T_{max} , increases with increasing frequency, and the activation energy, E_a , of the relaxational process may be determined from the slope of a semilog plot of frequency (f or ω) versus reciprocal peak temperature ($1/T_{\text{max}}$) as

$$\ln f = -\left(\frac{E_a}{R}\right)\frac{1}{T_{\text{max}}} + \ln f_0 \quad (5.37)$$

where f_0 is a constant obtained from the intercept. Typically, activation energies for low-temperature (i.e., secondary) relaxations are low (ca. 10 to 20 kcal mol^{-1}). In the example of the dynamic-mechanical spectra of poly(methyl methacrylate) shown in Figure 5-3, the activation energy of the β peak was reported to be approximately 17 kcal mol^{-1} . The activation energy for the γ relaxation of polysulfone (Figure 5-6) was reported to be $10.7 \text{ kcal mol}^{-1}$, in agreement with predictions of semiempirical molecular-orbital calculations of the energy barriers to rotation for the phenylene rings in the backbone of the polysulfone chain [6]. Corresponding activation energies for the glass transition, reflecting longer-range cooperative motions, are about an order of magnitude greater than those for secondary relaxations. For example,

the activation energy of the α (glass) relaxation of polysulfone is approximately 220 kcal mol⁻¹ [6]. High activation energies mean that the temperature location of the α (glass) relaxation is relatively insensitive to a change in frequency compared to secondary-relaxation processes. Principal relaxations and activation energies for a number of different polymers are given in several sources [7, 8].

5.1.2 Mechanical Models of Viscoelastic Behavior

An insight into the nature of the viscoelastic properties of polymers can be obtained by analyzing the stress or strain response of mechanical models using an ideal spring as the Hookean element and a dashpot as the viscous element. A dashpot may be viewed as a shock absorber consisting of a piston in a cylinder filled with a Newtonian fluid of viscosity η . The elemental models are a series combination of a spring and dashpot, the *Maxwell* element, and a parallel combination of a spring and dashpot, the *Voigt* element, as illustrated in Figure 5-7. In the following sections, relationships for the transient and dynamic responses of Maxwell and Voigt models are developed.

Maxwell Element. In the case of a series combination of a spring and dashpot, the total strain (or strain rate) is a summation of the individual strains (or strain rates) of the spring and dashpot. From Hooke's law ($\sigma = E\varepsilon$), the strain *rate* of an ideal elastic spring can be written as

$$\frac{d\varepsilon}{dt} = \left(\frac{1}{E} \right) \frac{d\sigma}{dt} \quad (5.38)$$

while the strain rate for the dashpot is obtained by rearranging Newton's law of viscosity (eq. (5.4)) as

$$\frac{d\varepsilon}{dt} = \frac{\sigma}{\eta}. \quad (5.39)$$

Therefore, the basic equation for strain rate in the Maxwell model is the summation of the strain rates for the spring and dashpot (eqs. (5.38) and (5.39)) as

$$\boxed{\frac{d\varepsilon}{dt} = \left(\frac{1}{E} \right) \frac{d\sigma}{dt} + \frac{\sigma}{\eta}}. \quad (5.40)$$

This differential equation can be solved for creep, stress relaxation, and dynamic response by applying the appropriate stress or strain function.

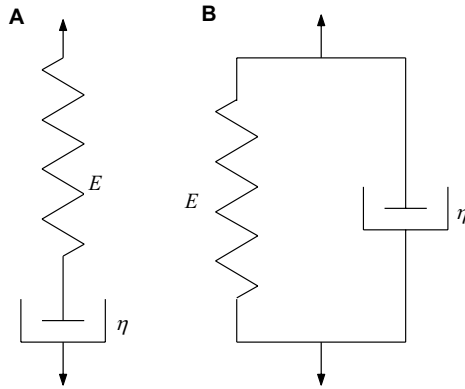


Figure 5-7 Maxwell (A) and Voigt (B) elements.

In a *creep* experiment (see Section 4.4.2), a *constant* stress, σ_0 , is applied instantaneously. Equation (5.40) then reduces to

$$\frac{d\varepsilon}{dt} = \frac{\sigma_0}{\eta}. \quad (5.41)$$

Rearrangement and integration of eq. (5.41) give

$$\varepsilon(t) = \left(\frac{\sigma_0}{\eta} \right) t + \varepsilon_0 \quad (5.42)$$

where ε_0 represents the *instantaneous* (i.e., $t = 0$) strain response of the spring element. The creep compliance function, $D(t)$, is then obtained as

$$D(t) = \frac{\varepsilon(t)}{\sigma_0} = \frac{t}{\eta} + \frac{\varepsilon_0}{\sigma_0} = \frac{t}{\eta} + D \quad (5.43)$$

where $D(= \varepsilon_0/\sigma_0)$ is the instantaneous compliance (of the spring). An alternative form of eq. (5.43) may be obtained by defining a *relaxation time*, τ , as

$$\tau = \frac{\eta}{E} = \eta D. \quad (5.44)$$

Equation (5.43) can then be represented in normalized form as

$$\frac{D(t)}{D} = \frac{t}{\tau} + 1. \quad (5.45)$$

In a *stress-relaxation* experiment (see Section 4.4.2), the strain (ε_0) is constant and, therefore, the strain rate is zero. Equation (5.40) then reduces to the first-order ordinary differential equation

$$\left(\frac{1}{E}\right)\frac{d\sigma}{dt} + \frac{\sigma}{\eta} = 0. \quad (5.46)$$

Rearrangement of eq. (5.46) and introduction of τ give

$$\frac{d\sigma}{\sigma} = -\left(\frac{1}{\tau}\right)dt. \quad (5.47)$$

Integration yields the stress response as

$$\sigma = \sigma_0 \exp\left(\frac{-t}{\tau}\right) \quad (5.48)$$

where σ_0 is the instantaneous stress response of the spring. The stress relaxation modulus, $E_r(t)$, is then obtained as

$$E_r(t) = \frac{\sigma}{\varepsilon_0} = \left(\frac{\sigma_0}{\varepsilon_0}\right)\exp\left(\frac{-t}{\tau}\right) = E \exp\left(\frac{-t}{\tau}\right) \quad (5.49)$$

where $E (= \sigma_0/\varepsilon_0)$ is the (Young's) modulus of the spring element.

To obtain an expression for the *dynamic-mechanical* response (i.e., complex compliance or modulus), the expression for complex stress, $\sigma = \sigma^0 \exp(i\omega t)$, is substituted into the Maxwell equation (eq. (5.40)) to give

$$\frac{d\varepsilon(t)}{dt} = \left(\frac{\sigma^0}{E}\right)i\omega \exp(i\omega t) + \left(\frac{\sigma^0}{\eta}\right)\exp(i\omega t). \quad (5.50)$$

Integration from time t_1 to t_2 gives

$$\varepsilon(t_2) - \varepsilon(t_1) = \left(\frac{\sigma^0}{E}\right)[\exp(i\omega t_2) - \exp(i\omega t_1)] + \left(\frac{\sigma^0}{\eta i\omega}\right)[\exp(i\omega t_2) - \exp(i\omega t_1)]. \quad (5.51)$$

Since the corresponding stress increment can be written as

$$\sigma(t_2) - \sigma(t_1) = \sigma^0 [\exp(i\omega t_2) - \exp(i\omega t_1)], \quad (5.52)$$

division of both sides of eq. (5.51) by this expression, and making use of τ , gives the complex compliance as

$$D^* = D - i \left(\frac{D}{\omega\tau} \right). \quad (5.53)$$

Therefore, the storage compliance obtained from the Maxwell model is simply the compliance of the spring

$$D' = D, \quad (5.54)$$

which is independent of time or frequency, while the loss compliance is

$$D'' = \frac{D}{\omega\tau}. \quad (5.55)$$

The corresponding expression for complex modulus, E^* , is obtained by recalling that E^* is the reciprocal of D^* and utilizing the complex conjugate of D^* as

$$E^* = \frac{1}{D^*} = \frac{1}{D - i \frac{D}{\omega\tau}} \times \frac{D + i \frac{D}{\omega\tau}}{D + i \frac{D}{\omega\tau}}. \quad (5.56)$$

Performing the multiplication, rearranging, and using the inverse relation $E = 1/D$ gives

$$E^* = E' + iE'' = \frac{E(\omega\tau)^2}{1 + (\omega\tau)^2} + i \left[\frac{E\omega\tau}{1 + (\omega\tau)^2} \right] \quad (5.57)$$

where

$$E' = \frac{E(\omega\tau)^2}{1 + (\omega\tau)^2} \quad (5.58)$$

and

$$E'' = \frac{E\omega\tau}{1 + (\omega\tau)^2}. \quad (5.59)$$

It follows from eqs. (5.58) and (5.59) that $\tan \delta$ for a Maxwell model is simply

$$\tan \delta = \frac{E''}{E'} = \frac{1}{\omega\tau}. \quad (5.60)$$

Voigt Element. For a parallel combination of a spring and dashpot, the Voigt model shown in Figure 5-7B, the strain on each element must be equal while the *stress is additive*. The fundamental relation for the Voigt model is, therefore,

$$\sigma = E\varepsilon + \eta \frac{d\varepsilon}{dt}. \quad (5.61)$$

Making use of the relaxation time (eq. (5.44)), the Voigt equation for *creep* deformation becomes a linear differential equation,

$$\frac{\sigma_0}{\eta} = \frac{\varepsilon(t)}{\tau} + \frac{d\varepsilon(t)}{dt} \quad (5.62)$$

which can be solved by using the integrating factor $\exp(t/\tau)$. Solving for $\varepsilon(t)$ gives the compliance function as

$$D(t) = D \left[1 - \exp\left(\frac{-t}{\tau}\right) \right] \quad (5.63)$$

where $D = 1/E$. In contrast to the Maxwell model, the Voigt equation cannot be solved in any meaningful way for stress relaxation because the dashpot element cannot be deformed instantaneously.

The response of a Voigt model to *dynamic* strain gives the relationships for the storage and loss compliance as

$$D' = \frac{D}{1 + (\omega\tau)^2} \quad (5.64)$$

and

$$D'' = \frac{D\omega\tau}{1 + (\omega\tau)^2}. \quad (5.65)$$

The forms of these relationships for compliance are the same as those for dynamic *moduli* (eqs. (5.58) and (5.59)) given by the Maxwell model.

Comparison of Simple Models. The two-element models approximate some of the viscoelastic properties of real polymers. Results are summarized in Table 5-1. In general, modulus is modeled best by the Maxwell element, while compliance is better represented by the Voigt element. The most significant limitation of these two models is that they employ only a single relaxation time (eq. (5.44)). This results in the prediction of only a *single transition* in modulus or compliance, whereas high-molecular-weight polymers exhibit both a glass-to-rubber and rubber-to-liquid tran-

sition. As would be expected, improvement is achieved by adding more elements, as discussed in the following section.

Table 5-1 Predictions of Viscoelastic Properties by the Maxwell and Voigt Models

Experiment	Maxwell Model	Voigt Model
Creep	$\frac{D(t)}{D} = 1 + \frac{t}{\tau}$	$\frac{D(t)}{D} = 1 - \exp\left(\frac{-t}{\tau}\right)$
Stress relaxation	$\frac{E(t)}{E} = \exp\left(\frac{-t}{\tau}\right)$	$\frac{E(t)}{E} = 1$
Dynamic mechanical	$\frac{D'}{D} = 1$	$\frac{D'}{D} = \frac{1}{1 + (\omega\tau)^2}$
	$\frac{D''}{D} = \frac{1}{\omega\tau}$	$\frac{D''}{D} = \frac{\omega\tau}{1 + (\omega\tau)^2}$
	$\frac{E'}{E} = \frac{(\omega\tau)^2}{1 + (\omega\tau)^2}$	$E' = E$
	$\frac{E''}{E} = \frac{\omega\tau}{1 + (\omega\tau)^2}$	$E'' = \omega\eta$

Multi-element Models. A multi-element model, particularly suited for modulus, is called the *Maxwell–Wiechert model*, which is a parallel combination of multiple Maxwell elements. In this model, the strains on each Maxwell element are equal and the stresses experienced by each Maxwell element are additive, as they are in the case of the single spring and dashpot in the simple Voigt model. For the two-element Maxwell–Wiechert model illustrated in Figure 5-8, the stress-relaxation modulus is given as

$$E(t) = E_1 \exp\left(\frac{-t}{\tau_1}\right) + E_2 \exp\left(\frac{-t}{\tau_2}\right) \quad (5.66)$$

where $\tau_1 = \eta_1 / E_1$ and $\tau_2 = \eta_2 / E_2$. By appropriate selection of values for E_i and τ_i , a reasonable representation of the glass and rubber plateau regions of the stress-relaxation modulus is obtained, as illustrated in Figure 5-9.

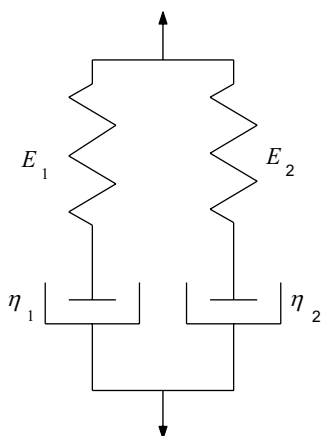


Figure 5-8 Representation of a two-element Maxwell–Wiechert model.

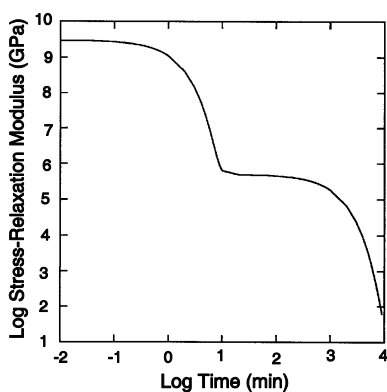


Figure 5-9 Prediction of stress-relaxation modulus, $E(t)$, as a function of dimensionless time (t/τ) for the two-element Maxwell–Wiechert model illustrated in Figure 5-8. Values for model parameters (eq. (5.66)) are $E_1 = 3 \times 10^9$ Pa, $E_2 = 5 \times 10^5$ Pa, $\tau_1 = 1$ min, and $\tau_2 = 10^3$ min.

Further improvement in terms of realistic slopes in the transition regions is obtained by adding additional Maxwell elements in the model and, therefore, providing a distribution of relaxation times as would be expected for a high-molecular-weight polymer with a broad distribution of molecular weights. In general, the stress-relaxation modulus of a Maxwell–Wiechert model consisting of N Maxwell elements can be written as the summation

$$E(t) = \sum_{i=0}^N E_i \exp\left(\frac{-t}{\tau_i}\right). \quad (5.67)$$

Corresponding equations can be written for dynamic moduli, as shown in Table 5-2.

Table 5-2 Predictions of Viscoelastic Properties by Two Multi-element Models, Maxwell–Wiechert and Voigt–Kelvin

Experiment	Maxwell–Wiechert Model	Voigt–Kelvin Model
Creep		$D(t) = \sum_{i=1}^N D_i \left[1 - \exp\left(\frac{-t}{\tau_i}\right) \right]$
Stress relaxation	$E(t) = \sum_{i=1}^N E_i \exp\left(\frac{-t}{\tau_i}\right)$	
Dynamic mechanical	$E' = \sum_{i=1}^N \frac{E_i (\omega \tau_i)^2}{1 + (\omega \tau_i)^2}$	$D' = \sum_{i=1}^N \frac{D_i}{1 + (\omega \tau_i)^2}$
	$E'' = \sum_{i=1}^N \frac{E_i \omega \tau_i}{1 + (\omega \tau_i)^2}$	$D'' = \sum_{i=1}^N \frac{D_i \omega \tau_i}{1 + (\omega \tau_i)^2}$

An alternative approach for a multi-element model is a *Voigt–Kelvin model*, which consists of a *series* arrangement of Voigt elements. A two-element Voigt–Kelvin model is illustrated in Figure 5-10. For N elements, the creep compliance can be written as a summation:

$$D(t) = \sum_{i=0}^N D_i \left[1 - \exp\left(\frac{-t}{\tau_i}\right) \right]. \quad (5.68)$$

Corresponding equations can be written for dynamic compliance as given in Table 5-2.

Relaxation and Retardation Spectra. In the limit of an infinite number of Maxwell elements in a Maxwell–Wiechert model, the summation given in eq. (5.67) may be replaced by an integral:

$$E(t) = \int_0^{\infty} E(\tau) \exp\left(\frac{-t}{\tau}\right) d\tau. \quad (5.69)$$

In this equation, $E(\tau)$ is a continuous function of the relaxation times. An alternative expression is given as

$$H(\tau) = \tau E(\tau) \quad (5.70)$$

where $H(\tau)$ is called the *relaxation-time distribution function*. Substitution of this relation into the integral and using $\ln \tau$ in place of τ gives

$$E(t) = \int_{\ln \tau = -\infty}^{\ln \tau = +\infty} H(\tau) \exp\left(\frac{-t}{\tau}\right) d \ln \tau . \quad (5.71)$$

Corresponding expressions can be written for the dynamic moduli.

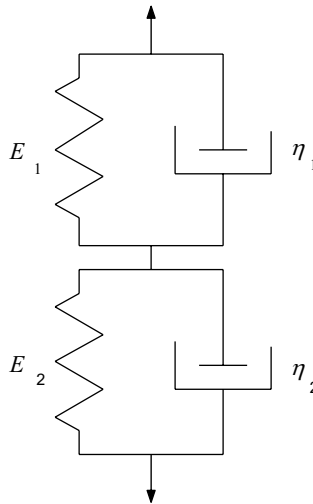


Figure 5-10 Representation of a two-element Voigt–Kelvin model.

An expression for compliance is obtained by considering an infinite number of Voigt elements in series (Voigt–Kelvin model)

$$D(t) = \int_{\ln \tau = -\infty}^{\ln \tau = +\infty} L(\tau) \left[1 - \exp\left(\frac{-t}{\tau}\right) \right] d \ln \tau , \quad (5.72)$$

where $L(\tau)$ is called the *retardation* spectrum function. Corresponding expressions can be written for the dynamic moduli.

Relaxation and retardation spectra characterize the viscoelastic properties of a polymer at a particular temperature. They can be calculated from one set of experimental data and then be used to predict the viscoelastic response under different experimental conditions. For example, the relaxation-time spectrum can be calculated from the temperature dependence of the dynamic loss modulus and then be used to calculate the temperature dependence of the stress-relaxation modulus. Such interre-

relationships minimize experimental work and provide a basis to test the consistency of experimental data.

5.1.3 Viscoelastic Properties of Polymer Solutions and Melts

Concentrated polymer solutions and melts also exhibit viscoelastic response. It is convenient to characterize this response in terms of a complex viscosity, η^* . This is defined by applying Newton's law of viscosity (eq. (5.4)) to the case of a dynamically applied *shear* strain, γ^* ($= \gamma_0 e^{i\omega t}$). The corresponding dynamic shear stress, τ^* , is then written as

$$\tau^* = \eta^* \frac{d\gamma^*}{dt} = i\omega\eta^* \gamma^*. \quad (5.73)$$

The complex viscosity can be written in a form analogous to dynamic compliance,

$$\boxed{\eta^* = \eta' - i\eta''}, \quad (5.74)$$

where η' is called the *dynamic viscosity* and is obtained from the values of the shear loss modulus (G'') and angular frequency, ω , as*

$$\eta' = \frac{G''}{\omega}. \quad (5.75)$$

The imaginary component of the viscosity, η'' , is obtained from the shear storage modulus, G' , as

$$\eta'' = \frac{G'}{\omega}. \quad (5.76)$$

The *Cox–Merz rule* provides an approximate relationship between the *steady-shear viscosity* in the limit of zero shear rate, η_0 (see Section 11.2.1), and the magnitude of the complex viscosity as

$$\eta_0 = |\eta^*| = \left[(\eta')^2 + (\eta'')^2 \right]^{1/2}. \quad (5.77)$$

* Equations (5.75) and (5.76) follow from eq. (5.73) as

$$G^* = G' + iG'' = \frac{\tau^*}{\gamma^*} = i\omega\eta^* = i\omega(\eta' - i\eta'') = \omega(\eta'' + i\eta').$$

Experimental Techniques. Commercial instrumentation to determine the stress response of polymeric solutions and melts to small (i.e., linear viscoelastic) static or dynamic shear strains is based on simple-shear geometries such as cone-and-plate, concentric (Couette) cylinder, and rotating parallel plates. The rate of applied strain for these instruments is low (10^{-4} to 10^3 s $^{-1}$). Two of these rheometers, cone-and-plate and concentric cylinder, are described in detail in Section 11.4 in relation to their importance in determining the *apparent viscosity* of polymer melts and concentrated solutions as a function of frequency or shear strain rate at low shear rates. Basic principles of rheometry are described in a variety of sources [9, 10].

The apparent viscosity, as defined by Newton's law of viscosity (eq. (5.4)), is obtained from steady-shear measurements as

$$\eta = \frac{\tau}{\dot{\gamma}}. \quad (5.78)$$

Values of complex viscosity or, equivalently, the real and imaginary components of the shear moduli, G' and G'' , are obtained by applying an *oscillatory* rather than steady shear to the cone in a cone-and-plate rheometer or to the cylinder in the case of a Couette rheometer.

Alternatively, the dynamic properties (i.e., G' and G'') of polymer solutions and melts can be obtained directly by using *steady-shear flow* in a rheometer employing an eccentric rotating-disk (ERD) geometry that is illustrated in Figure 5-11. In this rheometer design, the plates are parallel, but the axes perpendicular to the plates are offset by a preset distance, a . This offset results in a flow parallel to the plates that is periodic in time (i.e., dynamic flow), although the top plate is driven at a constant angular frequency, ω . The shear rate is given as

$$\dot{\gamma} = \left(\frac{a}{h} \right) \omega. \quad (5.79)$$

The dynamic moduli are determined from geometric parameters—axes offset (a), plate radius (R), and plate separation (h)—and forces measured in the orthogonal directions (F_x and F_y) as follows:

$$G' = \frac{F_y h}{a\pi R^2} \quad (5.80)$$

and

$$G'' = \frac{F_x h}{a\pi R^2}. \quad (5.81)$$

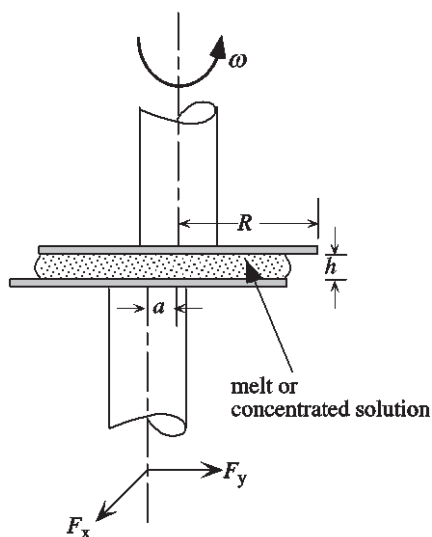


Figure 5-11 Eccentric rotating-disk (ERD) rheometer. In operation, a concentrated polymer solution or melt is sheared in the gap (h) between the two parallel plates of radius R (e.g., 2.5 cm) whose axes are offset by the distance a . The top plate is rotated at an angular frequency, ω (rad s^{-1}). Force can be measured in the orthogonal directions by means of transducers mounted in the plane of the bottom plate.

5.1.4 Dielectric Analysis

In place of a mechanical strain, viscoelastic response may be characterized by applying a time-dependent electric voltage to the sample. The voltage establishes an electrical field in the sample, which becomes electrically polarized. This means that any induced and permanent dipoles become oriented in the electric field. Polarization due to ionic conduction and the induction of a dipole moment of the molecule resulting from the distortion of the electron cloud of individual atoms is nearly instantaneous, while polarization due to the molecular motion and alignment of permanent dipoles in the electric field requires time. The polarization and ionic conduction result in the creation of a current whose amplitude depends upon frequency, temperature, and the dielectric properties of the material. As in the case of the stress response in dynamic-mechanical analysis, the frequency of the current is the same as the applied field but is shifted by the phase angle, δ . In dielectric analysis, the most important parameter for characterizing a sample is its *dielectric constant*, ϵ , which is defined next.

Theory. When a voltage (V) is applied across two electrodes between which a dielectric material is placed, a charge is established across the capacitor. This charge, Q (units of coulombs), is related to V and the capacitance (C) of the material (units of farads) as

$$Q = CV . \quad (5.82)$$

The capacitance may be expressed in terms of the capacitance of vacuum, C_0 , as

$$C = \varepsilon C_0 \quad (5.83)$$

where ε (dimensionless) is the dielectric constant, which is a function of temperature and time (or frequency). By definition, the dielectric constant for a vacuum is unity. The dielectric constant for air is only slightly higher at 1.0006, while that for water, which is capable of strong polarization, is 81 at room temperature and low frequency. Since polarization is time dependent, there is a *short-time* or *instantaneous response* for the dielectric constant, ε_U (or ε_0), that results from ion migration and induced polarization. The *long-time response*, ε_R (or ε_∞), represents the sum of contributions of the instantaneous response and the complete alignment of the permanent dipoles in the electric field.

The *charge density*, σ , is defined as

$$\sigma = \frac{Q}{A} \quad (5.84)$$

where A is the area of the plate electrodes. The charge density in the absence of a dielectric (i.e., a vacuum) between the electrodes is represented as σ_0 . This charge density is related to the *electric field*, E , which is defined as the ratio of the voltage across the capacitor and the distance between the electrodes as

$$E = \frac{V}{d} . \quad (5.85)$$

The relation between electric field and charge density is given by *Gauss's flux theorem*:

$$E = 4\pi\sigma_0 . \quad (5.86)$$

As previously discussed, the polarization that is time dependent, $P(t)$, contains an instantaneous component, P_U , due to dipole induction:

$$\lim_{t \rightarrow 0} P(t) = P_U . \quad (5.87)$$

The separate time-dependent (dipole-orientation) contribution to polarization is indicated as $P_D(t)$, giving the total polarization as

$$P(t) = P_D(t) + P_U. \quad (5.88)$$

From the limiting conditions at long time,

$$\lim_{t \rightarrow \infty} P(t) = P_R \quad (5.89)$$

and

$$\lim_{t \rightarrow \infty} P_D(t) = P_D, \quad (5.90)$$

it follows that

$$P_R = P_D + P_U. \quad (5.91)$$

The polarization at infinite time, P_R , is related to the charge density as

$$\sigma = \sigma_o + P_R. \quad (5.92)$$

Since

$$\sigma = \varepsilon_R \sigma_o \quad (5.93)$$

and (from eq. (5.86))

$$\sigma_o = \frac{E}{4\pi} \quad (5.94)$$

it follows that substitution of these equations into eq. (5.92) gives

$$\varepsilon_R - 1 = \left(\frac{4\pi}{E} \right) P_R. \quad (5.95)$$

Substitution of eq. (5.91) into eq. (5.95) then gives

$$\varepsilon_R - 1 = \left(\frac{4\pi}{E} \right) (P_D + P_U). \quad (5.96)$$

In analogy to the expression for polarization (eq. (5.91)), we may write

$$\varepsilon_R = \varepsilon_D + \varepsilon_U \quad (5.97)$$

and (following eq. (5.95))

$$\varepsilon_U - 1 = \left(\frac{4\pi}{E} \right) P_U. \quad (5.98)$$

The objective in the preceding development is to obtain expressions for the time dependency of the transient [i.e., $\varepsilon(t)$] or more commonly the dynamic [i.e., $\varepsilon(\omega, t)$] dielectric constant in response to a steady [i.e., $E(t)$] or oscillatory voltage [i.e., $E^*(\omega, t)$] applied to the electrodes. The approach is to assume that the time rate of change of the polarization is proportional to the magnitude of its displacement from its equilibrium value (P_R) as

$$\frac{dP(t)}{dt} = -\frac{P(t) - P_R}{\tau} \quad (5.99)$$

where τ is a time constant or relaxational time. From eq. (5.88), we may write

$$\frac{dP(t)}{dt} = \frac{dP_D}{dt}. \quad (5.100)$$

Substitution of eq. (5.100), eq. (5.88) for $P(t)$, and eq. (5.91) for P_R into eq. (5.99) gives

$$\frac{dP_D(t)}{dt} = -\frac{P_D(t) - P_D}{\tau}. \quad (5.101)$$

From eqs. (5.91), (5.95), and (5.98) it can be shown that

$$P_D = \frac{E}{4\pi} (\varepsilon_R - \varepsilon_U) \quad (5.102)$$

where $(\varepsilon_R - \varepsilon_U)$ is called the *dielectric relaxational strength*. Substitution of eq. (5.102) into eq. (5.101) and rearrangement gives the differential equation for a time-dependent electric field

$$\tau \frac{dP_D(t)}{dt} + P_D(t) = \frac{E(t)}{4\pi} (\varepsilon_R - \varepsilon_U). \quad (5.103)$$

For a frequency-dependent (i.e., sinusoidal) voltage

$$E^*(\omega, t) = E_0 \exp(i\omega t), \quad (5.104)$$

the differential equation of eq. (5.103) may be solved assuming that $t \gg \tau$, which indicates that steady-state conditions apply. The solution is given as

$$P_D^*(\omega) = \frac{(\varepsilon_R - \varepsilon_U) E^*(\omega)}{1 + i\omega\tau} \frac{1}{4\pi}. \quad (5.105)$$

A complex dielectric constant may be defined in terms of real and imaginary components, in a similar manner to dynamic compliance, as

$$\varepsilon^* = \varepsilon' - i\varepsilon'' \quad (5.106)$$

where

$$\tan \delta_e = \frac{\varepsilon''}{\varepsilon'}. \quad (5.107)$$

With analogy to eq. (5.102) and recognizing that ε_R is the only frequency-dependent component of the dielectric constant, we can write

$$\varepsilon^*(\omega) = \frac{4\pi P_D^*(\omega)}{E^*(\omega)} + \varepsilon_U. \quad (5.108)$$

Rearranging this equation for $P_D^*(\omega)$ and substitution of this expression into eq. (5.105) gives

$$\varepsilon^*(\omega) = \varepsilon_U + \frac{\varepsilon_R - \varepsilon_U}{1 + i\omega\tau}. \quad (5.109)$$

Multiplication of the numerator and denominator of the second term on the RHS of eq. (5.109) by its complex conjugate allows the real and imaginary components of ε^* to be resolved as

$$\varepsilon^*(\omega) = \varepsilon_U + \left(\frac{\varepsilon_R - \varepsilon_U}{1 + i\omega\tau} \right) \times \left(\frac{1 - i\omega\tau}{1 - i\omega\tau} \right) = \varepsilon_U + \frac{\varepsilon_R - \varepsilon_U}{1 + \omega^2\tau^2} - i \frac{\omega\tau(\varepsilon_R - \varepsilon_U)}{1 + \omega^2\tau^2}. \quad (5.110)$$

Comparison of this equation with eq. (5.106) gives

$$\varepsilon' = \varepsilon_U + \frac{\varepsilon_R - \varepsilon_U}{1 + \omega^2\tau^2} \quad (5.111)$$

and

$$\varepsilon'' = \frac{\omega\tau(\varepsilon_R - \varepsilon_U)}{1 + \omega^2\tau^2}. \quad (5.112)$$

As in the case of dynamic-mechanical oscillation of a Maxwell model (see Problem 5.4b), it is easily shown that ε'' exhibits a maximum at a frequency equal to the reciprocal of the relaxation time, τ , as shown by the plot of ε' (eq. (5.111)), ε'' (eq. (5.112)), and $\tan\delta_e$ versus frequency in Figure 5-12.

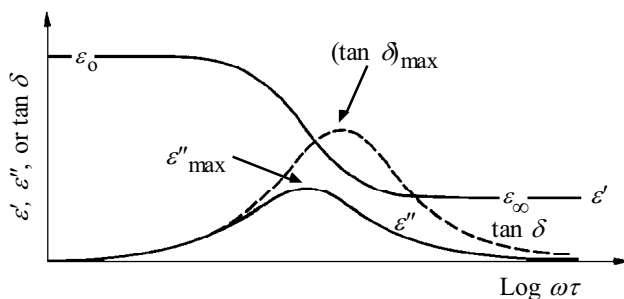


Figure 5-12 Illustration of the frequency dependence of the dielectric constant.

Equations (5.111) and (5.112) give a reasonable qualitative behavior of experimental ε' and ε'' with the limitation that the phenomenological model utilizes a single relaxation time, τ , whereas a distribution of relaxation times would be expected for high polymers. From the early work of Peter Debye, there have been a number of attempts to relate macroscopic properties of the dielectric, such as ε and P , with molecular properties, such as the dipole moment or molecular polarizability. A full description of these approaches is beyond the scope of this text, and the reader is encouraged to look at other reference sources such as the book by Daniels listed in Suggested Reading at the end of the chapter.

Experimental Methods. Values ε' and ε'' can be readily measured for polymer solutions, melts, and films over a wide range of frequencies (10^{-4} to 10^{10} Hz) by a variety of techniques. As a result of this wide frequency range, dielectric data can be plotted against frequency (i.e., frequency-plane measurements) at constant temperature in comparison with the temperature-plane plots typical for dynamic-mechanical measurements.

In the case of solid samples, a polymer film may be coated with an electrically conductive layer of gold or other metal to improve contact with the electrodes. The film is then placed in an electrode cell and immersed in a constant-temperature bath. The cell is connected to a frequency generator and typically to an electrical bridge to measure the electrical impedance of the sample. Frequently, a Schering impedance bridge, such as the one illustrated in Figure 5-13, is used over a frequency range from about 1 Hz to 10 MHz. A Schering bridge is similar to a Wheatstone bridge except that impedance, rather than resistance, is measured. By balancing the bridge, the equivalent capacitance, C_x , and resistance, R_x , of the sample are obtained. The parameters $\tan \delta_e$, ε' , and ε'' can then be determined as

$$\tan \delta = R_x C_x \omega, \quad (5.113)$$

$$\varepsilon' = \frac{C_x}{C_o (1 + \tan^2 \delta_c)}, \quad (5.114)$$

and

$$\varepsilon'' = \varepsilon' \tan \delta_c. \quad (5.115)$$

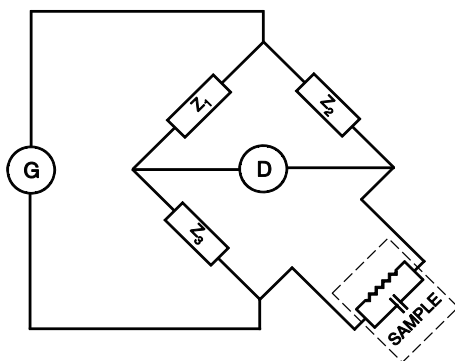


Figure 5-13 Representation of a dielectric test facility, a Schering bridge, that includes a frequency generator (G) and null detector (D). One or several of the bridge impedances are adjusted in order that the magnitude and the phase of the voltage drops across Z_1 and Z_2 are zero.

A plot of dielectric-loss (ε'') data for a polycarbonate sample as a function of frequency over a wide range of temperatures is shown in Figure 5-14A and B. In general, the glass-transition and secondary-relaxation processes can be investigated by dielectric measurements provided that there is polarizability in the side groups or main-chain repeating units. Dielectric measurements have also been used to study the cure process in thermoset composites by measurement of the dielectric constant at fixed frequency and temperature as a function of time.

Thermally Stimulated Current Analysis. Thermally stimulated current (TSC) analysis is a method related to dielectric spectroscopy that can be used to investigate amorphous transitions. In this technique, polymer dipoles are first oriented by applying a high potential across the sample at elevated temperatures (typically above T_g). The orientation is frozen by dropping the temperature below expected transitions while the potential is maintained. Next, the electric field is removed and the sample is heated. As the dipoles reorient, the resulting electric current due to the depolarization is measured as a function of temperature. Maxima appear at each transition due to the increased molecular mobility as temperature is increased. The resulting plot of thermally stimulated current against temperature is

very similar to that of the dynamic-mechanical loss data and can be used to identify secondary relaxations and glass transitions.

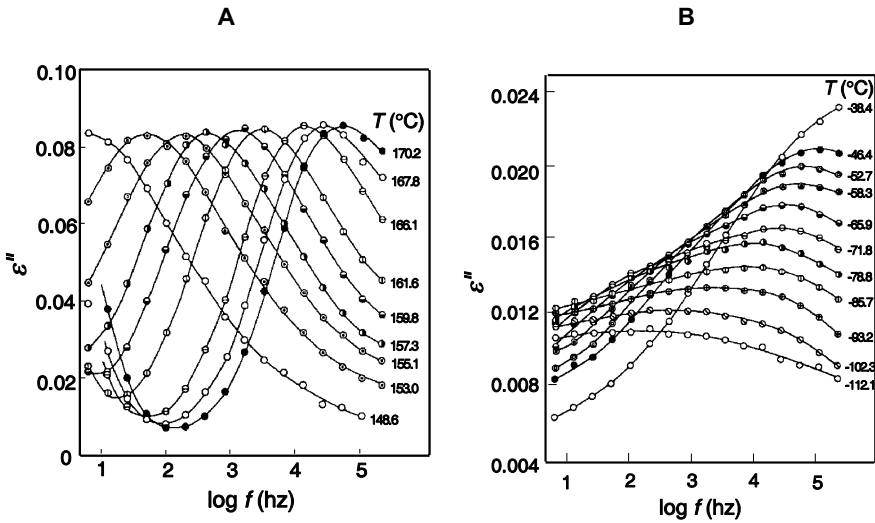


Figure 5-14 Plots of the dielectric loss constant (ϵ'') of polycarbonate as a function of frequency at different temperatures [11]. **A.** High-temperature data showing the α peak (i.e., the glass transition). **B.** Low-temperature data showing the secondary γ relaxation. The peak maxima are shown to increase in frequency with increasing temperature.

5.1.5 Dynamic Calorimetry

A variation of traditional differential scanning calorimetry (Section 4.3.2) is temperature-modulated DSC (TMDSC) [12, 13]. The principle behind TMDSC is the superimposition of a sinusoidal modulation of temperature upon the constant heating (or cooling) rate of conventional DSC operation. The sample temperature, T , is then given by

$$T = T_0 + q_0 t + A_T \sin(\omega t) \quad (5.116)$$

where T_0 is the initial temperature for the modulated scan, q_0 is the average heating rate, A_T is the amplitude of the temperature modulation, and ω is the angular frequency (rad min^{-1}) of the modulation. The time derivative of eq. (5.116) gives the heating rate modulation

$$q = q_0 + A_T \omega \cos(\omega t). \quad (5.117)$$

Fourier transformations of the modulated heating rate (q) and the heat-flow (HF) signals yield the average values $\langle q \rangle$ and $\langle HF \rangle$, the amplitudes A_q and A_{HF} of the heating rate and heat-flow signals, and the phase angle, ϕ , between these signals. From these values, average and complex heat capacities are obtained as

$$\langle C_p \rangle = \frac{\langle HF \rangle}{\langle q \rangle} \quad (5.118)$$

and

$$C_p^* = C_p' - iC_p'' \quad (5.119)$$

The magnitude of the complex heat capacity is determined from the signal amplitudes as

$$|C_p^*| = \frac{A_{HF}}{A_q} \quad (5.120)$$

The real (i.e., in-phase), C_p' , and imaginary (i.e., out-of-phase), C_p'' , components of the complex heat capacity are related to the magnitude and phase angle as

$$C_p' = |C_p^*| \cos \phi \quad (5.121)$$

and

$$C_p'' = |C_p^*| \sin \phi \quad (5.122)$$

These dynamic components of heat capacity are shown in comparison to a conventional DSC signal in Figure 5-15. In the TMDSC scan, the glass transition is identified by both a step change in C_p' and a peak in C_p'' in a manner similar to dielectric spectroscopy. In a conventional DSC scan, T_g is usually identified as the point of inflection in the specific heat or heat flow signal and is dependent upon the heating (or cooling) rate (see Section 4.3.4). In contrast, T_g determined from TMDSC measurements, like T_g determined by other dynamic techniques, is dependent upon the frequency of the modulation.

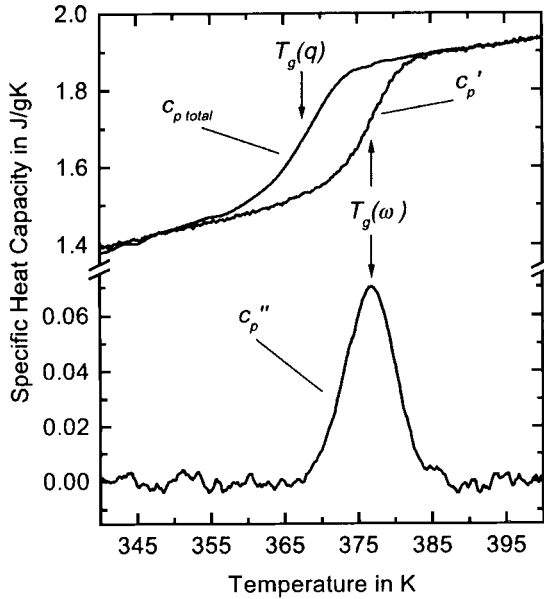


Figure 5-15 TMDSC scan of a polystyrene sample ($q_0 = -0.25 \text{ K min}^{-1}$; $A_T = 0.5 \text{ K}$, period $t_p = 60 \text{ s}$). A conventional DSC scan is shown by the top curve ($C_{p, \text{total}}$). Reprinted from S. Weyer, M. Merzlyakov, and C. Schick, *Application of an Extended Tool–Narayanaswamy–Moynihan Model. Part 1. Description of Vitrification and Complex Heat Capacity Measured by Temperature-Modulated DSC*. *Thermochimica Acta*, 2001. **377**: p. 85–96. Copyright 2001, with permission from Elsevier Science.

Alternatively, the response of TMDSC can be expressed as reversing and non-reversing heat flow as

$$\langle HF \rangle_{\text{rev}} = |C_p^*| q_0 \quad (5.123)$$

and

$$\langle HF \rangle_{\text{non-rev}} = \langle HF \rangle - \langle HF \rangle_{\text{rev}}. \quad (5.124)$$

For isothermal operation ($q_0 = 0$), as may be used in the study of thermoset cure, the reversing heat flow is zero (eq. (5.123)) and the non-reversing heat flow is the same as the total heat flow. One of the advantages of TMDSC has been its potential to separate reversible processes, such as the pseudo second-order glass transition, from non-reversing events (e.g., enthalpy recovery, recrystallization, and chemical reac-

tion occurring during cure). Exothermal events are detected only during the non-reversing signal.

5.1.6 Time–Temperature Superposition

Often, it is important to know how a material will behave (e.g., creep or stress relaxation) at a fixed temperature, but over a long time period (perhaps years) that may not be realistically accessible. Fortunately, long-time behavior can be evaluated by measuring stress-relaxation or creep data over a shorter period of time but at several different temperatures. Information from each of these different temperature curves may then be combined to yield a *master curve* at a single temperature by horizontally shifting each curve along the log time scale. This technique is called *time–temperature superposition* and is a foundation of linear viscoelasticity theory. In this procedure, the master curve is plotted as stress-relaxation modulus or creep compliance versus reduced time, t/a_T . The *shift factor*, a_T , is defined as the ratio of (real) time to reach a particular value of modulus at some temperature to the reference-scale time coordinate, t_r , corresponding to the same value of modulus in the master curve at the reference temperature, T_r ,

$$\boxed{a_T = \frac{t}{t_r}} \quad (5.125)$$

Stated more concisely, the time–temperature superposition principle says that

$$E(T, t) = E(T_r, t_r). \quad (5.126)$$

The procedure of horizontal shifting is illustrated for stress-relaxation and torsional–creep data for polycarbonate in Figure 5-16.

The dependence of the shift factor, a_T , on temperature is given by the *Williams–Landel–Ferry (WLF) relationship*

$$\boxed{\log a_T = \frac{-C_1(T - T_r)}{C_2 + T - T_r}} \quad (5.127)$$

where C_1 and C_2 are constants for a given polymer and T_r is the reference temperature. When T_r is taken to be the polymer T_g , as it often is, C_1 and C_2 may be approximated by the “universal” values of 17.44 and 51.6, respectively; however, significant deviations from these values may exist for some polymers (see Problem 5.7), as shown by values given for some common polymers in Table 5-3.

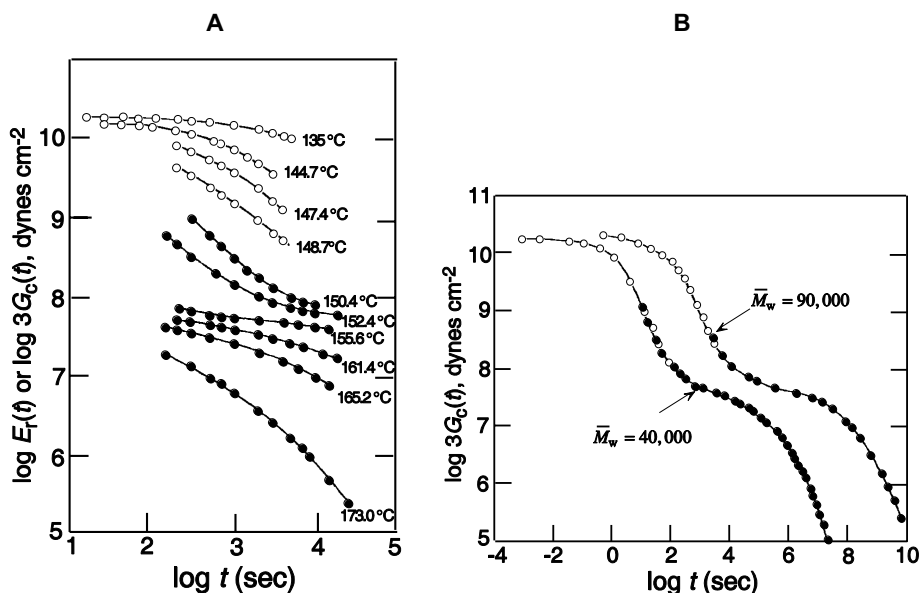


Figure 5-16 A. Modulus of polycarbonate ($\bar{M}_w = 90,000$) as a function of time and temperature from stress-relaxation (\bullet) and torsional-creep (\circ) measurements. B. Resulting master curve obtained by shifting both sets of data at a reference temperature of 150°C and for two different molecular-weight samples of polycarbonate ($\bar{M}_w = 40,000$ and 90,000). The master curve is shown to shift to higher times with increasing molecular weight. J. P. Mercer, et al., *Viscoelastic Behavior of the Polycarbonate of Bisphenol A*. *Journal of Applied Polymer Science*, 1965. **9**: p. 447–459.

Table 5-3 WLF Parameters of Some Common Polymers

Polymer	T_g (K)	C_1	C_2
Natural rubber	200	16.7	53.6
Polyisobutylene	202	16.6	104
Polyurethane	238	15.6	32.6
Poly(vinyl acetate)	304	17.4	43.4
Poly(ethyl methacrylate)	335	17.6	65.5
Poly(ethylene terephthalate), amorphous	343	17.1	31.7
Poly(ethylene terephthalate), crystalline	353	30.4	106.6
Poly(vinyl chloride)	353	16.2	49.7
Polystyrene	373	13.7	50.0

If C_1 and C_2 are not known, each curve may be horizontally shifted to the reference temperature curve until a value of modulus on the shifted curve coincides

with one on the reference curve.* The shift factor may then be calculated by use of the defining relationship for a_T given by eq. (5.125). The WLF parameters, C_1 and C_2 , may then be determined by plotting $(T - T_r)/\log a_T$ versus $(T - T_r)$, where rearrangement of eq. (5.127) gives

$$\frac{T - T_r}{\log a_T} = -\frac{1}{C_1}(T - T_r) - \frac{C_2}{C_1}. \quad (5.128)$$

Following this procedure, C_1 is obtained directly from the inverse of the slope, and C_2 can then be calculated from the value of C_1 and the intercept (C_2/C_1). It can be shown that C_1 and C_2 can be related to the fractional free volume at T_g (f_g) and the thermal-expansion coefficient of free volume (see Chapter 11, Appendix A.1).

As discussed in Section 4.1.2, Gibbs and DiMarzio have suggested that a true second-order transition should occur at a temperature (T_2) where the conformational entropy is zero. This would occur at an *equilibrium* glassy state that conceptually can be obtained by cooling from the melt at an infinitely slow rate. Therefore, the WLF relation can be used to determine the relationship between the thermodynamic transition temperature and the kinetic T_g by noting that shifting from a finite to an infinite time scale requires that the shift factor approach infinity or that the denominator in eq. (5.127) go to zero, where $T_r = T_g$ and $T = T_2$. This means that

$$T_2 = T_g - C_2 \approx T_g - 52 \quad (5.129)$$

using the universal value for C_2 . In other words, the true second-order transition temperature should lie approximately 52°C below the experimentally measured T_g .

The master curve for stress-relaxation modulus, shown in Figure 5-16B, illustrates the four characteristic regions of a high-molecular-weight polymer. At short times, the polymer behaves as a glassy material (glassy plateau), while at longer times the modulus sharply drops to the rubbery-plateau region. At sufficiently long times, the stress-relaxation modulus again rapidly falls. Conceptually, what is happening is that initially the polymer chains are entangled and unable to fully accommodate the applied strain on the sample. This results in a high apparent modulus. Eventually, sufficient time has elapsed at the experimental temperature for the chains to slip, and the sample adjusts to the load. The form of the master curve for stress relaxation is qualitatively similar to that of the plot of Young's modulus in

* It may be shown that for elastic chains in a network, the shear modulus is proportional to temperature and to density (i.e., chain concentration). Therefore, it may be necessary to introduce a small vertical shift to account for the dependence of modulus on both temperature and density (ρ). This correction may be expressed as

$$E(T_r, t_r) = \frac{\rho(T_r)T_r}{\rho(T)T} E(T, t).$$

Figure 4-19 where the units of the abscissa were temperature rather than time. The fact that time and temperature can be superimposed means that the change in modulus of the material with increasing time at constant temperature is equivalent to the change in modulus when measured at identical times but at increasing temperature.

5.1.7 Boltzmann Superposition Principle

Tensile (or shear) modulus and tensile (or shear) compliance are inversely related (see eq. 4.46). The same is true for complex modulus and complex compliance (see eq. (5.17)), but creep-compliance and stress-relaxation moduli are not as simply related; that is,

$$D(t) \neq \frac{1}{E_r(t)}.$$

This is because creep-compliance and stress-relaxation moduli are obtained by distinctly different experimental procedures. As discussed in Chapter 4, a fixed *load* is applied instantly at $t = 0$ in a creep experiment, while a fixed *strain* is applied instantaneously at $t = 0$ for stress-relaxation measurements.

A relationship between the creep-compliance and stress-relaxation moduli can be established by application of another fundamental statement of linear viscoelasticity, the *Boltzmann superposition principle*. This Boltzmann superposition principle states that the *total strain is a linear function of total applied stress*. In the case of a creep experiment, the strain is a function of the total load (stress) history in which each load makes an independent contribution to the creep. If a load, σ_0 , is instantaneously applied at time $t = 0$ and a second load, σ_1 , is applied at time $t = u_1$, as illustrated in Figure 5-17, then the strain at some time t' , where $t' > u_1$, is given by the Boltzmann superposition principle as

$$\varepsilon(t') = \sigma_0 D(t') + \sigma_1 D(t' - u_1). \quad (5.130)$$

In the general case of the application of a series of discrete loads, $\sigma_1, \sigma_2, \dots, \sigma_n$, applied at times $t = u_1, u_2, \dots, u_n$, the total resulting strain response in creep deformation is calculated from the tensile compliance function, $D(t)$, as

$$\varepsilon(t) = \sum_{i=1}^n \sigma_i D(t - u_i). \quad (5.131)$$

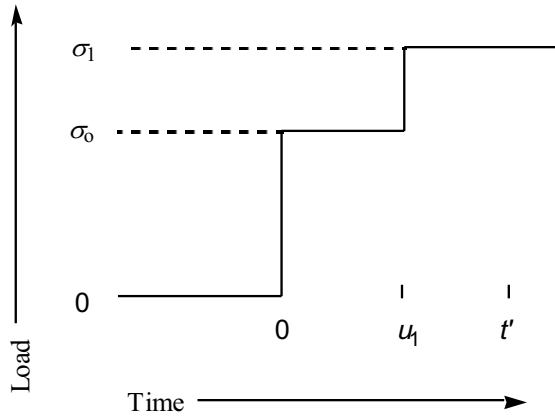


Figure 5-17 Stress history corresponding to the strain response given by eq. (5.130).

If the applied stress is some *continuous* function of time, $\sigma(t)$, application of the Boltzmann superposition principle gives the creep response in integral form as

$$\varepsilon(t) = \int_{-\infty}^t \left[\frac{\partial \sigma(u)}{\partial u} \right] D(t-u) du \quad (5.132)$$

where u is the time variable and integration covers the entire stress history ($-\infty < u \leq t$) of the sample. Using a convenient variable change, $a = t - u$, integration of eq. (5.132) by parts (see Appendix E at the end of this text) gives

$$\varepsilon(t) = D(0)\sigma(t) + \int_0^{\infty} \sigma(t-a) \left[\frac{\partial D(a)}{\partial a} \right] da. \quad (5.133)$$

The corresponding equations for stress relaxation are

$$\sigma(t) = \int_{-\infty}^t \left[\frac{\partial \varepsilon(u)}{\partial u} \right] E(t-u) du \quad (5.134)$$

and

$$\sigma(t) = E(0)\varepsilon(t) + \int_0^{\infty} \varepsilon(t-a) \left[\frac{\partial E(a)}{\partial a} \right] da. \quad (5.135)$$

5.1.8 Interrelationships between Transient and Dynamic Properties

A basis for relating the creep-compliance and stress-relaxation moduli is obtained by taking the Laplace transform of eqs. (5.132) and (5.134). A summary of the principles and basic relationships of Laplace transforms is included in Appendix E. It can be shown that the transformations of eqs. (5.132) and (5.134) give

$$\mathcal{L}[\varepsilon(t)] = p\mathcal{L}[\sigma(t)]\mathcal{L}[D(t)] \quad (5.136)$$

and

$$\mathcal{L}[\sigma(t)] = p\mathcal{L}[\varepsilon(t)]\mathcal{L}[E(t)] \quad (5.137)$$

where p is the Laplace variable. Substitution of eq. (5.136) into the RHS of eq. (5.137) gives the relationship between creep-compliance and stress-relaxation moduli in *transform space* (see Problem 5.3) as

$$\frac{1}{p^2} = \mathcal{L}[D(t)]\mathcal{L}[E(t)]. \quad (5.138)$$

The Boltzmann superposition principle also provides a means of interrelating dynamic (moduli) and transient (stress-relaxation) data. Utilizing eq. (5.134) and making a variable change in the form $s = t - u$ give

$$\sigma(t) = -\int_0^\infty \left[\frac{\partial \varepsilon(t-s)}{\partial s} \right] E(s) ds. \quad (5.139)$$

In dynamic oscillation,

$$\varepsilon(t-s) = \varepsilon^0 \exp[i\omega(t-s)] \quad (5.140)$$

and

$$\frac{\partial \varepsilon(t-s)}{\partial s} = \varepsilon(t)(-i\omega)\exp(-i\omega s). \quad (5.141)$$

Substitution of these equations into the integral of eq. (5.139), and noting that $\varepsilon(t)$ is not a function of s and, therefore, can be taken outside the integral, gives

$$\sigma(t) = i\varepsilon(t)\int_0^\infty \omega \exp(-i\omega s)E(s) ds. \quad (5.142)$$

Dividing both sides of this equation by $\varepsilon(t)$ and replacing the complex term by Euler's identity [$\exp(-i\omega s) = \cos \omega s - i \sin \omega s$] give the complex modulus as

$$E^* = \frac{\sigma(t)}{\varepsilon(t)} = \int_0^\infty \omega \sin(\omega s) E(s) ds + i \int_0^\infty \omega \cos(\omega s) E(s) ds . \quad (5.143)$$

Relating this equation to the customary form of E^* ($= E' + iE''$) gives the relationships between the stress-relaxation modulus, $E(s)$, and the storage and loss moduli as

$$E' = \omega \int_0^\infty \sin(\omega s) E(s) ds \quad (5.144)$$

and

$$E'' = \omega \int_0^\infty \cos(\omega s) E(s) ds . \quad (5.145)$$

The preceding equations may be recognized as the Fourier *sine* and *cosine* transforms of the stress-relaxation modulus function. This means that if the form of the stress-relaxation function is known, the dynamic moduli can be determined by taking the sine or cosine transforms of the function. Tables of these transforms are available in most handbooks of mathematical tables. For convenience, some important Fourier transforms are listed in Appendix E.

5.2 Introduction to Rubber Elasticity

In 1805, John Gough observed that the temperature of a rubber band would increase as it is stretched adiabatically. Also, if a weight is hung from the end of the rubber band and heat is applied, the rubber band will *decrease* in length rather than stretch, as observed for other materials such as common metals and gases as illustrated in Figure 5-18. It was not until the 1930s that an explanation for this behavior, known as the *Gough–Joule effect*, was provided by means of classical thermodynamics as described in the following section.

5.2.1 Thermodynamics

The first and second laws of thermodynamics applied to a reversible, equilibrium process provide the relationship between internal energy (U), entropy (S), and work (W) as

$$dU = TdS - dW . \quad (5.146)$$

For deformation of a rubber band, the work is a combination of pressure-volume expansion and the work due to the (tensile) force (f) applied to the rubber band, given as

$$dW = pdV - fd\ell \quad (5.147)$$

where the convention is that work done *by* the system (i.e., pressure-volume work) is positive and the work done *on* the system (i.e., force-displacement work) is negative. Enthalpy is related to the internal energy as

$$dH = dU + pdV. \quad (5.148)$$

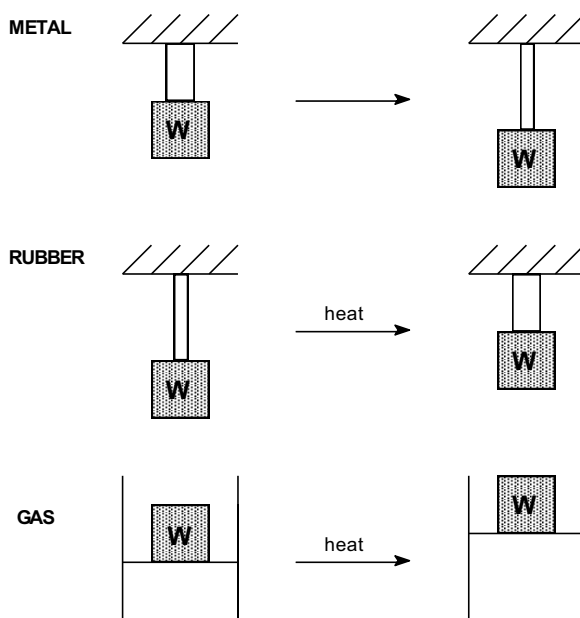


Figure 5-18 Illustration of the effect of heat on metal, rubber, and gas. Shaded boxes represent an applied load. Used with permission from J. E. Mark, *Rubber Elasticity*. The Journal of Chemical Education. **58**(11): 1981, p. 898–903. Copyright © 1981, Division of Chemical Education, Inc., American Chemical Society.

Substitution of eqs. (5.146) and (5.147) (in the form $pdV = dW + fd\ell$) into eq. (5.148) gives

$$dH = TdS + fd\ell. \quad (5.149)$$

At constant temperature and pressure, rearrangement of eq. (5.149) in terms of force and taking the (partial) derivative with respect to length at constant temperature and pressure give

$$f = \left(\frac{\partial H}{\partial \ell} \right)_{T,p} - T \left(\frac{\partial S}{\partial \ell} \right)_{T,p} . \quad (5.150)$$

Equation (5.150) shows that elastic force has both an enthalpic and entropic component ($f = f_e + f_s$).

In order to obtain an expression for the temperature dependence of force, we make use of the relation*

$$\left(\frac{\partial S}{\partial \ell} \right)_{T,p} = - \left(\frac{\partial f}{\partial T} \right)_{p,\ell} . \quad (5.151)$$

Substitution of eq. (5.151) into eq. (5.150) gives

$$f = \left(\frac{\partial H}{\partial \ell} \right)_{T,p} + T \left(\frac{\partial f}{\partial T} \right)_{p,\ell} . \quad (5.152)$$

Rearrangement of eq. (5.152) gives

$$\left(\frac{\partial f}{\partial T} \right)_{p,\ell} = \frac{f - (\partial H / \partial \ell)_{T,p}}{T} . \quad (5.153)$$

Equation (5.153) indicates that the slope of a force-temperature plot will be positive, as is usually observed for elastomers at moderate or higher extension, if

$$f > \left(\frac{\partial H}{\partial \ell} \right)_{T,p} .$$

This condition is satisfied except for very small extensions, as illustrated by Figure 5-19. It can be shown that the change of enthalpy due to deformation at constant temperature and pressure has both internal energy, U , and volume contributions as given by the expression

* Obtained from the reciprocity relationship for the exact differential equation for Gibbs free energy given as

$$dG = -SdT + Vdp + fd\ell .$$

$$\left(\frac{\partial H}{\partial \ell}\right)_{T,p} = \left(\frac{\partial U}{\partial \ell}\right)_{T,V} + T\left(\frac{\alpha}{\beta}\right)\left(\frac{\partial V}{\partial \ell}\right)_{T,p}. \quad (5.154)$$

Since elastomers are nearly incompressible, it is clear that the second term on the RHS of eq. (5.154) is very small. Furthermore, changes in internal energy due to conformation changes during deformation are also small. For these reasons, enthalpic contributions in rubber elasticity are generally insignificant and rubber-like behavior can be satisfactorily explained on the basis of entropic considerations alone. Conceptually, we can view polymer chains to be in an entropically favorable, disordered state when undeformed. During deformation, the chains become ordered and, therefore, an entropically driven force develops to restore the more favorable disordered conformational state.

The importance of entropy to the deformation of an ideal elastomer can be compared to that of an ideal gas. Heating a gas increases the driving force toward a state of maximum entropy. This means that an increase in temperature results in an increase in volume at constant pressure as was illustrated in Figure 5-18. Since the deformation of a compressed gas can be expressed as the reciprocal volume ($1/V$), we can say that an increase in the temperature of a gas at constant pressure results in a decrease in its deformation. This is analogous to the case of an elastomer whose measure of deformation is its length (ℓ), which decreases with an increase in temperature.

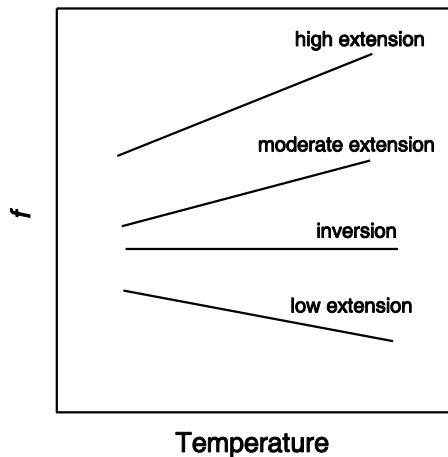


Figure 5-19 Thermoelastic behavior of elastomer at various elongations.

5.2.2 Statistical Theory

In the 1920s, Staudinger developed a thermodynamic expression for elastic force based upon polymer-chain statistics. The elastic force is related to the Helmholtz free energy, A , as

$$f = \left(\frac{\partial \Delta A}{\partial \ell} \right)_{T,V} \quad (5.155)$$

where $A = U - TS$ and ΔA represents the difference in Helmholtz free energy between the deformed and undeformed network ($\Delta A = A_d - A_u$). The entropy contribution is linked to the total number of conformations, Ω , available to the rubber network through the Boltzmann relation $S = k \ln \Omega$. An expression for Ω is obtained from the Gaussian radial-distribution function $\omega(r)$ for the i th chain in a network of N chains (see Section 3.1, eq. (3.5) and Figure 3-2) as

$$\Omega = \prod_{i=1}^N \omega(r_i). \quad (5.156)$$

The resulting equation for force is usually given in the form

$$f^* = G_o \left(\lambda - \frac{1}{\lambda^2} \right) \quad (5.157)$$

where f^* is the (nominal) stress, G_o is the shear modulus (one-third of the tensile modulus for incompressible materials), and λ is the principal *extension ratio*

$$\lambda = \frac{L}{L_o} = 1 + \varepsilon \quad (5.158)$$

where L_o is the original (undeformed) length of the elastomer and ε is the engineering or nominal strain.

The shear modulus, G_o , is proportional to temperature and to the number of chains in the elastomeric network (see eq. (4.49)). High crosslink density results in an increase in the number of network chains per unit volume and will, therefore, increase modulus. This will become apparent by comparing the stiffness of a lightly crosslinked rubber band with a highly crosslinked ebonite bowling ball.

As shown in Figure 5-20, the theory gives a good representation of the experimental stress-strain curve only for moderate strains ($\lambda = 1.5$). For larger extensions, the theory overestimates stress because the conformational state is no longer adequately predicted by the Gaussian-distribution model used in the derivation (eq. (5.156)). At still higher extensions ($\lambda > 6$), the observed stress rapidly rises due to the development of strain-induced crystallization. The increase in modulus is due to

the physical reinforcement effect of the crystallites. In general, the increase in modulus of an elastomer due to the presence of crystallites or the incorporation of fillers such as carbon black can be approximated by the *Guth–Smallwood equation*

$$\frac{E_f}{E_o} = 1 + 2.5\phi_f + 14.1\phi_f^2 \quad (5.159)$$

where E_f is the tensile (Young's) modulus of the filled elastomer, E_o is the modulus of the unreinforced elastomer, and ϕ_f is the volume fraction of the filler.

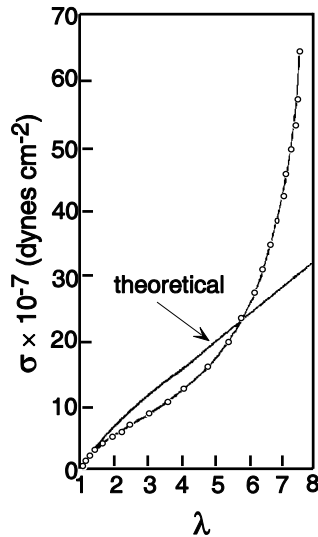


Figure 5-20 Comparison of the statistical-thermodynamic relationship (eq. (5.157) where $G_o = 4 \times 10^6$ dynes cm^{-2}) with the experimental stress-strain data (O) for natural rubber. Adapted from L. R. G. Treloar, *Stress-Strain Data for Vulcanized Rubber under Various Types of Deformation*. Transactions of the Faraday Society, 1944. **40**: p. 59.

5.2.3 Phenomenological Model

Another widely used model of rubber elasticity has its origin in continuum mechanics. It is known as the *Mooney–Rivlin equation*, given as

$$f^* = 2 \left(C_1 + \frac{C_2}{\lambda} \right) \left(\lambda - \frac{1}{\lambda^2} \right) \quad (5.160)$$

where C_1 and C_2 are empirical constants (distinct from the WLF constants) and f^* is given as

$$f^* = \frac{f}{A_d} \quad (5.161)$$

where A_d is the cross-sectional area of the undeformed elastomer. Values of C_1 and C_2 are obtained by plotting experimental stress-strain data in terms of the *reduced stress* [f^*] defined as

$$[f^*] = \frac{f^*}{\lambda - \lambda^{-2}} \quad (5.162)$$

versus $1/\lambda$. The intercept gives C_1 while the slope yields C_2 . Equation (5.160) is very useful for describing the stress-strain curves of elastomers over a wide range of extensions.

5.2.4 Recent Developments

The statistical theory of rubber elasticity is based upon a number of significant assumptions including:

- Crosslinking does not alter the chain dimensions from their unperturbed state.
- The end-to-end separation of network chains can be fit by a Gaussian distribution.
- Crosslink junctions are fixed at their mean positions and these junctions deform in the same ratio as the macroscopic deformation of the sample (i.e., *affine deformation*).

An alternative to the affine model is the “*phantom chain*” approximation whereby chains are permitted to pass through one another as if they had zero cross-sectional area. While the deformation of the mean position of the crosslink junctions is affine, the junctions are allowed to fluctuate about their mean positions. The phantom theory predicts moduli that are lower than predicted by the affine model. Both models predict that the modulus of a rubber network is independent of the deformation; however, experiments show that modulus actually decreases with an increase in λ as is correctly represented by the Mooney–Rivlin equation (eq. (5.160)), which owes its origin to continuum mechanics. Comparison of eq. (5.160) with the form of the statistical-theory result (eq. (5.157)) indicates that the λ -dependence of modulus is given as

$$[f^*] = 2C_1 + 2C_2\lambda^{-1} \quad (5.163)$$

where the Mooney–Rivlin constants are themselves independent of λ . More recent theoretical models, which are beyond the scope of this discussion, provide an improved model for the dependence of $[f^*]$ on λ and offer better insight into the molecular theory of rubber elasticity [14]. These include the constrained-junction and, later, the constrained-chain models for which the phantom-model prediction is approached as a limiting case at small deformations.

SUGGESTED READING

DIELECTRIC SPECTROSCOPY

Daniels, V. V., *Dielectric Relaxation*. 1967, London: Academic Press.

Runt, J. P., and J. J. Fitzgerald, *Dielectric Spectroscopy of Polymeric Materials: Fundamentals and Applications*. 1997, Washington DC: American Chemical Society.

DYNAMIC MECHANICAL SPECTROSCOPY

Boyer, R. F., *Dependence of Mechanical Properties on Molecular Motion in Polymers*. Polymer Engineering and Science, 1968. **8**(3): p. 161.

Gillham, J. K., *Characterization of Thermosetting Materials by Torsional Braid Analysis*. Polymer Engineering and Science, 1976. **16**(5): p. 353.

Gillham, J. K., *The TBA Torsion Pendulum: A Technique for Characterizing the Cure and Properties of Thermosetting Systems*. Polymer International, 1997. **44**: p. 262.

Gillham, J. K., and J. B. Enns, *On the Cure and Properties of Thermosetting Polymers Using Torsional Braid Analysis*. Trends in Polymer Science, 1994. **2**(12): p. 406.

Heijboer, J., *The Torsion Pendulum in the Investigation of Polymers*. Polymer Engineering and Science, 1979. **19**(10): p. 664.

RUBBER ELASTICITY

Boyce, M. C., and E. M. Arruda, *Constitutive Models of Rubber Elasticity: A Review*. Rubber Chemistry and Technology, 2000. **73**: p. 504.

Erman, B., and J. E. Mark, *Rubber-Like Elasticity*. Annual Review of Physical Chemistry, 1989. **40**: p. 351.

Flory, P. J., *Molecular Theory of Rubber Elasticity*. Polymer Journal, 1985. **17**(12): p. 1.

James, H. M., and E. Guth, *Simple Presentation of Network Theory of Rubber, with a Discussion of Other Theories*. Journal of Polymer Science, 1949. **4**: p. 153.

Kloczkowski, A., *Application of Statistical Mechanics to the Analysis of Various Physical Properties of Elastomeric Networks—a Review*. Polymer, 2002. **43**: p. 1503.

Mark, J. E., *Rubber Elasticity*. Journal of Chemical Education, 1981. **58**(11): p. 898.

Mark, J. E., *Experimental Determinations of Crosslink Densities*. Rubber and Chemistry Technology, 1982. **55**(13): p. 762.

Mark, J. E., and B. Erman, *Rubberlike Elasticity*. 1988, New York: John Wiley & Sons.

- Mark, J. E., and B. Erman, *Elastomeric Polymer Networks*. 1992, Englewood Cliffs: Prentice Hall.
- Nielsen, L. E., *Cross-Linking Effect on Physical Properties of Polymers*. Journal of Macromolecular Science—Reviews in Macromolecular Chemistry, 1969. **C3**(1): p. 69.
- Treloar, L. R. G., *Stress-Strain Data for Vulcanised Rubber under Various Types of Deformation*. Transactions of the Faraday Society, 1944. **40**: p. 59.
- Treloar, L. R. G., *The Physics of Rubber Elasticity*. 1958, Oxford University Press.

TEMPERATURE-MODULATED DSC

- Hutchinson, J. M., and S. Montserrat, *The Application of Temperature-Modulated DSC to the Glass Transition Region. II. Effect of a Distribution of Relaxation Times*. Thermochimica Acta, 2001. **377**: p. 63–84.
- Montserrat, S., and I. Cima, *Isothermal Curing of an Epoxy Resin by Alternating Differential Scanning Calorimetry*. Thermochimica Acta, 1999. **330**: p. 189–200.
- Ribeiro, M., and J.-P. E. Grolier, *Temperature Modulated DSC for the Investigation of Polymer Materials*. Journal of Thermal Analysis and Calorimetry, 1999. **57**: p. 253–263.
- Scherrenberg, R., V. Mathot, and P. Steeman, *The Applicability of TMDSC to Polymeric Systems. General Theoretical Description Based on the Full Heat Capacity Formulation*. Journal of Thermal Analysis, 1998. **54**: p. 477–499.
- Scherrenberg, R., V. Mathot, and A. Van Hemelrijck, *The Practical Applicability of TMDSC to Polymeric Systems*. Thermochimica Acta, 1999. **330**: p. 3–19.

VISCOELASTICITY

- Aklonis, A. A., and W. J. MacKnight, *Introduction to Polymer Viscoelasticity*. 2nd ed. 1983, New York: John Wiley & Sons.
- Ferry, J. D., *Viscoelastic Properties of Polymers*. 3rd ed. 1980, New York: John Wiley & Sons.
- Ferry, J. D., *Some Reflections on the Early Development of Polymer Dynamics: Viscoelasticity, Dielectric Dispersion, and Self-Diffusion*. Macromolecules, 1991. **24**(19): p. 5237–5245.
- McCrum, N. G., B. E. Read, and G. Williams, *Anelastic and Dielectric Effects in Polymeric Solids*, 1967, New York: John Wiley & Sons.
- Pearson, D. S., *Recent Advances in the Molecular Aspects of Polymer Viscoelasticity*. Rubber Chemistry and Technology, 1967. **40**: p. 439.
- Tschoegl, N. W., *The Phenomenological Theory of Linear Viscoelastic Behavior: An Introduction*, 1989, Berlin: Springer-Verlag.

PROBLEMS

- 5.1 Show that $|E^*| = \sigma^0 / \varepsilon^0$ and $|D^*| = 1/E^*$.

5.2 Show that the work per cycle per unit volume performed during dynamic tensile oscillation of a viscoelastic solid may be given as $\pi\sigma^0\varepsilon^0\sin\delta$ (eq. (5.30)).

5.3 Given the expression $G(t) = G_0 \exp(-t/\tau) + G_1$, show that the compliance function, $J(t)$, can be written in the form $J(t) = A - B \exp(-Ct/\tau)$, where A, B, and C are constants.

5.4 For a Maxwell model, show the following:

(a) The equation for complex modulus E^* (eq. (5.57)) can be obtained from the Fourier transform of the stress-relaxation modulus, E_r (eq. (5.49)).

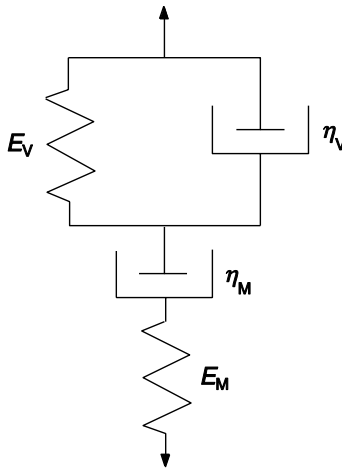
(b) A maximum in the loss modulus plotted as a function of frequency occurs at $\omega = 1/\tau$.

5.5 Given the four-element model illustrated below, derive an analytical solution for the strain behavior and sketch $\varepsilon(t)$ versus time under the following stress conditions:

$$t < 0 \quad \sigma = 0$$

$$0 \leq t < t_1 \quad \sigma = \sigma_0 \quad (\text{creep})$$

$$t_1 \leq t < t_2 \quad \sigma = 0 \quad (\text{creep recovery})$$



5.6 In the case of the expression for the dielectric loss constant given by eq. (5.112), the relaxation time can be assigned a temperature dependence of the form

$$\tau = \tau_0 \exp(H/RT)$$

where H is the activation energy. If ε'' assumes its maximum value at that temperature (T_{\max}) where $\omega = 1/\tau$, how can the value of H be determined given data in the form of a plot of ε'' versus T at different frequencies, f ?

5.7 Calculate the WLF shift factor, a_T , for polystyrene (PS) at 150°C given that the reference temperature is taken to be the T_g of PS, 100°C, and using (a) the “universal” values of the WLF parameters, C_1 and C_2 , and (b) the reported values of $C_1 = 13.7$ and $C_2 = 50.0$ K for PS.

5.8 If the maximum in the α -loss modulus of polystyrene at 1 Hz occurs at 373 K, at what temperature would the maximum occur at 110 Hz if the activation energy for this relaxation is 840 kJ mol⁻¹?

5.9 (a) Calculate the relaxation modulus, in SI units of GPa, at 10 seconds after a stress has been applied to three Maxwell elements linked in parallel using the following model parameters:

$$E_1 = 0.1 \text{ GPa} \quad \tau_1 = 10 \text{ s}$$

$$E_2 = 1.0 \text{ GPa} \quad \tau_2 = 20 \text{ s}$$

$$E_3 = 10 \text{ GPa} \quad \tau_3 = 30 \text{ s}$$

(b) Does this model give a realistic representation of stress relaxation behavior of a real polymer? Explain.

5.10 An elastomeric cube, 2 cm on a side, is compressed to 95% of its original length by applying a mass of 5 kg. What force is required to stretch a strip of the same elastomer by 50%? The initial length of the strip is 2 cm and its original cross-sectional area is 1 cm².

5.11 If the stress at 23°C of an ideal rubber is 100 psi when stretched to twice its original length, what would be the stress at a 50% extension?

5.12 The length of an ideal rubber band is increased 100% to 12.0 cm at 23°C. Stress on this rubber band increases by 0.2 MPa when it is heated to 30°C at 100% elongation. What is its tensile modulus in MPa at 23°C when it is stretched 2%?

5.13 Calculate the shear modulus (GPa) of a polymer sample in a torsion pendulum with a period of 1.0 s. The specimen is 10 cm long, 2 cm wide, and 7.5 mm thick and the moment of inertia is 5000 g cm².

5.14 For a two-phase system for which the complex shear modulus follows a log rule of mixtures, show that

$$\frac{G''}{G'} \cong \frac{G_1''}{G_1'} \phi_1 + \frac{G_2''}{G_2'} \phi_2.$$

REFERENCES

1. Nielsen, L. E., *Dynamic Mechanical Properties of High Polymers*. SPE Journal, 1960. **16**: p. 525–532.
2. Murayama, T., *Dynamic Mechanical Analysis of Polymeric Material*. 1978, Amsterdam: Elsevier.
3. Gillham, J. K., *Torsional Braid Analysis (TBA) of Polymers*, in *Development in Polymer Characterisation-3*, J. V. Dawkins, ed. 1982, Applied Science Publishers Ltd: London. p. 159–227.
4. Gillham, J. K., S. J. Stadnicki, and Y. Hazony, *Low-Frequency Thermomechanical Spectroscopy of Polymeric Materials: Tactic Poly(methyl methacrylate)*. Journal of Applied Polymer Science, 1977. **21**: p. 401–424.
5. O'Reilly, J. M., H. E. Bair, and F. E. Karasz, *Thermodynamic Properties of Stereoregular Poly(methyl methacrylate)*. Macromolecules, 1982. **15**: p. 1083–1088.
6. Fried, J. R., A. Letton, and W. J. Welsh, *Secondary Relaxation Processes in Bisphenol-A Polysulphone*. Polymer, 1990. **31**: p. 1032–1037.
7. McCrum, N. G., B. E. Read, and H. G. Williams, *Anelastic and Dielectric Effects in Polymeric Solids*. 1967, New York: John Wiley & Sons.
8. Fried, J. R., *Sub- T_g Transitions*, in *Physical Properties of Polymers Handbook*, J.E. Mark, ed. 2007, Springer: New York. p. 217–232.
9. Walters, K., *Rheometry*. 1975, London: Chapman and Hall.
10. Middleman, S., *The Flow of High Polymers*. 1968, New York: Interscience.
11. Matsuoka, S. and Y. Ishida, *Multiple Transitions in Polycarbonate*. Journal of Polymer Science: Part C, 1966. **14**: p. 247–259.
12. Reading, M., *Modulated Differential Scanning Calorimetry—A New Way Forward in Materials Characterization*. Trends in Polymer Science, 1993. **1**(8): p. 248–253.
13. Hutchinson, J. M., *Characterising the Glass Transition and Relaxation Kinetics by Conventional and Temperature-Modulated Differential Scanning Calorimetry*. Thermochimica Acta, 1998. **324**: p. 165–174.
14. Mark, J. E., *Molecular Theories of Rubberlike Elasticity and Some Recent Results on Model Networks and Unusual Fillers*. Kautschuk Gummi Kunststoffe, 1989. **42**(3): p. 191–193.

This page intentionally left blank

Polymer Degradation and the Environment

*P*olymers are susceptible to attack by a wide variety of naturally occurring and man-made agents. Some of these environmental agents and examples of polymers that are particularly susceptible to their action are listed in Table 6-1. In most cases, such environmental action is deleterious. For example, UV radiation and ozone can seriously degrade the unsaturated elastomers used in rubber tires. This degradation will limit the lifetime of the tire and could cause catastrophic failure. In practice, UV and ozone resistance is provided by adding various fillers and stabilizers to tire formulations (see Chapter 7).

In some cases, degradation may be a desirable goal. For example, it would be advantageous to be able to design plastic bottles and packaging film so that they rapidly degrade into environmentally safe by-products (e.g., carbon dioxide, water, and biomass) that will occupy less volume in a landfill. The challenge is to ensure that degradation does not occur during the normal shelf life of the plastic and that

cost and mechanical and other properties are not overly compromised to achieve biodegradability.

Table 6-1 Effects of Environmental Agents on Polymers

Agent	Susceptible Polymers	Examples
Biodegradation	Short-chain polymers, nitrogen-containing polymers, polyesters	Polyurethanes Polyether-polyurethane
Ionizing radiation	Aliphatic polymers having quaternary carbon atoms	Poly(methyl methacrylate) Polyisobutylene Polypropylene
Moisture	Heterochain polymers	Polyesters Polyamides Polyurethanes
Organic liquids and vapors	Amorphous polymers	Polystyrene Poly(methyl methacrylate)
Ozone	Unsaturated elastomers	Polyisoprene Polybutadiene
Sunlight	Photosensitive polymers	Polyacetals Polycarbonate

6.1 Polymer Degradation and Stability

Polymers can degrade by exposure to high temperature (thermal degradation), shear action (mechanodegradation), oxygen and ozone, electromagnetic (γ , UV) and ultrasonic radiation, moisture (hydrolysis), and chemical agents. Often, multiple exposures, such as a combination of moisture and heat or oxygen and light (photooxidation), can result in accelerated deterioration. Deterioration of plastics to normal environmental conditions is called *weathering*. Factors that contribute to weathering include radiation (UV, visible, and near-infrared), moisture, temperature cycling, and wind. Factors regulating the effects of temperature, oxygen, moisture, radiation, and chemical agents on the degradation of plastics are discussed in this section.

6.1.1 Thermal Degradation

In general, vinyl polymers are particularly susceptible to thermal degradation, which can occur either by chain scission involving the breakage of the backbone bonds to yield free-radical segments, or by non-chain scission, involving the elimi-

nation of a small molecule from a substituent group and subsequent double-bond formation. These two routes are illustrated for a vinyl polymer in Figure 6-1.

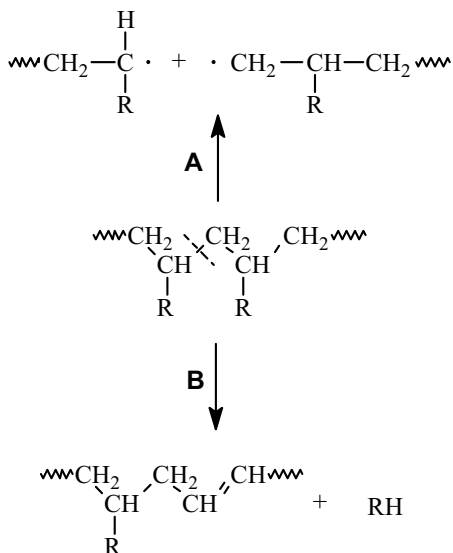
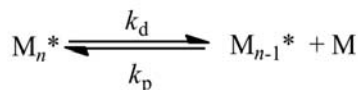


Figure 6-1 Illustration of thermal degradation of a vinyl polymer by (A) random chain scission and (B) non-chain scission mechanisms.

Chain Scission. Chain scission can occur by one of three mechanisms. These are (1) *random degradation*, where the chain is broken at random sites; (2) *depolymerization*, where monomer units are released at an active chain end; and (3) *weak-link degradation*, where the chain breaks at the lowest-energy bonds. In addition to thermal energy, degradation may be initiated by photochemical action, irradiation, or mechanical action.

Random homolytic cleavage of a polymer chain will result in a complex mixture of low-molecular-weight degradation products. Polyethylene and polypropylene degrade in this manner. In the case of 1,1-disubstituted vinyl polymers, the radical segments formed from the initial scission reaction will then depolymerize. This results in a gradual reduction in molecular weight and the production of monomer. Depolymerization may also be preceded by an initial scission at the chain end, as in the case of poly(methyl methacrylate).

The mechanism of *depolymerization* may be represented as



where k_d and k_p are the constants for depropagation and propagation, respectively, and M^* represents an active chain. At some temperature, called the *ceiling temperature*, T_c (see Section 2.2.1), the rates of propagation and depolymerization are equal and, therefore,

$$k_d [M_n^*] = k_p [M_{n-1}^*][M]. \quad (6.1)$$

If the molecular weight is high (i.e., $n \gg 1$), then M_{n-1} and M_n are indistinguishable and, therefore,

$$k_d = k_p [M]. \quad (6.2)$$

Expressing the rate constants in Arrhenius form then gives

$$A_d \exp\left(\frac{-E_d}{RT_c}\right) = A_p \exp\left(\frac{-E_p}{RT_c}\right)[M] \quad (6.3)$$

where A_d and A_p are called the collision frequency factors and E_d and E_p are the activation energies for depolymerization and polymerization, respectively. Rearrangement gives the following relationship for the ceiling temperature:

$$T_c = \left(\frac{E_p - E_d}{R \ln(A_p [M] / A_d)} \right). \quad (6.4)$$

The ceiling temperature varies widely with polymer structure, as illustrated by values given for several vinyl polymers in Table 6-2. For example, the ceiling temperature of polystyrene is 310°C but only 61°C for the 1,1-disubstituted vinyl polymer, poly(α -methylstyrene), which is much more sterically hindered at the radical site due to the presence of the methyl substituent at the α carbon site.

Whether or not a polymer will thermally depolymerize to yield monomer is only partly related to its ceiling temperature. Two other factors affecting depolymerization are the reactivity of the polymer-chain radicals in chain-transfer reaction and the activity of the available chain-transfer sites in the polymer. For example, polytetrafluoroethylene (PTFE) with a very high T_c (500°C) will produce almost a quantitative yield of monomer upon thermal degradation at temperatures *well below* T_c . The reason for this behavior is that the C–F bond of PTFE is very unreactive to a free-radical chain-transfer reaction and, as a result, the polymer provides no active chain-transfer sites to compete with the depolymerization process.

Table 6-2 Ceiling Temperatures of Some Common Vinyl Polymers

Polymer	Structure	T_c (°C)
Poly(α -methylstyrene)	$\left[\text{CH}_2 - \underset{\text{C}_6\text{H}_5}{\overset{\text{CH}_3}{\text{C}}} \right]$	61
Poly(methyl methacrylate)	$\left[\text{CH}_2 - \underset{\text{C}(=\text{O})\text{OCH}_3}{\overset{\text{CH}_3}{\text{C}}} \right]$	220
Polypropylene	$\left[\text{CH}_2 - \underset{\text{CH}_3}{\text{CH}} \right]$	300
Polystyrene	$\left[\text{CH}_2 - \underset{\text{C}_6\text{H}_5}{\text{CH}} \right]$	310
Polyethylene	$\left[\text{CH}_2 - \text{CH}_2 \right]$	400
Polytetrafluoroethylene	$\left[\underset{\text{F}}{\overset{\text{F}}{\text{C}}} - \underset{\text{F}}{\overset{\text{F}}{\text{C}}} \right]$	580

Non-chain Scission Reactions. One example of a common non-chain scission reaction is *dehydrohalogenation*, which results from the breakage of a carbon-halogen bond and the subsequent liberation of hydrogen halide. The most important example of a polymer that degrades by dehydrohalogenation is poly(vinyl chloride) (PVC). As illustrated in Figure 6-2, PVC undergoes dehydrochlorination at temperatures near and above its T_g (ca. 87°C) to yield hydrogen chloride and ultimately a *polyene* (i.e., conjugated double-bond) structure, which is accompanied by intense color formation. The presence of hydrogen chloride will accelerate the dehydrochlorination process, resulting in further property deterioration. PVC can be stabilized by adding compounds that interfere with the degradation process, neutralize hydrochloric acid as it is formed, trap free radicals, or react with double bonds to prevent subsequent chain scission. Commercial PVC resins usually contain organo-tin or similar thermal stabilizers (see Section 7.1.3). Another example of a commercial polymer that undergoes a non-chain scission reaction at high temperatures is

poly(vinyl alcohol) (PVA). Thermal degradation liberates acetic acid and results in polyene formation as in the case of PVC.

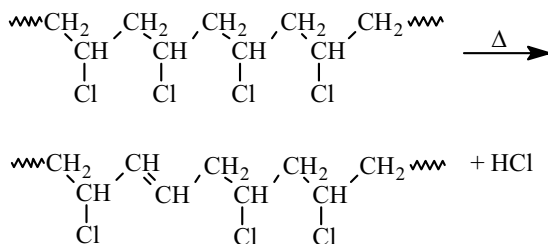


Figure 6-2 Partial dehydrochlorination of a repeating unit of PVC resulting in double-bond formation and the liberation of hydrogen chloride.

Polyacrylonitrile (PAN) is an interesting polymer with good gas-barrier properties suitable for packaging film (see Chapter 12). Although PAN can be solution-cast into film or solution-spun into textile (acrylic) fibers from organic solvents such as dimethylformamide (see Section 8.2.4), it cannot be melt-processed like other thermoplastics. This is because the nitrile ($-\text{C}=\text{N}$) groups of PAN undergo a cyclization reaction at elevated temperatures to yield a ladder-type polymer, as shown in Figure 6-3. This thermally modified form is deeply colored and insoluble but is important as the starting material in the production of some carbon and graphite fibers (see Section 7.1.2). Acrylonitrile finds use in thermoplastic and elastomer applications only as a copolymer with other monomers such as styrene and butadiene (e.g., ABS, SAN, NBR).

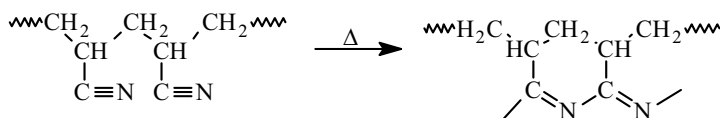


Figure 6-3 Cyclization of polyacrylonitrile at melt temperatures.

Strategies for Thermally Stable Polymers. Many flame-retardant additives as well as comonomers designed to improve the fire resistance of certain polymers are thermally labile and, therefore, the thermal stability of the polymer can be reduced. For use at high temperatures for extended periods of time, the most successful polymers are those with highly aromatic structures, especially those with heterocyclic rings. Resonance stabilization (with energies up to 16.7 kJ mol^{-1}) results in high main-chain bond strength and consequently high thermal stability. Examples of high-temperature polymers and their decomposition temperatures are given in Table 6-3.

Table 6-3 Examples of Thermally Stable Polymers

Polymer	Structure	T_d (°C) ^a
Aromatic polyester		480
Polybenzamide		500
Polybenzimidazole		650
Polypyrrole		660
Poly(<i>p</i> -phenylene)		660

^a Temperature at onset of weight loss in an inert atmosphere as determined by thermal gravimetric analysis (TGA).

Polymers having high-temperature stability as well as other high-performance properties are examples of specialty polymers designed for limited use in aerospace, electronics, and other applications and are discussed in Section 10.2. Unfortunately, the same factors that contribute to high-temperature stability of these polymers also translate to high T_g , high melt viscosity, and insolubility in common organic solvents, which make these polymers difficult or impossible to process by usual methods, such as extrusion and injection molding. Successful commercialization, therefore, always requires some compromise between thermal properties and processability.

6.1.2 Oxidative and UV Stability

With the exception of fluoropolymers, most polymers are susceptible to oxidation, particularly at elevated temperature or during exposure to ultraviolet light. Oxidation usually leads to increasing brittleness and deterioration in strength. Generally, the mechanism of oxidative degradation is free radical and is initiated by the ther-

mal or photolytic cleavage of bonds. The free radicals then react with oxygen to yield peroxides and hydroperoxides.

In general, unsaturated polyolefins are particularly susceptible to attack by oxygen and by ozone. The combined effect of light and oxygen (photooxidation) and the action of ozone (ozonolysis) on the degradation of a common elastomer, polyisoprene, are illustrated in Figures 6-4A and 6-4B, respectively. In both cases, an intermediate cyclic ozonide structure is formed. Subsequent breakage of the labile O–O bonds leads to chain scission and lower-molecular-weight polymer chains with carbonyl end groups. In the case of ozonolysis (Figure 6-4B), subsequent hydrolysis leads to chain scission and liberation of hydrogen peroxide.

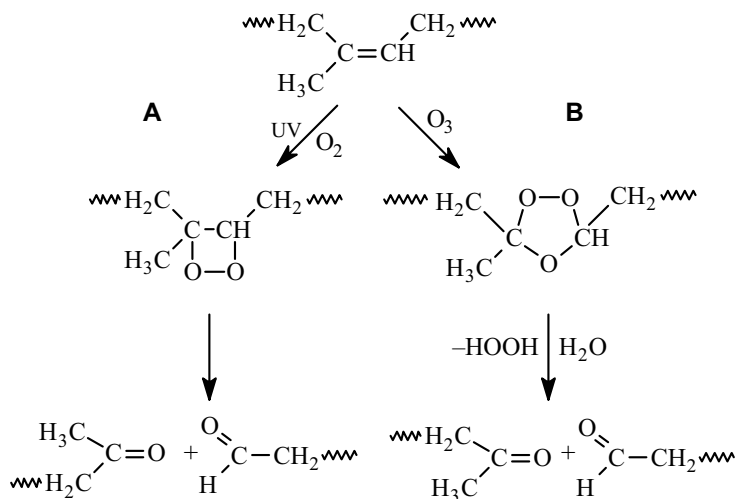


Figure 6-4 Degradation of polyisoprene by (A) photooxidation and (B) ozonolysis.

Oxidative degradation of saturated polymers can also occur through a complex series of reactions that involve the intermediate formation of peroxy radicals. Polystyrene is especially susceptible to photooxidative degradation. In this case, UV radiation is absorbed by the phenyl group, which can transfer the energy to nearby units along the polymer chain. Cleavage of the main chain can then occur with carbonyl-group formation. The result is yellowing and embrittlement of the plastic.

Commercial antioxidants include organic compounds like hindered phenols and aromatic amines, which act as free-radical scavengers, as well as agents that serve to suppress homolytic breakdown, such as organic phosphites. Effects of UV radiation may be reduced by incorporating additives, such as carbon black widely used in tire manufacture, that screen wavelengths in the UV range from 300 to 400 nm. Transparent thermoplastics like polycarbonate can be protected against yellowing and embrittlement from UV light by incorporating compounds, such as benzo-

phenone derivatives, that have a high extinction coefficient in the UV range and are able to convert absorbed radiation into heat without chemical change.

6.1.3 Chemical and Hydrolytic Stability

Solvent Crazing and Cracking. Virtually all thermoplastics in contact with organic liquids and vapors will fail at lower levels of stress or strain even if the interacting chemical is not ordinarily considered to be a solvent for the polymer. The effect of these chemicals is believed to be due to localized plasticization that allows the development of crazes or cracks (see Section 4.4.1) at reduced stress.

As discussed in Chapter 4, crazes consist mostly of voids that can absorb low-molecular-weight stress-cracking or stress-crazing agents. Plasticization reduces the effective T_g in the region of the craze and, therefore, increases the localized mobility of polymer chains and promotes craze and crack development. It is, therefore, not unexpected that the critical strain, ϵ_c , for solvent craze initiation is often closely related to the solubility parameter (see Section 3.2.6) of the agent in relation to that of the polymer. Minimum critical strains will be observed for solvents with solubility parameters close to that of the polymer. Under these circumstances, cracks will rapidly develop. The time for initiation of a craze depends on the rate of absorption, with the longest times to reach critical stress or strain observed for fluids of the highest viscosity. Crazes developing in the presence of a solvent grow more rapidly and to larger size than those grown in a solvent-free environment.

The relationship between solubility parameter and ϵ_c is illustrated for two engineering thermoplastics in Figure 6-5. The two polymers are (bisphenol-A) polysulfone and poly(2,6-dimethyl-1,4-phenylene oxide), whose solubility parameters were reported in this study [1] to be 10.7 and 8.6 (cal/cm³)^{1/2}, respectively. As shown, the minimum in ϵ_c is observed in the case of organic liquids whose solubility parameters approximate those of the two polymers (i.e., cracking agents); however, significant reduction in ϵ_c is observed for organic liquids whose solubility parameters fall on either side of the minima. Hansen solubility parameters (see Section 3.2.6) arranged in a 3-D plot of δ_d , δ_p , and δ_h can also be used to correlate environmental stress cracking. In addition to solubility, the diffusivity of the cracking/crazing agent can be an important factor in determining the rate of uptake [2]. Diffusivity, in turn, strongly depends on the size and shape of the sorbed molecule as discussed in Section 12.1.2.

Hydrolysis. Many polymers are susceptible to degradation due to the effect of water, particularly under acidic conditions. These include some naturally occurring polymers, such as polysaccharides and proteins, as well as some synthetic polymers, principally condensation polymers such as polyesters and polyamides. In general, vinyl polymers are not susceptible to hydrolysis. Factors that influence the susceptibility of a given polymer to hydrolysis include water permeability and solubility and

are determined by the chemical structure of the polymer and its physical state (e.g., crystallinity, glass-transition temperature, etc.). Autocatalysis of hydrolysis is possible if acidic or basic groups are produced by the polymer breakdown as in the case of polyesters. The hydrolysis of a polyester results in the formation of chain segments terminated by hydroxyl and carboxylic groups as follows:

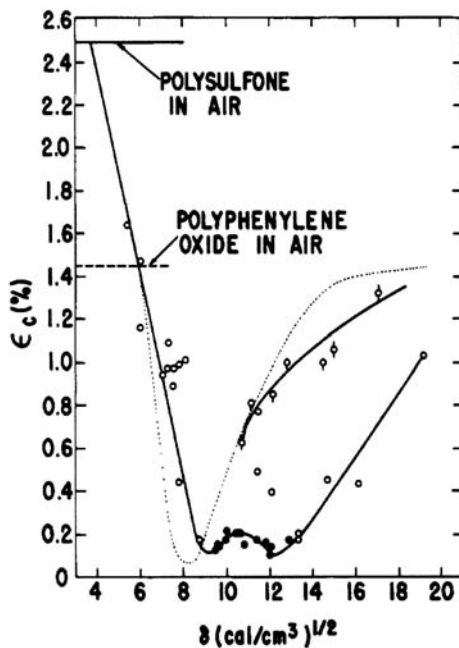
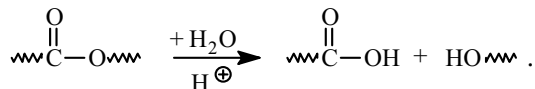
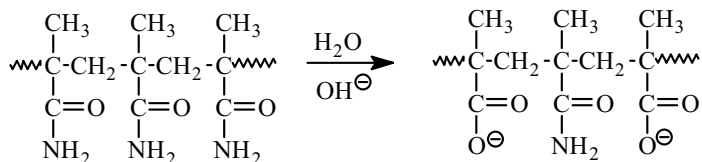


Figure 6-5 Plot of critical strain, ϵ_c , for crazing and cracking of polysulfone and poly(2,6-dimethyl-1,4-phenylene oxide) as a function of the solubility parameter, δ , of the cracking/crazing agent. Open circles represent crazing agents, while filled circles represent cracking agents. Open circles with single tabs are monohydric alcohols; those with double tabs are dihydric alcohols. Solid curves represent a fit of polysulfone data. The dotted curve fits data for poly(2,6-dimethyl-1,4-phenylene oxide) [3]. Reprinted with permission from R. P. Kambour, E. E. Romagosa, and C. L. Gruner, *Swelling, Crazing, and Cracking of an Aromatic Sulfone in Organic Media*. *Macromolecules*, 1972. **5**: p. 335. Copyright 1972 American Chemical Society.

Poly(vinyl esters) and poly(vinyl amides) are hydrolyzed to poly(vinyl carboxylic acids) under basic conditions. In these cases, hydrolysis will be less than complete because the presence of the negatively charged groups of the poly(carboxylic acid) retards the approach of the reagent (OH^-) to the adjacent ester or amide groups as illustrated for polymethacrylamide.



6.1.4 Effects of Radiation

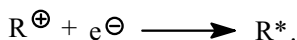
Many polymers are susceptible to degradation and crosslinking upon exposure to high-energy ionizing radiation (radiolysis) such as γ -radiation, electron beams, and X-rays. Sometimes, these effects can be used to an advantage. For example, integrated circuits can be prepared by microetching a polymeric coating of a silicon chip by electron-beam irradiation. The exposed silicon can then be doped. Radiation, particularly γ - and electron-beam radiation, can also be used to prepare graft copolymers. Radiation can also be used to polymerize a monomer in the solid state and to modify surfaces for adhesive bonding. In other cases, such as the use of plastics in space vehicles, nuclear power plants, and γ -sterilized medical disposables, polymers and composites selected for these applications must have good resistance to radiation. For example, it has been estimated that the total dosage of radiation for an object spending 30 years in space orbit is on the order of 10 mrad. Sterilization of medical disposables (e.g., syringes, surgical gowns, and labware) by γ -irradiation has become increasingly important due to the limitations of other methods, such as the inefficiency of steam sterilization and the suspected carcinogenesis of ethylene oxide used in "cold" sterilization.

Some polymers such as polystyrene and polysulfone are very radiation resistant, but others such as polypropylene will readily degrade upon irradiation. In general, polymers with aromatic rings such as polystyrene, aromatic polyamides, and polysulfones are extremely radiation resistant, as are thermosets such as epoxies, phenolics, and urethanes. Fibers that have good radiation resistance include poly(ethylene terephthalate) and aromatic polyamides. Among elastomers, polyurethanes have particularly good radiation resistance.

The primary event in radiation damage is the ejection of a high-energy electron:



This primary electron can then ionize additional molecules with the release of additional electrons in a chain reaction. An electronically excited state will result when a positively charged molecule is recombined with an available electron:



An excited state will also result when the energy transfer associated with interaction of the radiation with the material is insufficient to cause ionization. Excited states in polymers can decay by chemical reactions involving heterolytic bond cleavage producing ionic species or by homolytic bond cleavage of the main chain or substituent groups resulting in the formation of radical species. Radical lifetimes can be hours and even weeks at room temperature. This provides ample opportunity for the radicals to initiate crosslinking or to react with oxygen in the atmosphere. Whether only chain scission or crosslinking will occur depends upon the chemical structure of the polymer chain. In general, polymers having quaternary carbon atoms, such as polyisobutylene or poly(methyl methacrylate), undergo chain scission in an inert atmosphere, while crosslinking is more probable for polymers without quaternary carbon atoms, such as polyethylene and polystyrene. In the presence of oxygen, which can react with the free radicals that are generated upon irradiation, chain scission becomes the predominant mechanism. Antioxidants, which act as radical scavengers, are effective stabilizers for radiation-oxidative degradation.

6.1.5 Mechanodegradation

Polymer degradation can also result from the application of stress such as high shear deformation of polymer solutions and melts. In the case of solids, stress-induced degradation may result from comminution (grinding, milling, or crushing), machining, stretching, fatigue, tearing, abrasion, or wear. Mechanodegradation is particularly severe for high-molecular-weight polymers that exist in a highly entangled state. The result of stress-induced degradation is the generation of macroradicals originating from random chain rupture. In a process called *mastication*, natural rubber is softened by passing between spiked rollers, which also serve to disperse filler and other additives such as accelerators, vulcanizers, and antioxidants.

6.2 Management of Plastics in the Environment

At present, plastics account for roughly a quarter of all solid waste by volume in U.S. landfills versus about 40% for paper. At the present rate, U.S. landfill capacity could be exhausted in a decade or two. To reduce the volume of plastic waste that

goes to landfills, there are three alternatives: recycling, incineration, and biodegradation.

6.2.1 Recycling

Recycling of commercial plastics is an important contemporary issue from several aspects, such as the need to reduce the volume of plastic waste that is sent to landfills and the need to conserve non-renewable petroleum resources. Plastics, as well as paper and cardboard, represent a major portion of most trash. Many commodity plastics are now being recycled in the United States and Europe. These include poly(ethylene terephthalate) (PET) used in beverage containers, as well as polyolefins (i.e., polyethylene and polypropylene), polystyrene, and poly(vinyl chloride) (PVC) used in packaging.

There are two contemporary approaches to recycling. The obvious route is simply the reprocessing of waste plastics, which may take other forms and find different applications. For example, PET waste has been used in the manufacture of insulation boards in competition to the use of expanded polystyrene. In this process, waste PET containers are washed, shredded, ground into 5-mm particles, and dried to remove water that would initiate hydrolysis during processing. The particles are then mixed with a nucleating agent and an additive to increase melt viscosity (to facilitate the foaming process) and processed in a standard foam slab extruder unit, where an expansion gas is injected into the molten recycled PET just before it emerges from the extruder. Insulation boards prepared from waste PET have some advantages over expanded polystyrene, including lower smoke emission during burning. In addition, the high T_m (260°C) of PET makes it suitable for use as a hot-melt adhesive in the preparation of laminates.

The other method of recycling, which may have more potential, is called *tertiary recycling*.^{*} In this approach, chemical or thermal treatment is used to transform waste plastics into monomers that can then be used in the polymerization of virgin resin. Condensation polymers such as polyesters, nylons, and polyurethanes can be depolymerized by chemical processes such as glycolysis, methanolysis, and hydrolysis. Addition polymers, such as polyolefins, acrylics, and fluoroplastics, require thermal or catalytic cracking. In the United States, tertiary recycling has focused primarily on PET. Waste polyester resin collected from bottles, fibers, and film is heated with methanol and a catalyst under pressure to cause the depolymerization of PET into ethylene glycol and dimethyl terephthalate (DMT). DMT can be used as a replacement for *p*-xylene in the synthesis of PET (for details of the com-

^{*} “Primary” recycling refers to regrind, while “secondary” recycling is the process of physical or thermal reprocessing into a secondary product.

mercial production of PET, see Chapter 9). In Europe, attention has been directed toward an acid-catalyzed process that can convert nylon-6 recovered from worn carpets into caprolactam at temperatures ranging from 536° to 752°F.

The recycling of tires is another major issue for which good solutions are critically needed. In the United States alone, over 234 million tires are discarded annually. The majority of this volume is eventually sent to landfills, but as the number of available landfill sites decreases, alternative solutions must be sought. One approach is to extend the service life of tires (i.e., source reduction). Recycling of tires includes use of retreads and grinding into crumb for use in pads, mats, carpet backing, moisture barriers, rubber-modified asphalt, and sport tracks. Whole scraped tires can be used in a variety of non-transportation applications, such as erosion control, playgrounds, and artificial reefs. Also, there has been interest in processes that can utilize the significant energy content of scrap tires (up to 15,000 Btu per lb) to generate electricity and produce synthesis gas (H_2 and CO) for ammonia and methanol production. In such operations, the tires are first mixed with waste oil, such as used motor oil, at 700°F in a liquefaction reactor. A rotating screw is used to remove steel belts from the melt. During liquefaction, high-molecular-weight chains, as well as disulfide bridges formed during the vulcanization process, are broken and a liquid hydrocarbon mixture is produced. The liquid mixture is mixed with oxygen (gasification reactor) at 2500°F and 500 to 900 psia to produce synthesis gas and leave an inert slag.

Although the volume of plastics that are recycled is rapidly increasing, it is still small in comparison to that of aluminum and paper. Part of the reason for this low recycling rate is that the total cost of producing recycled plastics, including collecting and recycling, is typically 20% higher than for the virgin resins. In addition, thermosets that account for a significant fraction of the total volume of plastics cannot be recycled; however, it has been possible in some cases to granulate glass-reinforced thermosets into 2- or 3-cm particles for use as fillers in other fiber-reinforced composites.

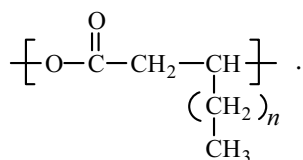
6.2.2 Incineration

Many plastics can be burned as cleanly as natural gas. Emissions include carbon dioxide, nitrogen oxides, and water vapor. As a pound of plastic produces 16,000 Btu when burned (more than twice the energy in a pound of coal), incineration can be used to generate energy, but not without serious attention to health issues. For example, some significant amounts of toxic compounds such as cadmium and other heavy metals will remain in the incinerator ash or can produce toxic emissions during combustion. Another problem is that the incineration of PVC, a significant component of many plastic wastes, may produce carcinogenic dioxins unless burned at very high temperatures.

6.2.3 Biodegradation

Biodegradable Polymers. Virtually no plastic is totally biodegradable. In fact, most polymers, including polyamides, polyfluorocarbons, polyethylene, polypropylene, and polycarbonate, are highly resistant to microbial attack. Among synthetic polymers, polyurethanes, especially polyether-polyurethanes, are susceptible to biological degradation. In general, naturally occurring polymers are more biodegradable than synthetic polymers. More specifically, polymers containing an ester functionality, particularly aliphatic polyesters, may be biodegradable. It is believed that biodegradation of these polymers proceeds by attack of the ester groups by nonspecific esterases produced by ground microflora combined with hydrolytic attack. Products of the degradation can be quickly metabolized by microorganisms. Complete biodegradation, or mineralization, occurs when all the polymer has been converted into gaseous products and/or biomass. Aerobic (in the presence of oxygen) and anaerobic (in the absence of oxygen) degradations yield similar degradation products; however, methane is produced in addition to water and carbon dioxide during anaerobic degradation.

One commercially important group of biodegradable polymers is the naturally occurring polyesters [4], the poly(β -hydroxyalkanoates), whose general structure is



Due to their biodegradability, polyhydroxyalkanoates have commercial potential as biomaterials as well as disposable plastic packaging materials. Originally identified in 1925, poly(β -hydroxybutyrate) (PHB), $n = 0$, is synthesized by the bacterium *Alcaligenes eutrophus*, which uses globules of PHB as an energy-storage medium analogous to fat in animals or starch in plants. The polymer is accumulated in discrete membrane-bound granules in the cytoplasm of the bacterium. PHB is a brittle polymer that is 100% isotactic and, therefore, highly crystalline (65% to 85%). The T_g of PHB is only 5° to 10°C while the crystalline-melting temperature is 175°C, which is close to its thermal decomposition temperature of 200°C. Poly(β -hydroxyalkanoates) with longer n -alkyl groups, such as poly(β -hydroxy-valerate) (PHV), $n = 1$, can be produced by *A. eutrophus* as well as another bacterium, *Pseudomonas oleovorans*, depending upon the type of carbon substrates available during the fermentation process.

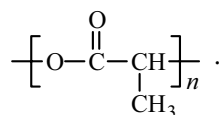
As shown by data given in Table 6-4, the principal difference in mechanical properties between PHB and the commodity thermoplastic, polypropylene, is the low extension-to-break of PHB. The toughness of PHB can be improved and its T_m

lowered with respect to its low thermal decomposition temperature by copolymerization with hydroxyvalerate. This copolymer is produced by *A. eutrophus* when grown in the presence of glucose and either propionic acid or valeric acid. Recently commercialized on a small scale, HB–HV copolymers are totally degradable to carbon dioxide and water by soil organisms in landfills or when composted with sewage. This plastic is expensive and may not be suitable for all applications, such as those that require long shelf life and for food-packaging applications where the propensity of PHB for bacterial growth is an obvious problem. One commercial use for PHB has been in the manufacture of shampoo bottles. HB–HV copolymers are suitable as matrices for controlled release of drugs due to their favorable biocompatibility and biodegradation properties. The relatively high cost of these biodegradable polymers may be reduced in the future by larger-scale production and advances in biotechnology. For example, the gene that synthesizes PHB has been recently identified, and it should, therefore, be possible to produce these polyesters in higher-productivity bacteria such as *E. coli* or even crop plants such as potatoes or turnips, which would then make PHB instead of starch.

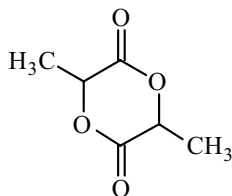
Table 6-4 Typical Properties of Polyhydroxybutyrate (PHB) Compared to Polypropylene (PP)

Property	PHB	PP
T_g (°C)	15	-10
T_m (°C)	175	176
Crystallinity (%)	80	70
Density (g cm ⁻³)	1.25	0.905
Flexural modulus (GPa)	4.0	1.7
Tensile strength (MPa)	40	38
Extension-to-break (%)	6	400
UV resistance	good	poor
Solvent resistance	poor	good

Another important biodegradable polyester is poly(lactic acid) (PLA):

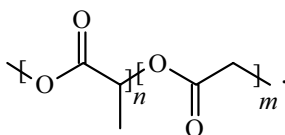


PLA can be polymerized from lactic acid or produced from corn- or rice-derived dextrose or from bacterially fermented starch obtained from food wastes such as potato peelings. The lactic acid is converted into lactide, a ring compound

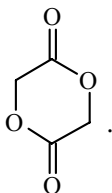


that is opened and polymerized to make PLA. Markets for PLA include fiber (apparel and carpeting) and packaging. PLA has good processability (e.g., can be thermoformed), high tensile strength and other desirable textile fiber properties, high odor barrier (important for food packaging), and resistance to grease, fats, and oils. PLA also has attractive deadfold characteristics suitable for confectionary wrapping. An advantage of PLA is that it degrades to lactic acid that can be metabolized in the body. For this reason, PLA finds important commercial use in a number of biomedical applications such as sutures, drug-delivery systems, and wound clips. It may also have some agricultural applications, such as timed-release coatings for fertilizers and pesticides and mulch films for moisture and heat retention and to reduce the weed population between rows of crops. In addition to the fact that PLA is derived from renewable agricultural resources, PLA can be composted and is, therefore, environmentally benign.

An important biodegradable copolymer is poly(lactide-*co*-glycolide) (PLGA):

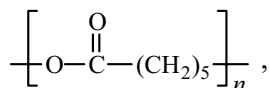


PLGA can be obtained from the copolymerization of lactide and glycolide:

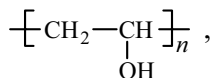


At compositions from about 25% to 75% GA, PLGA is amorphous and suitable for use in drug-delivery systems (see Section 12.2.1). PLGA has been considered as a substrate for incorporating hydroxyapatite (calcium phosphate hydroxide), the natural mineralization agent in bone, to develop artificial bone.

Other synthetic polymers that can be biodegraded (often with the help of specific microorganisms or addition of agents to promote chemical degradation) include polycaprolactone (PCL), a polyester,



poly(vinyl alcohol),



and cellulose and cellulose derivatives (see Section 8.2.2).

Biodegradation can also be used to dispose of unwanted monomers. For example, styrene is consumed by *P. aeruginosa* at the rate of 300 mg styrene/g bacteria/h [5]. Products of the biodegradation are biomass (the bacterial cellular matter formed during colony growth), carbon dioxide, and water.

Starch Additives. Another approach to biodegradability is to blend or graft a commercial thermoplastic with a naturally degradable material such as starch [6]. For example, starch can be blended with polyethylene during the blow molding of film for plastic bags. The expectation is that the starch will be eaten by soil microorganisms in a landfill and, therefore, the plastic matrix will be broken down into smaller particles. Starch obtained from corn is a glucose-based biopolymer consisting of linear amylose and highly branched, high-molecular-weight amylopectin (see Section 8.1.3). Advantages of starch are that it is inexpensive and totally biodegradable. Cornstarch granules retain about 6% to 20% moisture but are thermally stable up to 250°C in air. Extruded starch has a tensile strength of 20 to 30 MPa at 10% to 15% elongation. Acrylic and vinyl monomers, such as acrylic acid and styrene, can be grafted onto starch by ceric ion, Ce(IV), initiation.

One problem with this approach is that starch-filled plastics are weak and, therefore, more petroleum-based material may be required to provide adequate strength for such consumer products as grocery bags. Since disposable diapers and trash bags made from blended plastic may contain as little as 5% starch, the net result could be to introduce more plastic into the environment.

Biodegradation as a Practical Issue. Although biodegradation may have significant potential to alleviate some of the problems associated with plastic waste disposal, there remains some controversy as to whether any significant biodegradation will actually occur in modern, well-designed landfills. In order to store potentially hazardous materials, landfills are built to be free of moisture and airtight. Such anaerobic conditions, which serve to guard against the release of hazardous chemicals from landfills, also retard biodegradation. Another problem concerns the compatibility of the two major approaches to plastic waste management—biodegradation and recycling—since biodegradable polymers are not suitable candidates in the recycling of commingled plastics.

SUGGESTED READING

- Albertsson, A.-C., ed., *Degradable Aliphatic Polyesters*. Advances in Polymer Science, 2002. **157**: p. 1.
- Andrady, A. L., *Assessment of Environmental Biodegradation of Synthetic Polymers*. Journal of Macromolecular Science—Reviews in Macromolecular Chemistry and Physics, 1994. **C34**(1): p. 25.
- Garlotta, D., *A Literature Review of Poly(lactic acid)*. Journal of Polymers and the Environment, 2002. **9**: p. 63–84.
- Lenz, R. W., *Biodegradable Polymers*. Advances in Polymer Science, 1993. **107**: p. 1.
- Maharama, T., Y. S. Negi, and B. Mohanty, *Review Article: Recycling of Polystyrene*. Polymer—Plastics Technology and Engineering, 2007. **46**: p. 729.
- Nayak, P. L., *Biodegradable Polymers: Opportunities and Challenges*. Journal of Macromolecular Science—Reviews in Macromolecular Chemistry and Physics, 1999. **C39**(3): p. 481.
- Nelson, G. L., ed., *Fire and Polymers II: Materials and Tests for Hazard Prevention*. 1995, ACS Symposium Series, vol. 599: Washington, DC: American Chemical Society.
- Nguyen, T. Q., *Kinetics of Mechanochemical Degradation by Gel Permeation Chromatography*. Polymer Degradation and Stability, 1994. **46**: p. 99.
- Nir, M. M., J. Miltz, and A. Ram, *Update on Plastics and the Environment: Progress and Trends*. Plastics Engineering, March 1993, p. 73.
- Rader, C. P., S. D. Baldwin, D. D. Cornell, G.D. Sadler, and R. F. Stockel, eds., *Plastics, Rubber, and Paper Recycling*. 1995, ACS Symposium Series, vol. 609: Washington, DC: American Chemical Society.
- Rånby, B., *Basic Reactions in the Photodegradation of Some Important Polymers*. Journal of Macromolecular Science—Pure and Applied Chemistry, 1993. **A30**(9&10): p. 583.
- Sharma, R. R., and A. R. Ray, *Polyhydroxybutyrate, Its Copolymers and Blends*. Journal of Macromolecular Science—Reviews in Macromolecular Chemistry and Physics, 1995. **C35**(2): p. 327.
- Stein, R. S., *Polymer Recycling: Thermodynamics and Economics*. Macromolecular Symposium, 1998. **135**: p. 295.
- Swanson, C. L., R. L. Shogren, G. F. Fanta, and S. H. Imam, *Starch—Plastic Materials—Preparation, Physical Properties, and Biodegradability (A Review of Recent USDA Research)*. Journal of Environmental Polymer Degradation, 1993. **1**(2): p. 155.

REFERENCES

1. Kambour, R. P., E. E. Romagosa, and C. L. Gruner, *Swelling, Crazing, and Cracking of an Aromatic Copolyether-Sulfone in Organic Media*. Macromolecules, 1972. **5**: p. 335–340.

2. Hansen, C. M., and L. Just, *Prediction of Environmental Stress Cracking in Plastics with Hansen Solubility Parameters*. Industrial and Engineering Chemistry and Research, 2001. **40**: p. 21–25.
3. Bernier, G. A., and R. P. Kambour, *The Role of Organic Agents in the Stress Cracking and Cracking of Poly(2,6-dimethyl-1,4-phenylene oxide)*. *Macromolecules*, 1968. **1**: p. 393–400.
4. Lenz, R. W., Y. B. Kim, and R. C. Fuller, *Polyesters Produced by Microorganisms*. *Journal of Bioactive and Compatible Polymers*, 1991. **6**: p. 382–392.
5. Aalam, S., A. Paus, and J.-M. Lebeault, *High Efficiency Styrene Biodegradation in a Biphasic Organic/Water Continuous Reactor*. *Applied Microbiology and Biotechnology*, 1993. **39**: p. 696–699.
6. Inoue, Y., and N. Yoshie, *Structure and Physical Properties of Bacterially Synthesized Polyesters*. *Progress in Polymer Science*, 1992. **17**: p. 571–619.

Additives, Blends, Block Copolymers, and Composites

*T*ypically, commercial plastics are mixtures of one or more polymers and a variety of *additives* such as plasticizers, flame retardants, processing lubricants, stabilizers, and fillers. The exact formulation will depend upon the specific application or processing requirement. For example, poly(vinyl chloride) (PVC) is a thermally unstable polymer (see Section 6.1.1) having high modulus, or stiffness, typical of other glassy polymers at room temperature. In order to obtain a flexible-grade resin of PVC for use as packaging film or for wire insulation, the polymer must be blended with a plasticizer to reduce its T_g and with a small amount of an additive to improve its thermal stability at processing temperatures.

In many cases, certain properties of a polymer can be enhanced by blending it with another polymer. For example, the engineering thermoplastic, poly(2,6-dimethyl-1,4-phenylene oxide) (PPO), is a high- T_g polymer that is difficult to pro-

cess because of its susceptibility to thermal oxidation at high temperatures. Commercial resins of this polymer (Noryl) are blends of PPO and high-impact polystyrene (HIPS) and can also include different additives, such as lubricants, thermal stabilizers, flame retardants, or fillers. Since the T_g of PS (ca. 100°C) is lower than that of PPO (ca. 214°C), the overall T_g of the PPO/HIPS blend is lower than that of PPO alone and, therefore, the resin can be melt-processed at reduced temperatures where the oxidative instability of PPO is not a problem. The incorporation of HIPS also reduces the cost of this engineering resin and improves the impact strength of the blend.

Polymeric composites are physical mixtures of a polymer (the matrix) and a reinforcing filler (the dispersed phase) that serves to improve some mechanical property such as modulus or abrasion resistance. Fillers may be inorganic (e.g., calcium carbonate) or organic (graphite fiber or an aromatic polyamide such as Kevlar). Virtually any material can be used as the composite matrix, including ceramic, carbon, and polymeric materials. Typically, matrices for polymeric composites are thermosets such as epoxy or (unsaturated) polyester resin; however, some engineering thermoplastics with high T_g and good impact strength, such as thermoplastic polysulfones, have been used for composites. Principal applications for composites are in construction and transportation.

7.1 Additives

A variety of additives are widely used for thermoplastics, thermosets, and elastomers. The global market for plastics additives in 2011 was nearly \$40 billion and is expected to grow to about \$48 billion by 2016. Additives are sometimes grouped into four main functional categories—property modifiers, property extenders, stabilizers, and processing aids. Property modifiers represent the largest segment of the additives market. These include flame retardants, antioxidants, antimicrobials, plasticizers, blowing agents, and impact modifiers. Of these, plasticizers and flame retardants are the fastest-growing segment of this market. The plasticizer market is expected to grow by about 3.2% through 2016 and represents about 50% of the total additives market. In practice, additives are mixed with a polymer before processing by a variety of techniques, such as dry blending, extrusion, compounding, and other methods discussed later in Chapter 11.

7.1.1 Plasticizers

Plasticizers, particularly for PVC, constitute one of the largest segments of the additives market. The principal function of a plasticizer is to reduce the modulus of a polymer at the use temperature by lowering its T_g . The effect of a plasticizer on

modulus is illustrated by Figure 7-1. As shown, increasing the concentration of the plasticizer causes the transition from the high-modulus (glassy) plateau region to the low-modulus (rubbery) plateau region to occur at progressively lower temperatures. In addition, the transition of the plasticized polymer occurs over a wider range of temperatures than for the unplasticized polymer. Typically, plasticizers are low-molecular-weight organic compounds having a T_g in the vicinity of -50°C . In some cases, a miscible high-molecular-weight polymer having a low T_g (e.g., polycaprolactone or copolymers of ethylene and vinyl acetate) can be used as a plasticizer.

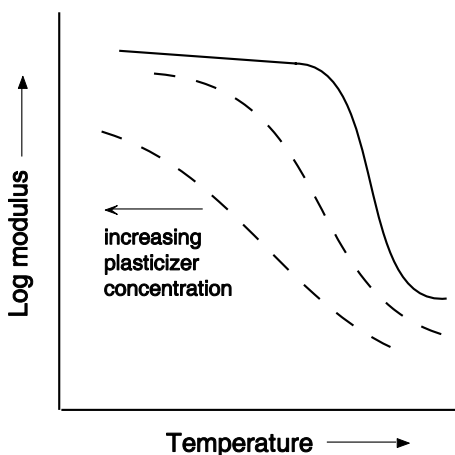


Figure 7-1 Effect of increasing plasticizer concentration on the modulus–temperature plot.

Requirements for an effective plasticizer include partial or complete miscibility with the host polymer and a low T_g . The T_g of the plasticized polymer depends upon the plasticizer concentration and the T_g of each component as estimated by a number of theoretical or empirical equations, such as the Kelley–Bueche equation [1] and others given in Section 4.3.4. Another commonly used relationship first proposed by Wood [2] to predict the T_g of random copolymers has been used to predict the T_g of plasticized polymers. The *Wood equation* has the form

$$T_g = \frac{T_{g,1} + (kT_{g,2} - T_{g,1})W_2}{1 - (1 - k)W_2}. \quad (7.1)$$

In this equation, k is considered to be an adjustable parameter and W_i is the weight fraction of component i where component 1 is typically the diluent. A related equation is the *Gordon–Taylor equation* [3]

$$T_g = \frac{T_{g,1}W_1 + KT_{g,2}W_2}{W_1 + KW_2} \quad (7.2)$$

where K is also commonly taken to be a fitting parameter. The Gordon–Taylor equation has been shown to be successful for fitting the T_g of random copolymers [4] and is also widely used to model the composition dependence of polymer mixtures and blends.

A very convenient equation relating T_g to the composition of a polymer mixture from known parameters (composition and individual polymer T_g) was given in Chapter 4 (eq (4.34)) as

$$\ln\left(\frac{T_g}{T_{g,1}}\right) = \frac{W_2 \ln(T_{g,2}/T_{g,1})}{W_1(T_{g,2}/T_{g,1}) + W_2}. \quad (7.3)$$

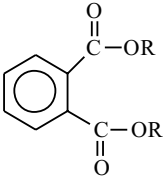
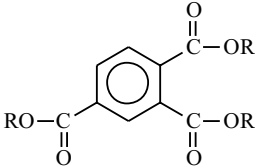
Equation (7.3) has been shown to be useful for a wide variety of polymer mixtures, including polymer blends, for which the T_g s of both components are roughly comparable, and plasticized polymers such as PVC, for which the T_g s of the polymer and plasticizer are widely apart. Comparisons between experimental and predicted T_g values are shown for two polymer blends and plasticized PVC in Figure 7-2.

In the case of plasticization, the actual reduction in polymer T_g per unit weight of plasticizer is called the plasticizer *efficiency*. High efficiency indicates that the plasticizer causes the glassy-to-rubbery transition to occur over a very broad temperature range. The problem with high-efficiency plasticizers is that they can diffuse out of the polymer in time due to their low miscibility with the polymer. Plasticizers that are susceptible to migration are said to have low *permanence*. Loss of plasticizer will lead to a gradual increase in brittleness as the T_g (and, therefore, the modulus) of the plasticized polymer slowly increases to that of the unplasticized (i.e., glassy) polymer. An example of a high-permanence (i.e., low-efficiency) plasticizer for PVC is tris(2-ethylhexyl)trimellitate, sometimes called trioctyl trimellitate (TOTM) (see Table 7-1); T_g data for PVC plasticized with TOTM are plotted in Figure 7-1.

When T_g reduction is obtained by compounding a polymer with a low- T_g compound, the process is called *external plasticization*. In some cases, plasticizer function can be obtained by copolymerizing the polymer with the monomer of a low- T_g polymer, such as poly(vinyl acetate). This process is called *internal plasticization*.

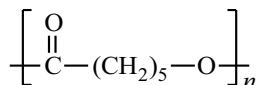
di-2-ethylhexyl adipate or dioctyl adipate (DOA); phosphates, such as tricresyl phosphate (TCP); and trialkyl trimellitates, such as tris(2-ethylhexyl trimellitate) or trioctyl trimellitate (TOTM). General structures for these classes of PVC plasticizers are shown in Table 7-1.

Table 7-1 Common Plasticizers for PVC

Plasticizer Classification	Chemical Structure	Examples ^a
Aliphatic diester	$\text{RO}-\overset{\text{O}}{\parallel}{\text{C}}-(\text{CH}_2)_n-\overset{\text{O}}{\parallel}{\text{C}}-\text{OR}$	DOA
Dialkyl phthalate		DOP, DIOP
Trialkyl phosphate	$\text{RO}-\overset{\text{O}}{\parallel}{\text{P}}(\text{OR})_2$	TCP
Trialkyl trimellitate		TOTM

^a Common names for plasticizers: DOP, dioctyl phthalate; DIOP, diisooctyl phthalate; DOA, dioctyl adipate; TCP, tricresyl phosphate; and TOTM, trioctyl trimellitate.

Examples of polymeric plasticizers include polycaprolactone (PCL):



with a T_g of -60°C and copolymers (and terpolymers) of ethylene with vinyl acetate, carbon monoxide, and sulfur dioxide. Polymeric plasticizers provide high permanence at the expense of low-temperature flexibility due to their higher T_g and low efficiency.

It has been observed that at low concentrations of plasticizer (e.g., 5% to 10%), modulus and tensile strength may sometimes be greater than that of the unplasticized polymer, while impact strength and permeability to gases and liquids may be lower. This behavior is opposite to that usually associated with plasticization and is, therefore, known as *antiplasticization*. If the plasticizer concentration is

raised above the antiplasticization range, the modulus and tensile strength will begin to fall, while the impact strength and permeability will increase (i.e., plasticization begins).

7.1.2 Fillers and Reinforcements

Fillers for thermoplastics and thermosets may be inert materials that serve to reduce resin cost and (to a lesser extent) improve processability or dissipate heat in exothermic thermosetting reactions. Examples of such fillers include wood flour, clay, talc, fly ash, sand, mica, and glass beads. Mica can also be used to modify the polymer's electrical- and heat-insulating properties. Other particulate fillers may be used to reduce mold shrinkage or to minimize electrostatic charging. These include graphite, carbon black, aluminum flakes, and metal and metal-coated fibers. For example, high loading of carbon fibers can provide electromagnetic interference (EMI) shielding for computer applications.

Reinforcing fillers are used to improve some mechanical property or properties, such as modulus, tensile or tear strength, abrasion resistance, and fatigue strength. For example, particulate fillers such as carbon black or silica are widely used to improve the strength and abrasion resistance of commercial elastomers. Fibers in the form of continuous strands, woven fabrics, and chopped (or discontinuous) fibers are used to reinforce thermoplastics and thermosets.

The typical fiber content of a polymer composite may range from 20% to 80% of the total weight. The most common form of fiber fillers is E-glass, typically used to reinforce thermosets, such as (unsaturated) polyester and epoxy resins. E-glass is a boroaluminosilicate glass having low alkali-metal content and containing small percentages of calcia (CaO) and magnesia (MgO). For special applications, such as in the manufacture of aerospace materials, fibers of boron, Kevlar (an aromatic polyamide or aramid), and especially carbon or graphite are preferred. Carbon and graphite fibers are obtained by the pyrolysis of organic materials such as polyacrylonitrile (PAN), rayon, or pitch. The highest mechanical properties are obtained by orienting the fibers at temperatures as high as 3000°C (graphite fibers). At the expense of higher cost and increased brittleness, these specialized fibers provide higher composite strength and modulus than glass-reinforced composites. Recently, there has been interest in using ultrahigh-molecular-weight polyethylene (see Chapter 10), having strength equal to an aramid fiber, as fiber reinforcement for epoxy and other matrices.

In addition to improvement in mechanical properties, composites may also offer weight reduction and improved conductivity, such as are provided by carbon or graphite fibers. Properties of typical fiber materials are given in Table 7-2. For highly demanding applications, microfibers or whiskers (synthetically grown single crystals) of alumina or silicon carbide may be used. Whiskers can have tensile strengths as high as 27.6 GPa (4 million psi) and moduli as high as 690 GPa (100

million psi). Other composite fillers recently being considered include buckminsterfullerene, C_{60} , which has been found to increase both T_g and thermal stability. Carbon nanotubes have extremely high modulus (up to 1.8 TPa) and are less brittle than carbon fiber. These can be used to make conductive composites suitable for electrostatic painting.

Table 7-2 Properties of Fibers Used in Composite Applications

Fiber	Tensile Modulus GPa ^a	Tensile Strength GPa ^a	Density g cm ⁻³
Boron	386	3.4–3.7	2.38–2.66
E-glass	72.4	3.45	2.55
S-glass	85.5	4.83	2.49
Graphite			
High-modulus	483–517	1.86	1.97
High-strength	234–255	2.83	1.77
Kevlar-49	138	2.76	1.44
Steel	407	4.14	7.81

^a To convert GPa to psi, multiply by 145,000.

7.1.3 Other Important Additives

In addition to plasticizers and fillers, the other important additives found in commercial plastics include thermal stabilizers, antioxidants, and UV-stabilizers to protect sensitive polymers against degradation due to processing temperatures and environmental attack. Other additives are used to improve fire resistance, to meet certain processing requirements (lubricants, curing and blowing agents, and catalysts for polymers prepared by reaction injection molding), to improve impact strength, to protect against exposure to bacteria and fungi, and to impart color. The specific formulation of a plastics resin is finely tailored to the end use of the resin. Formulations of plastic resins are usually given on the basis of parts per 100 unit weight of resin (phr), where the resin refers to the base polymer in the composition. The methods of action and some examples of these important additives are described in the following sections.

An important example of the use of plastics additives is PVC resin designed for potable water pipe extrusion. As shown by the data given in Table 7-3, PVC resin designed for this particular application can include eight or more different additives. All the components are blended using a dry blending technique in a specially designed mixer and then continuously extruded through an annular die. For the representative formulation given in Table 7-3, an acrylic-type processing aid may be used to provide a smooth extrudate, while calcium stearate and paraffin wax are present as lubricants. Since it is necessary to provide rigidity for pipe applications,

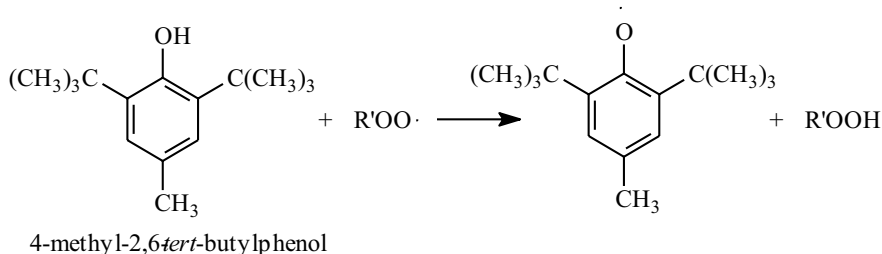
no plasticizers are used in this formulation. Ultrafine calcium carbonate is used as a reinforcing filler to provide high burst resistance. The choice of a thermal stabilizer depends upon consideration of toxicity levels since it is possible that plasticizer can diffuse out of the pipe into the water supply. For PVC pipe applications, alkyltin or antimony mercaptides are widely used stabilizers in the United States.

Table 7-3 Typical Formulation of a PVC Resin for Potable Water Pipe Extrusion

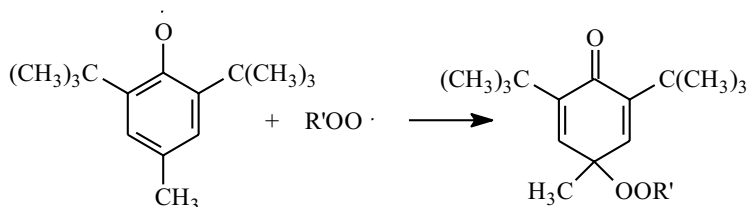
Component	Concentration (phr)
PVC (0.9 to 1.0 IV ^a)	100
Processing aids	1–5
Pigment	1–2
Calcium stearate	0.5–1.5
Paraffin wax	0.5–1
Alkyltin or antimony mercaptide	0.3–2.0
Impact modifier	0–10
Calcium carbonate	0–10

^a Inherent viscosity.

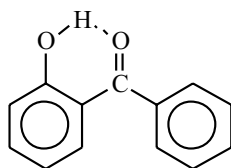
Stabilizers. Short-term stabilizers are those that are used to protect a polymer against the effects of temperature and oxygen during processing. These are typically low-molecular-weight compounds, such as hindered phenols and aromatic amines, which have high diffusivity in the polymer melt and serve as free-radical scavengers. Other antioxidants include those that serve to suppress homolytic breakdown such as organic phosphites. An example of an antioxidant that serves as a free-radical scavenger is 4-methyl-2,6-di-*tert*-butylphenol, which is used to inhibit the thermal oxidation of natural rubber. It functions by terminating free-radical sites formed as a result of thermal oxidation (see Section 6.1.1) by two routes: (1) abstraction of its hydroxyl hydrogen:



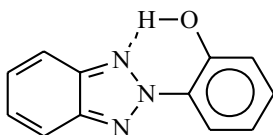
or (2) addition to the *para*-position of the aromatic ring:



Many polymers will absorb UV radiation in the wavelength from 290 to 400 nm. This absorbed energy can break bonds and initiate free-radical chain reactions that can lead to discoloration, embrittlement, and eventual degradation. UV stabilizers act to either absorb UV radiation or to deactivate free radicals and hydroperoxides as they are formed. As an example, carbon black, widely used in tire manufacture, provides good absorption in the UV range, as well as providing abrasion resistance and serving as a low-cost filler. Transparent thermoplastics like polycarbonate can be protected against yellowing and embrittlement from UV irradiation (photolysis) by incorporating compounds like benzophenone derivatives, such as *o*-hydroxybenzophenone:



These benzophenones have a high extinction coefficient in the UV range and are able to convert absorbed radiation to heat without chemical change. Benzotriazoles such as 2-(*o*-hydroxyphenyl)benzotriazole



are also widely used as UV absorbers.

Flame Retardants. When subjected to a sufficient heat flux for a sufficiently long time, all organic polymers will thermally degrade. Minimum radiant fluxes vary from about 16 to 34 kilowatts (kW) m^{-2} for polyurethane foam to 43 kW m^{-2} for polytetrafluoroethylene. In the absence of oxygen, thermal degradation is called *pyrolysis*. In the presence of oxygen, thermal degradation is called *oxidative pyrolysis* or *thermal-oxidative degradation*.

Flame retardants are added to alter the combustion process in some way. Strategies for effective flame retardants include the following:

- Inhibition of the vapor-phase combustion of the fuel gases
- Alteration of the thermal-degradation pathway by providing a low-energy process that promotes solid-state reactions leading to carbonization
- Formation of a protective coating to insulate against thermal energy

Classes of flame retardants include organochlorine compounds, organobromine compounds, organophosphorus, antimony oxides, boron compounds, and especially alumina trihydrate (ATH).

Biocides. In general, polyolefins and vinyl polymers are particularly resistant to bacterial attack (see Section 6.2.3) while natural rubber, cellulose and cellulose derivatives, and some polyesters are susceptible to microbial attack. A *biocide* is a chemical that controls or destroys bacterial growth. Alternative terminology includes bactericides, bacteristats, mildicides, fungicides, fungistats, germicides, and algicides. Important applications for biocides include latex paints and textiles. The ideal biocide is one that is toxic to the targeted microorganism but otherwise safe to humans and other animal life. For food packaging applications, biocides must be approved by the Food and Drug Administration in the United States. All biocides must be registered by the Environmental Protection Agency for use in the United States. Examples of industrial biocides include tributyltin oxide used in latex paints, textiles, and plastics and 10,10'-oxybisphenoxyarsine (OBPA) used in vinyl and urethane-polyolefin formulations.

Processing Additives. Lubricants are added to improve flow during processing by reducing melt viscosity (internal lubricants) or by reducing adhesion between metallic surfaces of the processing equipment and the polymer melt (external lubricants). Principal categories of lubricants include amides, esters, metallic stearates, waxes, and acids. The major market for processing lubricants is PVC, for which stearates are often used. Other lubricants include mineral oil and low-molecular-weight polyolefins. Organofunctional silicone fluids may be used as internal mold-release agents for reaction injection molding (RIM) of polyurethane (see Section 11.1.2).

Curing Agents. The term *curing* typically refers to the process of applying heat (and pressure) to change the properties of rubber or thermosetting resins. In the curing process, various additives (i.e., curing agents), including a number of sulfur-containing compounds, are used to promote the crosslinking of rubber (i.e., vulcanization) or the formation of a thermoset network (e.g., amines in the cure of epoxies). The process of network formation is discussed in detail in Chapter 9.

Colorants. Plastics can be colored by adding soluble dyes and inorganic and organic pigments that are dispersed in the plastic during processing. In the coloring of thermosets, dye dissolution or pigment dispersion must be completed before the

thermoset is fully formed. Classes of dyes that are used for plastics include azo compounds, anthraquinones, xanthenes, and azines. Among the most important inorganic pigments are iron oxides, cadmium, chrome yellow, and especially titanium dioxide (white).

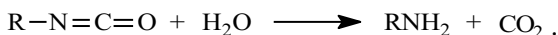
Heat Distortion and Impact Modifiers. Blends of one polymer with another having greater or lower T_g can be used to modify the T_g or heat-distortion temperature (HDT) of another polymer, as described in Section 7.2.2. Impact modifiers normally include high-impact polystyrene (HIPS), chlorinated polyethylene (CPE), and a variety of copolymers and terpolymers, such as SAN (styrene–acrylonitrile), ABS (acrylonitrile–butadiene–styrene), EVA (ethylene–vinyl acetate), MBS (methyl methacrylate–butadiene–styrene), and MABS (methyl methacrylate–acrylonitrile–butadiene–styrene). The mechanism of toughening is discussed in Section 7.2.2.

Antistatic Agents. Since most polymers are poor electrical conductors (see Section 12.3.1), static electrical charges can form on the surface of plastics. Such static charge buildup can present problems such as dust collection and sparking. Fortunately, hygroscopic additives called *antistats* are effective for dissipating static electrical charges. Antistats belong to either of two categories—external or internal. External, or topical, antistats are applied by spraying, wiping, or dipping the plastic surface, while internal antistats are compounded with the plastic during processing. In the case of internal antistats, the additive diffuses to the surface of the plastic where the hygroscopic additive absorbs moisture and, thereby, provides a conductive layer of water. Examples of antistatic agents include phosphate and fatty acid esters, polyhydric alcohol derivatives, sulfated waxes, ethoxylated and propoxylated aliphatics and aromatics, and especially quaternary ammonium compounds and amines.

Blowing Agents. Many plastics, such as polystyrene (expanded polystyrene) and polyurethanes, are foamed to provide insulating properties (rigid foam) or flexible products (flexible foam) for seat cushions and other applications. Gas production is achieved by adding a gas-producing compound called a *blowing agent* (or foaming agent). *Physical* blowing agents include volatile liquids such as short-chain hydrocarbons (e.g., pentanes, hexanes, and heptanes) and fluorocarbons (e.g., trichloromethane, tetrachloromethane, and trichlorofluoromethane) and gases such as nitrogen, carbon dioxide, and air that are added during processing. Volatilization results in the formation of a cellular structure through a phase change as the gas dissolved in the polymer at high pressure at processing conditions desorbs during depressurization. *Chemical* blowing agents (CBA) such as hydrazine derivatives are solid additives that generate gases when decomposed at processing temperatures. Unsaturated polyester is foamed by the use of a CBA. In some cases, gas production may occur by chemical reaction of the CBA with another component of the polymer system. Concern over emission of volatile organic compounds (VOCs), especially

chlorohydrocarbons, during processing has encouraged the development of safer alternatives to many of the physical blowing agents now used.

In the case of polyurethanes, flexible foams are produced by the production of carbon dioxide from the reaction of an isocyanate and water:



When the isocyanate is in excess, the resulting amine can react with another molecule of isocyanate to form a urea as shown:



Rigid foams are produced by use of a physical blowing agent, such as trichlorofluoromethane (refrigerant 11) or pentane. An important example of a rigid foam is expandable polystyrene (EPS) used for disposable drinking cups, cushioned packaging, and thermal insulation. The physical blowing agent used for EPS is typically pentane.

Compatibilizers. As discussed in the following sections, many polymers are immiscible and, therefore, phase-separate during processing. The mechanical properties of these immiscible blends are often poor due to inadequate interfacial strength between the dispersed phase and matrix. A variety of additives can be used to promote miscibility by reducing interfacial tension. Reactive compatibilizers chemically react with blend components and are, therefore, effective for many blend compositions. Nonreactive compatibilizers are typically block or graft copolymers of the blend homopolymers and are more specific in their action.

7.2 Polymer Blends and Interpenetrating Networks

7.2.1 Polymer Blends

The blending of two or more polymers has become an increasingly important technique for improving the cost/performance ratio of commercial plastics. For example, blending may be used to reduce the cost of an expensive engineering thermoplastic, to improve the processability of a high-temperature or heat-sensitive thermoplastic, or to improve impact resistance. Commercial blends may be homogeneous, phase-separated, or a bit of both.

Thermodynamics. Whether a particular polymer blend will be homogeneous or phase-separated will depend upon many factors, such as the kinetics of the mixing process, the processing temperature, and the presence of solvent or other addi-

tives; however, the primary consideration for determining miscibility of two polymers is a thermodynamic issue that is governed by the same (Gibbs) free-energy considerations that were discussed in Chapter 3 for polymer–solvent mixtures. The relationship between the change in Gibbs free energy due to mixing (ΔG_m) and the enthalpy (ΔH_m) and entropy (ΔS_m) of mixing for a reversible system was given as

$$\Delta S_m = \Delta H_m - T\Delta S_m. \quad (7.4)$$

If ΔG_m is positive over the entire composition range at a given temperature, the two polymers in the blend will separate into phases at equilibrium. For complete miscibility, two conditions are necessary: ΔG_m must be negative and the second derivative of ΔG_m with respect to the volume fraction of component 2 (ϕ_2) must be greater than zero

$$\left(\frac{\partial^2 \Delta G_m}{\partial \phi_2^2} \right)_{T,p} > 0 \quad (7.5)$$

over the entire composition range.

If $\Delta G_m < 0$, but eq. (7.5) is not satisfied (i.e., the appearance of local minima in the free-energy curve as shown in Figure 3-9), the blend will separate at equilibrium into two mixed-composition phases. This means that each phase (i.e., the dispersed and continuous phases) will contain some of each polymer. At a given temperature, equilibrium concentrations are given as a pair of isothermal points along the binodal ($\mu_i^A = \mu_i^B$), which is illustrated for a representative phase diagram in Figure 7-3.

In general, polymer blends can exhibit a wide range of phase behavior, including upper and lower critical solution temperatures (see Section 3.2.4), as illustrated by the liquid–liquid phase diagram given in Figure 7-3. At temperature T_1 , which is below the upper critical solution temperature (UCST) for phase separation located at T_2 , the equilibrium mixture will separate into two phases whose compositions lie on opposite sides of the *binodal* at T_1 . The binodal separates the stable (single phase) from the metastable state, while the *spinodal* marks the transition from the unstable to metastable region. At T_3 , which is above the UCST but below the lower critical solution temperature (LCST) located at T_4 , the blend is miscible at all compositions. Above the LCST (e.g., at T_5), two phases again coexist with compositions given by the upper binodal.

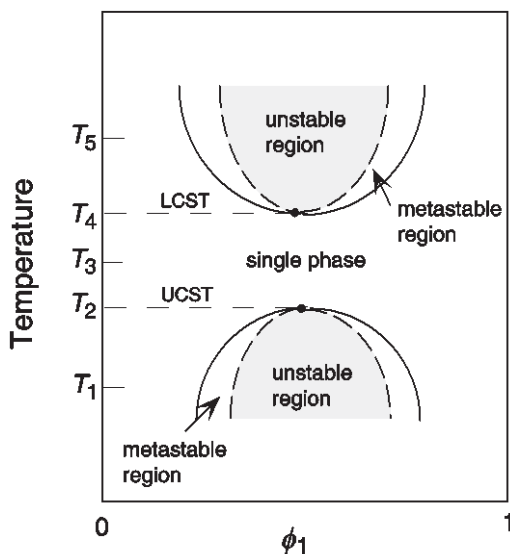


Figure 7-3 Idealized phase diagram for a polymer blend. The solid curve indicates a binodal, while the broken curve represents a spinodal separating the unstable and metastable regions. The upper critical (UCST) and lower critical solution (LCST) temperatures are located at T_2 and T_4 , respectively.

For polymer blends in the solid state, recent studies have shown that LCST behavior is quite common and needs to be considered during melt processing when elevated temperatures can cause phase separation and result in deleterious changes in the properties of the blend. An example of LCST phase behavior is a blend of polystyrene with the polycarbonate of tetramethylbisphenol-A [6]. In this case, a phase diagram was obtained by determining the temperature at which a particular blend composition first scatters light due to the incipient phase separation. Data obtained over the entire composition range are used to form a *cloud-point curve*. As shown by the data plotted in Figure 7-4, the LCST (assigned to the temperature at the minimum of the cloud-point curve) occurs near 240°C for this blend. This means that if the blend is melt-processed above 240°C, phase separation will occur. If the blend is heated above the LCST and rapidly cooled, the two-phase morphology will be retained in the solid state. As will be discussed shortly, thermal and mechanical properties will be very different depending on whether the blend forms a homogeneous mixture or a two-phase structure.

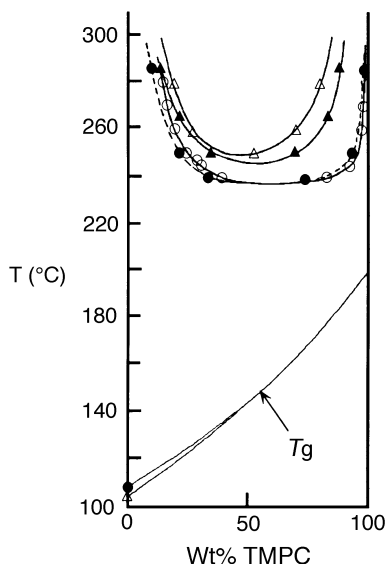


Figure 7-4 Phase behavior of TMPC/PS blends. Bottom curves show the dependence of T_g on the wt% of TMPC below the LCST. The top curves are cloud-point curves illustrating LCST behavior. The LCST shifts upward in temperature with decreasing PS molecular weight and the cloud-point curves are skewed toward the low-molecular-weight component, TMPC ($\bar{M}_w = 41,000$). Molecular weights (\bar{M}_w) of PS: (Δ), 42,000; (\blacktriangle), 59,000; (\circ), 180,000; and (\bullet), 320,000. Adapted with permission from K. H. Illers, W. Heckmann, and J. Hambrecht, *Untersuchung des Mischungsgleich-gewichts binärer Polymermischungen. I. Mischungen aus Polystyrol und Tetramethyl-bisphenol A-Polycarbonat*. *Colloid and Polymer Science*, 1984. **262**: p. 557–565. Copyright 1984 Springer-Verlag.

Compared to LCST phase behavior, UCST behavior is much more difficult to observe since a UCST may fall below the blend T_g , at which temperature all long-range (cooperative) segmental motions cease. Such chain mobility is required to achieve phase separation. For this reason, UCST behavior may be observed only in a solution of the blend in a low-molecular-weight solvent or under other special circumstances.

The bulk of experimental evidence indicates that most polymer pairs are immiscible. Immiscibility is a consequence of the very small combinatorial entropy change that results when two high-molecular-weight polymers are mixed. Scott [7] has extended the Flory–Huggins (F–H) lattice model (Section 3.2.1) to obtain an expression for ΔS_m for a polymer blend as

$$\Delta S_m = \left(\frac{RV}{V_r} \right) \left[\left(\frac{\phi_1}{x_1} \right) \ln \phi_1 + \left(\frac{\phi_2}{x_2} \right) \ln \phi_2 \right] \quad (7.6)$$

where R is the ideal gas constant, V is the volume of the blend, V_r is a reference volume (often taken as the molar volume of the smallest polymer repeating unit), ϕ_i is the volume fraction of polymer 1 or 2, and x_i is the degree of polymerization of polymer 1 or 2 relative to the reference volume. The corresponding equation for the Gibbs free energy of mixing is then

$$\Delta G_m = \left(\frac{RTV}{V_r} \right) \left[\left(\frac{\phi_1}{x_1} \right) \ln \phi_1 + \left(\frac{\phi_2}{x_2} \right) \ln \phi_2 + \chi_{12} \phi_1 \phi_2 \right] \quad (7.7)$$

where χ_{12} is the (Flory) interaction parameter of the blend of polymers 1 and 2.

Since the degree of polymerization (x_1 and x_2 appearing in the denominators on the RHS of eq. (7.6)) of high-molecular-weight polymers is large, ΔS_m is small. In order for ΔG_m (eq. (7.4)) to be negative as a necessary condition of miscibility, the enthalpic contribution to mixing, ΔH_m , must be either negative or zero, or have a small positive value. This implies that blend miscibility requires favorable interactions between the two blend polymers. Examples of favorable interactions include dispersive and dipole–dipole interactions, hydrogen bonding, or charge-transfer complexation.

As discussed in Chapter 3, the Flory–Huggins theory, although providing a useful basis for discussion, fails to correctly predict all aspects of polymer-blend behavior. For example, the F–H theory does not predict LCST behavior, which has been shown to occur. Good qualitative predictions of polymer phase behavior are, however, provided through the Flory equation of state (EOS) and other EOS models. For example, the effect of polymer molecular weight on the phase behavior of a binary polymer blend is qualitatively well represented using a modified form of the Flory EOS theory given by McMaster [8]. As shown in Figure 7-5, the LCST moves down in temperature as the molecular weight of either polymer in the blend decreases. This means that the region of miscibility increases with decreasing molecular weight, as may be expected from the favorable effect of decreasing molecular weight on increasing the combinatorial entropy of the blend. Also evident is the skewness of the binodal and spinodal curves when chain lengths of the molecular weight of the two polymers considerably differ. Specifically, the critical composition moves to the left as the ratio of chain lengths r_1/r_2 decreases. Figure 7-6 shows the effect of changes in the value of the interaction parameter on the phase diagram. As shown, the LCST moves to higher temperatures and the miscibility window (the area outside the binodal) widens as the interaction energy decreases.

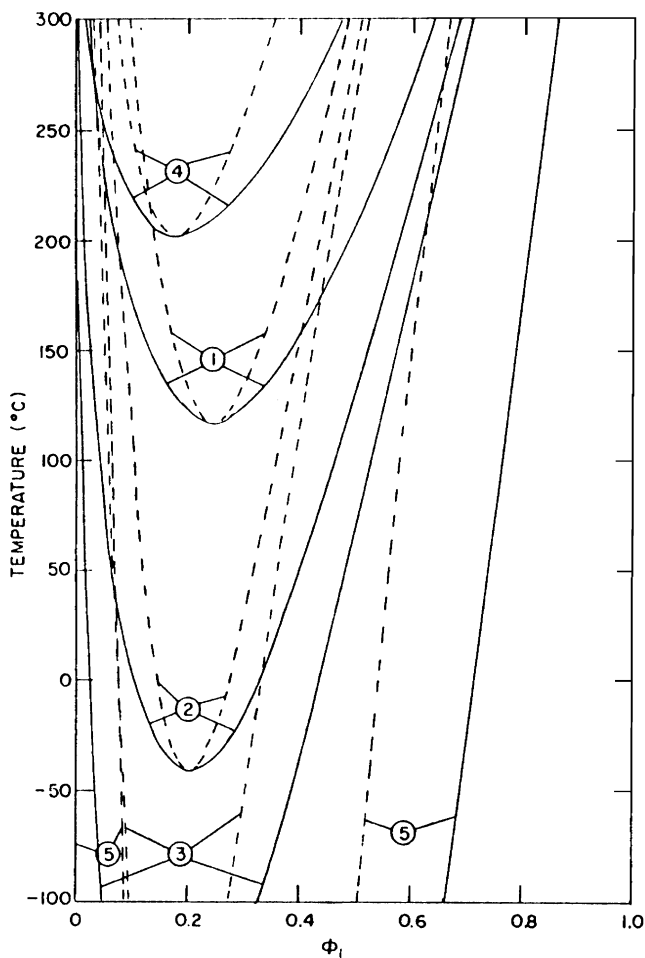


Figure 7-5 Effect of molecular weight of polymer 1 (curve 1, 30,000 molecular weight; curve 2, 50,000 molecular weight; and curve 3, 80,000 molecular weight) and polymer 2 (curve 4, 3000 molecular weight; curve 5, 6000 molecular weight) on the binodal (solid line) and spinodal (broken line) predicted by a modified version of the Flory EOS theory. Adapted with permission from L. P. McMaster, *Aspects of Polymer-Polymer Thermodynamics*. *Macromolecules*, 1973. **6**: p. 760–773. Copyright 1973, American Chemical Society.

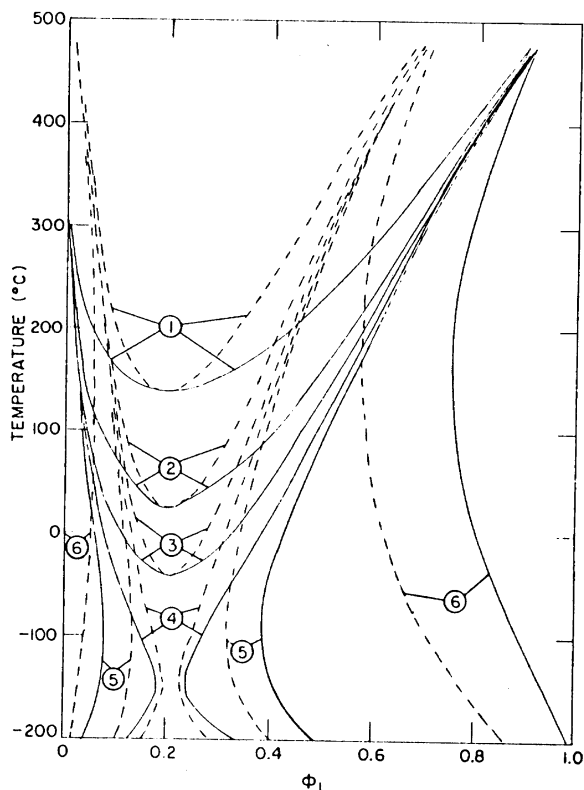


Figure 7-6 Effect of the value of the interaction energy on the binodal (solid line) and spinodal (broken line) predicted by a modified version of the Flory EOS theory. Values of X_{12} (cal cm^{-3}): curve 1, -0.050; curve 2, -0.100; curve 3, 0; curve 4, 0.005; curve 5, 0.010; and curve 6, 0.100. Adapted with permission from L. P. McMaster, *Aspects of Polymer-Polymer Thermodynamics*. Macromolecules, 1973. **6**: p. 760-773. Copyright 1973, American Chemical Society.

Recently, there has been interest in blends containing three-component polymers. The phase behavior of these ternary blends is difficult to determine experimentally as well as difficult to theoretically predict and to visualize. One way of representing their phase behavior is through the use of the triangular diagrams familiar to chemical engineers who have studied liquid-liquid equilibrium. The experimentally determined phase diagram [9] for ternary blends of PMMA, poly(ethyl methacrylate) (PEMA), and poly(styrene-*co*-acrylonitrile) (SAN) is shown in Figure 7-7. In this example, SAN (30 wt% acrylonitrile) is compatible (miscible) with PMMA and PEMA; however, PMMA and PEMA, themselves, are immiscible. In other words, two of the three polymer pairs are immiscible. As illustrated, there is a

moderately wide range of compositions (represented by the open circles lying outside the phase envelope) for which the three polymers can exist as homogeneous mixtures even though one polymer pair (PMMA/PEMA) is immiscible. In this study, evidence for phase homogeneity was deduced from detection of a single T_g (DSC measurements) for the blend.

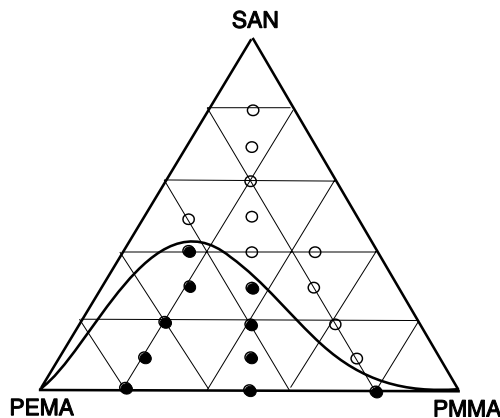


Figure 7-7 Triangular phase diagram for ternary blends of poly(methyl methacrylate) (PMMA), poly(ethyl methacrylate) (PEMA), and poly(styrene-co-acrylonitrile) (SAN). Filled circles (●) represent blend compositions that are phase-separated as indicated by the detection of multiple T_g s. Open circles (○) represent homogeneous compositions. Adapted from S. H. Goh and K. S. Siow, *Calorimetric Study of the Miscibility of Poly(styrene-co-acrylonitrile)/Poly(methyl methacrylate)/Poly(ethyl methacrylate) Ternary Blends*, *Thermochimica Acta*, 1985. **105**: p. 191–195, Copyright 1986, with permission from Elsevier Science.

Commercial Polymer Blends. Well-documented examples of miscible polymer blends are given in Table 7-4. Of these, the blends of poly(2,6-dimethyl-1,4-phenylene oxide)/PS and PVC/nitrile rubber (a copolymer of butadiene and acrylonitrile) are important commercially. Blends of poly(methyl vinyl ether)/PS and tetramethylbisphenol-A polycarbonate/PS, as mentioned earlier, have been reported to exhibit LCST at melt temperatures and have been widely used to study polymer-blend behavior. All these blends consist of only amorphous polymers, with the exception of PVC, which has a small degree of crystallinity (see Section 9.1.2).

In the case of poly(vinylidene fluoride) (PVDF) blends, PVDF can thermally crystallize depending upon blend composition and crystallization temperature. The second (amorphous) polymer in the blend (i.e., PEMA or PMMA) serves as a diluent, which lowers the crystalline-melting temperature, T_m , of the blend. From this information, the Flory interaction parameter can be obtained as discussed in Chapter 4 (eq. (4.4)). A plot of the T_g of the miscible [10] is shown in Figure 7-8.

Table 7-4 Examples of Miscible Polymer Blends

Polymer 1	Polymer 2
Polystyrene	Poly(2,6-dimethyl-1,4-phenylene oxide) Poly(methyl vinyl ether) Tetramethylbisphenol-A polycarbonate
Poly(vinyl chloride)	Polycaprolactone Nitrile rubber ^a
Poly(vinylidene fluoride)	Poly(ethyl methacrylate) Poly(methyl methacrylate)

^a For limited acrylonitrile content of the copolymer.

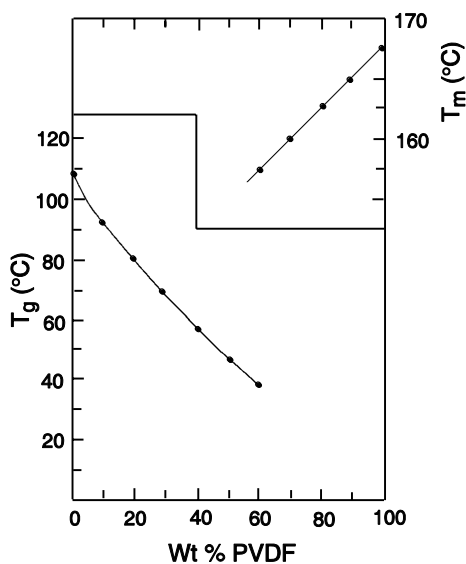


Figure 7-8 Experimental (DTA) values of T_g and T_m as a function of wt% of poly(vinylidene fluoride) (PVDF) in PVDF/PMMA blends. Adapted with permission from D. R. Paul and J. O. Altamirano, in *Copolymers, Polyblends, and Composites*, N. A. J. Platzer, ed., *Advances in Chemistry Series No. 142*, 1975, Washington, DC: American Chemical Society p. 371–385. Copyright 1975, American Chemical Society.

Properties of Blends. Properties of miscible polymer blends may be intermediate between those of the individual components (i.e., additive behavior), as is typically the case for T_g (see Figure 7-2). In other cases, blend properties may exhibit either positive or negative deviation from additivity, as illustrated by Figure 7-9. For example, both modulus and tensile strength of miscible polymer blends exhibit

a small maximum at some intermediate blend composition, while impact strength and permeability (see Chapter 12) will normally go through a broad minimum. This latter behavior has been attributed to a loss in free volume corresponding to a negative volume change of mixing (ΔV_m) due to favorable interactions between blend polymers.

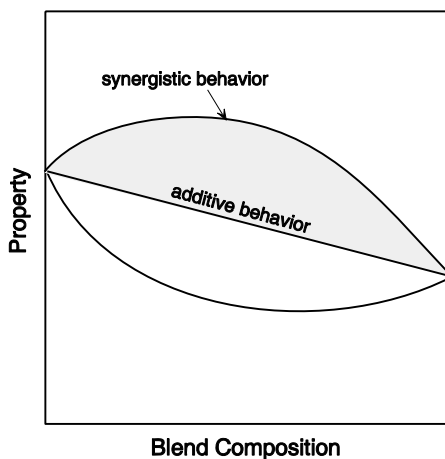


Figure 7-9 Illustration of three types of behavior for the dependence of miscible blend properties on composition.

7.2.2 Toughened Plastics and Phase-Separated Blends

The impact strength of brittle plastics such as PS can be significantly improved by incorporating a rubbery phase (e.g., polybutadiene) in the form of small ($< 0.01\text{-}\mu\text{m}$ -diameter) dispersed particles. Provided that adhesion between the dispersed phase and matrix polymer is good, the rubber particles can provide an energy-absorbing capability through a change in the mechanical-deformation process either through promotion of extensive shear yielding or craze formation (see Section 4.4.1) or through a combination of both. In the case of high-impact polystyrene (HIPS), interfacial adhesion is promoted by graft polymerization of butadiene with the polystyrene matrix.

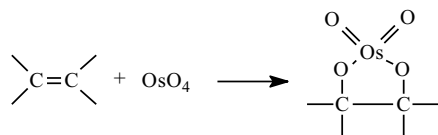
Figure 7-10 shows the complex morphology and extensive craze structure of a typical sample of HIPS that has undergone tensile deformation [11]. The phase structure is clearly seen in Figure 7-10A, which is a transmission electron micrograph of a sample that had been deformed, microtomed, and stained with osmium

tetroxide.* The light-colored areas contain the unstained polystyrene component of HIPS while the stained polybutadiene (PBD) regions appear as the darkened areas. It is noted that the dispersed PBD particles, which range in size from approximately 0.1 to 1.0 μm in diameter, contain significant amounts of occluded PS. These particles also appear to have become spheroidal as a result of the deformation process. The thin dark lines are the crazes (oriented perpendicular to the tensile direction) that have survived the microtoming and staining procedures. As a result of the removal of strain prior to sample preparation, the crazes have had an opportunity to relax or "heal" and therefore appear as thin, rather featureless structures. Extensive crazing is more clearly seen in Figure 7-10B, which shows a micrograph of the same sample that was obtained by deforming an unstained thin (0.1 μm) section that had been bonded to a copper cartridge inside the electron micrograph. In this case, the dispersed phase is less distinct due to the absence of staining; however, the craze microstructure is fully developed with the crazes interconnecting the dispersed PBD particles. As before, the crazes are oriented perpendicular to the tensile direction but the fibrils within the unrelaxed crazes are now clearly seen to be aligned in the tensile direction. This type of craze proliferation and bifurcation provides a means of energy dissipation (i.e., toughening) in the otherwise brittle PS matrix.

A higher-heat-distortion version of HIPS is ABS, which is an impact-modified styrene-acrylonitrile copolymer. Both HIPS and ABS are blended with other polymers to improve impact strength, as in the case of some commercial resins of polycarbonate (ABS-modified), PVC (ABS-modified), and poly(2,6-dimethyl-1,4-phenylene oxide) (HIPS-modified). Other polymeric impact modifiers include chlorinated polyethylene (CPE) and a variety of important copolymers including ethylene-vinyl acetate (EVA), methyl methacrylate-butadiene-styrene (MBS), and methyl methacrylate-acrylonitrile-butadiene-styrene (MABS).

Heat-distortion temperature (HDT) of a given polymer can sometimes be improved by blending with a high-HDT polymer. An example is the blend of PVC ($T_g \approx 85^\circ\text{C}$) and copolymers of styrene and maleic anhydride ($T_g \approx 116\text{--}123^\circ\text{C}$). Additional applications for heterogeneous (i.e., phase-separated) polymer blends include

* Osmium tetroxide (OsO_4) is a stain widely used to provide electron contrast for transmission electron microscopy of unsaturated polymers. This stain reacts with carbon double bonds as shown below and, in addition to providing increased electron density, serves to harden the rubbery component (e.g., polybutadiene in HIPS and ABS) and, therefore, facilitates sectioning by use of a cryogenic microtome.



coextruded textile polymers for the purpose of modifying some fiber property such as dyeability, self-crimping behavior, or antistatic character. In all these instances, acceptable mechanical properties of the blend require good interfacial adhesion between the continuous and dispersed phases. In the extreme case of macrophase-separated blends, mechanical properties as well as film clarity (i.e., transparency) may be unacceptable. In such cases, *compatibilizing agents* such as block copolymers containing one or two of the blend polymers may be useful to improve interfacial coupling.

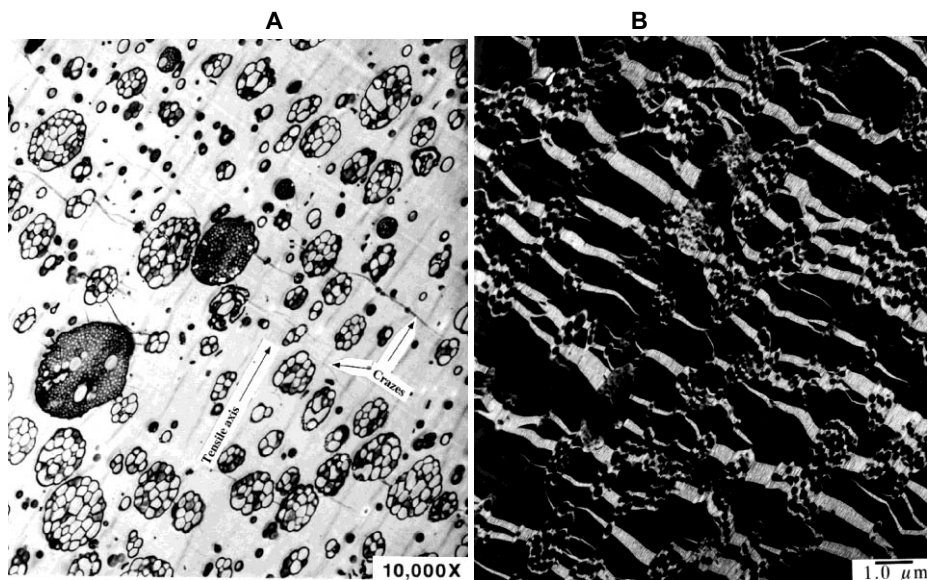


Figure 7-10 Transmission electron micrographs of high-impact polystyrene (HIPS). **A.** Stained microtomed section. **B.** In situ crazing using specimen deformation cartridge. Courtesy of R. C. Cieslinski, The Dow Chemical Company.

7.2.3 Interpenetrating Networks

Interpenetrating polymer networks or IPNs are combinations of two or more polymers in network form. At least one of the polymers is synthesized and/or cross-linked in the presence of the other. As such, IPNs share some of the advantages of both polymer blends and network polymers. If the two polymers in an IPN are thermodynamically immiscible, phase separation will occur as the monomer or monomers polymerize; however, the size of the dispersed phase will be smaller (10 to 100 nm) than would be the case for a physically mixed blend or for a block copolymer or graft of the two components. The controlled phase separation is due to

crosslinking restricting chain motion of the IPN. A wide range of morphologies is possible, depending upon the volume fraction of components, the viscosity of the phases, and the relative rates of crosslinking and phase separation.

Polymers that can be used in the preparation of IPNs include polyurethanes, polystyrene, poly(ethyl acrylate), and poly(methyl methacrylate). One of the earliest commercialized IPNs, used in many automotive applications, consists of polypropylene and ethylene–propylene–diene terpolymer (EPDM). If the ethylene segments of EPDM are sufficiently long to crystallize, the components are held together by crystalline domains of both polymers without the need of crosslinking (i.e., a thermoplastic IPN).

There are several ways by which IPNs can be prepared. For example, a *sequential IPN* is formed by first crosslinking one polymer. The crosslinked network is then swollen with a mixture of a monomer of the second polymer and a suitable crosslinking agent. The swollen film is then heated to initiate the polymerization and to crosslink the second (interpenetrating) network. An example of an IPN of poly(ethyl acrylate) (PEA) and polystyrene prepared in this way is illustrated in Figure 7-11.

If no crosslinking agent is used for the second polymer in the formation of a sequential IPN, only a single network of the initial polymer will result. In this case, the interpenetrating network is called a *semi-IPN*. *Gradient IPNs* are prepared by polymerizing the second monomer before equilibrium sorption occurs. *Simultaneous interpenetrating networks* (SINs) are formed when both polymers are synthesized and crosslinked simultaneously. Normally, SINs utilize polymers with different polymerization mechanisms (i.e., step and chain growth) to eliminate the possibility of copolymerization of the two monomers. Potential applications of IPNs include toughened plastics, ion-exchange resins, pressure-sensitive adhesives, soft contact lenses, controlled–release of drugs, and the preparation of novel membrane systems and sound- and vibration-damping material.

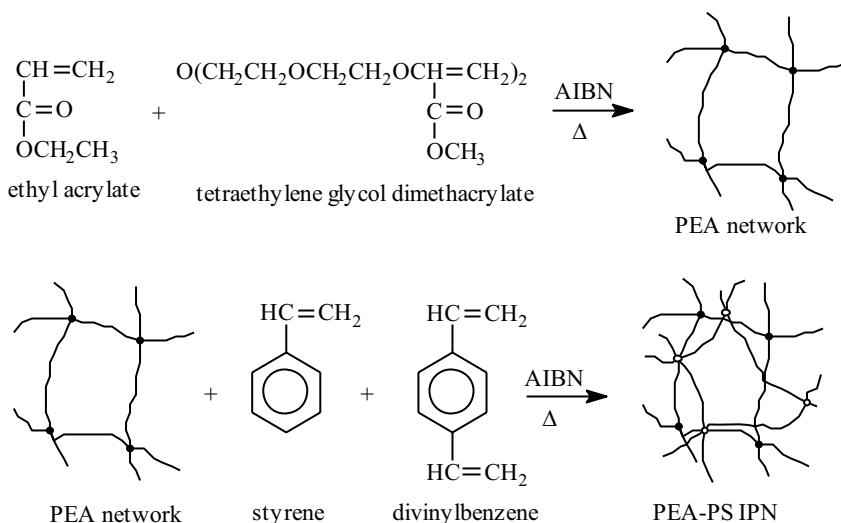


Figure 7-11 Preparation of a sequential interpenetrating network (IPN) by first polymerizing ethyl acrylate with a difunctional monomer, tetraethylene glycol dimethacrylate. The resulting PEA network is then swollen with styrene and divinylbenzene, which are subsequently polymerized to form an interpenetrating polystyrene network. The resulting IPN may be termed *cross-poly(ethyl acrylate)-inter-cross-polystyrene*, where the connectives *cross* and *inter* indicate crosslinked and interpenetrating, respectively. Adapted from L. W. Barrett and L. H. Sperling, *Today's Interpenetrating Polymer Networks*, Trends in Polymer Science, 1993. 1: p 45–49. Copyright 1993, with permission from Elsevier Science.

7.3 Block Copolymers

Polymerization of block and triblock copolymers by a number of different polymerization schemes including anionic, RAFT, group transfer, and click chemistry was covered in Chapter 2 (i.e., Sections 2.2, 2.4, and 2.5). Triblock copolymers such as polystyrene-*b*-polybutadiene-*b*-polystyrene (SBS) have applications as thermoplastic elastomers and are covered in Section 9.2.3. Amphiphilic triblock copolymers containing end blocks of hydrophilic polymers such as poly(ethylene oxide) or poly(2-alkyl-oxazolines) with a hydrophobic middle block such as polydimethylsiloxane or poly(ethyl ethylene) are being used to prepare biomimetic bilayers in which a variety of proteins are able to self-assemble into functional membrane

structures [12]. For all these reasons, how AB, ABA, and ABC* block copolymers self-organize into specific morphological structures in solution or in the melt and how different morphologies affect properties and function has significant importance. As discussed in Sections 2.2.1 and 2.2.2, physical blends of immiscible polymers will phase-separate at equilibrium. In the case of di- or triblock copolymers, the individual polymer blocks are prevented from complete macroscopic separation by their physical attachment to each other. The consequence is that the dimensions of the resulting structures are small (in the order of the radius of gyration). Energetically, phase separation is controlled by a competition between the drive to minimize the interfacial energy between immiscible polymers and the maximization of segmental entropy that decreases upon chain extension.

Self-assembly. In the case of diblock copolymers, such as polystyrene-*b*-polyisoprene and polystyrene-*b*-polybutadiene, the phase structure is controlled by the overall degree of polymerization, N , the overall volume fraction, f , and the Flory–Huggins interaction parameter (see Section (3.2.1)) between blocks A and B (χ_{AB}). The transition from a homogeneous melt to a micro-phase structure is termed the *order–disorder transition* and occurs at a critical value of the product χN . For a symmetric diblock copolymer where $f_A = f_B = 0.5$, this critical value is 10.5. Since χ is inversely proportional to temperature (see eq. (3.31), Section 3.2.1), a reduction in temperature will increase χ (and χN) and will eventually result in local ordering as shown by experimental data in Figure 7-12. Calculation of the phase diagram using self-consistent mean-field theory [13] shows good agreement with experimental results [14].

Due to their small dimensions, techniques such as TEM, SAXS, and small-angle neutron scattering (SANS) have been widely used for characterizing the morphology of block copolymers. TEM micrographs showing the morphology of two samples of polyisoprene-*b*-polystyrene (PI–PS) with different PI content and slightly different molecular weights are shown in Figure 7-13. The copolymer with the lower PI content (Figure 7-13a) exhibits lamellar microstructure while the copolymer with the higher PI content shows hexagonally packed cylinders (Figure 7-13b) in agreement with the predictions of self-consistent mean-field theory as mentioned in the previous paragraph.

* ABC block copolymers have three distinct polymer blocks—A, B, and C.

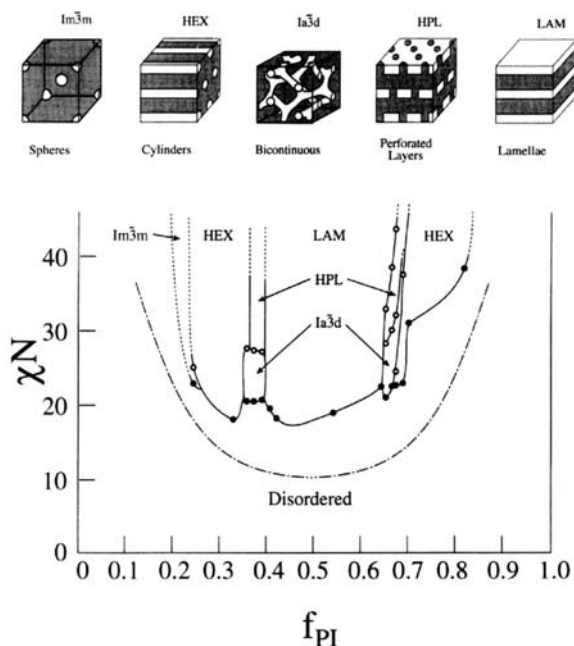


Figure 7-12 Experimental phase diagram for polyisoprene-*b*-polystyrene identifying regions of different morphologies such as body-centered close-packed spheres ($Im\bar{3}m$), hexagonal close-packed cylinders (HEX), and bicontinuous gyroid ($Ia\bar{3}d$) and lamellar structures (LAM). Reproduced with permission from A. K. Khandpur, et al., *Polyisoprene–Polystyrene Diblock Copolymer Phase Diagram near the Order–Disorder Transition*. *Macromolecules*, 1995. **28**: p. 8796–8806. Copyright 1995, American Chemical Society.

In the case of diblock containing one insoluble and one soluble block in water or other solvent, phase separation can occur in a variety of structures illustrated in Figure 7-14 [15]. The resulting geometry depends upon the concentration and the volume ratio between soluble and insoluble blocks (ISR). At a critical aggregation concentration (CAC), block copolymers begin to self-assemble into dispersed isotropic phases. The CAC decreases with increasing molecular weight and ISR composition. Assembled structures as diverse as polymer micelles and bilayer membranes can form (Figure 7-14). A key parameter is the packing parameter defined as

$$p = \frac{v}{a_0 d} \quad (7.8)$$

where v is the volume of the non-soluble block, a_0 is the surface area of the solvent-phobic block, and d is length of the solvent-phobic block. Amphiphilic ABA

triblock copolymers of hydrophilic poly(2-alkyl-2-oxazoline) end blocks and a central hydrophobic central (B) block of polydimethylsiloxane can form a polymeric vesicle or polymersome or a planar bilayer structure similar to a biological lipid bilayer [12]. A large number of protein channels can be incorporated into these membrane structures providing opportunities for sensor and other applications.

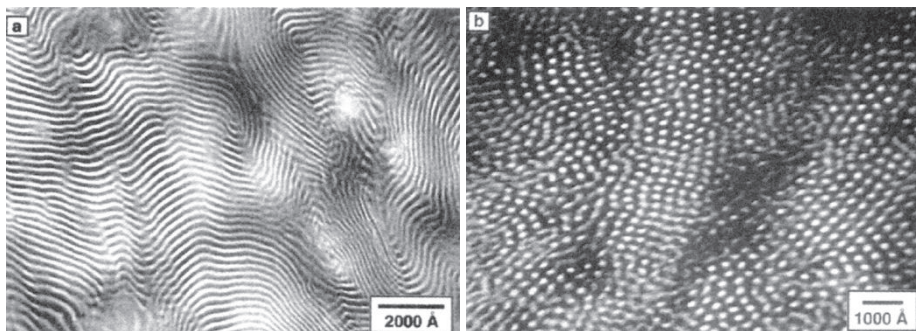


Figure 7-13 TEM micrographs of polyisoprene-*b*-polystyrene (PI-PS). (a) Lamellar morphology, $f_{PI} = 0.64$ ($M_n = 3.98 \times 10^4$); (b) hexagonally packed cylinders, $f_{PI} = 0.82$ ($M_n = 7.01 \times 10^4$). Specimens were annealed at 150°C in vacuum. Reproduced with permission from A. K. Khandpur et al., *Polyisoprene–Polystyrene Diblock Copolymer Phase Diagram near the Order–Disorder Transition*. *Macromolecules*, 1995. **28**: p. 8796–8806. Copyright 1995, American Chemical Society.

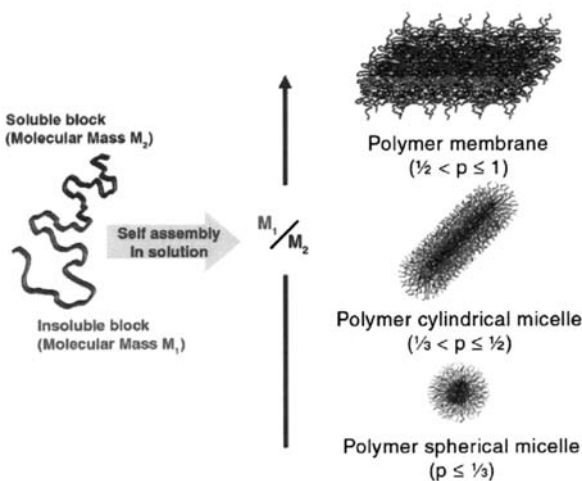


Figure 7-14 Morphological structures formed by amphiphilic triblock copolymers in solvent under different conditions. T. Smart et al., *Block Copolymer Nanostructures*, *Nano Today*, 2008. **3**(3–4): p. 38–46.

7.4 Composites

The first composite materials may have been bricks fashioned by the ancient Egyptians from mud and straw. Commercialization of composites can be traced to early in the twentieth century when cellulose fibers were used to reinforce phenolic and later urea and melamine resins. Probably the most familiar composite material today is Fiberglas, first introduced in the 1940s. Fiberglas is the trade name for a composite consisting of glass-fiber reinforcement of an unsaturated-polyester matrix. It is widely used to form large lightweight reinforced structures, such as the body of a Corvette, or the hull of a cabin cruiser, or as alternatives to heavy porcelain in the manufacture of bathtubs and shower stalls.

Composites are used in a wide range of applications, wherever high strength-to-weight ratios are important. Principal uses are found in the automotive, marine, and construction industries. In the majority of cases, especially those requiring high performance in the automotive and aerospace industries, the discontinuous phase or filler is in the form of a fiber. Typical fibers for composite applications include carbon or graphite, glass, aromatic polyamide (e.g., Kevlar), and others that were listed in Table 7-2. In some cases, the filler may be particulate—in the form of microspheres or flakes.

In most cases, composite matrices are thermosets, although there has been recent interest in composites made from thermoplastics and composites having carbon, ceramic, or metallic matrices for high-temperature and other demanding applications. The most important class of thermosets for composite use is epoxy (see Section 9.3.1). Although epoxy resins are inexpensive and easy to process, they are brittle and have relatively high moisture absorption, which can affect the strength of the filler–matrix interface. As discussed in the following sections, interfacial strength can be improved by the use of coupling agents, which are low-molecular-weight organic-inorganic compounds that serve to promote adhesion between the filler and matrix. In general, thermoplastics such as polysulfone offer higher impact strength than thermosets but are more susceptible to solvent attack and have higher creep compliance, which results in a loss of dimensional stability under load. Recently, some high-impact semicrystalline thermoplastics, such as polyetheretherketone (PEEK), have been evaluated for composite use due to their good solvent resistance and impact strength. Polyimides, which can be either thermoset or thermoplastic, are widely used in aerospace applications. Thermosetting polyimides provide easier processing and higher heat resistance, while thermoplastic polyimides offer greater toughness. Typical properties of some thermoset and thermoplastic matrices are compared in Table 7-5.

Composites are processed by a variety of methods, including compression and resin-transfer molding, which will be described in Chapter 11. Specialized processing operations for composite fabrication are filament winding and pultrusion,

which will be described in Section 7.4.2. These are used to prepare continuous fiber-reinforced composites with controlled fiber orientation.

Table 7-5 Properties of Composite Matrices

Property	Thermoset Epoxy	Thermoplastics		
		PI ^a	PSF ^b	PEEK ^c
Compressive strength, MPa	140	187	96	—
Density, g cm ⁻³	1.15–1.2	1.43	1.24	1.32
Modulus, GPa	2.8–4.2	3.2	2.5	3.9
Tensile strength, MPa	55–130	56	70	91
Thermal expansion coefficient, 10 ⁻⁶ per °C	45–65	50	—	47
Thermal conductivity, W (m K) ⁻¹	0.17–0.21	0.36	—	0.25
T_g , °C	130–250	370	185	143

^a PI, thermosetting polyimide.

^b PSF, bisphenol-A polysulfone (Udel P1700).

^c PEEK, polyetheretherketone; ca. 35% crystalline with T_m of 334°C.

The mechanical properties of composites are strongly influenced by the size, type, concentration, and dispersion of filler, as well as the extent of interfacial adhesion between the filler and matrix (i.e., continuous phase) and the properties of the matrix. The interrelationships between these variables are complex and only basic principles relating these parameters to the mechanical properties and ultimate performance of particulate and fiber-reinforced composites are developed in the following section.

7.4.1 Mechanical Properties

Modulus. The principal function of reinforcing fillers is to increase the modulus of the composite. This is typically accompanied by an increase in the heat-distortion temperature. The modulus of a glassy-polymer composite containing a rigid *particulate* filler may be estimated by use of the modified *Halpin–Tsai equation* given as

$$\frac{M}{M_m} = \frac{1 + AB\phi_f}{1 - B\psi\phi_f} \quad (7.9)$$

where M is the modulus (tensile, shear, or bulk) of the composite, M_m is the corresponding modulus of the unreinforced matrix polymer, A is a constant that depends on the filler geometry and the Poisson's ratio of the matrix, ϕ_f is the volume fraction of filler, ψ depends upon the maximum *packing* volume fraction of the filler (0.601

for random loose packing of spheres), and B is a function of A and the relative moduli of the filler (M_f) and matrix as

$$B = \frac{(M_f/M_m) - 1}{(M_f/M_m) + A}. \quad (7.10)$$

If the particulate filler is uniformly dispersed, the mechanical properties of a particulate-filled composite are independent of the testing direction (i.e., isotropic). By comparison, the properties of fiber-reinforced composites are dependent upon the direction of measurement—they are *anisotropic*. This is because fibers are usually uniaxially oriented or oriented randomly in a plane during the fabrication of the composite. The maximum modulus of the composite is obtained in the orientation direction. For uniaxially oriented fibers, the tensile (Young's) modulus measured in the orientation direction (the longitudinal modulus, E_L) is given by a simple rule of mixtures as

$$E_L = (1 - \phi_f)E_m + \phi_f E_f \quad (7.11)$$

where E_m is the tensile modulus of the matrix and E_f is the tensile modulus of the fiber (see Table 7-3). The modulus measured in the direction perpendicular to orientation (i.e., the transverse modulus, E_T) is typically much smaller than E_L . It can be expressed in the form of the modified Halpin–Tsai equation (eq. (7.9)) as

$$\frac{E_T}{E_m} = \frac{1 + AB\phi_f}{1 - B\psi\phi_f} \quad (7.12)$$

where A is equal to twice the aspect ratio (L/D) for uniaxially oriented fibers.

Strength. In general, composite strength, an ultimate property, depends upon many factors, such as the adhesive strength of the matrix-filler interphase, and, therefore, is not as easily modeled as is modulus. Interfacial strength may be reduced by the presence of water adsorbed on the filler surface or by thermal stresses resulting from a mismatch between the thermal coefficients of linear expansion for the filler and matrix polymer. Polymers have relatively high linear-expansion coefficients (60 to 80×10^{-6} per $^{\circ}\text{C}$ for PS) compared to fillers such as silica glass (0.6×10^{-6} per $^{\circ}\text{C}$) or graphite (7.8×10^{-6} per $^{\circ}\text{C}$).

Several relationships have been proposed to relate the ultimate strength of a *particulate-filled composite* (σ_u) to the ultimate strength of the unfilled matrix (σ_m). One such equation proposed by Schrage [16] is given as

$$\sigma_u = \sigma_m \exp(-r\phi_f) \quad (7.13)$$

where r is an interfacial factor (typically 2.66 for many composites). This provides a maximum value for strength (up to 35 to 40 vol % filler) and assumes good adhe-

sion between the dispersed filler and matrix. Strength of the composite will decrease with decreasing interfacial strength.

In the case of *fiber-reinforced composites*, strength, like modulus, depends on the orientation of the fiber with respect to the stress direction. The maximum strength is obtained for uniaxially oriented fibers when the fibers are oriented in the tensile (or longitudinal) direction, σ_L . In this case, the strength is given by the simple rule of mixtures in the same form as for modulus (eq. (7.11)):

$$\sigma_L = (1 - \phi_f) \sigma_m + \phi_f \sigma_f. \quad (7.14)$$

In contrast, the strength of the uniaxially oriented fiber composite is minimal when the strength is measured transverse to the fiber orientation, σ_T . This strength is strongly influenced by the strength of the interfacial bond and will be much lower than the longitudinal strength. As an approximation, σ_T may be approximated as one-half of the matrix strength, σ_m .

As an illustration of the effect of fiber reinforcement on composite properties, heat-distortion temperature and some mechanical properties of carbon- and glass-fiber composites of polyetheretherketone (PEEK), an engineering thermoplastic (see Section 10.2.3), are given in Table 7-6. As illustrated, reinforcement increases the heat-distortion temperature of PEEK from 148° to 300°C at 30% fiber loading. In addition, tensile strength and especially (flexural) modulus are increased considerably over corresponding values for the unfilled or “neat” resin due to the high modulus and strength of carbon and glass fibers (see Table 7-8). The modulus of the carbon-fiber composite is higher than that of the glass-fiber composite since the modulus of carbon and graphite fibers is greater than that of glass fibers up to a factor of nearly 5.

Table 7-6 Properties of PEEK Composites

Property	PEEK	30% Carbon Fiber	30% Glass Fiber
Flexural modulus (GPa) at 23°C	3.89	15.5	8.0
Heat-deflection temperature °C at 1.82 MPa (264 psi)	148	300	300
Tensile strength (MPa) at 23°C	91.0	146.0	140.0

Interfacial Adhesion and Coupling Agents. In practice, interfacial strength is improved by the use of low-molecular-weight organofunctional silanes (or titanates) such as those listed in Table 7-7, which act as a *coupling agent* bridging the matrix-filler boundary. Typically, these inorganic-organic additives have one or more hydrolyzable groups (e.g., hydroxyl or alkoxy) capable of silanol-group formation for bonding with mineral surfaces and a matrix-specific organofunctional group such as an epoxy functionality, which can react with, or promote adhesion to, the matrix resin. The most important of the coupling agents are the silanes that are

widely used in the form of aqueous dispersions to treat glass fiber and coarse particulate fillers.

Table 7-7 Common Coupling Agents

Type	Representative Structures
Epoxy silane	$\text{H}_2\text{C}-\overset{\text{O}}{\text{C}}-\text{CHCH}_2\text{OCH}_2\text{CH}_2\text{CH}_2\text{CH}_2-\text{Si}(\text{OCH}_3)_3$
Methacrylate	$\text{H}_2\text{C}=\overset{\text{CH}_3}{\text{C}}-\overset{\text{O}}{\underset{\text{O}}{\text{C}}}-\text{O}-\text{CH}_2\text{CH}_2\text{CH}_2-\text{Si}(\text{OCH}_3)_3$
Primary amine silane	$\text{H}_2\text{NCH}_2\text{CH}_2\text{CH}_2-\text{Si}(\text{OC}_2\text{H}_5)_3$
Titanate	$\left(\text{H}_2\text{C}=\overset{\text{CH}_3}{\text{C}}-\overset{\text{O}}{\underset{\text{O}}{\text{C}}}-\text{O} \right)_3 \text{TiOCH}(\text{CH}_3)_2$
Vinyl silane	$\text{CH}_2=\text{CH}-\text{Si}(\text{OCH}_3)_3$

The effect of coupling agents on the dry and wet flexural strength of glass-fiber-reinforced polyester is illustrated in Table 7-8. In this example, a silane-functional coupling agent is shown to greatly improve the flexural strength of the polyester composite, both in the dry state and after immersion in boiling water. Improved interfacial adhesion may also be achieved by modification or functionalization of the fiber surface. For example, the interfacial adhesion of ultrahigh-molecular-weight polyethylene may be improved by plasma treatment in pure oxygen.

Table 7-8 Flexural Strength of a Glass-Reinforced Polyester

Coupling Agent	Flexural Strength (GPa) ^a	
	Dry	2-Hour Boil
None	0.38	0.23
Vinyl silane	0.46	0.41
Methacrylate silane	0.62	0.59

^a To convert GPa to psi, multiply by 145,000.

Dynamic-Mechanical Properties. Dynamic-mechanical measurements (see Section 5.1.1) can be used to investigate the morphology of composites and phase-separated polymer blends through the “equivalent model” originally proposed by Takayanagi [17]. As illustrated in Figure 7-15, the dynamic-mechanical properties of any two-phase morphology, such as an immiscible blend, composite, laminate, or semicrystalline polymer, can be modeled as a series and parallel combination of contributions from the individual components—the matrix and dispersed phases.

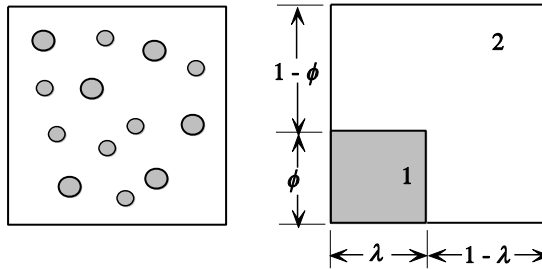


Figure 7-15 The equivalent model of Takayanagi [17]. An idealized two-phase system consisting of a dispersed phase (shaded regions) dispersed in a matrix of component 1 is shown at the left. This composite structure can be modeled as a unit cube ($1 \times 1 \times 1$) (pictured at right) with the dispersed phase (component 1) having dimensions of $\phi \times \lambda \times 1$ (i.e., the volume fraction is $\phi\lambda$).

The dynamic modulus of the composite can be modeled by resolving the equivalent model pictured at the right of Figure 7-15 as contributions from elements in series and parallel, as illustrated in Figure 7-16. Since elements A and B are in series, strains on these elements, or equivalently their weighted compliances, are additive and, therefore, we can write

$$D^* = \frac{1}{E^*} = (1 - \phi)D_A^* + \phi D_B^*. \quad (7.15)$$

Since element A is pure component 2 (the matrix component),

$$D_A^* = \frac{1}{E_A^*} = \frac{1}{E_2^*}. \quad (7.16)$$

Element B is a parallel combination of components 1 (dispersed component) and 2 (matrix) and, therefore, stresses or equivalently moduli are additive:

$$E_B^* = \frac{1}{D_B^*} = \lambda E_1^* + (1 - \lambda)E_2^*. \quad (7.17)$$

Substituting eqs. (7.16) and (7.17) into eq. (7.15) gives the final relationship for the dynamic compliance or modulus of the equivalent model as

$$D^* = \frac{1}{E^*} = \frac{1 - \phi}{E_2^*} + \frac{\phi}{\lambda E_1^* + (1 - \lambda)E_2^*}. \quad (7.18)$$

In eq. (7.18), ϕ and λ have the significance of fitting parameters, although the product ($\phi\lambda$) is equal to the *volume fraction* of the dispersed phase. The values of these fitting parameters obtained by fitting actual dynamic-mechanical data give a quali-

tative understanding of the morphology of the composite. For example, $\lambda = \phi$ indicates a uniformly dispersed phase, while $\lambda < \phi$ indicates agglomeration of dispersed phases.

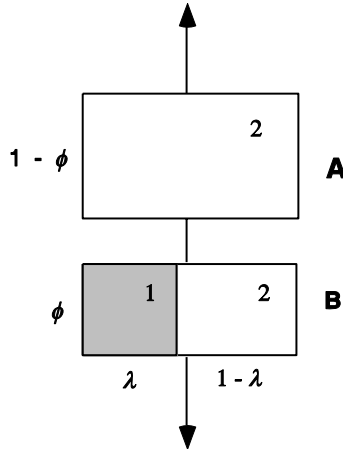


Figure 7-16 Parallel and series elements of equivalent model illustrated in Figure 7-15. Elements A and B are in series combination to the applied strain (arrows). Element B is composed of two elements (dispersed phase and matrix) in parallel.

7.4.2 Composite Fabrication

As previously indicated, composites can be fabricated by a variety of techniques, including compression and resin-transfer molding, which are discussed in Chapter 11. Composites used for nonstructural (i.e., non-load-bearing) applications are produced by using sheet-molding compound (SMC), bulk-molding compound (BMC), preform molding, injection molding, and spray-up. For the manufacture of composites for structural applications, two important processing methods are filament winding and pultrusion, which are reviewed here.

In general, BMC consists of styrenated unsaturated-polyester resin (unsaturated polyester containing styrene monomer, which is polymerized during the final cure process), a low-profile thermoplastic polymer, an inert filler such as calcium carbonate, glass fibers, a polymerization initiator, and other additives such as a lubricant (e.g., zinc stearate), and a maturation agent (e.g., MgO). BMC has the consistency of putty, which can be applied with a trowel. A related composite formulation is SMC, which is formed by combining styrenated polyester resin thickened by 1% of calcium or magnesium oxide, fillers, peroxides, and chopped glass fibers. The SMC is contained between layers of polyethylene film, which are removed at

the time of molding. In spray-up, glass fibers and a resin are simultaneously deposited in a mold. In this process, a roving (8 to 120 strands of glass fiber) is fed through a chopper and ejected into a resin stream. A preform refers to a preshaped composite formed by distribution of chopped fibers by air, water flotation, or vacuum over the surface of a preformed screen. A preform may also refer to a mat or cloth preformed to a specific shape on a mandrel or mock-up.

Filament Winding. A simple filament-winding operation is illustrated in Figure 7-17. Fibers are pulled from bobbins through a bath containing the composite resin, such as an epoxy or (unsaturated) polyester formulation, and then the impregnated fibers are wound onto a form (the mandrel) in some predetermined arrangement. Usually, fibers are E- or S-glass (see Table 7-3). Once the mandrel is uniformly covered to the desired thickness and fiber orientation, the composite is cured at an elevated temperature and the mandrel may be removed or left as an integral part of the composite. Filament winding may be used to prepare corrosion-resistant (fiber-glass) tanks and pipes. Employing advanced resin materials, filament winding is also being used to prepare high-performance composites for structural and other applications in the automotive and aerospace industries. The continuous reinforcement and controlled fiber orientation that can be achieved by filament winding provide a higher level of reinforcement than is possible by discontinuous reinforcement using individual fibers.

Pultrusion. A simplified diagram of a pultrusion operation is illustrated in Figure 7-18. Compared to filament winding, pultrusion is a completely continuous process operation since the cure step is online. This makes pultrusion a suitable process for commercial production lines producing a variety of composite shapes or profiles. A roving* of continuous fibers (e.g., E-glass) and a continuous-strand mat (typically glass/polyester) are combined and immersed in a resin bath before passing through a forming guide and the curing oven. The majority of composites that are pultruded are the fiber-glass variety prepared from unsaturated polyester resin and E-glass. Fiber loadings in pultrusion may range from 20% to 80%.

* When graphite or boron fibers are used in place of glass fibers, the term *tow* is used rather than roving.

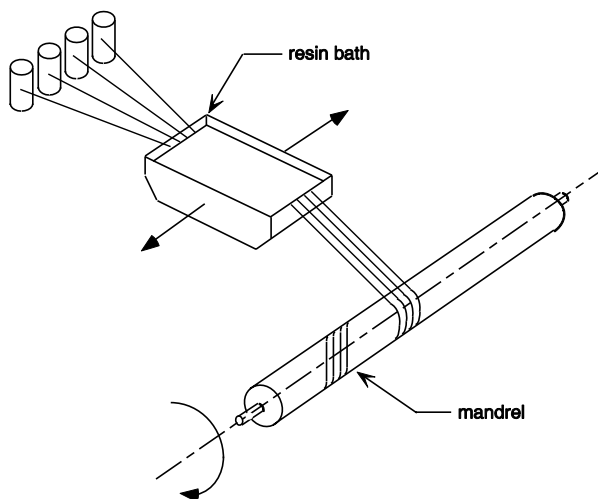


Figure 7-17 Filament-winding operation. Adapted from R. C. Hayes in *The Concise Encyclopedia of Polymer Science and Engineering*, J. I. Kroschwitz, ed. Copyright © 1990 by John Wiley & Sons. This material is used by permission of John Wiley & Sons, Inc.

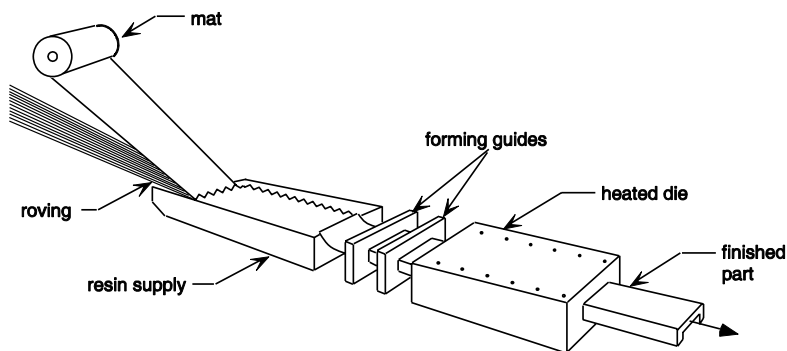


Figure 7-18 Pultrusion line. Adapted from D. Evans in *The Concise Encyclopedia of Polymer Science and Engineering*, J. I. Kroschwitz, ed. Copyright © 1990 by John Wiley & Sons. This material is used by permission of John Wiley & Sons, Inc.

7.5 Nanocomposites

One of the most rapidly growing areas of polymer technology is that of nanocomposites. Compared to more traditional composite materials described in the previous

section, the distinguishing characteristic of nanocomposites is the size of the reinforcing filler. In nanocomposites, this reinforcing filler (the nanofiller) is typically a carbon- or silicon-based high-aspect-ratio (10:1 to 1000:1) reinforcement that has one or more dimensions in the range from 1 to 100 nm (10 to 1000 Å). As covered in greater detail in Section 7.5.1, nanofillers include organically modified clay (montmorillonite or MMT), organically modified silicon–oxygen nanocages (POSS*), single- and multi-walled carbon nanotubes (CNTs), carbon nanofiber (CNF), graphene (single-sheet graphite), nanosilica (e.g., Aerosil), various metal oxides such as indium tin oxide (ITO), and graphite nanoparticles. Some of the attractive properties of nanocomposites include improved electrical and mechanical properties (e.g., increased strength and modulus without sacrificing impact properties), reduced gas and water permeability for barrier applications (e.g., packaging and fuel containment), increased thermal stability, flame resistance, and resistance to wear, elevated heat-distortion temperature, recyclability, potential for surface and interface modification, enhanced ionic conductivity, and improved processability (e.g., extrusion and molding). Other advantages include increased dimensional stability at elevated temperatures, better surface gloss, increased tear resistance of elastomers, optical transparency, accelerated cure of elastomers, and reduced shrinkage. Perhaps the earliest commercial nanocomposites were fabricated in the 1980s from nylon-6 and MMT by researchers at Toyota. Since the early work by Toyota, the market for nanocomposites has increased rapidly and is expected to reach 11 billion pounds by 2020 in the United States alone. In addition to nylon-6, nanocomposites have been prepared from many commodity and engineering-grade thermoplastics including nylon-11, polysiloxanes, poly(ethylene oxide), polyetherimide, some thermoplastic elastomers, and a variety of thermosets including epoxies, phenolic resins, and cyanate ester. Covered in the following section are MMT and the properties of nanocomposites of MMT. Section 7.5.2 provides coverage of other important nanofillers and their corresponding nanocomposites.

7.5.1 Montmorillonite Nanocomposites

Montmorillonite. The most common form of nano-reinforcement has been organoclay derived from montmorillonite (MMT). MMT is a naturally occurring 2:1 phyllosilicate with the same structure as talc and mica, but a different layer charge. Modification of the inorganic surface of MMT by organic treatment is used to increase dispersion in the polymer matrix. The crystal structure of MMT consists of 1-nm thin layers with a central octahedral sheet of alumina fused between two external silica tetrahedral sheets. These platelets have thicknesses of ~1 nm with as-

* Polyhedral oligomeric silsesquioxane or POSS, a trademark of Hybrid Plastics.

pect ratios (i.e., diameter:thickness) from 10:1 to 1000:1 and are arranged in stacks that can be separated (or exfoliated) during composite fabrication. Isomorphoic substitution within the layers (e.g., replacing Al^{3+} by Mg^{2+}) can be used to modify the charge-exchange capacity. The silicate sheets in MMT are separated by cations, typically sodium, as illustrated in Figure 7-19. These cations balance the overall charge. The sodium cation in the gallery can be exchanged with other cations such as lithium, potassium, and calcium. In water, large organic cations, such as an alkyl ammonium cation, can replace the sodium cation in the swollen layered silicates. Some specific examples include dimethyl distearyl ammonium chloride and dimethyl stearyl benzyl ammonium chloride. The choice of the alkyl group can be tailored to improve miscibility of MMT with a specific polymer matrix. For example, silicone rubber nanocomposites can be fabricated by ion-exchanging Na^+ /MMT with dimethyl ditallow ammonium bromide or hexadecyltrimethylammonium bromide. The ion-exchange process also increases the gallery height in relation to the molecular size of the organic cation.

For use in nanocomposites, the layered silicates of MMT are generally rendered organophilic by exchanging the Na^+ in a water-swollen layered silicate with an organic cation such as an alkyl ammonium ion. This ion-exchange process increases the gallery height in relation to the molecular size of the organic cation. The choice of an ammonium ion is influenced by its chemical compatibility with the composite matrix. Some examples include dimethyl distearyl ammonium chloride and dimethyl stearyl benzyl ammonium chloride. Organo-MMT nanocomposites of silicone rubber can be fabricated by ion-exchanging Na^+ /MMT with dimethyl ditallow ammonium bromide or hexadecyltrimethylammonium bromide.

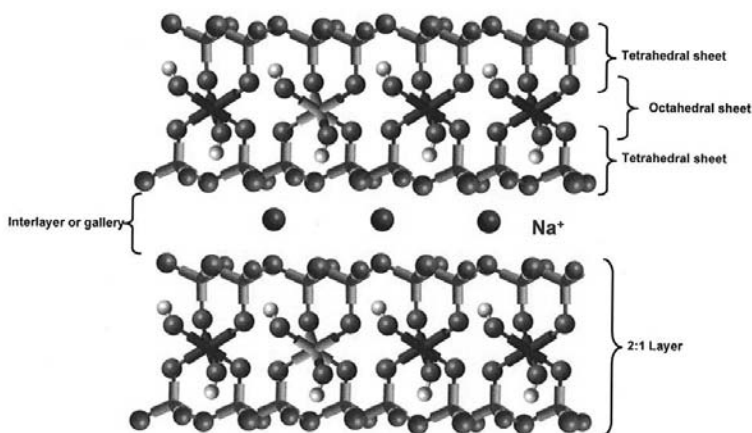


Figure 7-19 Structure of sodium montmorillonite. Courtesy of Southern Clay Product, Incorporated.

Processing. Various ways that polymer chains can be incorporated in organophilic layered silicates during melt processing are illustrated in Figure 7-20. Other than simply mixing the layered silicate with the polymer chains to form a microcomposite, individual polymer chains can be intercalated into each silicate layer. Alternatively, individual silicate layers can be separated (exfoliated). A nanocomposite also can be prepared by mixing the ion-exchanged layered silicate with a monomer followed by polymerization.

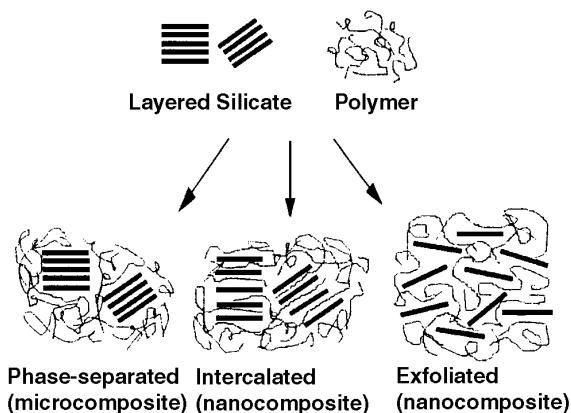


Figure 7-20 Three routes to polymer-silicate structures. From Günter Beyer, *Nanocomposites: a New Class of Flame Retardants for Polymers*, Polymer News. 2001, 25: p. 370. Copyright 2001. Reproduced with permission of Taylor & Francis, Inc., <http://www.routledge-ny.com>.

Properties. One of the unique advantages of nanocomposites, in general, is that property improvement can be significant at much smaller loading than for typical composites made with larger reinforcements such as glass and carbon fibers. This is clearly illustrated for nylon-6 in Figure 7-21 where the relative Young's modulus (ratio of composite modulus to matrix modulus) of a glass-fiber composite is compared to that of an MMT nanocomposite. As shown, the modulus of nylon-6 doubles at 8 wt% MMT compared to 20 wt% glass fiber that is required for the same reinforcement. Other properties of a nylon/MMT nanocomposite are given in Table 7-9. In addition to significant modulus increase, the heat-distortion temperature (HDT) is significantly increased as would be expected due to the reinforcement. While water absorption and impact strength are not significantly affected by MMT reinforcement, the coefficient of thermal expansion is significantly *reduced* while tensile strength is increased. In other studies, significant increases in HDT, modulus, and strength have been reported for MMT nanocomposites of bisphenol-A polysulfone at 3 wt% loading with little loss in elongation at break or impact strength [18]. At higher loading, exfoliation decreases and mechanical properties

decline. A modulus increase of about 50% has been reported for a polyimide/MMT nanocomposite [19] and about 100% for polydimethylsiloxane with only 1% MMT loading.

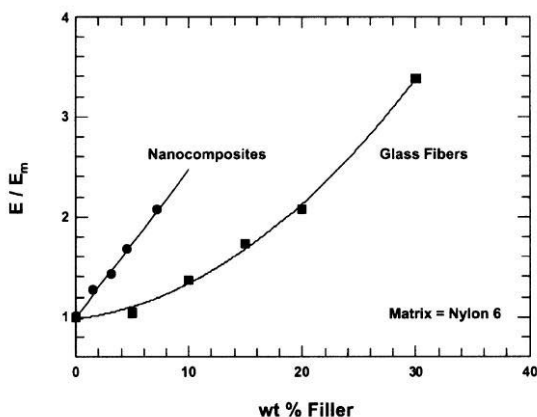


Figure 7-21 Comparison of relative modulus at different concentrations of glass fiber and MMT in nylon-6. Reproduced with permission from T. D. Fornes and D. R. Paul, *Modeling Properties of Nylon 6/Clay Nanocomposite Using Composite Theories*. Polymer, 2003. 4: p. 4993–5013.

Table 7-9 Representative Properties of a Nylon-6 Nanocomposite

Property	Nylon-6	Nanocomposite
Coefficient of thermal expansion ($\times 10^5$)	13	6.3
Heat-distortion temperature ($^{\circ}\text{C}$)	65	145
Tensile modulus (GPa)	1.1	2.1
Tensile strength (MPa)	69	107
Impact strength (kJ m^{-2})	2.3	2.8
Water absorption (%)	0.87	0.51

7.5.2 Buckyballs, Carbon Nanotubes, Graphene, and POSS

In addition to MMT, nanocomposites can be formed from a wide variety of nanofillers including those with a carbon base, principally fullerenes, nanotubes, and graphene. Another common nanofiller has the structure of a silicon–oxygen nanocage that can be functionalized with a wide variety of substituent groups including halogens and a number of organic groups such as methyl, ethyl, ethylene, and phenyl.

Buckyballs. The development of nanotechnology was greatly accelerated by the 1985 discovery of the formation of 60 carbon atom clusters when graphite was

vaporized by laser irradiation. This discovery was reported [20] by Richard Smalley and co-discoverers Robert Curl and Harold Kroto.* This work was an outcome of a study to investigate how long-chain carbon molecules may be formed in interstellar space. Smalley speculated that the resulting structure, subsequently termed a *buckyball* or buckminsterfullerene (C_{60}) was a polygon containing 60 vertices and 32 faces, of which 12 were pentagonal and 20 were hexagonal as illustrated by the soccer ball shown in Figure 7-22A and the simulation model in Figure 7-22B.

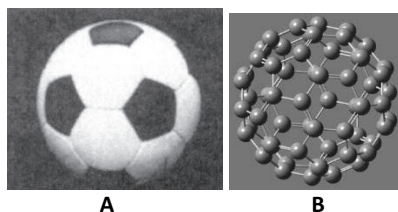


Figure 7-22 A. Type of soccer ball used by Smalley to illustrate his 1985 model. B. A computer-generated ball-and-stick representation of a buckyball.

Carbon Nanotubes. Carbon nanotubes (CNTs) are the hollow-fiber equivalent of the buckyball. The first single-walled carbon nanotube (SWNT) was produced in 1991 by Sumio Iijima [21] working at NEC in Japan. After the isolation of SWNTs was announced in 1993, Smalley found that by impregnating iron, cobalt, or nickel catalysts in graphite rods that had been used to prepare buckyballs using laser vaporization, an SWNT could be produced. Between 1993 and his untimely death in 2005, Smalley continued to improve the technology of making better CNTs, including producing them in solution and chemical-reacting them to attach functional groups. In general, CNTs provide an attractive combinations of high flexibility and strength combined with high stiffness and low density. SWNTs have diameters approximately 0.4 to 3 nm in diameter and exhibit good electrical properties but are relatively expensive to make.

The typical tensile strength of a CNT is in the range from 100 to 600 GPa or about two orders of magnitude greater than a typical carbon fiber (CF). Densities are approximately 1.3 g cm^{-3} compared to 1.8 to 1.9 g cm^{-3} for CF. Young's modulus is 1–5 TP, compared to 750 GPa for CF. CNTs can carry large current densities with thermal conductivities around 200 W/(mK) . For favorable interactions with a polymeric matrix, CNTs are chemically modified and require good dispersion that can be achieved through in situ polymerization of the matrix, shear mixing, the use of surfactants, and solution processing.

* For their work, Smalley, Curl, and Kroto shared the 1996 Nobel Prize in chemistry.

In addition to SWNTs, multi-walled CNTs (MWNTs) can be prepared. A comparison of computer-generated simulations of an SWNT and a double-walled CNT is shown in Figure 7-23. The projected 2014 market for CNTs given in Table 7-10 is roughly comparable for SWNTs and MWNTs with principal applications in electronics and automotive industries. At present, MWNTs are easier to produce on large scale than are SWNTs and are, therefore, less expensive. Outer diameters of MWNTs are in the range from 2 to 25 nm, significantly larger than SWNTs, with lengths in the range between 0.2 and 2 mm. A typical modulus of MWNTs is 1.8 TPa compared to 0.517 TPa for graphite. They are less brittle than graphite and have a tensile strength of 63 GPa (compared to 1.2 GPa for steel).

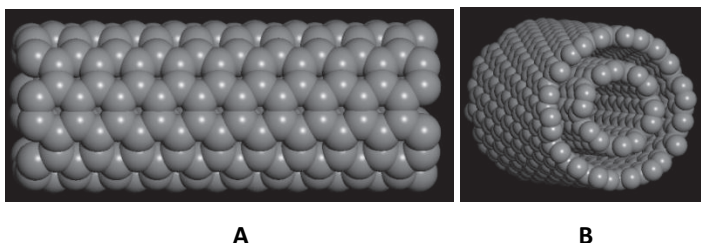


Figure 7-23 Computer simulations of (A) CPK representation of a single-wall CNT (side view); (B) CPK representation of a double-wall CNT (end view).

Table 7-10 Projected 2014 Market for Carbon Nanotubes (Total: \$1.07 Billion)

Total Demand	\$Billion
Type	
SWNT	600
MWNT	479
End Use	
Electronic	394
Automotive	165
Aerospace/defense	65
Other	445

Graphene. A recent addition to a growing list of important nanofillers is graphene. Graphene is a two-dimensional, one-atom-thick allotrope of sp^2 bonded carbon atoms packed in a honeycomb structure. Graphene samples of two to four layers in thickness can be prepared by an arc-discharge procedure. Graphene has many unusual properties including high electron transport (higher conductivity and thermal conductivity than copper but 25% of the weight), superior thermal conductivity, great mechanical strength, and remarkable flexibility and is an absolute barrier material. As shown in Figure 7-24, the tensile strength of an epoxy nanocomposite

containing 1 wt% graphene platelets (GPL) content exceeds that of the same epoxy nanocomposite containing 1 wt% SWNT or 1 wt% MWNT.

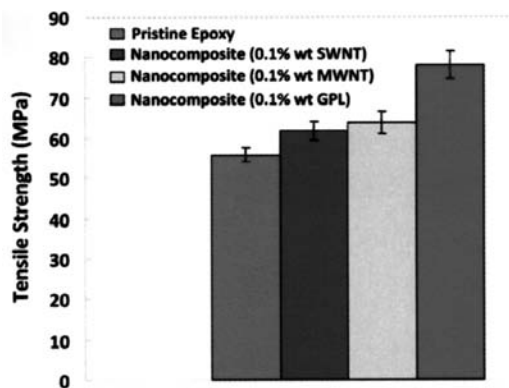


Figure 7-24 Uniaxial tensile testing of epoxy and epoxy nanocomposite with 0.1% of different nanofillers. Reproduced from M. A. Rafiee et al., *Enhanced Mechanical Properties of Nanocomposites at Low Graphene Content*. ACS Nano, 2009. **3**(12): p. 3884–3890.

The ultrahigh electron mobility of graphene and its room-temperature quantum Hall effect open unique opportunities for applications in electronics, particularly as a potential competitor to silicon-based devices. Potential applications include high-performance electronics, sensors, computer chips, and energy storage. Graphene was first produced by the mechanical exfoliation of graphite. Other approaches include liquid-phase exfoliation, unzipping carbon nanotubes, chemical vapor deposition, the epitaxial growth on electrically insulating substrates, mechanical exfoliation of graphene from bulk graphite, and the reduction of graphene derivatives (e.g., graphene oxide). A major technological challenge is the controlled production of large sheets. For their work with graphene, Andre Geim and Konstantin Novoselov shared the 2010 Nobel Prize in physics.

POSS. Polyhedral oligomeric silsesquioxane (POSS) can serve both as a multifunctional additive providing molecular-level reinforcement as well as a processing aid and flame retardant [22]. POSS is a cubic form of silica with dimensions in the range of 1 to 3 nm and eight organic groups at its vertices. A (T8) nanocage having all hydrogen substituents is shown in Figure 7-25. Larger nanocages having 10 (T10) and 12 (T12) Si atoms are available. T8 POSS has the formula $(\text{SiO}_{1.5})_8\text{R}_8$ where R represents a halogen atom or an organic group such as alkyl, aryl, cycloaliphatic, vinyl, nitrile, alcohol, isocyanate, glycidyl, or vinyl. A vinyl group can serve to copolymerize with other monomers or oligomers while other groups may serve to promote compatibility with the matrix. POSS nanocomposites exhibit elevated T_g

and decomposition temperature, increased thermal stability, higher modulus and melt strength, improved resistance to oxidation, and reduced flammability due to a significant reduction of the heat-release rate. Other advantages include increased service temperature, low density, low thermal conductivity, thermo-oxidative resistance, and aging resistance. Polymeric materials that have been used for POSS nanocomposites include epoxies, phenolic resins, polysiloxanes, polyimides, poly(propylene oxide), polycarbonate, polyethylene, polyurethanes, ethylene-propylene copolymers, poly(3-hydroxy alkenoates), and polypropylene.

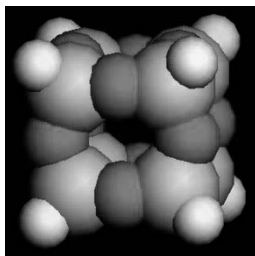


Figure 7-25 Computer representation (CPK model) of octahydrosilsesquioxane ($H_8Si_8O_{12}$). The hydrogen atoms can be replaced by a number of different groups to improve compatibility of the POSS filler with the polymer matrix.

SUGGESTED READING

BLENDS

- Bucknall, C. B., *Toughened Plastics*. 1977, London: Applied Science Publishers Ltd.
- Olabisi, O., *Interpretations of Polymer-Polymer Miscibility*. *Journal of Chemical Education*, 1981. **68**: p. 944.
- Olabisi, O., L. M. Robeson, and M. T. Shaw, *Polymer-Polymer Miscibility*. 1979, New York: Academic Press.
- Paul, D. R., and S. Newman, *Polymer Blends*. 1978, New York: Academic Press.
- Takayanagi, M., H. Harima, and Y. Iwata, *Viscoelastic Behavior of Polymer Blends and Its Comparison with Model Experiments*. 1963, *Memoirs of the Faculty of Engineering Kyushi University*, p. 1.
- Weber, M., *Polymer Blends: Materials with Versatile Properties*. *Macromolecular Symposium*, 2001. **163**: p. 235–250.

INTERPENETRATING NETWORKS

- Barrett, L. W., and L. H. Sperling, *Today's Interpenetrating Polymer Networks*. *Trends in Polymer Science*, 1993. **1**(2): p. 45.

Sperling, L. H., *Interpenetrating Polymer Networks and Related Materials*. 1981, New York: Plenum Press.

Sperling, L. H., *Interpenetrating Polymer Networks: An Overview*, in *Interpenetrating Polymer Networks*, D. Klempner, L. H. Sperling, and L. A. Utracki, eds., *Advances in Chemistry Series*. 1984, Washington, DC: American Chemical Society. **239**: p. 3–38.

BLOCK COPOLYMERS

Darling, S. B., *Directing the Self-Assembly of Block Copolymers*. *Progress in Polymer Science*, 1996. **32**: p. 1152.

Malinova, V., S. Belegirinou, D. de Bruyen Ouboter, and W. Meier, *Biomimetic Block Copolymer Membranes*. *Advances in Polymer Science*, 2010. **224**: p. 113.

COMPOSITES

Delmonte, J., *Technology of Carbon and Graphite Fiber Composites*. 1981, New York: Van Nostrand Reinhold.

Diefendorf, R. J., and E. Tokarsky, *High-Performance Carbon Fibers*. 1975, *Polymer Engineering and Science*. 1975, **15**: p. 150.

Lubin, G., ed., *Handbook of Composites*. 1982, New York: Van Nostrand Reinhold.

Nicolais, L., *Mechanics of Composites*. *Polymer Engineering and Science*, 1975. **15**: p. 137.

Nielsen, L. E., *Mechanical Properties of Polymers and Composites*. 1977, New York: Marcel Dekker, Inc.

Tsai, S. W., and H. T. Hahn, *Introduction to Composite Materials*. 1980, Westport: Technomic Publishing Company.

NANOCOMPOSITES

Brune, D. A., and J. Bicerano, *Micromechanics of Nanocomposites: Comparison of Tensile and Compressive Elastic Moduli, and Prediction of Effects of Incomplete Exfoliation and Imperfect Alignment on Modulus*. *Polymer*, 2002. **43**: p. 369.

Krishnamoorti, R., and R. Vaia, eds., *Polymer Composites: Synthesis, Characterization, and Modeling*. 2002, Washington, DC: American Chemical Society.

Paul, D. R., and L. M. Robeson, *Polymer Nanotechnology: Nanocomposites*. *Polymer*, 2008. **49**: p. 3187.

Slia, D., C. T. Hui, S. D. Burnside, and E. P. Giannelis, *An Interface Model for the Prediction of Young's Modulus of Layered Silicate-Elastomer Nanocomposites*. *Polymer Composites*, 1998. **19**: p. 608.

Vaia, R. A., and E. P. Giannelis, *Polymer Nanocomposites: Status and Opportunities*, *MRS Bulletin*, May 2001, p. 394.

PROBLEMS

7.1 Poly(2,6-dimethyl-1,4-phenylene oxide) (PPO) is blended with polystyrene. Compare the predictions of the inverse rule of mixtures and the logarithmic rule of mixtures (see Section 4.3.4) by plotting the calculated T_g of the blend against the weight fraction of PS. T_g values obtained from DSC measurements are as follows:

Wt% PPO	T_g (°C)
0	105
20	121
40	140
60	158
80	185
100	216

7.2 For a graphite-fiber composite of polysulfone containing 40 vol % filler, what are the maximum modulus and maximum strength that can be expected?

7.3. Draw the chemical structures for the following plasticizers:

(a) TCP

(b) TOTM

(c) DOA

(d) DIOP

7.4 Give your best estimate for the T_g of PVC plasticized with 30 phr of TOTM ($T_g = -72^\circ\text{C}$).

7.5 Explain why the curve representing the T_g of miscible TMPC/PS blends appearing in Figure 7-4 appears to diverge at low TMPC compositions.

7.6 Show that the Halpin–Tsai equation (eq. (7.9)) reduces to the simple law of mixtures

$$M = \phi_1 M_1 + \phi_2 M_2$$

when the Halpin–Tsai parameter A approaches infinity and reduces to the inverse rule of mixtures

$$\frac{1}{M} = \frac{\phi_1}{M_1} + \frac{\phi_2}{M_2}$$

when A approaches zero.

7.7 Inverse gas chromatography (see Section 3.2.5) can be used to determine an apparent Flory interaction, $\chi_{23,\text{app}}'$, using a solvent probe through the relationship [23]

$$\chi_{23,\text{app}}' \phi_2 \phi_3 = \ln \left(\frac{V_{g,\text{blend}}}{w_2 v_2 + w_3 v_3} \right) - \phi_2 \ln \left(\frac{V_{g,2}}{v_2} \right) - \phi_3 \ln \left(\frac{V_{g,3}}{v_3} \right)$$

where w and v are weight fraction and specific volume, respectively. Specific retention volumes for polystyrene (2), poly(2,6-dimethyl-1,4-phenylene oxide) (PPO) (3), and a 50/50 blend of PPO and polystyrene using toluene as the probe at 270°C are given below. From these data, calculate χ_{23} for the PPO/PS blend. Is this value consistent with the reported miscibility of this blend?

Coating	V_g (mL/g-coating)
PS	2.38
PPO	2.96
PPO/PS	2.42

7.8 Discuss the current market and methods of producing single-walled and multi-walled carbon nanotubes.

REFERENCES

1. Kelley, F. N., and F. Bueche, *Viscosity and Glass Temperature Relations for Polymer-Diluent Systems*. Journal of Polymer Science, 1961. **50**: p. 549–556.
2. Wood, L. A., *Glass Transition Temperatures of Copolymers*. Journal of Polymer Science, 1958. **28**: p. 319–330.
3. Gordon, M., and S. J. Taylor, *Ideal Copolymers and the Second-Order Transitions of Synthetic Rubbers. I. Non-Crystalline Copolymers*. Journal of Applied Chemistry, 1952. **2**: p. 493–500.
4. Penzel, E., J. Rieger, and H. A. Schneider, *The Glass Transition Temperature of Random Copolymers. I. Experimental Data and the Gordon-Taylor Equation*. Polymer, 1997. **38**(2): p. 325–337.
5. Fried, J. R., G. A. Hanna, and H. Kalkanoglu, *Compatibility Studies of PPO Blends*, in *Polymer Compatibility and Incompatibility—Principles and Practice*, K. Solc, ed. 1982, New York: Harwood Academic Publishers, p. 237–248.
6. Illers, K.-H., W. Heckmann, and J. Hambrecht, *Untersuchung des Mischungsgleichgewichts binärer Polymermischungen. I. Mischungen aus Polystyrol und Tetarmethyl-bisphenol A-Polycarbonat*. Colloid and Polymer Science, 1982. **262**: p. 557–565.
7. Scott, R. L., *The Thermodynamics of High Polymer Solutions. V. Phase Equilibria in the Ternary System: Polymer 1-Polymer 2-Solvent*. Journal of Chemical Physics, 1949. **17**: p. 279–284.
8. McMaster, L. P., *Aspects of Polymer-Polymer Thermodynamics*. Macromolecules, 1973. **6**: p. 760–773.

9. Goh, S. H., and K. S. Siow, *Calorithmic Study of the Miscibility of Poly(Styrene-co-Acrylonitrile)/Poly(Methyl Methacrylate)/Poly(Ethyl Methacrylate) Ternary Blends*. *Thermochimica Acta*, 1986. **105**: p. 191–195.
10. Paul, D. R., and J. O. Altamirano, in *Copolymers, Polyblends, and Composites*, N. A. J. Platzer, ed., 1975, Washington DC: American Chemical Society. p. 371–385.
11. Cieslinski, R. C., *Real-Time Deformation of Polymers in the Transmission Electron Microscope*. *Journal of Materials Science Letters*, 1992. **11**: p. 813–816.
12. Kita-Tokarczyk, K., et al., *Block Copolymer Vesicles—Using Concepts from Polymer Chemistry to Mimic Biomembranes*. *Polymer*, 2005. **46**: p. 3540–3563.
13. Matsen, M. W., and F. S. Bates, *Unifying Weak- and Strong-Segregation Block Copolymer Theories*. *Macromolecules*, 1996. **29**(4): p. 1091–1098.
14. Bates, F. S., and G. H. Fredrickson, *Block Copolymers—Designer Soft Materials*. *Physics Today*, February 1999. p. 32–38.
15. Smart, T., et al., *Block Copolymer Nanostructures*. *Nanotoday*, 2008. **3**(3–4): p. 38–46.
16. Schragger, M., *The Effect of Spherical Inclusions on the Ultimate Strength of Polymer Composites*. *Journal of Applied Polymer Science*, 1978. **22**: p. 2379–2381.
17. Takayanagi, M., H. Harima, and Y. Iwata, *Viscoelastic Behavior of Polymer Blends and Its Comparison with Model Experiments*. *Memoirs of the Faculty of Engineering, Kyushu University*, 1963. **23**: p. 113.
18. Sur, G. S., et al., *Synthesis, Structure, Mechanical Properties, and Thermal Stability of Some Polysulfone/Organoclay Nanocomposites*. *Polymer*, 2001. **42**: p. 9783–9789.
19. Tyan, H.-L., K.-H. Wei, and T.-E. Hsieh, *Mechanical Properties of Clay-Polyimide (BTDA-ODA) Nanocomposite via ODA-Modified Organoclay*. *Journal of Polymer Science: Part B: Polymer Physics*, 2000. **38**: p. 2873–2878.
20. Kroto, H. W., et al., *C₆₀: Buckminsterfullerene*. *Nature*, 1985. **318**: p. 162–163.
21. Iijima, S., *Helical Microtubules of Graphitic Carbon*. *Nature*, 1991. **354**: p. 56–58.
22. Koo, J. H., and L. A. Pilato, *Polymer Nanostructured Materials for High Temperature Applications*. *SAMPE Journal*, 2005. **41**(2): p. 7–19.
23. Al-Saigh, Z. Y., and P. Munk, *Study of Polymer-Polymer Interaction Coefficients in Polymer Blends Using Inverse Gas Chromatography*. *Macromolecules*, 1984: p. 803–809.

Biopolymers, Natural Polymers, and Fibers

*E*arly efforts during the growth of the plastics industry focused on the development of synthetic materials having comparable or superior properties to those of natural polymers. The first important advance was the development of nylon (synthetic silk) by Wallace Carothers at DuPont in 1938. In the commercial fiber industry, natural polymers such as cotton and silk, some chemically modified natural polymers including regenerated (e.g., viscose) cellulose and acetate, and synthetic polymers such as nylon are all important. With recent achievements in the mapping of the human genome and the beginning of the immense task of identifying and studying the function of many thousands of cellular proteins, an understanding of the structure and function of proteins and polynucleotides is becoming increasingly desirable for many disciplines outside the life sciences. These include materials and chemical engineering and computer science. In addition, there has been significant recent interest in the use of renewable resources such as chitin, an amino polysaccharide, to compete with other commodity thermoplastics. This chapter focuses first

on biopolymers and other naturally occurring polymers including proteins, polynucleotides, and polysaccharides. This coverage is followed by a section on natural and synthetic fibers.

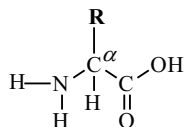
8.1 Biopolymers and Other Naturally Occurring Polymers

There are three main classes of biopolymers—proteins and polypeptides, polynucleotides, and polysaccharides. In biological systems, proteins have many roles including use as protective or supportive molecules in animals, as catalyst substrates, as oxygen-transporting molecules, and as regulators of chemical reactions in cells. Polynucleotides control such important functions as information storage and transfer, cell replication, and protein synthesis in living systems. The role of polysaccharides is primarily as skeletal reinforcement in plants and energy storage in both plants and animals.

Many naturally occurring polymers such as silk and cotton are utilized in their native form as textile fibers. Regenerated cellulose and cellulose derivatives are used in both fiber and film form as will be discussed in Section 8.2.2. Other naturally occurring polymers include keratin, collagen, elastin, fibronectin, and even polyisoprene (e.g., natural rubber). There are two other classes of naturally-occurring polymers that are important renewable resources and offer significant potential for commercial applications in many areas. These include agarose, made from seaweed, and chitin and its derivative, chitosan, which are obtained from the shells of shrimp and crabs.

8.1.1 Proteins

Proteins are heteropolymers containing up to 20 different types* of amino acids of the general structure



* The term *polypeptide* indicates a chain composed of a single amino acid while proteins contain two or more residues from any of the 20 genetically encoded amino acids in mammalian cells. A few organisms use 21 amino acids.

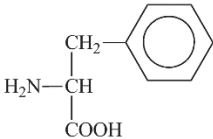
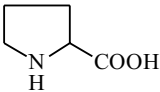
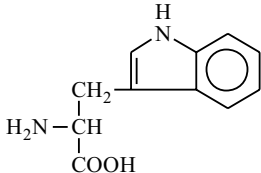
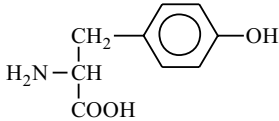
where R is a hydrogen atom in the case of the simplest amino acid glycine or any of a wide variety of substituent groups such as CH₃ (alanine) or an alkyl group as in the case of leucine. Identification of all 20 amino acids, including their common abbreviations, chemical structures, and characteristics, is given in Table 8-1. With the sole exception of glycine, amino acids are optically active chiral molecules due to the asymmetric C^α as identified above. All naturally occurring proteins contain L-amino acids.

Table 8-1 Naturally Occurring Amino Acids

Amino Acid	Symbol	Structure	Character
Alanine	Ala	$\begin{array}{c} \text{CH}_3 \\ \\ \text{H}_2\text{N}-\text{CH}-\text{COOH} \end{array}$	Nonpolar, hydrophobic
Arginine	Arg	$\begin{array}{c} \text{CH}_2(\text{CH}_2)_2\text{NHC}(\text{NH})\text{NH}_2 \\ \\ \text{H}_2\text{N}-\text{CH}-\text{COOH} \end{array}$	Basic
Asparagine	Asn	$\begin{array}{c} \text{CH}_2\text{CONH}_2 \\ \\ \text{H}_2\text{N}-\text{CH}-\text{COOH} \end{array}$	Polar, hydrophilic
Aspartic acid	Asp	$\begin{array}{c} \text{CH}_2\text{COOH} \\ \\ \text{H}_2\text{N}-\text{CH}-\text{COOH} \end{array}$	Acidic
Cysteine	Cys	$\begin{array}{c} \text{CH}_2\text{SH} \\ \\ \text{H}_2\text{N}-\text{CH}-\text{COOH} \end{array}$	Polar, hydrophilic
Glutamic acid	Glu	$\begin{array}{c} \text{CH}_2\text{CH}_2\text{COOH} \\ \\ \text{H}_2\text{N}-\text{CH}-\text{COOH} \end{array}$	Acidic
Glutamine	Gln	$\begin{array}{c} \text{CH}_2\text{CH}_2\text{CONH}_2 \\ \\ \text{H}_2\text{N}-\text{CH}-\text{COOH} \end{array}$	Polar, hydrophilic
Glycine	Gly	$\begin{array}{c} \text{H} \\ \\ \text{H}_2\text{N}-\text{CH}-\text{COOH} \end{array}$	Polar, hydrophilic
Histidine	His	$\begin{array}{c} \text{CH}_2-\text{Imidazole} \\ \\ \text{H}_2\text{N}-\text{CH} \\ \\ \text{COOH} \end{array}$	Polar, hydrophilic
Isoleucine	Ile	$\begin{array}{c} \text{CH}(\text{CH}_3)\text{CH}_2\text{CH}_3 \\ \\ \text{H}_2\text{N}-\text{CH}-\text{COOH} \end{array}$	Nonpolar, hydrophobic
Leucine	Leu	$\begin{array}{c} \text{CH}_2\text{CH}(\text{CH}_3)_2 \\ \\ \text{H}_2\text{N}-\text{CH}-\text{COOH} \end{array}$	Nonpolar, hydrophobic

(continues)

Table 8-1 Naturally Occurring Amino Acids (continued)

Amino Acid	Symbol	Structure	Character
Lysine	Lys	$\begin{array}{c} \text{CH}_2(\text{CH}_2)_3\text{NH}_2 \\ \\ \text{H}_2\text{N}-\text{CH}-\text{COOH} \end{array}$	Basic
Methionine	Met	$\begin{array}{c} \text{CH}_2\text{CH}_2\text{SCH}_3 \\ \\ \text{H}_2\text{N}-\text{CH}-\text{COOH} \end{array}$	Nonpolar, hydrophobic
Phenylalanine	Phe		Nonpolar, hydrophobic
Proline	Pro		Nonpolar, hydrophobic
Serine	Ser	$\begin{array}{c} \text{CH}_2\text{OH} \\ \\ \text{H}_2\text{N}-\text{CH}-\text{COOH} \end{array}$	Polar, hydrophilic
Threonine	Thr	$\begin{array}{c} \text{CH}(\text{CH}_3)\text{OH} \\ \\ \text{H}_2\text{N}-\text{CH}-\text{COOH} \end{array}$	Polar, hydrophilic
Tryptophan	Trp		Polar, hydrophilic
Tyrosine	Tyr		Polar, hydrophilic
Valine	Val	$\begin{array}{c} \text{CH}(\text{CH}_3)_2 \\ \\ \text{H}_2\text{N}-\text{CH}-\text{COOH} \end{array}$	Nonpolar, hydrophobic

Proteins, folded to unique compact states called native structures, perform various biological functions. Molecular weights of proteins can be as low as 6000 and as high as 1 million. The number of possible conformations that a protein can take is nearly astronomical—more than 10^{100} for a protein of only 100 amino acid residues.

In the cell, proteins are produced by an aqueous-phase polycondensation of amino acids in the ribosome. The amino acid sequence within the chain defines the

primary structure of the protein. This sequence determines the conformation, the *secondary* structure of the protein. The shape of the protein, determined by internal crosslinks and mutually attractive residues, constitutes the *tertiary* structure. For example, cysteine residues can form internal disulfide (S–S) crosslinks. The aggregation of individual polypeptide chains into a supramolecular structure defines the final or *quaternary* structure. Certain amino acids provide binding sites for nonprotein or prosthetic groups such as iron porphyrins (e.g., as found in hemoglobin and myoglobin) that serve to bind oxygen. These important groups complex with the imidazole component of histidine.

Fibrous proteins are tough, insoluble materials found in the protective and connective tissues of mammals, birds, and reptiles. Fibrous proteins include α -keratins, which are α -helix proteins found in hair, wool, horn, nails, feathers, and leather. Hydrogen bonding and disulfide bridges between cysteine residues provide strength and toughness. β -keratin collagens are found in animal connective tissue and tendons. Individual polypeptide chains form a loose helix that can hydrogen-bond with two other chains to create a triple-stranded rope.

All proteins can be classified into two categories—fibrous and globular. Globular proteins include the important biological proteins that regulate chemical reactions in the body. Globular proteins that are soluble in aqueous media include enzymes, antibodies, myoglobin, cytochrome C, serum albumin, and some hormones. These proteins contain both an α -helix and non-helical segments. As mentioned above, myoglobin is an iron-containing protein. It is composed of only 153 amino acids (molecular weight of 17,000) and is important as an oxygen-storing protein that is present in all animal tissues, particularly in whales and seals. It consists of a single polypeptide chain to which is attached one Fe(II)-porphyrin (heme) unit. Due to its simple structure and biological importance, myoglobin was the first protein whose structure was completely determined by John Kendrew in 1957 after 22 years of effort [1]. Another important protein is hemoglobin, which contains four myoglobin-like molecules arranged in a supramolecular structure. Lysozyme is an enzyme present in mucus or egg white that kills bacteria by attacking the cell wall. Lysozyme consists of a single polypeptide chain of 129 amino acid residues. The chain possesses four intramolecular cysteine crosslinks and three α -helices. Today, the structures of thousands of important proteins are known and readily available from sources such as the Protein Data Bank [2].

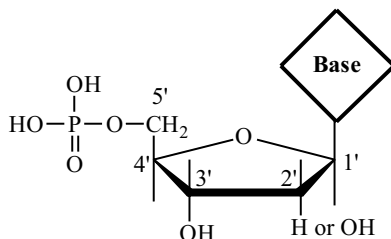
The importance of proteins in the understanding and treatment of human diseases has led to the growth of a newly defined field of investigation, *proteomics*. Proteomics is the study of protein function and the interactions of proteins with small molecules and other proteins. Following the completion of the Human Genome Project in 2000, proteomics has become the new frontier. There may be as many as 200,000 proteins in the human genome. The total deciphering of the human proteome will be a more demanding task than mapping the human genome. Proteomics will focus on an understanding of where proteins are located in the cell, when they are present during the life of a cell, at what concentration, for how long, and

what other proteins they functionally interact with. Since most diseases are a result of protein malfunction, proteomics should lead to new advances in medical science.

Protein Synthesis. In the laboratory, proteins can be synthesized by a sequential addition of amino acids to crosslinked, chloromethylated polystyrene beads (see Section 2.4.1) by a procedure developed by Bruce Merrifield in the 1960s [3]. As discussed in Section 2.5.4, proteins can also be synthesized through a process involving gene-splicing of bacterial DNA. Synthetic human insulin can also be made in this way. Some synthetic polypeptides can be synthesized by a condensation reaction of some simple amino acids such as glycine, alanine, or phenylalanine. In a living cell, proteins are synthesized at ribosomal sites by the RNA-initiated process described in the following section.

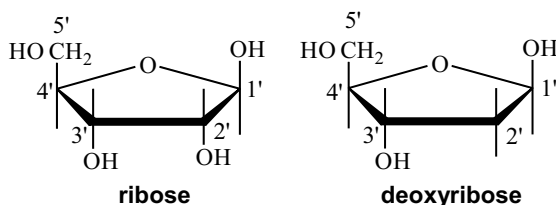
8.1.2 Polynucleotides

Two main types of polynucleotides, or nucleic acids, occur in nature—deoxyribonucleic acid (DNA) and ribonucleic acid (RNA). DNA provides the storage sites for genetic information within the chromosomes of the cell nucleus. RNA molecules transmit information coded into their structure to the ribosomes where protein synthesis occurs. A single nucleotide, the monomer with which polynucleotides are built, consists of three parts—a phosphoric acid residue, a cyclic five-carbon (pentose) sugar, and a heterocyclic organic base, either a purine or pyrimidine, as illustrated below.



One of two types of sugar molecules, ribose or deoxyribose, is found in polynucleotides. The central difference between ribose and deoxyribose is the type of substituent group at the 2' carbon position. As shown next, ribose has a hydroxyl group at the 2' position; both substituents at the 2' position in deoxyribose are hydrogen atoms.*

* For simplicity, hydrogen atoms are not explicitly shown but are understood to be present at all open positions.



Only D-ribose is found in RNA while deoxy-D-ribose is unique for DNA.

The heterocyclic bases include two purines—adenine (A) and guanine (G)—and three pyrimidines—thymine (T), cytosine (C), and uracil (U). Structures of the five bases are shown in Table 8-2. Thymine, adenine, guanine, and cytosine are found in DNA; adenine, guanine, cytosine, and uracil are present in RNA. Thymine is, therefore, unique to DNA while uracil is unique to RNA. Sugar units of different nucleotides are joined by phosphate-hydroxyl linkages between the 3' and 5' carbons to form the polynucleotide. Representative skeletal chains for RNA and DNA are illustrated in Figure 8-1.

Table 8-2 Purine and Pyrimidine Bases Found in Nucleic Acids

DNA Only	DNA and RNA			RNA Only
<p>Thymine</p>	<p>Adenine</p>	<p>Guanine</p>	<p>Cytosine</p>	<p>Uracil</p>

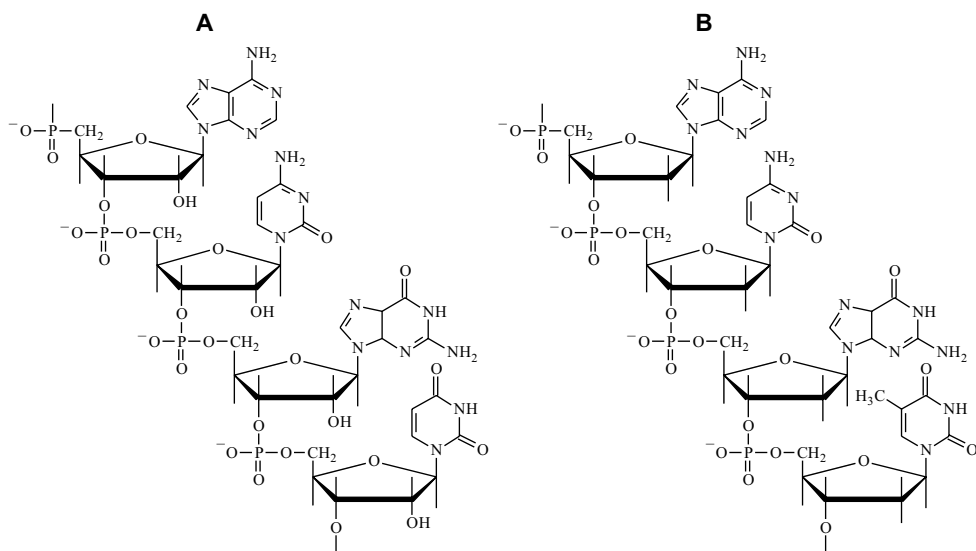


Figure 8-1 (A) A representative four-nucleotide segment of RNA with an A-C-G-U base sequence. (B) A four-nucleotide segment of DNA with an A-C-G-T sequence segment.

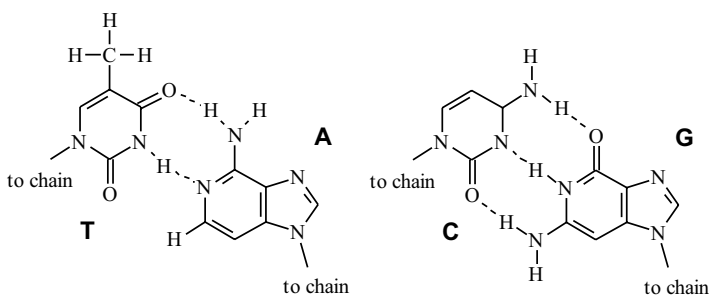


Figure 8-2 Hydrogen bonding between complementary base pairs in DNA.

A typical DNA molecule is extremely large. Molecular weights can range from several million to more than several hundred million corresponding to several thousand to hundreds of thousands of nucleotides. Within a cell, a DNA molecule exists in a very compact conformation, but when stretched out, a typical DNA molecule can form a thread several feet in length. As deduced by Watson and Crick from an analysis of the X-ray diffraction patterns of highly oriented DNA fibers obtained by Maurice Wilkins in 1953 [4, 5], DNA exists in the form of a right-handed helix with two complementary chains running in opposite directions. The helix undergoes one complete turn every 34 Å. The helical structure is stabilized by

the formation of hydrogen bonds between two complementary base pairs along the chain—either an A–T or a C–G combination as illustrated in Figure 8-2. As shown, two hydrogen bonds link adenine to thymine while three hydrogen bonds links guanine to cytosine. An illustration of a DNA double helix is shown in Figure 8-3.

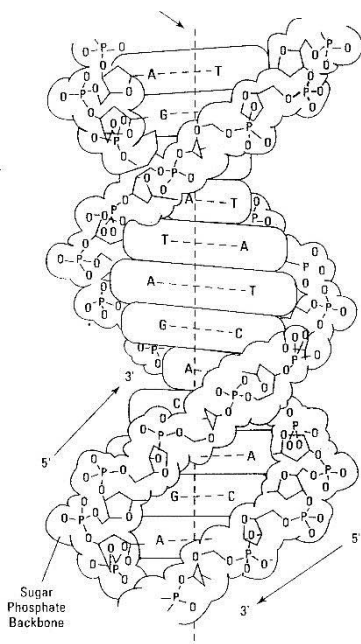


Figure 8-3 Structure of a DNA double helix. Arrows show the direction of phosphate linkages connecting 3' to 5' carbons on contiguous deoxyribose sugar residues. Adenine, thymine, guanine, and cytosine are hydrogen bonded to their complementary base pairs (see Figure 8-2) and stacked at right angles to the axis of the helix (top arrow). Reproduced from J. Yin, *Chemical Engineering Progress*, November 1999, p. 65–74, with permission from the American Institute of Chemical Engineers.

As discussed, RNA differs from DNA in the type of sugar (i.e., ribose in RNA and deoxyribose in DNA) and in the uniqueness of one pyrimidine base (i.e., thymine in DNA and uracil in RNA). Unlike DNA, RNA exists as a single helix and, therefore, does not possess the complementary base-pairing characteristic of DNA. RNA molecules are also significantly lower in molecular weight. Three forms of RNA are involved in protein synthesis. These are transfer RNA (t-RNA), messenger RNA (m-RNA), and ribosomal RNA (r-RNA). Messenger RNA accounts for about 5% to 10% of the cell's total RNA. The function of m-RNA is to receive genetic code from the DNA in the genes (the transcription process) and to transmit that in-

formation to the ribosomes where protein synthesis occurs.* The sequence of bases of the m-RNA is complementary to a portion of one DNA strand unwound from a DNA pair in the cell nucleus. For example, an A–T–C–G–T sequence in DNA will be transcribed to a U–A–G–C–U sequence in m-RNA. Transfer RNA molecules are relatively small, only about 70 to 80 repeating units in length.

Protein synthesis in the ribosome is a rapid process whereby as many as 150 amino acid residues can be assembled in a matter of seconds. The ribosomes are nearly spherical particles, about 200 Å in diameter, that are scattered through the cell protoplasm. These are formed from certain proteins and high-molecular-weight ribosome-RNA (r-RNA). The synthesis process involves four steps. Initially, amino acid molecules become enzymatically bound to t-RNA by an esterification reaction. There is at least one t-RNA for each amino acid; however, several different t-RNA molecules can attach to the same amino acid. Then an initiation complex is formed between the t-RNA ester and the m-RNA, whose code directs the sequential linkage of amino acids in the ribosome. Construction of the protein begins with a reaction between the carboxylic acid end of the first amino acid and the amino residue of the second amino acid that is coded by the m-RNA. Both m-RNA– and t-RNA–peptide chains are moved along the ribosome to position the next coded site. Finally, when the last coded instruction from the m-RNA has been followed, the completed protein separates from the ribosome.

It is clear that only four bases—adenine, uracil, guanine, and cytosine—must code for at least 20 different amino acids (see Section 8.1.1). This means that a sequence of at least three nucleotides, the codon, must provide the minimal code for a single amino acid. Such a three-base or triplet sequence represents 64 (4^3) combinations. Since there are only 20 genetically coded amino acids, some redundancy must be built into the coding process. This is a helpful protection against harmful mutations. As shown in Table 8-3, some amino acids (arginine, leucine, and serine) are coded for as many as six different triplet combinations while tryptophan and methionine are each coded by a single triplet (A–U–G and U–G–G, respectively). As also illustrated by Table 8-3, some codons provide a start or stop instruction to the protein synthesis process.

* A gene is a sequence in DNA that codes for a protein. In the human, there can be as many as 100,000 to 150,000 genes.

Table 8-3 Codon Assignments for Individual Amino Acids in Protein Synthesis

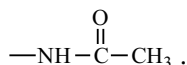
		SECOND POSITION					
		U	C	A	G		
F I R S T P O S S I T I O N	U	Phenylalanine	Serine	Tryosine	Cysteine	U C A G	T H I R D P O S I T I O N
		Leucine		STOP	STOP		
				STOP	Tryptophan		
	C	Leucine	Proline	Histidine	Arginine	U C A G	
				Glutamine			
	A	Isoleucine	Threonine	Asparagine	Serine	U C A G	
				Lysine	Arginine		
	G	Valine	Alanine	Aspartic acid	Glycine	U C A G	
				Glutamic acid			

^a And START.

8.1.3 Polysaccharides

Polysaccharides, which include cellulose, starch, and glycogen, are cycloliner polyethers formed by the condensation of sugar molecules. Degrees of polymerization can range from 30 to 100,000. Common types of sugar molecules found in cellulose and starch include two cyclic forms of glucose, or glucopyranoses. These are α -D-glucose (α -D-glucopyranose) and β -D-glucose (β -D-glucopyranose), whose chemical structures are shown in Figure 8-4. In cellulose, starch, and glycogen, the glucose residues are condensed via the hydroxyl groups at the 1 and 4 positions on adjacent molecules. Another important polysaccharide, chitin, an amino polysaccharide found in insect and some shellfish exoskeletons, is formed from 2-acetamido-2-deoxy-D-glucose (*N*-acetyl-D-glucosamine). Chitin differs from cellu-

lose only in the substitution of the hydroxyl group on the 2-carbon with the *N*-acetyl group



Cellulose and chitin are the most important naturally occurring polymeric materials due to their abundance, accessibility, low cost, and nontoxic, attractive properties including biodegradability and biocompatibility.

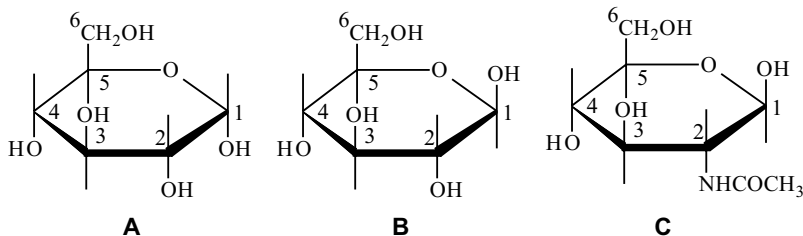


Figure 8-4 Sugars found in common polysaccharides. **A.** α -D-glucose; **B.** β -D-glucose; **C.** 2-acetamido-2-deoxy-D-glucose.

Cellulose. Cellulose is one of the most abundant organic materials found in nature. Cotton, in its purified form, is 94% cellulose with only small amounts of related products (e.g., hemicellulose and pectin). Wood contains about 50% cellulose. Plant cell walls and fibers are all made from cellulose. Cellulose is formed through the 1,4- β -linkage of glucose units. A typical chain of cellulose is composed of 200 to 6000 anhydroglucose units, each of which contains three hydroxyl groups and are linked by an acetal bridge (see Figure 8-5). Corresponding molecular weights are 300,000 to 1,000,000. Cellulose consists of fully extended chains that are strongly hydrogen bonded into sheets of a highly crystalline matrix. Cellulose is, therefore, an insoluble, infusible (i.e., degrades before melting) polymer and fibers and films are obtained only by chemically modifying cellulose, as discussed in Section 8.2.2.

Starch. Starch is the principal energy storage polysaccharide in photosynthetic plants. Most starches have two structurally different forms—amylose, a linear polymer having degrees of polymerization between 100 and 6000, and a high concentration of amylopectin, a highly branched fraction. Branches in amylopectin are 12 to 15 glucose residues in length and occur at every sixth to twelfth backbone residue. Amylose consists of 1,4- α linked glucose units compared to the 1,4- β linked glucose in cellulose. In water, amylose forms a helical conformation. Glycogen, which is more heavily branched than amylopectin, is used as an energy-storage mechanism in animal tissues.

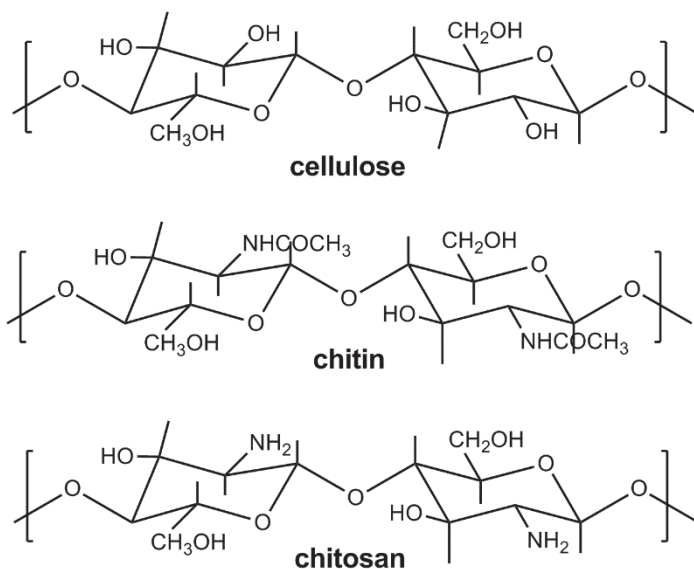


Figure 8-5 Chemical structures of cellulose, chitin, and chitosan.

Chitin. As mentioned earlier, a chitin molecule consists of 2-acetamido-2-deoxy-D-glucose units connected through a β (1-4) linkage, as shown in Figure 8-5.* Chitin occurs in two structural forms. The less abundant form is β -chitin, characterized by weak intermolecular forces due to the parallel arrangement of chitin molecules; α -chitin has stronger interactions due to its antiparallel arrangement. The high nitrogen content of chitin makes it useful as a chelating agent. Chitin is obtained as a waste product from the processing of seafood.

The chemical modification of chitin, as in the case of cellulose (see Section 2.4.2), is difficult due to its limited solubility. Chitin can be transformed into chitosan† that has free amino groups by deacetylating chitin. The degree of deacetylation is typically in the range from 70% to 95%. Deacetylation of chitin was reported as early as 1859 by Rouget, who boiled chitin in a concentrated hydroxide solution. The first U.S. patents reporting the production of chitosan and the preparation of film and fiber from chitosan were issued in 1934.

A comparison of the chemical structures of cellulose, chitin, and chitosan is shown in Figure 8-5. One of the most useful properties of chitosan is its ability to chelate harmful metal ions such as copper, lead, mercury, and uranium from waste

* Poly- β (1 \rightarrow 4)-2-acetamido-2-deoxy-D-glucopyranose.

† Poly- β (1 \rightarrow 4)-2-amino-2-deoxy-D-glucopyranose.

water. Membranes prepared from chitosan can be used for water clarification, filtration, and controlled release. Chitosan is insoluble in water and in alkali and organic solvents but is soluble in most solutions of organic acids, such as acetic and formic acid, at a pH below 6.

Reactions of Polysaccharides. Polysaccharides can be hydrolyzed to oligosaccharides and glucose. Hydrolysis can occur by enzymatic action such as the action of amylase on the amylose fraction of starch. Polysaccharides can also be hydrolyzed by non-enzymatic processes including their hydrolysis in aqueous acid.

The available hydroxyl groups of cellulose provide sites for chemical modification including esterification and etherification. Such reactions have a significant effect on the properties and usefulness of cellulose. For example, cellulose nitrate is produced by the nitration of cellulose in a mixture of nitric acid and sulfuric acid. Cellulose acetate is obtained by reacting cellulose with acetic acid or acetic anhydride (see Section 2.4.2). Cellulose ethers can be prepared by reacting alkali-cellulose* with an alkyl halide such as methyl chloride. Methylcellulose is soluble in water and used as an adhesive, a foam stabilizer, and a binder in ink. Carboxymethylcellulose is obtained from the reaction of alkaline cellulose with chloroacetic acid or chloroacetate as shown by Figure 8-6. The sodium form of carboxymethylcellulose is called cellulose gum. It is also water soluble and is used as a thickening, binding, and stabilization agent in foods and other applications.

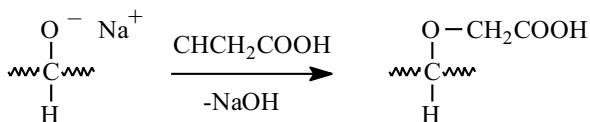


Figure 8-6 Preparation of carboxymethylcellulose by a reaction of sodium cellulose with chloroacetic acid.

Rayon, regenerated cellulose, can be made by two processes. These are the xanthate process, an esterification reaction with aqueous sodium hydroxide and carbon disulfide, and the cuprammonium process, which uses ammonium hydroxide and copper oxide to dissolve cellulose as described in Section 8.2.2.

8.1.4 Naturally Occurring Elastomers

Elastin. Elastin is a protein rich in glycine, alanine, and valine. Molecular weight is typically greater than 70,000. Its structure is mostly that of a random coil with some

* Sodium cellulose formed by reacting cellulose with aqueous sodium hydroxide.

α -helix structure. It has properties similar to those of rubber and imparts elasticity to arterial walls and ligaments. Crosslinking of elastin is achieved through the formation of a desmosine structure by four lysine side chains, as illustrated in Figure 8-7.

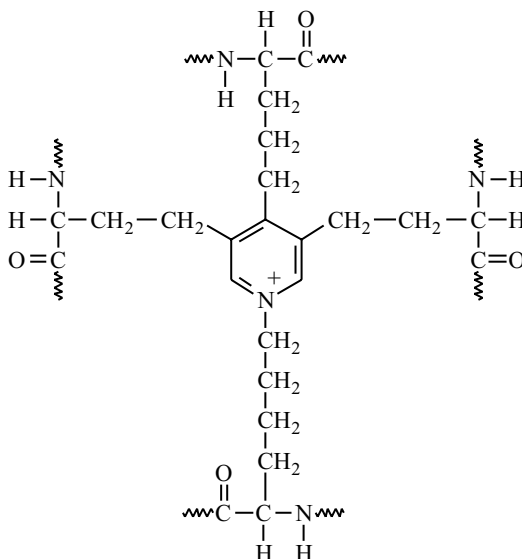
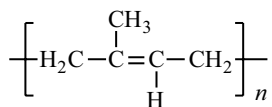
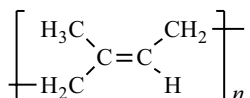


Figure 8-7 Central desmosine structure of an elastin network.

Polyisoprenes. Several geometric isomers (see Section 1.2.3) of polyisoprene

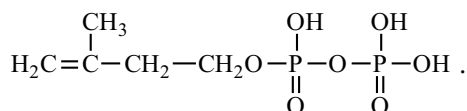


are produced by trees and plants. As described in Section 9.2.1, these can also be commercially obtained by standard polymerization techniques. Depending upon their stereochemistry, some naturally occurring polyisoprenes are suitable to use either as hard plastic material (e.g., gutta percha and balata) or as elastomers (*Hevea brasiliensis* or natural rubber). Both gutta percha (*Palaquium oblongifolium*) and balata (*Mimusops globosa*) are obtained from trees, although from different regions of the globe. The hardness of these polyisoprenes is attributed to their *trans*-configuration



which facilitates chain packing and results in reduced chain flexibility. Gutta percha was used as early as 1850 for cable insulation. Both gutta percha and balata find limited applications as covers for golf balls but, more recently, as material for orthopedic splints. Both *cis*- and *trans*-1,4-polyisoprene are found in chicle (*Achras sapota*) used as a base for chewing gum.

Cis-1,4-polyisoprene is a flexible or rubbery polymer obtained from the tree *Hevea brasiliensis* (Hevea rubber). In nature, Hevea or natural rubber (NR) is obtained by the enzymatic polymerization of isopentylpyrophosphate



It is harvested as a latex containing about 35% rubber and 5% solids (e.g., proteins, sugars, resins, and salts). The rubber is obtained by coagulation of the latex. Natural rubber can also be obtained, although at a reduced yield, from a variety of plants including guayule, which grows in the southwestern United States and northern Mexico. By sulfur vulcanization, a process patented by Charles Goodyear in 1844 (see Section 9.2.1), individual chains of *cis*-1,4-polyisoprene can be crosslinked through the formation of disulfide bonds to provide elastomeric properties suitable for tires and other applications.

8.2 Fibers

Fibers are typically semicrystalline polymers that can be spun into long strands that have high strength-to-weight ratios for textile as well as composite applications (see Section 7.4). They are prepared by the melt or solution spinning of both synthetic polymers (e.g., polyesters, nylons, polyolefins, and acrylic polymers such as polyacrylonitrile) and naturally occurring polymers, principally cellulose in the form of rayon (regenerated cellulose) and cellulose acetate.

8.2.1 Natural and Synthetic Fibers

Naturally Occurring Fibers. Fibers obtained from natural resources were used for textile applications long before the first polymer was synthesized in the laboratory. These fibers include those derived from vegetables or plants, such as cotton and jute, and those obtained as animal products, especially wool and silk. The principal component of vegetable or plant fibers is cellulose whose structure was shown in Figure 8-5. With the exception of silk, the principal component of animal fibers is

keratin—a natural cellular system of fibrous proteins that serves as the protective outer barrier (e.g., skin, hair, and scales) for high vertebrates. The protein of a silk filament, which is produced by the silkworm (the caterpillar of a small moth belonging to the species *Bombyx mori*), is *fibroin*, which has a simpler structure than keratin.

Representative properties of some important natural fibers are given in Table 8-4. The tensile strength of a fiber is usually expressed in terms of *tenacity*, which is stress per unit of linear density. SI units of tenacity are Newtons per tex where tex is the weight of the fiber in grams per 1000 m.*

Table 8-4 Representative Properties of Some Natural and Synthetic Fibers (at 65% Relative Humidity)

Fiber	Tenacity at Break, (N/tex) ^a	Extension at Break, (%)	Elastic Modulus (N/tex ^a)	Specific Gravity
Natural Fibers				
Wool	0.09–0.15	25–35	2.2–3.1	1.30
Cotton	0.26–0.44	4–10	9–30	1.54
Cellulosics				
Cellulose ^b	0.12–0.33	10–30	3.7–5.8	1.50–1.54
Cellulose acetate ^c	0.09–0.13	25–40	2.2–3.5	1.30–1.35
Non-cellulosics				
Polyester ^d	0.35–0.53	15–30	7.9	1.38
Nylon ^d	0.40–0.71	15–30	3.5	1.14
Acrylic ^d	0.40–0.44	15–20	5.3–6.2	1.17
Olefin (PP)	0.44–0.79	15–30	2.6–4.0	0.90

^a To convert N/tex to g/den, multiply by 11.3.

^b From viscose process.

^c Secondary acetate (DS less than 2.4).

^d Continuous filament.

Synthetic Fibers. Synthetic fibers are generally semicrystalline polymers that are capable of being spun into filaments of length-to-diameter ratios in excess of 100. Usually, fibers are uniaxially oriented during the spinning process (melt, dry, or wet) to give materials of high tenacity. Fibers may be spun from the melt or from a concentrated solution (i.e., wet or dry spinning) as described in Section 8.2.4. Textile *yarns* of synthetic polymers are produced by twisting several continuous fibers together to form a uniform structure with all filaments aligned parallel to the yarn axis.

Commercially processed fibers may be classified as cellulosic or non-cellulosic. *Cellulosics*, regenerated cellulose (rayon) and cellulose acetate (acetate),

* An older term was the denier (d), which is the number of grams per 9000 m.

are derived from naturally occurring cellulose through chemical reaction and modification. The *non-cellulosics* (polyester, nylon, polyolefin, and acrylic) are all synthetic polymers. They clearly constitute the largest part of the commercial market, as shown by the production data given in Table 8-5. Over recent years, cellulosic fibers represent only a small and decreasing share of the U.S. fiber market over the past decade; overall, the size of the synthetic fiber market in the United States has been decreasing. The methods of synthesis and the spinning techniques used to prepare synthetic fibers are presented in the following sections.

Table 8-5 U.S. Production of Synthetic Fibers in 2012^a

Fiber	Thousands of Metric Tons ^b	Annual Change %, 2002–2012
Cellulosics (acetate and rayon)	27	-10.3
Non-cellulosics		
Nylon	562	-6.6
Olefin	1021	-3.1
Polyester	1203	-2.2

^aAdapted from Chemical and Engineering News, July 1, 2013, p. 44.

^bConversion: 2206.6 lbs per metric ton.

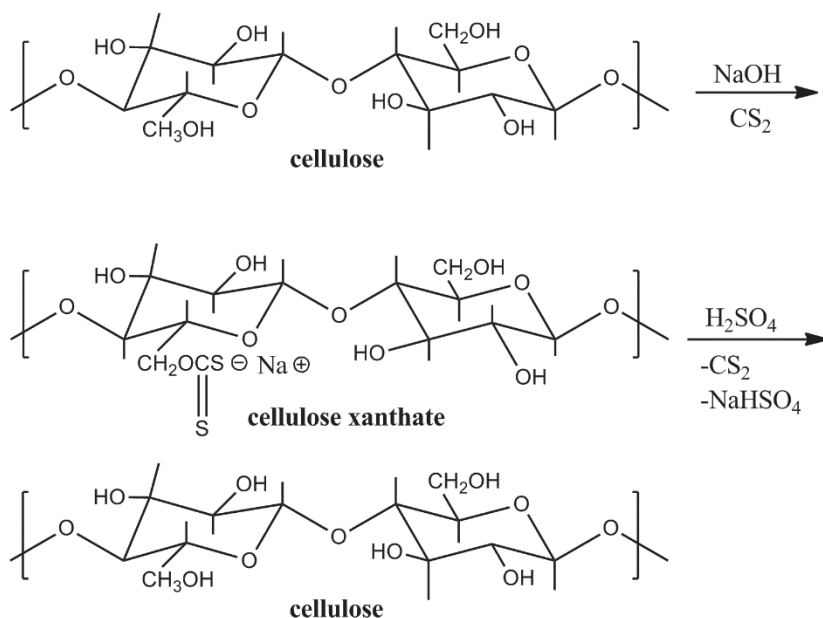


Figure 8-8 Viscose process for the production of regenerated cellulose.

8.2.2 Cellulosics

Cellulose. Cellulose for fiber applications is obtained from wood pulp and short fibers left from cotton recovery. The rigid chain of cellulose is strongly hydrogen bonded and highly crystalline. For these reasons, cellulose is essentially insoluble and infusible (i.e., degrades before melting) and, therefore, fibers and films can be obtained only by chemically modifying cellulose, as discussed next. Cellulose in fiber (rayon) or film (cellophane) form is usually obtained by the viscose process, which dates from the 1920s.* The approach is to regenerate cellulose from an intermediate soluble form, which is called *cellulose xanthate*. In this highly capital- and energy-intensive process, cellulose pulp (wood pulp or cotton linters) is treated with a concentrated (18%) aqueous sodium hydroxide solution at room temperature. During treatment, cellulose is oxidatively degraded to lower molecular weight and is partially solubilized. After an aging period, the slurry is reacted with carbon disulfide (CS₂) to produce cellulose xanthate, whose structure is shown in Figure 8-8. Typically, about one in every six hydroxyl groups is reacted during this process. The yellow colloidal dispersion (viscose) of cellulose xanthate is spun into an aqueous bath of an acid (sulfuric) and a salt (NaHSO₄), which convert the xanthate back to cellulose, now in fiber form. During spinning, the fiber can be stretched to impart greater strength for textiles and tire cord applications. Fibers obtained from regenerated cellulose are hydrophilic and have less developed crystalline structure than natural cellulose. Typical properties of cellulose fibers are included in Table 8-4. A problem with rayon and its derivatives is their flammability, which necessitates the addition of flame retardants.

Cellulose Derivatives. As shown in Figure 8-9, a cellulose derivative of important fiber and film properties, cellulose triacetate, is obtained by reacting cellulose with glacial acetic acid in the presence of acetic anhydride and traces of sulfuric acid in refluxing methylene chloride. Although CTA is still moderately crystalline, it has higher solubility than native cellulose and can be wet spun from a methylene chloride–alcohol mixture into toluene. This derivative can be partially hydrolyzed to give cellulose diacetate (CA), which can be dry spun from acetone. The secondary acetate groups of CTA are the least stable and, therefore, will hydrolyze first. About 65% to 75% of the acetate groups are left unhydrolyzed in commercial cellulose acetate. Cellulose acetate was first produced in 1865 and rapidly replaced its more volatile relative, cellulose nitrate. Large-scale production of cellulose acetate began during World War I.

* In the cuprammonium process, cellulose is dissolved in a solution of ammonium hydroxide and copper oxide. The regenerated fiber is then obtained by extrusion into water. Although the cuprammonium process is simpler than the xanthate process, it is less preferred due to the cost of lost copper during processing.

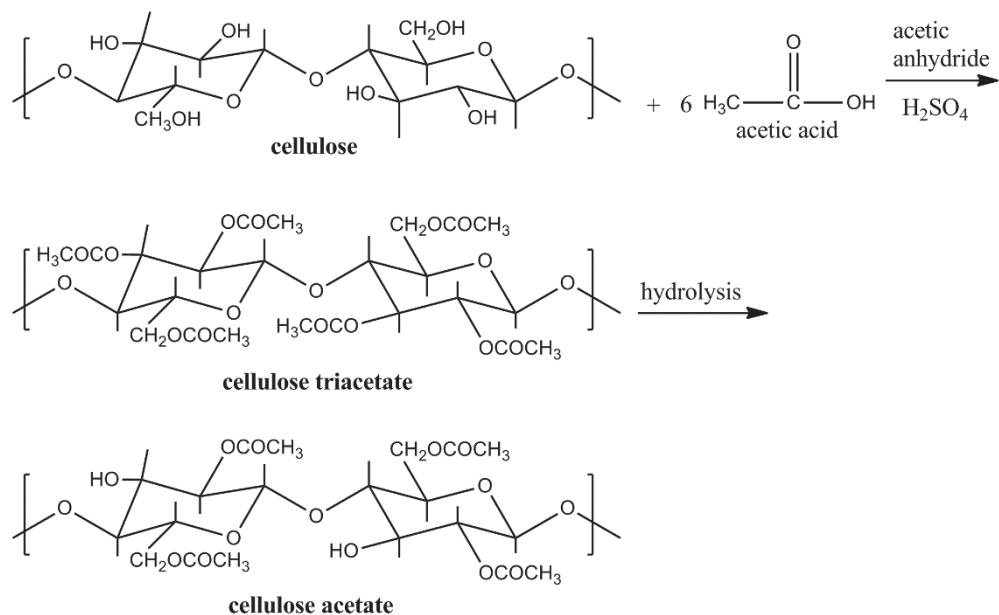
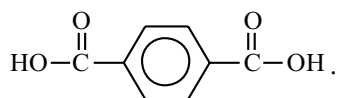


Figure 8-9 Acetylation of cellulose and partial hydrolysis of cellulose triacetate to yield cellulose diacetate.

8.2.3 Non-cellulosics

Polyesters. A polyester fiber is defined as one composed of at least 85 wt % of an ester of a dihydric alcohol (HOROH) and terephthalic acid whose structure is



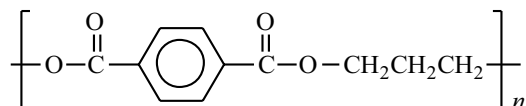
Of all possible polyester combinations, poly(ethylene terephthalate) (PET) is by far the most important and is the largest-volume synthetic fiber (see Table 8-5) although film (Mylar) and bottle applications are also important (as discussed in Section 9.1.3). The first polyester fibers became commercially available in the United States in 1953 (DuPont Dacron). About 61% of PET produced for fiber applications is used for apparel. Staple blends of polyester and cotton are used for permanent-press garments. The remaining production finds applications in tire cord and home furnishing.

Poly(ethylene terephthalate) has a relatively low T_g (ca. 69°C) but a high T_m (ca. 265°C) with moderate crystallinity. Mechanical properties of polyester fiber were compared with other commercial fibers in Table 8-4. For fiber applications,

typical molecular weights range from 10,000 to 15,000. Higher molecular weights provide high-strength fibers for industrial applications. Polyester is resistant to many solvents and to weak mineral acid. In addition, polyester fibers are abrasion and oxidation resistant and display good lightfastness.

Properties of polyester fibers can be modified by copolymerization or by blending with a variety of additives. For example, dyeability can be improved by copolymerization with small amounts of comonomers such as adipic acid and isophthalic acid, which increase the amorphous content available for dye penetration. Additives are widely used to enhance properties such as fire retardancy (e.g., bromine or phosphorous compounds) and antistatic properties (e.g., carbon and PEG).

A next-generation polyester is poly(trimethylene terephthalate) or PTT,



obtained by the polycondensation of terephthalic acid and 1,3-propanediol (in place of ethylene glycol used in the manufacture of PET). This polyester may provide superior dyeability, better stretch, and better softness than PET for apparel applications and better wear and stain resistance for carpet use. Poly(trimethylene terephthalate) may also find a small market in engineering resin and film applications.

Polyamides. The fibers with the next largest sales volume are the polyamides, which find major uses in carpets, apparel, tire reinforcement, and various industrial applications. These are either A–A/B–B condensation polymers prepared from diamines and dicarboxylic acids or A–B condensation polymers prepared from lactams (see Section 2.1). Aliphatic polyamides are called *nylons*. When at least 85% of the amide groups are attached to aromatic groups, the polyamides are called *aramids*. Aramids (e.g., Nomex and Kevlar) are expensive, high-performance fibers that are not used for consumer textile applications. Instead, they find important use as reinforcing fibers for composites, substitutes for asbestos, and material for tire cords (see Chapters 7 and 10). In addition to fiber applications, nylons are available as engineering thermoplastics that can be injection molded into a wide variety of products such as gear wheels, electrical switches and connectors, ski shoes, and automotive coolant tanks.

Principal among the A–A/B–B aliphatic polyamides is nylon-6,6 (or PA 66),* more descriptively called poly(hexamethylene adipamide). Nylon-6,6 is synthesized

* Nylons are designated by the number of carbons in the chain. The first and second numbers in the name of A–A/B–B polyamides such as nylon-6,6 refer to the number of carbons in the diamine and dicarboxylic acid, respectively. For example, a nylon prepared from hexamethylene diamine (6 carbons) and adipic acid (10 carbons) would be designated as nylon-6,10.

by the step-growth polymerization of hexamethylene diamine and adipic acid. An exact stoichiometric equivalence of functional groups is achieved by the formation of an intermediate hexamethylene diammonium adipate salt, as shown in Figure 8-10. A slurry of 60% to 80% of recrystallized salt is heated rapidly, thereby releasing steam, which is air-purged from the reaction vessel. The temperature is then raised to 220°C and finally to 280°C near the end of monomer conversion (80% to 90%). The pressure of steam generated during the polymerization is maintained at 1.38 to 1.72 MPa (200 to 250 psi). At this point, pressure is reduced to atmospheric and heating is continued until the polymerization is complete. Small concentrations of monofunctional acids, such as 0.5 mol % of aluric or acetic acid, can be added to the polymerization mixture to control molecular weight. Other nylons of less commercial importance may be made by using difunctional acids of longer or shorter chains.

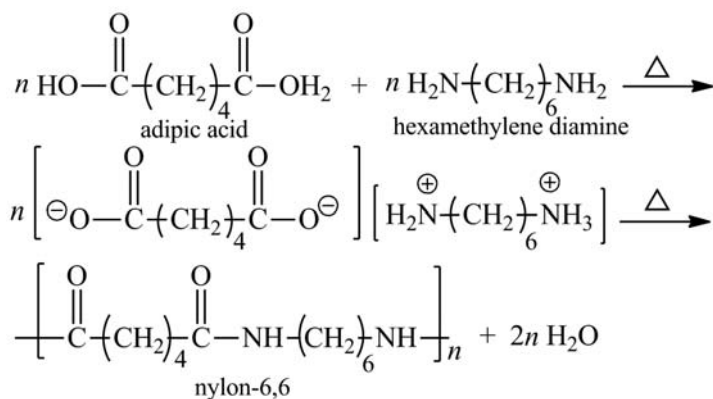


Figure 8-10 Synthesis of nylon-6,6 by means of the A–A/B–B step-growth polycondensation of adipic acid and hexamethylene diamine following intermediate salt formation.

Other important polyamides are obtained by the ring-opening polymerization of lactams. Poly(ϵ -caprolactam), or nylon-6 (PA 6), represents about 25% of the total nylon production. High-molecular-weight nylon-6 may be obtained from the anionic polymerization of ϵ -caprolactam using strong bases such as sodium hydride or commercially by the hydrolytic polymerization of ϵ -caprolactam, as shown in Figure 8-11. Although the actual mechanism of the latter scheme is not fully understood, it is believed to involve a mixed chain- and step-growth mechanism involving the intermediate formation of the amino acid obtained from the ring opening of caprolactam.

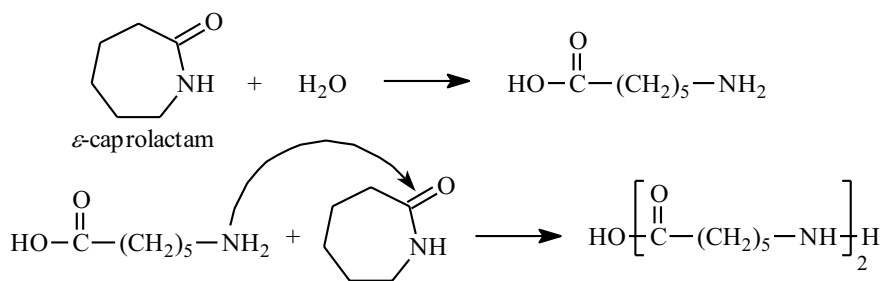


Figure 8-11 Hydrolytic polymerization of ϵ -caprolactam to the dimer. High-molecular-weight nylon-6 is obtained by the subsequent addition of caprolactam.

Acrylics. Acrylic fibers, primarily used for apparel (70%) and home furnishings (30%), are copolymers of principally acrylonitrile (AN). Polyacrylonitrile (PAN) alone cannot be used for thermoplastic applications because it undergoes cyclization at processing temperatures, as discussed in Section 6.1.1. The resulting “ladder” polymer can be used as a starting material for the preparation of graphite filaments, which are obtained by further heat treatment at elevated temperatures (see Section 7.1.2). Acrylonitrile (AN) finds use in thermoplastic and elastomeric applications only as a copolymer with other monomers such as styrene (e.g., ABS, SAN, and NBR). Like PVC, PAN is insoluble in its own monomer, which means that the polymer will precipitate during bulk polymerization. It can also be solution polymerized by free-radical mechanism in water or dimethyl formamide (DMF) with ammonium persulfate as an initiator. The homopolymer can be dry spun from DMF directly from the polymerization reactor (or wet spun from DMF into water). Fibers are also made from copolymers with styrene, vinyl acetate, vinyl chloride, vinylpyridine, acrylic esters, and acrylamide. Fibers with greater than 85% AN content are termed *acrylic*, while those with lower AN composition (35% to 85%) are called *modacrylic*. The presence of the nitrile group ($-\text{C}\equiv\text{N}$) in acrylic fibers results in strong intermolecular hydrogen bonding, allowing for high fiber strength.

Olefinics. Olefinic fibers are those that contain at least 85% of any olefin such as ethylene or propylene, the latter being the more common. Olefin fibers are used for home furnishings, such as carpet and upholstery, as well as some industrial applications, such as rope and geotextiles (used in soil engineering for separation, drainage, reinforcement, and filtration). Mechanical properties of polypropylene fibers were compared with other commodity fibers in Table 8-4. Generally, the advantages of olefin fibers include low cost and light weight, while disadvantages include susceptibility to compressive creep and UV degradation. Olefin fibers are hydrophobic and are resistant to most solvents. Unfortunately, these same properties impede dyeing. Acid-dyeable olefin fibers can be prepared by blending the polyolefin with a copolymer, which provides suitable dye sites such as poly(vinyl-

toluene-*co*- α -methylstyrene), which significantly adds to the cost. Usually, olefin fibers are colored by blending the polyolefin with pigments prior to spinning.

8.2.4 Fiber-Spinning Operations

Three processes are commonly used to form polymeric fibers. These include spinning of a polymer melt, called melt spinning, and two processes that are used to spin fibers from a concentrated polymer solution—dry and wet spinning. Polyamide, polyester, and polyolefin fibers are typically obtained by the melt-spinning process. Solution spinning is used for cellulosic and acrylic fibers.

Melt Spinning. What may be viewed as the most direct process is melt spinning, developed in the late 1930s. During a melt-spinning operation, illustrated in Figure 8-12, a polymer is melted or extruded, clarified by a filter, and pumped by means of a gear pump through a die having one or more small holes. This die is called a *spinneret*. The extruded fiber leaving the spinneret is then cooled and may be uniaxially stretched by take-up rollers called *godets* rotating at different speeds. Fiber stretching orients the fiber chains or crystallites and, therefore, serves to increase modulus and strength in the longitudinal direction. Finally, the cooled oriented fiber is wound onto a spin bobbin for subsequent fiber treatment, such as texturing* and dyeing, before being woven into fabric. The most important classes of polymers that are melt spun include the polyolefins (e.g., polyethylene and polypropylene), polyamides (e.g., nylon-6 and nylon-6,6), and polyester (PET). The relatively high melt viscosity of the polyolefins requires the use of an extruder rather than a gear pump, such as may be used for nylons. Typically, PET is melt spun at 286°C through a spinneret containing 24 orifices having 0.5-mm diameters. The average extrusion velocity is 1 to 20 m min⁻¹.

* In a texturing operation, straight fiber filaments are twisted or kinked to impart a property called *crimp*, which results in fabrics that have a more pleasing touch similar to those prepared from naturally produced fibers such as wool.

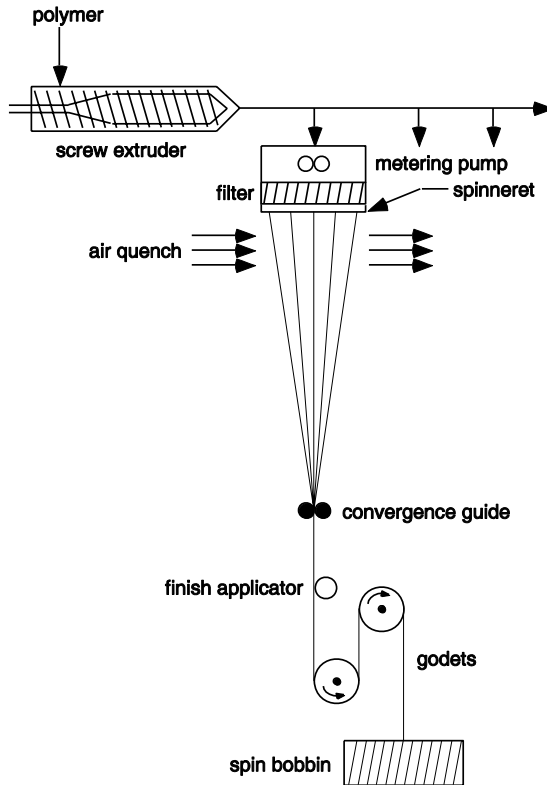


Figure 8-12 Melt spinning of synthetic polymers. Adapted from J. E. McIntyre and M. J. Denton, *Fibers, Manufacture*, in *The Concise Encyclopedia of Polymer Science and Engineering*, J. I. Kroschwitz, ed. 1990, New York: John Wiley & Sons. Copyright © 1990 John Wiley & Sons. This material is used by permission of John Wiley & Sons, Inc.

Dry and Wet Spinning. Polymer concentrations in solutions used for dry or wet spinning are typically in the range of 20 to 40 wt%. During a *dry-spinning* process, illustrated in Figure 8-13, the solution is filtered and pumped through a spinneret into a spinning cabinet (up to 25 ft. in length) through which heated air is passed. Solvent from the fiber rapidly evaporates into the airstream and is then carried out of the spinning cabinet for future solvent recovery. For this purpose, volatile solvents such as acetone and carbon disulfide are sometimes used. Water has been used as a solvent for the dry spinning of fibers from poly(vinyl alcohol) (PVA). The dried fiber is then oriented and wound onto a bobbin. The speed of a dry-spinning line can be very high compared to melt- or wet-spinning operations—up to 1000 m min^{-1} . Commodity fibers that are dry spun include cellulose acetate and acrylics.

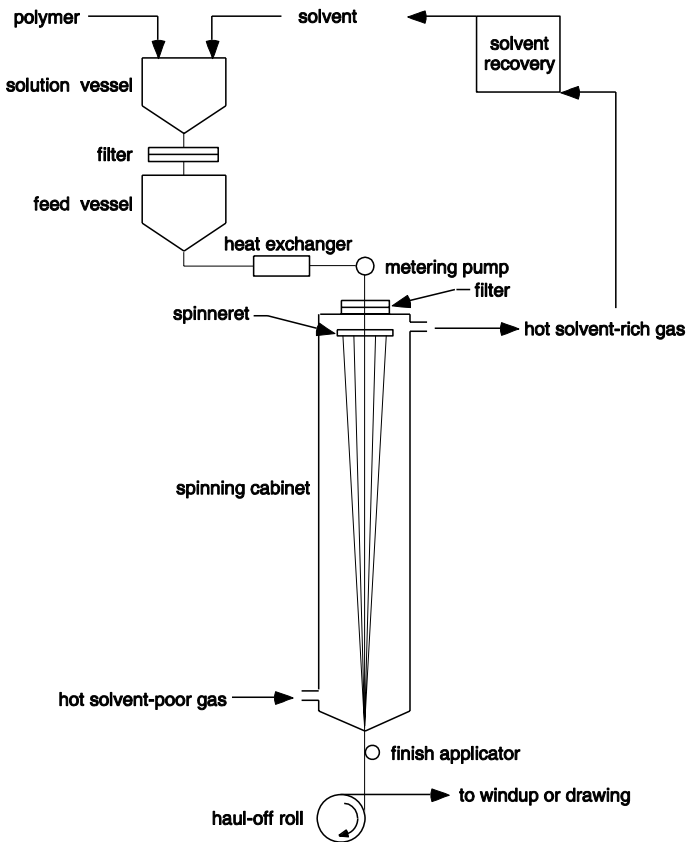


Figure 8-13 A process for the dry spinning of synthetic fibers. Adapted from J. E. McIntyre and M. J. Denton, *Fibers, Manufacture*, in *The Concise Encyclopedia of Polymer Science and Engineering*, J. I. Kroschwitz, ed. 1990, New York: John Wiley & Sons. Copyright © 1990 John Wiley & Sons. This material is used by permission of John Wiley & Sons, Inc.

Wet spinning, one of the oldest fiber-production methods, differs from dry spinning in that fiber formation results from the coagulation of the polymer solution by immersion in a nonsolvent such as water. As illustrated in Figure 8-14, the spinneret is directly immersed in the nonsolvent bath. Since the coagulation process is slow, the linear velocity of a wet-spinning line is much slower than either melt- or dry-spinning operations; however, high productivity can be obtained by spinning multiple fibers from a single spinneret. The viscose process used to prepare regenerated cellulose (rayon) fiber (see Section 8.2.2) is a wet-spinning process that employs chemical modification of the side groups of cellulose in both the solution and coagulation steps to control solubility properties. Wet spinning has been used to

obtain fibers of PVA, poly(vinyl chloride), and polyacrylonitrile (PAN). In the case of PAN, fibers can be wet spun from a dimethylformamide (DMF) solution into dimethylacetamide (DMAC) or from 50% sodium thiocyanate into aqueous 10% sodium thiocyanate. Polyurethane elastomers such as Spandex (see Section 9.2.2) can be wet spun from DMF solution into water.

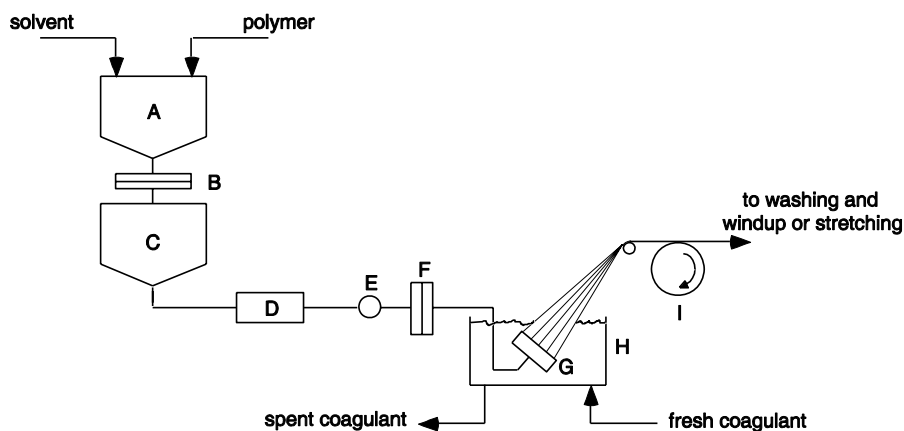


Figure 8-14 Wet-spinning process. A, solution vessel; B and F, filters; C, feed vessel; D, heat exchanger; E, metering pump; G, spinneret; H, spin bath containing coagulant; I, haul-off roll. Adapted from J. E. McIntyre and M. J. Denton, in *The Concise Encyclopedia of Polymer Science and Engineering*, 1990. J. I. Kroschwitz, ed. 1990, New York: John Wiley & Sons. Copyright © 1990 John Wiley & Sons. This material is used by permission of John Wiley & Sons, Inc.

For some specialized applications, such as the spinning of hollow-fiber membranes for gas or liquid separation (see Section 12.1.4), the extruded fiber may first pass through air before entering the bath. If the parameters of the spinning process, such as the concentration of the spinning solution, temperature, and extent of air drying, are properly chosen, it is possible to spin asymmetric fibers having a dense thin skin on top of a thick microporous support layer. The thin top layer provides high flux and good selectivity.

Electrospinning. Polymer fibers with diameters in the nanoscale to microscale range can be produced by electrospinning. This is accomplished by feeding a charged polymer solution or melt through a small aperture toward a grounded collecting plate located about 5 to 30 cm from the electrospinning jet. Diameters as small as 100 nm can be obtained by this process. Solvent evaporates during the electrospinning operation and any residual charges on the fiber dissipate with time.

Crystalline morphology and molecular orientation may be controlled by using a rotating disk collector. Polymers that have been electrospun include polyoxymethylene, poly(ethylene oxide), polystyrene, nylon-6, polyacrylonitrile, SBS, and poly(ethylene terephthalate) (PET). An electron micrograph of a mat of electrospun PET fibers is shown in Figure 8-15. Applications for nanospun fibers include scaffolds for tissue engineering, wound dressings, and controlled drug release.

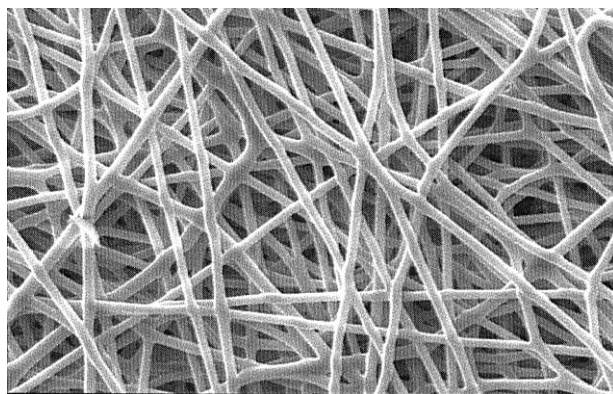


Figure 8-15 Electron micrograph of melt electrospun poly(ethylene terephthalate). Reproduced from J. Lyons and F. Ko, *Melt Spinning of Polymers: A Review*. *Polymer News*, 2005. **30**: p.1-9. Reproduced by permission of Taylor and Francis, Inc., <http://www.routledgeny.com>.

SUGGESTED READING

BIOPOLYMERS

- Klug, A., *The Discovery of the DNA Double Helix*. *Journal of Molecular Biology*, 2004. **335**: p. 3.
- Skolnick, J., and A. Kolinski, *Computer Simulations of Globular Protein Folding and Tertiary Structure*. *Annual Review of Physical Chemistry*, 1989. **40**: p. 207.
- Watson, J. D., *The Double Helix*. 1968, New York: Atheneum,

NATURALLY OCCURRING POLYMERS

- Doelker, E., *Cellulose Derivatives*. *Advances in Polymer Science*, 1993. **107**: p. 199.
- Li, Q., E. T. Dunn, E. W. Grandmaison, and M. F. A. Goosen, *Applications and Properties of Chitosan*. *Journal of Bioactive and Compatible Polymers*, 1992. **7**: p. 370.
- Ravi Kumar, M. N. V., *A Review of Chitin and Chitosan Applications*. *Reactive and Functional Polymers*, 2000. **46**: p. 1.
- Roberts, G. A. F., *Chitin Chemistry*. 1992, London: Macmillan.

FIBERS

- Grayson, M., ed., *Encyclopedia of Textiles, Fibers and Nonwoven Fabrics*. 1984, New York: Wiley-Interscience.
- Lewin, M., and E. M. Pearce, eds., *Handbook of Fiber Science and Technology*, vol. IV: Fiber Chemistry. 1985, New York: Marcel Dekker.
- Lyons, J., and F. Ko, *Melt Spinning of Polymers: A Review*. *Polymer News*. 2005. 30: p. 170.

PROBLEMS

- 8.1** The characteristic ratios of cellulose and amylose are reported to be 36 and 5, respectively. Based upon this information, what can you say about the relative flexibility of amylose and cellulose? What structural characteristics contribute to this difference between conformations? Explain why amylose is soluble in water while cellulose is not.
- 8.2** What specific polymers or blends of polymers are used for olefin, nylon, and polyester fibers in carpet applications? What are the advantages and disadvantages of each?
- 8.3** How do the thermal and mechanical properties of Nomex and Kevlar compare and how are these differences related to their chemical structure? Which polymer would be expected to have the larger characteristic ratio? How can the molecular weight of these polymers be determined?
- 8.4** Why can starch but not cellulose be digested by humans? How do cows digest cellulose?
- 8.5** One of the most interesting computational challenges is the molecular simulation of protein folding. Review what has been done and what are the most difficult obstacles.

REFERENCES

1. Kendrew, J. C., et al., *A Three-Dimensional Model of the Myoglobin Molecules Obtained by X-Ray Analysis*. *Nature*, 1958. **81**: p. 662–666.
2. Berman, H. M., D. S. Goodell, and P. E. Bourne, *Protein Structures: From Famine to Feast*. *American Scientist*, 2002. **90**: p. 350–359.
3. Merrifield, R. B., *Solid Phase Peptide Synthesis. I. The Synthesis of a Tetrapeptide*. *Journal of the American Chemical Society*, 1963. **85**: p. 2149–2154.

4. Wilkins, M. H. F., et al., *Helical Structure of Crystalline Deoxyribose Nucleic Acid*. *Nature*, 1953. **172**: p. 750–762.
5. Wilkins, M. H. F., et al., *Helical Structure of Crystalline Deoxyribose Nucleic Acid*. *Nature*, 1953. **172**: p. 759–763.

Thermoplastics, Elastomers, and Thermosets

*A*s discussed in Chapter 1, polymers may be categorized as plastics (thermoplastics or thermosets), fibers, or synthetic rubber. Of the total synthetic polymer production in the United States, commodity thermoplastics account for the largest share of the market. Thermoplastics are followed by fibers (see Section 8.2), synthetic elastomers, and thermosets. The most commercially important thermoplastics include polyolefins (i.e., polyethylene and polypropylene), PVC, and the styrenics (e.g., PS, HIPS, SAN, and ABS). The principal feature of both thermosets and conventional elastomers that distinguishes them from thermoplastic materials is the formation of a network structure upon fabrication. This network may be formed by covalent or sometimes physical links that connect individual molecules. If only a few such links are formed, the material can be deformed but will return to its original shape upon release of the applied force, provided the force is less than required

to rupture the bonds. Polymers that have limited or no crystallinity, have low softening temperatures (glass-transition temperatures in the range from -50° to -70°C), and can be crosslinked in the above manner are candidates for elastomer applications. Polymeric materials that have a high density of crosslinks and are, therefore, infusible, insoluble, and dimensionally stable under load are thermosets.

9.1 Commodity Thermoplastics

Thermoplastics are polymers that can be melt processed by a variety of methods, including extrusion and molding. Thermoplastics are used for a wide range of applications, such as film for packaging, photographic and magnetic tape, beverage and trash containers, upholstery, and a variety of automotive parts. As shown by the data given in Table 9-1, the largest sales volume thermoplastics are the polyolefins followed by polypropylene, poly(vinyl chloride) and copolymers of vinyl chloride. Other important thermoplastics include poly(ethylene terephthalate), which is used for packaging applications (e.g., plastic bottles) and as an important fiber (i.e., polyester fiber) as discussed in Section 8.2.3. Engineering-grade polyesters that reach a more specialized market are reviewed in Section 10.1.8. The synthesis and properties of these important commercial thermoplastics are given in the following sections.

Table 9-1 U.S. Production of Thermoplastics in 2012^a

Thermoplastic	Thousands of Metric Tons ^{ba}	Annual Change %, 2002–12
Polyethylenes		
LDPE	3123	-1.5
LLDPE	6098	1.7
HDPE	8046	1.1
Polypropylene	7405	-0.4
Polystyrene	2473	-2.0
PVC and copolymers	6944	0.0

^a Adapted from Chemical and Engineering News, July 12, 2013, p. 65–66.

^b Conversion: 2206.6 lbs per metric ton.

9.1.1 Polyolefins

The polyolefins include various grades of polyethylene, differentiated on the basis of their crystallinity (i.e., density), and polypropylene. A comparison of the properties of polypropylene and the two extreme polyethylene grades—low-density (LDPE) and high-density polyethylene (HDPE)—are given in Table 9-2.

Table 9-2 Properties of Commodity Polyolefins

Property	ASTM	LDPE	HDPE	PP
Specific gravity	D792	0.91–0.93	0.94–0.97	0.90–0.91
Crystallinity, %	—	50–70	80–95	82
Melt temperature, °C	—	98–120	127–135	165–171
Tensile strength, MPa ^a	D638	4.1–16	21–38	31–41
Tensile modulus, GPa ^b	D638	0.10–0.26	0.41–1.24	1.10–1.55
Elongation-to-break, %	D638	90–800	20–130	100–600
Impact strength, notched Izod, J m ^{-1 c}	D256	No break	27–1068	21–53
Heat-deflection temperature, °C, at 455 kPa (66 psi)	D648	38–49	60–88	225–250

^aTo convert MPa to psi, multiply by 145.

^bTo convert GPa to psi, multiply by 1.45×10^5 .

^cTo convert J m⁻¹ to lb_f in.⁻¹, divide by 53.38.

Polyethylene. Ethylene, one of the most important petrochemicals, may be polymerized by a variety of techniques to produce products as diverse as low-molecular-weight waxes and highly crystalline, high-molecular-weight polyethylene (HDPE). The first commercialized polyolefin (1939) was a low-crystallinity, low-density polyethylene (LDPE) produced in 1939 by ICI in England. The majority of LDPE produced today in the United States is used as thin film for packaging, while the remaining production finds use in wire and cable insulation, coatings, and injection-molded products.

Low-density polyethylene is produced by free-radical bulk polymerization using traces of oxygen or peroxide as the initiator. Polymerization is conducted either in high-pressure autoclaves or in continuous tubular reactors operating at temperatures near 250°C and pressures as high as 3000 atm. Since the heat of ethylene polymerization is high (105 kJ mol⁻¹), the exotherm needs to be carefully controlled. For this reason, the polymerization may be conducted in several stages, each employing low conversion.

Small amounts of polar comonomers such as acrylates, vinyl esters, and vinyl ethers may be added during the polymerization process to modify product properties, particularly to impart low-temperature flexibility through the reduction of crystallinity. For example, low-molecular-weight copolymers of ethylene and vinyl acetate (EVA) have been used as polymeric plasticizers for PVC (see Section 7.1.1). The incorporation of small amounts (<7%) of vinyl acetate results in polyethylene films (modified LDPE) having better toughness, clarity, and gloss. Copolymers of ethylene and vinyl alcohol (EVOH) provide better processability and moisture resistance and high gas-barrier properties for packaging applications. Films made from copolymers of ethylene and ethyl acrylate have outstanding tensile strength, elongation-to-break, clarity, resistance to stress cracking, and flexibility at low temperatures. Copolymers of ethylene and methacrylic acid, particularly neutralized in

the form of sodium or zinc salts, are called ionomers. Ionomers exhibit extreme toughness and abrasion resistance (see Section 10.2.2).

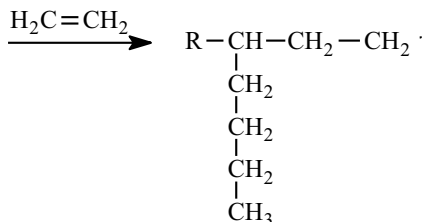
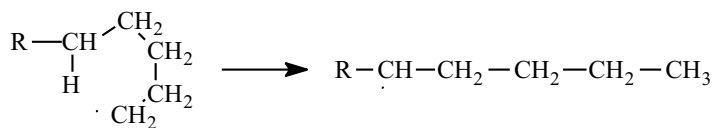
Molecular weights of LDPE typically fall in the range between 6000 and 40,000. Different molecular-weight grades are sold on the basis of their *melt index* (ASTM D1238). Melt index refers to the weight (in grams) of polymer extruded over a specified time interval and temperature through an extrusion die* in a plastometer that is fitted with a standard dead-weight piston and cylinder. For extrusion at 190°C in 10 min, typical melt indices of LDPE range from 0.1 to 109. In an oxygen-initiated polymerization, molecular weight can be reduced by simply increasing the oxygen concentration.

The free-radical polymerization of ethylene produces a highly branched molecule. The number of these branches may be as high as 30 per 500 monomer units. Most of these are short-chain alkyl groups such as ethyl and butyl, which are produced by an intramolecular “back-biting” mechanism illustrated in Figure 9-1A. At higher conversions and at lower pressures, long-chain branches (i.e., hexyl or longer) may be produced through a chain-transfer mechanism as illustrated in Figure 9-1B. Branching acts as defects that reduce crystallinity, as evidenced by the low density and low crystalline-melting temperature (T_m) of LDPE compared to HDPE (see Table 9-2). Branching can be reduced by increasing the pressure of the polymerization. For example, nearly linear polyethylene can be produced by free-radical polymerization at pressures approaching 5000 atm.

Alternatively, polyethylene with reduced branching can be obtained by polymerizing ethylene in the presence of a number of coordination catalysts (see Section 2.2.3). The first catalysts (Philips-type) consisted of chromium oxide (CrO_3) supported on aluminum oxide (Al_2O_3) or a silica–alumina base. Polymerization is conducted at 100 atm and 200°C in hydrocarbon solvents in which the catalysts are insoluble (i.e., heterogeneous solution polymerization). Alternative schemes employ Ziegler-type catalysts, which are typically complexes of aluminum trialkyls and titanium or other transition-metal halides, originally triethyl aluminum and titanium tetrachloride [1–3]. Compared to the Philips-type supported catalysts, Ziegler catalysts generally require lower temperatures and pressures, (i.e., 60° to 75°C and 1 to 10 atm) to obtain high-molecular-weight linear polymers.

*ASTM D1238 specifies a capillary die of 2.0955 mm in diameter and 8.0 mm in length.

A



B

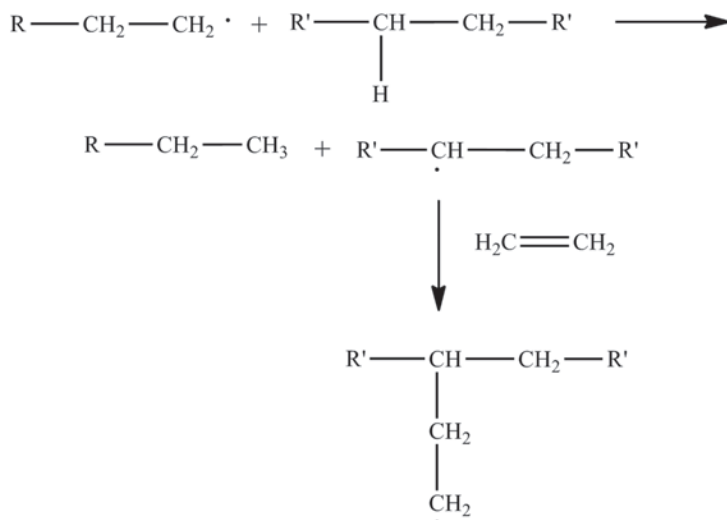


Figure 9-1 Mechanisms of branching during the free-radical polymerization of low-density polyethylene. **A.** Formation of an *n*-butyl (C_4H_9) branch by an intramolecular “back-biting” mechanism. **B.** Formation of long-chain branches via an intermolecular chain-transfer mechanism. Long alkyl end chains are represented by R and R'.

Ethylene can also be polymerized by metallocene polymerization (see Section 2.2.3) [4–7]. Although metallocene catalysts are significantly more expensive than Ziegler–Natta catalysts, they can provide sufficiently high activity to be competitive. The first high-activity metallocene catalyst system for ethylene polymerization, bis(cyclopenta-dienyl)zirconium dichloride (Cp_2ZrCl_2)–MAO, was reported by Sinn

and Kaminsky in 1980 [8]. The process produced a linear high-density polyethylene with narrow-molecular-weight distribution and opened the way for the use of other metallocene and non-metallocene [3] transition-metal catalysts for olefin polymerizations. Metallocene catalysts are also able to incorporate comonomers, such as butene-1, hexene-1, and octene-1, much more efficiently than is otherwise possible [4].

Typical properties of HDPE were given in Table 9-2. The principal commercial applications for HDPE include blow-molded containers, crates, pails, drums, gas tanks, and blown film. Polyethylene with molecular weights as high as 5 million (i.e., ultrahigh-molecular-weight polyethylene, UHMW) has been used for specialty applications, particularly for medical use such as artificial hip replacements (see Section 10.2.3).

Approximately 30 years ago, another low-pressure process (Unipol) was developed for the polymerization of ethylene. This process produces what may be considered a third-generation hybrid polyethylene (see Section 2.3.5)—a linear low-density polyethylene (LLDPE) produced at low pressure. Branches are linear alkanes that are shorter than those of LDPE. One advantage of LLDPE over LDPE is a faster cycling time during the molding of containers and lids. LLDPE is frequently blended with LDPE for film and sheet production. In recent years, the production of LLDPE represents about one-third of the combined world production of both LDPE and LLDPE. LLDPE produced by metallocene polymerization (see Section 2.2.3) provides superior mechanical and heat-sealing properties compared to conventionally produced LLDPE [5]. In addition to LDPE, LLDPE, and HDPE, other commercial grades of polyethylene include medium-density polyethylene or MDPE and very-low-density polyethylene or VLDPE ($\rho < 0.915 \text{ g cm}^{-3}$).

Polypropylene. The polyolefin with the largest sales volume is polypropylene (PP), properties of which are included in Table 9-2. Polypropylene is a lightweight, moderately high- T_m plastic that finds use in the manufacture of pipe, sheet, and blow-molded containers and as a textile fiber (see Section 8.2.3). In general, α -olefins such as PP cannot be polymerized by either radical or ionic catalysts. While atactic PP can be produced by use of a Lewis acid or organometallic compound, the product is a branched, rubbery polymer ($T_g = -20^\circ\text{C}$) at ambient temperature with no important commercial applications. In the 1950s, Natta showed that Ziegler-type catalysts could be used to produce stereoregular PP with high crystallinity; however, in contrast to the polymerization of HDPE, the coordination polymerization of α -olefins is slower and more critically dependent on the nature of the catalyst. The commercial plastic, first introduced in 1957, was highly isotactic (i.e., *i*-PP). High-molecular-weight (150,000 to 1,500,000) *i*-PP can be obtained by using a heterogeneous catalyst of modified titanium (III) chloride with a co-catalyst or activator, usually an organoaluminum compound such as diethylaluminum chloride. Catalysts are slurried in a hydrocarbon mixture, which helps to facilitate heat transfer in batch or continuous reactors operating at temperatures of 50° to 80°C and pressures of 5

to 25 atm. Hydrogen, which acts as a chain-transfer agent, may be used to moderate molecular weight. Syndiotactic PP (*s*-PP) can be produced by using homogeneous Ziegler–Natta catalysts at lower temperatures; however, recent interest in *s*-PP has grown with the development of metallocene catalysts (see Section 2.2.3) [3–6]. Metallocene polymerization of propylene, using catalysts such as isopropyl(Cp)(fluorenyl)ZrCl₂–MAO [9], produces polypropylene with extremely high syndiotacticity ($[\text{rrrr}] > 90\%$) and a T_m near 150°C. Compared to its isotactic counterpart, *s*-PP has a slightly lower T_m and is more susceptible to solvent attack.

In comparison to HDPE, commercial grades of *i*-PP have a higher T_m , slightly lower crystallinity, and better crack resistance. Unlike polyethylene, whose lowest-energy conformation is the extended planar zigzag (see Chapter 1), the pendant methyl groups of PP require a more complicated conformation whereby three monomer units constitute a single turn in a helix. Its higher T_m allows PP to be used in products that must be steam sterilized. One disadvantage of PP is the susceptibility of its methyl groups to thermooxidative degradation.

9.1.2 Vinyl Polymers

Polystyrene. Polystyrene (PS) was first produced in quantity by Dow in 1938. Today, styrenic polymers, principally general-purpose (GP-PS) and impact grades of polystyrene (HIPS), constitute about 14% of the total thermoplastics market (see Table 9-1). Properties of different grades of PS are given in Table 9-3. Commercial (atactic) PS is produced by free-radical polymerization in bulk or suspension with peroxides or trace oxygen as initiators. Exotherm control in bulk polymerization can be achieved by using multiple-step polymerizations—an initial low conversion in a stirred-tank reactor followed by high conversion in a tubular reactor operating with an increasing temperature gradient.

The principal use for PS has been packaging, where it is receiving increasing competition from PP. An especially important application for styrenic polymers is the manufacture of foam and bead for insulation and packaging materials. The first expandable PS (EPS) was produced in England in 1943. Today, the worldwide consumption of EPS is estimated at 1.6 million tons. EPS is a closed-cell structure made from PS beads and a hydrocarbon propellant or blowing agent such as isopentane and butane (see Section 7.1.3). For construction use, flame-retardant grades of EPS can be produced by adding <1% of brominated aliphatic compounds such as hexabromocyclododecane (HBCD).

One advantage of PS for packaging and related applications is that it can be reprocessed fairly easily. For example, the use of 30% to 50% clean scrap is common practice in the manufacture of thermoformed packaging, and used coffee cups can be recycled as regrind for use in the core of three-layer sheet for new cup production.

Table 9-3 Properties of Styrenic Polymers

Property	ASTM	GP-PS	HIPS	ABS
Specific gravity	D792	1.04–1.05	1.03–1.06	1.03–1.58
Tensile strength, MPa ^a	D638	36.6–54.5	22.1–33.8	41.4–51.7
Tensile modulus, GPa ^b	D638	2.41–3.38	1.79–3.24	2.07–2.76
Elongation-to-break, %	D638	1–2	13–50	5–25
Impact strength, notched Izod, J m ^{-1c}	D256	13.3–21.4	26.7–587	160–320
Heat-deflection temperature, °C at 455 kPa (66 psi)	D648	75–100	75–95	102–107

^aTo convert MPa to psi, multiply by 145.

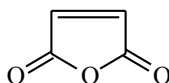
^bTo convert GPa to psi, multiply by 1.45×10^5 .

^cTo convert J m⁻¹ to lb_f in.⁻¹, divide by 53.38.

Polystyrene is especially susceptible to photooxidative degradation (see Section 6.1.2), which results in brittleness and yellowing. Degradation is initiated by the phenyl group, which absorbs UV radiation from sunlight. This energy is transferred to other sites along the polymer chain, resulting in bond cleavage, radical formation, and reaction with oxygen to form hydroperoxide and carbonyl groups.

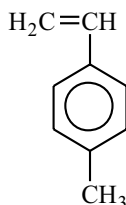
Stereospecific Polystyrene. As mentioned above, commercial-grade polystyrene is the atactic polymer (*a*-PS) produced by free-radical polymerization. An isotactic PS (*i*-PS) was first prepared by Natta in 1955 using a Z–N catalyst consisting of titanium tetrachloride and triethylaluminum [10]. Isotactic PS is moderately crystalline with a T_m of $\sim 230^\circ\text{C}$ but is more brittle and expensive than *a*-PS. For these reasons, *i*-PS was never commercialized. In 1986, syndiotactic PS (*s*-PS) was obtained by a metallocene polymerization (see Section 2.2.3) [11]. Unlike *i*-PS, *s*-PS has some advantages in properties over commercial-grade *a*-PS. These include better high-temperature performance ($T_m \approx 277^\circ\text{C}$), better toughness, lower permeability (i.e., improved barrier properties), and good chemical resistance. These advantages are offset by a higher price compared to commodity-grade PS. Current potential markets for *s*-PS include some electrical and electronics applications where *s*-PS can compete with poly(butylene terephthalate) (PBT) (see Section 10.1.8). Other areas may include some specialized products requiring thin walls and long, difficult flow paths during injection molding.

Styrene Copolymers. Disadvantages of GP-PS include its high brittleness and low T_g . To some extent, these limitations can be addressed through copolymerization. For example, copolymerization of styrene with maleic anhydride



provides slightly higher heat-distortion temperature, while copolymerization of styrene with acrylonitrile (i.e., SAN copolymer) provides higher strength and chemical resistance. Impact modification of PS can be obtained through the incorporation of polybutadiene. For example, high-impact PS (HIPS) is produced by the emulsion polymerization of styrene in a polybutadiene or styrene-butadiene (SBR) latex. The resulting toughened PS consists of a glassy matrix of PS in which are dispersed small domains (~ 0.005 -cm diameter) of polybutadiene. High interfacial adhesion, important for high strength, is achieved through graft polymerization of styrene, which occurs during the preparation of HIPS. ABS resins (see Section 10.1.2) are produced by blending latex emulsions of SAN and NBR (acrylonitrile-butadiene rubber) or by grafting styrene and acrylonitrile onto polybutadiene in latex form. Properties of SBR and NBR elastomers are reviewed in the following section. Polystyrene can be crosslinked by copolymerizing styrene with limited amounts of divinylbenzene. Applications of crosslinked PS beads include gel-permeation chromatography (see Section 3.3.4) and ion-exchange resins (see Section 2.4.1).

Other Styrenic Polymers. The monomer *p*-methylstyrene (PMS)



can be synthesized from toluene and ethylene by a zeolite process in high yield. This monomer can be polymerized by techniques similar to those used for PS to give poly(*p*-methylstyrene) that has a lower density, a slightly higher heat-distortion temperature, better flame retardancy, and faster molding cycles than conventional GP-PS. Stereospecific poly(*p*-methylstyrene) can be polymerized using metallocene catalysts [4].

Poly(vinyl chloride). As Table 9-1 indicates, PVC and copolymers of vinyl chloride are among the largest-volume commodity thermoplastics. Annual U.S. production is estimated at about 69 million metric tons. Poly(vinyl chloride) (PVC) is available in two general grades, rigid and flexible. Rigid-grade PVC is used as sheet, pipe, and window profiles and for other molded parts. Flexible-grade PVC is obtained by blending PVC with low- T_g plasticizers as discussed in Section 7.1.1. Applications of plasticized PVC include wire coating, upholstery, floor coverings, film, and tubing. Commercial PVC is a clear, moderately tough, low-crystallinity ($T_g = 87^\circ\text{C}$; $T_m = 212^\circ\text{C}$) material with low to moderate molecular weight (25,000 to 150,000). Properties of rigid- and flexible-grade PVC are summarized in Table 9-4.

Table 9-4 Representative Properties of Commercial Grades of PVC

Property	ASTM	Rigid	Flexible
Specific gravity	D792	1.03–1.58	1.16–1.35
Tensile strength, MPa ^a	D638	41.4–51.7	22.1–33.8
Tensile modulus, GPa ^b	D638	2.41–4.14	1.79–3.24
Elongation-to-break, %	D638	2–80	13–50
Impact strength, notched Izod, J m ⁻¹ ^c	D256	21.4–1068	26.7–587
Heat-deflection temperature, °C at 455 kPa (66 psi)	D648	57–82	75–95

^aTo convert MPa to psi, multiply by 145.

^bTo convert GPa to psi, multiply by 1.45×10^5 .

^cTo convert J m⁻¹ to lb_f in.⁻¹, divide by 53.38.

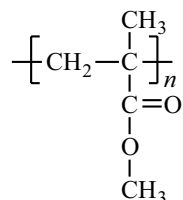
Polymerization of commercial-grade PVC is conducted by free-radical polymerization principally by suspension polymerization techniques, although emulsion polymerization and, more recently, bulk polymerization methods are also used. PVC is insoluble in its own monomer and, therefore, the polymer precipitates during bulk polymerization or within the monomer droplets in the case of suspension polymerization. If the suspension polymerization is performed under moderate pressure and then vented at the stage of high monomer conversion, a porous “dry-blend” resin is produced. Such resins are able to absorb large amounts of a plasticizer before becoming sticky and are, therefore, used in preparing flexible-grade PVC formulations.

The polymerization temperature is typically around 50°C for commercial PVC resins since higher temperatures can lead to minor branching and excessive formation of hydrochloric acid through dehydrochlorination, while lower temperatures result in polymers of high syndiotactic content. Dehydrochlorination, which starts at about 100°C, is also a serious problem when unstabilized PVC is heated above its T_g , as during melt processing (see Section 6.1.1). The thermally initiated dehydrochlorination reaction produces hydrochloric acid, which further accelerates dehydrochlorination, leading to intense color formation and eventual deterioration of polymer properties. It was for these reasons that the first commercial vinyl resins produced between 1928 and 1930 were copolymers of vinyl chloride with vinyl acetate, vinyl ethers, and acrylic esters. Today, thermal stability of the homopolymer is improved by adding organotin and other compounds.

Properties of PVC can be modified through chemical modification, copolymerization, or blending. For example, PVC may be chlorinated (i.e., CPVC) to increase its heat-distortion temperature for applications such as a hot-water pipe. A flexible film can be obtained by copolymerizing vinyl chloride with vinylidene chloride (Saran) or vinyl acetate. Vinyl acetate may also be grafted onto the PVC chain. The toughness of PVC can be improved by blending with high-impact resins

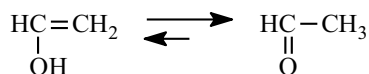
such as ABS (acrylonitrile–butadiene–styrene) and MBS (methyl methacrylate–butadiene–styrene) (see Section 7.2.2).

Poly(methyl methacrylate). Among other commercially important vinyl polymers are poly(methyl methacrylate) (PMMA) and to a lesser extent poly(vinyl acetate) and its derivatives. Commercial-grade PMMA



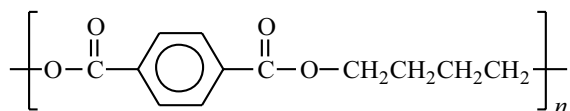
is an amorphous polymer of moderate T_g (105°C), with high light transparency and good resistance to acid and environmental deterioration. It is commercially polymerized by free-radical initiators such as peroxides and azo compounds in suspension or in bulk (e.g., cast polymerization) for sheet and molding compounds or for more specialized applications such as hard contact lenses. PMMA may also be polymerized anionically (see Section 2.2.2) at low temperatures to give highly isotactic ($T_g = 45^\circ\text{C}$; $T_m = 160^\circ\text{C}$) or highly syndiotactic ($T_g = 115^\circ\text{C}$; $T_m = 200^\circ\text{C}$) polymers. PMMA finds major applications in the automotive industry (e.g., rear lamps, profiles, and light fixtures), as acrylic sheet for bathtubs, advertisement signs, and lighting fixtures, and as composite material for kitchen sinks, basins, and bathroom fixtures.

Poly(vinyl acetate). Poly(vinyl acetate) (PVAC) ($T_g = 29^\circ\text{C}$), which may be polymerized by free-radical emulsion or suspension polymerization, finds limited applications in adhesives and also as the starting material for the production of poly(vinyl alcohol) (PVAL) and poly(vinyl butyral) (PVB), as discussed in Section 2.4.2. Poly(vinyl alcohol), which is used as a stabilizing agent in emulsion polymerization and as a thickening and gelling agent, cannot be directly polymerized because its monomer is isomeric with acetaldehyde, as shown below.



Commercially, PVAL is produced by the hydrolysis of PVAC in concentrated methanol. PVAL can be partially reacted with butyraldehyde to give PVB, which in its plasticized form is used as the inner layer of windshield safety glass. About 25% of the PVAL repeating units are left unreacted to provide strong adhesion to the glass.

time, a promising alternative to PET for molding applications appeared to be poly(butylene terephthalate) (PBT)



which crystallized faster than the available grades of PET. Although much interest was directed toward developing PBT for molding (as well as fiber) use during the 1970s, the market for moldable PBT did not develop to the extent originally envisioned due to several issues, including problems with postmolding warpage. In the late 1970s, interest was directed toward the development of faster-crystallizing grades of PET suitable for molding applications such as packaging (soft drink and custom bottles and thermoformed trays). The current usage of PBT has been in the guise of an engineering thermoplastic along with several other polyesters, such as polyarylates (see Section 10.1.8) and liquid-crystalline polyesters (Section 10.2.6) for use in specialized applications.

The traditional route to the production of commercial PET is through two successive ester-interchange reactions, as shown in Figure 9-2. The first step (Figure 9-2A) is the ester interchange of dimethyl terephthalic acid (DMT) and ethylene glycol at temperatures near 200°C during which methanol is removed and an oligomeric product ($n = 1 - 4$) is obtained. In the second-stage esterification (Figure 9-2B), increasing temperature causes the formation of high-molecular-weight PET during which ethylene glycol is distilled off.

The total world production of PET was approximately \$23 billion in 2010 and is expected to increase to about \$48 billion by 2016. The largest segments of this market are fibers, plastic bottles, and films (magnetic recording tape and photographic). The market for molding grades of PET is particularly strong as a result of the relative ease with which PET can be recycled [12]. Although recycled PET cannot be used directly for beverage bottles, it can be used in the manufacture of other products, such as insulation boards, or can be thermally or chemically decomposed to its monomers, which can be used for the polymerization of virgin resin (see Section 6.2.1).

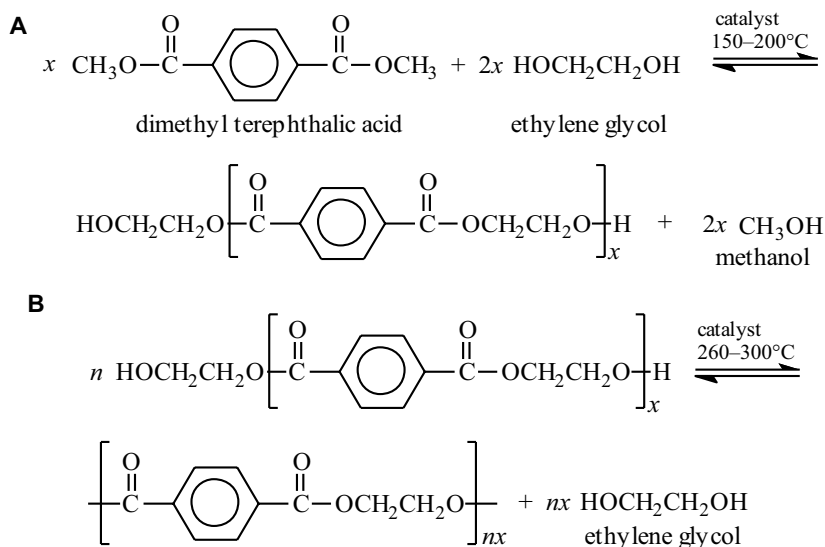
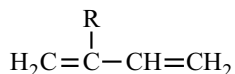


Figure 9-2 Two steps in the polymerization of poly(ethylene terephthalate). **A.** Ester interchange of dimethyl terephthalic acid and ethylene glycol. **B.** High-temperature esterification to yield high-molecular-weight polymer and ethylene glycol as a by-product.

9.2 Elastomers

Elastomers can be broadly classified as belonging to one of three groups: diene elastomers, nondiene elastomers, and thermoplastic elastomers. Diene elastomers such as polybutadiene, polyisoprene, and polychloroprene are polymerized from monomers containing two sequential double bonds (a diene) having the structure



where R represents a substituent group such as a hydrogen atom (in the case of polybutadiene), a chlorine atom (in polychloroprene), or a methyl group (in polyisoprene). As discussed in the following section, polymerization results in a repeating unit containing a single double bond that can provide a site for subsequent crosslinking (i.e., vulcanization). Typically, the most significant segment of the U.S. market for synthetic rubber is styrene-butadiene rubber (SBR), followed by polybutadiene and EP rubber.

Nondiene elastomers include polyisobutylene, polysiloxanes (silicone rubber), and a number of specialty elastomers, such as polyurethane (Spandex), and fluoroelastomers, such as Viton. Nondiene elastomers have no unsaturated sites and, therefore, crosslinking requires alternative methods to vulcanization, such as the use of trifunctional monomers in the case of condensation polymerizations (e.g., polysiloxanes), by the use of free-radical initiators, or by copolymerization with a small amount of a diene monomer (e.g., butadiene).

Thermoplastic elastomers such as SBS terpolymer are thermoplastics that contain rigid (“glassy”) and soft (“rubbery”) segments that can be thermally processed, unlike chemically crosslinked elastomers. Upon cooling, the soft and rigid segments phase-separate into physically distinct domains whereby the rigid domains serve as physical anchors for the rubbery segments and, thereby, provide a restoring force when the thermoplastic elastomer is stretched. The methods of synthesis and the properties of these three classes of elastomers are reviewed in the following sections. Principles of rubber elasticity were developed in Section 5.2.

9.2.1 Diene Elastomers

One way to form an elastomeric network is by the chemical bonding of two unsaturated carbons located on adjacent polymer molecules. Elastomers containing unsaturated sites include some of the most important synthetic rubbers, such as polybutadiene, polyisoprene, and polychloroprene. As shown in Figure 9-3, conjugated dienes such as isoprene and chloroprene can be polymerized to give either a 1,2-, 3,4-, or 1,4-polymer. In the case of 1,4-polymers, both *cis* and *trans* configurations are possible. In the case of the polymerization of 1,3-butadiene, for which there is no asymmetric substitute group, the 1,2- and 3,4- structures are identical. The proportion of each type of structure incorporated into the polymer chain influences both thermal and physical properties and is controlled by the conditions and method of polymerization. For example, butadiene can be polymerized by free-radical addition (see Chapter 2) at low temperature to give a polymer that is mostly *trans*-1,4- with only about 20% 1,2- structure. As the polymerization temperature is increased, the amount of *cis*-1,4- structure increases, while the proportion of 1,2- structure remains about the same.

Dienes can also be prepared by anionic polymerization using lithium or organolithium initiators like *n*-butyllithium in nonpolar solvents like pentane or hexane to yield polymers with high *cis*-1,4 content. The proportion of *cis*-1,4 structure decreases when higher alkali-metal initiators or more polar solvents are employed. Stereoregularity can also be controlled by use of selective coordination catalysts like Ziegler–Natta (see Section 2.2.3) or heterogeneous Alfin catalysts, which are combinations of alkenyl sodium compounds, alkali metal halides, and an alkoxide. Use of the latter system gives high-molecular-weight, high *trans*-1,4-content polymers.

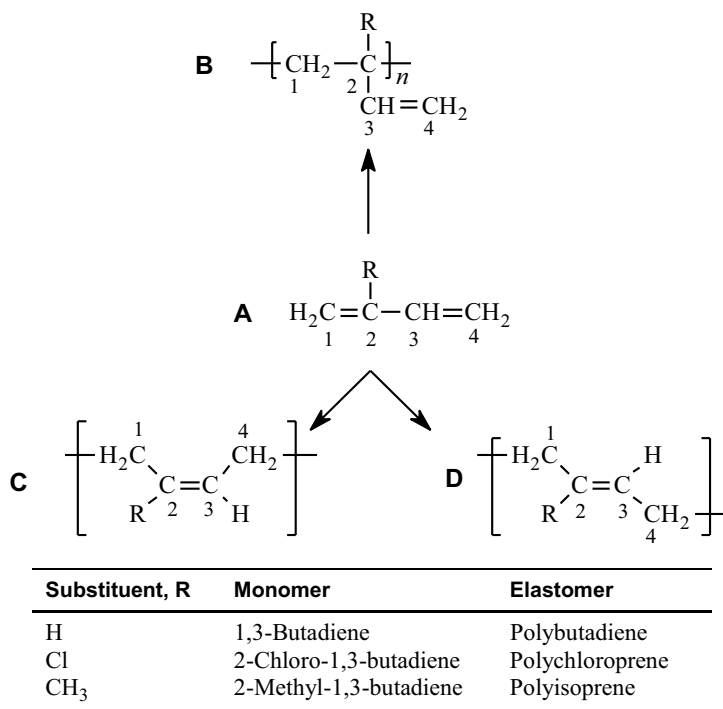


Figure 9-3 Polymerization of diene monomer (A) to yield 1,2- (B), *cis*-1,4- (C), and *trans*-1,4- structures (D). Different elastomers are obtained depending upon the substituent group, R.

Butadiene-Based Elastomers. Of all synthetic elastomers, polybutadiene (BR) and butadiene copolymers enjoy the largest sales share. In particular, styrene-butadiene copolymers (SBR) now have the largest share of the entire synthetic elastomer market in the United States. The principal use of both BR and SBR is in the production of tires and tire products, which are typically blends of both natural and synthetic rubbers. Polybutadiene has good resilience and abrasion resistance and low heat buildup—important properties for tire applications.

SBR is a highly random copolymer of butadiene and 10% to 25% styrene. The addition of styrene results in a lower price and contributes to the good wearing and bonding characteristics of SBR. In addition, strength, abrasion resistance, and blend compatibility are improved over BR alone. Like BR, SBR can be polymerized by a free-radical mechanism in emulsion either at 30° to 60°C (hot rubber) or near 0°C (cold rubber). A typical composition of the butadiene portion of SBR is approximately 70% of *trans*-1,4-polybutadiene, 15% to 20% of *cis*-1,4-polybutadiene, and 15% to 20% of 1,2-polybutadiene. Coordination copolymerization in solution yields

an SBR product (stereo SBR) that has a higher molecular weight, narrower molecular-weight distribution, and higher *cis*-1,4- content than emulsion-polymerized SBR.

Butadiene can also be copolymerized with 15% to 40% acrylonitrile in either hot or cold free-radical emulsion polymerization. The resulting elastomer, NBR or *nitrile rubber*, has improved oil and aromatic solvent resistance and, therefore, can be used as material for gaskets, tubing, O-rings, and gasoline hose. NBR, whose production was 180 million pounds in the United States during 2001, can also be used as a blend component in tire manufacture.

Polyisoprene. As discussed in Section 8.1.4, polyisoprene occurs in nature but can also be produced synthetically. Natural rubber (NR) or Hevea rubber used in tire manufacture is nearly all *cis*-1,4-polyisoprene. The synthetic equivalent of *cis*-1,4-polyisoprene (IR) can be obtained by polymerizing 2-methyl-1,3-butadiene (Figure 9-3) with Ziegler–Natta and Alfin catalysts. High *trans*-content polyisoprene may also be obtained by appropriate catalyst selection. IR has many of the good properties of its naturally occurring counterpart including high resilience, strength, and abrasion resistance. As in the case of most other diene-based elastomers, IR has poor resistance to attack by ozone, gasoline, oil, and organic solvents.

Polychloroprene. Another important diene-based elastomer is polychloroprene (neoprene), or CR. Compared to the other elastomers in this class, CR exhibits good resistance to attack by oxygen, ozone, oil, and gas. For these reasons, CR is used primarily as material for gaskets, tubing, O-rings, seals, and gasoline hose. The commercial material is mostly *trans*-1,4-polychloroprene produced by free-radical emulsion polymerization of 2-chloro-1,3-butadiene (Figure 9-3).

Metathesis Elastomers. At present, polynorbornene and polyoctenamer are two commercial elastomers produced by ring-opening metathesis polymerization (see Section 2.5.1). These specialty elastomers offer high oil absorptivity (polynorbornene) and high strength (polyoctenamer). Recent advances have shown that other elastomers, including polybutadiene as well as block and graft copolymers, can be made by metathesis [13, 14].

Vulcanization. Uncrosslinked rubber products such as natural rubber obtained from the latex of the *Hevea brasiliensis* tree are tacky, gummy materials, much like chewing gum, having none of the resiliency and permanent set we normally associate with commercial rubber products such as rubber bands, rubber hose, and tires. To obtain a network structure, diene elastomers are crosslinked by use of peroxides, ionizing radiation, and especially sulfur or sulfur-containing compounds. An illustration of a crosslinked elastomeric network is shown in Figure 9-4.

In the traditional method of vulcanization, which dates back to 1839, the rubber compound is heated with elemental sulfur. Sulfur bridges between individual elastomer molecules are formed by what is believed to be an ionic mechanism involving addition to the double bond. Concentration of sulfur in the vulcanized prod-

uct is typically 3 parts per hundred (pph) parts of elastomer compared to about 30 pph in highly crosslinked, hard rubber such as ebonite. The traditional vulcanization process is slow and inefficient as long sulfur bridges and cyclic sulfur structures can form. The process is improved by addition of accelerators such as thiuram disulfides, dithiocarbamates, and benzothiazoles. Activators such as zinc oxide and stearic acid serve to reduce the concentration of cyclic sulfide units and promote the formation of shorter-chain sulfide bridges. In addition to these additives, typical formulations for commercial rubber may include antioxidants and reinforcing fillers (see Section 7.1).

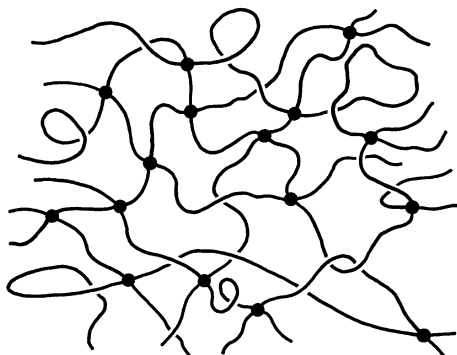
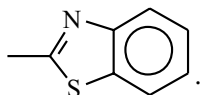


Figure 9-4 Idealized representation of a crosslinked elastomeric network. Filled circles indicate crosslink points (e.g., polysulfide bridges). Reproduced from J. E. Mark and B. Erman, *Rubberlike Elasticity—A Molecular Primer*. 1988, New York: John Wiley & Sons, with permission of James E. Mark.

A typical formulation for the vulcanization of a diene is given in Table 9-5. In this formulation, the fatty acid (e.g., stearic acid) and zinc oxide serve as the vulcanization activators. It is believed that the activators form a salt that complexes with the accelerator. Through this process, the accelerator forms a monomeric polysulfide as illustrated in Figure 9-5. The Ac group indicated in Figure 9-5 is an organic radical derived from the accelerator. An example is the benzothiazolyl group



This monomeric polysulfide then reacts with an unsaturated site of an elastomer chain to produce a rubber polysulfide and finally with another chain to form a polysulfide bridge. Typical molecular weight between crosslink points ranges from approximately 4000 to 10,000 where the molecular weight of individual chains is on the order of 100,000 to 500,000.

Table 9-5 Typical Vulcanization Ingredients for a Polydiene

Component	Phr
Accelerator	0.5–2
Sulfur	0.5–4
Fatty acid	1–4
Zinc oxide	2–10

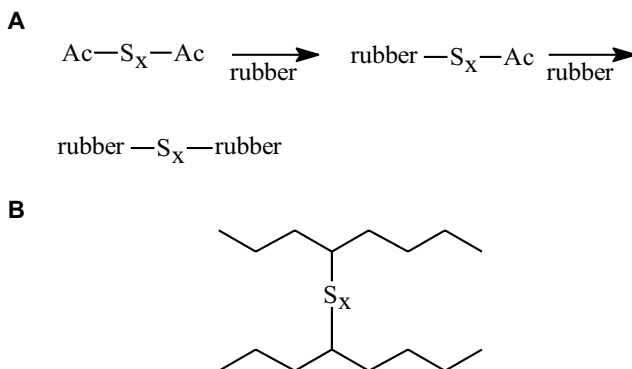


Figure 9-5 Vulcanization process. **A.** A polysulfide formed by reaction of elemental sulfur with an accelerator reacts with individual rubber chains to form a polysulfide bridge. **B.** Polysulfide bridge between two rubber chains.

9.2.2 Nondiene Elastomers

A number of important elastomers do not have the unsaturated chain structure characteristic of the diene elastomer. These nondiene elastomers include polyisobutylene (butyl rubber), polysiloxane (silicone rubber), fluoroelastomers such as Viton, polyurethane elastomers such as Spandex, and elastomers derived from ethylene and propylene (EP and EPDM elastomers). In two cases—*butyl rubber* and *EPDM*—a small amount of diene monomer that provides a site for vulcanization is included by means of copolymerization. For the other nondiene elastomers, free-radical initiators or polyfunctional monomers are used for network formation. The absence or low concentration of double bonds in the main chain of these elastomers results in high resistance to attack by oxygen and ozone and superior chemical resistance of these specialty rubbers compared to diene elastomers.

Polyisobutylene. Polyisobutylene or butyl rubber is produced as a copolymer (*IIR rubber*) containing about 0.5% to 2% isoprene, which provides the necessary unsaturation sites for vulcanization. Butyl rubber exhibits outstanding resistance to attack by oxygen and ozone and exhibits low gas permeability. For these reasons, it finds principal usage in weather stripping and inner tubes. High-molecular-weight

butyl rubber may be prepared by low-temperature cationic polymerization using Lewis acids like aluminum chloride in chlorocarbon solvents such as chloromethane.

Polysiloxanes. Silicone elastomers have both high-temperature and oxidative stability, flexibility at low temperatures, good electrical properties, and resistance to weathering and oil. Typical applications include wire and cable insulation, surgical implants, gasket material and seals, and aircraft tubing. Polysiloxanes can be prepared by the hydrolysis of dichlorosilanes such as dimethyldichlorosilane, as shown in Figure 9-6. This process is unsatisfactory for obtaining high-molecular-weight polymer because of a tendency to form cyclic siloxanes, typically trimers and tetramers. High-molecular-weight polymer suitable for elastomer applications can be obtained by subsequent base-catalyzed ring-opening polymerization of the cyclic products. Crosslinked siloxane elastomers may be obtained by cohydrolysis of dichlorosilanes with alkyl-trichlorosilanes, which provide an additional functional group for polymerization. Alternatively, polydimethylsiloxane can be crosslinked by the use of peroxides. The efficiency of the vulcanization step is greatly enhanced by incorporation of unsaturated sites through copolymerization with vinyl-group-containing siloxanes such as vinylmethylsilanol.

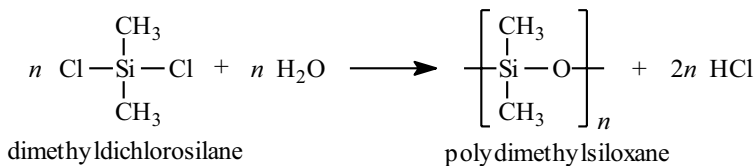


Figure 9-6 Polymerization of polydimethylsiloxane by the hydrolysis of dimethyldichlorosilane.

Fluoroelastomers. Most fluoroelastomers are obtained by high-pressure, free-radical emulsion polymerizations using organic or inorganic initiators. Most are copolymers of fluorinated polyolefins (tetrafluoroethylene and hexafluoropropylene) with vinylidene fluoride. Examples of common fluoroelastomers are given in Table 9-6. Fluorocarbon elastomers are capable of meeting demanding service applications, including operation over a broad temperature range and exposure to a wide range of chemicals and petroleum products. Uses include hose, tubing, O-rings, and gaskets in automotive, petrochemical, petroleum, and hydraulic applications. Fluoroelastomers are compounded with various fillers, processing aids, accelerators, and curatives and then extruded into the desired form such as tubing or O-ring cord. The extrudate is then postcured at 200° to 260°C for up to 24 h to achieve maximum mechanical properties.

Table 9-6 Examples of Fluoroelastomers

Fluoroelastomer	Trademarks
Poly(vinylidene fluoride- <i>co</i> -hexafluoropropylene)	Viton, Fluorel
Poly(vinylidene fluoride- <i>co</i> -hexafluoropropylene- <i>co</i> -tetrafluoroethylene)	Viton, Fluorel
Poly[vinylidene fluoride- <i>co</i> -tetrafluoroethylene- <i>co</i> -perfluoro(methyl vinyl ether)]	Viton
Poly[tetrafluoroethylene- <i>co</i> -perfluoro(methyl vinyl ether)]	Kalrez
Poly(tetrafluoroethylene- <i>co</i> -propylene)	Aflas
Poly(vinylidene fluoride- <i>co</i> -chlorotrifluoroethylene)	Kel-F

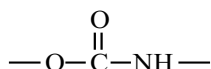
Polyurethanes. Polyurethanes (PUR) were developed by Otto Bayer and coworkers at I. G. Farbenindustrie in 1937. These polymers have high strength, good resistance to gas, oil, and aromatic hydrocarbons, high abrasion resistance, and excellent resistance to oxygen and ozone but are susceptible to microbial attack. Applications include shoe soles, solid tires, and impellers. Although the majority of polyurethane usage is for rigid and flexible foams first produced in the 1950s, about 15% of polyurethane production is targeted for elastomer applications. Basics of urethane chemistry and the preparation of polyurethane elastomers are discussed in this section.

In general, polyurethanes can be prepared either by the step-growth polymerization of diisocyanates with dihydroxyl (diol) compounds or, less commonly, by the reaction of bischloroformates with diamines. Both routes are illustrated in Figure 9-7. As shown, the step-growth polymerization of a diisocyanate with a diol, unlike the bischloroformate reaction, occurs without liberation of a low-molecular-weight by-product. The high reactivity of the isocyanate group enables polyurethanes to be processed by reaction injection molding (RIM) as discussed in Section 11.1.2.

Isocyanates, the esters of isocyanic acid (HNCO), can be aliphatic, cycloaliphatic, or polycyclic. Typical diisocyanates include methylene-4,4'-diphenyl-diisocyanate (MDI), toluene-2,4-diisocyanate (TDI),* and hexamethylene diisocyanate (HMI), whose structures are shown in Table 9-7. Diols are typically low-molecular-weight (e.g., 2000 to 3000) hydroxyl-terminated polyesters or polyethers such as polytetrahydrofuran (PTHF). Isocyanates or hydroxyl compounds with functionalities greater than 2 can be used to introduce branched groups or cross-links. Characteristic of all polyurethanes is the presence of the carbamate group[†]

* Often used as a mixture with its 2,6-isomer.

† An early term for polyurethanes was polycarbamate, from carbamic acid (RNHCO₂H).



in the chain backbone. Depending upon the chemical composition of the reactants (i.e., R, R'), the polyurethane chain may also include ester, ether, amide, or urea groups.

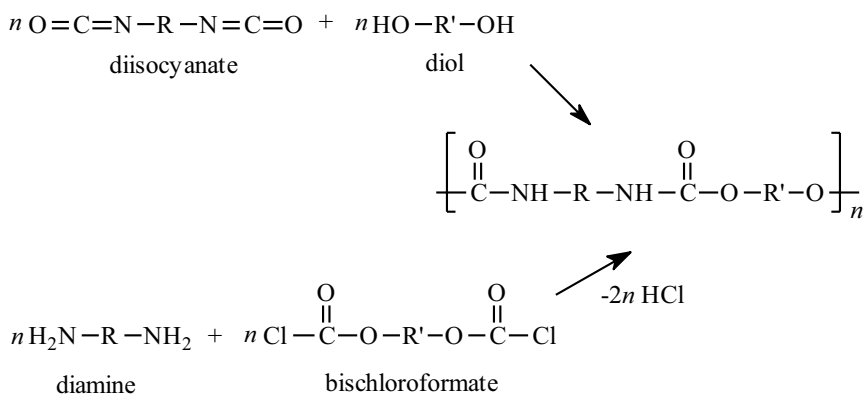
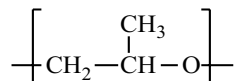
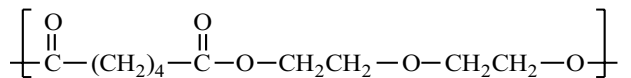


Figure 9-7 Routes to the synthesis of polyurethanes from diisocyanates (top) and bischloroformates (bottom).

Polyurethane elastomers can be obtained by the formation of $(\text{AB})_n$ -block copolymers consisting of alternating “soft” and “hard” segments. Typically, polyurethane elastomers are prepared by reacting an excess of an aromatic diisocyanate (e.g., MDI or TDI) with a hydroxy-terminated polyether or polyester (2000 to 3000 molecular weight) to yield an isocyanate-terminated prepolymer. An example of a commonly used polyether is poly(propylene glycol)



while a typical polyester is poly(diethyleneglycol adipate)



Polyester-based polyurethanes are less expensive and have better oxidative and high-temperature stability than do polyether-based polyurethanes, which have better hydrolytic stability and better low-temperature flexibility. As illustrated in Figure 9-8, the prepolymer can then be reacted with a diamine, such as ethylenediamine,

which acts as a chain extender to give the high-molecular-weight elastomer through a urea linkage as shown below.

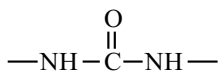
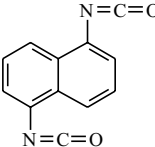
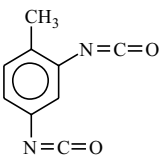


Table 9-7 Examples of Typical Diisocyanates

Diisocyanate	Abbrev.	Structure
Hexamethylenediisocyanate	HMI	$\text{O=C=N—(CH}_2\text{)}_6\text{—N=C=O}$
4,4'-Methylene-bis(cyclohexylisocyanate)	H_{12}MDI	$\text{O=C=N—}\langle\text{cyclohexane ring}\rangle\text{—CH}_2\text{—}\langle\text{cyclohexane ring}\rangle\text{—N=C=O}$
Methylene-4,4'-diphenyldiisocyanate	MDI	$\text{O=C=N—}\langle\text{phenyl ring}\rangle\text{—CH}_2\text{—}\langle\text{phenyl ring}\rangle\text{—N=C=O}$
Naphthalene-1,5-diisocyanate	NDI	
Toluene-2,4-diisocyanate	TDI	

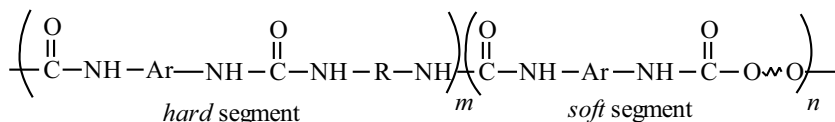
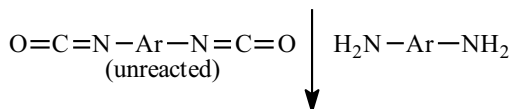
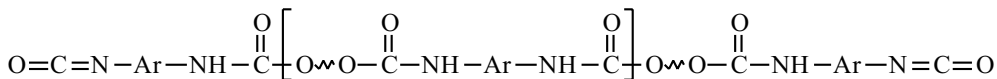
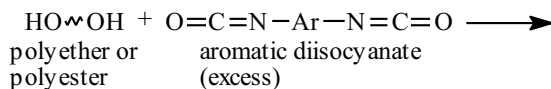
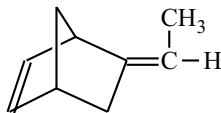


Figure 9-8 Synthesis of an elastomeric polyurethane for fiber applications.

The soft blocks of the copolymer are the flexible polyether/polyester segments, which constitute the bulk of the elastomer and form an amorphous continuous phase whose T_g is below normal-use temperature. Intermolecular hydrogen bonding between urethane groups results in domain association of hard blocks ($T_g > T_{use}$), which serve as physical anchor sites or crosslinks providing a restorative force when these elastomers are stretched. When the polyurethane elastomer is stretched, the soft segments elongate and crystallize until tension is released. Polyurethane elastomers are easily dyed and have high strength and chemical resistance, good abrasion and mar resistance, and elastic recovery. They are stable to attack by hydrocarbons and oxygen, although they are susceptible to strong acids and oxygenated solvents like ketones. Uses for polyurethane elastomers include foundation garments, surgical hose, and swimsuits.

Elastomers from Polyolefins. Random copolymers of ethylene and propylene (EPM rubber) can be prepared by use of soluble Ziegler–Natta catalysts (see Section 2.2.3) at controlled ethylene-propylene monomer concentration. The random placement of monomer units limits crystallinity and results in a rubbery material that can be crosslinked with peroxides through hydrogen abstraction and subsequent radical combination. Alternatively, an unsaturated terpolymer (EPDM rubber) can be prepared from ethylene, propylene, and unconjugated dienes like dicyclopentadiene, cyclooctadiene, 1,4-hexadiene, and ethylidene norbornene



These unsaturated terpolymers may be vulcanized by traditional means. EPM and EPDM have good resistance to acids, good weatherability and color stability, and good electrical stability. They can be used as substitutes for SBR and neoprene in automotive applications such as in tires, radiator hose, gaskets, and seals. EPM and EPDM are also used in wire and cable insulation, weather stripping, and in footwear. Blends of polypropylene and EPDM are used as material in the manufacture of car bumpers.

9.2.3 Thermoplastic Elastomers

Commercial elastomers can be made without the formation of the permanent crosslinks that are normally created through vulcanization. In place of covalent bonds, rigid-domain structures are used to create a network structure, as illustrated in Figure 9-9. These are typically the crystalline or glassy phases associated with the crystalline or glassy blocks of block copolymers or result from associations formed through the creation of secondary bonds such as hydrogen bonding between chemical groups in different molecules. Since these domains are physical in nature, they

are normally reversible and therefore elastomers belonging to this class are thermoplastic and can be fabricated by conventional molding techniques. Thermoplastic elastomers can be made from polyurethanes (discussed in Section 9.2.1), polyesters, polyolefins, and styrenic block copolymers. The absence of a separate vulcanization step and easy recycling of these materials have led to rapid commercialization of thermoplastic elastomers over the past 30 years.

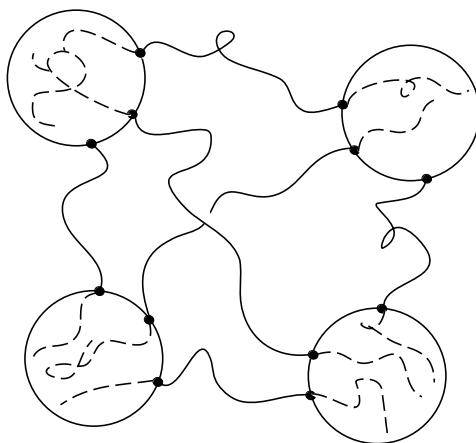


Figure 9-9 Representation of glassy domains in a thermoplastic elastomer such as SBS, polystyrene-*block*-polybutadiene-*block*-polystyrene. Circles represent physically separated domains of high glassy polymer (e.g., polystyrene) content that serve as physical crosslinks. Glassy domains are interconnected by the elastomeric (e.g., polybutadiene) segments. Adapted from L. H. Sperling, *Introduction to Physical Polymer Science*. Copyright © 1986 John Wiley & Sons. This material is used by permission of John Wiley & Sons, Inc.

SBS Elastomers. The most commercially important thermoplastic elastomers are ABA block copolymers composed of a high-molecular-weight (50,000 to 100,000) polystyrene end block and a central block of low-molecular-weight (10,000 to 20,000) polybutadiene (YSBR) or other olefins such as isoprene and ethylene-butylene. When cooled from the melt to below their glass-transition temperature, the polystyrene blocks phase-separate to form rigid glassy domains that act as physical crosslinks for the elastomeric olefin blocks. These block copolymers are prepared by anionic “living” polymerization as discussed in Section 2.2.2. As a class, they have higher tensile strength than SBR rubber but have limited heat resistance. YSBR can be hydrogenated to improve weather and temperature resistance. Blends of styrenic thermoplastic elastomers are used in rubber bands, toy products, shoe soles, and gasket material. YSBR containing 30% polybutadiene content may be blended with PS to produce a resin suitable for thermoforming plas-

tic drinking cups. PS alone is too brittle to withstand the high extension resulting from thermoforming (see Section 11.1.2).

Olefinic Elastomers. Olefinic thermoplastic elastomers, prepared by use of Ziegler–Natta catalysts (see Section 2.2.3), include *polyallomers*, which are block copolymers of polypropylene (the hard, crystalline block) and a second olefinic block, usually ethylene or ethylene and a diene (EPDM). EPDM block copolymers are attractive replacements for neoprene in oil-resistant wire and cable insulation due to their superior processability and coloration properties.

Copolyesters. Thermoplastic copolyesters consist of a hard (crystalline) polyester block, such as that formed by the reaction of terephthalic acid and butanediol, and a soft block of an amorphous long-chain polyester (e.g., polytetramethylene ether glycol) soft block. Like thermoplastic polyurethanes, thermoplastic copolyesters have good hydrocarbon and abrasion resistance. Applications include wire and cable insulation, gaskets, seals, hose, and automotive parts.

9.3 Thermosets

Principal commercial thermosets include epoxies, polyesters, and formaldehyde-based resins (i.e., phenol–formaldehyde, urea–formaldehyde, and melamine–formaldehyde). Typically, phenol resins constitute the largest segment of the thermoset market, followed by urea resins, unsaturated polyesters, and melamine resins.

9.3.1 Epoxies

Epoxies are formed by a two-stage process. Initially, a low-molecular-weight prepolymer is prepared by a base-catalyzed step-growth reaction of a dihydroxy compound such as bisphenol-A with an epoxide, typically epichlorohydrin, as illustrated in Figure 9-10. The prepolymer molecular weight is increased and the network is formed during a separate cure step, as shown in Figures 9-11 and 9-12. Amines, usually aromatic, may be used to cause ring opening of the end epoxide groups through nucleophilic addition (Figure 9-11). Carboxylic acid anhydrides such as phthalic acid anhydride can react with pendant hydroxyl to give ester acids, which can then react with epoxide or other hydroxyl groups to create additional ester groups (Figure 9-12). Epoxy resins have high chemical and corrosion resistance, outstanding adhesion properties, low shrinkage upon cure, and good electrical properties. Principal applications for these resins include protective coatings, composite matrices, and adhesives.

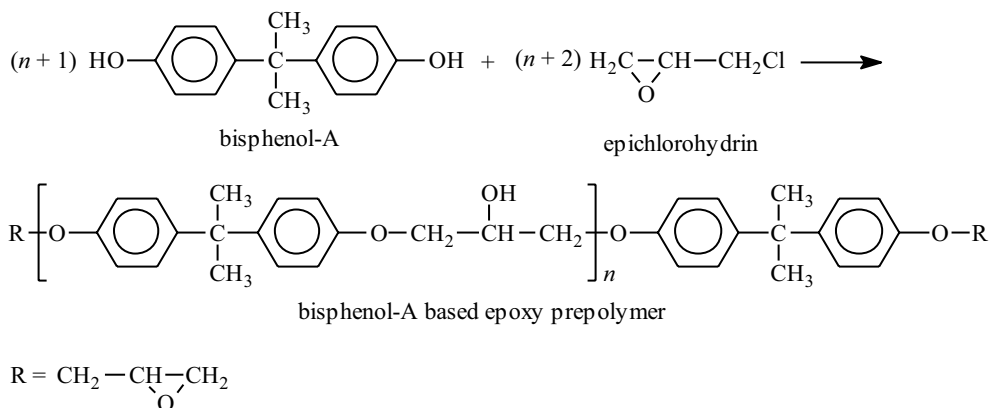


Figure 9-10 Epoxy prepolymer formed from bisphenol-A and epichlorohydrin.

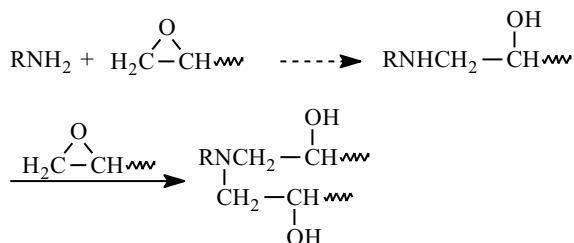


Figure 9-11 Cure of an epoxy resin by reaction of the prepolymer with an amine.

9.3.2 Unsaturated Polyesters

Polyester resins are widely used in construction and marine applications. Network formation distinguishes polyester resins from linear (thermoplastic) polyesters such as PET. Crosslinking is achieved either by use of polyols such as glycerol, as in the case of saturated polyesters (glyptal), or by the use of unsaturated dicarboxylic acids, such as maleic anhydride in the case of unsaturated polyester resins. Glyptal, which is used mainly as an adhesive or modified with natural or synthetic oils (oil-modified alkyds) for coatings, is formed by the reaction of glycerol and phthalic anhydride, as shown in Figure 9-13. The reaction is allowed to continue until a viscous liquid is obtained. The liquid can then be transferred to a mold for further network development (hardening).

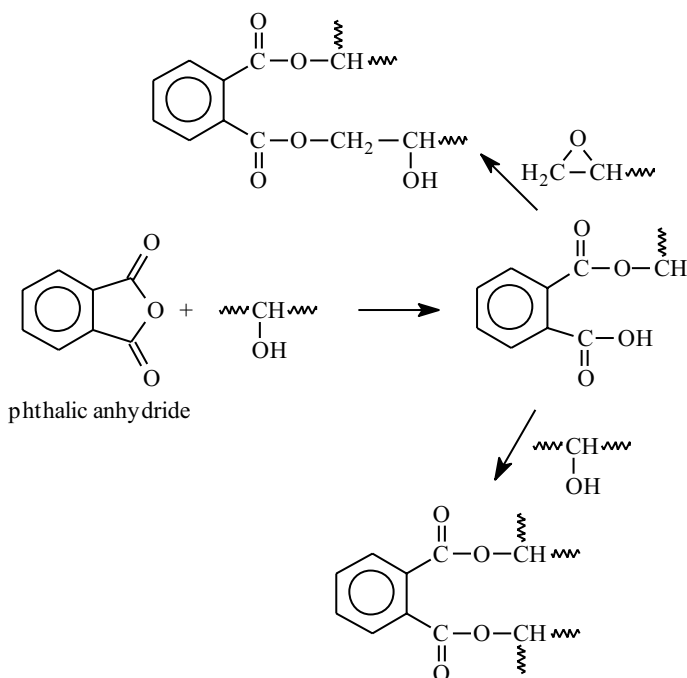


Figure 9-12 Cure of an epoxy resin by reaction of the prepolymer with an anhydride.

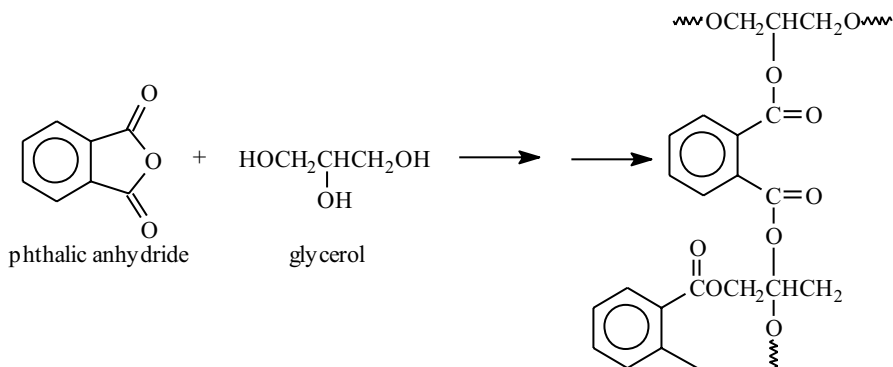


Figure 9-13 Formation of a glyptal resin.

Unsaturated polyester resins, which are used as the matrix component of glass-fiber composites, can be obtained by copolymerization of both saturated acids (e.g., phthalic anhydride) and unsaturated acids (e.g., maleic anhydride) with a diol such

as propylene glycol or diethylene glycol, as illustrated in Figure 9-14. Incorporation of the saturated acid serves to decrease crosslink density and consequently resin brittleness. Fumaric acid may be used in place of maleic acid to increase impact resistance. The low-molecular-weight product is soluble in styrene, which can then polymerize in the presence of peroxides at the double-bond sites of the prepolymer.

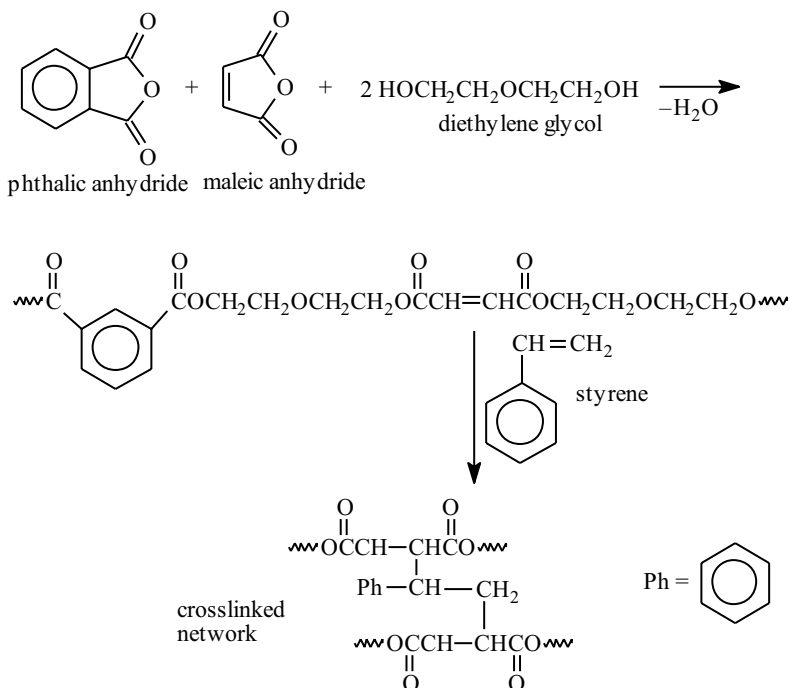


Figure 9-14 Formation of an unsaturated polyester resin.

9.3.3 Formaldehyde Resins

Formaldehyde is used in the production of two different but related classes of thermosets—phenoplasts and aminoplasts. *Phenoplasts*, or phenolic (PF) resins, are produced by the condensation of phenol (or resorcinol) and formaldehyde. These were the first synthetic thermosets. About 41% of PF resins are used in plywood manufacture and about 14% in insulation. Other applications include lacquers and varnishes, molding compounds, and laminates (e.g., wall panels and table tops).

Aminoplasts are prepared from the condensation of either urea (UF resins) or melamine (MF resins) with formaldehyde. Applications of aminoplasts are similar to those of phenoplasts; they also include the treatment of textile fibers for improv-

ing their shrink and crease resistance and their use to increase the wet strength of paper. In terms of sales volume, UF resins are the most important. Like phenolic resins, they can be used in molding, laminating, and adhesive applications, especially where the darker color of phenolics may be objectionable, such as in interior-grade plywood. They also find use in the manufacture of electrical switches and plugs and insulating foam. MF resins are harder and more chemical, temperature, and moisture resistant than UF resins but are more expensive. Typical applications for MF resins include decorative plastic dinnerware, laminated worktops, and electrical fittings. Formaldehyde-based resins may be used as unmodified compounds or may be compounded with additives such as wood flour or glass fibers that serve as reinforcing fillers.

Phenoplasts. Phenolic resin was the first totally synthetic coating material. It was commercialized in 1909 as Bakelite, a replacement for cellulose nitrate [15, 16]. Phenolic resins may be prepared by either a base-catalyzed addition of formaldehyde to phenol (resole formation) or by an acid-catalyzed reaction (novolac formation). The first step in resole formation is the reaction of phenol and excess formaldehyde under basic conditions to form mono-, di-, and trimethylolphenols. The formation of monoethylolphenol is illustrated in Figure 9-15. Under these conditions, phenol is present as a resonance-stabilized anion, and substitution is exclusively *ortho* and *para*. Upon heating, the methylolphenols condense to give a low-molecular-weight prepolymer called a *resole* (see Figure 9-16), which contains a large number of free methylol groups and is soluble in base. Further heating of the resole at elevated temperatures and under basic, neutral, or slightly acidic conditions yields the final high-molecular-weight network called the *resite*.

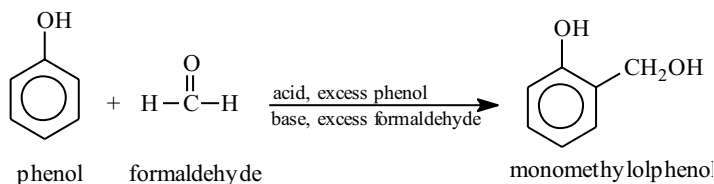


Figure 9-15 Reaction of phenol and formaldehyde to yield monomethylolphenol. Formation of dimethylolphenols and trimethylolphenols is also possible.

Resole formation can also be obtained by an initial acid-catalyzed reaction of formaldehyde with excess phenol. The mechanism involves protonation of the carbonyl group of formaldehyde, followed by electrophilic aromatic substitution at the *ortho* and *para* positions of phenol. Under acidic conditions, further reaction yields a low-molecular-weight, fusible but insoluble prepolymer called a *novolac* whose structure is illustrated in Figure 9-17. Unlike resole (Figure 9-16), novolac contains no residual hydroxymethyl groups. The high-molecular-weight network, the *resite*,

is obtained from the novolac by heating with additional formaldehyde, paraformaldehyde, or hexamethylenetetramine.

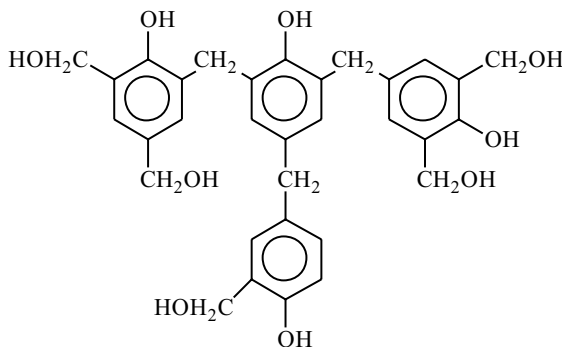


Figure 9-16 Representative structure of a resole.

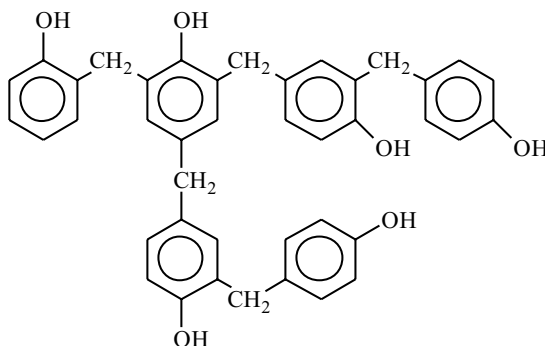


Figure 9-17 Representative structure of a novolac.

Aminoplasts. The first step in the production of UF resins is the nucleophilic addition of urea to formaldehyde to give methylol derivatives, as illustrated in Figure 9-18, in a manner similar to the initial stages of phenolic-resin production. Subsequent condensation of these derivatives gives the final high-molecular-weight resin. The UF resin may be a true network structure, such as that shown in Figure 9-19A, or a colloidal dispersion of UF condensates (Figure 9-19B), which are stabilized by association with excess formaldehyde.

As illustrated by Figure 9-20, the initial step in the preparation of MF resin is a condensation of formaldehyde and melamine similar to that of urea and formaldehyde (Figure 9-18). A difference is that the majority of amino groups of melamine form *dimethylol* derivatives rather than monomethylol derivatives, as in the case of UF resins. In the final stage of resin production, methylol groups condense with

amino groups to form methylene bridges, which link the prepolymer chains in a rigid network structure, as illustrated in Figure 9-21.

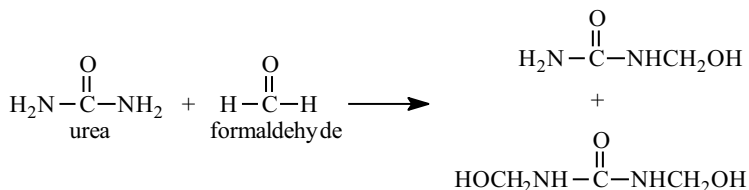


Figure 9-18 Reaction of urea and formaldehyde to yield methylol derivatives as the first step in the production of urea-formaldehyde resins.

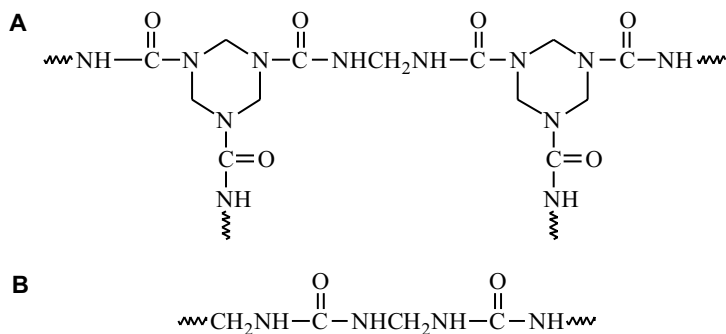


Figure 9-19 Structures proposed for a fully cured UF resin. **A.** Network model. **B.** Oligomeric UF condensates in the colloidal dispersion mode.

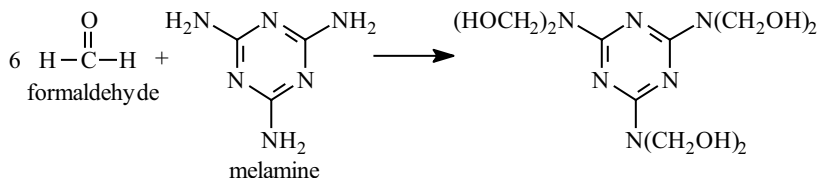


Figure 9-20 Condensation of melamine and formaldehyde to yield the dimethylol derivative of melamine.

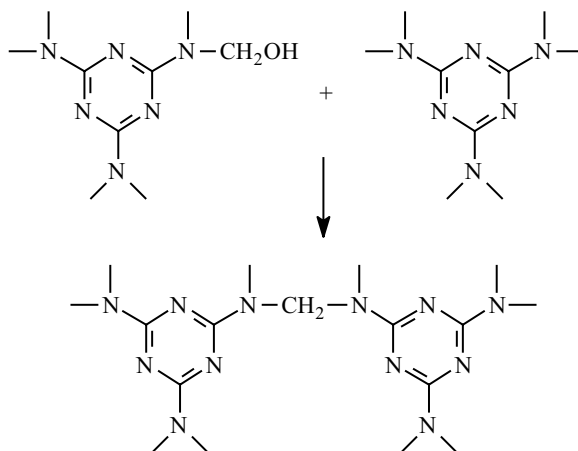


Figure 9-21 Formation of MF-resin network.

SUGGESTED READING

THERMOPLASTICS

- Braun, D., *PVC—Origin, Growth, and Future*. Journal of Vinyl and Additives Technology, 2001. 7: p. 168.
- Endo, K., *Synthesis and Structure of Poly(vinyl chloride)*, Progress in Polymer Science, 2002. 7: p. 202.
- Gilbert, M., *Crystallinity in Poly(vinyl chloride)*. Journal of Macromolecular Science—Review in Macromolecular Chemistry and Physics, 1994. C34: p. 77.
- Imanishi, Y., and N. Naga, *Recent Developments in Olefin Polymerizations with Transition Metal Catalysts*. Progress in Polymer Science, 2001. 26: p. 1147.
- Jog, J. P., *Crystallization of Polyethylene Terephthalate*. Journal of Macromolecular Science, Chemistry and Physics, 1995. C35: p. 531.
- Makino, T., *Poly(vinyl chloride) and Environmental Issues*. Polymer Recycling, 2000. 5: p. 223.
- Nass, L. I., and C. A. Heiberger, eds., *Encyclopedia of PVC*. 2nd ed. 1986, New York: Marcel Dekker.
- Prasad, A. V., and R. P. Singh, *Recent Developments in the Degradation and Stabilization of High-Impact Polystyrene*. Journal of Macromolecular Science, Reviews in Macromolecular Chemistry and Physics, 1997. C37: p. 581.
- Vogl, O., *Polyolefins: Synthesis and Structure*. Journal of Macromolecular Science—Pure and Applied Chemistry, 1998. A35: p. 1017.
- Vogl, O., *Polypropylene: An Introduction*. Journal of Macromolecular Science—Pure and Applied Chemistry, 1999. A36: p. 1547.

Xie, T., K. B. McAuley, J. C. C. Hsu, and D. W. Bacon, *Gas Phase Ethylene Polymerization: Production Processes, Polymer Properties, and Reactor Modeling*, Industrial and Engineering Chemistry Research, 1994. **33**: p. 449.

ELASTOMERS

Améduri, B., B. Boutevin, and G. Kostov, *Fluoroelastomers: Synthesis, Properties and Applications*, Progress in Polymer Science, 2001. **26**: p. 105.

Clarson, S. J., and J. A. Semlyen, eds., *Siloxane Polymers*. 2003, Englewood Cliffs: Prentice Hall.

Hamed, G. R., *Reinforcement of Rubber*. Rubber Chemistry and Technology, 2000. **73**: p. 524.

Mark, J. E., *Silicon-Containing Polymers*. Advances in Chemistry Series, 1990. **224**; p. 47.

Morawetz, H., *History of Rubber Research*. Rubber and Chemical Technology, 2000. **73**: p. 405.

Wirpsza, Z., *Polyurethanes: Chemistry, Technology and Applications*. 1993, London: Ellis Horwood.

PROBLEMS

- 9.1 Discuss the uses of thermosets in the construction industry.
- 9.2 Natural rubber is sometimes epoxidized. Describe the reaction and the use of epoxidized rubber.
- 9.3 Compare the mechanical and thermal properties and costs of PET and poly(trimethylene terephthalate) (PTT).^{*} Can PTT be used as a substitute for PET in engineering thermoplastic applications?
- 9.4 Describe the chemical routes to obtain the following monomers:
 - (a) bischloroformates from dihydroxy compounds
 - (b) hexamethylene diisocyanate from hexamethylene diamine
 - (c) naphthalene diisocyanate from naphthalene

^{*} See Section 8.2.3.

REFERENCES

1. Ziegler, K., et al., *Das Mulheimer Normaldruck-Polyethylene-Verfahren*. *Angewandte Chemie*, 1955. **67**(19,20): p. 541–547.
2. Soga, K., and T. Shiono, *Ziegler–Natta Catalysts for Olefin Polymerizations*. *Progress in Polymer Science*, 1997. **22**: p. 1503–1546.
3. Sinn, H., and W. Kaminsky, *Ziegler–Natta Catalysts*. *Advances in Organometallic Chemistry*, 1980. **18**: p. 99–149.
4. Imanishi, Y., and N. Naga, *Recent Developments in Olefin Polymerizations with Transition Metal Catalysts*. *Progress in Polymer Science*, 2001. **26**: p. 1147–1198.
5. Hamielec, A. E., and J. B. P. Soares, *Polymerization Reaction Engineering—Metallocene Catalysts*. *Progress in Polymer Science*, 1996. **21**: p. 651–706.
6. Kaminsky, W., *New Polymer by Metallocene Catalysis*. *Macromolecular Chemistry and Physics*, 1996. **197**: p. 3907–3945.
7. Kaminsky, W., and M. Arndt, *Metallocenes for Polymer Catalysis*. *Advances in Polymer Science*, 1997. **127**: p. 144–187.
8. Sinn, H., et al., *Ziegler–Natta Catalysts*. *Angewandte Chemie, International Edition in English*, 1980. **19**: p. 369.
9. Ewen, J. A., et al., *Syndiotactic Propylene Polymerization with Group 4 Metallocenes*. *Journal of the American Chemical Society*, 1988. **110**: p. 6255–6256.
10. Natta, G., and D. Corradini, *Kristallstruktur des isotaktischen Polystyrols*. *Makromolekulare Chemie*, 1955. **16**: p. 77–80.
11. Ishihara, N., M. Kuranoto, and M. Uoi, *Stereospecific Polymerization of Styrene Giving the Syndiotactic Polymers*. *Macromolecules*, 1988. **21**: p. 3356–3360.
12. Awaja, F., and D. Pavel, *Recycling of PET*. *European Polymer Journal*, 2005. **41**: p. 1453–1477.
13. Stinson, S. C., *Olefin Polymerization by Metathesis Expanding in Many New Directions*. *Chemical & Engineering News*, 1987. **65**(17): p. 41–43.
14. Brandrup, J., E. H. Immergut, and E. A. Grulke, eds. *Polymer Handbook*. 4th ed. 1999, New York: John Wiley & Sons.
15. Baekeland, L. H., *The Synthesis, Constitution, and Uses of Bakelite*. *Journal of Industrial and Engineering Chemistry*, 1909. **1**: p. 149–161.
16. Baekeland, L. H., and H. L. Bender, *Phenol Resins and Resinoids*. *Industrial and Engineering Chemistry*, 1925. **17**(3): p. 225–237.

This page intentionally left blank

Engineering and Specialty Polymers

*E*ngineering and specialty thermoplastics offer outstanding properties in one or more areas when compared with commodity thermoplastics such as polystyrene and polyolefins (see Chapter 9). Advantages may include high thermal stability or excellent chemical resistance, low creep compliance, and high tensile, flexural, and impact strength. Not unexpectedly, these properties come at a premium in price. In many cases, these polymers can be used as replacements for metals, particularly where a high strength-to-weight ratio is an important consideration, such as in automotive and aerospace applications.

The classification between engineering and specialty plastics is somewhat arbitrary. For purposes of discussion, the term *engineering plastics* will refer to those polymers that are used in the manufacture of premium plastic products where high-temperature resistance, high impact strength, chemical resistance, or other special properties are required. The important engineering plastics are normally considered to include aliphatic polyamides (nylon-6 and nylon-6,6), ABS resin, polycarbonate,

poly(phenylene oxide), acetal, polysulfones, poly(phenylene sulfide), engineering polyesters, and fluoroplastics. Properties of some of these engineering thermoplastics are given in Table 10-1. By comparison, *specialty plastics* are significantly more expensive but achieve very high performance in one or more areas. These plastics find limited but critical use in aerospace composites, as membranes for gas and liquid separations (see Section 12.1), as flame-retardant textile fabrics for firefighters and race car drivers, and as material for sutures and surgical implants. The most important class of specialty plastics is the polyimides. Other specialty polymers include polyetherimide, poly(amide-imide), polybismaleimides, polybenzimidazoles, ionic polymers, poly(aryl ether ketones), polyphosphazenes, polyarylates and related aromatic polyesters, ultrahigh-molecular-weight polyethylene and other specialty polyolefins, and dendritic polymers.

Table 10-1 Representative Properties of Some Important Engineering Thermoplastics

Property	PA-6 ^a	PA-6,6 ^a	ABS ^b	PC	PPO	Acetal	PSF	PPS
Specific gravity (D 792)	1.12– 1.14	1.13– 1.15	1.03– 1.06	1.20	1.06	1.42	1.24	1.34
Tensile strength, MP ^c (D 638)	69	76	41–52	66	66	66–83	70	74
Tensile modulus, GPa ^d (D 638)	0.69	NA	2.1–2.8	2.4	2.4	3.6	2.6	3.3
Elongation-to- break, % (D 638)	300	300	5–25	110	20– 60	25–75	50– 100	3
Flexural strength, MPa ^d (D 790)	34	42	76–90	93	93	97	106	138
Flexural modulus, GPa ^d (D 790)	9.7	12–28	26–28	23	25– 28	26–30	27	41
Impact strength, notched Izod, m ⁻¹ e (D 265)	160	112	160– 320	854	96– 267	69– 123	160– 320	11
HDT, °C at 455 kPa (66 psi) (D 648)	150– 185	180– 240	102– 107	138	137	124	150– 175	137

^a Moisture conditioned.

^b Medium-impact grade.

^c To convert MPa to psi, multiply by 145.

^d To convert GPa to psi, multiply by 1.45×10^5 .

^e To convert J m⁻¹ to lb_f in.⁻¹, divide by 53.38.

10.1 Engineering Plastics

10.1.1 Polyamides

Polyamides can have either all aliphatic- or all aromatic-chain backbones. The aliphatic polyamides, particularly nylon-6 and nylon-6,6, are the most widely used engineering thermoplastics. In addition to their important fiber applications (see Section 8.2.3), aliphatic polyamides may be used as molded parts for automotive and other applications. Commercial nylon resins for molding applications may be modified for improved flame retardancy and impact strength, or reinforced with minerals or glass fibers to increase modulus as well as to lower cost. Fibers made from aromatic polyamides, such as Nomex and Kevlar, provide outstanding high-temperature resistance and high tensile strength for use as fire-retardant fabric and for tire cord. As a class, polyamides exhibit excellent resistance to wear and abrasion, a low coefficient of friction, good resilience, and high impact strength. Properties of nylon-6 and nylon-6,6 are given in Table 10-1. The chemical structures of the repeating units of the most important aliphatic and aromatic polyamides and the monomers from which they are polymerized are given in Table 10-2.

Table 10-2 Chemical Structures of Important Polyamides

Monomer(s)	Polymer	Structure
Caprolactam	Poly(ϵ -caprolactam) (nylon-6)	$\left[\text{NH}-\overset{\text{O}}{\parallel}{\text{C}}-(\text{CH}_2)_5 \right]$
Hexamethylene diamine adipic acid	Poly(hexamethylene adipamide) (nylon-6,6)	$\left[\text{NH}-(\text{CH}_2)_6-\text{NH}-\overset{\text{O}}{\parallel}{\text{C}}-(\text{CH}_2)_4-\overset{\text{O}}{\parallel}{\text{C}} \right]$
Hexamethylene diamine sebacic acid	Poly(hexamethylene sebacamide) (nylon- 6,10)	$\left[\text{NH}-(\text{CH}_2)_6-\text{NH}-\overset{\text{O}}{\parallel}{\text{C}}-(\text{CH}_2)_8-\overset{\text{O}}{\parallel}{\text{C}} \right]$
Isophthaloyl chloride <i>m</i> - phenylenediamine	Poly(<i>m</i> -phenylene isophthalamide) (Nomex)	$\left[\text{HN}-\text{C}_6\text{H}_3-\text{NH}-\overset{\text{O}}{\parallel}{\text{C}}-\text{C}_6\text{H}_3-\overset{\text{O}}{\parallel}{\text{C}} \right]$
Terephthaloyl chloride <i>p</i> -phenylenediamine	Poly(<i>p</i> -phenylene ter- ephthalamide) (Kevlar)	$\left[\text{HN}-\text{C}_6\text{H}_4-\text{NH}-\overset{\text{O}}{\parallel}{\text{C}}-\text{C}_6\text{H}_4-\overset{\text{O}}{\parallel}{\text{C}} \right]$

All nylons are water sensitive due to the hydrogen-bonding character of the amide groups. For example, nylon-6,6 absorbs about 9% water during equilibrium at ambient temperature and 100% relative humidity. Water absorption decreases

with decreasing amide-group concentration in the polymer backbone as in the case of nylon-11 (1.9% water absorption) obtained by the ring-opening polymerization of 11-aminoundecanoic acid. Water acts as a plasticizer, which reduces tensile strength and modulus (and, therefore, dimensional stability), while increasing elongation-to-break and consequently toughness. Care must be taken to reduce water content of nylon resins to below 0.3% before melt processing to avoid embrittlement due to hydrolytic degradation.

Nylon-6,6 and nylon-6 dominate the non-fiber polyamide market. Nylon-6,6 has higher rigidity, but nylon-6 is more weather and thermally resistant. Due to its good barrier properties, nylon-6 film is used for packaging of some oxygen-sensitive foods. Other aliphatic nylons having more specialized markets include nylon-11, nylon-12, and nylon-4,6. For example, nylon-11 and nylon-12 have been used in the manufacture of fuel lines and compressed-air brake tubing.

Aromatic Polyamides. In the 1960s, aromatic polyamides, often called *aramids*, were developed to improve the heat and flammability resistance of nylons. Poly(*m*-phenylene isophthalamide) (Nomex) is a highly heat-resistant nylon (decomposes at about 370°C) obtained by the solution or interfacial polymerization of a *meta*-substituted aromatic diacid chloride and diamine, as illustrated in Figure 10-1. Nomex may be used as a substitute for asbestos in many applications, such as flame-resistant protective clothing and hot-gas filtration equipment. Nomex in the form of thin pads has been used to isolate the fragile sintered silica-fiber mats of the space shuttle from stress and vibration during flight.

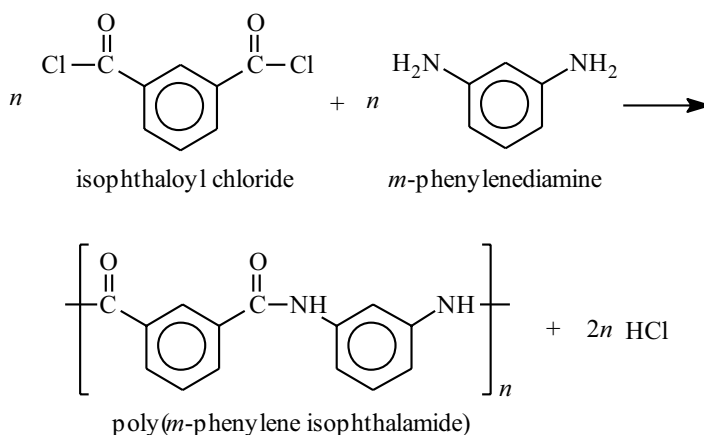


Figure 10-1 Synthesis of an aromatic polyamide, poly(*m*-phenylene isophthalamide) (Nomex).

The corresponding linear aromatic polyamide, poly(*p*-phenylene terephthalamide) (PPT) (Kevlar) (see Table 10-2), decomposes only above 500°C. Fibers of Kevlar have higher strength and modulus than steel on an equal weight basis. It has been used as a substitute for steel in belted radial tires (i.e., aramid fiber) and in the manufacture of mooring lines, as well as bullet-resistant vests and other protective clothing. Kevlar fiber is also used in the manufacture of fiber-reinforced plastics (see Chapter 7). Fabric made from Kevlar has been used as the skin covering for the first human-powered aircraft, the *Gossamer Albatross*, which was flown across the English Channel.

10.1.2 ABS

Another important thermoplastic with a major market share is ABS, which represents a resin containing acrylonitrile, butadiene, and styrene. ABS is a high-impact, high-HDT grade of polystyrene (see Table 10-1) that, together with the thermoplastic nylons, marks the boundary in price and performance between commodity and engineering thermoplastics. Uses for ABS include automotive applications, consumer products including small and large appliances, and business machines and telecommunications where good impact strength at moderate cost is required.

ABS was first developed in the 1950s by grafting a styrene-acrylonitrile copolymer (SAN) onto semi-crosslinked particles of polybutadiene (PBD). The PBD component of ABS increases impact strength over that of SAN alone. Developments during the 1960s led to a variety of methods to obtain ABS, including bulk, emulsion, and suspension polymerizations, although emulsion processes (free-radical polymerization of styrene and acrylonitrile in the presence of PBD or butadiene copolymers) are still the most widely used. A typical ABS formulation contains <15% butadiene and <20% acrylonitrile. The morphology of an ABS resin, as can be seen by scanning electron microscopy aided by staining the unsaturated sites of the butadiene component, varies with the production process. In general, immiscibility of PBD with SAN results in phase separation whereby PBD is dispersed in the form of small PBD particles contained within a matrix of SAN, as shown in Figure 10-2. Rubber particles produced by bulk or suspension processes are larger (0.5 to 5 μm) than those produced by emulsion methods (0.1 to 1 μm). Graft polymerization of SAN and PBD provides good interfacial adhesion between the dispersed and matrix phases. When ABS is mechanically deformed, the PBD particles act to modify the deformation process by either promoting craze formation (see Figure 10-2) or shear banding (see Section 4.4.1). As a result, the total energy-to-fail (i.e., impact strength) of ABS is increased over that of unmodified PS or SAN.

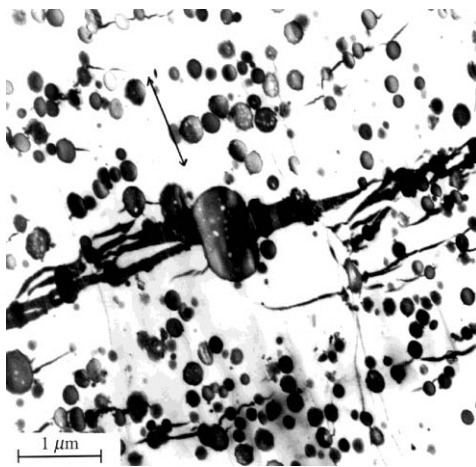


Figure 10-2 Electron micrograph of a section cut parallel to the surface of a deformed sample of ABS. The arrow shows the direction of applied strain. The dispersed phase (dark regions) consists of PBD particles. Crazes appear as dark lines running across the photograph. These craze structures are oriented perpendicular to the strain direction and pass through a number of PBD particles. Reproduced from M. Matsuo, *Polymer Engineering & Science*, 1969, **9**, p. 206 (1969). © 1969 Society of Plastics Engineering, Inc. Reprinted by permission of John Wiley & Sons, Inc.

10.1.3 Polycarbonates

The polycarbonate obtained from bisphenol-A is the engineering thermoplastic with the second-highest sales volume. Polycarbonate (PC) is an amorphous polymer with attractive engineering properties (see Table 10-1), including high impact strength, low moisture absorption, low combustibility, good dimensional stability, and high light transmittance (up to 88%). The latter property has resulted in the application of PC as an impact-resistant substitute for window glass. Another important application for PC is its use as the material for compact discs. Among the disadvantages of PC are its limited chemical and scratch resistance and a tendency to yellow with long-term ultraviolet exposure. These problems have been addressed by the introduction of silicone-coated and free-radical stabilized polycarbonate resins.

Polycarbonate can be synthesized by the polycondensation of bisphenol-A and phosgene, as shown in Figure 10-3. For each repeating unit that is formed, two molecules of hydrogen chloride are liberated. Alternatively, if the *sodium salt* of bisphenol-A is used in the polymerization, the by-product becomes sodium chloride rather than hydrogen chloride. This is an obvious advantage because the salt will precipitate out of the organic solvent used in the polymerization and, therefore, can

be easily and safely removed. In contrast, the production of strongly acidic hydrogen chloride requires special consideration for disposal and in the selection of construction material used in the polymerization reactor.

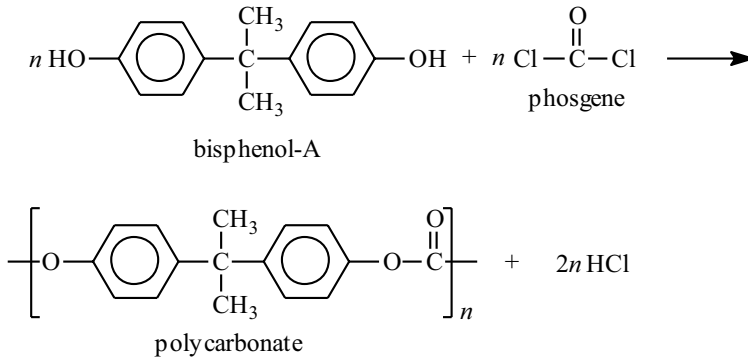
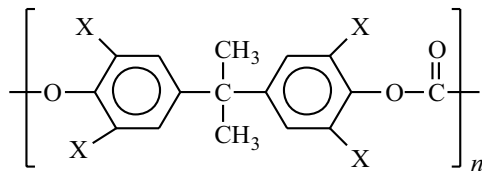


Figure 10-3 Synthesis of bisphenol-A polycarbonate by the polycondensation of bisphenol-A and phosgene.

Other polycarbonates can be polymerized by modified interfacial condensation or by melt transesterification of tetrasubstituted bisphenols. These polycarbonates have the general structure



where X represents a halogen, especially bromine, or a methyl group. One example is tetramethylbisphenol-A polycarbonate (TMPC), X = CH₃, which has a higher heat-distortion temperature (HDT) and better hydrolytic stability than PC. The HDT or T_g is a result of the greater rigidity of the TMPC chain due to the steric hindrance of the substituent methyl groups. One disadvantage of TMPC is its low impact resistance; however, this may be improved through blending with impact-resistant resins such as HIPS, ABS, and MBS (see Section 7.2.2). The styrene component of these impact modifiers forms a homogeneous phase with TMPC. Impact-modified grades of TMPC can also be used to increase the HDT of PVC. Tetrabromobisphenol-A polycarbonate (TMBPC), X = Br, can be blended with PC to increase HDT. Copolymers of bisphenol-A and tetrabromobisphenol-A or tetrachlorobisphenol-A provide better flame retardancy. The polycarbonate obtained from cyclohexanonebisphenol can be blended with PC to increase the HDT from 160° to 205°C.

10.1.4 Modified Poly(phenylene oxide)

Another large-sales-volume engineering thermoplastic having substantially higher HDT than PC is poly(2,6-dimethyl-1,4-phenylene oxide) or PPO, which is obtained from the free-radical, step-growth, oxidative-coupling polymerization of 2,6-xyleneol [1], as shown in Figure 10-4.

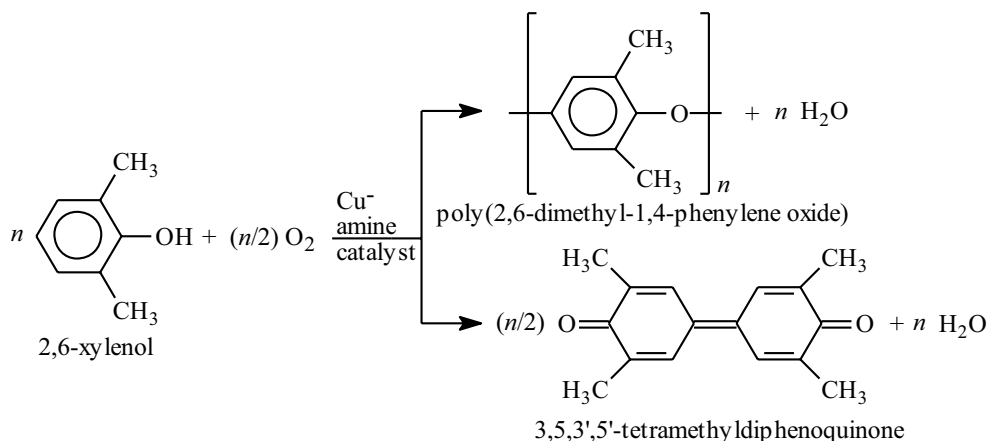


Figure 10-4 Oxidative-coupling polymerization of 2,6-xyleneol. 3,5,3',5'-tetramethyldiphenylidenequinone (DPQ) is a by-product of this polymerization. The concentration of DPQ impurity depends upon the choice of catalyst and conditions of the polymerization. For example, the yield of DPQ is about 3 wt% using a cupric formate and pyridine catalyst.

A related polymer, poly(2,6-diphenyl-1,4-phenylene oxide), originally considered for fiber applications, has limited commercial use as a packing for GC columns. A good review of oxidative-coupling polymerization and the commercialization of PPO has been given by Hay [2]. PPO has many attractive properties (see Table 10-1), including high impact strength, chemical stability to mineral and organic acids, and low water absorption. A limitation that had restricted its commercialization is its high glass-transition temperature ($T_g \approx 214^\circ\text{C}$) in relation to the susceptibility of its methyl groups to thermal oxidation, which poses problems for melt processing. For these reasons, commercial resins (Noryl) are made by blending PPO with high-impact polystyrene (HIPS), which serves to reduce the processing temperature, although heat-distortion temperature is reduced as well. Like impact-modified grades of TMPC, the styrene component of HIPS forms a homogeneous phase with PPO. Noryl resins are also available in flame-retardant and filled grades and are used in many electrical and automotive applications.

In addition to PPO/HIPS blends, commercial resins of PPO and polyamides (PA) are available for improved thermal stability required for certain electrical and electronics applications. In this case, a compatibilizer (see Section 7.1.1) such as a PA-grafted styrene–maleic anhydride copolymer serves to improve blend properties. Blends of PPO with polyesters and polyolefins offer better dimensional stability than PPO/PA resins at the expense of lower thermal stability.

10.1.5 Acetal

Polyacetal, sometimes known simply as acetal or as polyformaldehyde and polyoxymethylene (POM), may be the first universal polymer. In 1987, mass spectral data revealed the presence of POM in the gas cloud of Halley's comet. On earth, POM may be obtained by the anionic or cationic polymerization of formaldehyde or by the cationic ring-opening polymerization of trioxane, as shown in Figure 10-5. The highly regular chain structure of polyacetal contributes to its high crystallinity and excellent chemical resistance. Properties of a typical acetal resin are given in Table 10-1.

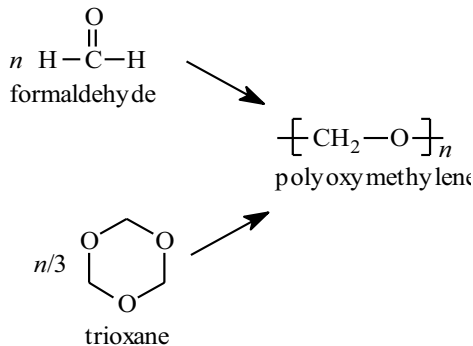


Figure 10-5 Two routes for the synthesis of polyoxymethylene.

Acetal is degraded by UV radiation, leading to color change and loss of toughness and tensile strength; however, acetal can be stabilized against UV degradation by the usual UV absorbers and hindered-amine light stabilizers (HALS). Carbon black and titanium dioxide fillers are also effective for light and UV screening. A particularly attractive property of acetal is its high dimensional stability (creep resistance), which allows acetal to be used as a replacement for metals in gears and machine parts. Rubber-toughened grades of polyacetals are available for applications where higher impact strength, flexural strength, and tensile-fracture resistance are desired. Automotive and electrical/electronic use accounts for approximately two-thirds of worldwide acetal production. Another important consideration for the

continued growth of acetal resins is that acetal can be chemically recycled to monomer.

10.1.6 Polysulfones

Polysulfones comprise a class of engineering thermoplastics with high thermal, oxidative, and hydrolytic stability and good resistance to aqueous mineral acids, alkalis, salt solutions, oils, and greases. Their high biocompatibility and ability to be sterilized by a variety of techniques make them highly suitable for medical applications [3]. Polysulfones also have high permeability and permselectivity which make them attractive as membrane polymers in gas separations (see Section 12.1.2). Chemical structures and representative properties of three aromatic polysulfones are given in Tables 10-3 and 10-4, respectively.

Table 10-3 Chemical Structures of Commercial Polysulfones

Polysulfone	Structure of Repeating Unit
Polysulfone	
Polyethersulfone	
Polyphenylsulfone	

Table 10-4 Representative Properties of Commercial Polysulfones

Property	PSF	PES	PPS
Specific gravity (D 1505)	1.25	1.37	1.29
Tensile strength at yield, MPa ^a (D 638)	70.3	84.1	71.7
Tensile modulus, GPa ^b (D 638)	2.48	2.70	2.14
Elongation to break, % (D 638)	50–100	40–80	60
Flexural strength, MPa ^a (D 790)	106	129	85.5
Flexural modulus, GPa ^b (D 790)	2.69	2.57	2.30
Impact strength (notched Izod), J m ⁻¹ D 256 ^c	69	85	641
HDT, °C, at 455 kPa (66 psi) (D 648)	174	203 ^d	200–204

^a To convert MPa to psi, multiply by 145.

^b To convert GPa to psi, multiply by 1.45×10^5 .

^c To convert J m⁻¹ to lbf in.⁻¹, divide by 53.38.

^d Reported at 1.82 MPa (264 psi).



Figure 10-8 UDEL polysulfone is used for the transparent containers holding the potassium hydroxide electrolyte of a nickel–cadmium battery for electrical backup in railroad applications. The polysulfone container is unaffected by the alkaline electrolyte and is resistant to shock, vibration, and moisture. Courtesy of Solvay Advanced Polymers, L.L.C.

10.1.7 Poly(*p*-phenylene sulfide)

Poly(*p*-phenylene sulfide) (PPS), or poly(thio-1,4-phenylene), is another important engineering thermoplastic with many attractive properties (Table 10-1), such as outstanding chemical resistance, good electrical properties, excellent flame retardance, low coefficient of friction, and high transparency to microwave radiation. As illustrated in Figure 10-9, PPS can be prepared by the polycondensation of *p*-dichlorobenzene and sodium sulfide.

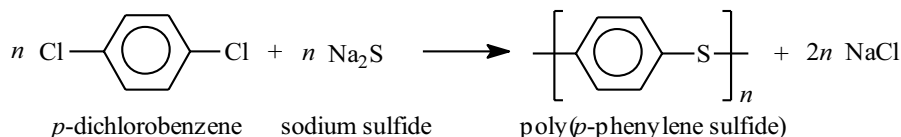


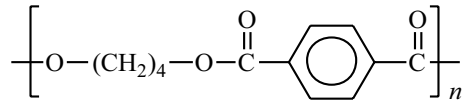
Figure 10-9 Synthesis of poly(*p*-phenylene sulfide).

PPS is highly crystalline with a relatively high melting temperature (285°C) and is insoluble in organic solvents below 200°C. This means that special processing techniques must be used to manufacture products from this engineering resin. For example, PPS coatings are obtained by spraying an aqueous *slurry* of PPS particles and heating the coated object to temperatures above 370°C. PPS can be injection- and compression-molded at high temperatures (300° to 370°C) at which PPS particles soften and undergo an apparent crosslinking reaction to yield a totally

insoluble product. Principal applications of PPS include cookware, bearings, and pump parts for service in various corrosive environments. PPS is frequently produced as reinforced grades (typically filled with glass fiber and mixtures of minerals such as talc and chalk) that have higher strength and HDT.

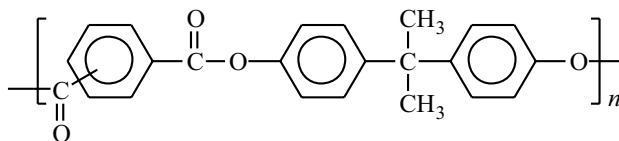
10.1.8 Engineering Polyesters

The slow rate of crystallization of poly(ethylene terephthalate) (PET), which is widely used as a textile fiber (see Section 8.2.3), normally results in poor surface quality and release properties of molded parts. Modified grades of PET have enabled penetration of this polyester into the beverage-bottle market and use in other molding applications (see Section 9.1.3). In the non-bottle market, PET is in competition with a related engineering polyester, poly(butylene terephthalate) (PBT)



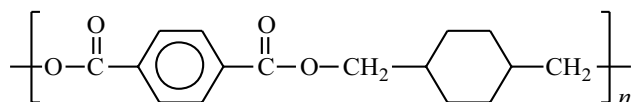
which was introduced by several companies in the early 1970s. Principal applications for PBT include injection-molded parts for electrical and electronic use and for automotive markets. Both polyesters, like polycarbonates, are moisture sensitive (hydrolytic instability) but have high strength, rigidity, and toughness, excellent dimensional stability, low coefficient of friction, abrasion resistance, and good resistance to chemicals and grease.

In the late 1970s, an all-aromatic polyester (polyarylate, PAR) produced by the condensation polymerization of bisphenol-A and mixed phthalic acids



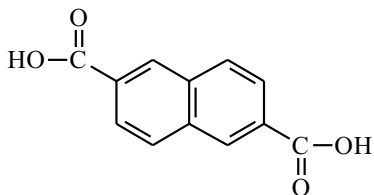
was marketed in the United States. Unlike PET and PBT, polyarylate is amorphous and has high clarity, as well as high heat-distortion temperature (T_g in the range of 150° to 200°C), UV stability, inherent flame retardance, and good electrical properties. Typical outdoor applications for polyarylate include solar collectors, safety devices, construction, and transportation. Other uses include the manufacture of plastic parts for electronic and electrical hardware such as lighting fixtures. Unfortunately, a variety of factors, including competition with polysulfone and polycarbonate and poor processability, have virtually eliminated the market for PAR.

Another engineering polyester gaining recent interest is poly(dimethylene cyclohexane terephthalate) (PCT)

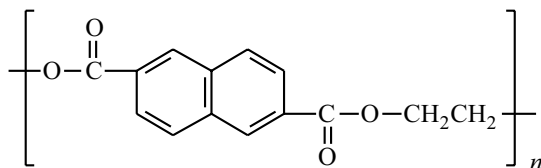


which has high thermal stability and finds applications in some electronic components. Like PET, PCT crystallizes slowly and, therefore, nucleating agents and “hot” oil-cooled molds must be used in order to process PCT in a reasonable time scale.

Recently, interest has focused on the monomer naphthalene dicarboxylate (NDC)



which can be copolymerized with DMT to yield a copolyester with better barrier and heat resistance for bottle and packaging applications. NDC can also be polymerized (with ethylene glycol) to yield poly(ethylene naphthalate) (PEN)

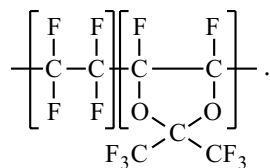


which can be blended with PET to improve properties. PEN can be extruded and blow-molded and has better mechanical strength, higher heat and chemical resistance, better dimensional, thermal, UV, and hydrolytic stability, and improved barrier properties compared to PET. The higher thermal resistance of PEN (T_g of 120°C compared to approximately 78°C for PET) expands the potential market for polyester bottles to those such as baby food jars that need to be steam-sterilized. Current applications for PEN include industrial fiber cord for rubber reinforcement, blood evacuation tubing, and electronic film, such as long-lasting video-recording tape. Other potential markets include electrical and electronic parts (e.g., motor insulation, magnetic tapes, and capacitors) and microwaveable packaging for medical and other applications.

10.1.9 Fluoropolymers

Among the most important fluoropolymers is polytetrafluoroethylene (PTFE or Teflon), obtained by the emulsion free-radical polymerization of tetrafluoroethylene (TFE). Teflon was accidentally discovered by Roy J. Plunket and Jack Rebok who had been working on new refrigerants at DuPont in 1938. On the morning of April 6, Plunket and Rebok noticed that TFE gas stored in a high-pressure vessel in dry ice solidified into a smooth, waxy white powder that seemed impervious to liquids and could not be charred or melted under ordinary conditions. Commercially produced PTFE, introduced in 1950, is highly dense (2.1 to 2.3 g cm⁻³) with high-temperature stability, low-temperature flexibility, an extremely low coefficient of friction, low dielectric constant and dissipation factor, and chemical inertness. Many of these properties are similar to those of PPS described earlier. Also like PPS, PTFE is extremely difficult to process by conventional techniques. Limited processability is attributed to its extremely high crystallinity and high crystalline-melting temperature ($T_m = 327^\circ\text{C}$), resulting from its highly regular structure and unusually high molecular weight. For coating applications, PTFE is sintered at high temperature and pressure. Recently, researchers at ETH in Zurich have shown that it is possible to melt-process PTFE from medium-viscosity/molar mass micropowders, obtained by γ - or electron-beam irradiation, into a product with good mechanical properties [4].

Improvement in melt processability can also be obtained by incorporating a small concentration of a comonomer such as hexafluoropropylene (Teflon FEP), ethylene (ETFE), or more perfluoroalkoxy (PFA) fluorocarbon resins. In these cases, copolymerization serves to reduce crystallinity. A more recent example of an important TFE copolymer is “amorphous” Teflon (TEFLON-AF)



This fluoropolymer can be made by statistical copolymerization of TFE with a fluorinated cyclic ether, perfluoro-(2,2-dimethyl-1,3-dioxole). Incorporation of the cyclic ether prevents crystallization and contributes to better processability, although at a sacrifice in some properties.

In addition to PTFE, several other partially fluorinated polymers listed in Table 10-5 have achieved commercial importance. These include polychlorotrifluoroethylene (CTFE or Kel), which is also available as a copolymer with ethylene or vinylidene fluoride. Applications include electrical insulators, gaskets and seals, and pump parts. Poly(vinylidene fluoride) (PVDF or Kynar), also available as a copolymer with hexafluoroisobutylene (HFIB), is a crystalline polymer ($T_m = 170^\circ\text{C}$) that

finds primary applications in coatings, gasket material, wire and cable insulation, and extruded vinyl siding for houses. Poly(vinyl fluoride) (PVF or Tedlar) is another highly crystalline polymer ($T_m = 197^\circ\text{C}$) that can provide tough, flexible films with excellent outdoor weatherability and good abrasion and stain resistance. Applications include protective coatings for materials that are used in the building industry.

Table 10-5 Chemical Structures of Some Important Fluoropolymers

Fluoropolymer	Repeating Unit
Polytetrafluoroethylene	$-\left[\text{CF}_2-\text{CF}_2 \right]-$
Fluorinated ethylene-propylene copolymer (FEP)	$-\left[\text{CF}_2-\text{CF}_2 \right]_m - \left[\text{CF}_2-\underset{\text{CF}_3}{\text{CF}} \right]_n-$
Polychlorotrifluoroethylene (CTFE)	$\left[\begin{array}{c} \text{Cl} \\ \\ \text{CF}_2-\text{C} \\ \\ \text{F} \end{array} \right]$
Poly(vinylidene fluoride) (PVDF)	$\left[\begin{array}{c} \text{F} \\ \\ \text{CH}_2-\text{C} \\ \\ \text{F} \end{array} \right]$
Poly(vinyl fluoride) (PVF)	$\left[\begin{array}{c} \text{F} \\ \\ \text{CH}_2-\text{CH} \end{array} \right]$

Fluorinated polymers also find significant applications as highly thermally and chemically resistant elastomers, as discussed in Section 9.2.2. These include amorphous copolymers of vinylidene fluoride and hexafluoropropylene, which can be crosslinked in the presence of diamines and basic oxides through dehydrofluorination followed by amine addition. Elastomers can also be made from copolymers of TFE and perfluoroalkyl vinyl ethers, such as perfluoromethyl vinyl ether, and copolymers of vinylidene fluoride and hexafluoroisobutylene. Network formation can be achieved by incorporation of comonomers containing nitrile pendant groups, which when heated can form triazine structures.

10.2 Specialty Polymers

Specialty polymers have small but important commercial markets in the aerospace and electronics industries and as materials for biomedical applications. The most important of these include polyimides, ionomers, polyaryletherketones, polyorganophosphazenes, certain aromatic polyesters and high-performance fibers, polyacetylenes and other electrically conductive polymers, and dendrimers.

10.2.1 Polyimides and Related Specialty Polymers

Polyimides represent an important class of high-temperature, solvent-resistant polymers. Typical uses for polyimides include electronics, sleeve bearings, and valve seatings, and as the matrix component of graphite composites for compressor vanes in jet engines and other aerospace applications. Often, polyimides are formed by a two-stage process. The first step involves the polycondensation of an aromatic dianhydride and aromatic diamine to form an intermediate poly(amic acid). Dehydration of the poly(amic acid) at elevated temperatures yields the polyimide (PI) structure. A representative polymerization of a polyimide is shown in Figure 10-10. Unlike the intermediate poly(amic acid), the cured (i.e., fully imidized) PI is insoluble and infusible and has high temperature and oxidative stability and good electrical-insulation properties and radiation resistance.

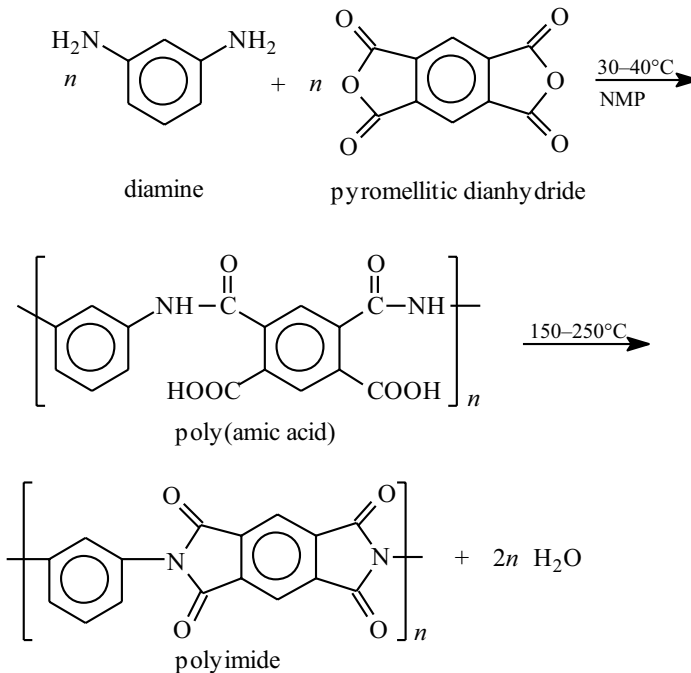
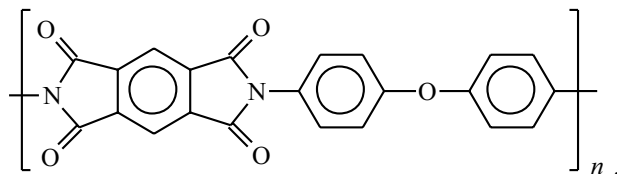
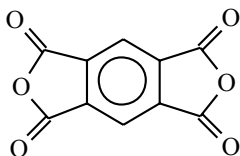


Figure 10-10 Polymerization of a polyimide.

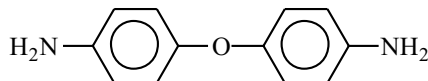
A large variety of PI structures are possible, limited only by the number of available dianhydrides and diamines. An example of a commercially important PI is a polypyromellitimide available as film called Kapton (DuPont), whose imidized structure is



Kapton is obtained by the condensation polymerization of pyromellitic anhydride



and 4,4-diamino diphenyl ether



Properties of Kapton are given in Table 10-6.

Table 10-6 Properties of a Polyimide, Polyetherimide, and Poly(amide-imide)

Property	PI ^a	PEI ^b	PAI ^c
Density (g cm ⁻³)	1.42	1.27	1.42
% Elongation at 23°C			15
at yield		7–8	
at break	70	60	
Flexural modulus (GPa), tangent at 23°C		3.31	5.0
Flexural strength (MPa)	—	—	241
HDT, °C at 1.82 MPa (264 psi)	—	200	278
Impact strength, Izod (J m ⁻¹)			
notched	—	53.4	144
unnotched	—	1335	1068
Tensile modulus (GPa), 1% secant	3.0	3.0	4.8
Tensile strength (MPa) at 23°C, at yield	172	105	192
<i>T_g</i> (°C)	385	217	—
Water absorption, % over 24 h and RT and 40% RH	2.9	0.25	0.33

^a Kapton H.

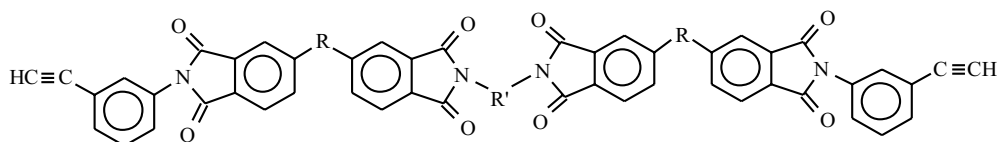
^b Ultem 1000.

^c Torlon 4203L; contains 3% TiO₂ and 0.5% fluorocarbon.

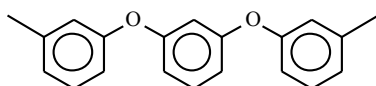
Some disadvantages of these “imidizable” polyimides are the limited shelf life of the precursor poly(amic acids) and possible structural weakness of the fully im-

idized product due to void formation as a result of water release in the curing process. In addition, some thermoplastic polyimides are available. These polyimides are fully imidized but can be melt-processed at high temperatures or can be solution-cast. Solubility in relatively nonpolar liquids is achieved by incorporation of aromatic polyether linkages in the backbone or pendant phenyl and alkyl groups introduced through appropriate selection of the aromatic diamine.

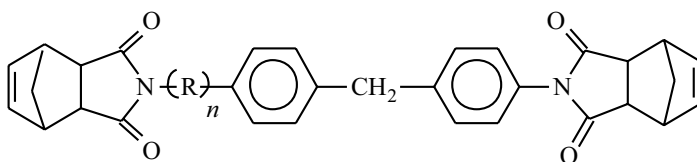
Another approach to PI synthesis, particularly suited for structural composites, is the use of thermoset PIs. A thermoset PI is one prepared by heating a fully imidized PI-prepolymer having a reactive functional group at each end that can react with another prepolymer. An example of a thermoset PI is Thermid resin, which uses acetylene-terminated prepolymers for network formation. The structure of Thermid is given as



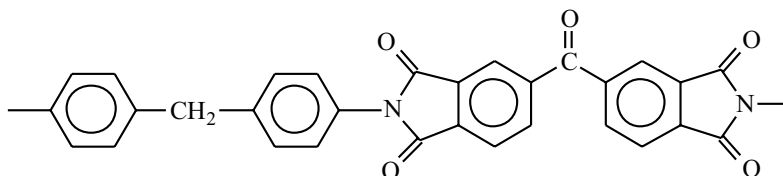
where R is a carbonyl (C=O) or a hexafluoropropane (6F) functionality, $C(CF_3)_2$, and R' is the aromatic group



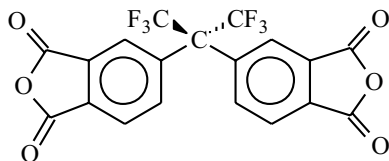
Another important example of a thermoset PI is PMR-15, which has been widely used as the matrix for graphite composites for aerospace applications. PMR-15 uses a norbornene end functionality for network formation



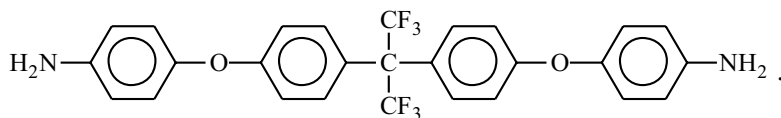
where R ($n \approx 2$) has the aromatic structure



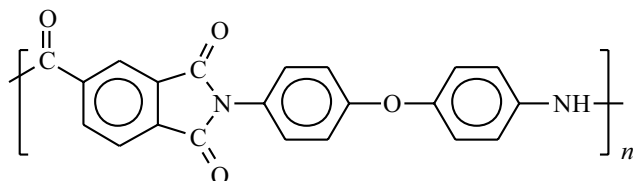
In general, polyimides having excellent thermal and thermooxidative stability (although at much higher cost) can be obtained from fluorinated dianhydrides, especially 6FDA*



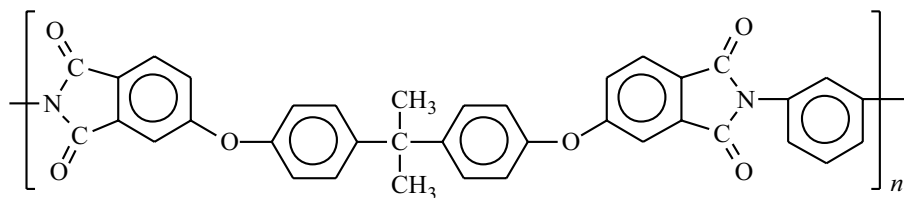
or fluorinated diamines such as 2,2-bis[(4-aminophenoxy)phenyl]hexafluoropropane



Poly(amide-imide) and Polyetherimide. To improve the melt processability of polyimides, the basic imide structure can be combined with more flexible aromatic groups, such as aromatic ethers and amides. For example, poly(amide-imide) (PAI) (e.g., Torlon)



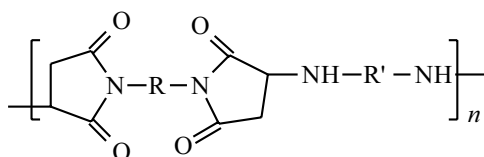
is obtained from the polycondensation of trimellitic anhydride (TMA) and an aromatic diamine (e.g., 4,4'-oxydianiline). Another imide-type engineering thermoplastic is polyetherimide (PEI, Ultem), obtained by a nitro-displacement reaction [5] involving bisphenol-A, 4,4'-methylene-dianiline, and 3-nitrophthalic anhydride.



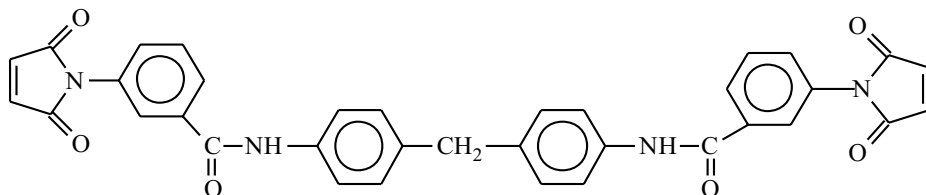
* 5,5'-(2,2,2-trifluoro-1-(trifluoromethyl)ethylidene)-bis(1,3-isobenzofuranedione).

Both PAI and PEI have high heat-distortion temperature, tensile strength, and modulus. Properties of a representative polyimide (Kapton H) and two representative grades of PEI and PAI are compared in Table 10-6. Once imidized, Kapton is no longer melt-processable, unlike PAI and PEI, which are compromised by lower softening temperatures (T_g or HDT). Kapton has an HDT of 357°C and a continuous-use temperature of ca. 270°C. One advantage of PAI and PEI over Kapton is their lower water absorption, which is especially important for composite applications. Applications for PAI and PEI include high-performance electrical and electronic parts, microwave appliances, and under-the-hood automotive parts.

Polybismaleimides. A related imide-type polymer is the polybismaleimide (Kerimid, Kinel). A repeating unit can be represented as



where R and R' represent a variety of aromatic groups. Polybismaleimide is obtained by a (Michael) *addition* of diamine to the unsaturated sites at the ends of a bismaleimide having a structure similar to



Applications for polybismaleimides include use as composite resin for filament winding and laminates (see Chapter 7), friction pads, gears, and bearings.

Polybenzimidazole. Polybenzimidazole (PBI)* is a product of the polycondensation of an aromatic tetramine and an aromatic dicarboxylic acid or derivative [6]. An example of the synthesis of a polybenzimidazole is given in Figure 10-11. As a class, polybenzimidazoles have very high thermal and hydrolytic stability but are often infusible. PBI can be used in fiber form for high-temperature composite and other applications (see Section 10.2.8). It is also being actively considered as a fuel-cell membrane as discussed in Section 12.1.2.

* Poly[2,2'-(*m*-phenylene)-5,5'-bibenzimidazole].

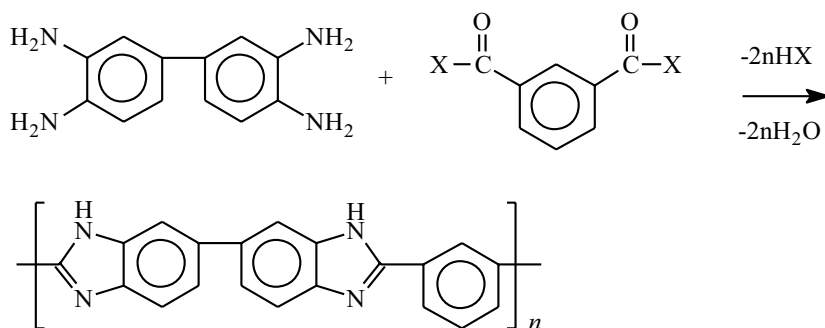


Figure 10-11 Synthesis of a polybenzimidazole from 3,3'-diaminobenzidine and an aromatic dicarboxylic acid. X represents one of several possible reactive sites including OH, Cl, OCH₃, and OC₆H₅.

Ladder Polymers. At the extreme in high-temperature stability are polymers that incorporate highly fused-ring backbones such as polyimidazopyrrolones. They are obtained by a two-step cure process involving the initial condensation of an aromatic tetracarboxylic acid and aromatic tetramine (Figure 10-12). Such materials, which are sometimes known as *ladder polymers* because their fused-ring structure resembles the rungs of a ladder, are capable of withstanding temperatures in excess of 500°C (see also Section 6.1.1). The first ladder polymers were synthesized in the mid-1960s due to their potential for high thermal stability. More recently, conjugated ladder polymers have been studied for their linear and nonlinear optical properties (see Section 12.4.1) [7].

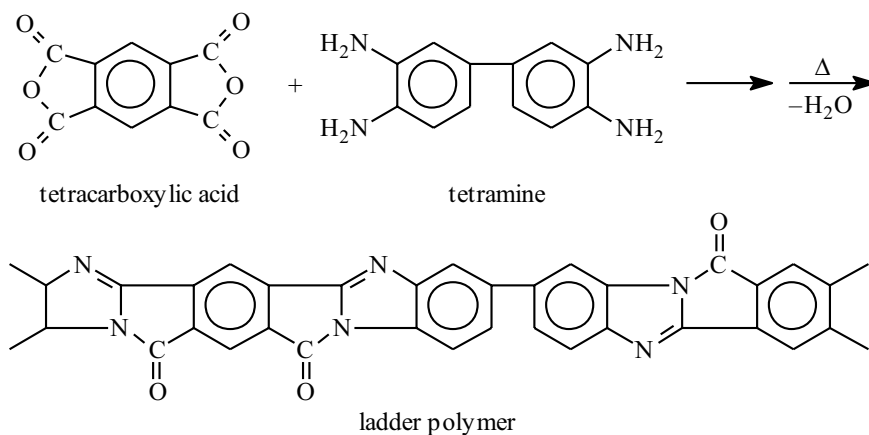
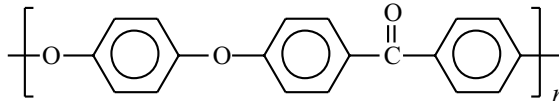


Figure 10-12 Polymerization of a ladder polymer, polyimidazopyrrolone.

10.2.2 Polyaryletherketones

A important entry into the engineering thermoplastic market is the poly(aryl ether ketones) (PAEK), of which polyetheretherketone (PEEK, Victrex)



is the most important [8]. As indicated by the data given in Table 10-7, PEEK is semicrystalline but can be melt-processed at elevated temperatures. Attractive properties include good abrasion resistance, low flammability and emission of smoke and toxic gases, low water absorption, and resistance to hydrolysis, wear, radiation, and high-temperature steam. The high solvent resistance, good impact strength, and good thermal stability (maximum continuous working temperature of 260°C) of PEEK make it a good candidate as a thermoplastic matrix for graphite composites (see Section 7.3). Other applications include solvent-resistant tubing for chromatography, wire and cable insulation for hostile environments, and magnet-wire coating.

High-molecular-weight PEEK can be synthesized by the solution polycondensation of alkali bisphenates with activated aromatic dihalides (typically difluoride) at high temperatures, as shown in Figure 10-13. A wide variety of other arylene ether homopolymers and copolymers with T_g values ranging from 114° to 310°C can be prepared by the nucleophilic displacement of aromatic dihalides and potassium bisphenates [9].

Table 10-7 Typical Properties of PEEK

Property	Value
T_g (°C)	143
HDT, °C at 1.82 MPa (264 psi)	148
Crystallinity, %	
Typical	20–35
Maximum	48
Heat of fusion, ΔH_f (J g ⁻¹)	130–161
Density (g cm ⁻³)	
Amorphous	1.263
Crystalline	1.400
Water absorption, % over 24 h and 40% RH	0.15
Solubility parameter (cal/cm ³) ^{1/2}	9.5
Tensile strength (MPa) at 23°C	91.0
Elongation at 23°C, %	150
Flexural modulus at 23°C, GPa	3.89
Impact strength, Charpy (J m ⁻¹)	1388

10.2.4 Ionic Polymers

Ionic sites may be introduced into polymers through chemical modification or copolymerization. Ionic polymers derived from synthetic organic polymers and containing up to 10 to 15 mol % ionic content are called *ionomers*. Those with higher ionic content are called *polyelectrolytes*. Polyelectrolytes are soluble in water but insoluble in common organic solvents. Typical applications for ionomers include ion-exchange resins, membranes for liquid and facilitated gas separations, superacid catalysts, and most importantly as separators in chloralkaline electrolytes.

Ionic sites are typically pendant carboxylic or sulfonic acid groups that are partially or completely neutralized to form the polymeric salt. Counterions may be sodium, zinc, ammonium, or a halide. Typical nonionic polymer backbones include polyethylene, polystyrene, and copolymers of fluorocarbons such as TFE. Due to the general incompatibility of ionic and nonionic segments, micro-phase separation of the ionic groups is typical of ionic polymers. Small aggregates consisting of only ionic material are termed *multiplets*, while larger aggregates that also include nonionic material are called *clusters*. Multiplets, consisting of only a few ions or ion pairs, act as moderately strong, temporary, ionic crosslinks. The larger clusters also act as mechanical reinforcement.

The introduction of ionic groups can have significant effects on the properties of polymers. For example, ionic sites can increase T_g , modulus, and melt viscosity. The extent of property modification depends upon the dielectric constant of the backbone, the position and type of ionic group, the type of counterion, ionic concentration, and the degree of neutralization. The concentration of ionic groups and the strength of interaction between the anion and cation determine the increase in T_g with a relationship given as

$$T_g = \frac{cq}{a} \quad (10.1)$$

where c is the concentration of ionic repeat units in the backbone, q is the charge of the counterion, and a is the distance of closest approach between the centers of charge of anion and cation. Generally, T_g is observed to increase 2° to 10°C per mol % of ionic repeat units.

Ionomers. A common commercial ionomer is Surlyn, a copolymer of ethylene and about 15% methacrylic acid. About 33% of the methacrylic acid comonomers are neutralized with sodium hydroxide to produce the sodium salt, as illustrated in Figure 10-14. Ionic bonding provides a tough material, often used for covering golf balls as a replacement for gutta percha, in packaging applications such as a coating for safety bottles to store hazardous chemicals, and in the manufacture of automotive bumper strips and guards.

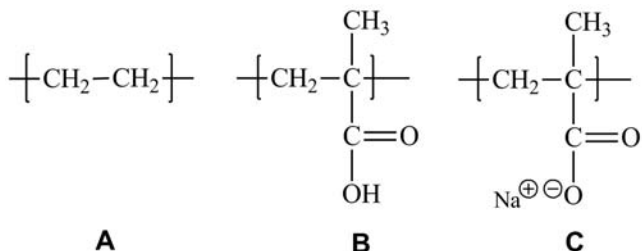


Figure 10-14 Comonomer units in Surlyn A. **A.** Ethylene. **B.** Methacrylic acid. **C.** Sodium salt of methacrylic acid.

Another important class of ionomers is the *perfluorosulfonate ionomers* (PFSI). These are copolymers of TFE and a perfluorinated vinyl ether containing a terminal sulfonyl fluoride (SO_2F) group, as shown in Figure 10-15. The most important commercial PFSI product is Nafion ($y = 1$ in Figure 10-15) manufactured by DuPont, while a related PFSI ($y = 0$) has been developed by Dow Chemical Company. Commercial PFSI films are extruded but can also be solution-cast under special conditions. After film formation, the sulfonyl fluoride groups are converted to sulfonate groups by reaction with sodium or potassium hydroxide, with further conversion to the commercial sulfonic acid (SO_3H) form (Nafion-H). Other ionic forms (e.g., Na^+ , Li^+ , K^+ , Ag^+ , Ca^{2+} , and Al^{3+} salts) can be obtained by ion exchange with the appropriate salts. Nafion has selective permeability to ions and can, therefore, be used in the production of chlorine and caustic by electrolysis of salt solutions; it has also been evaluated for use in many other applications, such as a membrane for gas separations, organic electrosynthesis, fuel cells, electrodes, separation of amino acids, controlled drug release, and biosensors (see Section 12.1.2).

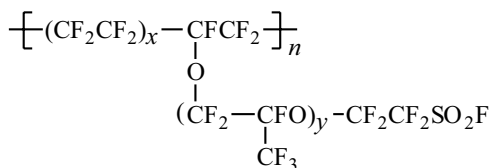
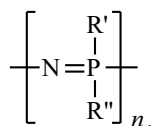


Figure 10-15 Structure of Nafion perfluorinated ionomer.

10.2.5 Inorganic Polymers

In addition to the polysiloxanes (Section 9.2.2), there are several other polymers having an all-inorganic backbone that have commercial potential for some specialized applications. These include poly(organophosphazenes) and polysilastyrene.

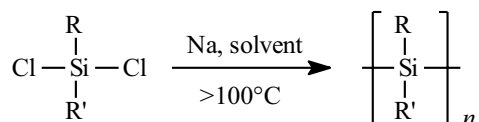
Poly(organophosphazenes). The structure of a poly(organophosphazene) repeat unit, having substituent groups R' and R'' , is



Symmetric substitution (i.e., $\text{R}' = \text{R}''$) yields crystalline polymers while asymmetric substitution ($\text{R}' \neq \text{R}''$) yields noncrystalline rubbery materials suitable for elastomer application. Properties range from highly solvent-resistant, low-temperature flexible elastomers to glassy materials that can be fabricated in film and fiber form. Potential applications of poly(organophosphazenes) include elastomers, coatings, and biomedical encapsulation [11, 12].

Poly(organophosphazenes) may be prepared by substitution of poly(dichlorophosphazene), which is obtained from the radiation or plasma polymerization of hexachlorocyclotriphosphazene. The intermediate polymer, poly(dichlorophosphazene), is unstable due to its high susceptibility to hydrolysis. In the presence of even atmospheric moisture, poly(dichlorophosphazene) decomposes to ammonium phosphates and phosphoric acids. Fortunately, the active chlorine sites can be readily substituted by nucleophiles such as alkoxides, aryloxides, and amines to yield a wide variety of high-molecular-weight polymers that are chemically and thermally stable. Various synthesis routes to prepare poly(organophosphazenes) were discussed in Section 2.4.1.

Polysilanes. Polysilanes, or polysilylenes, are inorganic polymers with an all-silicon backbone. They can be polymerized by a Wurtz-type reaction of a dichlorosilane [13, 14]



where R and R' are organic substituents. Depending upon the type of side group, polysilanes can be amorphous or highly crystalline. Glass-transition temperatures can range from -50° to 120°C . Polysilanes have good high-temperature thermal stability (up to 250°C or more), are inert to oxygen, and are resistant to hydrolysis. Applications include use as UV photoresists, polymeric photoinitiators, nonlinear optical material, and ceramic precursors. A silane copolymer, polysilastyrene, can be prepared from the solution copolycondensation of dimethyldichlorosilane and phenylmethyldichlorosilane. It is highly soluble and can be spun into fibers, which when heated in an inert atmosphere at very high temperature are converted to a variety of gaseous by-products and β -silicon carbide filaments, as shown in Figure 10-16. Silicon-carbide fibers have extreme strength, as well as exceptional chemical and heat resistance, which makes them suitable for many aerospace applications.

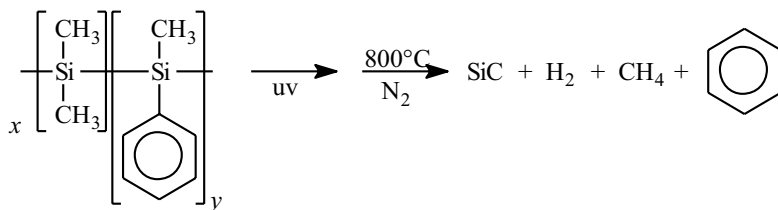


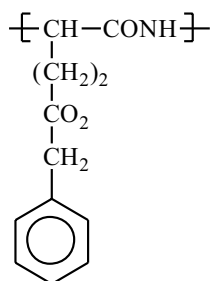
Figure 10-16 Pyrolysis of polysilastyrene to give silicon carbide.

10.2.6 Liquid-Crystalline Polymers

Low-molecular-weight liquid crystals have been known since 1888 when it was shown that heating could cause certain cholesteryl esters to change their optical state from colored and opaque to clear. Flory suggested in 1956 that polymers containing long, rigid units could form anisotropic ordered solutions above some minimum concentration depending upon temperature and the axial (length/diameter) ratio, x , of the polymer chain [15]. According to Flory's lattice theory, the threshold volume fraction, ϕ , is given as

$$\phi = \frac{8}{x} \left[1 - \frac{2}{x} \right] \approx \frac{8}{x} \quad (10.2)$$

for high values of x . Above the critical threshold volume fraction, a stable anisotropic phase is formed from solutions and melts of rod-like polymers. In 1974, liquid-crystal behavior for a polymeric system was first observed in a concentrated solution of poly(benzyl L-glutamate)



which forms a rod-like α -helical conformation in a variety of organic solvents.

The rigid units or *mesogens* of a liquid-crystalline polymer (LCP) can lie along the polymer backbone or be attached to the backbone as a substituent group (i.e., side-chain LCP) [16]. Polymers that form liquid-crystalline organization in solution are termed *lyotropic*, while those that form from the melt are called *thermotropic*. There are three recognized categories of liquid-crystalline structures. As

illustrated in Figure 10-17, the most ordered structure, the *smectic state*, is observed when all the mesogens are arranged in a parallel and lateral order. The smectic state is rare and has been observed only for thermotropic polymers. More common for polymers is the *nematic state*, in which there is parallel but not lateral order. Aromatic polyamides (aramid) form a nematic liquid-crystalline state in concentrated solution. If mesogens are oriented parallel to one another but the directions vary from one layer to another, the liquid-crystal structure is termed *cholesteric*.

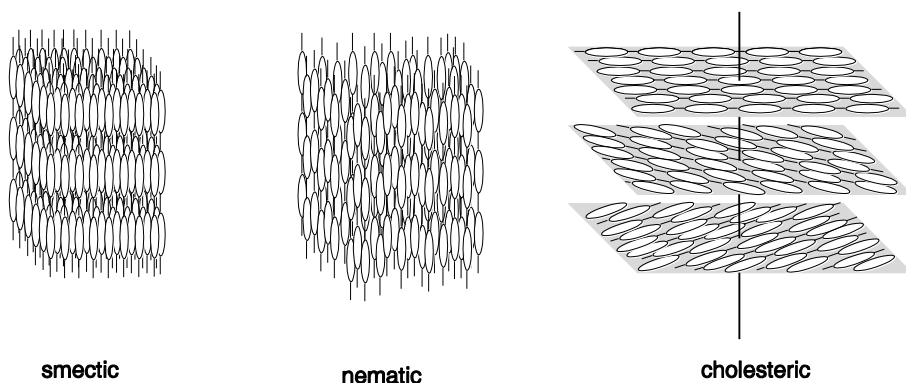
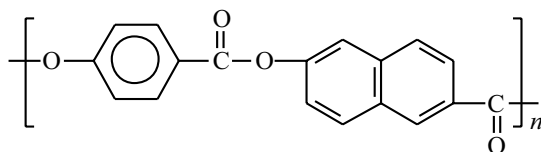
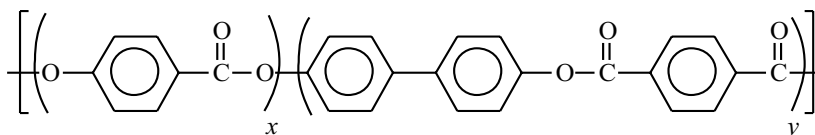


Figure 10-17 Liquid-crystal structures: smectic, nematic, and cholesteric. From R. W. Lenz and J.-I. Jin, *Liquid Crystal Polymers: A New State of Matter*. Polymer News, 1986. **11**: p. 201 Copyright 1986. Reproduced by permission of Taylor & Francis, Inc. <http://www.routledge.com>.

Liquid-crystalline polyesters and copolyesters may have been recognized as early as 1965. Liquid-crystal polyesters have highly aromatic structures such as Vectra (Hoechst Celanese)



and the thermotropic polyester Xydar (Amoco)



that is made from the polycondensation of *p*-hydroxybenzoic acid (HBA), *p,p'*-biphenol, and terephthalic acid. Such stiff-chain structures lead to ordering of the chains of LCPs in a manner similar to low-molecular-weight liquid crystals.

In general, LCPs are manufactured in a stepwise polycondensation by either a batch or continuous process. The LCP is then mixed with various additives and extruded. A majority of the LCPs sold are reinforced with 30% to 40% glass filler having polymeric sizing to provide a strong interface between the fiber and matrix. Unreinforced grades are injection-molded for specialty applications.

Properties of a part molded from an LCP are highly dependent upon the morphology of the part, which is determined by the conditions of processing. Injection-molded parts exhibit highly oriented skins, with rigid chains oriented in the direction of flow. The core zone beneath this skin is less ordered. This morphology results in very good properties (particularly in the direction of flow) and very high dimensional stability. Other attractive properties of LCPs include exceptional oxygen and barrier properties (100 times that of PETP), very high thermal stability, high modulus and strength, good dimensional stability, and high chemical and solvent resistance. Properties of Xydar are compared to those of a molding-grade PET in Table 10-8.

Table 10-8 Comparison of Properties of PET with Liquid-Crystalline Polyester

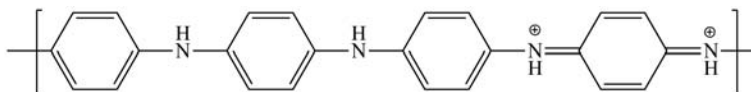
Property	PET ^a	LC Polyester ^b
Tensile strength, MPa	81	126
Tensile modulus, GPa	2.8	8.3
Elongation, %	4–70	5
Flexural strength, MPa	3.0	131
Flexural modulus, MPa		13.1
Izod impact strength, J m ⁻¹		
notched		208
unnotched		454
Density, g cm ⁻³		1.35
<i>T</i> _m , °C (or Vicat softening point)	235	358
HDT at 1.8 MPa, °C	80	337

^a Arnite.

^b Xydar.

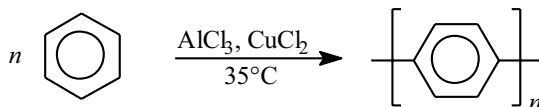
At the moment, the high cost of liquid-crystalline polyesters has limited these resins to specialty applications such as electronic components (e.g., computer memory modules), housings for light-wave conductors, a variety of aerospace applications, and filaments to compete with aramid fibers. This situation could change as monomer costs are reduced through increasing production and supply.

peroxydisulfate. Polyaniline can exist in several oxidation states with vastly different conductivities (ranging from 10^{-11} to 10^2 S cm^{-1}). Only the emeraldine salt of polyaniline



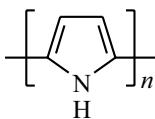
is electrically conductive.

Poly(*p*-phenylene) (PPP) can be prepared by the Freidel–Crafts polymerization of benzene

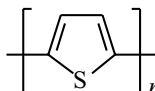


and by other synthesis routes to yield a structurally regular polymer with high strength, solvent resistance, and excellent thermal and thermal oxidative stability [17]. PPP can be converted from an electrical insulator to a highly conductive charge-transfer complex by doping with strong electron donors or acceptors.

Polypyrrole (PPy)

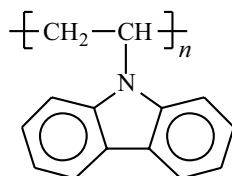


and polythiophene (PT)



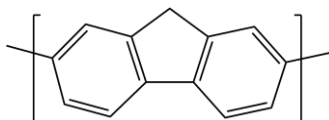
are related in structure and properties. Polypyrrole is obtained by the electropolymerization of pyrrole as a highly colored, dense conducting film while polythiophene can be polymerized by the anodic oxidation of thiophene. Unlike polyacetylene, polypyrrole and polythiophene can be synthesized in the doped form and are very stable in air. Unfortunately, their conductivities are lower than that of polyacetylene (see Section 12.3.1).

Photoconductive Polymers. Some polymers become conductive when illuminated. The ability to become photoconductive has great importance for the xerographic-copier, laser-printer, and duplicator industries. The most important example of a photoconductive polymer is poly(*N*-vinylcarbazole) (PVK)



which can be polymerized by free-radical and cationic mechanisms. Both amorphous (free-radical) and tactic PVK can be prepared. Amorphous PVK has a T_g of 227°C and a density of 1.184 g cm^{-3} . In the dark, PVK is an insulator; however, it becomes conductive when exposed to UV radiation. Incorporation of sensitizing dyes or electron acceptors extends the photoconductive response to the visible and near-IR region. In general, photoconductivity can be attributed to the ability to generate free-charge carriers (electron hole) by the absorption of radiation and the subsequent transport of these carriers to the electrodes.

Polyfluorenes. Polyfluorenes are a class of conjugated polymers with both photoactive and electroactive properties with important applications in light-emitting diodes, field-effect transistors, and polymer solar cells [18]. A typical structure of polyfluorene is shown below.



Fluorene can be polymerized by either oxidative coupling or electropolymerization.

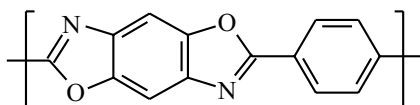
10.2.8 High-Performance Fibers

In addition to the aramids, Kevlar and Nomex (see Section 10.1.1), there are several other rigid-rod polymers that can be spun into fibers for high-temperature composite and related applications. These include polybenzimidazole (PBI), polybenzobisoxazole (PBO), and polybenzobisthiazole (PBT).

As discussed in Section 10.2.1, polybenzimidazole is obtained from the polycondensation of an aromatic tetramine and an aromatic dicarboxylic acid or derivative. The most important of the polybenzimidazoles is poly[2,2'-(*m*-phenylene)-5,5'-bibenzimidazole], shown in Figure 10-11. This polymer is obtained from the polycondensation of tetraaminobiphenyl and diphenyl isophthalate in poly(phosphoric acid) (PPA) in a two-stage process at high temperature [19]. Fiber may be dry-spun from solution in dimethylacetamide and drawn under high temperature to obtain a very high-tensile-strength fiber. PBI has high-temperature stability (in excess of 400°C) and excellent chemical resistance. It will burn only in a high-oxygen-content atmosphere ($>48\%$ oxygen). Applications include many of those for which

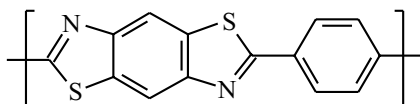
Kevlar may be used, including flue-gas filtration, and generally as a substitute for asbestos.

A related polymer is polybenzobisoxazole (PBO)*



which can be prepared by the polycondensation of 4,6-diamino-1,3-benzenediol dihydrochloride and terephthalic acid in PPA.

Polybenzobisthiazole (PBT)[†]



is obtained from the polycondensation of 2,5-diamino-1,4-benzenedithiol dihydrochloride in PPA.

10.2.9 Dendritic Polymers

Dendritic macromolecules may be classified into dendrons, dendrimers, and hyperbranched polymers. Dendrons and dendrimers are typically prepared by multistep reactions while hyperbranched polymers are synthesized by a one-step self-polymerization of AB_x -type multi-functional monomers where A and B are mutually reactive functional groups [20]. Hyperbranched polymers have a fractal pattern of chemical bonds but branches do not emanate from a central core and may be comb-shaped as an example [21, 22]. The word *dendrimer* comes from the Greek *dendron* meaning “tree” and *meros* meaning “part.” Dendrimers have a spherical or globular form similar to that of an ice crystal with many individual branches radiating from the center. A representative dendrimer is shown in Figure 10-19. Some dendrimers can have diameters of more than 10 nm and molecular weights exceeding 1 million. Dendrimers can provide some interesting opportunities. For example, dendrimers can penetrate biological membranes and carry a variety of chemicals or drugs in their low-density interiors. They can be used to remove pollutants from water, serve as nanoscale catalysts and reaction vesicles, control drug release, and moderate chemical reactions. Applications for hyperbranched polymers include coatings, pigment dispersants, and adhesives.

* Poly(*p*-phenylene-2,6-benzoxazole-diyl).

[†] Poly(*p*-phenylene-2,6-benzobisthiazole-diyl).

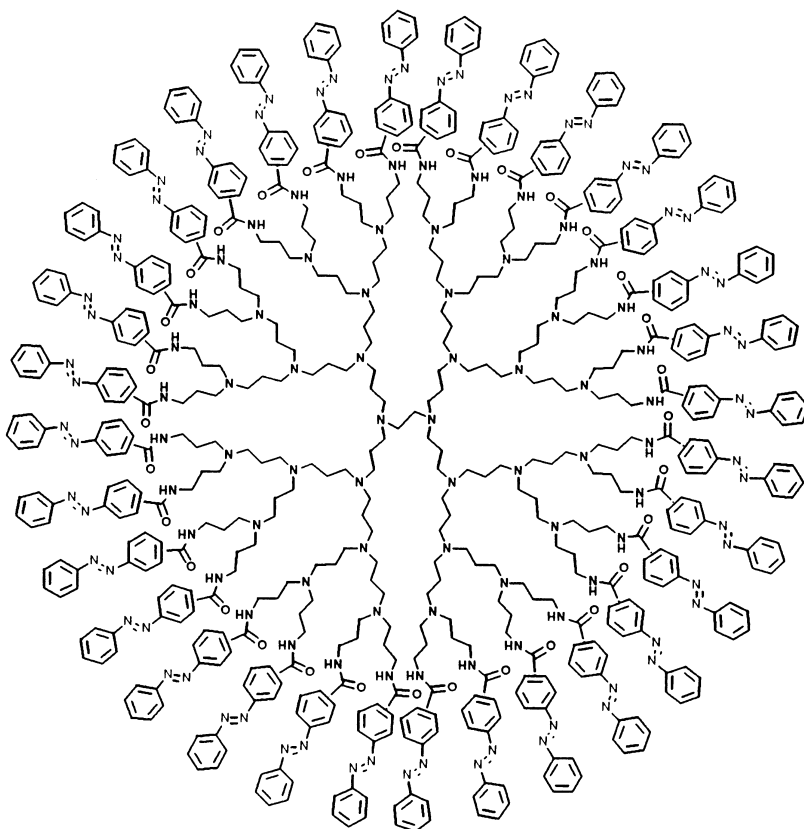


Figure 10-19 Azobenzene dendrimer. Reprinted from F. Vögtle, S. Gestermann, R. Hesse, H. Schwier, and B. Windisch, *Functional Dendrimers*. Progress in Polymer Science, 2000. **25**: p 987–1041. Copyright 2000, with permission from Elsevier Science.

SUGGESTED READING

ENGINEERING PLASTICS

Cebe, P., *Review of Recent Developments in Poly(phenylene sulphide)*. Polymers and Polymer Composites, 1995. **3**: p. 239.

Clarson, S. J., and J. A. Semlyen, *Siloxane Polymers*. 1993, Englewood Cliffs: Prentice Hall.

Feiring, A. F., J. F. Imbalzano, and D. L. Kerbow, *Developments in Commercial Fluoroplastics*. Trends in Polymer Science, 1994. **2**: p. 26.

- LeGrand, D. G., and J. T. Bendler, eds., *Handbook of Polycarbonate Science and Technology*. 2000, New York: Marcel Dekker, Inc.
- Lopez, L. C., and G. L. Wilkes, *Poly(p-phenylene sulfide)—An Overview of an Important Engineering Thermoplastic*. *Journal of Macromolecular Chemistry—Reviews in Macromolecular Chemistry and Physics*, 1989. **C29**: p. 83.
- Masamoto, J., *Modern Polyacetals*. *Progress in Polymer Science*, 1993. **18**: p. 1.
- Rao, V. L., *Polyether Sulfones*. *Journal of Macromolecular Science, Chemistry and Physics*, 1999. **C39**: p. 655.
- Rigby, R. B., *Polyetheretherketone PEEK*, *Polymer News*, 1984. **9**: p. 325.

SPECIALTY PLASTICS

- Baziun, C. G., and A. Eisenberg, *Ion-Containing Polymers: Ionomers*. *Journal of Chemical Education*, 1981. **58**: p. 938.
- Brostow, W., *Properties of Polymer Liquid Crystals: Choosing Molecular Structures and Blending*. *Polymer*. 1990. **31**: p. 979.
- Dyson, R. W., ed., *Specialty Polymers*. 1987, New York: Chapman and Hall.
- Genies, E. M., A. Boyle, M. Lapkowski, and C. Tsintavis, *Polyaniline: A Historical Survey*, *Synthetic Metals*, 1990. **36**: p. 139.
- Gleria, M., and R. De Jaeger, *Aspects of Phosphazene Research*. *Journal of Inorganic Organometallic Polymers*, 2001. **11**: p. 1.
- Hodd, K., *Trends in High Performance Polymers. Part I—Linear High Performance Polymers*. *Trends in Polymer Science*, 1993. **1**(5): 129.
- Lopyrev, V. A., G. F. Myachina, O. I. Shevaleyevskii, and M. L. Khidekel, *Polyacetylene Review*. *Polymer Science USSR*, 1988. **30**(10): p. 2151.
- Mittal, K. L., ed., *Polyimides: Synthesis, Characterization, and Applications*, vols. 1–2. 1984, New York: Plenum Press.
- Negi, Y. S., and P. V. Adhyapak, *Developments in Polyaniline Conducting Polymers*. *Journal of Macromolecular Science—Polymer Reviews*, 2002. **C42**: p. 35.
- Preston, J., *High-Strength/High-Modulus Fibers from Aromatic Polymers*. *Journal of Chemical Education*, 1981. **58**: p. 935.
- Samuel, J., T. Xavier, and T. Kurian, *Ionomers*, *Progress in Rubber and Plastics Technology*, 2000. **16**: p. 1.
- Scherf, U., and D. Neher, eds., *Polyfluorenes*. *Advances in Polymer Science*, vol. 212. 2008, Heidelberg: Springer Verlag.
- Sroog, C. E., *Polyimides*. *Progress in Polymer Science*, 1991. **16**: p. 561.
- Takekoshi, T., *Polyimides*. *Advances in Polymer Science*, 1990. **94**: p. 1.
- Tomalia, D. A., and J. M. J. Fréchet, *Discovery of Dendrimers and Dendritic Polymers: A Brief Historical Perspective*. *Journal of Polymer Science, Polymer Chemistry Education*, 2002. **40**: p. 2719.
- Vögtle, F., S. Gestermann, R. Hesse, H. Schwierz, and B. Windisch, *Functional Dendrimers*. *Progress in Polymer Science*, 2000. **25**: p. 987.

PROBLEMS

10.1 How is Kevlar synthesized? What is the reason why Nomex was developed before Kevlar?

10.2 Using the material developed in this chapter, suggest the best polymer candidate for each of the following applications and explain your selection:

- (a) Bullet-proof armor
- (b) Precision plastic gear
- (c) Microwave tray
- (d) Carbonated beverage container
- (e) Solvent-resistant O-ring
- (f) Observation window for a deep-dive submarine
- (g) Golf ball cover
- (h) Polymeric anode

10.3 Why is PBI an attractive candidate for fuel-cell membranes while the related polymers PBO and PBT are not?

REFERENCES

1. Hay, A. S., *Polymerization by Oxidative Coupling. II. Oxidation of 2,6-Disubstituted Phenols*. Journal of Polymer Science, 1962. **58**: p. 581–591.
2. Hay, A. S., *The SPE International Award Address—1975 Polymerization by Oxidative Coupling—an Historical Review*. Polymer Engineering and Science, 1976. **16**(1): p. 1–10.
3. Dickinson, B. L., *UDEL Polysulfone for Medical Applications*. Journal of Biomaterials Applications, 1988. **3**(4): p. 605–634.
4. Tervoort, T., et al., *Melt-Processible Poly(tetrafluoroethylene)*. Macromolecules, 2000. **33**(17): p. 6460–6465.
5. Takekoshi, T., *Synthesis of High Performance Aromatic Polymers via Nucleophilic Nitro Displacement Reaction*. Polymer Journal, 1987. **19**(1): p. 1912–02.
6. Vogel, H., and C. S. Marvel, *Polybenzimidazoles, New Thermally Stable Polymers*. Journal of Polymer Science, 1961. **50**: p. 511–539.
7. Wang, C.-S., *Properties of Conjugated Ladder Polymers*. Trends in Polymer Science, 1993. **1**(7): p. 199–205.
8. Nguyen, H. X., and H. Ishida, *Poly(aryl-ether-ketone) and Its Advanced Composites: A Review*. Polymer Composites, 1987. **8**(2): p. 57–73.
9. Hergenrother, P. M., B. J. Jensen, and S. J. Havens, *Poly(arylene ethers)*. Polymer, 1988. **29**(2): p. 358–369.

10. Kelley, J. M., *Ultra-High Molecular Weight Polyethylene*. Journal of Macromolecular Science, 2002. **C42**(3): p. 355–371.
11. Singler, R. E., N. S. Schneider, and G. Hagnauer, *Polyphosphazenes: Synthesis Properties—Applications*. Polymer Engineering and Science, 1975. **15**(5): p. 321–338.
12. Allcock, H. R., *Polyphosphazenes*. Journal of Inorganic and Organometallic Polymers, 1992. **2**(2): p. 197–211.
13. West, R., *The Polysilane High Polymers*. Journal of Inorganic and Organometallic Polymers, 1986. **300**: p. 327–346.
14. Miller, R. D., and J. Michl, *Polysilane High Polymers*. Chemical Reviews, 1989. **89**(6): p. 1359–1410.
15. Flory, P. J., *Statistical Thermodynamics of Semi-Flexible Chain Molecules*. Proceedings of the Royal Society of London, Series A, Mathematical and Physical Science, 1956. **234**(1196): p. 73–83.
16. Lenz, R. W., and J.-I. Jin, *Liquid Crystal Polymers: A New State of Matter*. Polymer News, 1986. **11**: p. 200–204.
17. Gin, D. L., and V. P. Conticello, *Poly(p-phenylene): New Directions in Synthesis and Application*. Trends in Polymer Science, 1996. **4**(7): p. 2172–22.
18. Leclerc, M., *Polyfluorenes: Twenty Years of Progress*. Journal of Polymer Science: Part A: Polymer Chemistry, 2001. **39**: p. 2867–2873.
19. Moelter, G. M., R. F. Tetreault, and M.J. Hefferon, *Polybenzimidazole Fiber*. Polymer News, 1983. **9**: p. 134–138.
20. Dvornic, P. R., and D. A. Tomalia, *Starburst Dendrimers: A Conceptual Approach to Nanoscopic Chemistry and Architecture*. Macromolecular Symposium, 1994. **88**(1): p. 123–148.
21. Jikei, J., and M.-A. Kakimoto, *Hyperbranched Polymers: A Promising New Class of Materials*. Progress in Polymer Science, 2001. **26**: p. 1233–1285.
22. Kim, Y. H., and O. Webster, *Hyperbranched Polymers*. Journal of Macromolecular Science—Polymer Reviews, 2002. **C42**(1): p. 55–89.

Polymer Processing and Rheology

*P*olymer melts and concentrated solutions exhibit both viscous and elastic properties. The viscoelastic properties of polymeric solids were the principal topics of discussion in Chapter 5. In this chapter, the viscoelastic properties of polymer melts and concentrated solutions, particularly in relation to polymer-processing operations, are described. Viscous properties determine such processing parameters as the form of the velocity profile, the magnitude of the pressure drop, and the amount of heat generation (i.e., viscous heating) during extrusion through a die. Elastic behavior is responsible for such extrusion phenomena as die swell, melt fracture, and nonzero exit pressure. The fundamentals of polymer-processing operations and the basics of polymer rheology are presented in this chapter.

11.1 Basic Processing Operations

Polymer-processing operations may be classified into five broad categories—extrusion, molding, spinning, calendaring, and coating. Of these, extrusion is perhaps the most widely used. Applications of extrusion include the continuous production of plastic pipe, sheet, and rods. Molding is normally a batch process, principally in the form of injection- and compression-molding operations used to make plastic parts as diverse as the cap to a ballpoint pen and a fiber-reinforced bathtub. Other important processing methods include the fiber spinning of textiles (discussed in Section 8.2.4), the calendaring of plastic sheet, and the deposition of organic coatings on plastic sheet. Two specialized methods of preparing fiber-reinforced composites—filament winding and pultrusion—were discussed in Chapter 7.

11.1.1 Extrusion

A form of extrusion was probably first used in England at the end of the eighteenth century to produce seamless lead pipe. In 1845, a ram-driven device was used to extrude threads of gutta percha and to produce pipe from shellac and gutta percha. The first submerged cable laid across the English Channel in 1851 was an insulated copper conductor produced by what may be the first application of a commercial wire-coating operation. Screw-driven extruders were developed in the second half of the nineteenth century, and twin-screw extruders appeared in the late 1930s.

The two principal components of an extrusion operation are the extruder and the die. As illustrated in Figure 11-1, the extruder consists of a hopper that holds the resin stock (usually in the form of small pellets or powder) and the extruder barrel, which can be conceptually divided into three sections on the basis of function. These are called the *feed*, *compression*, and *metering* sections. In the feed section, the solid feed is conveyed by the rotating screw from the hopper to the compression zone where the resin begins to melt due to the action of electrical heaters attached to the barrel wall. By the time the resin reaches the metering zone all the resin has melted, and the shearing action of the screw rotating against the inner wall of the extruder barrel forces the melt out of the extruder and through a die. The die shapes the extrudate to the desired form. For example, a die with an opening in the form of an annulus (i.e., two concentric cylinders) is used to extrude pipe; a capillary die is used to extrude rods; and a slit die having a rectangular opening is used to extrude sheet. A specially designed capillary die is used to coat wire with a layer of plastic insulation (see Section 11.5.2).

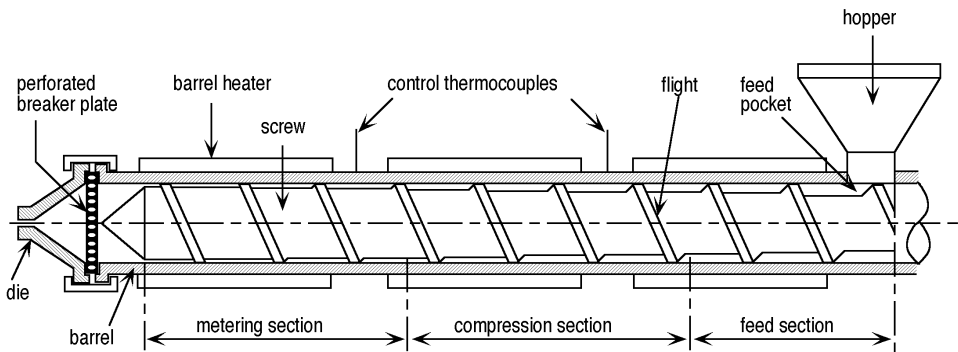


Figure 11-1 Illustration of a single-screw extruder. Adapted from N. G. McCrum, C. P. Buckley, and C. B. Bucknall, *Principles of Polymer Engineering*. 1988, Oxford: Oxford University Press.

In commercial polymer production, powder from a polymerization reactor may be fed directly to an extruder that has an opening for venting volatiles—a process called *devolatilization*. Examples of volatile contaminants include residual monomer and solvent that may be used during the polymerization process. The extruded melt is then passed through a capillary die, cooled, and chopped to form small pellets. These pellets are easier and safer to handle than the powder and can be shipped, stored, dried, and finally fed into the hopper of another extruder or injection-molding machine to produce the final product.

The extruder illustrated in Figure 11-1 has a single screw that is tapered so that the distance between the bottom of the screw channel and the wall of the barrel decreases as the metering section is reached. This provides increasing shear rate (see Section 11.5.1) as the melt is forced toward the exit of the extruder. This is advantageous since the viscosity of polymer melts and concentrated polymer solutions decreases with increasing shear rate, as discussed in Section 11.2.1. Extruders equipped with twin screws that rotate in opposite directions are used when even higher shear rates are needed, as in the case of temperature-sensitive, high-viscosity polymer melts.

11.1.2 Molding

Molding is one of the earliest and most important processing operations. These include compression, transfer, injection, reaction injection, thermoforming, blow, and rotational molding, which are included in this section.

Compression Molding. In many ways, compression molding is the least expensive and simplest of all polymer-processing operations. An early form of compression molding was used by the ancient Chinese to form articles from paper-mâché. During the early nineteenth century, compression molding was used in the United States and other countries to mold rubber parts and cases made from a composite of gum shellac and woody fibers. In 1907, Leo Baekeland employed a compression-molding process to produce phenol–formaldehyde (i.e., phenolic) resins [1].

Today, compression molding and a related technique, transfer molding, are the principal methods of molding thermosets such as phenolic resins, alkyds, and unsaturated polyesters (see Section 9.3.2). Injection molding, described in the next section, is the preferred method for molding thermoplastics, except in the case of molding large parts where the cost of transfer molding or injection molding may be excessive compared to that of compression molding. The compression-molding process is fairly simple. First, the resin is placed in the bottom half of an open, heated mold. Next, the top half of the mold is placed over the bottom half and pressure is applied to cause the molten resin to completely fill the mold cavity, while the excess resin is forced out of the mold as *flash*. Presses with clamping capacities from 5 to 4000 tons are available for manual and semiautomatic operation. An illustration of a compression-molding operation is shown in Figure 11-2.

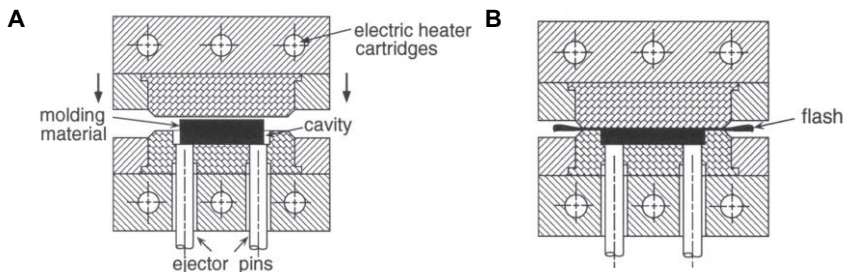


Figure 11-2 Compression-molding process. **A.** View of an open mold with molding material in place. **B.** Closed mold showing formed part and flash formed from excess resin. Adapted from J. L. Hull, *Compression and Transfer Molding*, in *The Concise Encyclopedia of Polymer Science and Engineering*, 1990. J. I. Kroschwitz, ed. Copyright © 1990 by John Wiley & Sons. This material is used by permission of John Wiley & Sons, Inc.

Transfer Molding. In the case of *transfer* (or *plunger*) molding, the mold is closed prior to resin entry. A simplified diagram of a transfer-molding process is shown in Figure 11-3. A plunger is used to force a predetermined amount of molten resin from an open *transfer pot* through a small opening in the mold. After the mold is opened (Figure 11-3C), ejector pins are used to push the molded part out of the mold. The residual (i.e., uninjected molding resin) is called the *cull*. Molding cycles

tend to be shorter than for compression molding because mold temperatures can be higher and the premelted polymer flows more easily through the mold, typically under lower pressure. For these reasons, transfer molding is used to mold parts with intricate geometries and to mold fragile parts or when an insert is used in the mold and the flow of granular molding material during compression molding would otherwise damage or displace the insert.

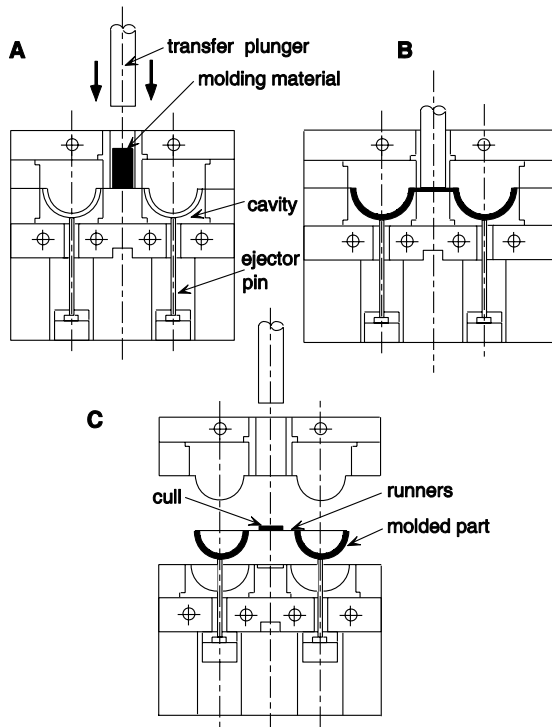


Figure 11-3 Transfer-molding operation. **A.** Transfer pot is loaded while mold is in closed position. **B.** Plunger pushes molding material into mold form. **C.** Mold opens and ejector pins push out molded part. Adapted from J. L. Hull, Compression and Transfer Molding, in *The Concise Encyclopedia of Polymer Science and Engineering*, 1990. J. I. Kroschwitz, ed. Copyright © 1990 by John Wiley & Sons. This material is used by permission of John Wiley & Sons, Inc.

In the case of molding thermoset resins, the molding compound is first placed in the cavity of the compression mold or the transfer pot of a transfer-molding process and heated (ca. 150°C) to provide sufficient flow for mold filling. Pressure (e.g., 2000 psi or 13.4 MPa) is then applied over sufficient time to allow the resin to cure (i.e., crosslink).

Injection Molding. Another important polymer-processing operation is injection molding. The principle behind injection molding dates back to 1856 when E. Pelouze of the United States developed a die-casting machine for forcing molten metal into a die by mechanical or hydraulic means. The development of the first injection-molding machine for thermoplastics was a result of ivory shortages during the Civil War. In 1868, the Phelan and Collender Co., a producer of billiard balls, offered an impressive award of \$10,000 to anyone who could produce a satisfactory substitute for ivory. In 1869, John Wesley Hyatt, a printer from Boston, invented the material celluloid (cellulose nitrate) to replace ivory. Celluloid was the world's first commercial synthetic resin and was used to produce products as diverse as billiard balls and dentures. In 1872, John and his brother Isaiah patented a simple extrusion device consisting of a steam-heated cylinder, a hydraulic plunger, and a discharge nozzle to extrude rods and tubes from cellulose nitrate.

As illustrated in Figure 11-4, one type of a modern injection-molding operation uses a reciprocating screw to melt a measured volume of feed introduced through the hopper. After a sufficient time has elapsed to form a homogeneous melt, the rotation of the screw ceases, and the melt is rammed into a mold under high pressure by a hydraulically driven thrust of the screw. The amount of resin that can be molded may vary with a particular machine from a few grams to a few kilograms, with clamping forces up to 5000 tons.

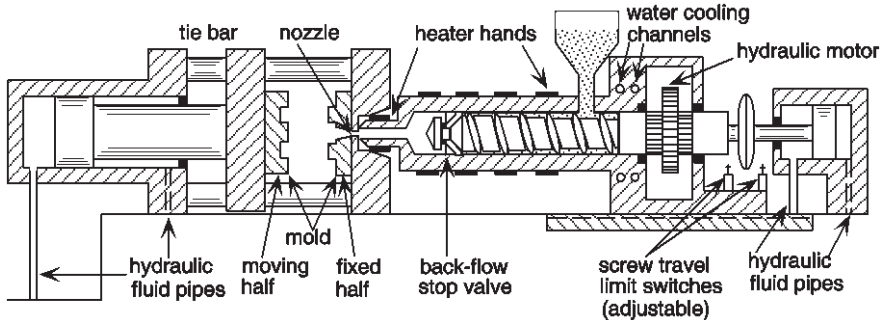


Figure 11-4 Illustration of a reciprocating-screw injection-molding machine and mold. Adapted from N. G. McCrum, C. P. Buckley, and C. B. Bucknall, *Principles of Polymer Engineering*. 1988, Oxford: Oxford University Press.

A mold may be used to produce a single part such as a computer keyboard or several smaller parts simultaneously (i.e., multi-impression molds). As an illustration, the cross section of a multi-impression mold to produce plastic boxes is shown in Figure 11-5A. The resulting molded assembly after removal from the mold is illustrated in Figure 11-5B. Anyone who has ever built a plastic model airplane is already familiar with the features of an injection-molded assembly. The thick sec-

tion through which the molten resin is forced from the nozzle of the injection-molding machine and first enters the mold is called the *sprue*. From the sprue, the melt is pushed through *runners*, which evenly distribute the melt to each mold cavity. The narrow point of attachment of the runner to the mold cavity is called the *gate*. After the mold is totally filled, it is cooled and opened to release the molded assembly. The molded parts are then broken from their attachment at the gates, and scrapped sprues, runners, and gates may be recycled to the molding operation. Molds must be able to withstand significant pressures and high temperatures and produce parts with close tolerances after numerous and rapid operations. For these reasons, great care must be exercised in mold design and manufacture. This usually represents a significant expenditure of capital, which contributes significantly to the total price of the molded part.

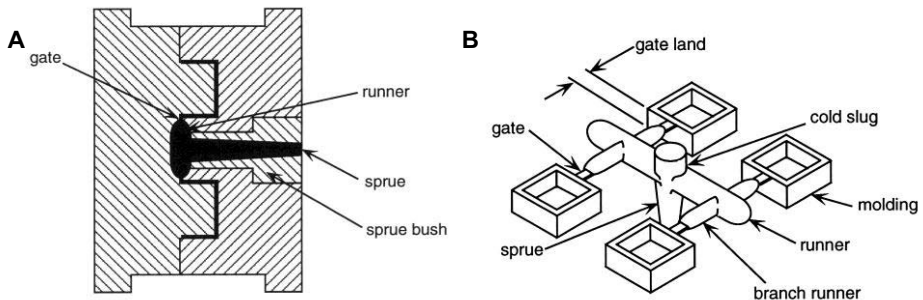


Figure 11-5 **A.** Typical mold design used in a multi-impresion injection-molding process for the production of plastic boxes in this example. **B.** Removed mold assembly showing boxes and plastic scrap (i.e., sprue and runners). Adapted from N. G. McCrum, C. P. Buckley, and C. B. Bucknall, *Principles of Polymer Engineering*. 1988. Oxford: Oxford University Press.

There are several variations of the basic design of the reciprocating-screw injection-molding machine illustrated in Figure 11-4. For example, a less common design often used for thermoplastics is called the screw pot or *two-stage* screw. In this variation of the injection-molding process, the operations of the extruder screw and injection plunger are separated. A fixed (i.e., non-reciprocating) screw is used to melt the resin, which flows into a separate injection chamber and plunger assembly. The reciprocating-screw design is preferred for molding thermosets and elastomers and for heat-sensitive thermoplastics.

Reaction Injection Molding. Reaction injection molding or RIM is a relatively new process (developed in Germany during the late 1960s) whereby the polymer is simultaneously synthesized and molded into the finished product. An illustration of a RIM process is shown in Figure 11-6. At the start of the process, exact quanti-

ties of monomers (including catalyst and other additives) are metered into a mixing unit and rapidly forced into the mold, where most of the polymerization occurs. In contrast to injection molding, temperatures and clamping pressures in a RIM process are relatively low, allowing the use of inexpensive aluminum tooling. Other advantages of RIM include low energy consumption, rapid start-up time, and its suitability for the manufacture of large articles such as automotive bumpers. Disadvantages include the risk of worker exposure to noxious, high-vapor-pressure reagents such as diisocyanates, which are used in the RIM production of polyurethane.

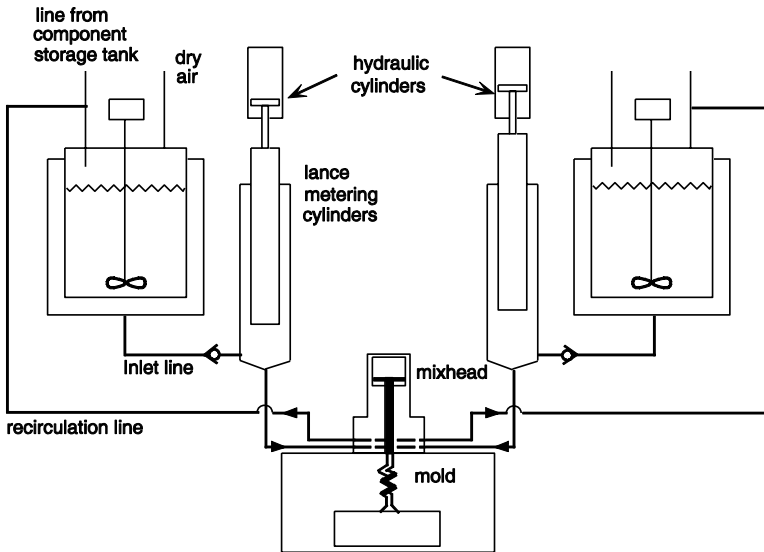


Figure 11-6 Illustration of a reaction injection-molding process showing separate tanks for polymerization reagents. Adapted from L. T. Manzione, Reaction Injection Engineering, in *The Concise Encyclopedia of Polymer Science and Engineering*, 1990. J. I. Kroschwitz, ed. Copyright © 1990 by John Wiley & Sons. This material is used by permission of John Wiley & Sons, Inc.

Due to the need for a controlled and rapid polymerization process, RIM is suited only for condensation-type polymers with favorable polymerization kinetics. Examples of polymers that can be processed in this way include polyamides, epoxies, and especially polyurethanes, which represent more than 95% of total RIM production. Polyurethanes are prepared by reacting diisocyanates with diols and chain extenders as discussed in Section 9.2.2. The majority of the RIM-produced polyurethane is used for elastomer applications (e.g., automotive bumpers and fascia), with the remainder used for structural foam. In addition, milled glass and short glass fi-

bers can be added during RIM to provide reinforcement to the molded part. This process, called reinforced RIM or RRIM, was developed in the 1970s.

Thermoforming. Thermoforming is an operation borrowed from metallurgy. In thermoforming, a plastic sheet is heated until it softens and is then formed to the shape of a mold preform by application of external air pressure or by pulling a vacuum (i.e., vacuum forming) between the sheet and the mold, as illustrated in Figure 11-7. Ancient Egyptian craftsmen who softened tortoise shells to form a variety of shapes may have been the first thermoformers, but it was not until 1938, with the production of blister packaging from cellulose acetate sheet, that the modern thermoforming industry began. Applications for thermoforming in today's plastics industry range from the high-volume production of plastic drinking cups to the production of plastic bed liners of half-ton pickup trucks.

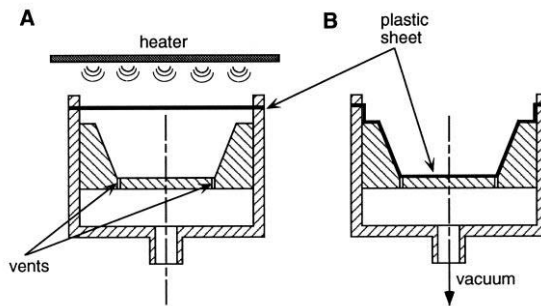


Figure 11-7 Vacuum-forming operation. **A.** Flat sheet is heated. **B.** Softened sheet is forced to fit the mold contour by evacuating the space between the sheet and the mold. Adapted from R. J. Crawford, *Plastics Engineering*. 1990, Danvers, MA: Elsevier Science, p. 200. Copyright 1981, with permission from Elsevier.

Blow Molding. Blow molding uses a gas (e.g., air or sometimes nitrogen) to expand a hot preform, or *parison*, against the form of a mold cavity to produce a hollow object. Blow molding may date back to 1880 when John Wesley Hyatt used this technique to produce baby rattles. Plastic bottles, automotive fuel tanks, toy tricycles, and other consumer products are made in this way. The first plastic bottle was blow-molded from polyethylene in 1943. Two types of processes are used for blow molding—*injection* and *extrusion*.

Injection blow molding is used primarily to produce small bottles and other parts. In this process, a parison is first injection-molded around a core rod in a preform mold and then transferred to a bottle blow-mold cavity. In the cavity, air expands the parison to the shape of the bottle.

For larger bottles and plastic tanks, an *extrusion blow-molding* process is used, as illustrated in Figure 11-8. In this process, the plastic resin is first extruded

as a tube (i.e., the parison) and is then captured by two halves of a mold in a continuous process. A blowpin is inserted, the mold is closed, and air is forced into the parison through the blowpin to expand the parison to the form of the mold cavity.

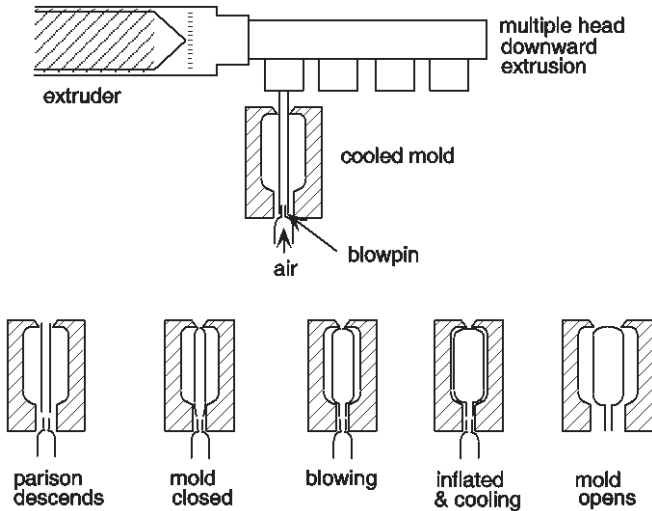


Figure 11-8 Extrusion blow-molding process in the production of plastic bottles. Adapted from D. H. Morton-Jones Kluwer, *Polymer Processing*. 1989, Kluwer Academic Publishers, Figures 6.1 and 6.2, p.128. Copyright 1989, D. H. Morton-Jones, Kluwer Academic Publishers.

Rotational Molding. Rotational molding, or rotomolding, uses centrifugal force to force-coat the inside of a mold with molten resin. The process is relatively simple, inexpensive to operate, and particularly suited for molding very large objects—the largest reported is an 85-m³ tank. The forerunner of the modern rotational-molding process was called slush molding, developed by the rubber industry to produce gloves, boots, and other items from plastisols. In slush molding, the liquid was first poured into a hot mold. Once the layer of plastic solidified, excess liquid was poured off.

In a typical rotational-molding operation, the mold cavity is first charged with a predetermined amount of resin powder or liquid. It is then closed and biaxially rotated in an oven. Finally, the mold is removed and cooled. Rotational molding produces little or no flash, thereby eliminating trimming operations and wasted resin. In addition, rotational molding produces very uniform wall thickness as well as strong corner sections, which may be difficult to obtain by other methods.

11.1.3 Calendering

Calendering is another method, in addition to extrusion, that can be used to produce plastic sheets. As illustrated in Figure 11-9, molten polymer is compressed in the small gap (the nip region) between two heated cylinders rotating in opposite directions. Sheets with widths up to 6 ft and a thickness as small as 0.002 in. can be produced at speeds up to 300 ft min^{-1} . The bulk of U.S. calendering output is poly(vinyl chloride) (PVC), including flexible sheet and film and blends and copolymers of PVC. Calenders can also be used to impart a finish (e.g., gloss or roughness) to a preformed plastic sheet or to laminate two sheets.

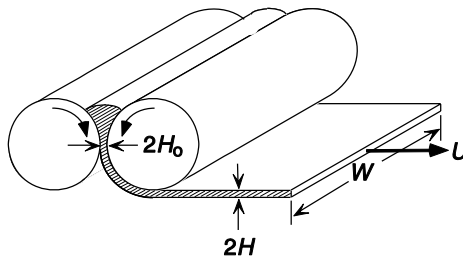


Figure 11-9 Simplified representation of a calendering process. Adapted from J. M. McKelvey, *Polymer Processing*. 1982, New York: John Wiley & Sons, with permission of the author.

11.1.4 Coating

Many different types of processes can be used to coat a thin layer of liquid (e.g., polymer melt or solution) onto a moving sheet, called the *web*. Examples of coatings include the deposition of

- Photographic emulsion on a cellulosic web
- Magnetic surface on poly(ethylene terephthalate) for recording and computer tape
- Polymer layer on a metal foil for capacitor applications
- Finishes and backings on textile fibers and fabrics

Examples of different coating operations are illustrated in Figure 11-10. In *roll coating* (Figure 11-10A), the lower roll picks up liquid from a bath and delivers it to a second roll or directly to the moving web. The thickness of the coating depends upon properties of the liquid (i.e., viscosity, etc.) and the spacing between the rolls

through which the web moves. This spacing may be controlled directly or indirectly by controlling pressure between the two rolls.

Another important type of coating operation is called *blade coating*. In this process, a flexible blade is used to directly meter the coating liquid onto a moving web from the fluid reservoir, or the blade is combined with a roll-coating operation, as shown in Figure 11-10B. The blade is flexible and pressure developed under the blade determines the coating thickness.

The most direct method to apply a coating is by direct extrusion onto the moving web, as shown in Figure 11-10C. This process is sometimes called *curtain coating* and is often used in conjunction with UV curing. The thickness of the coating is determined by the speed of the web and the volumetric output of the extruder.

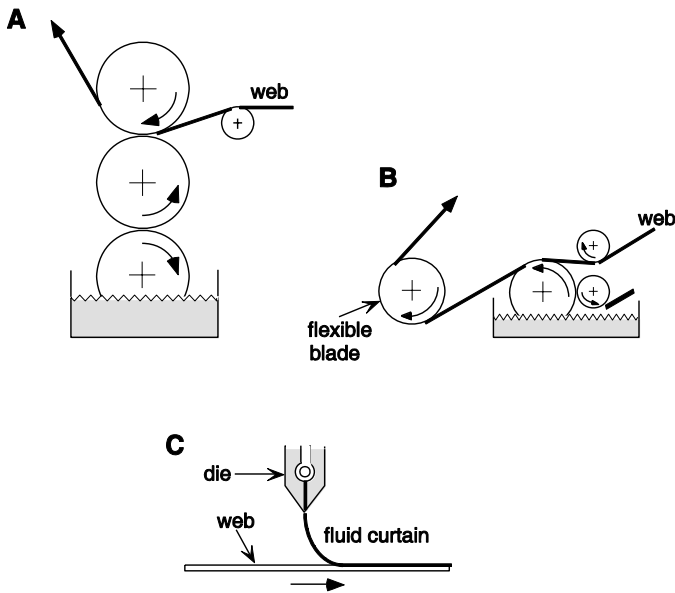


Figure 11-10 Examples of coating process. **A.** Roll coating. **B.** Blade coating. **C.** Curtain coating. After S. Middleman, *Fundamentals of Polymer Processing*. 1977, New York: McGraw-Hill. Reproduced with permission of the author.

11.2 Introduction to Polymer Rheology

The viscous flow of a Newtonian fluid is described by *Newton's law of viscosity* given for shear flow as

$$\tau = \mu \frac{d\gamma}{dt} \quad (11.1)$$

where τ is shear stress, μ is the Newtonian viscosity coefficient, and γ is the shear strain. The time dependence of shear strain is called the *shear strain rate* or simply shear rate:

$$\dot{\gamma} \equiv \frac{d\gamma}{dt} \quad (11.2)$$

A *simple flow* is defined as one in which *only one* of the three components of the velocity vector

$$\mathbf{u} = (u_1, u_2, u_3) \quad (11.3)$$

is nonzero. The subscripts 1, 2, and 3 identifying the three components of the velocity vector, u_i , refer to the axes of the particular coordinate system used to analyze the flow process (i.e., x , y , and z in rectangular coordinates; r , θ , and z in cylindrical coordinates; and r , θ , and ϕ in spherical coordinates).

An example of a simple shear flow is Couette shear flow between two infinitely wide parallel plates, as illustrated in Figure 11-11. To analyze this simple flow, it is convenient to establish a rectangular-coordinate system having its x -axis fixed in the bottom plate and oriented along the shear direction, with the y -axis perpendicular to the plate surface. In this case, the shear strain, γ , is defined as the ratio of the deformation of a differential element in the x -direction (dx) to that in the y -direction (dy) during shear. It is easily shown that the shear *rate* in plane Couette flow is equal to the velocity gradient as

$$\dot{\gamma} \equiv \frac{d\gamma}{dt} = \frac{d}{dt} \left(\frac{dx}{dy} \right) = \frac{d}{dy} \left(\frac{dx}{dt} \right) = \frac{du_x}{dy} \quad (11.4)$$

where u_x is the velocity of the fluid in the x -direction. The *maximum* shear rate occurs at the moving plate surface and is given as U/H , where U is the constant (maximum) velocity of the upper plate moving in the x -direction and H is the distance of separation between the two plates. The *minimum* shear rate is zero, which occurs at the bottom (stationary) plate (i.e., $y = 0$) assuming there is *no slip* of the fluid layer at the plate surface; therefore, $u_x(0) = 0$.

As illustrated in Figure 11-11 and later discussed in Section 11.3.2, the velocity, u_x , is a linear function of the y -coordinate. In the case of Newtonian fluids such as water and mineral oil, the viscosity, μ , is a function of temperature and pressure but is *independent* of $\dot{\gamma}$. In contrast, the viscosity of non-Newtonian fluids such as concentrated polymer solutions and polymer melts is a function of temperature, pressure, and $\dot{\gamma}$. In addition, the viscosity of polymer solutions and melts exhibits a

strong dependence on molecular weight. These unique aspects of polymer rheology are discussed in the following section.

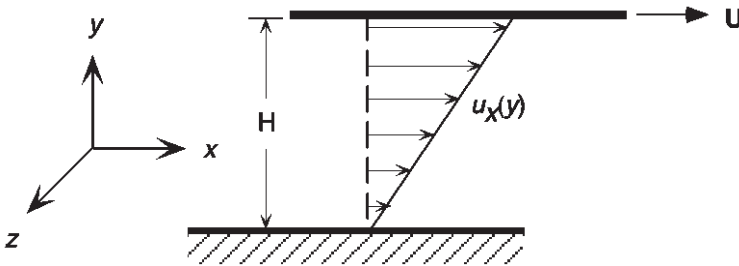


Figure 11-11 Representation of simple shear flow (plane Couette flow) between parallel plates whereby the upper plate is moving at a constant velocity (U).

11.2.1 Non-Newtonian Flow

Shear-Rate Dependence. The non-Newtonian or *apparent viscosity*, η^* , of polymer solutions and melts is defined following Newton's law of viscosity (eq. (11.1)) as

$$\tau = \eta(\dot{\gamma})\dot{\gamma}. \quad (11.5)$$

Equation (11.5) is called the *generalized Newtonian fluid* (GNF) model. The actual analytical relationship between τ and $\dot{\gamma}$ and, therefore, the dependence of η on $\dot{\gamma}$ are given by the *constitutive equation* of the material. Melts of high-molecular-weight polymers and their concentrated solutions display three characteristic regions, as illustrated in Figure 11-12. At low shear rates, η is nearly independent of

* Since τ and $\dot{\gamma}$ are the shear stress and shear rate, respectively, the viscosity defined by eq. (11.5)

$$\eta = \frac{\tau}{\dot{\gamma}}$$

is the *shear viscosity*. An extensional or Trouton viscosity is defined by the corresponding expression for tensile stress and strain as

$$\eta_T = \frac{\sigma}{\dot{\epsilon}}.$$

The extensional viscosity and its dependence upon the tensile strain rate are important in modeling processing operations where significant extensional flow occurs, such as converging flow in a runner during injection molding and during calendering and blow-molding operations. Extensional viscosity may also have significant importance to the drag-reduction properties of dilute polymer solutions (see Section 11.2.6).

$\dot{\gamma}$ (i.e., Newtonian behavior) and approaches a limiting zero shear rate value of η_0 . At higher $\dot{\gamma}$, η decreases with increasing $\dot{\gamma}$. Fluids that display this behavior are termed *shear thinning*. Finally, η once again approaches a limiting Newtonian plateau, η_∞ , at very high $\dot{\gamma}$.

The molecular basis for shear-thinning behavior is the effect of shear on entanglements, as illustrated in Figure 11-13. At low shear rates, the entanglements impede shear flow and, therefore, viscosity is high. As the shear rate increases, chains begin to orient in the flow direction and disentangle from one another—the viscosity begins to drop. Finally, the molecules become fully oriented in the flow direction at very high shear rates. At this point, stable entanglements are no longer possible and the viscosity reaches a low level that is again independent of shear strain rate. This second Newtonian plateau region is observed in the case of polymer solutions but is rarely observed for polymer melts because the shear rates required for chain orientation in the melt are so high that the chains actually can be broken (i.e., shear-induced degradation or mechanodegradation; see Section 6.1.5). In rare cases, viscosity may *increase* with increasing shear rate. Fluids that exhibit this behavior are called shear thickening (or dilatant). Examples of shear-thickening behavior are generally limited to concentrated suspensions such as PVC pastes and polymer melts that undergo shear-induced crystallization.

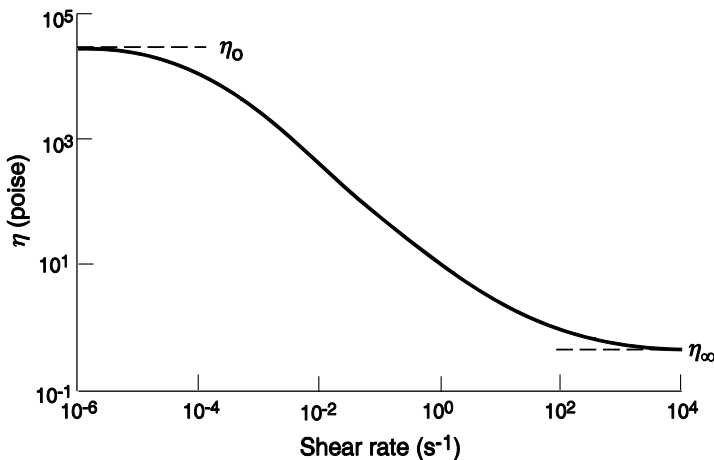


Figure 11-12 Typical dependence of apparent viscosity, η , of a polymeric melt on shear rate, $\dot{\gamma}$, showing the zero-shear viscosity, η_0 , plateau. Adapted from H. A. Barnes, J. F. Hutton, and K. Walters, *An Introduction to Rheology*. 1989, Elsevier Science. Copyright 1989, Elsevier Science.

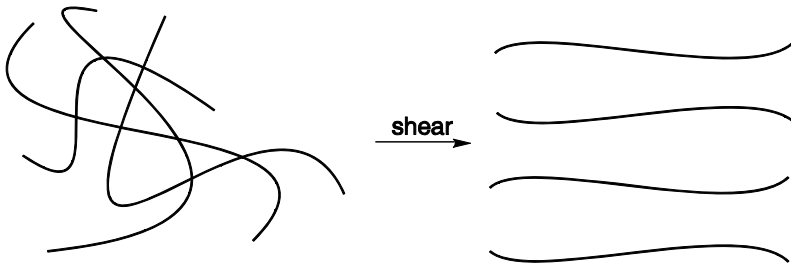


Figure 11-13 Idealized view of the effect of shear on the entanglements of melts and concentrated polymer solutions.

Molecular-Weight Dependence. The significance of entanglements to shear-thinning flow suggests that molecular weight and the critical molecular weight for entanglements, M_c (see Section 4.1.1), should significantly influence the rheological properties of polymers. It has been shown that the zero-shear viscosity, η_0 , is directly related to the weight-average molecular weight, \bar{M}_w , when $\bar{M}_w < M_c$ but follows a 3.4 power dependence on \bar{M}_w when $\bar{M}_w \geq M_c$. In addition, the onset of shear-thinning behavior occurs at progressively lower $\dot{\gamma}$ as molecular weight increases, as shown by viscosity data for polystyrene ($M_c = 31,200$) given in Figure 11-14.

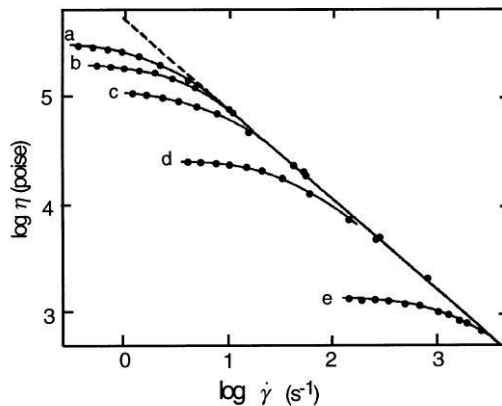


Figure 11-14 Effect of increasing molecular weight on the dependence of polymer viscosity on $\dot{\gamma}$ for polystyrene at 183°C. Molecular weights: (a) 242,000; (b) 217,000; (c) 179,000; (d) 117,000; and (e) 48,500. Adapted from R. A. Stratton, *The Dependence of Non-Newtonian Viscosity on Molecular Weight for "Monodisperse" Polystyrene*. *Journal of Colloid and Interface Science*, **22**: p. 517–530. Copyright 1966, with permission from Elsevier Science.

Temperature Dependence. The temperature dependence of the apparent viscosity of a polymer melt follows a typical *Arrhenius relationship* at high temperatures, ca. 100°C above T_g , as given by

$$\eta = \eta_r \exp \left[\frac{E}{R} \left(\frac{1}{T} - \frac{1}{T_r} \right) \right] \quad (11.6)$$

where η_r is the viscosity at some reference temperature, T_r , E is the activation energy (typically 21 to 210 kJ mol⁻¹), and R is the ideal gas constant. At lower temperatures, in the vicinity of the glass-transition temperature, approximately $T_g < T < T_g + 100^\circ\text{C}$, viscosity increases much more rapidly with decreasing temperature than is given by the Arrhenius expression. In this case, the temperature dependence of melt viscosity can be obtained by the WLF equation (see Section 5.1.6) as

$$\log \left[\frac{\eta(T)}{\eta(T_g)} \right] = \log a_T = \frac{-C_1(T - T_g)}{C_2 + T - T_g} \quad (11.7)$$

where $\eta(T_g)$ is the viscosity at T_g . Figure 11-15 shows the fit of experimental data for polycarbonate, for which excellent agreement between experimental viscosities and those predicted by the WLF equation is observed over the temperature range from $T_g + 55^\circ\text{C}$ to $T_g + 185^\circ\text{C}$ [2].

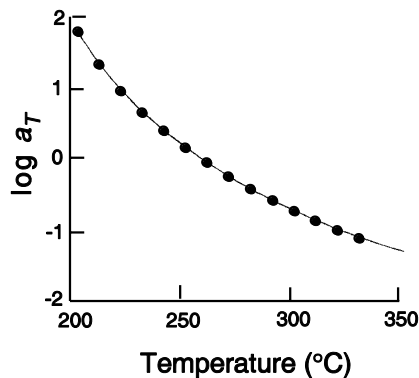


Figure 11-15 WLF fit (curve) of the shift factor, $a_T = \eta(T)/\eta(260^\circ\text{C})$, for polycarbonate at a reference temperature of 260°C. Adapted from P. Lomellini, *Viscosity-Temperature Relationships of a Polycarbonate Melt: Williams—Landel—Ferry versus Arrhenius Behaviour*. Makromolekulare Chemie, 1992. **193**: p. 6979, with permission of the publisher.

As discussed in Chapter 4, one view of the glass transition is that it is an iso-viscous state where the viscosity at T_g , $\eta(T_g)$, is approximately 10^{12} Pa-s (10^{13} poise) [3]. Use of eq. (11.7) provides a means of relating the WLF parameters, C_1 and C_2 , to the free volume, V_f , and the thermal-expansion coefficient, α , of the polymer as shown in Appendix A.1 of this chapter.

Pressure Dependence. Unlike the case for the glass-transition temperature, viscosity can be significantly affected by pressure. This pressure dependence may be an important consideration in the design of some processing operations, such as injection molding for which mold pressures can be very high. At constant temperature, the effect of pressure on viscosity can be approximated by the relation

$$\ln\left(\frac{\eta}{\eta_r}\right) = \beta(p - p_r) \quad (11.8)$$

where η_r is a reference viscosity corresponding to some reference pressure, p_r , and β is a pressure coefficient in the range of 0.87 to 4.93×10^{-8} Pa $^{-1}$ (0.6 to 3.4×10^{-4} psia $^{-1}$). As an example, the viscosity of a polystyrene melt at 250°C will nearly double with an increase in pressure from 13.8 to 27.6 MPa (2000 to 4000 psi). Often, in the modeling of processing operations, it is necessary to neglect the effect of pressure in order to obtain analytical or even numerical solutions that are manageable, as discussed in Section 11.3.

Time Dependence. Shear-thinning (and shear-thickening) behavior is considered to be reversible providing no thermal or mechanical degradation has occurred. In some cases, the subsequent flow behavior of a previously sheared fluid may depend upon the prior shear history and the time allowed for recovery. A fluid whose viscosity is reduced by prior deformation or decreases with time under conditions of constant stress or shear rate is called *thixotropic* [4]. Eventually, the viscosity will recover (increase) once the stress is removed. An example of a thixotropic fluid is non-drip latex paint. Similarly, a fluid whose viscosity has increased as a result of prior deformation history or increased in time under application of constant stress or strain is called *antithixotropic*. As will be shown shortly, the successful modeling of polymer-processing operations is difficult enough without introducing time-dependent viscosity terms, and no attempt to do so will be made here.

11.2.2 Viscosity of Polymer Solutions and Suspensions

Solution Viscosity. For very dilute solutions, polymer coils are widely separated and do not overlap, as illustrated in Figure 11-16. At a critical concentration, c^{**} , marking the transition from the extremely dilute to dilute regions, the hydrodynamic volumes of individual coils start to touch. As concentration is further increased ($c >$

c^*), coils begin to overlap and finally entanglements are formed that increase viscosity.

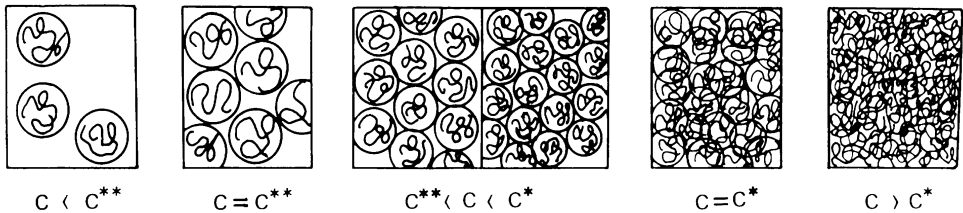


Figure 11-16 Critical concentration regions showing transition from the extremely dilute region ($c < c^{**}$) where polymer coils are isolated to the dilute region ($c > c^*$) where coils become entangled. Reproduced from A. Dondos and C. Tsitsilianis, *Viscoelastic Study of Extremely Dilute Macromolecular Solutions: Critical Concentration c and the Intrinsic Viscosity of the Polystyrene through Scaling Laws. The Value of the Huggins Constant*, Polymer International, 1992. **28**: p. 151–156. Copyright Society of Chemical Industry. Reproduced with permission. Permission is granted by John Wiley & Sons Ltd. on behalf of the SCI.

The critical concentration, c^* , may be marked by an abrupt increase in the relative viscosity increment* (eq. 3.104). This transition is shown for cellulose acetate (CA) in dimethyl sulfoxide (DMSO) in Figure 11-17. The critical transition concentration was found to be 3.7 g dL^{-1} and approximately independent of the solvent^[5], although a dependence of c^* on the molecular weight of CA would be expected.

* The relative viscosity increment is also known as the specific viscosity, η_{sp} .

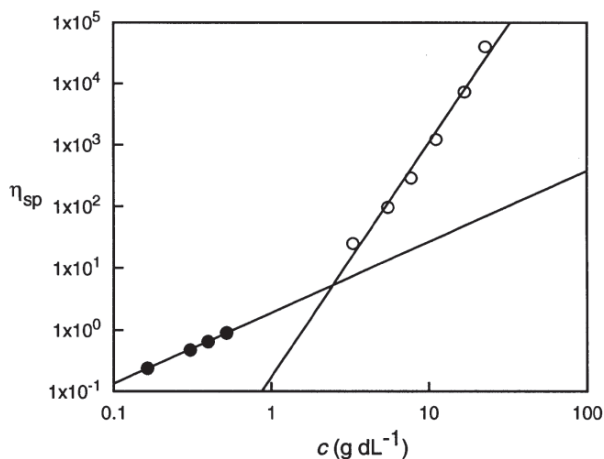


Figure 11-17 Concentration dependence of the specific viscosity, η_{sp} of dilute and moderately concentrated solutions of cellulose acetate in dimethyl sulfoxide [5]. The intersection of straight lines that are drawn through the dilute-solution (\bullet) and concentrated-solution (\circ) data marks the critical concentration, c^* (ca. 3.7 g dL^{-1} in this case).

Below c^* , viscosity is proportional to concentration, but above c^* , viscosity is approximately proportional to the *fifth power* of concentration. In general, the effect of molecular weight and solution concentration of viscosity can be modeled as [6]

$$\eta = K(c\rho)^\alpha M^\beta \quad (11.9)$$

where K is a constant and α and β are parameters; the ratio β/α is usually in the range from 0.54 to 0.74.

The presence of a solvent (or plasticizer) has two effects on polymer viscosity in the concentrated solution region: the solvent (1) lowers the T_g and (2) increases the molecular weight between entanglements, M_e (see Section 4.1.1), as

$$M_e = \frac{M_e^o}{\phi} \quad (11.10)$$

where M_e^o is the molecular weight between entanglements for the undiluted polymer and ϕ is the volume fraction of solvent. As polymer concentration increases, polymer solutions become more non-Newtonian as the number of entanglements increases, as illustrated for concentrated solutions of polystyrene in *n*-butyl benzene in Figure 11-18. The data show that viscosity of a concentrated polymer solution rapidly increases with increasing polymer concentration. In addition, the onset of shear-thinning behavior occurs at lower shear rate with increasing concentration.

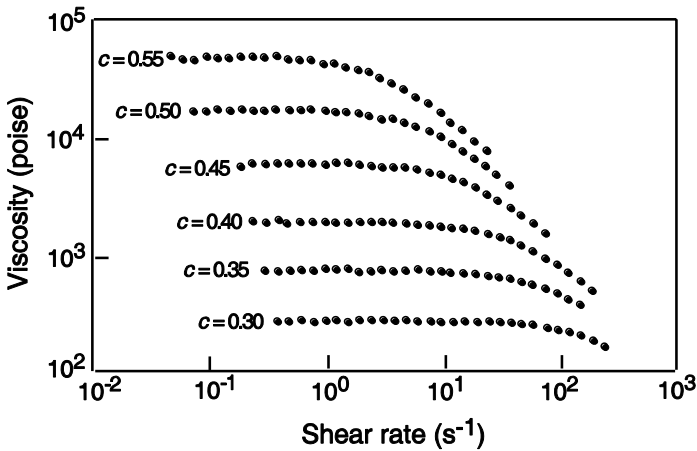


Figure 11-18 Viscosity of polystyrene (411,000 molecular weight) in *n*-butyl benzene at different concentrations (c , units of g cm^{-3}) as a function of shear strain-rate ($\dot{\gamma}$) at 30°C . Adapted from W. W. Graessley, R. L. Hazleton, and L. R. Lindeman, *The Shear-Rate Dependence of Viscosity in Concentrated Solutions of Narrow-Distribution Polystyrene*, Transactions of the Society of Rheology, 1967. 11: p. 267–285 (1967), with permission of the publisher.

Viscosity of Suspensions. In many cases, concentrated polymer solutions and melts may contain particulate or fiber fillers. For example, commercial rubber formulations usually contain carbon black. Poly(vinyl chloride) for floor tile or wire insulation applications typically contains rigid fillers such as calcium carbonate. A *plastisol* is a suspension of polymer particles in a liquid plasticizer, while a *latex* is a suspension of polymer particles in water. In all these cases, suspended particles affect the rheological properties of the suspension.

In 1906, Einstein theorized that the viscosity of dilute suspensions in a Newtonian liquid can be expressed as

$$\eta = \eta^0 (1 + k_E \phi) \quad (11.11)$$

where η^0 is the viscosity of the suspending liquid, k_E is called the Einstein coefficient, and ϕ is the volume fraction of suspended particles. The Einstein coefficient depends upon the geometry of the dispersed phase as well as the orientation of fibers and other nonspherical fillers. In the case of spherical fillers, such as calcium carbonate, k_E is 2.5. Equation (11.11) indicates that the relative viscosity, η/η^0 , depends only upon the concentration of filler and is independent of the size and nature of the particles. Over the years, many other equations have been proposed with various degrees of success. One of the best, proposed by Mooney, is given as

$$\ln(\eta/\eta^0) = \frac{k_E \phi}{1 - \phi/\phi_m} \quad (11.12)$$

where ϕ_m is the maximum packing (volume) fraction, which varies from 0.065 for rod-shaped particles to 0.7405 for hexagonal close-packed spheres. It may be noted that even Newtonian fluids such as water become non-Newtonian at moderate concentrations of suspended particles. Some suspensions such as lattices and plastisols exhibit yield (Bingham) behavior, as discussed in the following section.

11.2.3 Constitutive Equations

In order to model a simple-flow geometry as a prelude to handling more complicated processes such as extrusion, it is necessary to begin with some reasonable model for the relation between shear stress and shear rate (eq. (11.5)). The most widely used relationship is the *power-law* (or Ostwald–de Waele–Nutting) model given as

$$\tau = m\dot{\gamma}^n \quad (11.13)$$

where m is called the *consistency* and n is the *power-law index*. For a given polymer, m is a decreasing function while n is an increasing function of increasing temperature, which means that the melt becomes more Newtonian (i.e., less shear thinning) with an increase in temperature. It follows from the GNF model given by eq. (11.5) that the dependence of apparent viscosity, η , on $\dot{\gamma}$ for a power-law fluid (PLF) is

$$\eta = m\dot{\gamma}^{n-1}. \quad (11.14)$$

Equation (11.14) indicates that, when $n = 1$, η is independent of $\dot{\gamma}$. This means that Newton's law of viscosity may be considered to be a special case (i.e., $n = 1$ and $m = \mu$) of the more general PLF model. For shear-thinning behavior, $n < 1$. Representative values of the power-law parameters, m and n , and the $\dot{\gamma}$ range for which they are applicable are given for several commercially important polymers in Table 11-1. Some non-Newtonian fluids require an application of a threshold (or yield) stress, τ_y , before flow will begin. Such fluids are termed *Bingham* fluids and may be viewed as having some internal structure that collapses at τ_y . Examples include some suspensions, slurries, pulps, and ketchup. If the viscous response is Newtonian once the yield stress has been reached, the constitutive equation for a Bingham fluid can be written as

$$\tau = \tau_y + \mu\dot{\gamma}. \quad (11.15)$$

Table 11-1 Power-Law Parameters for Some Representative Polymers

Polymer	T (°C)	$\dot{\gamma}$ Range (s ⁻¹)	m (N s ^{n} m ⁻²)	n
Polycarbonate	180	100–1000	8.39×10^3	0.64
	200	100–1000	4.31×10^3	0.67
	220	100–1000	1.08×10^3	0.80
Polypropylene	180	100–400	6.79×10^3	0.37
	190	100–3500	4.89×10^3	0.41
	200	100–4000	4.35×10^3	0.41
Polystyrene	190	100–4500	4.47×10^4	0.22
	210	100–4500	2.38×10^4	0.25
	225	100–5000	1.56×10^4	0.28

It is clear that eq. (11.14) is suitable for representing the dependence of viscosity on shear rate only in the shear-thinning region where a plot of $\log \eta$ versus $\log \dot{\gamma}$ is linear. Since this is normally the $\dot{\gamma}$ range for most important processing operations, particularly extrusion and injection molding (see Table 11-2), this restriction is seldom significant considering the simplicity of the model. Other constitutive equations, such as the Carreau model [7], are available to fit data over a more extensive $\dot{\gamma}$ range but, typically, make the solution to processing problems more difficult.

Table 11-2 Typical $\dot{\gamma}$ Range for Polymer Processing Operations

Operation	$\dot{\gamma}$ Range (s ⁻¹)
Compression molding	1–10
Calendering	10–10 ²
Extrusion	10 ² –10 ³
Injection molding	10 ³ –10 ⁴

11.2.4 Elastic Properties of Polymeric Fluids

A unique and important characteristic of polymer melts and concentrated solutions is their elastic recovery after shear deformation. When polymer chains are oriented in the flow direction, there is an entropic driving force for the chains to recover their random coil conformation upon cessation of the stress. For example, chains undergoing shear deformation during flow in a capillary will recover their original equilibrium conformations at the exit of a capillary where stress goes to zero. This gives rise to *die swell* whereby the diameter of the extruded fiber is larger than the diameter of the capillary. As an illustration, the die swell of polyethylene extruded through a capillary die is shown in Figure 11-19.

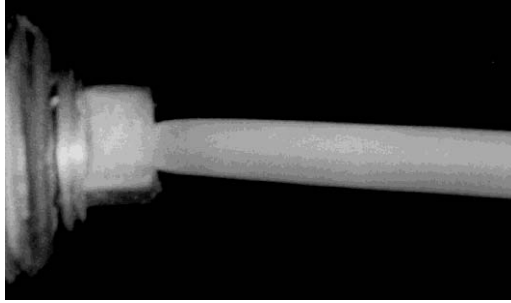


Figure 11-19 Die swell of high-density polyethylene exiting a circular tube at 180°C. Reprinted from C. D. Han, *Rheology in Polymer Processing*. 1976, New York: Academic Press. p. 3. Copyright 1976 Academic Press.

Quantitatively, elastic response is expressed in terms of *normal stresses*. Both stress and strain are second-order tensors and can be represented by a 3×3 matrix having nine components. For example, the stress tensor, τ , in an arbitrary coordinate system with axes 1, 2, and 3 (equivalent to x , y , and z in rectangular coordinates; r , z , and θ in cylindrical coordinates; or r , θ , and ϕ in spherical coordinates) is given as

$$\boldsymbol{\tau} = \begin{pmatrix} \tau_{11} & \tau_{12} & \tau_{13} \\ \tau_{22} & \tau_{22} & \tau_{23} \\ \tau_{31} & \tau_{32} & \tau_{33} \end{pmatrix}. \quad (11.16)$$

The first and second subscripts of each stress component, τ_{ij} , in the matrix identify the row (the direction of the force vector) and the column (the normal to the plane on which the component of force acts), respectively. The stress tensor (as well as the strain tensor,* which can be written in an analogous fashion) is symmetrical. This means that $\tau_{ij} \equiv \tau_{ji}$ and, therefore, only six of the total of nine stress components are independent. The normal stress components are those lying along the diagonal of the matrix where $i \equiv j$ (i.e., τ_{11} , τ_{22} , τ_{33}). The orientation of normal stresses for a cubical fluid element in simple plane shear is illustrated in Figure 11-20.

* The rate-of-deformation tensor is given as

$$\boldsymbol{\Delta} = \begin{pmatrix} \Delta_{11} & \Delta_{12} & \Delta_{13} \\ \Delta_{21} & \Delta_{22} & \Delta_{23} \\ \Delta_{31} & \Delta_{32} & \Delta_{33} \end{pmatrix}$$

for which the components of the tensor are symmetric, $\Delta_{ij} \equiv \Delta_{ji}$.

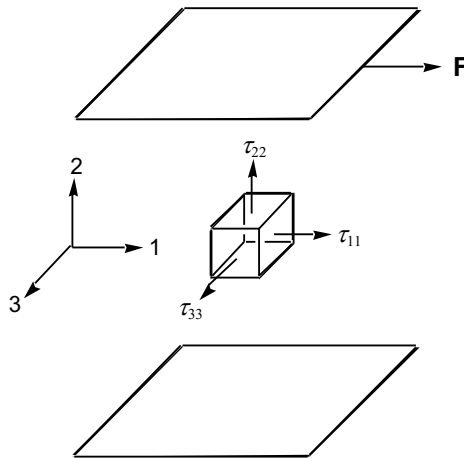


Figure 11-20 Normal stresses generated at the faces of a cubical element of fluid undergoing simple shear (shear stress τ_{12}).

When considering normal stresses, it is convenient to define two *normal-stress differences* that, like apparent viscosity, are functions of $\dot{\gamma}$. These are the *first* (or primary) *normal-stress difference*

$$\tau_{11} - \tau_{22} = \Psi_1(\dot{\gamma})\dot{\gamma}^2 \quad (11.17)$$

and the *second normal-stress difference*

$$\tau_{22} - \tau_{33} = \Psi_2(\dot{\gamma})\dot{\gamma}^2 \quad (11.18)$$

where Ψ_1 and Ψ_2 are called the first and second normal-stress coefficients, respectively, which are also functions of $\dot{\gamma}$. The apparent viscosity, η , and the two normal-stress coefficients are the three *material functions* that describe the complete shear response (viscous and elastic) of polymeric fluids.

In terms of their importance to polymer processing, the first normal-stress difference is the more significant of the two. It is responsible for the swelling of extrudate exiting a die (called *die swell*, the Barus effect, or puffup) and for a nonzero pressure drop that has been observed to occur at the die exit (see Section 11.4.1). By comparison, the second normal-stress difference is small (only 10% to 15% of the magnitude of the first normal-stress difference) and has a negative sign. Both normal-stress differences can be measured directly at low $\dot{\gamma}$ by modern rheological instruments such as cone-and-plate and parallel-plate rheometers, which have sensitive force transducers mounted in the three directions orthogonal to the plane of shear. Basic concepts of rheometry are covered in Section 11.4. For evaluation of normal-stress effects at higher $\dot{\gamma}$ typical of actual processing operations, online rheometers such as a slit die (rectangular die) attached to an extruder may be used.

By reading pressures along the length of the die using flush-mounted pressure transducers, the exit pressure may be determined by extrapolation of a plot of pressure versus die length. Correlations may then be used to relate die swell to exit pressure for given operating conditions.

11.2.5 Melt Instabilities

It has been widely recognized that polymer extrudates of a wide variety of shapes including tubing, rods, and other profiles can develop distortions at some critical shear flow rates. This general phenomenon of distorted extrudates is called *melt fracture*. Distortions can take the form of bamboo, spirals, or “sharkskin” as shown in Figure 11-21. Although this behavior has been widely observed, the cause of sharkskin and other forms of melt fracture is still a controversial subject [8]. A recent explanation attributes sharkskin formation to chain disentanglement at the die wall in the exit region [9]. This may be due to a combination of interfacial slip and cohesive failure.

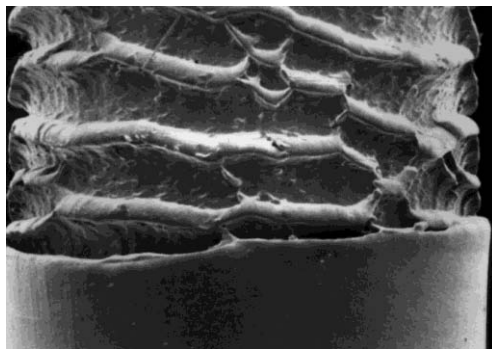


Figure 11-21 Scanning electron micrograph showing the onset of sharkskin in an extruded LLDPE rod (0.76 mm in diameter). Reproduced from M. M. Denn, *Pressure Drop Flow Rate Equation for Adiabatic Capillary Flow with a Pressure- and Temperature-Dependent Viscosity*. Polymer Engineering and Science, 1981. **21**: p. 65–68, by permission of the publisher.

11.2.6 Drag Reduction

It has been observed that dilute solutions (1 to 100 ppm) of many high-molecular-weight (>100,000) linear polymers can reduce turbulent friction in fluid flow by as much as 70% to 80%. This *drag reduction* was first observed in 1948 for flow in a circular pipe [10]. The most effective drag-reducing agents are flexible and high-

molecular-weight polymers. Poly(ethylene oxide) (PEO) is widely used as a drag-reducing polymer in aqueous solutions. Another water-soluble polymer that is effective as a drag-reducing agent is polyacrylamide. Some naturally occurring polymers such as guar and xanthan are also effective drag reducers. The *oil-soluble* polymer polyisobutylene (PIB) is effective for drag reduction of crude oil [11]. Suspensions of some fibers, including nylons, can also impart good drag reduction in turbulent flow.

Although the exact mechanism of drag reduction is still unclear, it is possible that drag reduction may be related to extensional flow. During flow, long polymer chains become disentangled and oriented in the direction of flow. Extensional viscosity (see Section 11.2.1) significantly increases and a form of strain-rate hardening occurs, which imposes a maximum limit on the strain rate. The high extensional viscosity reduces turbulent fluctuations (probably through the suppression of the roll-wave motion and vortex stretching in the sublayer) and, thereby, reduces friction.

Applications for drag reduction include those for which reduced friction in fluid flow is important. For example, a small amount of a water-soluble polymer can be injected into sewers during periods of heavy rain to upgrade flow and, thereby, prevent flooding. A drag-reducing polymer can also be injected at the bow of a ship to decrease friction and increase speed or be used to decrease pressure drop in water lines for firefighting.

11.3 Analysis of Simple Flows

Polymer-processing operations like extrusion, injection molding, pultrusion, roll coating, blow molding, and others are too complicated to model rigorously. Fortunately, most processing operations can be broken down into a set of simpler flow processes for which analytical or numerical solutions can be obtained using various simplifying approximations and constraints. In this way, it is possible to understand how process variables such as screw speed and temperature in an extruder affect performance variables such as volumetric output. A complete discussion of the modeling of polymer processes is well beyond the scope of this chapter and the reader is encouraged to consult the excellent texts by Han, McKelvey, Middleman, and Tadmor and Gogos that are cited in the Suggested Reading at the end of this chapter. In the next sections, a general development of this subject is given along with some important results to serve as an introduction to the subject.

All polymer-processing operations involve the flow of polymer solutions or melts under a pressure gradient, shear deformation, or both. Since concentrated polymer solutions and polymer melts are non-Newtonian fluids, it is necessary to know the exact relationship between stress and strain—the constitutive equation—

in order to analyze flow through even the simplest geometry. As mentioned earlier, the PLF model is the one most frequently used. The simplest geometries to model are those for which (1) edge effects can be neglected, (2) flow is isothermal, and (3) a coordinate system (rectangular, cylindrical, or spherical) can be selected such that there is only one nonzero component of the velocity vector (i.e., flow is visco-metric). Examples include pressure flow through long capillaries and between infinitely wide parallel plates. Simple *shear* flows* include those created by long concentric cylinders of which one cylinder is rotating or moving along the axial direction and between infinitely wide parallel plates of which one is moving at a constant velocity and is parallel to the other.

The solution to a simple-flow model is usually in the form of an expression for velocity as a function of the coordinate parameter(s) of the system. For example, the velocity in the axial (z) direction (i.e., along the length of a capillary) is a function of the radial distance from the centerline, $u_z(r)$, as discussed in the following section. In cases where the flow is directed out of the system, as it is in pressure flow through a capillary, the velocity profile can be used to obtain an expression for the volumetric flow rate.

In general, any solution to a flow problem must satisfy the conservation of momentum (i.e., the dynamic equations), conservation of mass (i.e., the continuity equations), and conservation of energy (i.e., the energy equations). The solutions given in the following examples of pressure and shear flow are obtained with the assumptions that the flow is isothermal, laminar, fully developed, steady, and incompressible. In addition, it is assumed that all body forces such as gravity can be neglected. The imposition of isothermal conditions is an especially major constraint, especially since processing operations are seldom isothermal and the flow of viscous polymer melts results in the generation of heat (i.e., viscous dissipation). The advantage of the restraint of isothermal flow is that it removes the energy equations from consideration in the solution and, therefore, greatly simplifies the task.† Taken

* A simple shear flow is formally defined as one for which a coordinate system can be chosen such that there is a nonzero component of velocity in only one direction

$$\mathbf{u} = (u_1, 0, 0)$$

and the rate-of-deformation tensor is given as

$$\Delta = \dot{\gamma} \begin{pmatrix} 0 & 1 & 0 \\ 1 & 0 & 0 \\ 0 & 0 & 0 \end{pmatrix}$$

where $\dot{\gamma}$ is the shear rate (a scalar).

† The energy equation for an incompressible fluid is written in Cartesian coordinates as

$$\rho \hat{C}_p \left(\frac{\partial T}{\partial t} + u_j \frac{\partial T}{\partial x_j} \right) = \frac{\partial}{\partial x_j} \left(k \frac{\partial T}{\partial x_j} \right) + \tau_{ij} \frac{\partial u_i}{\partial x_j}$$

together, these assumptions mean that only *one* dynamic equation usually needs to be solved for a particular problem.

The dynamic equations for an *incompressible* fluid of density ρ subject to an external force field, \mathbf{f} , are written in Cartesian coordinates as

$$\rho \left(\frac{\partial u_i}{\partial t} + u_j \frac{\partial u_i}{\partial x_j} \right) = \frac{\partial T_{ij}}{\partial x_j} + \rho f_i \quad (11.19)$$

where u is velocity, t is time, f is a body force (e.g., gravity), and the summation is over all j —the coordinate parameters x , y , and z . This means that there are three dynamic equations for each coordinate system. The parameter T_{ij} appearing in eq. (11.19) is a component of the *total* stress tensor and is defined as

$$T_{ij} = \tau_{ij} - p\delta_{ij} \quad (11.20)$$

where τ_{ij} is the component of the shear-stress tensor (see eq. (11.16)) corresponding to T_{ij} and sometimes called the dynamic (or deviatoric) stress tensor; p is (hydrostatic) pressure; and δ_{ij} is called the Kronecker delta, a component of a unity tensor* (where $\delta_{ij} = 1$ for $i = j$ and $\delta_{ij} = 0$ for $i \neq j$).

The continuity equation for an incompressible fluid is written in Cartesian coordinates as

$$\frac{\partial u_i}{\partial x_i} = 0. \quad (11.21)$$

The complete expressions for the dynamic and continuity equations in Cartesian and cylindrical coordinates are given in Appendix A.2 at the end of this chapter.

Velocity is introduced into the solution of a process-flow problem through its relationship to strain (e.g., eq. (11.4)) and the constitutive equation (eq. (11.5)), which relates the stress, τ , and shear strain rate.† For simple isothermal flows, where

where \hat{C}_p is the heat capacity per unit mass and k is the thermal conductivity. The dynamic and energy equations are usually coupled through the velocity terms, making the solution of differential equations especially difficult. Numerical solutions are available for adiabatic conditions, but, in general, temperature effects are very difficult to handle for non-Newtonian flow.

* The unity tensor is formally given as

$$\delta = \begin{pmatrix} 1 & 0 & 0 \\ 0 & 1 & 0 \\ 0 & 0 & 1 \end{pmatrix}.$$

† It should be noted that the well-known Navier–Stokes equations are just a special case of the more general dynamic equations—one for which the incompressible fluid is Newtonian and, therefore,

there is only one nonzero component of the velocity vector, the problem reduces to the solution of a single differential equation provided by the dynamic equations.

The terms within parentheses on the left-hand side of eq. (11.19) are called the *inertial* terms and usually can be neglected.* This is particularly fortunate since the second of the inertial terms introduces nonlinearity to the set of partial differential equations. Since we are also neglecting body forces, what remains of eq. (11.19) is a much simpler relationship:

$$\frac{\partial T_{ij}}{\partial x_{ij}} = 0. \quad (11.22)$$

Another assumption, and one that is very good, is that there is *no slip* between the fluid and the surface of the flow geometry. This no-slip assumption provides one or two boundary conditions for the solution of the differential equation. The example of pressure flow through a capillary given in the next section serves to illustrate this general approach for solving a fluid-flow problem.

11.3.1 Pressure (Poiseuille) Flow

Flow through a Capillary. Analysis of simple pressure flow through a tube or capillary is important in the modeling of extrusion through a capillary die and in the measurement of melt viscosity by means of a capillary rheometer, as discussed in Section 11.4.1. As discussed in the previous section, it is helpful to assume that flow is isothermal, fully developed, incompressible, laminar, and steady. For an infinitely long, horizontal tube for which undeveloped flow in the entrance region and gravitational forces can be ignored, the dynamic equations are reduced to the single differential equation (see Problem 11.8)

$$\frac{\partial p}{\partial z} = \frac{1}{r} \left[\frac{\partial}{\partial r} (r \tau_{rz}) \right] \quad (11.23)$$

where z is chosen to be the direction of flow (the axial direction). Substitution of the PLF constitutive equation (eq. (11.13)) in the form

$$\tau_{rz} = m \dot{\gamma}_{rz}^n = m \left(\frac{du_z}{dr} \right)^n \quad (11.24)$$

$$\tau_{ij} = \mu \dot{\gamma}_{ij}.$$

* Note that all derivatives with respect to time (e.g., the first of the inertial terms) become zero when the flow is assumed to be steady in time.

into eq. (11.23) and integration twice give the velocity of a PLF as

$$u_z(r) = \left(\frac{nR}{1+n} \right) \left(\frac{R\Delta p}{2mL} \right)^{1/n} \left[1 - \left(\frac{r}{R} \right)^{(1+n)/n} \right] \quad (11.25)$$

where R is the tube radius, $\Delta p/L$ is the pressure drop across the capillary per unit length, and r is the radial distance from the centerline (see Problem 11.9). Boundary conditions are obtained by realizing that the velocity at the surface (i.e., at $r = R$) of the capillary wall is zero, given a condition of no-slip, and the maximum velocity

$$u_z^{\max} = \left(\frac{nR}{1+n} \right) \left(\frac{R\Delta p}{2mL} \right)^{1/n} \quad (11.26)$$

occurs at the centerline ($r = 0$) and, therefore, $du_z/dr = 0$ (i.e., $\dot{\gamma} = 0$ at the centerline of the capillary). Division of eq. (11.25) by eq. (11.26) gives the velocity profile in dimensionless form as

$$\frac{u_z}{u_z^{\max}} = 1 - \left(\frac{r}{R} \right)^{(1+n)/n}. \quad (11.27)$$

As shown in Figure 11-22, the velocity profile of a PLF becomes flatter (i.e., more plug flow) with decreasing n (i.e., with increasing shear-thinning behavior).

The volumetric flow rate, Q , through the capillary can be obtained by integrating the velocity function (eq. (11.25)) as

$$Q = \int_{r=0}^R \pi r u_z(r) dr = \left(\frac{\pi R^3}{1+3n} \right) \left(\frac{R\Delta p}{2mL} \right)^{1/n}. \quad (11.28)$$

For the special case of a Newtonian fluid for which $m = \mu$ and $n = 1$, eq. (11.28) reduces to the familiar *Hagen–Poiseuille equation*

$$Q = \frac{\pi R^4 \Delta p}{8\mu L}. \quad (11.29)$$

Similar models can be developed for isothermal pressure flow through other simple-flow geometries such as an annulus or infinitely wide parallel plates. Respectively, these approximate the flow through tubing (i.e., annular die) and sheet (i.e., slit) dies used in extrusion. The exact form of the relationship between Q and the pressure drop, Δp , is called the *die characteristic*. As will be discussed in Section 11.5.1, a *screw characteristic*, which relates the volumetric output of an extruder as a function of different variables such as the extruder screw speed and geometry, may be obtained by modeling extruder operation as combined pressure and shear flow in a rectangular duct. Simultaneous solution of the die and screw charac-

teristics gives the operating conditions of pressure and flow rate for the coupled operation of the extruder and die. For completeness, the die characteristics for a PLF in different die geometries are summarized in Table 11-3.

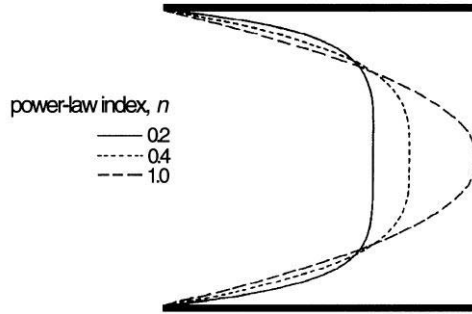


Figure 11-22 Velocity profile of a power-law fluid during isothermal pressure flow through a capillary as a function of the power-law index (n). Adapted from *An Introduction to Rheology*, H. A. Barnes, J. F. Hutton, and K. Walters, p. 34, Copyright 1989, with permission from Elsevier.

Table 11-3 Die Characteristics for a Power-Law Fluid in Pressure Flow

Geometry	Die Characteristic
Capillary	$Q = \left(\frac{n\pi R^3}{1+3n} \right) \left(\frac{R\Delta p}{2mL} \right)^{1/n}$
Annulus ^a	$Q = \left(\frac{n\pi R_o}{1+2n} \right) (R_o - R_i)^{2+1/n} \left(\frac{\Delta p}{2mL} \right)^{1/n} F(n, \kappa)$
Parallel plates ^b	$\frac{Q}{W} = \left[\frac{nH^2}{2(1+2n)} \right] \left(\frac{H\Delta p}{2mL} \right)^{1/n}$
Rectangular duct ^c	$Q = WH^2 \left(\frac{W\Delta p}{2mL} \right)^{1/n} S_p$

^a R_i , inner radius; R_o , outer radius; F is a function of n and the aspect ratio of the annulus, $\kappa = R_i/R_o$.

^b Infinitely wide parallel plates where H represents the separation of plates and W is unit width.

^c This is an example of a non-simple flow geometry; S_p is a shape factor that is a function of n and the aspect ratio, W/H .

11.3.2 Drag Flow

Plane Couette Flow. An example of a simple shear flow is plane (Couette) flow between two infinitely wide parallel plates as used as an example in Section 11.2 and illustrated in Figure 11-11. In this case, the top plate is driven at a constant velocity, U , in the x -direction while the bottom plate is fixed. Since the plates are infinitely wide, there are no edge effects and, therefore, the only nonzero component of the velocity vector is the x -component. This is an example of a *viscometric flow* as were the previous cases for simple pressure flows. Assuming that there is *no slip* of the fluid at the surface of the two plates and the vertical distance between the two plates is given as H , the velocity of the fluid element, u_x , at the top surface (i.e., $y = H$) is U , while the velocity at the bottom plate (i.e., $y = 0$) is zero. With these boundary conditions, the velocity profile is linear and *independent of the fluid type* (or constitutive equation). Specifically, the solution of the (x -component) dynamic equation gives the velocity of each fluid element as

$$u_x = \left(\frac{y}{H} \right) U. \quad (11.30)$$

The volumetric flow rate, Q , per unit width is then obtained from the velocity equation as

$$\frac{Q}{W} = \int_0^H u_x dy = \frac{UH}{2}. \quad (11.31)$$

As was the case for the velocity profile, the volumetric flow rate is independent of the fluid constitutive relationship—it is the same whether the fluid is Newtonian or a PLF.

Axial Annular Couette Flow. An important geometry that can be used as a model of a processing operation (e.g., wire coating as illustrated in Section 11.5.2) consists of two concentric cylinders of which the inner cylinder (e.g., the wire) is pulled at a constant linear velocity, U , as illustrated in Figure 11-23.

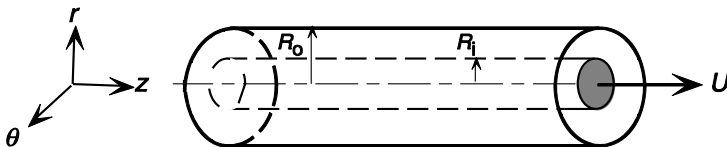


Figure 11-23 Representation of axial annular Couette flow. The inner cylinder is pulled at a velocity, U .

A solution of this problem for a Newtonian fluid is easily obtained and gives

$$\frac{u_z}{U} = \frac{\ln(r/R_o)}{\ln \kappa} \quad (11.32)$$

where $\kappa = R_i/R_o$. The solution for a PLF is given as*

$$\frac{u_z}{U} = \frac{1}{\kappa^q - 1} \left[\left(\frac{r}{R_o} \right)^q - 1 \right] \quad (11.33)$$

where

$$q = 1 - \frac{1}{n}. \quad (11.34)$$

The volumetric flow rate is then obtained as

$$Q = 2\pi \int_{R_i}^{R_o} r u_z(r) dr. \quad (11.35)$$

Using eq. (11.33) and performing the integration give the following relationship for Q (in dimensionless form) of a power-law fluid in axial annular Couette flow:

$$\frac{Q}{2\pi R_o (R_o - R_i) U} = \frac{1}{q+2} \frac{1 - \kappa^{q+2}}{(1 - \kappa)(\kappa^1 - 1)} - \frac{1 + \kappa}{2(\kappa^q - 1)}. \quad (11.36)$$

In this case, Q has the general significance of the volume of coating extruded on the wire per unit time. The complete analysis of an actual wire-coating operation is more complicated than indicated above because it involves the superposition of a pressure flow on the drag flow. The pressure flow is introduced as a result of the attachment of an extruder to the wire-coating die.

11.4 Rheometry

The relationship between stress and shear rate, and therefore the dependence of apparent viscosity upon shear rate, can be determined over a wide temperature range by a variety of techniques that utilize some of the simple pressure or shear geometries discussed in the previous section. These include capillary and Couette rheome-

* In the case of axial annular Couette flow, the solutions for u_z and Q for a Newtonian fluid cannot be obtained from the PLF results by letting $n = 1$ ($q = 0$) and must be obtained independently.

try, which are based upon simple pressure flow through a capillary and simple shear flow through two rotating, concentric cylinders, respectively. Other common methods include cone-and-plate and parallel-plate rheometry, which can also give information concerning normal stresses through measurements by force transducers mounted in the direction normal to the plane of shear. Slit rheometers, which can be used to measure exit pressures in pressure flow through a rectangular channel, can be used to measure normal stress under typical processing conditions. The basics of capillary, Couette, and cone-and-plate rheometry are presented in this section. A complete discussion of rheometry can be found in a number of excellent texts such as those by Nielsen, Middleman, and Walters cited in the Suggested Reading at the end of this chapter.

11.4.1 Capillary Rheometer

In addition to providing a model for flow of a non-Newtonian fluid through a capillary die, an understanding of pressure flow through a tube may be used to determine the apparent viscosity of a polymer melt as a function of $\dot{\gamma}$. This method is called *capillary rheometry* and can be used over the $\dot{\gamma}$ range from 1 to 10^5 s^{-1} , which includes most polymer-processing operations (see Table 11-2). As can be shown by a simple force balance on a fluid element in the capillary, the shear stress ($\tau_{rz} \equiv \tau_{rz}$) given as

$$\tau = \frac{r\Delta p}{2L} \quad (11.37)$$

depends only upon the pressure drop and distance from the centerline—it is totally independent of whether the fluid is Newtonian or non-Newtonian (see Problem 11.6).

The experimental procedure requires the measurement of Q as a function of Δp through a capillary of known dimensions. The capillary is attached to a reservoir containing the polymer solution or melt, as illustrated in Figure 11-24. Pressurization of the reservoir forces the fluid through the capillary. From the value of Δp , the shear stress at the tube wall, τ_w (the maximum stress in capillary flow), is calculated as

$$\tau_w = \frac{R\Delta p}{2L}. \quad (11.38)$$

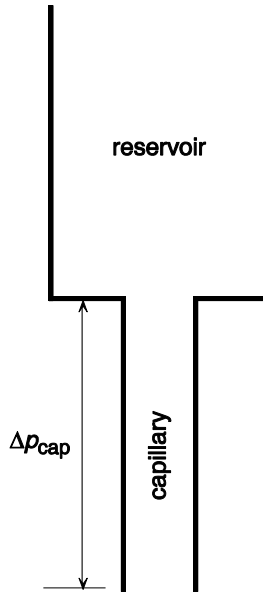


Figure 11-24 Pressure reservoir and capillary showing the overall pressure drop across the capillary (Δp_{cap}).

A second parameter used in the analysis of capillary-rheometry data is the *apparent shear rate*, ϕ , which is calculated from the experimentally measured volumetric flow rate, Q , as

$$\phi = \frac{4Q}{\pi R^3}. \quad (11.39)$$

As in the case for τ_w , ϕ is independent of the constitutive relation of the fluid; however, the exact form of the relationship between ϕ and $\dot{\gamma}$ is dependent upon the fluid model. For example, $\dot{\gamma}_w \equiv \phi$ for a Newtonian fluid. In the case of a PLF, it may be shown that the shear rate at the wall is given as

$$\dot{\gamma}_w = \frac{3n+1}{4n} \phi. \quad (11.40)$$

The apparent viscosity for any non-Newtonian fluid is then calculated from values of the model-independent expression for τ_w (eq. (11.38)) and the model-dependent expression for $\dot{\gamma}$ (e.g., eq. (11.40)) through the GNF model (eq. (11.5)) as

$$\eta = \frac{\tau_w}{\dot{\gamma}_w}. \quad (11.41)$$

If the fluid behavior is power law over the entire experimental range of $\dot{\gamma}$, a plot of $\log \tau_w$ versus $\log \phi$ will be linear with slope equal to the power-law index, n , and an intercept of $\log m'$, which is related to the consistency, m , as*

$$m = m' \left(\frac{4n}{3n+1} \right)^n. \quad (11.42)$$

Values of $\dot{\gamma}$ for each ϕ can then be calculated from knowledge of n and use of eq. (11.40).

One problem with the use of capillary rheometry is that the equations given above were obtained by assuming the usual model conditions: that the flow in the capillary is isothermal, fully developed, incompressible, laminar, and steady. The most difficult assumption to realize (and the one that is most easy to accommodate) is that the flow is fully developed over the entire length of the capillary. As shown in Figure 11-25, a significant pressure drop can occur at the entrance region of the capillary due to the extra stress needed to support the non-axial components of the velocity profile that result from the flow of the fluid from the large-diameter reservoir into the narrow capillary. For this reason, the pressure drop is not linear over the entire length of the capillary. Entrance effects can usually be neglected if the capillary is sufficiently long (e.g., $L/D > 200$); however, capillaries used in melt rheometry are typically short and, therefore, the experimental data need to be corrected for any entrance effects.

* It follows from eq. (11.24) in the form $\tau_w = m\dot{\gamma}_w^n$ and from eq. (11.40) that $\log \tau_w = n \log \phi + \log m'$.

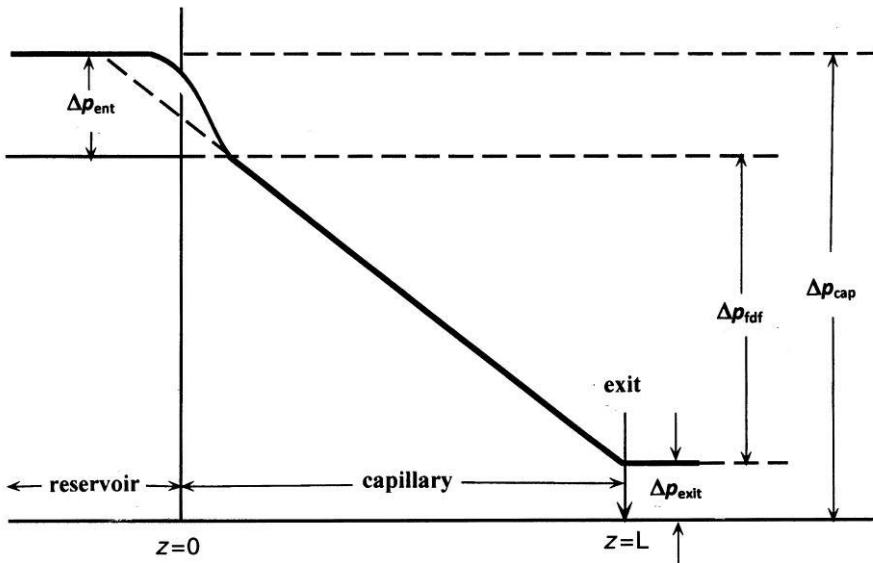


Figure 11-25 Pressure profile in reservoir and capillary (see Figure 11-23) showing the pressure drop in the entrance region between the reservoir and capillary, Δp_{ent} , the pressure drop across the capillary, and the exit pressure, p_{exit} .

Bagley [12] has suggested that entrance effects can be handled by assuming that the *effective* length of the capillary is greater than the actual length and, therefore, the shear stress at the wall can be corrected as

$$\tau_w^c = \frac{R\Delta p}{2(L + \varepsilon R)} \quad (11.43)$$

where ε is an empirical parameter obtained by extrapolating a plot of Δp versus the capillary aspect ratio, L/R , to zero pressure drop at constant $\dot{\gamma}$ for capillaries of different lengths as shown in Figure 11-26. Procedures for incorporating the effects of viscous heating and pressure on capillary flow have been proposed [13, 14] but are not usually undertaken.

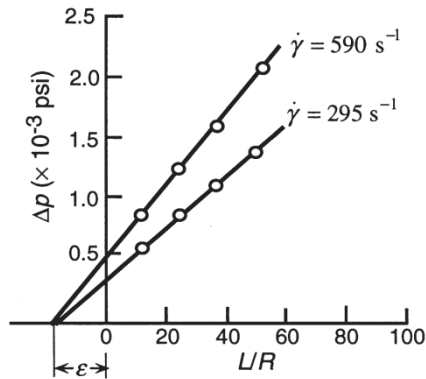


Figure 11-26 Bagley plot of pressure drop along a capillary versus capillary aspect ratio, L/R , at two different values of $\dot{\gamma}$. Adapted by special permission from M. H. Wohl, *Instruments for Viscosity*. Chemical Engineering, March 25, 1968. p. 99–104. Copyright © 1968, by Access Intelligence, New York 10005.

11.4.2 Couette Rheometer

Another example of a simple shear flow is circular Couette flow whereby a cylinder of radius R_i is driven at a constant angular velocity of Ω (usual units of rad s^{-1}) within an outer concentric cylinder of radius R_o as illustrated in Figure 11-27.

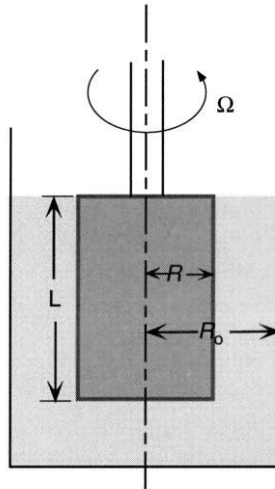


Figure 11-27 Couette rheometer.

The solution to this flow problem is simplified by using cylindrical coordinates and assuming that the cylinders have infinite length so that edge effects can be neglected.* Using the assumption of nonslip of the fluid at the surface of the two cylinders, the boundary conditions are

$$u_{\theta}(r = R_i) = R_i \Omega \quad (11.44)$$

and

$$u_{\theta}(r = R_o) = 0. \quad (11.45)$$

Unlike the case for plane Couette flow, the velocity profile is dependent upon the rheological properties of the fluid. The general solution for the θ component of the velocity vector for a PLF (eq. (11.13)) is

$$\frac{u_{\theta}}{R_i \Omega} = \left(\frac{r}{R_i} \right) \frac{1 - (R_o/r)^{2/n}}{1 - \kappa^{-2/n}} \quad (11.46)$$

where $\kappa = R_i/R_o$ is the aspect ratio. Again, this is an example of a viscometric flow where the remaining components of the velocity vector (i.e., u_r and u_z) are zero. For a Newtonian fluid ($n = 1$) such as water or mineral oil, eq. (11.46) reduces to

$$u_{\theta} = \frac{\Omega R_i^2}{R_i^2 - R_o^2} \left(r - \frac{R_o^2}{r} \right). \quad (11.47)$$

The expressions for shear stress and shear rate are

$$\tau = \frac{M}{2\pi r^2 L} \quad (11.48)$$

and

$$\dot{\gamma} = \frac{2\Omega R_i^2 R_o^2}{r^2 (R_i^2 - R_o^2)} \quad (11.49)$$

where M is the measured torque and L is the (submerged) length of the inner cylinder.

* Corrections can be made for edge effects by taking data for cylinders of different lengths in a manner similar to the Bagley correction for capillary data.

11.4.3 Cone-and-Plate Rheometer

Another important method of measuring the rheological properties of polymer solutions and melts is the cone-and-plate rheometer, which is illustrated in Figure 11-28. Either steady-shear or dynamic-viscosity data (see Section 5.1.3) can be obtained by this method. The cone angle, β , is typically very small (1 to 3 radians)—much smaller than is suggested by Figure 11-28. At these low angles, the shear rate is given as

$$\dot{\gamma} = \frac{\Omega}{\beta} \quad (11.50)$$

where Ω is the angular velocity of the cone. Dynamic viscosity can be obtained by applying an oscillatory shear on the cone. The shear stress, τ , is determined as

$$\tau = \frac{3M}{2\pi R_c^3} \quad (11.51)$$

where M is the measured torque on the cone having radius R_c . The apparent viscosity is then obtained from steady-shear measurements as

$$\eta = \frac{\tau}{\dot{\gamma}}. \quad (11.52)$$

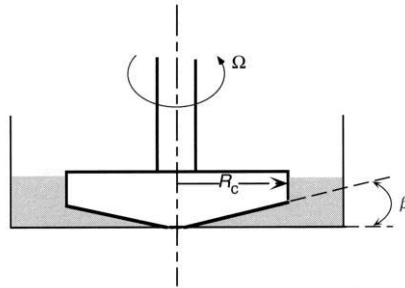


Figure 11-28 Idealized illustration of a cone-and-plate rheometer.

11.4.4 Rheometry of Polymer Solutions and Melts

Cone-and-plate, Couette cylinder, and also parallel-plate and eccentric rotating-plate rheometers can measure apparent viscosity over a low to moderate range of shear rates (e.g., 10^{-4} to 10^3 s^{-1}). Slit and capillary rheometers operate at high shear rates typical of many processing operations such as extrusion (see Table 11-2). Measurements using a variety of rheometers (e.g., cone-and-plate, slit, and capillary

rheometers) can be used to cover the entire range of shear rates, as illustrated in Figure 11-29.

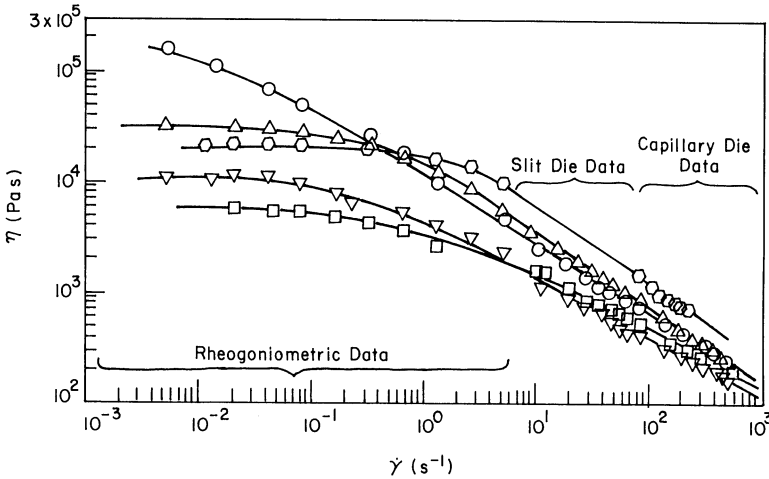


Figure 11-29 Viscosity versus shear rate for polymer melts at 200°C showing ranges of shear rate over which rheogoniometric (cone-and-plate), slit-die, and capillary rheometric measurements apply. Data for (○) high-density polyethylene, (Δ) polystyrene, (◐) poly(methyl methacrylate), (∇) low-density polyethylene, and (◻) polypropylene. Reprinted from C. D. Han, *Rheology in Polymer Processing*. 1976, New York: Academic Press. p. 108. Copyright 1976, Academic Press.

11.5 Modeling of Polymer-Processing Operations

11.5.1 Extrusion

Most complex polymer-processing operations can be reduced to a number of simple flow operations (see Section 11.3), which can be more easily solved. This is true for processing operations such as wire coating, blow molding, calendering, extrusion, and others. A full discussion of the modeling of polymer-processing operations is beyond the scope of this chapter and the reader is encouraged to consult any of a number of excellent texts cited in the Suggested Reading at the end of this chapter. As an illustration of the general approach, the basics of the modeling of extrusion are given in this section.

As discussed in Section 11.1.1, an extruder has three zones—feed, compression, and metering. In the modeling of extrusion, the metering section is the easiest

to analyze because the screw is conveying a homogeneous melt compared to solid pellets in the feed zone and a complex mixture of pellets and molten polymer in the compression zone. Clearly, a complete modeling of the extrusion process requires a coupled analysis of all three zones; however, the simpler treatment required to model the metering zone serves to illustrate how basic rheological principles developed in Sections 11.2 and 11.3 can be applied to tackle more complex processing problems.

To analyze flow in the metering zone, an approximation that is made (i.e., the lubrication approximation) is that rotation of the screw in the extruder shears the melt along the screw channel in a manner similar to plane Couette flow (Section 11.3.2) as described below. When no die is attached to the extruder, shear flow is the only consideration and the modeling is particularly easy. This is called a condition of *open discharge*. When a die (e.g., capillary, slit, or annular) is attached to the extruder, a pressure drop is produced across the die (pressure flow) and flow through the extruder is a combination of shear flow along the screw channel and pressure flow (back flow) against the extrusion direction. The volumetric flow, Q , therefore can be expressed as a simple combination of drag (shear) and pressure flows as*

$$Q = Q_d - Q_p. \quad (11.53)$$

From eq. (11.53), it is clear that the case of open discharge (i.e., $Q_p = 0$) results in the maximum extruder output. Simple pressure flow through various die geometries has been discussed in Section 11.3.1. Expressions were given for isothermal flow of both Newtonian and power-law fluids. In these cases, Q was given as some function of the pressure drop across the die (see Table 11-3). These relationships were called the die characteristics.

In order to obtain an expression for a screw characteristic (Q versus Δp), it is necessary to make some assumptions about the extruder screw geometry that allow the flow to be modeled as plane Couette flow. An illustration of a simple screw geometry is shown in Figure 11-30. If the diameter of the screw, D , is much greater than the channel depth, B ,[†] and the screw is assumed to have constant depth along the extruder barrel, the screw channel can be visually unwrapped from the screw barrel to give a long rectangular channel, as illustrated in Figure 11-31. Drag flow along the screw channel can then be modeled as plane shear flow with the barrel wall shearing fluid in the channel. Due to the presence of the channel walls, the flow is not a simple flow such as plane Couette flow between two infinitely wide

* Back flow due to leakage between the top of the screw flight and barrel wall is usually neglected. This expression is strictly true for Newtonian fluids for which the two flows are not coupled as they would be in the case of non-Newtonian flow.

[†] The flight clearance, δ , is usually considered to be negligible with respect to B .

parallel plates as discussed in Section 11.3.2. Plane Couette flow may be a reasonable assumption, however, if the width, W , of the channel is much greater than the channel height, B .

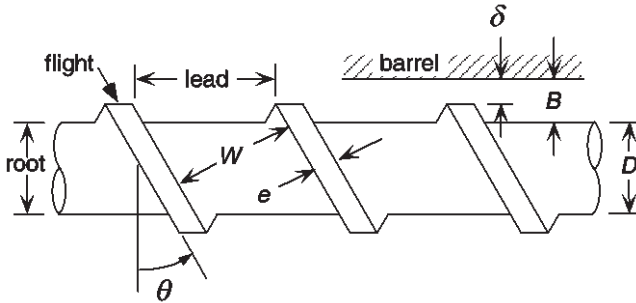


Figure 11-30 Illustration of extruder-screw geometry. Adapted from S. Middleman, *Fundamentals of Polymer Processing*. 1977, New York: McGraw-Hill Book Company. Reproduced with permission of Stanley Middleman.

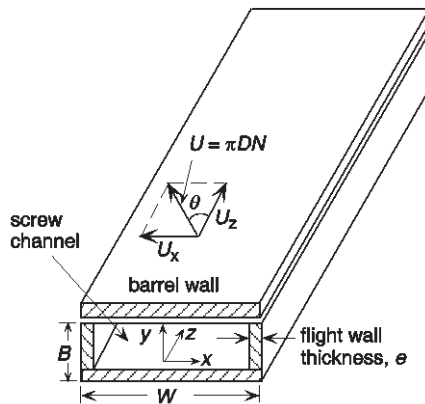


Figure 11-31 Geometry of an unwrapped screw channel.

In order to simplify the analysis of the extrusion process, the flow can be assumed to be isothermal and the fluid to be Newtonian. Under these conditions and using the geometric approximations that $W \gg B$ and $D \gg B$, the screw characteristic, a combination of both drag and pressure flows along the screw channel, is given as

$$Q = AN - C \frac{\Delta p}{\mu} \quad (11.54)$$

where N is the screw speed (in rpm) and μ is the Newtonian viscosity. The parameters A and C are determined by the geometry of the screw (see Figure 11-30) as

$$A = \frac{1}{2} \pi D W B \cos \theta \quad (11.55)$$

and

$$C = \frac{W B^3}{12 Z} \quad (11.56)$$

where Z is the screw channel length, which is related to the overall length of the extruder, L , and angle of the flight, θ , as

$$Z = \frac{L}{\sin \theta}. \quad (11.57)$$

For Newtonian fluids, the die characteristic can be put in the general form

$$Q = \frac{k}{\mu} \Delta p \quad (11.58)$$

where k is a function of the geometry for a given die (e.g., capillary, annulus, or slit), as given in Table 11-4. For Newtonian fluids, the die characteristic is a linear function of Δp , as was the screw characteristic. A plot of Q versus Δp for the screw (eq. (11.54)) and that for the die (eq. (11.58)) will intersect at a point that defines the *operating parameters* of Q and Δp for the combined operation of the extruder and die. Alternatively, Δp can be obtained analytically for extrusion of a Newtonian fluid by employing the mass balance between the extruder and die

$$Q_{\text{extruder}} = Q_{\text{die}}. \quad (11.59)$$

Substitution of eqs. (11.54) and (11.58) into eq. (11.59) gives the operating pressure drop as

$$\Delta p = \frac{\mu A N}{k + C}. \quad (11.60)$$

Once Δp is obtained from eq. (11.60), Q can then be calculated from either eq. (11.54) or eq. (11.58).

The *power* consumption for extrusion of a Newtonian fluid under isothermal conditions is given as

$$P = E \mu N^2 Z + A N \Delta p \quad (11.61)$$

where Δp is the operating pressure and E is a parameter determined from the screw geometry as

$$E = \left(\frac{\pi^3 D^3}{B} \right) \sin \theta (1 + 3 \sin^2 \theta). \quad (11.62)$$

Table 11-4 Die Parameters, k

Die	Expressions for k
Capillary	$\pi R^4/8L$
Annulus	$\left(\pi R_o^4/8L \right) \left[1 - \kappa^4 - \frac{(1 - \kappa^2)^2}{\ln(1/\kappa)} \right]$
Slit ^a	$WH^3 F_p/12L$

^a F_p is a shape factor that is an infinite series as a function of the aspect ratio, W/H ; F_p goes to unity in the limit as W/H goes to zero (equivalent to pressure flow through infinitely wide parallel plates).

Alternatively, the screw characteristic may be expressed in a dimensionless form by defining the variables

$$\Pi_Q = \frac{Q}{U_z BW} \quad (11.63)$$

and

$$\Pi_p = \frac{\Delta p B^2}{\mu U_z Z} \quad (11.64)$$

where U_z is the linear velocity of the screw barrel along the screw channel (the z -direction), given as

$$U_z = \pi DN \cos \theta. \quad (11.65)$$

In the case of a Newtonian fluid in isothermal flow, a plot of Π_Q versus Π_p is linear, as shown in Figure 11-31. The limiting case of open discharge, which provides the maximum extruder output, is given by $\Pi = 0$ for which $\Pi = 1/2$, as shown by the plot of Figure 11-32. This means that Q for open discharge in Newtonian flow is

$$Q = \frac{1}{2} U_z BW \quad (11.66)$$

which is the equivalent expression for drag Couette flow of a Newtonian fluid between two infinitely wide, parallel plates (eq. (11.31)). In the case of the extruder,

the two parallel plates are taken to be the bottom of the screw channel and the inner surface of the extruder barrel (where the lubrication approximation has been made that $W \gg B$ and $D \gg B$).

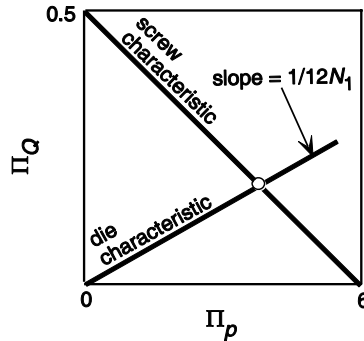


Figure 11-32 Plot of dimensionless screw and die characteristics for isothermal Newtonian flow. Adapted from S. Middleman, *Fundamentals of Polymer Processing*. 1977, New York: McGraw-Hill Book Company. Reproduced with permission of Stanley Middleman.

The die characteristic for isothermal Newtonian flow can also be put in dimensionless form as

$$\Pi_Q = \frac{\Pi_p}{12N_1} \quad (11.67)$$

where N_1 is given as

$$N_1 = \frac{C}{k}. \quad (11.68)$$

In eq. (11.68), C is a function of screw geometry (eq. (11.56)) and k is a function of the die geometry, as given in Table 11-4. The dimensionless die characteristic is included in the plot of the screw characteristic shown in Figure 11-32. For given die and screw geometries, Newtonian viscosity, and screw speed, the intersection of the dimensionless screw and die characteristics defines the operating parameters of volumetric screw output, Q , and pressure drop, Δp . This information can then be used to determine the power requirement for the extruder given by eq. (11.61).

The assumptions of both isothermal and Newtonian flow may be viewed as rather extreme for the modeling of the extrusion of a non-Newtonian fluid; however, they form a reasonable basis for refinement. As was given in Table 11-3, die characteristics are available for the isothermal flow of power-law fluids. Numerical solutions are also available for combined pressure and drag flow of a PLF in a chan-

nel. From this information, the screw characteristics for PLF flow can be obtained as shown in dimensionless form in Figure 11-32.

As shown, the relationship between Π_o and Π_p is no longer linear except in the case when the power-law index, n , is unity; this is the limiting case for isothermal Newtonian flow, as illustrated in Figure 11-33. Similar nonlinearity would follow for the die characteristics and, therefore, an analytical solution for Δp as given in eq. (11.60) for a Newtonian fluid is not possible. In the graphical solution, the intersection of the dimensionless die and screw characteristics defines the operating parameters, Q and Δp , for the combination of extruder and die, as illustrated for Newtonian fluid flow in Figure 11-32. Further refinements to include adiabatic flow of a power-law fluid in the screw channel have also been made and give a better picture of actual extrusion operation.

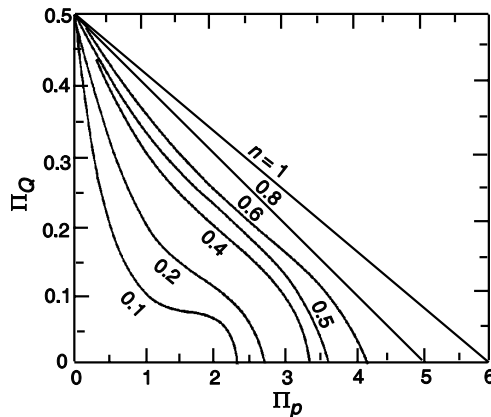


Figure 11-33 Dimensionless screw characteristics for isothermal power-law flow. Adapted from S. Middleman, *Fundamentals of Polymer Processing*. 1977, New York: McGraw-Hill Book Company. Reproduced with permission of Stanley Middleman.

11.5.2 Wire Coating

To coat a wire with an insulating polymer coating, a bare copper wire is pulled through a capillary die attached to an extruder. As a first approximation, wire coating can be modeled as axial annular drag flow as illustrated in Figure 11-34. A solution can be obtained for both Newtonian and non-Newtonian fluids with or without an imposed pressure drop. The objective of this analysis is to obtain an expression for the thickness of the coating, h , given the geometry (i.e., length, L , and diameter, D) of the die channel, the operating parameters of the die (e.g., temperature and axial velocity of the wire, U), and the properties of the fluid (e.g., viscosity at a specif-

ic temperature and shear rate in the case of a non-Newtonian fluid). Alternatively, analysis of this operation can provide insight into how changes in different operational or design parameters can affect the final coating thickness of the insulation or how parameters must be set to achieve a specified thickness. The most realistic but most difficult problem is annular drag flow of a PLF under a pressure drop; however, the simpler case of annular drag flow of a Newtonian fluid under conditions of open discharge as developed below serves to illustrate the general approach to this modeling problem.

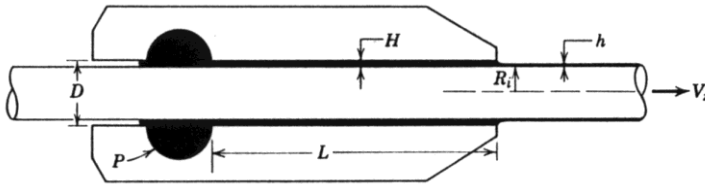


Figure 11-34 Representation of a wire-coating operation. Reproduced from J. M. McKelvey, *Polymer Processing*. 1962, New York: Wiley & Sons, with permission of James M. McKelvey.

The mass flow rate of the coating, \dot{m}_c , can be obtained as

$$\dot{m}_c = V_z A_c \rho \quad (11.69)$$

where V_z is the axial velocity of the wire through the die, ρ is the density of the coating at the temperature at the outlet of the die, and A_c is the cross-sectional area of the coating. Given the radius of the wire, R_i , and the thickness of the coating, h , eq. (11.69) becomes

$$\dot{m}_c = V_z S \left[(R_i + h)^2 - R_i^2 \right] \rho. \quad (11.70)$$

A mass balance equates the mass flow rate of the extruded coating with the mass flow rate due to drag flow in the die

$$\dot{m}_d = \rho' Q \quad (11.71)$$

where ρ' is the polymer density at the temperature *inside* the die and Q is the volumetric flow rate due to axial annular drag flow of the wire in the die. The solution for Q of a PLF was given in eq. (11.36). As indicated in Section 11.3.2, it is not possible to get Q for a Newtonian fluid directly from eq. (11.36) simply by setting $n = 1$. The actual solution for a Newtonian fluid is given as

$$Q = -2\pi R (R - R_i) \frac{2\kappa^2 \ln \kappa - \kappa^2 + 1}{4(1 - \kappa) \ln \kappa} \quad (11.72)$$

where

$$\kappa = \frac{R}{R_i}. \quad (11.73)$$

Substitution of eq. (11.73) into eq. (11.72) and then equating the mass flow rate ($\dot{m}_c = \dot{m}_d$) give a quadratic equation whose solution is

$$h' = \frac{h}{R_i} = \left[1 - \frac{2\rho'}{\kappa\rho} \left(\frac{1}{\kappa} - 1 \right) F(\kappa) \right]^{1/2} - 1 \quad (11.74)$$

where h' is a dimensionless coating thickness and

$$F(\kappa) = \frac{2\kappa^2 \ln \kappa - \kappa^2 + 1}{4(1 - \kappa) \ln \kappa}. \quad (11.75)$$

An interesting result revealed by eq. (11.74) is that the coating thickness for a Newtonian fluid is primarily a function of die and wire diameters but is independent of wire velocity and the fluid viscosity.

For a PLF, the dimensionless thickness for isothermal flow is given by

$$h' = \left[1 - \frac{2\rho'}{\kappa\rho} \left(\frac{1}{\kappa} - 1 \right) H(\kappa, q) \right]^{1/2} - 1 \quad (11.76)$$

where

$$H(\kappa, q) = \frac{1}{q+2} \frac{1 - \kappa^{q+2}}{(1 - \kappa)(\kappa^q - 1)} - \frac{1 + \kappa}{2(\kappa^q - 1)} \quad (11.77)$$

and

$$q = 1 - \frac{1}{n}. \quad (11.78)$$

Again, coating thickness is independent of wire velocity but now depends upon the power-law index, n , (i.e., viscosity) of the fluid. As temperature increases, it would be expected that n should increase (i.e., become less shear thinning) and, therefore, h' should increase.

In the case of both combined drag and pressure flow, the total volumetric flow is additive ($Q = Q_d + Q_p$) for a Newtonian fluid only. The solution to this problem shows that increasing pressure drop across the die increases the coating thickness. The result for a PLF is a bit more difficult to obtain as it requires a solution to the dynamic equations (see Appendix A.2) for u_z . Solutions are available in many poly-

mer processing texts such as the excellent one cited in the Suggested Reading at the end of this chapter.

APPENDICES

A.1 RELATIONSHIP BETWEEN THE WLF PARAMETERS AND FREE VOLUME

The Doolittle equation [15, 16] relates viscosity to the fractional free volume, f , which is defined as

$$f = \frac{V_f}{V} \tag{A.1}$$

where V is the actual volume of the polymer at some temperature, T . The Doolittle equation is given as

$$\ln \eta(T) = \ln A + B \left(\frac{1}{f} - 1 \right) \tag{A.2}$$

where A and B are constants. The corresponding equation for $T = T_g$ is then

$$\ln \eta(T_g) = \ln A + B \left(\frac{1}{f_g} - 1 \right) \tag{A.3}$$

where f_g is the fractional free volume at T_g . The fractional free volume, f , at a given temperature, T , is related to f_g as

$$f = f_g + \alpha_f (T - T_g) \tag{A.4}$$

where α_f is the thermal-expansion coefficient of the free volume

$$\alpha_f = \left(\frac{\partial V_f}{\partial T} \right)_p \tag{A.5}$$

Substitution of eqs. (A.2) to (A.4) into eq. (11.7) gives

$$\log a_T = \log \frac{\eta(T)}{\eta(T_g)} = - \left(\frac{B}{2.303 f_g} \right) \left[\frac{T - T_g}{(f_g / \alpha_f) + T - T} \right] \tag{A.6}$$

Comparison of the form of eq. (A.6) with the WLF expression (eq. 5.127) for $\log a_T$ gives the following relationships for the WLF parameters:

$$C_1 = \frac{B}{2.303f_g} \quad (\text{A.7})$$

and

$$C_2 = \frac{f_g}{\alpha_f}. \quad (\text{A.8})$$

Since the thermal-expansion coefficient of free volume is not generally available,* the thermal-expansion coefficient of the melt, easily determined by dilatometry (Section 4.3.2), may be used.

A.2 DYNAMIC AND CONTINUITY EQUATIONS

A.2.1 CARTESIAN COORDINATES

x-Component:

$$\rho \left(\frac{\partial u_x}{\partial t} + u_x \frac{\partial u_x}{\partial x} + u_y \frac{\partial u_x}{\partial y} + u_z \frac{\partial u_x}{\partial z} \right) = -\frac{\partial p}{\partial x} + \left(\frac{\partial \tau_{xx}}{\partial x} + \frac{\partial \tau_{yx}}{\partial y} + \frac{\partial \tau_{zx}}{\partial z} \right) + \rho g_x \quad (\text{A.9})$$

y-Component:

$$\rho \left(\frac{\partial u_y}{\partial t} + u_x \frac{\partial u_y}{\partial x} + u_y \frac{\partial u_y}{\partial y} + u_z \frac{\partial u_y}{\partial z} \right) = -\frac{\partial p}{\partial y} + \left(\frac{\partial \tau_{xy}}{\partial x} + \frac{\partial \tau_{yy}}{\partial y} + \frac{\partial \tau_{zy}}{\partial z} \right) + \rho g_y \quad (\text{A.10})$$

z-Component:

$$\rho \left(\frac{\partial u_z}{\partial t} + u_x \frac{\partial u_z}{\partial x} + u_y \frac{\partial u_z}{\partial y} + u_z \frac{\partial u_z}{\partial z} \right) = -\frac{\partial p}{\partial z} + \left(\frac{\partial \tau_{xz}}{\partial x} + \frac{\partial \tau_{yz}}{\partial y} + \frac{\partial \tau_{zz}}{\partial z} \right) + \rho g_z \quad (\text{A.11})$$

Continuity equation:

$$\frac{\partial u_x}{\partial x} + \frac{\partial u_y}{\partial y} + \frac{\partial u_z}{\partial z} = 0 \quad (\text{A.12})$$

A.2.2 CYLINDRICAL COORDINATES

r-Component:

* Although the thermal expansion coefficient of free volume can be obtained by positron annihilation spectroscopy and from molecular simulation, data are extremely limited at this time.

$$\rho \left(\frac{\partial u_r}{\partial t} + u_r \frac{\partial u_r}{\partial r} + \frac{u_\theta}{r} \frac{\partial u_r}{\partial \theta} - u_z \frac{\partial u_r}{\partial z} \right) = -\frac{\partial p}{\partial r} \quad (\text{A.13})$$

θ -Component:

$$\rho \left(\frac{\partial u_\theta}{\partial t} + u_r \frac{\partial u_\theta}{\partial r} + \frac{u_\theta}{r} \frac{\partial \theta}{\partial u_\theta} - \frac{u_r u_\theta}{r} + u_z \frac{\partial u_\theta}{\partial z} \right) = -\frac{1}{r} \frac{\partial p}{\partial \theta} + \left[\frac{1}{r^2} \frac{\partial}{\partial r} (r^2 \tau_{r\theta}) + \frac{1}{r} \frac{\partial \tau_{\theta\theta}}{\partial \theta} + \frac{\partial \tau_{\theta z}}{\partial z} \right] + \rho g_\theta \quad (\text{A.14})$$

z -Component:

$$\rho \left(\frac{\partial u_z}{\partial t} + u_r \frac{\partial u_z}{\partial r} + \frac{u_\theta}{r} \frac{\partial u_z}{\partial \theta} + u_z \frac{\partial u_z}{\partial z} \right) = -\frac{\partial p}{\partial z} + \left[\frac{1}{r} \frac{\partial}{\partial r} (r \tau_{rz}) + \frac{1}{r} \frac{\partial \tau}{\partial \theta} + \frac{\partial \tau_{zz}}{\partial z} \right] + \rho g_z \quad (\text{A.15})$$

Continuity equation:

$$\frac{1}{r} \frac{\partial}{\partial r} (r u_r) + \frac{1}{r} \frac{\partial u_\theta}{\partial \theta} + \frac{\partial u_z}{\partial z} = 0 \quad (\text{A.16})$$

SUGGESTED READING

- Aharoni, S. M., *Critical Concentration for Intermolecular Interpenetration and Entanglements*. Journal of Macromolecular Science: Part B: Physics: 1978. **B15**: p. 347.
- Alberino, L. M., *Reaction Injection Molding: Review and Overview*. Polymer News, 1985. **11**: p. 135.
- Barnes, H. A., J. F. Hutton, and K. Walters, *An Introduction to Rheology*. 1989, Amsterdam: Elsevier.
- Choi, H. J., and M. S. Jhon, *Polymer-Induced Turbulent Drag Reduction*. Industrial and Engineering Chemistry Research, 1996. **35**: p. 2993.
- Darby, R. *Taking the Mystery Out of Non-Newtonian Fluids*. Chemical Engineering, March 2001, p. 66.
- Denn, M. M., *Extrusion Instabilities and Wall Slip*. Annual Review of Fluid Mechanics, 2001. **33**: p. 265.
- Han, C. D., *Rheology in Polymer Processing*. 1976, New York: Academic Press.
- McCrum, N. G., C. P. Buckley, and C.B. Bucknall, *Principles of Polymer Engineering*. 1988, New York: Oxford University Press.
- McKelvey, J. M., *Polymer Processing*. 1962, New York: John Wiley & Sons.
- Middleman, S., *The Flow of High Polymers*. 1968, New York: Interscience Publishers.

- Middleman, S., *Fundamentals of Polymer Processing*. 1977, New York: McGraw-Hill Book Company.
- Morton-Jones, D. H., *Polymer Processing*. 1989, London: Chapman and Hall.
- Nielsen, L. E., *Polymer Rheology*. 1977, New York: Marcel Dekker, Inc.
- Tadmor, Z., and C. G. Gogos, *Principles of Polymer Processing*. 1979, New York: John Wiley & Sons.
- Walters, K., *Rheometry*. 1975, London: Chapman and Hall.
- Wilkes, G. L., *An Overview of the Basic Rheological Behavior of Polymer Fluids*. *Journal of Chemical Engineering*, 1981. **58**: p. 880.

PROBLEMS

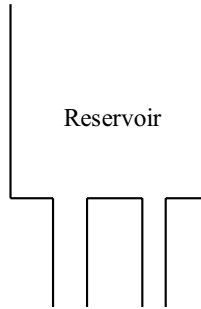
11.1 Poly(vinyl acetate) (PVAc) is extruded at 180°C at constant temperature through a capillary rheometer having a ram (reservoir) diameter of 0.375 in. and a capillary with an inside diameter of 0.041 in. and length of 0.622 in. The data provided give the efflux time to extrude 0.0737 in.³ at different ram loads. Using the following data:

Ram Load (lb _f)	Efflux Time (min)
97.5	5.32
145	1.58
217	0.31
250	0.17

- (a) Determine the power-law parameters n and m for PVAc and state all assumptions used to obtain your results.
- (b) Plot the apparent viscosity, η , in units of Pa·s versus the nominal shear rate at the wall, $\dot{\gamma}_w$ (s⁻¹), using logarithmic coordinates.

11.2 Plot the dimensionless velocity profile for polystyrene flowing in a capillary at 483 K.

11.3 As illustrated, two capillaries of identical length are connected to the same liquid reservoir in which a power-law fluid is held. The tubes differ in radii by a factor of 2. When a pressure is applied to the reservoir, the volumetric flow rates from the two tubes differ by a factor of 40. What is the value of n ? How different are the nominal shear rates in the two cases?



11.4 Molten polystyrene flows through a circular tube at 210°C under a pressure drop of 1000 psi. Given that the inside diameter of the tube is 0.25 in. and that the tube is 3 in. in length, calculate the following:

- (a) The (nominal) shear stress at the wall in units of N m^{-2}
- (b) The (nominal) shear rate at the wall in s^{-1}
- (c) The volumetric flow rate in $\text{cm}^3 \text{ s}^{-1}$

Assume that flow is isothermal, steady, and fully developed.

11.5 (a) Given that tensile (Trouton's) viscosity is defined as

$$\eta_T = \frac{\sigma}{\dot{\epsilon}}$$

where σ and ϵ are the *true* tensile stress and *true* strain, respectively, show that

$$\ln L = \left(\frac{1}{\eta_T} \right) \sigma t + \ln L_0$$

when viscosity is independent of $\dot{\epsilon}$ and L_0 is the *initial* length of the sample.

(b) A strip of polyisobutylene (800,000 molecular weight) is subjected to a fixed tensile load at ambient conditions. Initially, the sample is 0.699 cm wide, 6.0 cm long, and 0.155 cm thick. The strip is hung vertically and a mass of 75 g is attached to the bottom of the strip. The sample length is then recorded as a function of time with the following measurements:

Time (min)	1	2	3	6	12	15	18	21	24
Length (cm)	6.90	7.00	7.10	7.25	7.48	7.60	7.69	7.79	7.90

Plot the data given in the form of $\ln L$ versus σt and determine the value of η_T in SI units. Comment on the probable phenomenological significance of the actual intercept of the plot obtained by extrapolating the linear portion of the data.

11.6 Show that eq. (11.37), which defines shear stress in pressure flow through a capillary, is correct by balancing pressure force and shear force in a cylindrical element.

11.7 A 2-in. melt extruder is pumping a *Newtonian fluid* through a slit die for which the form factor, F_p , is 0.5. The viscosity, μ , of the fluid at operating conditions is $0.2 \text{ lb}_f\text{-s in.}^{-2}$. The dimensions of the slit die are 1 in. in width, 0.8 in. in height, and 3 in. in length. The geometric parameters for the extruder are given in the following table:

Extruder Geometry	
Extruder length, L_{ext}	14.75 in.
Screw diameter, D	1.982 in.
Channel depth, B	0.166 in.
Flight angle, θ	30°
Channel width, W	11 in.

If the extruder is rotating at 60 rpm under isothermal conditions, determine the following:

- (a) Pressure drop, Δp , in psi
- (b) Volumetric flow rate, Q , in units of $\text{in.}^3 \text{ min}^{-1}$
- (c) Power, P , required to operate the extruder in hp ($1 \text{ hp} = 550 \text{ ft-lb}_f \text{ s}^{-1}$)

11.8 Using the dynamic equations for cylindrical coordinates given in Appendix A.2.2 of this chapter, show how eq. (11.23) can be obtained making the usual assumptions of isothermal, steady, fully developed, laminar flow through a capillary. State any additional assumptions necessary to obtain eq. (11.23).

11.9 Derive eq. (11.25) for the velocity profile of a power-law fluid for pressure flow through a capillary.

11.10 Derive eq. (11.46) for the velocity u_θ of a power-law fluid in a Couette rheometer.

11.11 Derive eqs. (11.72) and (11.74) for the axial annular Couette flow of a Newtonian fluid in a wire-coating die.

11.12 A Newtonian fluid having a viscosity of 15,000 poise is to be coated on a wire having a diameter of 0.06 in. through an annular die of 0.08-in. inside diameter. The length of the die is 1.25 in. Assuming isothermal flow, calculate the required pressure drop (in psi) across the die to produce a uniform coating having a thickness of 0.06 in. The wire is moving at a velocity of 100 ft min^{-1} . What is the nominal shear rate in the die?

11.13 Derive eq. (11.76) for a PLF in a wire-coating operation.

REFERENCES

1. Baekeland, L. H., *The Synthesis, Constitution, and Uses of Bakelite*. Journal of Industrial and Engineering Chemistry, 1909. **1**: p. 149–161.
2. Lomellini, P., *Viscosity-Temperature Relationships of a Polycarbonate Melt: Williams–Landel–Ferry versus Arrhenius Behaviour*. Makromolekulare Chemie, 1992. **193**: p. 69–79.
3. Cohen, M. H. and D. Turnbull, *Molecular Transport in Liquids and Glasses*. Journal of Chemical Physics, 1959. **31**(5): p. 1164–1169.
4. Mewis, J., *Thixotropy—A General Review*. Journal of Non-Newtonian Fluid Mechanics, 1979. **6**: p. 1–20.
5. Wang, C. S. and J. R. Fried, *Viscoelastic Properties of Concentrated Cellulose Acetate Solutions*. Journal of Rheology, 1992. **36**(5): p. 929–945.
6. Onogi, S., et al., *Effects of Molecular Weight and Concentration on Flow Properties of Concentrated Polymer Solutions*. Journal of Polymer Science, Polymer Symposium, 1966. **15**(1): p. 381–406.
7. Carreau, P. J., *Rheological Equations from Molecular Network Theories*. PhD Dissertation, Department of Chemical Engineering, University of Wisconsin. 1992.
8. Wang, S.-Q., P. A. Drda, and Y.-W. Inn, *Exploring Molecular Origins of Sharkskin, Partial Slip, and Slope Change in Flow Curves of Linear Low Density Polyethylene*. Journal of Rheology, 1996. **40**(5): p. 875–898.
9. Pudjijanto, S. and M. M. Denn, *A Stable “Island” in the Slip-Stick Region of Linear Low-Density Polyethylene*. Journal of Rheology, 1994. **38**(6): p. 1735–1744.
10. Toms, B. A., *Observations on the Flow of Linear Polymer Solutions through Straight Tubes at Large Reynolds Numbers*. Proceedings of the International Congress on Rheology, 1948. **2**: p. 135–141.
11. Burger, E. D., L. G. Chorn, and T. K. Perkins, *Studies of Drag Reduction Conducted over a Broad Range of Pipeline Conditions When Flowing Prudhoe Bay Crude Oil*. Journal of Rheology, 1980. **24**: p. 603–636.
12. Bagley, E. B., *End Corrections in the Capillary Flow of Polyethylene*. Journal of Applied Physics, 1957. **28**(5): p. 624–627.
13. Kamal, M. R. and H. Nyun, *Capillary Viscometry: A Complete Analysis Including Pressure and Viscous Heating Effects*. Polymer Engineering and Science, 1980. **20**(2): p. 109–119.
14. DeKee, D. and R. F. Wissbrun, *Polymer Rheology*. Physics Today, June 1998. p. 24–29.
15. Doolittle, A. K., *Studies in Newtonian Flow. II. The Dependence of the Viscosity of Liquids on Free Space*. Journal of Applied Physics, 1951. **22**(12): p. 1471–1475.
16. Doolittle, A. K., *Studies in Newtonian Flow. III. The Dependence of the Viscosity of Liquids on Molecular Weight and Free Space (in Homogeneous Series)*. Journal of Applied Physics, 1952. **23**(2): p. 236–239.

This page intentionally left blank

Polymers for Advanced Technologies

As was covered in previous chapters, plastics find important applications for commodity products such as textiles, tires, and packaging. Polymers, particularly thermosets, also find widespread use for composite applications in the automotive, marine, and aerospace industries. Many of these markets have now matured so future growth is expected to be small; however, there are many more applications for polymers that may be less obvious but have great potential and offer challenges for new technologies and growth. Some of these include polymeric membranes for the purification of air and water, for important separations in the chemical and biotech industries, and for proton conduction in fuel cells. Polymers also have important applications in medicine, including uses in controlled drug delivery, artificial organs, and protein synthesis. Some polymers can be made to be electrically conductive and offer potential for the semiconductor industry. Other important specialized applications for polymers include their use as lightweight electrodes and electrolytes for batteries and photovoltaic devices in solar energy conversion. Some newly

developed polymers exhibit unusual optical properties that have attracted significant interest from the defense industries. This chapter seeks to present a picture of these emerging areas in polymer science and engineering.

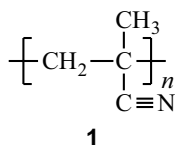
12.1 Membrane Science and Technology

The solubility and diffusivity of gases and liquids in polymers can vary by many orders of magnitude depending upon the chemical structure of the polymer and its conformation, crystallinity, and chain mobility. These differences provide opportunities for the use of polymers in many applications including the separation of gases and liquid mixtures, proton transport through fuel-cell membranes, and food packaging where a barrier is needed against the damaging effects of moisture and/or oxygen.

12.1.1 Barrier Polymers

Good barrier materials for gas and water vapor are important for packaging film, plastic beverage bottles, and the encapsulation of electronic parts (see Section 12.3.6). As an approximate rule of thumb, a polymer with a permeability, or permeability coefficient (P),* less than 10^{-11} cm³-cm/cm²-s cmHg at 0% humidity at 25°C is considered to be a barrier polymer. In general, polymers with high nitrile functionality like polyacrylonitrile (PAN) and the related polymer, polymethacrylonitrile (PMAN, structure 1), have high gas-barrier properties [1]. Because of its attractive CO₂ barrier properties, poly(ethylene terephthalate) is used as the material in the manufacture of plastic bottles for carbonated beverages. As shown by data given in Table 12-1, polyolefins such as polyethylene and polypropylene that are very hydrophobic are good water barriers. Low-density polyethylene film is used as cereal-box liners (O₂ and moisture barrier). Some polar polymers like poly(vinyl alcohol) are very good gas barriers but poor water barriers. Other polymers like poly(vinylidene chloride) (Saran) have both low gas and low water permeability. Polymers that have appreciable water solubility will swell and subsequently exhibit higher gas permeability (i.e., lower gas-barrier properties) when wet than when dry. Salame [2] has proposed a simple group-contribution scheme, the Permachor method, for estimating gas and liquid permeability, particularly for barrier polymers. A review of this approach is included in Chapter 13 (Section 13.1.3).

* Permeability is defined as the amount of a gas passing through a polymer film of unit thickness, per unit area, per second, and at a unit pressure difference.

Table 12-1 Permeability Coefficients of Selected Polymers at 25°C^a

Polymer	$P(\text{O}_2)^b$	$P(\text{water})^c$
Poly(vinyl alcohol)	~0.0001	~5000
Polyacrylonitrile	~0.002	2.45
Poly(vinylidene chloride)	0.012	~0.052
Polymethacrylonitrile	0.012	3.32
Poly(ethylene terephthalate)	0.42	3.2
Poly(vinyl chloride)	0.48	2.5
Poly(vinyl acetate)	3.3	107
Polypropylene	10.8	0.42
Polyethylene (LDPE)	2930.0	0.83
Polyisobutylene	90.0	9.2
Polydimethylsiloxane	~3000	80.5

^a Data taken from ref. [1].

^b $P \times 10^{11}$ cm³-cm/cm²-sec cmHg at 0% humidity

^c $P \times 10^{11}$ g-cm/cm² sec cmHg

12.1.2 Membrane Separations

Although the major uses of membranes are in the production of potable water by reverse osmosis and the separation of industrial gases, membranes can be used for many other important applications. These include the filtration of particulate matter from liquid suspensions, air, and industrial flue gas and the separation of liquid mixtures, such as the dehydration of ethanol azeotropes. More specialized applications include ion separation in electrochemical processes, membrane dialysis of blood and urine, artificial lungs and skin, the controlled release of therapeutic drugs, the affinity separation of biological molecules, membrane-based sensors for gas and ion detection, and membrane reactors. Although membranes can be prepared from metals, ceramics, and microporous carbon and glass, polymeric membranes have great versatility and are widely used. The applications and mechanisms of transport in polymeric membranes are outlined in this section.

Filtration. The most obvious use of membranes is in the filtration of solid particles such as dust, salts, bacteria, and some large viruses from liquids or air streams. As illustrated in Figure 12-1, large organic molecules such as starch and large-diameter bacteria (e.g., *Staphylococcus*) can be filtered by membranes having pore diameters in the range from ca. 1 to 10 μm . Membranes having pore diameters

in the range of 0.01 to 10 μm are called *microfilters*, while those with smaller pore diameters in the range of 10 \AA to 1000 \AA are called *ultrafilters*. Ultrafilters are suitable for filtering smaller particles, including some bacteria and viruses, as well as some moderately sized organic molecules like sugars. For example, heat-sensitive medical serums can be *cold-sterilized* by microfiltration or ultrafiltration to remove bacterial contamination. Microporous membranes of polypropylene are being evaluated for the removal of SO_2 from flue gas and for the removal of suspended solids and clarification of industrial sewage. Examples of other industrial applications for microfiltration and ultrafiltration are given in Table 12-2.

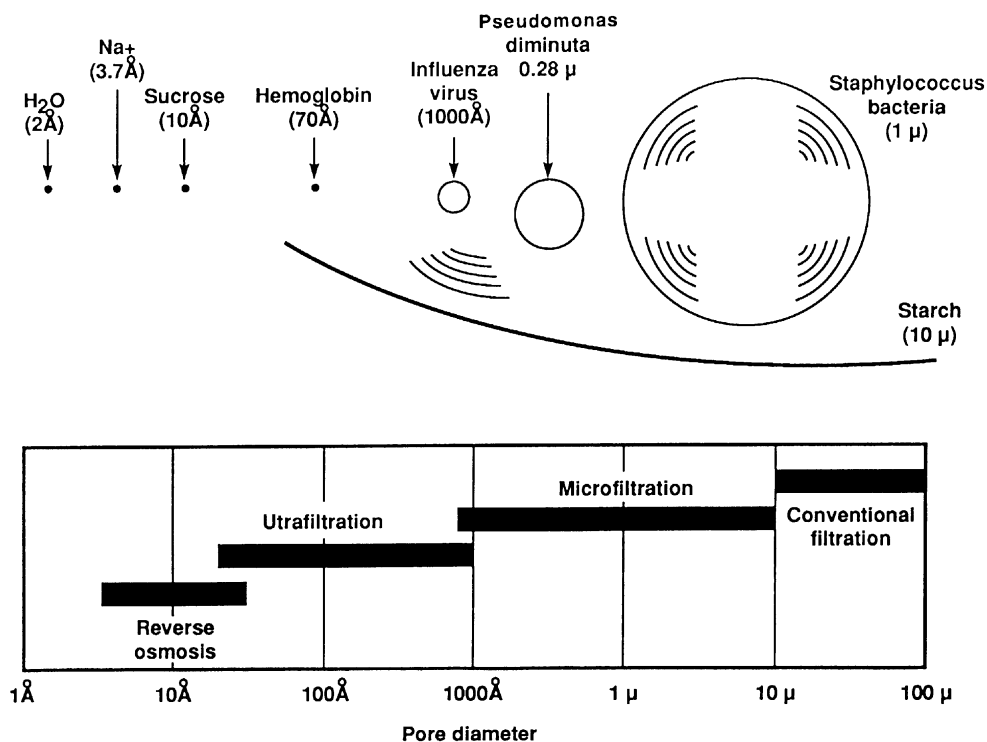


Figure 12-1 Pore sizes and terminology used in filtration. Courtesy of Membrane Technology and Research, Inc., Menlo Park, CA.

Table 12-2 Industrial Applications for Microfiltration and Ultrafiltration Membranes

Industry	Examples
Biotechnology	Product separation from fermentation broth and blood/plasma filtration
Electrocoating	Electrocoat paint filtration
Food	Clarification of apple juice and egg-white concentration
Pharmaceutical	Cold sterilization by removal of microorganisms such as bacteria and yeast cells from aqueous solutions
Semiconductor/electronics	Production of 18 megohm·cm or ultrapure water
Waste management	Oil–water separation and metals recovery

At the extreme limit of filtration is a process called *reverse osmosis* (or hyperfiltration), which is used to obtain potable water from brackish water or salt water. The process is termed “reverse” osmosis since water would be expected to diffuse from the side of low salt concentration to that of high concentration in normal osmosis. In reverse osmosis, a pressure drop up to several thousand psi is used to offset the osmotic pressure differential between fresh and salt water. For successful reverse-osmosis (RO) operation, the diameter of any pores that may be present in the dense separating layer of an RO membrane must be no larger than ca. 5 to 20 Å in order to retain dissolved microsolute such as salt ions while allowing water to freely transport through the membrane. A polymer frequently used for preparing RO membranes is cellulose triacetate, although some other polymers such as aromatic polyamides and sulfonated polysulfone have been used.

Another growing area in membrane filtration is nanofiltration (NF). The performance of NF membranes falls between that of RO and UF membranes with pore sizes in the area of 10 Å and nominal molecular-weight cutoffs in the range from 100 to 200. Nanofilters are usually prepared as thin-film composite membranes consisting of a thin separating layer containing negatively charged hydrophilic groups attached to a UF-membrane support. Polymers suitable for the separating layer include cellulose acetate, polyamides, poly(vinyl alcohol), and sulfonated polysulfone and polyethersulfone. As illustrated by Figure 12-2, NF membranes retain sugars and some multivalent salts (e.g., MgSO_4) but pass many monovalent salts (e.g., NaCl) and undissociated acids. Salt rejection is due to electrostatic interactions between ions and the separating layer. Applications for NF membranes include the demineralization of water, the removal of heavy metals, and the removal of lignin and related impurities from wood-pulp streams. Advantages of NF membranes over RO membranes are higher water flux and improved fouling resistance against hydrophobic colloids, proteins, and oils.

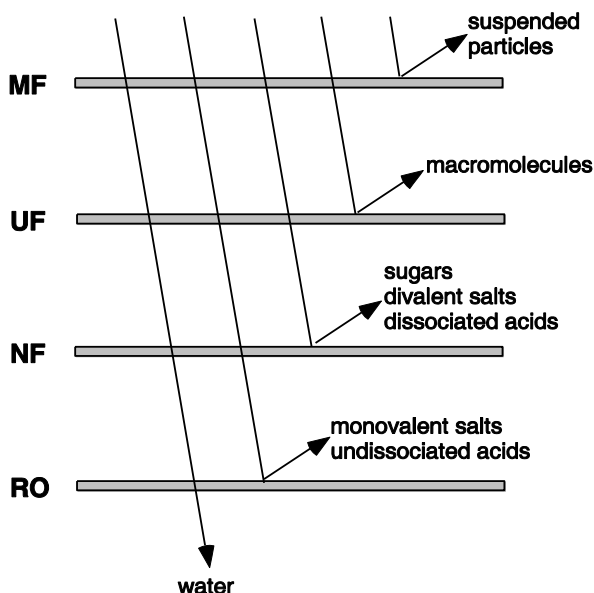


Figure 12-2 Comparison of the rejection performance of microfiltration (MF), ultrafiltration (UF), nanofiltration (NF), and reverse-osmosis (RO) membranes to solutes of different sizes and charge. Adapted from L. P. Raman, M. Cheryan, and N. Rajagopalan, *Chemical Engineering Progress*, March 1994, with permission of the American Institute of Chemical Engineers.

Gas Separations. The potential of using polymeric membranes to separate mixtures of gases may have been realized as early as 1866 when Thomas Graham reported that the oxygen content of atmospheric air could be enriched from 21% to 41% by permeation through a membrane of natural rubber. The first commercial membrane for the large-scale separation of gas mixtures was introduced in 1979. As indicated by Table 12-3, there are several important industrial applications where membrane operations can be competitive with more traditional methods of gas separations, such as cryogenic separation and pressure-swing adsorption (PSA). These include oxygen enrichment of air, hydrogen separation from carbon monoxide and other gases, removal of carbon dioxide from natural gas, and the reduction of organic vapor concentration in air. Other smaller-scale applications include the preservation of food such as apples and bananas during transport by blanketing with low-oxygen-content air, the generation of inert gases for safety purposes, and the dehydration of gases.

Table 12-3 Applications for Polymeric Membranes in Gas Separations

Separations	Suitable Polymers
O ₂ /N ₂	Silicone rubber Polysiloxane- <i>block</i> -polycarbonate Polysulfone Ethylcellulose Poly[(1-trimethylsilyl)-1-propyne] Polypyrrolone Polytriazole Polyaniline
H ₂ from CO, CH ₄ , N ₂	Polysulfone
Acid gases (e.g., CO ₂ and H ₂ S) from hydrocarbons	Cellulose acetate Poly(vinyl chloride) Polysulfone Polyetherimide
Hydrocarbon vapors from air	Silicone rubber

Although ultraporous (i.e., molecular sieve) carbon and certain metallic (e.g., palladium, palladium–silver alloys, and microporous aluminum) as well as ceramic membranes have been used for gas separation, polymers have particularly high selectivity for many important gas mixtures and are easily fabricated into a variety of membrane configurations, such as flat-film, hollow-fiber, and composite membranes consisting of a thin polymer film on a macroporous support. For example, hollow-fiber membranes of polysulfone are used commercially to adjust the H₂/CO ratio in process syn gas for methanol synthesis and the H₂/N₂ ratio in ammonia purge gas.

The selection of a polymer for a particular gas-separation application is guided by the permeability (P_A) and its permselectivity (α_{AB}) for that gas as defined next. The driving force for transport of the gas through the membrane is the pressure drop (Δp) between the high-pressure upside and low-pressure downside of the membrane. Pressure drops may be as high as 2000 psi (13.8 MPa) in certain circumstances.

The *permeability* is defined as the ratio of flux (J_A) to pressure drop as

$$P_A \equiv \frac{J_A \ell}{\Delta p} \quad (12.1)$$

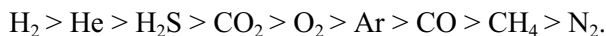
where ℓ is membrane thickness. The most commonly used unit of gas permeability is the barrer that has the value $10^{-10} \text{ cm}^3 \text{ (STP)-cm}/(\text{cm}^2\text{-s-cmHg})$.

The *permselectivity* of a polymeric membrane for one gas (A) over another gas (B) is given by the ratio of their permeabilities

$$\alpha_{AB} = \frac{P_A}{P_B} \quad (12.2)$$

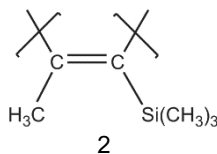
When the permeabilities are measured for pure gases, the permeability ratio is called the *ideal* permselectivity. Since gas mixtures are usually nonideal, especially under high pressure, the actual permselectivity expressed as the ratio of permeabilities for each gas in the mixture may be quite different from the ideal value. Nonetheless, permselectivities are usually reported as ideal values because pure gas permeabilities are more frequently available.

In general, permeability of a polymer for a gas increases with decreasing size and increasing solubility (or condensability) of the gas. The relative permeability of a gas is usually independent of polymer structure and is given in the order of decreasing gas permeability as



As shown by values given in Table 12-4, permeability and, to a lesser extent, permselectivity vary widely with polymer structure and physical state (i.e., rubber, glass, or crystalline).

Generally, permeability is higher while permselectivity is lower for rubbery polymers than for glassy polymers, although a few exceptions exist. An important exception is poly[1-(trimethylsilyl)-1-propyne] (PTMSP, structure 2).



PTMSP is a glassy polymer having higher gas permeability than polysiloxane and almost all other rubbery polymers [3]. This unusually high permeability has been attributed to its high gas diffusivity due to very high free volume. Unfortunately, high free volume leads to an inability of the polymer to differentiate gas molecules on the basis of size and, as a result, permselectivity is low. This inverse relationship between permeability and permselectivity—highly permeable polymers are not selective—is a general one for all polymers [4]. Particularly attractive membrane candidates for a specific gas separation such as O_2/N_2 and CO_2/CH_4 are those polymers whose values of permeability and permselectivity fall near the upper boundary of experimental data as illustrated by the log–log plot of the O_2/N_2 separation factor (α) versus the oxygen permeability separation in Figure 12-3.

Table 12-4 Gas Permeability and Permselectivity of Representative Polymers (at 25° to 35°C)

Polymer	$P(O_2)^a$	$P(O_2)/P(N_2)$	$P(CO_2)^a$	$P(CO_2)/P(CH_4)$
Rubbery Polymers				
Butyl rubber	1.3	3.9	5.8	6.6
Natural rubber	24	3.0	134	4.7
Silicone rubber	610	2.2	4553	3.4
Semicrystalline Polymers				
Low-density polyethylene ($\rho = 0.9164$)	2.9	3.0	12.6	4.3
High-density polyethylene ($\rho = 0.964$)	0.4	2.9	1.7	4.4
Poly(ethylene terephthalate) ^b	0.04	4.5	0.30	—
Glassy Polymers				
Cellulose acetate	0.68	3.4	5.5	28
Polysulfone	1.3	5.2	4.9	23
Polycarbonate	1.5	5.2	6.0	23
Polystyrene	2.6	3.3	10.5	—
Poly(2,6-dimethyl-1,4-phenylene oxide)	18	5.0	59	15
Poly(4-methylpentene-1)	29	4.4	93	—
Poly[1-(trimethylsilyl)-1-propyne]	7200	1.7	19,000	4.4

^a Permeability in barrers [10^{-10} cm³(STP)-cm/(cm²-s-cmHg)].

^b $X_c = 0.50$.

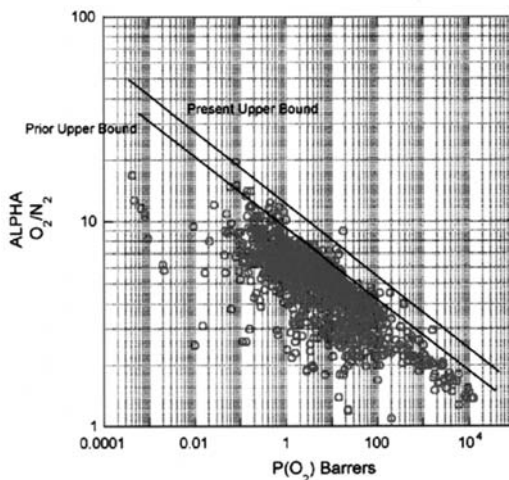


Figure 12-3 Log-log plot of the separation factor for O_2/N_2 versus the permeability coefficient of oxygen. Solid lines represent current and earlier upper boundaries. Reproduced with permission from L. M. Robeson, *The Upper Bound Revisited*. *Journal of Membrane Science*, 2008. **320**: p. 390–400.

Liquid Separations. Membranes can be used effectively to separate liquid mixtures (e.g., water–organic and organic–organic) in competition with traditional chemical processes such as distillation, adsorption, liquid–liquid extraction, and fractional crystallization. One important membrane operation termed *pervaporation* uses a pressure drop (reduced pressure on the downside) to separate components from a liquid mixture on the basis of preferential solubility and diffusivity in a manner fundamentally similar to gas separation.

In pervaporation, the (liquid) feed mixture is pumped *across* the membrane surface. As illustrated by Figure 12-4, crossflow operation reduces the potential for fouling and concentration polarization by providing a rapid flow at the membrane surface to sweep away contaminating particles and to encourage mixing at the membrane–liquid interface.

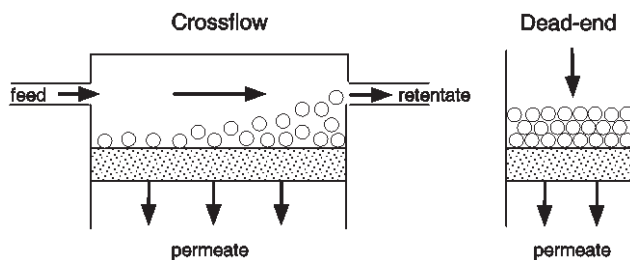


Figure 12-4 Illustration of a crossflow membrane process (left) compared to dead-end filtration (right).

A representative process flow chart for pervaporation is illustrated in Figure 12-5. Vacuum (i.e., vacuum pervaporation) or reduced pressure (i.e., sweep-gas pervaporation) is applied at the downside of the membrane. Separation occurs by selective solution diffusion (see Section 12.1.3) and subsequent evaporation at the downside and is driven by the partial-pressure gradient between the liquid feed and the permeate vapor. The permeate vapor phase is condensed and recovered as the product stream. The portion of the feed that is not permeated is called the *retentate*.

Related processes include *pertraction*, by which the permeate is dissolved in a circulating carrier fluid rather than being vaporized, and vapor permeation or *evapomeation*, where the feed stream is a vapor or vapor–gas mixture and, therefore, no phase change occurs during the process. In general, pervaporation can be used to separate structural isomers, to separate components from azeotropic and close boiling mixtures, to recover trace substances, and to displace the equilibrium of a chemical reaction. Commercial uses of pervaporation include the concentration of ethanol produced by the fermentation of biomass (e.g., starch, sugar, and cellulose), the removal of trace organic compounds from water supplies, and the separation of mixtures of organic compounds. Vapor permeation (i.e., evapomeation) may be used to remove trace organic compounds from air or in hybrid distillation processes

whereby a separate membrane stage may be used in addition to more traditional distillation processes. The choice between pervaporation and other separation processes such as distillation is largely controlled by economics. In pervaporation, the principal form of energy utilization is the heat of vaporization of the permeate. Economics are particularly favorable for pervaporation in the case of the separation of azeotropic mixtures such as ethanol and water.

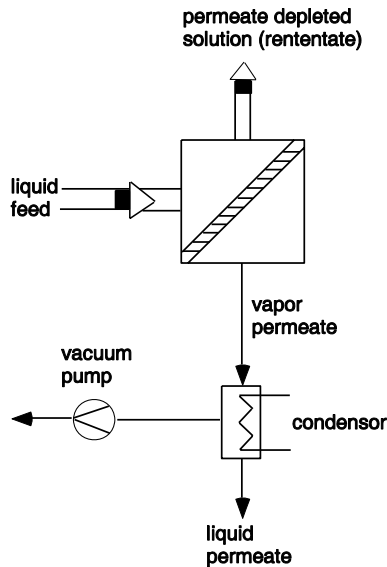


Figure 12-5 Schematic of membrane-pervaporation process. A binary liquid mixture passes crossflow over a polymeric membrane and the permeate, enriched in the more permeable component, is vaporized on the downside (low-pressure side), condensed, and collected. Courtesy of Membrane Technology and Research, Inc., Menlo Park, CA.

Membranes for pervaporation may be dense (homogeneous) membranes, asymmetric membranes, or composite membranes consisting of a thin permselective polymeric layer covering a microporous support. For alcohol–water separation, cellulose derivatives provide high permeability with moderate selectivity. Poly(vinyl alcohol) (PVA), used as a graft copolymer or as the separating layer in a composite membrane, has preferential permeability to water over alcohols or other organic molecules, while silicone rubber is more permeable to alcohols (also aldehydes and ketones) than to water.

Flux in pervaporation is a function of a diffusion term (D_0), the concentration of the penetrant (C_i), and the strength of penetrant-membrane (polymer) interaction (γ) and is inversely dependent on membrane thickness (ℓ) as

$$J_i = \frac{D_o}{\gamma \ell} [\exp(\gamma C_i) - 1]. \quad (12.3)$$

The selectivity for component A over B in a binary liquid mixture may be expressed by the *separation factor* (α_{AB})

$$\alpha_{AB} = \frac{y_A/y_B}{x_A/x_B} \quad (12.4)$$

or by the *enrichment factor* (β_A), the ratio of concentrations (typically in mass units) of the preferentially pervaporating species (A) in the permeate and feed

$$\beta_A = \frac{y_A}{x_A} \quad (12.5)$$

where x_A and y_A represent the concentration in the feed (i.e., liquid phase) and permeate (i.e., vapor phase), respectively.

Other Separations. In addition to the major membrane processes—filtration, gas separation, and pervaporation—several other fundamental membrane operations are important to the chemical and biomedical industries, such as those listed in Table 12-5. Processes like electrodialysis that can be used to desalt ionic solution use ion-exchange membranes, which are swollen gels or microporous membranes carrying a fixed positive or negative charge. For example, anion-exchange membranes have fixed positive charges (typical charge density of 2 to 4 milliequivalents per gram of membrane) that bind anions from solution. Separation is based upon exclusion of co-ions (same charge as fixed ions of the membrane).

An important application for membranes is in electrochemical processes such as the production of caustic, as shown in Figure 12-6. In this process, water enters at the cathode compartment while saturated brine (NaCl) is fed to the anode compartment. Electrodes are separated by a perfluorosulfonate ionomer membrane such as Nafion (see Section 10.2.4), which has a low diffusion coefficient for Cl^- and a high diffusion coefficient for Na^+ . Water is decomposed at the cathode to produce concentrated sodium hydroxide and hydrogen. At the anode, chloride ions are reduced to chlorine, while the sodium ions are able to permeate the membrane to the cathode compartment, and the anions (Cl^- and OH^-) are excluded. The mechanism of transport through perfluorosulfonate ionomer membranes is briefly discussed in Section 12.1.3.

Table 12-5 Other Membrane Processes

Process	Applications	Driving Force	Membrane Type	Applications
Dialysis	Separation of colloids and other large particles from inorganic ions and other small particles	Concentration gradient	Hydrophilic ultrafilters	Artificial kidney Plasma purification; caustic recovery in the viscose process
Electrodialysis	Separation of ions having opposite charges	Electrical potential	Ion exchange	Concentration of electrolyte solutions; desalting
Electro-osmosis	Treatment of colloidal suspensions and sludge in effluent and waste streams	Electrical potential	Ion exchange	Dewatering

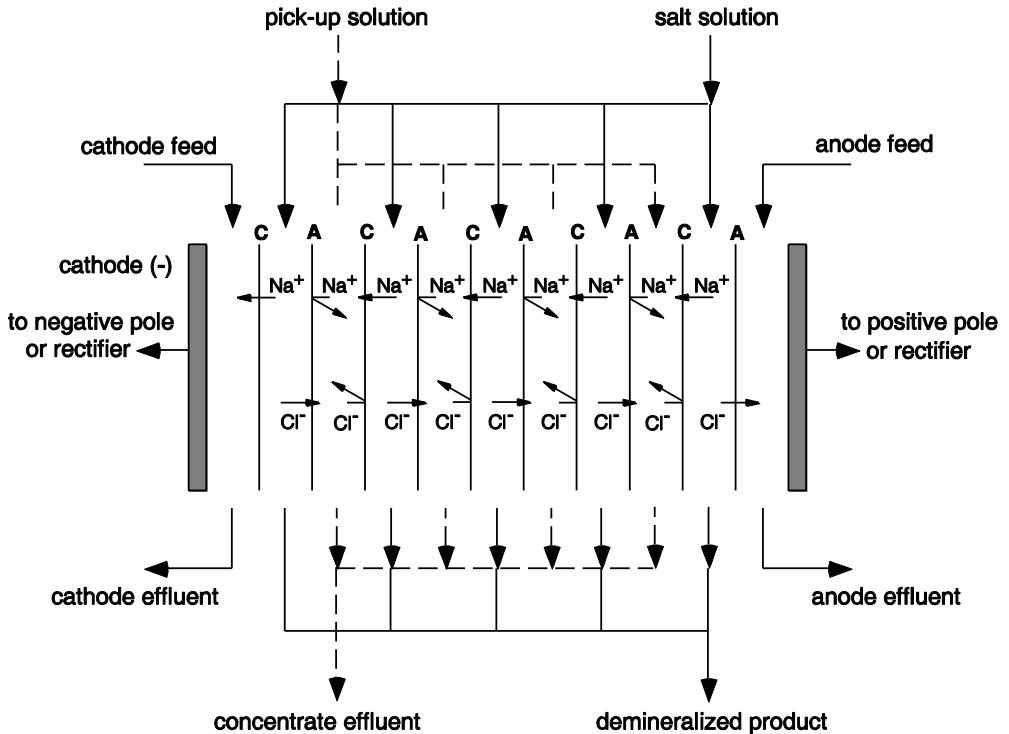


Figure 12-6 Typical chlor-alkali cell used in the production of caustic. Courtesy of Membrane Technology and Research, Inc., Menlo Park, CA.

Fuel Cells. Polymeric membranes also have important potential in the development of efficient and inexpensive fuel cells that could be used to power electric cars and have other important aerospace and military applications. An illustration of a proton-exchange fuel cell is shown in Figure 12-7. At the anode, hydrogen is ionized. Electrons produced by the ionization travel through the external circuit (i.e., the electric motor) and return to the cathode, where they combine with oxygen to form oxygen ions. These reactions are accelerated by the platinum catalyst. The hydrogen ions (i.e., protons) travel through a polymer membrane to the cathode, where they combine with the oxygen ions to form water. As in the case of the chlor-alkali process, perfluorosulfonate ionomers such as Nafion are effective membrane polymers for fuel-cell applications. In addition to the use of hydrogen for fuel cells, natural gas, hydrocarbons, and methanol may be used as fuel. In the case of direct methanol fuel-cell applications, an aqueous methanol solution is delivered to the anode (air to the cathode). Carbon dioxide and water are by-products. A problem in the selection of a fuel cell membrane has been methanol crossover (diffusion from the anode to the cathode) [5], which is a particular problem for Nafion through which methanol easily diffuses. In this case, a variety of sulfonated polymers including some polyphosphazenes (see Section 10.2.5) show promise.

12.1.3 Mechanisms of Transport

The two principal modes of transport that can occur in membrane separations are *size exclusion* in the case of porous membranes and *solution diffusion* in the case of nonporous or dense membranes. Size exclusion is determined by the diameter of the pore in relation to the penetrant size and diffusional path (i.e., mean free path in the case of gases). Size exclusion may be used to separate particles as large as 10 μm or as small as a couple of angstroms in the case of gas molecules. The size and (Lennard-Jones)* collision parameters for several industrially important gas molecules are given in Table 12-6.

* The potential energy, U , is the work required to bring two gas molecules from infinite distance to some separation distance, r , as illustrated:

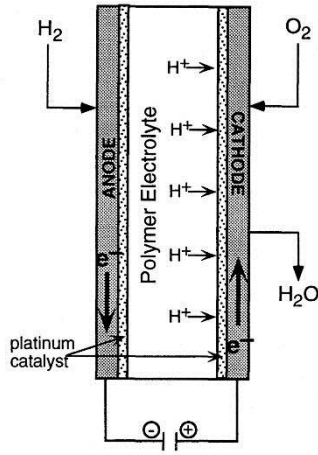
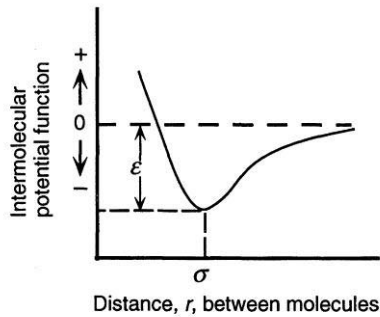


Figure 12-7 Illustration of a typical fuel-cell configuration.



The Lennard-Jones or 6-12 potential function is given as

$$U = 4U = 4\epsilon \left[\left(\frac{\sigma}{r} \right)^{12} - \left(\frac{\sigma}{r} \right)^6 \right]$$

where ϵ is the depth of the potential well and σ is the distance of separation at which the potential energy reaches a minimum.

Table 12-6 Kinetic Diameters and Lennard-Jones Potential Well Depth^a of Important Gases

Gas:	He	H ₂	CO ₂	O ₂	N ₂	CO	CH ₄
Kinetic diameter (Å)	2.6	2.89	3.3	3.46	3.64	3.76	3.80
ϵ/k (K)	10.2	59.7	195	107	71.4	91.7	149
σ (Å)	2.55	2.83	3.94	3.47	3.80	3.69	3.76

^aSee text footnote for identification of the Lennard-Jones parameters ϵ/k and σ .

Transport through nonporous membranes is controlled by the solubility and diffusivity of the penetrant in the polymer matrix. In this regard, the transport of gases through a glassy polymer differs from that in a rubbery polymer. This is a result of an additional mode of sorption that is available in glassy polymers—the filling of Langmuir-type microvoids or regions of localized high free volume present in the glassy state. A discussion of diffusion through porous media and the solution-diffusion model is presented in the following sections, as are two other more specialized membrane-transport processes—facilitated and coupled transport and transport through perfluorosulfonate ionomers.

Transport through Porous Media. As illustrated in Figure 12-8, the mechanism of flow of gas molecules through porous membranes depends upon the size of the pores in relation to the *mean free path* of the gas molecules. The mean free path represents the average distance traversed by gas molecules between collisions. The Knudsen number (N_{Kn}) is defined as the ratio of the mean free path to the mean pore diameter. When the Knudsen number is small, flow is inversely proportional to the viscosity of the fluid (gas). This is called *viscous flow*, illustrated in Figure 12-8A. In contrast, *Knudsen flow* occurs when the Knudsen number is large (i.e., for small pore sizes). In this case, molecules diffusing within the pores collide much more frequently with the pore walls than with themselves (Figure 12-8B). The Knudsen diffusion coefficient is inversely proportional to the *square root* of the molecular mass (M) of the diffusing species following the relationship

$$D_{Kn} = \frac{d}{3} \left(\frac{2RT}{M} \right)^{1/2} \quad (12.6)$$

where d is the pore diameter. Although some separation can be achieved by selective Knudsen flow of gas molecules, permselectivity is small unless the molecules are very different in size. A third mechanism occurs when the pore diameter is small compared to the molecular diameters of the diffusing molecules. This is termed *molecular sieving* (Figure 12-8C). Small molecules can also diffuse through dense molecules (Figure 12-8D) through a solution-diffusion mechanism discussed in the following section.

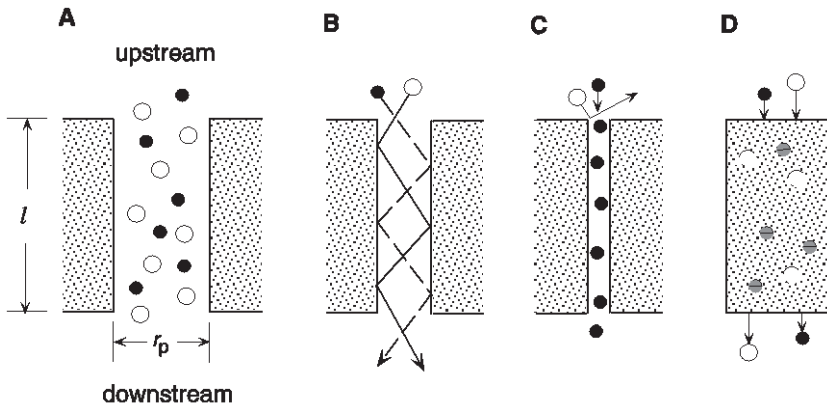


Figure 12-8 Illustration of the membrane transport of two differently sized molecules by various mechanisms. From left to right: **(A)** viscous flow through large pores of radii r_p (no separation); **(B)** Knudsen flow (separation based upon difference in molecular weights); **(C)** molecular sieving (separation due to relative diffusive rates and surface sorption on pore walls); and **(D)** solution-diffusion transport through a dense membrane (separation based upon relative solubility and diffusivity).

Solution-Diffusion Transport. The predominant mechanism of transport for industrial gas- and liquid-separating membranes involves the dissolution and subsequent diffusion of molecules in a nonporous or dense membrane. In general, the permeability can be represented as the product of the solubility, S , and diffusivity, D , coefficients of the penetrant in the polymer membrane as

$$P = SD \quad (12.7)$$

The mechanism of penetrant *solubility* in a polymeric membrane depends upon the activity of the penetrant and whether the polymer is in the rubbery or glassy state. The solubility of organic vapors at very low activities and gases at low to moderate pressures in liquids and rubbery polymers is given by *Henry's law* expressed as

$$C = Sp \quad (12.8)$$

where C is the concentration of sorbed penetrant (typically units of cc of gas at STP per cc of polymer) and p is the pressure. In general, the solubility of a gas increases with its condensability. More condensable gases are those with higher boiling points or critical temperatures, such as CO_2 . At higher penetrant activities, as is the case for organic vapors and highly condensable gases like CO_2 at moderate to high pressures, Henry's law no longer applies. In this case, the Flory-Huggins lattice model (see Section 3.2.1) may be used to represent the observed increase in solubility with

increasing pressure in rubbery polymers (i.e., $T > T_g$). An illustration of this behavior is shown in Figure 12-9, which plots the sorbed concentration of CO_2 in a silicone elastomer against pressure. Below approximately 400 psia, sorption is adequately represented by the linear relationship given by Henry's law. At higher pressures, the sorbed concentration increases at an increasing rate as modeled by the Flory–Huggins theory.

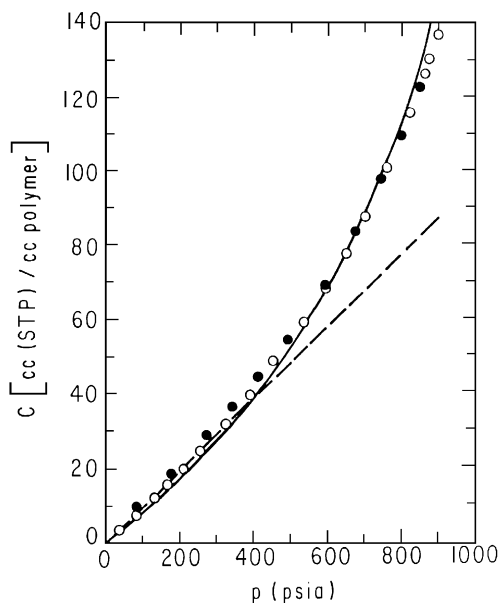


Figure 12-9 Sorption isotherm of CO_2 in silicone rubber at 35°C . Data points give CO_2 concentrations measured at different pressures during sorption (\circ) and desorption (\bullet). The solid line represents the fit by the Flory–Huggins equation; the broken line represents Henry's law behavior. Reprinted with permission from G. K. Fleming and W. J. Koros, *Macromolecules*, 1986. **19**: p. 2285. Copyright 1986, American Chemical Society.

Below T_g and at low to moderate gas pressures, the sorption isotherm curves *downward* with increasing pressure, as illustrated by the data for polysulfone in Figure 12-10. The most successful model for sorption in glassy polymers is given by the *dual-mode* model [6], which postulates that an additional (Langmuir) mode of sorption is possible by the filling of microvoids in the glassy state. The total sorbed concentration is then a summation of Henry's law dissolution (C_D) and Langmuir-type hole-filling (C_H) contributions as

$$C = C_D + C_H = k_D p + \frac{C_H' b p}{1 + b p} \quad (12.9)$$

The parameters characterizing dual-mode sorption are the Henry's law coefficient, k_D , the Langmuir or hole-filling capacity of the glass, C_H' , and the hole-affinity parameter, b . Dual-mode parameters for representative polymers are given in Table 12-7.

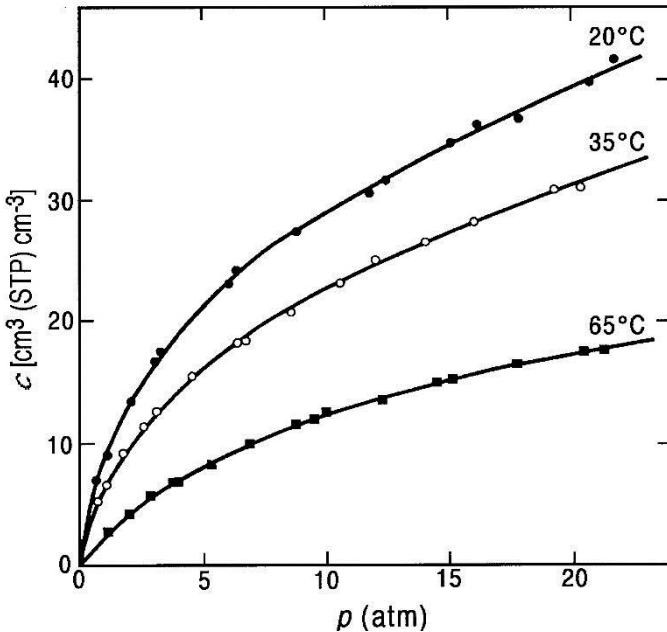


Figure 12-10 Sorption isotherm of CO_2 in a glassy polymer, polysulfone ($T_g = 186^\circ\text{C}$), showing dual-mode behavior. As temperature is decreased from 65° to 20°C , the isotherm becomes increasingly nonlinear as the Langmuir capacity increases with increasing $T - T_g$. Adapted from Y. Maeda and D. R. Paul, *Effect of Antiplasticization on Gas Sorption and Transport. I. Polysulfone*. *Journal of Polymer Science: Part B: Polymer Physics*, 1987. **25**(5): p. 957. Copyright © 1987 John Wiley & Sons. Reprinted by permission of John Wiley & Sons, Inc.

As discussed earlier, the Henry's law coefficient, k_D , is strongly influenced by the condensability of the gas. For example, k_D is especially high for CO_2 (see Table 12-7), which is a very condensable gas. In turn, the condensability of a gas can be related to ϵ/k , the well depth of the Lennard-Jones potential-energy plot for a gas.

Values of ε/k were given for some gases in Table 12-6. For a given polymer, k_D is exponentially related to ε/k as [7]

$$\ln k_D = \ln k_D^\circ + m \frac{\varepsilon}{k} \quad (12.10)$$

where k_D° is a constant for a given polymer and temperature and m is the slope ($\sim 0.01 \text{ K}^{-1}$) of a plot of $\ln k_D$ versus ε/k . The second contribution to solubility for glassy polymers—the Langmuir capacity, C_H' —depends upon the size and distribution of microvoids and, therefore, can be related to the free volume of the glass. Free volume is determined by the stiffness and molecular dimensions of the polymer chain and the extent of undercooling of the glass.

Table 12-7 Representative Dual-Mode Parameters for Sorption of Nitrogen, Methane, and Carbon Dioxide in Important Gas-Separating Polymers at 35°C

Polymer	k_D (cm ³ (STP)/cm ³ -atm)	C_H' (cm ³ (STP)/cm ³)	b (atm ⁻¹)
Cellulose acetate^a			
CO ₂	1.43	34.2	0.197
Polycarbonate			
N ₂	0.0909	2.11	0.0564
CO ₂	0.685	18.81	0.262
Poly(2,6-dimethyl-1,4-phenylene oxide)			
CH ₄	0.33	18.1	0.11
CO ₂	0.95	27.5	0.25
Poly(methyl methacrylate)			
N ₂	0.020	1.902	0.043
CH ₄	0.102	8.507	0.046
CO ₂	0.944	19.680	0.158
Polysulfone			
N ₂	0.0753	9.98	0.0156
CO ₂	0.664	17.8	0.326
Poly(vinyl chloride)			
N ₂	0.0169	0.451	0.0448
CO ₂	0.587	8.939	0.2094

^aData obtained at 30°C.

The fundamental law for transport through a flat membrane is given by *Fick's first law* as

$$J = -D \frac{dC}{dx} \quad (12.11)$$

where J is the flux (units of mass per unit time), D is the diffusion coefficient, and dC/dx is the concentration gradient of penetrant across the membrane. Integration of eq. (12.11) from $x = 0$ to $x = \ell$, using Henry's law for C (eq. (12.8)), and assuming that D is independent of concentration, gives

$$J = \frac{SD}{\ell}(p_2 - p_1) \quad (12.12)$$

where p_1 and p_2 are the pressure at the low- and high-pressure sides of the membrane, respectively. Substitution of $P = SD$ (eq. (12.7)) into eq. (12.12) gives

$$J = \frac{P}{\ell} \Delta p \quad (12.13)$$

which is equivalent to eq. (12.1).

Equations (12.11) and (12.12) strictly apply to the diffusion of gases at low to moderate pressures through rubbery polymers where Henry's law is valid and the diffusion coefficient is independent of concentration. For glassy polymers, the concentration of gases at low to moderate pressures is no longer given by Henry's law but by the dual-mode model (eq. (12.9)). The most successful approach to predict gas permeability in glassy polymers, the *partial immobilization* theory [8], is based upon the dual-mode model, which postulates that there are two populations of sorbed gas—the Henry's law dissolution component and Langmuir sites. In the partial immobilization theory, each population is assigned separate diffusion coefficients, for which Fick's first law can be written as

$$J = -D_D \left(\frac{dC_D}{dx} \right) - D_H \left(\frac{dC_H}{dx} \right) \quad (12.14)$$

where D_D and D_H are the diffusion coefficients for the Henry's law dissolution and hole populations, respectively. Generally, the diffusion coefficient for gas molecules contained in the Langmuir sites is smaller than that for the Henry's law regions. For example, $D_D = 5.15 \times 10^{-8} \text{ cm}^2 \text{ s}^{-1}$ and $D_H = 5.83 \times 10^{-9} \text{ cm}^2 \text{ s}^{-1}$ for polycarbonate at 35°C. Integration of eq. (12.14) and using the dual-mode model for C_D and C_H (eq. (12.9)) gives the expression for permeability as

$$P = k_D D_D \left(1 + \frac{FK}{1 + bp_2} \right) \quad (12.15)$$

where

$$F = \frac{D_H}{D_D} \quad (12.16)$$

and

$$K = \frac{C_H' b}{k_D}. \quad (12.17)$$

Equation (12.15) was obtained by assuming a pressure of p_2 at the high-pressure side of the membrane and zero pressure at the downside. For the example of polycarbonate cited above, the ratio of the diffusion coefficients, F , given by eq. (12.16), is 0.113. It is noted that as temperature increases to above T_g the polymer passes from the glassy to the rubbery state (see Section 4.3) and the Langmuir-capacity term, C_H' , and, therefore, K , goes to zero, and $P = k_D D \equiv SD$ (eq. (12.8)).

Both the permeability and diffusion coefficients can be determined by measuring the amount, Q_t , of permeant passing through a membrane at some time, t , as illustrated in Figure 12-11. From the steady-state transport rate, $(dQ_t/dt)_{ss}$, the permeability is determined as

$$P = \left(\frac{\ell}{p_2 A} \right) \left(\frac{dQ_t}{dt} \right)_{ss} \quad (12.18)$$

where A is the surface area of the membrane of thickness ℓ . The diffusion coefficient, which influences the initial or transient permeation behavior of the membrane, is obtained from measurement of the *time lag* (θ), which is the extrapolated value of Q_t , as shown in Figure 12-11. In the partial-immobilization model, the diffusion coefficient is related to the time lag as

$$\theta = \frac{\ell^2}{6D} \left[1 + f(K, F, bp_2) \right] \quad (12.19)$$

where $f(K, F, bp_2)$ is a function of the dual-mode parameters and pressure. For rubbery polymers where $C_H' = 0$, this term is zero and, therefore, the diffusion coefficient is simply obtained as

$$\boxed{D = \frac{\ell^2}{6\theta}}. \quad (12.20)$$

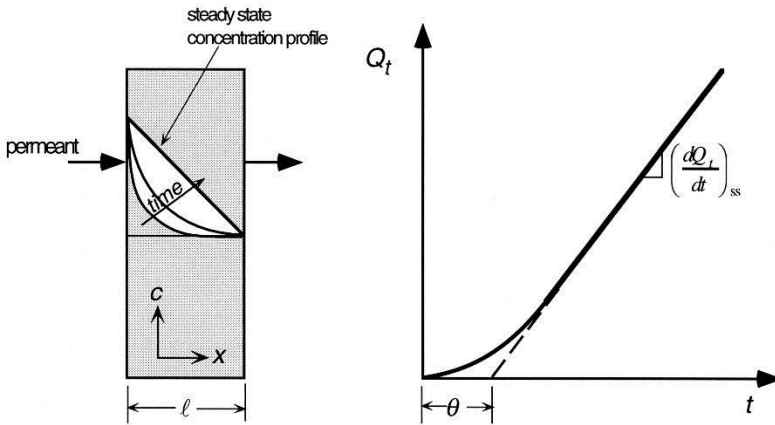


Figure 12-11 Plot of the amount of permeant versus time for a flat film illustrated at the left. The slope of the linear portion of the curve gives the steady-state permeability, while the intercept with the time axis yields the time lag, θ , from which the apparent diffusion coefficient can be obtained (eq. (12.20)). The increase in permeant concentration in the film up to the attainment of steady state is illustrated at the left.

Facilitated and Coupled Transport. As described in the previous sections, the basis of separation by filtration is particle size, while gas separation and pervaporation use differences in solute solubility and diffusivity to separate components from a mixture. In contrast, transport in two related processes—facilitated and coupled transport—is by means of a carrier mechanism. In both processes, a macroporous membrane (e.g., Celgard macroporous polypropylene) containing a free mobile carrier separates two liquid phases. The carrier, which is insoluble in the liquid phase, is contained in the membrane pores by capillary attraction. In facilitated transport, the carrier interacts with the permeant at the membrane–liquid interface. The permeant-carrier complex diffuses through the membrane and the permeant is released at the opposite membrane–liquid interface. An example of facilitated transport is the transport of oxygen by hemoglobin, as illustrated in Figure 12-12A. In the case of coupled transport, a chemical reaction occurs at the interface of the membrane and liquid phases, and mass flux occurs in both directions, as illustrated for $\text{Cu}^{2+}/\text{H}^+$ transport in Figure 12-12B. One practical problem with facilitated and coupled transport is the instability of the membrane, as the carrier may diffuse out of the pores of the macroporous membrane with time.

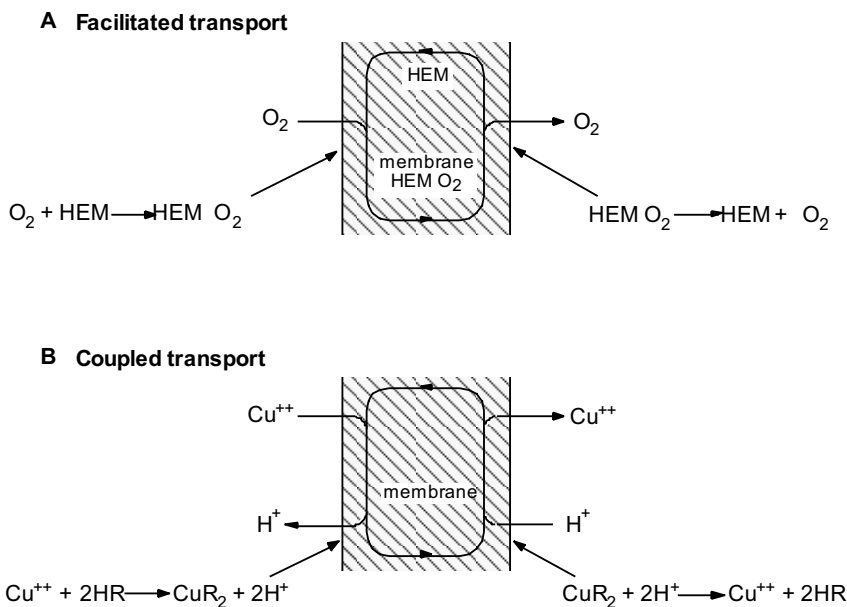
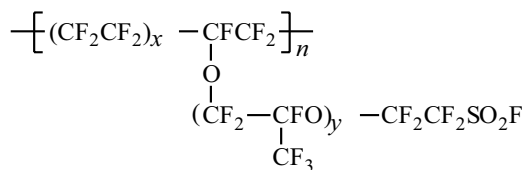


Figure 12-12 A. Facilitated transport of oxygen. B. Coupled transport of cupric and hydrogen ions. (Courtesy of Membrane Technology and Research, Inc., Menlo Park, CA).

Transport through Perfluorosulfonate Ionomers. As mentioned earlier, a class of polymers frequently used for a number of membrane-separation processes, including the chlor-alkali process, fuel cells, facilitated gas transport, and liquid separations, is the perfluorosulfonate ionomers (PFSI). As discussed in Section 10.2.2, PFSIs are copolymers of tetrafluoroethylene and a perfluorinated vinyl ether containing a terminal sulfonyl fluoride (SO_2F) group (structure 3).



3

The most important commercial PFSI product is Nafion ($y = 1$), which is produced as film by melt extrusion. After film formation, the sulfonyl fluoride groups are converted to sulfonate groups by reaction with sodium or potassium hydroxide, with further conversion to the commercial sulfonic acid (SO_3H) form (Nafion-H). Other ionic forms (e.g., Na^+ , Li^+ , K^+ , Ag^+ , Ca^{2+} , Al^{3+} salts) can be obtained by ion

exchange with the appropriate salts. The importance of Nafion to chlor-alkali production is its selective permeability to ions. The morphology of Nafion membranes has been extensively studied to understand its transport properties. A widely accepted theory is the cluster-network model [9] illustrated in Figure 12-13. According to this model, the ionic sites (SO_3^-) of the pendant groups phase-separate from the polytetrafluoroethylene backbone to form clusters approximately 4 nm (40 Å) in diameter and connected by short, narrow channels. The ionic channels provide a relatively free diffusional path for cations such as Na^+ , for which it is highly selective. By the same reasoning, small polar molecules such as water and aliphatic alcohols easily pass through the ionic channels, while the diffusion of larger nonpolar molecules is restricted.

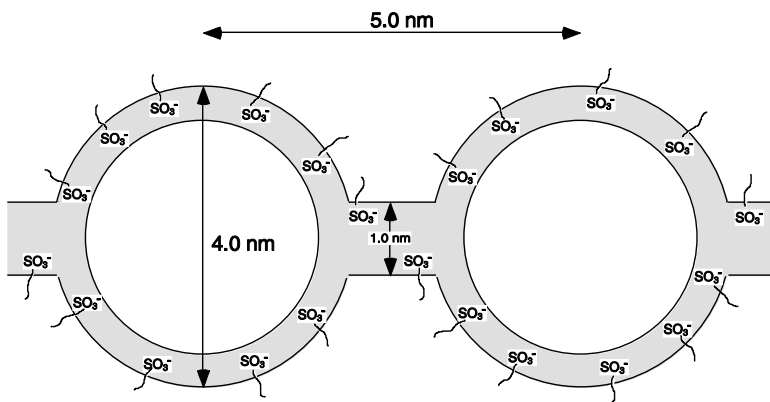


Figure 12-13 Illustration of the cluster-network model of perfluorosulfonate membranes [9].

12.1.4 Membrane Preparation

Dense membranes may be formed by any of the methods normally used to prepare films. These include melt extrusion, compression molding, and solution casting (see Chapter 11). As described next, procedures to prepare microporous and asymmetric membranes that consist of an integral dense skin covering a microporous substrate require significant art, as well as a basic understanding of polymer morphology and solution thermodynamics.

Microporous Membranes. Techniques that can be used to prepare microporous and ultraporous membranes are summarized in Table 12-8. Some microporous membranes suitable for ultrafiltration and microfiltration applications are prepared by stretching a semicrystalline polymer film such as a polyolefin (e.g., Celgard polypropylene) or polytetrafluoroethylene (e.g., Gore-Tex) in the solid

state. Stretching forces a separation of crystalline lamellae (see Section 4.2.1) and results in the creation of slit-like pores, typically $0.2 \mu\text{m}$ in length and $0.02 \mu\text{m}$ in width. Total porosity of such microporous membranes may be 40%.

Table 12-8 Methods Used to Prepare Microporous and Ultraporous Membranes

Method	Description
Leaching	Extraction of solid pore formers
Phase inversion	Phase separation of a ternary mixture of polymer, solvent, and nonsolvent
Sintering	Melting of a semicrystalline polymer powder
Stretching	Combined stretching and annealing of extruded semicrystalline film
Thermally induced phase separation	Cooling a mixture of a polymer with a latent solvent to a point of thermal separation of the mixture followed by extraction of the latent-solvent phase
Track etching	Irradiation of polymer films resulting in the production of fission fragments followed by caustic etching

Pore structure can also be obtained by leaching solids dispersed in a solid material by use of a suitable extraction solvent. For example, porous (“thirsty”) glass (e.g., Vicor glass) can be prepared by extracting boron-containing compounds and alkali metal oxides from hollow glass fibers with dilute hydrochloric acid. A pore size of approximately 40 \AA and a 40% void volume can be obtained by this procedure.

Microporous membranes can be prepared from a wide variety of thermoplastics by irradiation. This process is called nucleation track etching. When radioactive elements decay, fission fragments including heavy positive ions are produced that can penetrate polymers to significant depths. For example, fission fragments from ^{252}Cf can penetrate polycarbonate to a depth of $20 \mu\text{m}$ while those from ^{235}U will penetrate to a depth of 10 to $12 \mu\text{m}$. Collision of the fragments with polymer chains results in chain scission along the penetration path (see Chapter 6). These radiation-degraded polymer molecules are then etched from the film by treatment with acid or base. If the films are sufficiently thin compared to the depth of penetration, the combination of track formation and etching results in the creation of cylindrical pores that pass completely through the film and have a narrow pore-size distribution. Typical pore diameters fall in the range from 0.02 to $20 \mu\text{m}$. In addition to polycarbonate, other polymers that can be track-etched include poly(ethylene terephthalate), cellulose acetate, cellulose nitrate, and poly(methyl methacrylate).

Asymmetric-Membrane Formation. In order to ensure favorable economics for membrane separations compared to other, more traditional separation techniques, it is necessary to achieve both high selectivity *and* high flux. While permea-

bility and selectivity of dense membranes are intrinsic properties of the membrane material, flux can be increased by decreasing the membrane thickness (eq. (12.12)). Since membranes must be sufficiently strong to withstand significant pressure drops (e.g., potentially as high as 2000 psi in some applications), there is a limit to how thin a membrane can be and still provide the necessary strength under operating conditions. A major technological advance that has addressed this problem was the development of asymmetric membranes in 1960 by Loeb and Sourirajan [10] for reverse-osmosis applications. As described next, these membranes are prepared by a phase-inversion process that produces a thin, dense surface layer or *skin* and a thick, macroporous substrate. The skin, which may be only 0.1 to 1 μm in thickness, provides the separating function while the substrate provides the mechanical strength. An electron micrograph of a typical asymmetric fiber is shown in Figure 12-14.

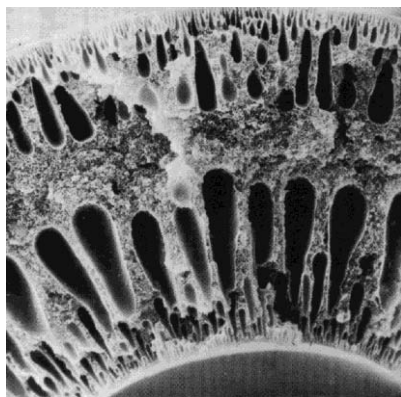


Figure 12-14 Photomicrograph of a cross section of an asymmetric hollow-fiber membrane showing large macrovoids in a porous substructure and a thin, dense skin on the outer and inner surfaces of the fiber. Reprinted with permission from J. M. S. Henis and M. K. Tripodi, *The Developing Technology of Gas Separating Membranes*. Science, 1983. **220**: p. 11. Copyright 1983 American Association for the Advancement of Science.

There are four techniques by which asymmetric membranes can be prepared—dry, wet, thermal, and polymer-assisted. All involve the phase separation of a moderately concentrated polymer solution to form a gel in which the polymer becomes the continuous phase and solvent molecules coalesce to form pockets. Removal of the solvent from these pockets leaves voids, which constitute the macroporous structure of the asymmetric membrane. Phase inversion can be induced either by the action of a nonsolvent such as water (i.e., chemically induced) or by a change in temperature (i.e., thermally induced), which causes the membrane solution to become thermodynamically unstable and consequently to phase-separate (see Chapter 3).

In the dry process of membrane formation, a polymer, solvent, and nonsolvent are mixed to give a composition within the miscible or single-phase region of the triangular diagram, as shown in Figure 12-15. The solution is then evaporated to dryness. As the volatile components (i.e., solvent and nonsolvent) are lost, the overall composition moves into the miscibility gap and phase separation occurs. In the wet process, a polymer solution is partially evaporated and then coagulated in a nonsolvent, typically water.

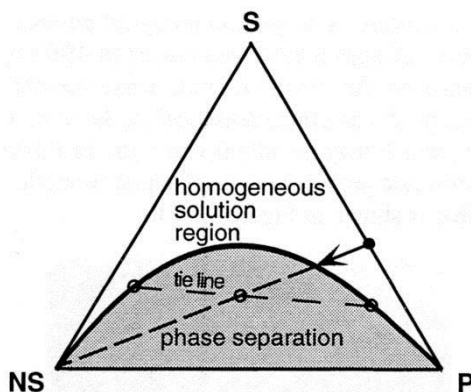


Figure 12-15 Phase diagram of a ternary mixture containing polymer (P), solvent (S), and nonsolvent (NS) at constant temperature. When a nonsolvent is added to a concentrated polymer solution whose composition is indicated by the filled circle along the S–P side, the overall composition of the mixture follows the line connecting this point and the NS vertex. When the composition reaches the phase envelope, phase separation (coagulation) begins. The composition of the two equilibrium phases is given by a tie line through the point on the phase diagram representing the overall composition of the ternary mixture, as shown.

The thermal process or thermally induced phase separation (TIPS) utilizes a “latent” solvent and a decrease in temperature to cause phase separation. A latent solvent is one that has a high-boiling-point, low-molecular-weight solvent for the polymer at some high temperature (e.g., 220°C) but a nonsolvent at lower temperature. Examples of latent solvents include *N*-tallowdiethanolamine (TDEA), menthol, and sulfolane. The polymer and latent solvent are melt-blended, cast into a film or extruded as a fiber, and then cooled to induce phase separation. As shown in Figure 12-16, phase separation occurs when the temperature is lowered to below the upper critical solution temperature (UCST). After phase inversion, the latent solvent (the pore former) is then extracted by another solvent (a nonsolvent for the polymer). Membrane morphology is determined by many parameters, such as the polymer concentration, solution temperature, and rate of cooling. Phase separation within the spinodal results in phase separation by a mechanism called *spinodal decomposition*.

Spinodal decomposition results in a “lacy” membrane structure. Phase separation within the metastable region located between the spinodal and binodal occurs by nucleation and growth and leads to an open pore structure. Microporous membranes of high-density polyethylene, polypropylene, polystyrene, and poly(2,6-dimethyl-1,4-phenylene oxide) can be prepared by this procedure.

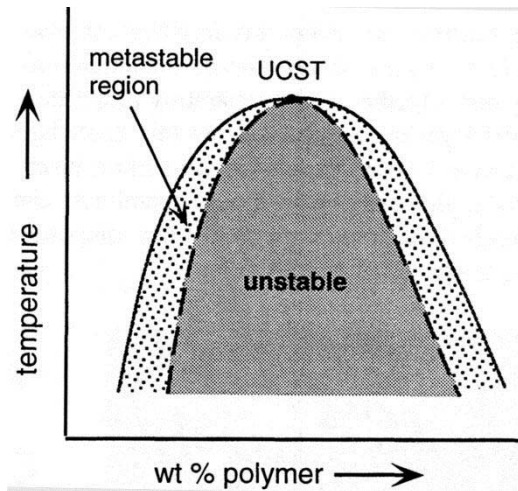


Figure 12-16 Phase diagram of a polymer solution illustrating phase separation as temperature decreases below the upper critical solution temperature (UCST). The binodal is indicated by the solid curve; the spinodal is represented by the broken curve.

The polymer-assisted method of membrane formation utilizes a mixture of *two* physically compatible but immiscible polymers dissolved in a common solvent. This means that the two polymers form a homogeneous solution with the solvent at low to moderately high polymer content but do not form a homogeneous mixture in the solid state. When the solution is cast and the solvent evaporated, phase separation of the two polymers results. The polymer with lower concentration in the blend will form the dispersed phase in a continuous phase of the polymer present in higher concentration. The art is to select the dispersed-phase polymer to be soluble in some convenient solvent (usually water) that is not a solvent for the polymer forming the continuous phase. An example of a water-soluble polymer that is used for this purpose is poly(*N*-vinylpyrrolidone) (PVP). After casting and drying, the dispersed phase is extracted out of the membrane by the solvent. The resulting membrane will have a skinless, microporous structure suitable as a substrate for the preparation of composite membranes.

Coated Asymmetric and Composite Membranes. Although asymmetric membranes have great potential as highly efficient membranes for gas separations,

small defects or pores can develop in the skin layer during their preparation. These pinholes permit the free passage of gas molecules through the membrane, resulting in reduced separation. Such pores need to be only approximately 10 Å or more in diameter to cause a significant decrease in selectivity. The problem of achieving defect-free skinned membranes was solved by Henis and Tripodi [11] who showed that coating an asymmetric fiber with a thin layer of a highly permeable polymer such as silicone rubber plugged the open pores and forced separation to occur through the dense, separating region of the skin.

Membranes with attractive flux and permselectivity can also be prepared by using a microporous membrane (e.g., a skinned asymmetric membrane) as a support for casting a thin film of another polymer with the desired separation properties. A composite membrane with a very thin separating layer can be obtained by this procedure. Alternatively, lamination and plasma polymerization can be used to prepare the surface layer. The membrane flux and permselectivity of a coated asymmetric or composite membrane can be related to membrane morphology and the individual transport properties of the components by analogy to an electrical-resistance network, as illustrated by Figure 12-17.

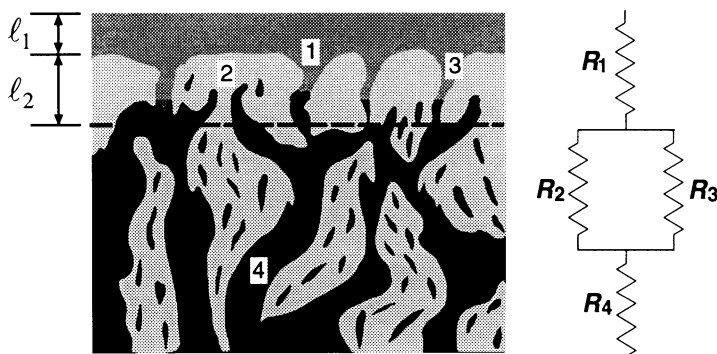


Figure 12-17 The resistance model of coated asymmetric membranes: coating (1), dense layer (2), pore (3), and substrate (4). Adapted from M. S. Henis and M. K. Tripodi, *Composite Hollow Fiber Membranes for Gas Separation: The Resistance Model Approach*. *Journal of Membrane Science*, 1981. **8**: p. 233. Copyright 1981, with permission from Elsevier.

In the resistance model, the permeation flux

$$Q_i = \left(\frac{P_i}{\ell} \right) A \Delta p \quad (12.21)$$

is equated with electrical current, I , and the driving force or pressure drop, Δp , across the membrane with the electrical potential, E . In an electrical network, the resistance, R_e , is related to I and E by Ohm's law

$$R_e = \frac{E}{I}. \quad (12.22)$$

It follows that the analogous resistance to permeation, R_p , is given as

$$R_p = \left(\frac{\ell}{P_i} \right) A. \quad (12.23)$$

The coated membrane illustrated in Figure 12-17 is equivalent to a resistor (dense coating layer, 1) in series with two parallel resistors (i.e., the dense layer, 2, and the pore region, 3, of the skin) and with the porous substrate, 4. The total resistance of the network is then given as

$$R_T = R_1 + \frac{R_2 R_3}{R_2 + R_3} + R_4. \quad (12.24)$$

The substrate is typically sufficiently porous to pose no significant resistance to permeation (i.e., $P_4 A_4$ is very large) and, therefore, R_4 may be safely neglected. To simplify the analysis, it may be assumed that the smaller pores in the skin are filled completely with the coating material to the depth of the skin (ℓ_2) although it can be shown that, in usual circumstances, complete filling is not required for the coating to be effective. Furthermore, the pore area, A_3 , is typically only a small fraction of the total surface area of the fiber (i.e., $A_2 \gg A_3$) and, therefore, $A_2 \approx A_1$. Using these assumptions, the resulting equation for total membrane flux becomes [11]

$$\frac{Q_i}{A_2 \Delta p} = \left(\frac{P}{\ell} \right)_i = \left[\frac{\ell_1}{P_{1,i}} + \frac{\ell_2}{P_{2,i} + P_{1,i} (A_3/A_2)} \right]^{-1}. \quad (12.25)$$

Values of P/ℓ for the coating and substrate polymers may be easily obtained from steady-state permeability measurements of dense films of the two materials and the fiber morphology (e.g., A_3/A_2 , ℓ_1 , and ℓ_2) can be determined by electron microscopy.

Module Fabrication. For commercial separations of liquids and gases and for purification and desalination of seawater, membranes with very large surface areas (10^3 to 10^7 m²) and high area-to-volume ratios (packing density) are needed to meet flux requirements. A hollow-fiber membrane module illustrated in Figure 12-18 gives the highest packing densities (10^4 to 10^5 m² m⁻³). Other configurations include spiral-wound, plate-and-frame, tubular, and capillary. Typical module designs used

for reverse osmosis (RO), pervaporation (PV), gas permeation (GP), ultrafiltration (UF), electrodialysis (ED), and microfiltration (MF) are given in Table 12-9.

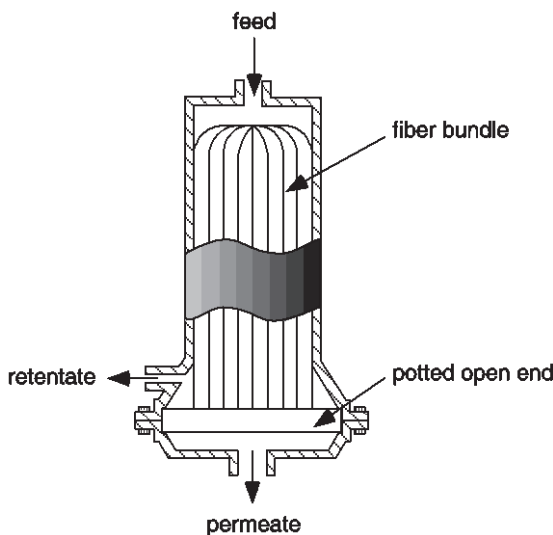


Figure 12-18 Cutaway view of a typical hollow-fiber membrane module. Adapted from K. Scott, *Membrane Separation Technology*. 1990, Oxford: STI.

Table 12-9 Preferred Module Designs for Major Membrane Separations

Module Type	Separation ^a
Capillary	UF, MF
Hollow-fiber	RO, GP, PV
Plate-and-frame	PV, UF, ED
Spiral-wound	RO, PV, GP
Tubular	UF, MF

^a Code: RO, reverse osmosis; GP, gas permeation; PV, pervaporation; UF, ultrafiltration; ED, electrodialysis; MF, microfiltration.

Hollow-fiber modules are frequently used for commercial RO and gas separations. The typical o.d. of hollow fiber ranges from 80 to 200 μm with a wall thickness of 20 μm or greater. These fibers are made (melt or wet spinning) from polyamide, cellulose triacetate, and sulfonated polysulfone for RO applications and usually polysulfone for gas separations. Seals for membrane bundles are usually made from epoxy. Modules containing fibers of larger diameters are sometimes called *capillary modules* and are used for UF (and MF) applications. Typical polymers used for UF capillary modules include polysulfone, polyacrylonitrile, and chlorinated polyolefins. In all cases, process streams must be pretreated to remove large par-

ticles that can plug pores or chemicals that can dissolve or craze the polymeric fibers or lead to swelling or leakage of the seal materials.

The principal application for *spiral-wound membranes* has been reverse osmosis. As illustrated in Figure 12-19, spiral-wound modules are prepared by sandwiching alternate layers of flat sheet membranes, spacers, and porous material around an inner porous permeate-collection tube. The feed flows axially along the sandwich in the channels, approximately 1.0 mm in depth, formed by the spacers, while the permeate flows radially to the collection tube. Spiral-wound membrane modules designed for RO separations are typically about 1 m in length and 0.2 m in diameter and can accommodate flow rates up to 28 m³ per day and pressures up to 40 bars.

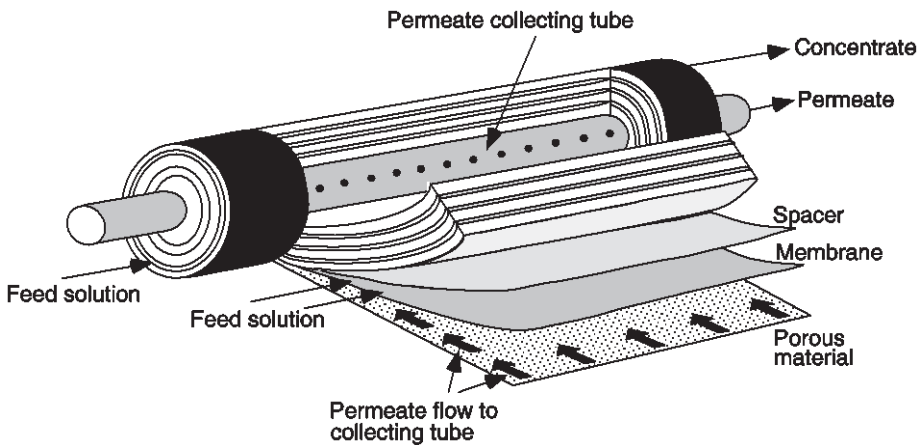


Figure 12-19 Spiral-wound membrane modules. Adapted from K. Scott, *Membrane Separation Technology*. 1990, Oxford: STI.

In cases where feeds cannot be pretreated to remove potential fouling contaminants or where the module must be steam-sterilized, a tubular-membrane module, as illustrated in Figure 12-20, is sometimes used. The module, which looks much like a shell-and-tube heat exchanger, consists of an inner membrane tube surrounded by porous supporting tubes. In some cases, the membrane may be inorganic (e.g., ceramic) rather than organic to meet the more aggressive environments in which such modules are used. Such units can be easily cleaned and can be steam-sterilized; however, pressure losses are high and productivity is low compared to hollow-fiber and spiral-wound units. Principal applications for tubular-membrane modules are UF and MF.

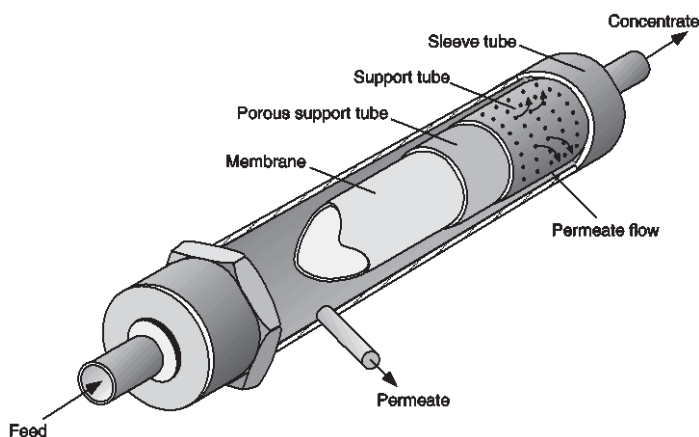


Figure 12-20 Tubular-membrane module. Adapted from K. Scott, *Membrane Separation Technology*. 1990, Oxford: STI.

12.2 Biomedical Engineering and Drug Delivery

Polymers are widely used in medicine as materials in the manufacture of sutures, vascular grafts, intravascular stents, artificial organs, orthopedic implants, and prosthetic devices. Polymers also find applications in controlled release of drugs as an alternative to more traditional metal amalgams. Depending upon the application, polymers for biomedical use must be biocompatible and excel in properties specific for the specific application such as selective permeability, biodegradability, and high strength or modulus. The biocompatibility of a polymeric material depends upon the degree of adsorption of plasma proteins to the polymer surface and upon the interaction of these proteins with cell receptors. Protein adsorption can be reduced by increasing hydrophilicity or steric repulsion using plasma film deposition and by the grafting of water-soluble polymers, such as the radiation grafting of *N*-allylacrylamide. Segmented polyurethanes and poly(urethane-urea) are examples of polymers having good biocompatibility that can be further improved through grafting of heparin, a D-glucosamine polysaccharide.

Polymers that have been used in medical applications include PVC, polypropylene, some acrylics, and polystyrene. Radiation-sterilizable and environmentally safe grades of PVC have given this polymer a significant share of the medical plastics market. Polypropylene has been used in sterilizable medical packaging and drug-delivery devices. Recent metallocene polyolefins (see Section 2.2.3) provide some advantages for medical applications including superior optical clarity, ductility at low temperature, and low residual concentration of polymerization catalysts. The attractive properties of metallocene-polymerized syndiotactic polystyrene (see

Section 9.1.2) such as its high thermal stability open opportunities for use as sterilizable trays, surgical instruments, and dental equipment.

Polymers can be used in the treatment of diseases including cancer [12] through facilitated and safe delivery of drugs (e.g., paclitaxel), proteins, and genetic material such as DNA (gene therapy). As illustrated in Figure 12-21, hydrophilic polymers may be used to link a specific drug (Figure 12-21a), to engulf a protein (Figure 12-21b) or a recombinant DNA sequence (Figure 12-21c), and to enclose a poorly soluble (hydrophobic) drug within a micelle (Figure 12-21d) or a dendrimer (Figure 12-21e). Natural and synthetic polymers and copolymers that have been evaluated for these applications include poly(ethylene glycol) (PEG), *N*-(2-hydroxypropyl) methacrylate copolymers, poly(vinyl pyrrolidone), poly(ethyleneimine) (PEI, structure 4), polyphosphazenes, hyaluronic acid, chitosan, dextran, poly(aspartic acid), poly(L-lysine) (PLL, structure 5), and poly(lactic-*co*-glycolic acid). PEG, being nontoxic and non-immunogenic, is a particularly common polymer used in graft and block copolymers. PEG is often used to water-solubilize a variety of drugs, proteins, and several nanoparticles. Triblock copolymers of PEG with poly(ϵ -caprolactone) (PCL), PEG-*b*-PCL-*b*-PEG, and with poly(D,L-lactic acid-*co*-glycolic acid), PEG-*b*-PLGA-*b*-PEG, can form polymeric micelles that can encapsulate a drug. A commonly used dendrimer is polyamidoamine (PAMAM). Applications of polymers in controlled drug delivery, gene therapy, antibiotic fibers and fabrics, tissue engineering, kidney dialysis, and artificial organs are discussed in the following sections.

12.2.1 Controlled Drug Delivery

Controlled drug delivery, or controlled release, provides two important potential applications for the use of polymers in the effective management of medical drugs in the body. The first of these is *controlled release* whereby a steady therapeutic concentration of the drug is maintained. Current examples of the use of controlled drug release include the delivery of contraceptives and the treatment of glaucoma. The other application is *site-directed* drug delivery whereby a polymer serves as a carrier to bring a drug to a specific site in the body, such as a site of infection, a diseased organ, or a collection of malignant cells.

Drugs can be delivered in a variety of traditional forms such as tablets, pills, capsules, liquids, and injections. While polymers are sometimes used as binders to modify consistency or to contain a specific dosage, they can also be used to deliver and target drugs in some applications. Polymers for such applications must be biocompatible and be able to biodegrade into products that are nontoxic and biocompatible themselves. Those that meet these requirements include a number of hydrolysable polyesters such as PLA and PGA and block copolymers of the two. Other choices include polyanhydrides, polyphosphoesters, poly(amino acids), and chitosan. PEG has been used to attach drugs. Styrene-isobutylene block copolymers

have been used as a cardiac stent coating for the controlled delivery of the drug Taxol (paclitaxel), which serves to prevent the narrowing of the arteries due to restenosis whereby the migration of vascular smooth-muscle cells can restrict blood flow.

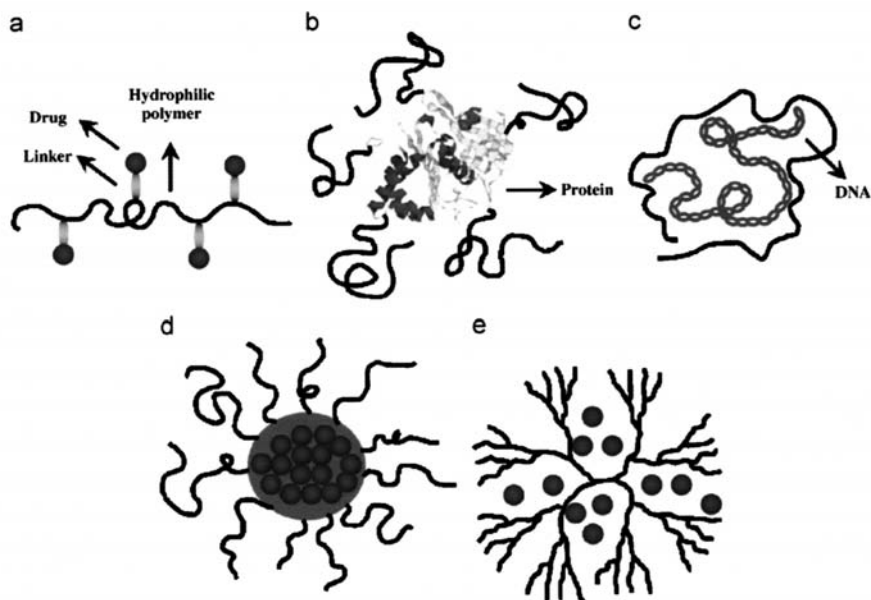
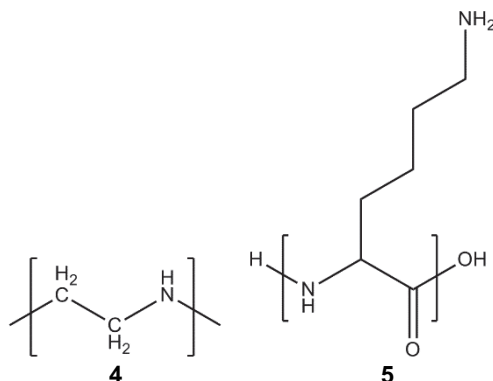


Figure 12-21 Illustration of polymeric nanomedicines: (a) polymer–drug conjugates; (b) polymer–protein conjugates; (c) polymer–DNA conjugates; (d) polymeric micelles; and (e) dendrimers. Reproduced from J. H. Park et al., *Polymeric Nanomedicine for Cancer Therapy*. Progress in Polymer Science, 2008. **33**: p. 113–137. Copyright 2008, with permission from Elsevier.

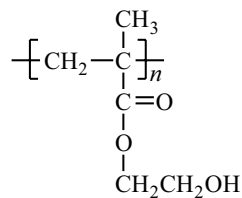


The rate of drug release can be controlled by diffusion, reaction, or solvent. In *diffusion control*, the driving force for diffusion is the concentration gradient across the delivery device, which can be a reservoir or matrix system. In the reservoir system, the drug is encapsulated by a polymeric membrane, which can be either microporous or nonporous. Delivery is constant in time if the drug core is maintained at a saturated level. In the case of a matrix system, the drug is dissolved or dispersed in a polymer. In contrast to the reservoir system, the release rate in a matrix device will decrease with time as the distance the drug has to travel from within the matrix increases due to depletion of drug concentration at the surface of the device. Polymers that have been used for diffusion-controlled devices include polydimethylsiloxane and poly(ethylene-*co*-vinyl acetate).

Reaction-controlled systems utilize biodegradable polymers as a means of delivery. The drug can be physically dispersed in the polymer, which gradually degrades in the body as a result of hydrolysis or enzymatic attack. Alternatively, the drug can be chemically linked to a polymer chain by a suitable spacer group that provides a biodegradable link. For reaction-controlled delivery, poly(lactide-*co*-glycolide) is particularly attractive because its breakdown products, lactic and glycolic acids, are biologically safe.

In *solvent-controlled* delivery, drug release is regulated by the permeation of water through the polymer. This may be achieved by the use of a simple osmotic pump, as illustrated in Figure 12-22. In this example, the drug core is enclosed by a semipermeable membrane that allows water to penetrate into the device due to osmotic pressure. The drug solution is dispersed through the orifice of the device at a rate equal to the rate of water uptake.

Another type of a solvent-activated system for controlled release uses polymeric *hydrogels*, which are water-swollen crosslinked polymer networks. The drug is incorporated in hydrogel polymer in the dry (glassy) state. When introduced in an aqueous environment, the polymer swells. The resulting gel provides a medium favorable for drug diffusion. A commonly used hydrogel is prepared from poly(2-hydroxyethyl methacrylate) (HEMA, structure 6) crosslinked by copolymerization with a difunctional polymer. Since PHEMA is water soluble, the crosslinked network will swell to form a gel containing about 35% water in an aqueous environment. In addition to controlled-release applications, PHEMA is used in the manufacture of soft contact lenses.



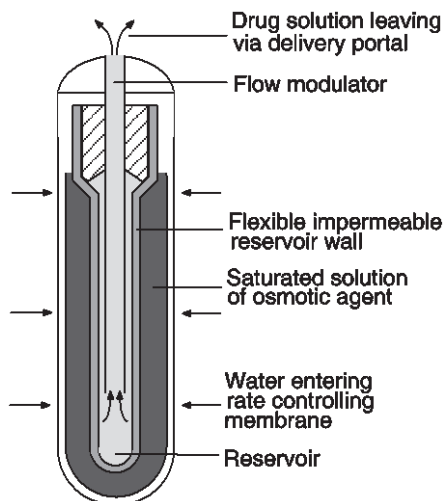


Figure 12-22 Illustration of an osmotic pump used in controlled drug delivery. Reprinted with permission from ASTM Standardization News, October 1986. Copyright ASTM International, 100 Barr Harbor Drive, West Conshohocken, PA 19428.

Although the technology for *site-directed drug delivery* is still in its infancy, some examples illustrate its potential. One application uses a block copolymer of poly(ethylene glycol) (PEG) and poly(aspartic acid) as the drug carrier. PEG provides the carrier solubility, while the poly(amino acid) is used to attach an anti-cancer drug (e.g., adriamycin).

12.2.2 Gene Therapy

Gene therapy employs the transfer of genetic material, primarily plasmid DNA, to modify defective genes or to replace missing ones as an approach to treating disease. Carriers for this genetic material may be a recombinant virus or a synthetic vector such as a lipid, a polypeptide such as polylysine (shown in structure 5), or polymers that can complex with DNA (a polyplex). Viruses used as vectors can be made non-replicant (and, therefore, non-pathogenic) by replacing a part of the genome with a therapeutic gene. While viral vectors are extremely efficient due to the inherent engineering of a virus, there is a significant risk that the recombinant virus may revert to a wild-type virulent form. Fatalities have been reported in some clinical trials. For this reason, there is significant interest in developing safe synthetic vectors such as polymers. While polymeric vectors pose fewer risks, they are significantly less efficient than virial vectors. Early issues with this approach include low

12.2.3 Antimicrobial Polymers

Antimicrobial polymers, sometimes called biocidal polymers, constitute a class of functionalized polymers that are able to inhibit the growth of bacteria and other microorganisms. Applications include biocidal fabrics and films, water sanitation, the prevention of infection in medical and dental practice, and the prevention of bacterial contamination in the food industry. An extensive review of the area has been given by Kenaway et al. [14]. To be effective, a polymeric biocide must be able to adsorb on the negatively charged cell membrane of a bacterium, disrupt the cell membrane, and cause lysis and cell death. In this way, they mimic the action of certain proteins such as gramicidin and magainin. Polymers that provide biocidal function include chitosan, polymeric quaternary ammonium materials, halogenated polystyrene–divinylbenzene sulfonamides, and polyurethanes having surface-active alkylammonium chloride end groups. Recently, a variety of nanocomposites containing silver nanoparticles, bioactive agents intercalated in montmorillonite (MMT, Section 7.5), and functionalized polyhedral oligomeric silsesquioxane (POSS) also have shown promise for their antimicrobial efficacy.

12.2.4 Tissue Engineering

The ability to repair or regenerate tissue has great importance for growing skin for the repair of burned areas, for the repair of damaged tendons, and for the growth of stem cells, as examples. For this purpose, it is necessary to support growing cells on a suitable *scaffold* structure. The scaffold serves as an immobilizing and protective site for transplanted cells and to direct cell growth through the transport of growth factors and other hormones and nutrients. The naturally occurring protein collagen is an excellent biomaterial for scaffold construction [15] but issues of contamination and infection limit its use as a scaffold material. An alternative approach is the use of biocompatible polymers for the construction of scaffolds to repair and regenerate tissue defects [16]. There are a number of requirements for polymers for such applications. They must be biodegradable, non-antigenic, non-carcinogenic, nontoxic, non-teratogenic, and biocompatible [17]. Polymers and copolymers that have been evaluated for scaffolds include trimethylene polycarbonates, polyphosphazenes, polyurethanes, polyfumarate, polyorthoester, poly(glycerol sebacate), polypyrrole, polyacrylates, poly(ether ester amide), poly(amido amine), and poly[(D,L-lactic acid)-*co*-(glycolic acid)] (PLGA).

12.2.5 Kidney Dialysis and Artificial Organs

Kidney Dialysis. One of the important medical applications of polymeric membranes is kidney dialysis, used to remove low-to-moderate-molecular-weight compounds from blood. These include sodium chloride, potassium chloride, urea, creatinine, and uric acid. At the same time, larger molecules necessary for life, such as cellular particles and plasma proteins, must be retained. The driving force for dialysis is a concentration gradient. Polymers suitable for kidney dialysis include cellophane (regenerated cellulose) that can be prepared in the form of small-diameter (ca. 200- μm) hollow fibers approximately 17 cm in length. As many as 10,000 of these fibers are used in a typical dialysis module. Practical problems that are encountered in operation include concentration polarization and clogged pores due to the adsorption of plasma proteins.

Artificial Organs. Some polymers can be used to manufacture artificial organs such as artificial kidneys, pancreases, and lungs. Artificial tendons and muscles have also been developed. A concern is always thrombus (clot) formation when foreign substances are in contact with blood. Heparin, a sulfonated glycosaminoglycan having anticoagulation properties, can be grafted onto the polymer surface to impart thrombo-resistance.

12.3 Applications in Electronics and Energy

Polymers can be electrically conductive or, doped with conductive fillers, can also be made photoconductive. These properties provide important applications such as polymeric electrodes in batteries, photovoltaics for solar cells, electronic shielding, encapsulation, and dielectrics as discussed in this section.

12.3.1 Electrically Conductive Polymers

In general, polymers have very poor electrical conductivity. In fact, some polymers such as polytetrafluoroethylene are good electrical insulators. In the 1800s, it was observed that the conductivity of natural rubber—normally an excellent insulator—could be significantly increased by adding carbon black, which is naturally conductive. In the 1930s, natural rubber filled with acetylene black was used in antistatic devices in hospitals and other facilities to reduce the danger of sparks resulting from the buildup of static electricity.

Before 1973, only one polymer—polysulfurnitride (SN)_x—was known to have any appreciable conductivity ($\sim 10^3$ S cm⁻¹).^{*} As in the case of natural rubber, it was found that this conductivity could be increased significantly by doping with an electron acceptor such as bromine ($\sim 10^4$ S cm⁻¹).[†] Unfortunately, interest in this polymer was less than it would otherwise be because of the explosive nature of its precursor monomer, S₂N₂.

By the late 1970s, researchers in the United States and Japan had shown that the electrical conductivity of an organic polymer—polyacetylene—could also be increased by a factor of 10^{12} (to $\sim 10^3$ S cm⁻¹) when it was doped with an electron donor such as an alkali–metal ion or an electron acceptor such as arsenic pentafluoride (AsF₅) or iodine.[‡] The conductivity of doped polyacetylene is comparable to that of copper on an *equal weight basis*. A comparison of the electrical conductivities and specific gravities of several polymers, common metals, and carbon is made in Table 12-10.

Table 12-10 Conductivities of Polymers and Metals

Material	Conductivity ^a (S cm ⁻¹)	Specific Gravity
Silver	10^6	10.5
Copper	6×10^5	8.9
Aluminum	4×10^5	2.7
Polyacetylene (doped)	1.5×10^5	1
Platinum	10^5	21.4
Polythiophene (doped)	10^4	1
Mercury	10^4	13.5
Carbon fiber	500	1.7–2
Carbon-black-filled polyethylene	10	1
Polymer electrolyte ^b	10^{-4}	1
Polytetrafluoroethylene (Teflon)	10^{-18}	2.1–2.3
Polyethylene	10^{-22}	0.9–0.97

^a Units of siemens (S) per cm.

^b Ionic conductivity.

^{*} The basic unit of conductivity (the inverse of resistivity) is siemens (S) per cm. A siemens is a reciprocal ohm (i.e., $1 \text{ S} = \Omega^{-1}$). As an illustration, the conductivity of polytetrafluoroethylene, an excellent insulator, is approximately 10^{-18} S cm⁻¹.

[†] Polysulfurnitride has been observed to become superconductive (~ 108 S cm⁻¹) at temperatures approaching absolute zero. (~ 0.3 K).

[‡] In 2000, Alan J. Heeger, Alan C. MacDiarmid, and Hideki Shirakawa shared the Nobel Prize in chemistry for their discovery and development of conductive polymers.

More recently, conductivity has been demonstrated for doped versions of poly(*p*-phenylene) (PPP), polypyrrole (PPy), polythiophene (PT), and polyaniline (PANI). The synthesis and properties of polyacetylene and these other conductive polymers were reviewed in Section 10.2.7. Although the electrical conductivities of many of these other polymers are lower than those polyacetylene, they have the advantage of being more stable against the effects of oxygen and moisture. As shown by the chemical structure of the repeating units of these polymers in Table 12-11, a common feature that makes these polymers capable of transporting electrical charge is a conjugated π -electron consisting of alternating single and double bonds along the polymer chain backbone or ring structure. It is believed that doping results in an electron imbalance, and the extended π -conjugated structure of the conductive polymer allows the new electron population to move along the backbone when an electric potential is applied.


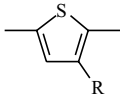
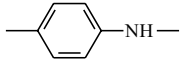
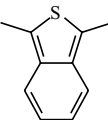
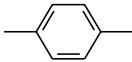
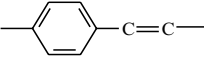
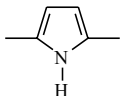
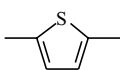
In general, conductivity increases with decreasing *band gap*, which is the amount of energy needed to promote an electron from the highest occupied molecular orbital (HOMO), the valence band, to the lowest unoccupied molecular orbital (LUMO), empty band, immediately above it. The empty band is the conduction band. Metals have zero band gaps, while insulators like many polymers have large band gaps (1.5 to 4 eV), which impede electron flow. By careful design of the chemical structure of the polymer backbone, it may be possible to obtain band gaps as low as 0.5 to 1 eV. Currently, the lowest band gap observed for a polymer is ~ 1 eV reported for polyisothianaphthalene (see Table 12-11).

12.3.2 Polymeric Batteries

Potential applications of conductive polymers are significant since they are generally lighter, more flexible, and easier to fabricate than many of the materials they seek to replace. An important example is the use of polymers as both cathodes and solid electrolytes in batteries for automotive and other applications as alternatives to lead-acid batteries. A diagram of a typical lithium-polymer battery is shown in Figure 12-23. Potential advantages of polymeric batteries include high reliability, light weight, non-leakage of electrolyte solution, ultrathin-film form, flexibility, and high energy density (up to 100 W dm^{-3}). Polyacetylene, poly(*p*-phenylene), polypyrrole, and polyaniline can be used as the cathode material, with a lithium-aluminum alloy as the anode. Lithium-poly(*p*-phenylene) batteries can deliver current densities as high as 50 mA cm^{-2} , achieve efficiencies up to 91% during charging and discharging, and have theoretical energy densities of 320 W-h kg^{-1} . Examples of polymers used in the formulation of solid electrolytes include poly(alkyl sulfide)s, polyphosphazenes (see Section 10.2.5) having oligo(oxyethylene) side groups, and especially poly(ethylene oxide). Salts that are added to form the electrolyte include a number of lithium salts having low crystal lattice energies, such as lithium tetrafluoroborate

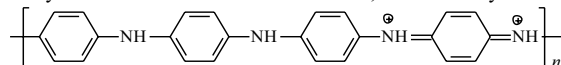
(LiBF₄), lithium hexafluoroarsenate (LiAsF₆), lithium perchlorate (LiClO₄), and lithium trifluoromethanesulfonate, sometimes called lithium triflate (LiCF₃SO₃).

Table 12-11 Chemical Structures and Conductivities of Some Electrically Conductive Polymers

Conductive Polymer	Repeating Unit	Dopants	Conductivity ^a (S cm ⁻¹)
<i>trans</i> -Polyacetylene		I ₂ , Br ₂ , Li, Na, AsF ₅	10 ⁴
Poly(3-alkyl-thiophene)		BF ₄ ⁻ , ClO ₄ ⁻ , FeCl ₄ ⁻	10 ³ – 10 ⁴
Polyaniline ^b		HCl	200
Polyisothianaphthalene		BF ₄ ⁻ , ClO ₄ ⁻	50
Poly(<i>p</i> -phenylene)		AsF ₅ , Li, K	10 ³
Poly(<i>p</i> -phenylene vinylene)		AsF ₅	10 ⁴
Polypyrrole		BF ₄ ⁻ , ClO ₄ ⁻ , tosylate ^c	500–7500
Polythiophene		BF ₄ ⁻ , ClO ₄ ⁻ , tosylate, ^c FeCl ₄ ⁻	10 ³

^a Approximate maximum conductivity of doped polymer.

^b Polyaniline exists in four oxidation states, of which only the emeraldine salt



is a good conductor requiring only protonic doping of the imine nitrogen as shown.

^c *p*-Methylphenylsulfonate.

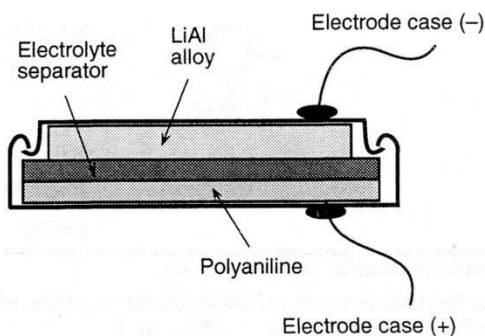


Figure 12-23 Illustration of a rechargeable battery using a polymeric cathode (polyaniline). The anode is a lithium–aluminum alloy, while the electrolyte can be a solution (e.g., propylene carbonate) of an appropriate salt or a solid polymer electrolyte (e.g., Li–PEO). Courtesy of M. G. Kanatzidis.

Other possible uses of conductive polymers include sensors, conductive paints, semiconductor circuits, low-current wires, electromechanical actuators, and photovoltaic (PV) material for use in solar cells as described in the following section. Applications of conductive polymers in photonic applications, including use in light-emitting diodes, as nonlinear optical material, variable-transmission (“smart”) windows, and electrochromic displays, are covered in Section 12.4.

12.3.3 Organic Photovoltaic Polymers

The potential of using light to produce electricity has been known since 1839 when Edmond Becquerel discovered that a current could be produced when a silver chloride electrode immersed in an electrolytic solution was connected to a counter metal electrode that was illuminated with white light. The current era in photovoltaic (PV) technology began in 1954 when scientists from Bell Laboratories [18] showed that *solar cells* based on *p-n* junctions in single crystals of silicon could be used to produce electricity. Efficiencies* of these early inorganic photovoltaic (IPV) solar cells were in the range from 5% to 6%. Traditional applications included satellite power and roof-top power sources. Today, commercial Si-based solar cells can have overall power conversion efficiencies up to about 20%.

* Solar cell efficiency (%) = $\frac{\text{Power out (W)} \times 100\%}{\text{Area (m}^2\text{)} \times 1000 \text{ W/m}^2}$.

Another class of solar-cell materials, organic photovoltaics (OPV), includes photovoltaic polymers (PPVs). Polymeric solar cells (PSCs) provide several advantages over inorganic photovoltaic devices such as ease of fabrication using solution-based processing, low weight, and the flexibility to conform to the shape of a variety of supporting structures. Applications are diverse and include roof shingles, solar curtains, and even solar backpack chargers; however, current efficiencies of PSCs, with highest reported [19] efficiencies of around 10%, are currently much lower than those of Si-based solar cells (>20%).

The mechanisms of photoconversion also differ between IPV and OPV solar cells [20]. In the case of IPV solar cells, light absorption leads to the creation of *free* electron–“hole” pairs. In contrast, *excitons* [21] are formed in OPV solar cells. Excitons, electrically neutral quasiparticles, are mobile excited states consisting of a *bound* electron and a hole. The exciton radius is considered to be ~1 nm with binding energy ~0.4 to 1.0 eV. Excitons can transmit energy without transporting net charge. They can be dissociated at interfaces of materials with different electron affinities. Blending conjugated polymers with high-electron affinity molecules in bulk-heterojunction (BHJ) solar cells, illustrated in Figure 12-24, promotes rapid exciton dissociation.

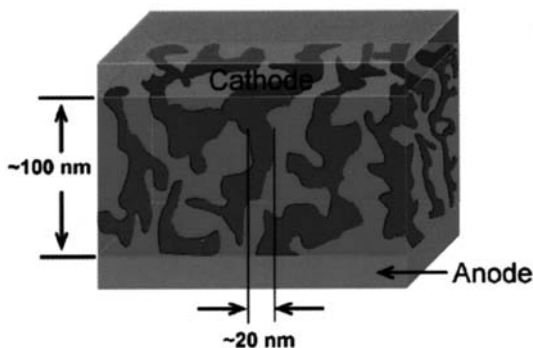
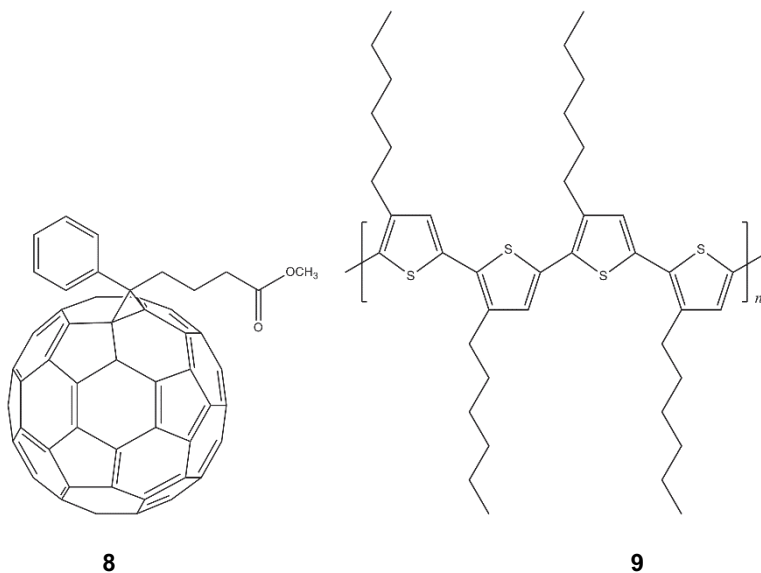


Figure 12-24 Illustration of a typical BHJ morphology showing acceptor–donor interfacial regions. Reproduced with permission from X. Yang and J. Loos, *Toward High Performance Polymer Solar Cells: The Importance of Morphology Control*. *Macromolecules*, 2007. **40**(5): p. 1353–1362, Copyright 2007 American Chemical Society.

Electron acceptors are typically a fullerene* or a chemically modified fullerene such as 1-(3-methoxy-carbonyl)propyl-1-phenyl-[6,6]-methanofullerene (PCBM). Donor polymers include those that have π -conjugation such as poly(3-hexylthio-

* Fullerenes are also called a buckminsterfullerene, buckyball, or simply C_{60} .

phene) (P3HT) and poly(1,4-phenylenevinylene) (PPV), poly[oxa-1,4-phenylene-(1-cyano-1,2-vinylene)-(2-methoxy-5-(3',7'-dimethyloctyloxy)-1,4-phenylene-1,2-(2-cyano-vinylene)-1,4-phenylene] (PCNEPV), and poly[2-methoxy-5-(3',7'-dimethyloctyl-oxy)-1,4-phenylenevinylene] (MDMO-PPV). At the molecular level, conjugated polymers such as P3HT become electron donors as electrons are promoted to the antibonding π^* band upon photoexcitation. Structures of PCBM, P3HT, PCNEPV, and MDMO-PPV, are shown in structures 8–11, respectively. A more detailed look at a representative BHJ solar cell using an MDMO-PPV electron donor and a PCBM electron-acceptor is illustrated in Figure 12-25. Important considerations for the design of high-efficiency BHJ solar cells include (a) a broad absorption range and strong absorption coefficient in the solar spectrum; (b) a bicontinuous network with domain width less than twice the exciton diffusion length; and (c) high donor-acceptor interfacial area to facilitate exciton dissociation and transport of separated charges to their respective electrodes [22].



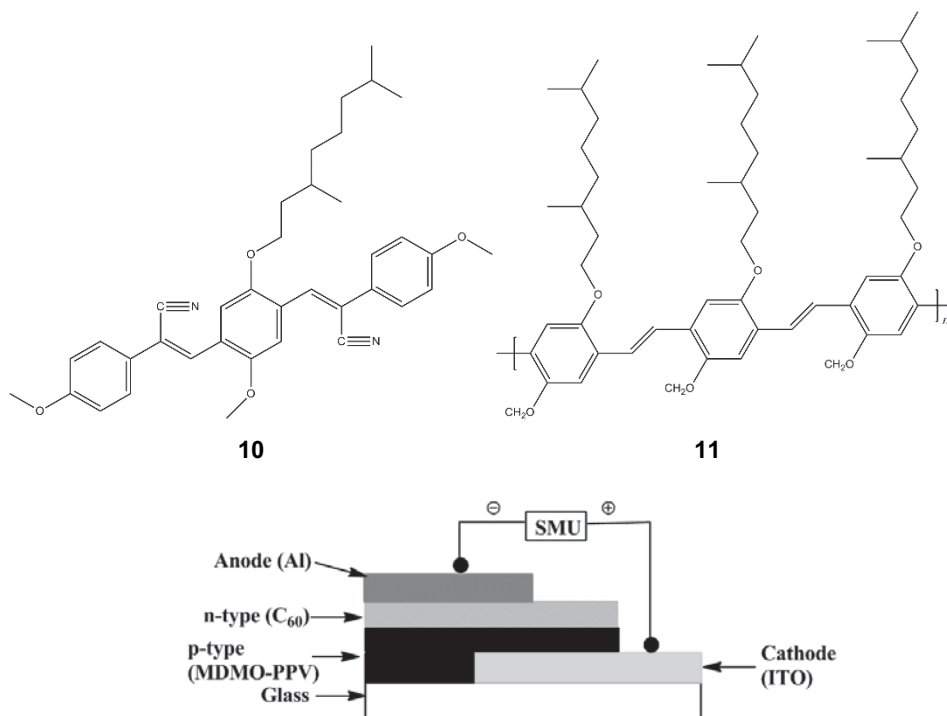


Figure 12-25 Detailed illustration of an MDMO-PPV/fullerene BHV. In this example, the cathode is a coating of indium tin oxide (ITO) on glass, the anode is aluminum, and SMU is an abbreviation for source measurement unit. Adapted from C. J. Brabec, N. S. Sariciftci, and J. C. Hummelen, *Plastic Solar Cells*. Advanced Functional Materials, 2001. **11(1)**: p. 15–26.

12.3.4 Electronic Shielding

Undesirable signals in the radio frequency (RF) range emitted by many electrical devices such as computers can interfere with normal RF reception. This behavior is called electromagnetic interference (EMI). Regulations from the Federal Communications Commission (FCC) have placed restrictions on RF transmissions by computers and other electrical devices. Unfilled polymers, typically insulating material, provide very little EMI shielding capability. There are two basic approaches that can be used to achieve EMI shielding for plastic enclosures. One includes coating the plastic with a conductive metal; the other involves blending the plastic with conductive fiber or particles. Generally, carbon- and metal-filled composites such as PVC filled with aluminum flakes provide suitable housings for low-emission electronic devices.

12.3.5 Dielectrics

A current challenge in materials science is the development of low-dielectric-constant or low- k materials to replace SiO_2 . Silicon dioxide ($k = 4.2$) is an inadequate insulator to prevent “cross talk” between the closely spaced copper wire of the latest generation of semiconductors. For the 0.10- μm circuit lines required for the next-generation computer chips, k must be 2.5 or lower. Some polymers, particularly porous polymers, may be able to meet these needs with k values as low as 1.9. A variety of polymers have been proposed for low- k materials. These include polyimides, heteroaromatic polymers, poly(aryl ethers), and fluoropolymers. Polyimides, such as Kapton (see Section 10.2.1), had been used from the early 1970s to the late 1980s as inter-metal dielectrics. The dielectric constants of polytetrafluoroethylene and some of its derivatives (Section 10.1.9) are among the lowest of all polymers (between 1.9 and 2.1). In general, fluorine substitution decreases the dielectric constant of a polymer including polyimides. One of the biggest challenges may be thermal stability as the low- k polymers must be able to withstand temperatures of 400° to 450°C for several hours during annealing steps required to provide void-free copper deposits. Practically, this means that the thermal decomposition temperature must be far in excess of 500°C. Fabrication techniques include chemical vapor deposition (CVD), plasma-enhanced CVD, and spin coating.

12.3.6 Electronic Encapsulation

Polymers are used to provide integrated-circuit devices with a protective seal against moisture, radiation, and ion contamination. Thermosets, thermoplastics, and elastomers are all used as encapsulants. Included among thermosets are thermosetting polyimides, epoxies, unsaturated polyesters, and alkyd resins, as reviewed in Section 9.3. Candidates among thermoplastic encapsulants are poly(vinyl chloride), polystyrene, polyethylene, fluoropolymers, and acrylics. Elastomers can include silicone rubber and polyurethanes. For the most critical applications, epoxies and polyimides are favored.

12.4 Photonic Polymers

The next technological revolution may be the widespread use of optical rather than electronic devices for both storage and processing of data. Optical technology has the advantages of both speed and compactness of storage space. Optical storage of computer data is already common (i.e., CD-ROM and WORM drives) and ways to use optical devices for processing data are being explored. Among materials that are

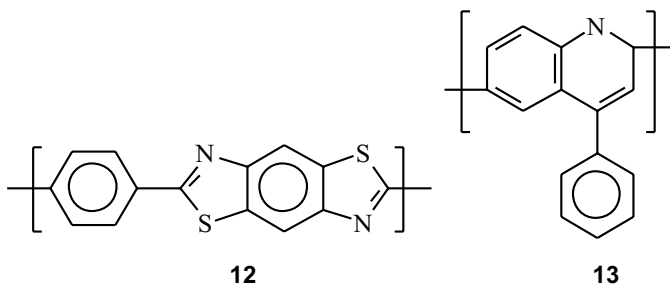
suitable for optical technology are polymers that exhibit *nonlinear optical* (NLO) properties. This means that their optical properties vary with the intensity of the light compared to ordinary glass, which is linear in its optical properties. Photore sponsive sunglasses that change tint with the intensity of sunlight are examples of NLO materials.

12.4.1 Nonlinear Optical Polymers

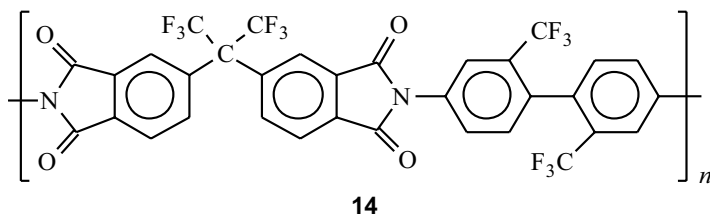
Unlike other materials, the refractive index of a nonlinear optical (NLO) material is not constant but a function of the intensity of the incident light striking it. For NLO effects to be observed, the light must be coherent and intense such as is produced by a laser. NLO behavior can be first-order or second-order depending upon whether nonlinear effects are dependent upon the first-order hyperpolarizability tensor term, $\chi^{(2)}$, or the second-order hyperpolarizability term, $\chi^{(3)}$, in the equation for the polarizability (P) of the bulk material

$$P = \chi^{(1)}E + \chi^{(2)}E \cdot E + \chi^{(3)}E \cdot E \cdot E + \dots \quad (12.26)$$

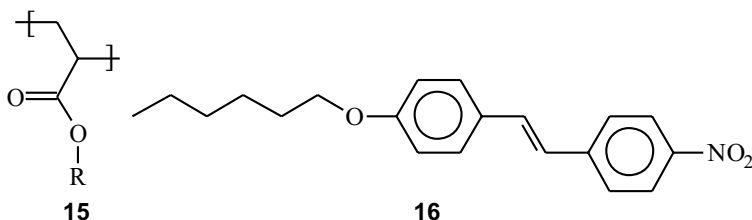
where E is the external electric field. Third-order nonlinear materials are important for optical signal processing. Materials that have significant third-order NLO behavior have a small optical band gap, high concentration of easily polarizable electrons, and a large effective conjugation length. Polymers that exhibit third-order nonlinearity include many of the conductive polymers listed in Table 12-11 such as polyacetylene, poly(*p*-phenylene vinylene) (PPV), polythiophene (PT), and polyaniline (PANI). Others include poly(*p*-phenylene benzo-bisthiazole) (PBZT, structure 12) and polyquinoline (PPQ, structure 13). Other possibilities include modified rigid-rod polyimides with NLO-active side groups.



In general, molecules with π -electron structures can exhibit NLO effects when these electrons are optically excited. In the case of polymers, these π -electron structures can be part of the main-chain backbone, as for example in the case of the 6F-polyimide (structure 14, see Section 10.2.1).



The NLO functionality can also be incorporated as a side chain, as in the case of an acrylate polymer (structure 15) having a substituent group (R) that contains a 4-methoxy-4'-nitrostilbene moiety connected by a six-carbon spacer (structure 16)



12.4.2 Light-Emitting Diodes

A light-emitting diode (LED) is a crystalline semiconductor chip that glows. Only red and green were available colors for the first LEDs introduced in the 1960s. An organic light-emitting diode, or OLED, is made of sheets of polymer semiconductor material resembling plastic, as shown in Figure 12-26. Polymer LEDs were discovered by Richard Friend and coworkers at Cambridge University in 1989 and now provide a full palette of light. The first polymer exhibiting light emission, green-yellow in color, was PPV (see Table 12-11), which had low efficiency and short lifetime. Substitution of the phenylene ring of PPV with alkoxy groups (structure 17) such as illustrated below results in emission in the orange-red range while poly(*p*-phenylene) emits blue light. LEDs can provide light at very high efficiency (up to 75% of electric consumption can be converted to light). Polymers like the substituted polythiophene, poly[3-(4-octylphenyl)-2,2'-bithiophene] (structure 18), will luminesce with polarized light when an electric current is passed through them. A variety of polymer configurations including block copolymers, side-chain polymers, and even dendrimers (see Section 10.2.9) provide opportunities for LEDs.

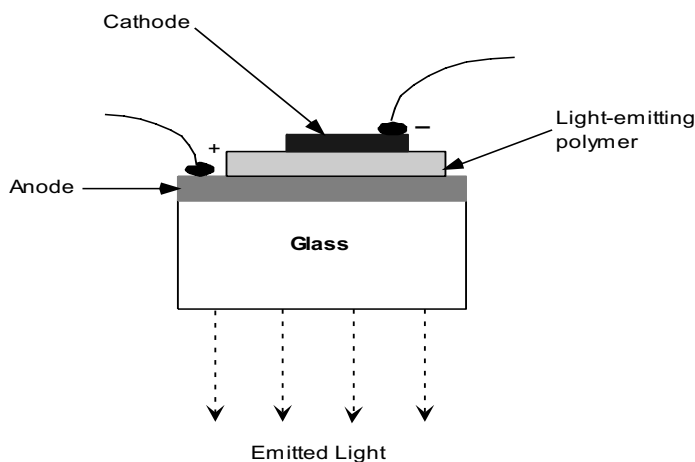
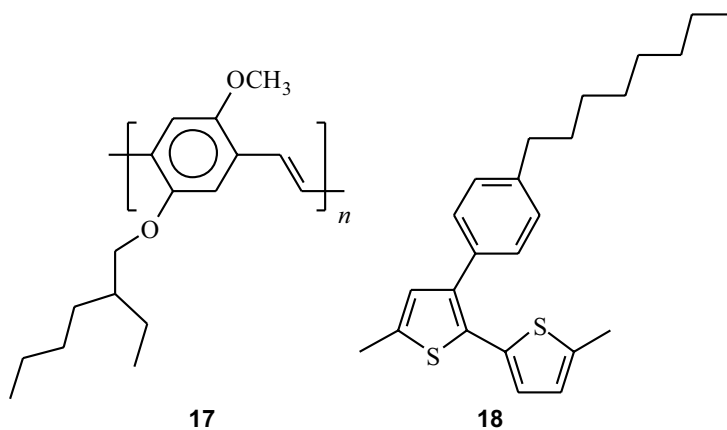


Figure 12-26 Basic design of a polymer LED.



12.5 Sensor Applications

Polymers have been used to replace other materials such as inorganic semiconductors, metals, catalysts, and solid electrolytes in a variety of sensing devices [23–25]. These include many diverse applications such as pH measurements, gas sensing, explosives detection, humidity measurements, and biosensing. In many of these cases, the physical or electrical response of semiconducting polymers to a specific molecule, the *analyte*, provides the basis for sensing.

In the design of chemical sensors, a receptor site that provides some form of molecular recognition for a given analyte is connected to a signaling unit. The binding event results in a property change that can be measured. The chemosensor can be modified by changing its binding constant and selectivity and through modification of the transduction efficiency between the binding event and the resulting signal. The signal can be electrical resulting from changes in capacitance or resistance or optical through changes in fluorescence or absorption. Two related approaches to forming a generic chemical sensor from a thiophene polymer structure are illustrated in Figure 12-27. A specific crown ether receptor that can be used for sodium cation detection is illustrated in Figure 12-28. Conformation twisting of the polythiophene can result in a drop in conductivity of 10^5 or more.

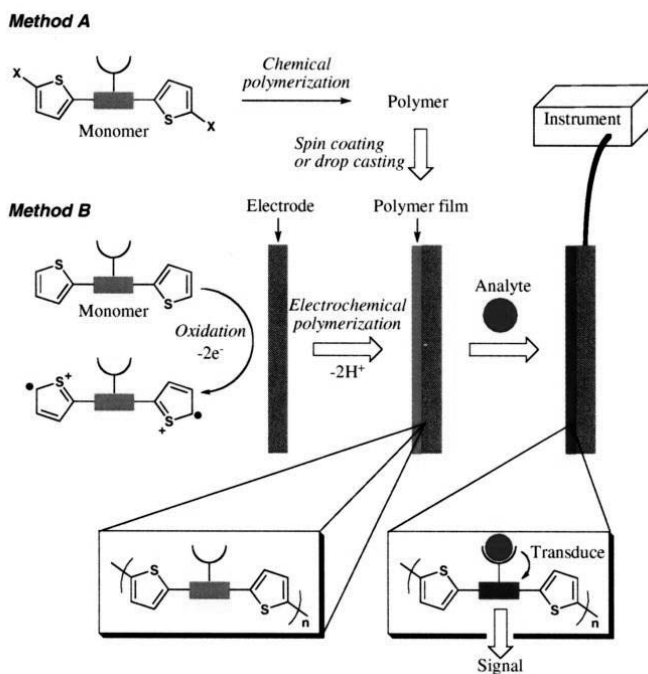


Figure 12-27 Illustration of two related approaches to developing a chemical sensor using a semiconducting polymer containing receptor sites. In Method A, a thiophene derivative is spin-coated or drop-coated on a suitable electrode. In Method B, the monomer is polymerized on the electrode using anodic electrochemical polymerization. Reproduced from K. Sugiyasu and T. M. Swager, *Conducting Polymer-Based Chemical Sensors: Transduction Mechanisms*. Bulletin of the Chemical Society of Japan, 2007. **80**(11): p. 2074–2083.

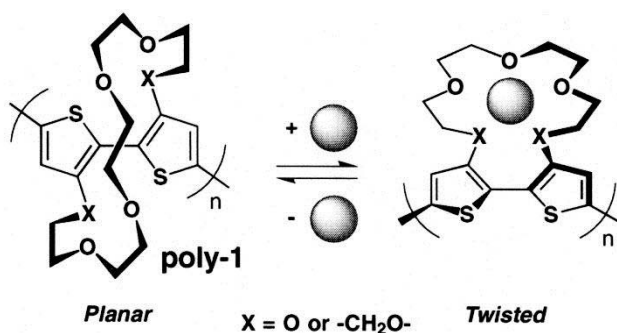
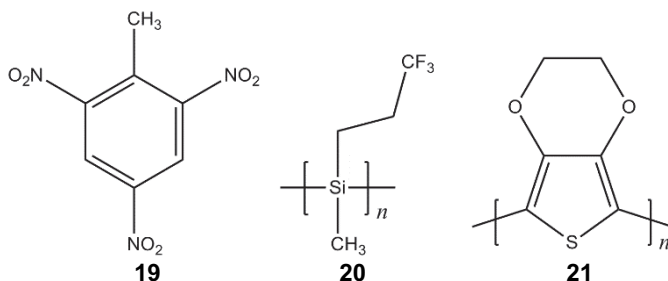


Figure 12-28 Conformation changes induced upon the insertion of an alkali metal cation inside a crown-ether-modified polythiophene. Reproduced from K. Sugiyasu and T. M. Swager, *Conducting Polymer-Based Chemical Sensors: Transduction Mechanisms*. Bulletin of the Chemical Society of Japan, 2007. **80**(11): p. 2074-2083.

Explosives Detection. An important application of chemical sensors is the detection of nitroaromatic explosives [26], especially trinitrotoluene (TNT, structure 19), which is an ingredient of many explosives and also poses environmental health risks. Nitroaromatics are electron accepting while conjugated polymers are electron donors. On this basis, nitroaromatic analytes can act as electron acceptors for photoexcited electrons of conjugated polymers including substituted polyacetylenes, poly(*p*-phenylenevinylenes), poly(*p*-phenyleneethynylenes), and polymeric porphyrins. In the presence of nitroaromatics, polymers such as poly(3,3,3-trifluoropropylmethylsilane) (PTFPMS, structure 20) exhibit photoluminescence quenching that provides another means for detection.

Gas Sensors. Conjugated polymers such as polyaniline, polypyrrole, and poly(3,4-ethylenedioxythiophene) (PEDOT, structure 121) also can be used in sensing devices for gases such as CO, H₂, NH₃ (an electron donor), and NO₂ (an electron acceptor) as well as airborne organic vapors such as halocarbons, alcohols, and ethers [27].



SUGGESTED READING

MEMBRANES

- Baker, R. W., J. G. Wijmans, and J. H. Kaschemekat, *The Design of Membrane Vapor–Gas Separation Systems*. *Journal of Membrane Science*, 1998. **151**: p. 55.
- Belfort, G., *Synthetic Membrane Processes*. 1984, Orlando: Academic Press.
- Brüschke, H., *Industrial Application of Membrane Separation Processes*. *Pure and Applied Chemistry*, 1995. **67**: p. 993.
- Comyn, J., *Polymer Permeability*. 1985, London: Elsevier Applied Science Publishers.
- Crank, J., *The Mathematics of Diffusion*. 1975, New York: Oxford University Press.
- Crank, J., and G. S. Park, *Diffusion in Polymers*. 1968, London: Academic Press.
- Feldman, D., *Polymer Barrier Films*. *Journal of Polymers and the Environment*, 2002. **9**: p. 49.
- Feng, X., and R. Y. M. Huang, *Liquid Separation by Membrane Pervaporation: A Review*. *Industrial and Engineering Chemistry and Research*, 1997. **36**: p. 1048.
- Gilron, J., and A. Soffer, *Knudsen Diffusion in Microporous Carbon Membranes with Molecular Sieving Character*. *Journal of Membrane Science*, 2002. **209**: p. 339.
- Henis, J. M. S., and M. K. Tripodi, *The Developing Technology of Gas Separating Membranes*. *Science*, 1983. **220**: p. 11.
- Ho, W. S., and K. K. Sirkar, eds., *Membrane Handbook*. 1992, New York: Van Nostrand Reinhold.
- Huang, R. Y. M., *Pervaporation Membrane Separation Processes*. 1991, Amsterdam: Elsevier.
- Kesting, R. E., *Synthetic Polymeric Membranes*. 1985, New York: John Wiley & Sons.
- Kesting, R. E., and A. K. Fritzsche, *Polymeric Gas Separation Membranes*. 1993, New York: John Wiley & Sons.
- Koros, W. J., ed., *Barrier Polymers and Structures*. ACS Symposium Series 423. 1990, Washington, DC: American Chemical Society.
- Koros, W. J., and G. K. Fleming, *Membrane-Based Gas Separation*. *Journal of Membrane Science*, 1993. **83**: p. 1.
- Koros, W. J., *Membranes: Learning a Lesson from Nature*. *Chemical Engineering Progress*. October 1995, p. 68.
- Matsuura, T., *Synthetic Membranes and Membrane Separation Processes*. 1994, Boca Raton: CRC Press.
- Mulder, M., *Basic Principles of Membrane Technology*. 1991, Dordrecht: Kluwer Academic Publishers.
- Park, J. H., S. Lee, J.-H. Kim, K. Park, K. Kim, and I. C. Kwon, *Polymeric Nanomedicine for Cancer Therapy*. *Progress in Polymer Science*, 2008. **33**: p. 113.
- Paul, D. R., *Gas Sorption and Transport in Glassy Polymers*. *Berichte der Bunsengesellschaft für Physikalische Chemie*, 1979. **83**: p. 294.

- Phair, J. W., and S. P. S. Badwal, *Materials for Separation Membranes in Hydrogen and Oxygen Production and Future Power Generation*. Science and Technology of Advanced Materials Science, 2006. **M7**: p. 792–805.
- Strathmann, H., *Membrane Separation Processes: Current Relevance and Future Opportunities*. AIChE Journal, 2001. **47**: p. 1077.
- Wynn, N., *Pervaporation Comes of Age*. Chemical Engineering Progress. October 2001, p. 66–72.

BIOMEDICAL APPLICATIONS

- Bajpai, A. K., S. K. Shukla, S. Nhanu, and S. Kankane, *Responsive Polymers in Controlled Drug Delivery*. Progress in Polymer Science, 2008. **33**: p. 1088.
- Dash, M., F. Chiellini, R. M. Ottenbrite, and E. Chiellini, *Chitosan—a Versatile Semi-Synthetic Polymer in Biomedical Applications*. Progress in Polymer Science, 2011. **36**: p. 981.
- De Bartolo, L., S. Morelli, A. Bader, and E. Drioli, *Evaluation of Cell Behaviour Related to Physico-Chemical Properties of Polymeric Membranes to Be Used in Bioartificial Organs*. Biomaterials, 2002. **23**: p. 2485.
- Graham, N. B, and D. A. Wood, *Hydrogels and the Biodegradable Polymers for the Controlled Delivery of Drugs*. Polymer News, 1982. **8**: p. 230.
- Jagur-Grodzinski, J., *Biomedical Application of Functional Polymers*. Reactive and Functional Polymers, 1999. **39**: p. 99.
- Jagur-Grodzinski, J., *Polymers for Targeted and/or Sustained Drug Delivery*. Polymers for Advanced Technologies, 2009. **20**: p. 595.
- Jeong, J. H., *Molecular Design of Functional Polymers for Gene Therapy*. Progress in Polymer Science, 2007. **32**: p. 1239.
- Kenawy, E.-R., S. D. Worley, and R. Broughton, *The Chemistry and Applications of Antimicrobial Polymers: A State-of-the Art Review*. Biomacromolecules, 2007. **8**(5): p. 1360.
- Khandare, J., and T. Minko, *Polymer–Drug Conjugates: Progress in Polymeric Prodrugs*. Progress in Polymer Science, 2006. **31**: p. 359.
- Kost, J., *Hydrogels for Controlled Delivery of Bioactive Agents*. Polymer News, 1995. **20**: p. 73.
- Langer, R., and N. A. Peppas, *Advances in Biomaterials, Drug Delivery, and Bionanotechnology*. AIChE Journal, 2003. **49**(12): p. 2990.
- Langer, R., and J. P. Vacanti, *Tissue Engineering*. Science, 1993. **260**: p. 920.
- Martina, M., and D. W. Hutmacher, *Biodegradable Polymers Applied in Tissue Engineering Research: A Review*. Polymer International, 2007. **56**: p. 145.
- Mulligan, R. C., *The Basic Science of Gene Therapy*. Science, 1993. **260**: p. 926.
- Ottenbrite, R. M., ed., *Polymeric Drugs and Drug Administration*. ACS Symposium Series 545. 1994, Washington, DC: American Chemical Society.
- Pack, D. W., A. S. Hoffman, S. Pun, and P. S. Stayton, *Design and Development of Polymers for Gene Delivery*. Nature Reviews: Drug Discovery, 2005. **4**: p. 581.
- Park, J. H., S. Lee, J.-H. Kim, K. Park, K. Kim, and I. C. Kwon, *Polymeric Nanomedicine for Cancer Therapy*. Progress in Polymer Science, 2008. **33**: p. 113.

- Schaffert, D., and E. Wagner, *Gene Therapy Progress and Prospects: Synthetic Polymer-Based Systems*. Gene Therapy, 2008. **15**: p. 1131.
- Stamatialis, D. F., B. J. Papenburg, M. Girones, S. Saiful, S. N. M. Bettahalli, S. Schmitmeier, and M. Wessling, *Medical Applications of Membranes: Drug Delivery, Artificial Organs, and Tissue Engineering*. Journal of Membrane Science, 2008. **308**: p. 1.
- Sugibayashi, K., and Y. Morimoto, *Polymers for Transdermal Drug Delivery Systems*. Journal of Controlled Release, 1994. **29**: p. 177.
- Suzuki, M., and O. Hirasa, *An Approach to Artificial Muscle Using Polymer Gels Formed by Micro-Phase Separation*. Advances in Polymer Science, 1993. **110**: p. 241.
- Wong, S. Y., J. M. Pelet, and D. Putman, *Polymer Systems for Gene Delivery—Past, Present, and Future*. Progress in Polymer Science, 2007. **32**: p. 799.

ELECTRONICS AND ENERGY

- Goetzberger, A., C. Hebling, and H.-W. Schock, *Photovoltaic Materials, History, Status, and Outlook*. Materials Science and Engineering, 2003. **40**: p. 1.
- Hadziioannou, G., and G. G. Malliaras, eds., *Semiconducting Polymers: Chemistry, Physics and Engineering*. 2007, Weinheim: Wiley-VCH.
- Heeger, A. J., *Charge Storage in Conducting Polymers: Solitons, Polarons, and Bipolarons*. Polymer Journal, 1985. **17**: p. 201.
- Heeger, A. J., *Semiconducting and Metallic Polymers: The Fourth Generation of Polymeric Materials*. Synthetic Metals, 2002. **125**: p. 23.
- Hoppe, H., and N. S. Sariciftci, *Organic Solar Cells: An Overview*. Journal of Materials Research, 2004 **19**(7): p. 1924.
- Huang, J.-C., *EMI Shielding Plastics: A Review*. Advanced Polymer Technology, 1995. **14**: p. 137.
- Kaner, R. B., and A. G. MacDiarmid, *Plastics That Conduct Electricity*. Scientific American, February 1988, p. 106.
- Ku, C. C., and R. Liepins, *Electrical Properties of Polymers*. 1987, Munich: Hanser Publications.
- MacDiarmid, A. G., *Synthetic Metals: A Novel Role for Organic Polymers*. Synthetic Metals, 2002. **125**: p. 11.
- Margolis, J. M., ed., *Conductive Polymers and Plastics*. 1989, New York: Chapman and Hall.
- Patel, J. S., *Liquid Crystal: Materials for Displays*. Annual Review of Materials Science. **23**: p. 269.

PHOTONICS

- Jacobson, S., P. Landi, T. Findakly, J. Stamatoff, and H. Yoon, *Nonlinear Optical Polymers in Advanced Photonics*. Journal of Applied Polymer Science, 1994. **53**: p. 649.
- Lee, K.-S., ed., *Polymers for Photonics Applications I*. Advances in Polymer Science 158. 2002, Berlin: Springer-Verlag.
- Reinhardt, B. A., *The Status of Third-Order Polymeric Nonlinear Optical Materials: Directions and Philosophy of Polymer Research for Nonlinear Optics in the U.S. Air Force Wright Laboratory*. Trends in Polymer Science, January 1993, p. 4.

PROBLEMS

12.1 An asymmetric hollow fiber of polysulfone has a surface pore area, A_3/A_2 , of 1.9×10^{-6} and an effective skin thickness of 1000 Å. If the fiber is coated with a 1- μm layer of silicone rubber, calculate the effective P/ℓ for the coated membrane for CO_2 and the permselectivity for CO_2/CH_4 .

12.2 What pore size is required for Knudsen flow of oxygen and nitrogen through a porous membrane? What would be the ratio of diffusion coefficient, $D(\text{O}_2)/D(\text{N}_2)$, for the permeation of air through this membrane? How does this ratio compare to that for the permeation of air through a polysulfone hollow-fiber membrane? How does this ratio of diffusion coefficients compare to the ideal permselectivity, $\alpha(\text{O}_2, \text{N}_2)$, reported for oxygen/nitrogen through the polysulfone membrane?

12.3 What are the limitations, if any, to the statement that $P = SD$ (eq. (12.7))?

12.4 What are the principal applications of pervaporation in the chemical industry? For these cases, how do the economics of pervaporation compare with more traditional separation methods in the United States and in Europe?

12.5 What are the principal applications for polymeric fuel-cell membranes? What are their advantages and limitations compared to other proton-conduction membranes?

12.6 For encapsulation of islet cells for medical implants in humans, what polymers would be most suitable? Discuss your choices.

REFERENCES

1. Salame, M., *Transport Properties of Nitrile Polymers*. Journal of Polymer Science, Polymer Symposium, 1973. **41**: p. 1–15.
2. Salame, M., *Prediction of Gas Barrier Properties of High Polymers*. Polymer Engineering and Science, 1986. **26**(22): p. 1543–1546.
3. Nagai, K., et al., *Poly[1-(trimethylsilyl)-1-propyne] and Related Polymers: Synthesis, Properties, and Functions*. Progress in Polymer Science, 2001. **26**: p. 721–798.
4. Robeson, L. M., *The Upper Bound Revisited*. Journal of Membrane Science, 2008. **320**: p. 390–400.
5. Heinzl, A., and V. M. Barragan, *A Review of the State-of-the-Art of the Methanol Crossover in Direct Methanol Fuel Cells*. Journal of Power Sources, 1999. **84**: p. 70–74.
6. Vieth, W. R., J. M. Howell, and J. H. Hsieh, *Dual Sorption Theory*. Journal of Membrane Science, 1976. **1**: p. 177–220.
7. Teplyakov, V., and P. Meares, *Correlation Aspects of the Selective Gas Permeabilities of Polymeric Materials and Membranes*. Gas Separation and Purification, 1990. **4**: p. 66–74.
8. Paul, D. R., and W. J. Koros, *Effect of Partially Immobilizing Sorption on Permeability and the Diffusion Time Lag*. Journal of Polymer Science: Polymer Physics Edition, 1976. **14**: p. 675–685.

9. Gierke, T. D., and W. Y. Hsu, *The Cluster-Network Model of Ion Clustering in Perfluorinated Membranes*, in *ACS Symposium Series*, A. Eisenberg and H. L. Yeager, eds. 1982, Washington DC: American Chemical Society, p. 283–307.
10. Loeb, S., and S. Sourirajan, *Sea Water Determination by Means of a Semiempirical Membrane*. University of California, Los Angeles, Report No. 60-60, 1960.
11. Henis, J. M. S., and M. K. Tripodi, *Composite Hollow Fiber Membranes for Gas Separation: The Resistance Model Approach*. *Journal of Membrane Science*, 1981. **8**(3): p. 233–246.
12. Park, J. H., et al., *Polymeric Nanomedicine for Cancer Therapy*. *Progress in Polymer Science*, 2008. **33**: p. 113–137.
13. Pack, D. W., et al., *Design and Development of Polymers for Gene Delivery*. *Nature Reviews: Drug Discovery*, 2005. **4**: p. 581–593.
14. Kenaway, E.-R., S. D. Worley, and R. Broughton, *The Chemistry and Applications of Antimicrobial Polymers: A State-of-the-Art Review*. *Biomacromolecules*, 2007. **8**(5): p. 1359–1384.
15. Martino, A. D., M. Sittinger, and M. V. Risbud, *Chitosan: A Versatile Biopolymer for Orthopaedic Tissue-Engineering*. *Biomaterials*, 2005. **26**: p. 5983–5990.
16. Shoichet, M. S., *Polymer Scaffolds for Biomaterials Applications*. *Macromolecules*, 2010. **43**: p. 581–591.
17. Martina, M., and D. W. Hutmacher, *Biodegradable Polymers Applied in Tissue Engineering Research: A Review*. *Polymer International*, 2007. **56**: p. 145–157.
18. Chapin, D. M., C. S. Fuller, and G. L. Pearson, *A New p-n Junction Photocell for Converting Solar Radiation into Electrical Power*. *Journal of Applied Physics*, 2012. **25**: p. 676–677.
19. Chen, H.-Y., et al., *Polymer Solar Cells with Enhanced Open-Circuit Voltage and Efficiency*. *Nature Photonics*, 2009. **3**: p. 649–653.
20. Gregg, B. A., and M. C. Hanna, *Comparing Organic to Inorganic Photovoltaic Cells: Theory, Experiment, and Simulation*. *Journal of Applied Physics*, 2003. **93**(6): p. 3505–3614.
21. Liang, W. Y., *Excitons*. *Physics Education*, 1970. **5**(4): p. 226–228.
22. Liang, Y., and L. Yu, *A New Class of Semiconducting Polymers for Bulk Heterojunction Solar Cells with Exceptionally High Performance*. *Accounts of Chemical Research*, 2010. **43**(9): p. 1227–1236.
23. Dai, L., P. Soundararajan, and T. Kim, *Sensors and Sensor Arrays Based on Conjugated Polymers and Carbon Nanotubes*. *Pure and Applied Chemistry*, 2002. **74**(9): p. 1753–1772.
24. Adhikari, B., and S. Majumdar, *Polymers in Sensor Applications*. *Progress in Polymer Science*, 2004. **29**: p. 699–766.
25. Lange, U., N. V. Roznyatovskaya, and V. M. Mirsky, *Conducting Polymers in Chemical Sensors and Arrays*. *Analytica Chimica Acta*, 2008. **614**: p. 1–26.
26. Toal, S. J., and W. C. Troglor, *Polymer Sensors for Nitroaromatic Explosives Detection*. *Journal of Materials and Chemistry*, 2006. **16**: p. 2871–2883.
27. Bai, H., and G. Shi, *Gas Sensors Based on Conducting Polymers*. *Sensors*, 2007. **7**: p. 267–307.

This page intentionally left blank

Correlations and Simulations in Polymer Science

*M*any properties of polymers can be easily measured by use of relatively simple instrumentation as discussed in earlier chapters. Standardized testing methods have been formulated by the American Society of Testing Methods (ASTM). A partial listing of these standards for plastics and rubber is given in Appendix C. When a polymer has not yet been synthesized or perhaps is unavailable or in quantities too small to fully test, a variety of approaches can be used to accurately *predict* polymer properties. In addition, these methods can be used to investigate how systematic structural changes such as the substitution of different chemical groups may affect polymer properties. Early approaches include group-contribution methods that have been successfully used to predict the properties of small molecules [1]. This approach has been adapted for polymers by van Krevelen [2, 3] whereby the repeat unit is divided into individual atoms or small chemical groups such as methyl or

phenyl groups that contribute incrementally to a specific property. Another successful approach for predicting polymer properties makes use of topological and geometrical parameters [4]. This approach offers a reliable alternative method to group-contribution methods and is particularly valuable in cases when specific chemical groups are unavailable in more traditional group-contribution methods. In some cases, artificial neural networks (ANNs) have been used to predict properties or to optimize processing operations using a set of descriptors and a large (training) set of experimental data. A fourth approach is the use of molecular simulations that can provide information on physical, mechanical, and transport properties. The accuracy of simulations depends upon the quality of a molecular mechanics force field that describes the potential-energy surface of the atomistic system. A successful polymer force field requires extensive parameterization for a large number of molecules using experimental data for validation and is applicable for a wide variety of polymers. Each of these approaches is described in the sections that follow.

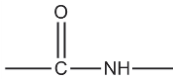
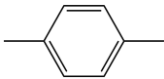
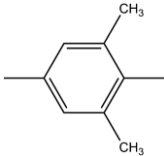
13.1 Group-Contribution Methods

As mentioned in the previous paragraph, an extensive collection of group-contribution methods for estimating polymer properties has been given by van Krevelen [2, 3]. Important applications of group-contribution methods include predictions of mechanical properties, surface energy, viscosity, density, thermal expansion coefficient, heat capacity, glass-transition temperature, crystalline-melt temperature, permeability, solubility parameters, free volume, and chemical potential. In this section, only a few of the more common group-contribution methods are illustrated. For more extensive treatment of group-contribution methods including comparisons of experimental and predicted properties, refer to the treatise by van Krevelen [2] and other sources.

13.1.1 Volumetric Properties

An important physical property that can be obtained by group contributions is specific or molar volume that provides an estimation of polymer density. As shown by selected values in Table 13-1, group-contribution increments are available to calculate specific volumes of glassy, rubber, and crystalline states at 298 K and consequently density as illustrated in Example 13.1. Group-contribution methods given by van Krevelen also can be used to calculate the van der Waals volume of a polymer, from which the fractional free volume can be obtained as shown in Example 13.2.

Table 13-1 Representative van Krevelen [2] Values for Molar Volume Increments (Bivalent Groups) at 298 K

Group	$V_{a,i}^a$ (cm ³ /mol)	$V_{c,i}^a$ (cm ³ /mol)	V_w (cm ³ /mol)
—CH ₂ —	16.37	14.68	10.23
—CF ₂ —	23.7	21	14.8
—C(CH ₃) ₂ —	49.0	44.0	30.7
—Si(CH ₃) ₂ —	67.5	60.6	42.2
—CH(CH ₃)—	32.72	29.35	20.45
—CH(CN)—	30.7	27.5	21.5
—CH(C ₆ H ₅)—	84.16	75.48	52.6
—CH=CH—	27.0	24.3	16.9
—CH=CCl—	41.0	37.0	25.7
—CH=C(CH ₃)—	<i>cis</i> 43	40	27.2
	<i>trans</i> 43	37	
—O—	<i>al</i> ^b (8.5)	(7.9)	(5.5)
	<i>ar</i> ^b (8.0)	(7.1)	(5.0)
	(21)	(18.7)	18.9 (13)
—COO—	<i>gen</i> ^c 23	21.5	15.2
	<i>acr</i> ^c 20.5	18.4	
—OCOO—	31	27	18.9
	65.5	59	43.3
	104	94	65.6

^a Subscripts a and c on $V_{a,i}$, and $V_{c,i}$ correspond to the fully amorphous and fully crystalline states, respectively; V_w is the van der Waals molar volume.

^b *al*, aliphatic oxygen; *ar*, aromatic oxygen.

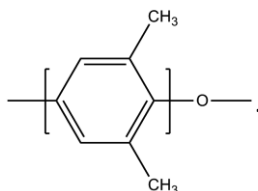
^c *gen*, general; *acr*, acrylic.

Example 13.1

Calculate the specific density of poly(2,6-dimethyl-1,4-phenylene oxide) using group-contribution methods.

Solution

The repeating unit of poly(2,6-dimethyl-1,4-phenylene oxide) is



Poly(2,6-dimethyl-1,4-phenylene oxide) is an *amorphous* polymer with a T_g of 214°C (see Section 10.1.4). The molecular weight of the repeating unit is $8(12.011) + 15.9994 + 8(1.00794) = 120.151$. Using values from Table 13-1, the molar volume is calculated to be $104 + 8.0 = 112.0 \text{ cm}^3/\text{mol}$. Specific volume is then calculated as

$$V_a = 112 \frac{\text{cm}^3}{\text{mol}} \frac{\text{mol}}{120.2 \text{ g}} = 0.9318 \frac{\text{cm}^3}{\text{g}}$$

Specific density is then calculated as $1/0.9318 = 1.073 \text{ g/cm}^3$. This value is in excellent agreement with a reported experimental value of 1.06 g/cm^3 at 296 K [5].

Van der Waals Volume. The van der Waals volume, V_w , of a molecule is the atomistic space occupied by the molecule. Values for selected van der Waals volume increments are included in Table 13-1 for bivalent groups (i.e., two valence connection sites) and in Table 13-2 for non-bivalent groups (one, three, or four valence connection sites). An important use of V_w is the estimation of *fractional free volume* (FFV) defined as

$$\text{FFV} = \frac{V - V_o}{V} \quad (13.1)$$

where V is the specific volume of the polymer at a given temperature and V_o is the volume occupied by the polymer chains. The FFV directly relates to important polymer properties such as viscosity and diffusivity or permeability as given by the equation

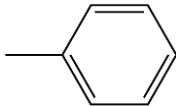
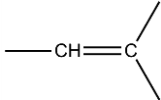

$$P = A \exp\left(\frac{-B}{\text{FFV}}\right). \quad (13.2)$$

Bondi [6] has suggested that an occupied “volume,” V_o , can be obtained from the van der Waals volume of the various groups comprising the polymer repeat unit as

$$V_o = 1.3 \sum_{k=1}^N (V_w)_k \quad (13.3)$$

where N is the total number of groups in the repeat unit.

Table 13-2 Representative van Krevelen [2] Values for van der Waals Volume Increments (non-Bivalent Groups) at 298 K

Group	V_w^a (cm ³ /mol)
—H	3.44
—CH ₃	27.2
—C≡N	14.7
—OH	8.0
—F	5.7
—Cl	al 11.6 ar 12.0
	45.85
—C≡	(8)
	13.5
	16.6

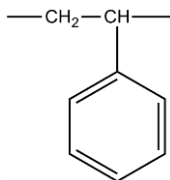
^a *al*, aliphatic oxygen; *ar*, aromatic oxygen.

Example 13.2

Calculate the fractional free volume (FFV) of atactic polystyrene (aPS) using only group contributions.

Solution

The repeating unit of PS is



Group Contribution	V_a	V_w
—CH ₂ —	16.37	10.23
—CH(C ₆ H ₅)—	84.16	52.6

The molar volume, V , of *a*-PS is obtained by summing the group contributions of V_a taken from Table 13-1 as 100.53 (16.37 + 84.16) cm³/mol. Similarly, the van der

Waals volume obtained by summing the group contributions, V_w (Table 13-1), is 62.83 cm³/mol (10.23 + 52.6). The occupied volume is then obtained from eq. (13.3) as $V_o = 1.3 \times 62.8 = 81.7$ cm³/mol. Finally, the FFV is obtained from eq. (13.1) as

$$\text{FFV} = \frac{V - V_o}{V} = \frac{100.5 - 81.7}{100.5} = \frac{18.8}{100.5} = 0.187.$$

This value compares favorably with a value of 0.177 reported by Thran et al. [7].

13.1.2 Glass-Transition Temperature

Correlations to predict the glass-transition temperature (T_g) have been reviewed by Fried [8]. Van Krevelen [2] has summarized some early approaches. A simple correlation used by van Krevelen for T_g is given as

$$T_g = \frac{\sum_i Y_{g,i}}{M} = \frac{Y_g}{M} \quad (13.4)$$

where Y_g is the molar glass-transition function (units of K·kg/mol), $T_{g,i}$, and M is the molecular weight (kg/mol) of the structural unit. In evaluation of a set of nearly 600 polymers, it was observed that Y_g depends upon the nature of other groups present in the structural unit and, therefore, correction terms must be added in the numerator for different functional groups. A plot of predicted versus experimental T_g values for 55 vinyl and aromatic-backbone polymers over the temperature range from about 200 to 441 K is shown in Figure 13-1. Agreement for this group of polymers is quite satisfactory ($R^2 = 0.8177$). The calculation of the T_g of bisphenol-A polycarbonate from group contribution is shown next in Example 13.3.

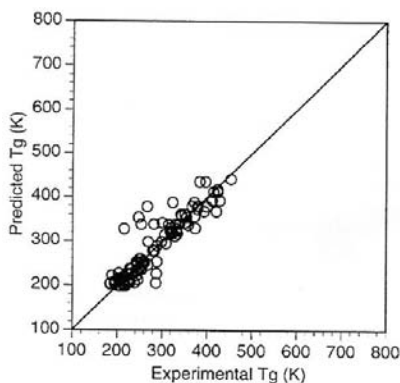
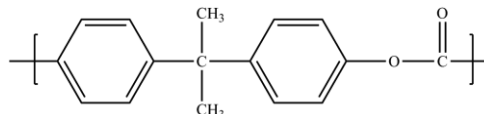


Figure 13-1 Plot of predicted (eq. (13.4)) versus experimental T_g of 55 polymers reported by van Krevelen [2].

Example 13.3

Calculate the T_g of bisphenol-A polycarbonate (PC) using van Krevelen's parameters. The repeating unit structure of PC is shown below.

**Solution**

The selected structural groups for PC and their corresponding molecular weights and molar glass-transition functions (van Krevelen [2] parameters) are shown in the table below.

Group	$Y_{g,i}^a$	M_i
	20	60.0
	87	194.3
$\Sigma =$	107	254.3

^a Units of $Y_{g,i}$ are K·kg/mol.

The molecular weight of the repeating unit is then calculated as $60.0 + 194.3 = 254.3$ and the corresponding sum of the molar glass-transition functions is 107. The T_g is then calculated from eq. (13.4) as

$$T_g = \frac{\sum_i Y_{g,i}}{M} = \frac{107 \text{ K kg/mol}}{254.3 \text{ kg/kmol}} \times \frac{1000 \text{ mol}}{\text{kmol}} = 421 \text{ K.}$$

This value compares favorably with reported experimental values [5] ranging from 413 to 424 K.

13.1.3 Permeability

The permeability of glassy and rubbery polymers has been discussed in Section 12.1.2. Several approaches have been proposed to predict polymer permeability from chemical group contributions. For example, Salame [9, 10] has proposed that gas permeability, particularly for low-permeability (i.e., barrier) polymers, can be

predicted from the value of the polymer Permachor, π , calculated from the relationship

$$\pi = \frac{1}{N} \sum_i (N_i \cdot \Pi_i) \quad (13.5)$$

where N is the total number of characteristic groups per structural unit, N_i is the number of i groups in the structural unit, and Π_i is the increment of group i contributing to the Permachor. Representative values of incremental Permachor values are given in Table 13-3.

Once the Permachor is calculated from the structure, the permeability at 298 K, $P(298)$, for nitrogen and other gases is then obtained from the equation

$$P(298) = P^*(298) \exp(-s\pi) \quad (13.6)$$

where $P^*(298)$ is the permeability (in SI units of $\text{cm}^3(\text{STP}) \text{ cm}/\text{cm}^2\text{-s-Pa}$)* of the gas in natural rubber and s is a scaling factor ($s = 0.12$ for O_2 , N_2 , and CO_2). In the case of nitrogen, $\log P^*(298)$ is -12. Once the permeability for nitrogen has been calculated, permeabilities of O_2 and CO_2 can be approximated by relative permeabilities averaged for many polymers using nitrogen as the standard gas (e.g., $P(\text{N}_2):P(\text{O}_2):P(\text{CO}_2)::1:3.8:24$). Although Permachor values are valid only for amorphous polymers, corrections are available to account for crystallinity [2]. As shown in Figure 13-2, there is excellent agreement between experimental permeability values for O_2 , N_2 , and CO_2 and permeabilities predicted from Permachor values. Example 13.4 illustrates the use of the Permachor approach to predict the oxygen permeability of polydimethylsiloxane. It is important to recognize that the extent of success for the Permachor method, like other group-contribution methods such as that for estimating T_g or the solubility parameter as shown in the following section, is limited by the availability of group contributions for structural units of less common but still important engineering and specialty polymers such as polyimides and polyphosphazenes (see Section 10.2.5) that have hundreds of possible chemical variations. Several alternative approaches for permeability prediction are available [2, 4].

* The unit $\text{cm}^3(\text{STP})$ is the amount of gas in units of cm^3 at standard temperature and pressure (i.e., 273 K, 1 bar).

Table 13-3 Selected Group Contributions to the Molar Permachor^a

Group	Π_i
—CH ₂ —	15
—CF ₂ —	120
—CH(CH ₃)—	15
—CH(CN)—	205
—C(CH ₃) ₂ —	-20
—Si(CH ₃) ₂ —	-116
-CH(<i>i</i> -butyl)-	-1
—CH=CH—	-12
—CH=CCl—	33
—CH=C(CH ₃)—	-30
—O—	70
	309
O	
—C—NH—	(wet 210)

^a Values taken from Salame [10].

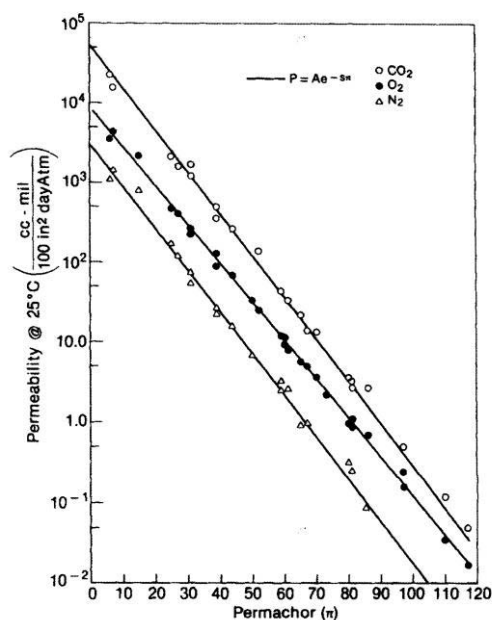
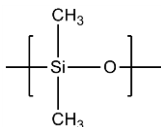


Figure 13-2 Correlation of gas permeability to polymer Permachor. Experimental data are given for oxygen (●), nitrogen (Δ), and carbon dioxide (○). Reproduced from M. Salame, *Prediction of Gas Barrier Properties of High Polymers*. Polymer Engineering and Science, 1986. **26**(22): p. 1543–1546. Reprinted by permission of John Wiley & Sons, Inc.

Example 13.4

Calculate the oxygen permeability of polydimethylsiloxane (PDMS)



using the molar Permachor values listed in Table 13-3.

Solution

The Permachor is calculated using eq. (13.5) as

$$\pi = \frac{1}{2}[(1)(-116) + (1)(70)] = -23.$$

Next the nitrogen permeability is obtained from eq. (13.6) as

$$P(298) = (10^{-12}) \exp[(-0.12)(-23)] = 1.58 \times 10^{-11} \text{ cm(STP) cm/cm}^2\text{-s-Pa.}$$

Finally, oxygen permeability is obtained from the relative permeability of O₂ to N₂ (a factor of 3.8), giving the following permeability value:

$$P(298) = 3.8 \times 1.58 \times 10^{-11} = 6.0 \times 10^{-11} \text{ cm(STP) cm/cm}^2\text{-s-Pa.}$$

An experimental value of the oxygen permeability of PDMS at 308 K is reported as $9.33 \times 10^{-8} \text{ cm}^3(\text{STP}) \text{ cm/s cm}^2 \text{ cmHg}$ [11]. Conversion of pressure units from cmHg to Pa (Appendix D, Table D-2) results in a $P(298)$ value of $7.00 \times 10^{-11} \text{ cm}^3(\text{STP}) \text{ cm/cm}^2\text{-s-Pa}$, in good agreement with the experimental value of $6.0 \times 10^{-11} \text{ cm}^3(\text{STP}) \text{ cm/cm}^2\text{-s-Pa}$ cited above.

13.1.4 Solubility Parameter

The concept of the solubility parameter was introduced in Section 3.2.6. Solubility parameters of polymers can be estimated by use of one of several group-contribution methods, such as those given by Small [12] and by Hoy [13]. Calculation of δ by a group-contribution method requires the value of a molar attraction constant, F_i , for each chemical group in the polymer repeat unit. Values of F_i have been obtained by regression analysis of physical property data for a large number of organic compounds (e.g., 640 compounds in Hoy's method). In the case of Small's method, all compounds for which hydrogen bonding occurs (e.g., hydroxyl compounds, amines, and carboxylic acids) were excluded. A listing of some important molar attraction constants is given in Table 13-4.

Table 13-4 Molar Attraction Constants at 25°C

Group	Molar Attraction Constant, F ($(\text{MPa})^{1/2} \text{ cm}^3 \text{ mol}^{-1}$)		
	Small [12]	Hoy [13]	Van Krevelen [2]
-CH ₃	438	303	420
-CH ₂ -	272	269	280
>CH-	57	176	140
>C<	-190	65.5	0
-CH(CH ₃)-	495	(479)	560
-C(CH ₃) ₂ -	686	(672)	840
-CH=CH-	454	497	444
>C=CH-	266	422	304
Phenyl	1504	1398	1517
<i>p</i> -Phenylene	1346	1442	1377
-O- (ether)	143	235	256
-OH	—	462	754
-CO- (ketone)	563	538	685
-COO- (ester)	634	668	512
-OCOO- (carbonate)	—	(904)	767
-CN	839	726	982
-N=C=O	—	734	—
-NH-	—	368	—
-S- (sulfide)	460	428	460
-F	(250)	84.5	164
-Cl (primary)	552	420	471
-Br (primary)	696	528	614
-CF ₃ (<i>n</i> -fluorocarbon)	561	—	—
-Si-	-77	—	—

The solubility parameter of a polymer can then be calculated from the molar attraction constants and the molar volume of the polymer, V (units of $\text{cm}^3 \text{ mol}^{-1}$), from the relationship

$$\delta = \frac{\sum_{i=1} F_i}{V} \quad (13.7)$$

where the summation is taken over all groups in the repeating unit. As shown earlier (Section 13.1.1), the molar volume can be obtained from group contributions as well. Chemical groups can be atoms, particularly halogens or small uniquely identifiable groups in the polymer repeating unit such as methyl, methylene, and phenyl groups as shown in Table 13-4. Calculated values of solubility parameters for some

common solvents and polymers have been tabulated in a number of publications [2, 14, 15]. Some representative values are given in Table 13-5. A sample calculation using Small's method is given next in Example 13.5.

Table 13-5 Solubility Parameters of Some Common Solvents and Polymers

	Solubility Parameter, δ^a	
	(MPa) ^{1/2}	(cal cm ⁻³) ^{1/2}
Solvents		
<i>n</i> -Hexane	14.9	7.28
Carbon tetrachloride	17.8	8.70
Toluene	18.2	8.90
Benzene	18.6	9.09
Chloroform	19.0	9.29
Tetrahydrofuran	19.4	9.48
Chlorobenzene	19.6	9.58
Methylene chloride	20.3	9.92
1,4-Dioxane	20.5	10.0
<i>N</i> -Methyl-2-pyrrolidone	22.9	11.2
Dimethylformamide	24.8	12.1
Methanol	29.7	14.5
Water	47.9	23.4
Polymers		
Polyisobutylene	15.5	7.58
Polysulfone	20.3	9.92
Poly(vinyl chloride)	21.5	10.5
Polystyrene	22.5	11.0
Poly(methyl methacrylate)	22.7	11.1
Cellulose acetate	25.1	12.3
Polyacrylonitrile	25.3	12.4
Poly(vinyl acetate)	25.7	12.7

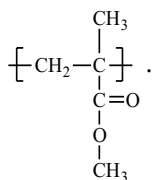
^a Calculated from Hansen solubility parameters using eq. (13.7) at 25°C; conversion: 1 MPa^{1/2} = 0.489 (cal cm⁻³)^{1/2}.

Example 13.5

Estimate the solubility parameters, in units of (MPa)^{1/2}, for poly(methyl methacrylate) (PMMA) by the method of Small [12]. The density of PMMA is reported to be 1.188 g cm⁻³ at 25°C.

Solution

The structure of the PMMA repeat unit is



From the available chemical groups listed in Table 13-4, the molar-attraction constant for the repeating unit of PMMA can be obtained as follows:

Group	F	Number of Groups	$\sum F_i$
-CH ₃	438	2	876
-CH ₂ -	272	1	272
>C<	-190	1	-190
-COO- (ester)	634	1	634
			1592

The formula weight of a PMMA repeating unit is calculated from atomic weights (Appendix F) as follows:

$$\begin{array}{rcl} \text{C:} & 5 \times 12.01115 & = 60.06 \\ \text{O:} & 2 \times 15.9994 & = 32.0 \\ \text{H:} & 8 \times 1.00797 & = 8.06 \\ & & \hline & & 100.12 \end{array}$$

Using the density of PMMA given in the problem statement, the molar volume, V , is then calculated as

$$\frac{200.12}{1.188} = 84.28 \text{ cm}^3 \text{ mol}^{-1}.$$

The solubility parameter is then calculated as

$$\delta_i = \frac{\sum F_i}{V_i} = \frac{1592}{84.28} = 18.9 \text{ MPa}^{1/2}.$$

This value is within about 17% of the value of 22.7 MPa^{1/2} given in Table 13-5 for PMMA. Recalculation of the solubility parameter using Hoy's and van Krevelen's group contributions given in Table 13-4 gives values of 19.1 and 19.4 MPa^{1/2}, respectively, which are a little closer to the reported experimental value.

13.1.5 Activity Coefficients

As discussed in Chapter 3, once a value for the interaction parameter is known or can be estimated, the activity of a solvent in a polymer solution can be estimated by means of the Flory–Huggins equation. It is also possible to *predict* activity through a variety of chemical group-contribution methods [16]. The most fully developed of these methods is UNIFAC-FV [17]. The acronym UNIFAC stands for *UNIQUAC Functional-group Activity Coefficients*, which had been widely used for the prediction of vapor–liquid equilibrium (VLE) for mixtures of low-molecular-weight components [18], and FV represents a free-volume contribution originating from the Flory equation-of-state theory (see Section 3.2.3). UNIQUAC, itself, is an acronym for *Universal Quasi-Chemical equations*, which provides good representation of both vapor–liquid equilibrium (VLE) and liquid–liquid equilibrium (LLE) for binary and multicomponent mixtures of nonelectrolytes using one or two adjustable (energy) parameters per binary pair [19]. The difference between UNIQUAC and UNIFAC, or UNIFAC-FV, is that UNIFAC uses the solution-of-functional-groups (SOG) concept [20] to obtain group-contribution parameters (the adjustable parameters in UNIQUAC) from knowledge of the chemical groups comprising the mixture components in a manner similar to the way that solubility parameters are calculated by the methods of Small or Hoy as discussed in the previous section.

In the UNIFAC-FV approach, solvent activities may be calculated as contributions from three sources—a combinatorial (entropy) term, a residual (enthalpic) term, and a (Flory equation-of-state*) free-volume term as

$$\ln a_1 = \ln a_1^C + \ln a_1^R + \ln a_1^{FV}. \quad (13.8)$$

The combinatorial term is given as

$$\ln a_1^C \approx \ln \phi_1' + (1 - \phi_1') + \frac{z}{2} M_1 q_1' \left[\ln \left(\frac{\theta_1'}{\phi_1'} \right) - 1 + \frac{\phi_1'}{\theta_1'} \right] \quad (13.9)$$

where ϕ_1' is the segment volume fraction, θ_1' is the surface area fraction, z is the coordination number of the lattice (taken to be 10), and M_1 is the molecular weight of component 1 (i.e., the solvent in a polymer solution). The parameter q_1' in eq. (13.9) is related to the van der Waals surface area as

$$q_1' = \frac{1}{M_1} \sum_{k=1}^N \nu_k^{(1)} Q_k \quad (13.10)$$

* See Chapter 3, Section 3.2.3.

where $\nu_k^{(1)}$ is the number of functional groups of type k in the solvent and Q_k is a group area parameter obtained from the (Bondi) van der Waals group surface area, A_{wk} , and normalized to a methylene unit of polyethylene as

$$Q_k = \frac{A_{wk}}{2.5 \times 10^9}. \quad (13.11)$$

The surface area fraction, θ_1' , is calculated from q_1' as

$$\theta_1' = \frac{q_1' w_1}{\sum_{j=1}^N q_j' w_j} \quad (13.12)$$

where the summation in the denominator of eq. (13.12) is taken over all N components of the mixture. Similarly, the segment volume fraction of the solvent, q_1' , is calculated from the weight fractions and the group volume parameter of each component of the mixture, r_j' , as

$$\phi_1' = \frac{r_1' w_1}{\sum_{j=1}^N r_j' w_j} \quad (13.13)$$

where the relative van der Waals volume is given as

$$r_1' = \frac{1}{M_1} \sum_{k=1}^N \nu_k^{(1)} R_k \quad (13.14)$$

and $\nu_k^{(1)}$ is the number of groups (an integer) of type k in the solvent and R_k is the normalized van der Waals group volume, V_{wk} , evaluated as

$$R_k = \frac{V_{wk}}{15.17}. \quad (13.15)$$

The molar group area parameter, Q_k , given by eq. (13.11), and the molar group volume parameter, R_k , are available for most structural groups as well as for some common solvents, such as water, carbon disulfide, and dimethylformamide. These group parameters are continuously updated and new ones added in the literature [21]. Some representative values of Q_k and R_k are given in Table 13-6.

It is noted that the first two terms on the RHS of eq. (13.9) are essentially the combinatorial terms of the Flory–Huggins (F–H) equation (eq. 3.37) with the exception that segment rather than volume fractions are used. The remaining two terms serve to correct for the effect of molecular shape. The difference between the combinatorial activity given by eq. (13.9) and that of the F–H expression is usually

small when segment fractions are used in place of volume fractions in the F–H expression.

Table 13-6 Molar Group Area (Q_k) and Volume (R_k) Parameters^a

Main Group	Subgroup	R_k	Q_k	Sample Group Assignment
CH ₂	CH ₃	0.9011	0.848	Hexane
	CH ₂	0.6744	0.540	<i>n</i> -Butane
	CH	0.4469	0.228	2-Methylpropane
	C	0.2195	0.000	Neopentane
C=C	CH ₂ =CH	1.3454	1.176	Hexene-1
	CH=CH	1.1167	0.867	Hexene-2
	CH ₂ =C	1.1173	0.988	2-Methyl-1-butene
	CH=C	0.8886	0.676	2-Methyl-2-butene
	C=C	0.6605	0.485	2,3-Dimethylbutene
CH ₂ CO	CH ₃ CO	1.6724	1.448	Butanone
	CH ₂ CO	1.4457	1.180	Pentanone-3
ACH ^b	ACH	0.5313	0.400	Naphthalene
	AC	0.3652	0.120	Styrene
ACCH ₂	ACCH ₃	1.2663	0.968	Toluene
	ACCH ₂	1.0396	0.660	Ethylbenzene
	ACCH	0.8121	0.348	Cumene
SiO		1.1044	0.466	Polysiloxane
OH		1.0000	1.200	Propanol-2
CH ₃ OH		1.4311	1.432	Methanol
H ₂ O		0.9200	1.400	Water
CHCl ₃		2.8700	2.410	Chloroform
HCON(CH ₃) ₂		3.0856	2.736	<i>N,N</i> -Dimethylformamide
SiO		1.1044	0.466	Octamethyl cyclotetrasilane

^a Supplementary material to ref. [21]

^b The prefix A indicates that the group is contained in an *aromatic* structure.

The residual contribution to the activity of the solvent in UNIQUAC is given as

$$\ln a_1^R = M_1 q_1' \left[1 - \ln \left(\sum_{i=1}^N \theta_i' \tau_{i1} \right) - \sum_{i=1}^N \left(\theta_i' \tau_{1i} / \sum_{j=1}^N \theta_j' \tau_{ji} \right) \right] \quad (13.16)$$

where the two *adjustable* parameters, τ_{ij} and τ_{ji} , are given as

$$\tau_{ij} = \exp \left[- \left(\frac{u_{ij} - u_{jj}}{RT} \right) \right] \quad (13.17)$$

and

$$\tau_{ji} = \exp \left[- \left(\frac{u_{ji} - u_{ii}}{RT} \right) \right]. \quad (13.18)$$

The parameter u_{ij} is the potential energy of aN i - j pair.

In UNIFAC, the *residual* term is replaced by the SOG concept as

$$\ln a_1^R = \sum_{\text{all groups}} \nu_k^{(1)} \left[\ln \Gamma_k - \ln \Gamma_k^{(1)} \right] \quad (13.19)$$

where Γ_k is the group residual activity (or activity coefficient) and $\Gamma_k^{(1)}$ is the group residual activity (or activity coefficient) of group k in a reference solution containing only solvent molecules (for normalization so that $a_1 \rightarrow 1$ as $w_1 \rightarrow 1$). The group activation term, Γ_k or $\Gamma_k^{(1)}$, is obtained from the expression

$$\ln \Gamma_k = M_k Q'_k \left[1 - \ln \left(\sum_{\text{all groups}} \Theta'_m \Psi_{mk} \right) - \sum_{\text{all groups}} \frac{\Theta'_m \Psi_{km}}{\sum_{\text{all groups}} \Theta'_n \Psi_{nm}} \right] \quad (13.20)$$

where Θ'_m is the *area fraction* of group m , calculated in a similar way to that of θ_j' :

$$\Theta'_m = \frac{Q'_m W_m}{\sum_{n=1}^N Q'_n W_n}. \quad (13.21)$$

In eqs. (13.20) and (13.21), M_k is the molecular weight of the functional group k , Q'_m is the group-area parameter per gram such that $Q'_m = Q_m/M_m$, and W_m is the weight fraction of group m in the mixture. The *group-interaction parameter*, Ψ_{mn} , is given by

$$\Psi_{mn} = \exp \left[- \left(\frac{U_{mn} - U_{mm}}{RT} \right) \right] = \exp \left(\frac{a_{mn}}{T} \right) \quad (13.22)$$

where U_{mn} is a measure of the energy of interaction between groups m and n . The group-interaction parameters, a_{mn} and a_{nm} ($a_{mn} \neq a_{nm}$), for each pair of groups have been compiled and continuously revised, principally by fitting experimental VLE or LLE data for low-molecular-weight compounds. Representative values of the group-interaction parameters derived from VLE data are given in Table 13-7. In tables of group-interaction parameters, each major group contains several subgroups with their own R_k and Q_k values (Table 13-6), but *all subgroups have identical group-interaction parameters*.

Table 13-7 Representative Values of the Group-Interaction Parameters, a_{nm} and a_{mn} (K)^a

	CH ₂	C=C	ACH	ACCH ₂	OH	CH ₂ CO	CH ₃ OH	SiO
CH ₂	0.0	86.02	61.13	76.50	986.5	476.4	697.2	252.7
C=C	-35.36	0.0	38.81	74.15	524.1	182.6	787.6	n.a.
ACH	-11.12	3.446	0.0	167.0	636.1	25.77	637.4	238.9
ACCH ₂	-69.70	-113.6	-146.8	0.0	803.2	-52.10	603.3	n.a.
OH	156.4	457.0	89.60	25.82	0.0	84.00	-137.1	n.a.
CH ₂ CO	26.76	42.92	140.1	365.8	164.5	0.0	108.7	n.a.
CH ₃ OH	16.51	-12.52	-50.00	-44.50	249.1	23.39	0.0	n.a.
SiO	110.2	n.a.	234.4	n.a.	n.a.	n.a.	n.a.	n.a.

^a Supplementary material to ref. [21].

For polymer–solvent systems, Oishi and Prausnitz [17] have shown that the *free-volume* contribution appearing in eq. (13.8) can be a significant *positive* contribution to the total activity and used the Flory EOS (where $X_{12} = 0$) to obtain

$$\ln a_1^{\text{FV}} = 3c_1 \ln \left[\frac{(\tilde{v}_1^{1/3} - 1)}{(\tilde{v}_M^{1/3} - 1)} \right] - c_1 \left[\left(\frac{\tilde{v}_1}{\tilde{v}_M} - 1 \right) \left(1 - \frac{1}{\tilde{v}_1^{1/3}} \right)^{-1} \right]. \quad (13.23)$$

In this equation, $3c_1$ represents the number of external degrees of freedom per solvent (i.e., component 1) molecule (c_1 is usually set to 1.1), subscript M refers to the mixture, and \tilde{v} is the reduced volume as defined in Chapter 3 (eq. (3.47)). Oishi and Prausnitz have suggested calculating the reduced volume for the solvent as

$$\tilde{v} = \frac{v_1}{15.17br_1'} \quad (13.24)$$

where b is a proportionality factor of order unity (often taken as 1.28). The reduced volume of the mixture, \tilde{v}_M , is calculated by assuming that the volume of the liquid mixture is additive. For a binary mixture of solvent and polymer (component 2), \tilde{v}_M is given as

$$\tilde{v}_M = \frac{v_1 w_1 + v_2 w_2}{15.17b(r_1' w_1 + r_2' w_2)}. \quad (13.25)$$

UNIFAC-FV has been very successful in the prediction of solvent activities for polymer solutions [16], as illustrated for polyisobutylene/benzene in Figure 13-3. Although the UNIFAC-FV approach was developed to improve predictions of activities or activity coefficients for polymeric systems, it also has been used for mixtures of low-molecular-weight compounds with reasonable success. Free-volume contributions can be important even for mixtures of low-molecular-weight

components if the characteristic temperatures (T^*) differ significantly, as in the case of gas/hydrocarbon mixtures, for example. As an illustration of UNIFAC-FV, the calculation of the activity of benzene in polyisobutylene is shown in Example 13.6

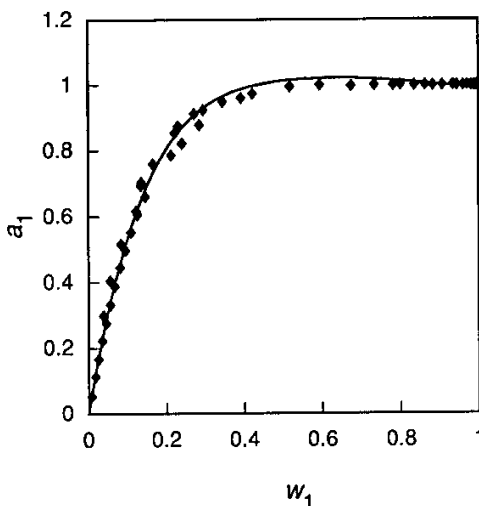
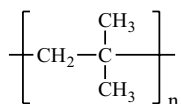


Figure 13-3 Comparison of experimental data for the activity of benzene (a_1) as a function of its weight fraction (w_1) in polyisobutylene at 25°C with predictions (—) of UNIFAC-FV [16].

Example 13.6

Using UNIFAC-FV, calculate the activity of benzene in polyisobutylene (PIB)



at 25°C when the weight fraction of benzene is 0.1.

Solution

Component	ρ (g mL ⁻³)	M	Main group	Sub-group	R_k	Q_k	No. of Groups
Benzene	0.8736	78.11	ACH	ACH	0.5313	0.400	6
PIB	0.9169	56.07	CH ₂	C	0.2195	0.0	1
			CH ₂	CH ₂	0.6744	0.540	1
			CH ₂	CH ₃	0.9011	0.848	2

Combinatorial contribution:

$$q'_1 = \frac{1}{78.11} 6(0.400) = 0.03073$$

$$r'_1 = \frac{1}{78.11} 6(0.5313) = 0.04081$$

$$q'_2 = \frac{1}{56.07} [1(0) + 1(0.540) + 2(0.848)] = 0.03987$$

$$r'_2 = \frac{1}{56.07} [1(0.2195) + 1(0.6744) + 2(0.9011)] = 0.04808$$

$$\theta'_1 = \frac{0.03073(0.1)}{0.0307(0.1) + 0.03987(0.9)} = 0.07888$$

$$\phi'_1 = \frac{0.04081(0.1)}{0.04081(0.1) + 0.04808(0.9)} = 0.08618$$

$$\ln a_1^c = \ln(0.08618) + (1 - 0.08618) + \frac{10}{2} (78.11)(0.03073) \left[\ln \left(\frac{0.07888}{0.08618} \right) - 1 + \frac{0.08618}{0.07888} \right]$$

$$= -1.4831$$

Residual contribution:

$$W_{\text{ACH}} = 0.1$$

$$W_{\text{CH}_3} = 0.9 \frac{15.025(2)}{56.07} = 0.4823$$

$$W_{\text{CH}_2} = 0.9 \frac{14.0169}{56.07} = 0.2250$$

$$W_{\text{C}} = 0.9 \frac{12.001}{56.07} = 0.1926$$

$$Q'_{\text{ACH}} = \frac{Q_{\text{ACH}}}{13.0089} = \frac{0.4}{13.0089} = 0.03075$$

$$Q'_{\text{CH}_3} = \frac{Q_{\text{CH}_3}}{15.025} = \frac{0.848}{15.025} = 0.05644$$

$$Q'_{\text{CH}_2} = \frac{Q_{\text{CH}_2}}{14.0169} = \frac{0.540}{14.0169} = 0.03853$$

$$Q'_{\text{C}} = \frac{Q_{\text{C}}}{12.001} = \frac{0}{12.001} = 0$$

$$\Theta'_{\text{ACH}} = \frac{Q'_{\text{ACH}} W_{\text{ACH}}}{Q'_{\text{ACH}} W_{\text{ACH}} + Q'_{\text{CH}_3} W_{\text{CH}_3} + Q'_{\text{CH}_2} W_{\text{CH}_2} + Q'_{\text{C}} W_{\text{C}}} = \frac{0.003075}{0.03897} = 0.07892$$

$$\Theta'_{\text{CH}_3} = \frac{Q'_{\text{CH}_3} W_{\text{CH}_3}}{Q'_{\text{ACH}} W_{\text{ACH}} + Q'_{\text{CH}_3} W_{\text{CH}_3} + Q'_{\text{CH}_2} W_{\text{CH}_2} + Q'_{\text{C}} W_{\text{C}}} = \frac{0.02722}{0.03897} = 0.6986$$

$$\Theta'_{\text{CH}_2} = \frac{Q'_{\text{CH}_2} W_{\text{CH}_2}}{Q'_{\text{ACH}} W_{\text{ACH}} + Q'_{\text{CH}_3} W_{\text{CH}_3} + Q'_{\text{CH}_2} W_{\text{CH}_2} + Q'_C W_C} = \frac{0.008669}{0.03897} = 0.2225$$

$$\Theta'_C = \frac{Q'_C W_C}{Q'_{\text{ACH}} W_{\text{ACH}} + Q'_{\text{CH}_3} W_{\text{CH}_3} + Q'_{\text{CH}_2} W_{\text{CH}_2} + Q'_C W_C} = 0$$

Note that interaction parameters are only between main groups, and in this case there are only two main groups—ACH (benzene) and CH₂ (C, CH₂, and CH₃ subgroups)—in PIB. This greatly reduces the number of calculations for the residual contribution to the activity of benzene as follows:

$$\Psi_{\text{ACH,CH}_2} = \exp\left(-\frac{a_{\text{ACH,CH}_2}}{T}\right) = \exp\left(-\frac{11.12}{298}\right) = 1.0380 = \Psi_{\text{ACH,CH}_3} = \Psi_{\text{ACH,C}}$$

$$\Psi_{\text{CH}_2,\text{ACH}} = \exp\left(-\frac{a_{\text{CH}_2,\text{ACH}}}{T}\right) = \exp\left(-\frac{61.13}{298}\right) = 0.8145 = \Psi_{\text{CH}_3,\text{ACH}} = \Psi_{\text{C,ACH}}$$

$$\begin{aligned} \ln \Gamma_{\text{ACH}} = & M_{\text{ACH}} Q'_{\text{ACH}} \left[1 - \ln(\Theta'_{\text{ACH}} \Psi_{\text{ACH,ACH}} + \Theta'_{\text{CH}_3} \Psi_{\text{CH}_3,\text{ACH}} + \Theta'_{\text{CH}_2} \Psi_{\text{CH}_2,\text{ACH}} + \Theta'_C \Psi_{\text{C,ACH}}) - \right. \\ & \frac{\Theta'_{\text{ACH}} \Psi_{\text{ACH,ACH}}}{\Theta'_{\text{ACH}} \Psi_{\text{ACH,ACH}} + \Theta'_{\text{CH}_3} \Psi_{\text{CH}_3,\text{ACH}} + \Theta'_{\text{CH}_2} \Psi_{\text{CH}_2,\text{ACH}} + \Theta'_C \Psi_{\text{C,ACH}}} - \\ & \frac{\Theta'_{\text{CH}_3} \Psi_{\text{ACH,CH}_3}}{\Theta'_{\text{ACH}} \Psi_{\text{ACH,CH}_3} + \Theta'_{\text{CH}_3} \Psi_{\text{CH}_3,\text{CH}_3} + \Theta'_{\text{CH}_2} \Psi_{\text{CH}_2,\text{CH}_3} + \Theta'_C \Psi_{\text{C,CH}_3}} - \\ & \frac{\Theta'_{\text{CH}_2} \Psi_{\text{ACH,CH}_2}}{\Theta'_{\text{ACH}} \Psi_{\text{ACH,CH}_2} + \Theta'_{\text{CH}_3} \Psi_{\text{CH}_3,\text{CH}_2} + \Theta'_{\text{CH}_2} \Psi_{\text{CH}_2,\text{CH}_2} + \Theta'_C \Psi_{\text{C,CH}_2}} - \\ & \left. \frac{\Theta'_C \Psi_{\text{ACH,C}}}{\Theta'_{\text{ACH}} \Psi_{\text{ACH,C}} + \Theta'_{\text{CH}_3} \Psi_{\text{CH}_3,\text{C}} + \Theta'_{\text{CH}_2} \Psi_{\text{CH}_2,\text{C}} + \Theta'_C \Psi_{\text{C,C}}} \right] = \\ & 0.400 \left[1 - \ln(0 + 0.2225 \cdot 0.8145 + 0.6986 \cdot 0.8145 + 0.07892) - \right. \\ & \frac{0.07892(1)}{0.07892(1) + 0.6986(0.8145) + 0.2225(0.8145) + 0} - \\ & \left. \frac{(0.6986 + 0.2225)(1.0380)}{0.0789(1.0380) + 0.6986(1) + 0.2225 + 0} \right] = 0.4 \left[1 - \ln(0.8292) - 1.0615 \right] = 0.05036 \end{aligned}$$

$$\ln \Gamma_{\text{ACH}}^{(1)} = 0$$

$$\ln a_1^{\text{R}} = 6(0.05036 - 0) = 0.3022$$

Free-volume contribution:

$$\bar{v}_1 = \frac{1.145}{15.17(1.28)0.04081} = 1.445$$

$$\bar{v}_M = \frac{1.1447(0.1) + 1.0906(0.9)}{15.17(1.28)[0.04081(0.1) + 0.04808(0.9)]} = 1.1920$$

$$\ln a_1^{\text{FV}} = 3(1.1) \ln \left[\frac{1.445^{1/3} - 1}{1.1920^{1/3} - 1} \right] - 1.1 \left[\left(\frac{1.445}{1.1920} - 1 \right) \left(1 - \frac{1}{1.445^{1/3}} \right)^{-1} \right] = 0.528$$

Total activity of benzene:

$$\ln a_1 = -1.483 + 0.302 + 0.528 = -0.653; \quad a_1 = 0.520$$

These results show that the residual or enthalpic contribution to the activity is relatively small compared to the combinatorial contribution. This should be expected on the basis of the non-polar nature of PIB and benzene. As shown by a comparison of experimental activities with calculated values in Figure 13-3, UNIFAC-FV very accurately predicts the activity of benzene in PIB due to the extensive parameterization of UNIFAC for many compounds.

13.2 Topological Indices

Another method of predicting polymer properties is the topological approach developed by Bicerano [4, 22]. This approach uses simple connectivity indexes and other structural descriptors where the emphasis is on the use of additive contributions over individual atoms and bonds rather than chemical groups. This method is limited to amorphous, uncrosslinked, isotropic polymers containing any of nine atoms (i.e., C, N, O, H, F, Si, S, Cl, and Br). All that is required is the structure of the repeat unit and its molecular weight. Details of the procedures required are given in Bicerano's book [4] and have been incorporated in the commercial software program Synthia.* Properties that can be calculated include the van der Waals volume (V_w), molar volume, solubility parameter, glass-transition temperature, coefficient of volumetric thermal expansion, molar volume as a function of temperature, molar heat capacity at constant pressure, permeability (O_2 , N_2 , CO_2), molar diamagnetic susceptibility, molar refraction, dielectric constant, thermal conductivity, viscosity, activation energy for viscous flow, characteristic ratio, critical molecular weight for entanglement, mechanical properties (Young's modulus, volume resistivity, brittle fracture stress, bulk modulus, shear yield stress, shear modulus), refractive index, and surface tension. Hand calculations are tedious as illustrated by the example of polystyrene given in Bicerano's reference article [22] but lend themselves nicely to computer implementation.

In general, the most basic information required is the structure of the repeat unit of the polymer chain from which the molecular weight of the repeat unit can be calculated. For polystyrene (PS) whose repeat unit structure is shown in Figure

* Available through Materials Studio (Accelrys).

13-4, the molecular weight per repeat unit is 104.15 g/mol. The first step is the calculation of the total number of rotational degrees of freedom of the polymer repeat unit. The total number is obtained from the sum of the total number of backbone degrees of freedom and the total number of side-group degrees of freedom using a set of specific rules to define a rotational unit. In the case of PS, there is a total of two rotatable backbone bonds in the backbone and just one rotational side-group bond (i.e., the bond connecting the phenyl ring and the backbone) for a total of three rotational degrees of freedom as shown in Figure 13-4. The next step is the calculation of the length of the polymeric repeat unit in its fully extended conformation (i.e., the planar zig-zag conformation in the case of PS) as shown in Figure 13-4. This is obtained by calculating the length of a triangle with two sides formed by the C–C bonds 1 and 2 (1.54 Å in length) connected by an angle of 109.5°. For PS, this value is 2.54 Å.

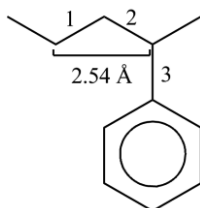


Figure 13-4 Representation of the repeat unit structure of polystyrene showing the two rotatable backbone bonds (1 and 2) and the rotatable side-group bond (3). For clarity, carbon and hydrogen atoms have been omitted. The length of the repeat unit, based upon the planar zig-zag conformation of the backbone chain, is 2.54 Å.

The next step is the calculation of the connectivity indices. These include the two zeroth-order indices, ${}^0\chi$ and ${}^0\chi^v$, defined in terms of *atom* descriptors and two first-order indices, ${}^1\chi$ and ${}^1\chi^v$, defined in terms of *bond* descriptors. The zeroth-order indices are calculated from the atomic indices, δ_i and valence atomic indices, δ_i^v , as

$${}^0\chi \equiv \sum (1/\sqrt{\delta}) \quad (13.26)$$

and

$${}^0\chi^v \equiv \sum (1/\sqrt{\delta^v}) \quad (13.27)$$

where the summation is made over all the vertices of the hydrogen-suppressed repeat unit. Bond indices are calculated from the atomic indices as

$$\beta_{ij} \equiv \delta_i \delta_j \quad (13.28)$$

and

$$\beta_{ij}^v \equiv \delta_i^v \delta_j^v. \quad (13.29)$$

The first-order (bond) connectivity indices are obtained from the bond indices as

$${}^1\chi \equiv \sum (1/\sqrt{\beta}) \quad (13.30)$$

and

$${}^1\chi^v \equiv \sum (1/\sqrt{\beta^v}). \quad (13.31)$$

The atomic indices, δ , and valence atomic indices, δ^v , are obtained from tables of values that depend upon the type and hybridization (Hyb) of atoms at the vertices and the total number of hydrogen atoms (N_H) at these sites. Some representative values are given in Table 13-8. Application of these rules to the example of PS is shown by values marked on a repeat unit in Figure 13-5. Using these values gives values of the zeroth-order indices, ${}^0\chi$ and ${}^0\chi^v$, and the first-order indices, ${}^1\chi$ and ${}^1\chi^v$ from eq. (13.26) through eq. (13.31). The calculated values are ${}^0\chi = 5.40$, ${}^0\chi^v = 4.67$, ${}^1\chi = 3.97$, and ${}^1\chi^v = 3.02$. Once these values are available, various physical, thermal, and mechanical properties can be calculated from the appropriate equation given by Bicerano [4]. As an example, density can be obtained from the repeat molecular weight, M , and the amorphous molar volume at 298 K, $V(298)$, as

$$\rho = \frac{M}{V(298)} \quad (13.32)$$

where

$$V(298) = 3.642770 {}^0\chi + 9.798697 {}^0\chi^v - 8.542819 {}^1\chi + 21.693912 {}^1\chi^v + 0.978655 N_{MV} \quad (13.33)$$

and N_{MV} is calculated from the overall chemical composition of the repeat unit. Predicted physical and thermal properties of PS calculated by Bicerano's method are compared with experimental values in Table 13-9. In general, agreement is very good.

Table 13-8 Selective Atomic and Valence Atomic Indices [22]

Atom	Hyb	N_H	δ	δ^v
C	sp^3	3	1	1
		2	2	2
		1	3	3
		0	4	4
	sp^2	2	1	2
		1	2	3
N	sp^3	0	3	4
		1	1	3
		0	2	4
O	sp^3	2	1	4
		1	2	4
	sp^2	0	3	5
		1	1	4
Si	sp^3	0	2	5
		1	1	5
		0	2	6
Cl	—	0	1	6
		1	3	1/3
		0	4	4/9
		0	1	7/9

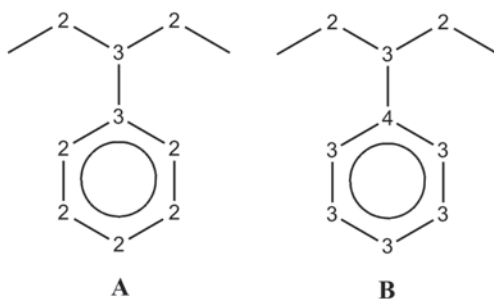


Figure 13-5 Atomic (A) and valence atomic (B) connectivity indices marked at the vertices of a PS repeat unit. Values taken from Table 13-8.

Table 13-9 Comparison Between Experimental Physical and Thermal Properties and Properties Estimated by Bicerano's Method [22]

Property	Predicted Value	Experimental Value
ρ , g cm ⁻³	1.07	1.05
δ , (J cm ⁻³) ^{0.5}	19.5, 20.1	17.4- 19.0
T_g , K	382	373
C_p^g , (298), J/(mole K)	133.5	126.5
$\Delta C_p(T_g)$	26.8	30.8
γ , dyn cm ⁻¹ at 298 K	39.4, 41.0, 43.6	40.7

13.3 Artificial Neural Network

An artificial neural network (ANN) is a computing system composed of a number of highly connected processing elements or nodes that process input data and predict specific output data in a way roughly similar to the function of brain neurons. Each neural network has a learning process that typically includes a set of training data for which the output is known. A schematic representation of a simple ANN is illustrated in Figure 13-6. This neural network has five input nodes (X_1 , X_2 , X_3 , X_4 , and X_5), one output node (Y_1), and four hidden nodes represented by the shaded circles. During operation of the ANN, each of the input variables is assigned a weight, W_i . As shown, each input node is able to provide signals to the other nodes. The weighted sum of all the signals is then transformed by a specific function. The output variable can be changed by adjusting the weights to each node.

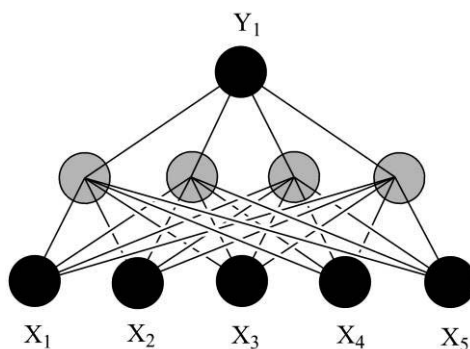


Figure 13-6 Illustration of a simple neural network consisting of five input nodes (X_1 through X_5), four hidden nodes (shaded circles), and a single output node (Y_1).

Each node beyond the input layer takes as its input a linear combination of the outputs. For example, the input to some i th node in the hidden layer, I_i , can be written as

$$I_i = \sum_j w_{ij} X_j + \theta_i \quad (13.34)$$

where X_j is the output of the j th node, θ_i is a parameter termed the *bias*, w_{ij} is the connection weight between the nodes, and the summation is over all the nodes in the previous layer. Weights can have positive or negative values. The calculated input is then transformed to calculate the output of the nodes. A common transform function is an S-shaped sigmoid function such as

$$y(x) = -\frac{a}{c[1 - \exp(-bx)]}. \quad (13.35)$$

Radial and threshold transfer functions also have been used. Weights are iteratively changed in proportion to the differences between the obtained outputs and target values in the training set. A set of input and known output values constitutes a training set for the network whereby the connection weights and biases are adjusted to minimize the prediction error. While several neural-network configurations are possible, a commonly used approach is the back-propagation neural network (BPNN). There are at least three hierarchical layers of neural nodes in a BPNN—an input layer, a middle or hidden layer, and an output layer as illustrated in Figure 13-6. In this configuration, each layer is fully connected to the next layer. The number of nodes in the hidden layer can be adjusted depending upon the complexity of the problem and the size of the input information.

Traditional applications of ANNs include speech recognition and synthesis, pattern recognition, market forecasting, process modeling, and property prediction. The last two have significant applications in polymer science and technology and include the design of compression molding, blow molding, and injection molding and such diverse property predictions as density, permeability, solvent activity, the compressibility factor, phase equilibria, permeability, dielectric dissipation factor, lower critical solution temperatures, estimation of kinetic rate constants in metallocene polymerization, and failure prediction of composites. ANNs have also been combined with topological indices to predict polymer properties [23]. An example [24] of the application of ANNs to predict polymer T_g is discussed next.

Prediction of T_g . As discussed earlier, group-contribution methods can be used with good success but only if the specific chemical groups of the target polymer are available in the correlation. There have been a number of approaches using different polymer descriptors, typically obtained from computational chemistry cal-

culations. One recent example [24] is the prediction of T_g using molecular descriptors obtained from density functional theory (DFT) calculations. Descriptors include total energy, C_v , molecular average polarizability, the energy of the highest occupied molecular orbital, and entropy. Experimental T_g values for a total of 113 polyacrylates and polystyrenes were used for this study. From these, 58 polyacrylates were selected for training a three-layer BPNN. The 23 polyacrylates and 32 polystyrenes were used to evaluate the performance of the neural network. In Figure 13-7, results are presented in a plot of calculated versus experimental T_g values. As illustrated, agreement is good. Specifically, the root-mean-square error for the prediction set was 17 K.

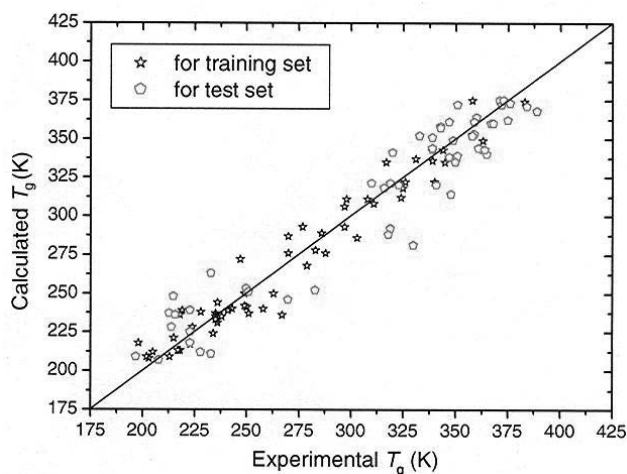


Figure 13-7 Plot of calculated versus experimental T_g obtained by using an ANN of chemical descriptors. Reproduced from W. Liu and C. Cao, *Artificial Neural Network Prediction of the Glass Transition Temperature of Polymers*. Colloid and Polymer Science, 2009. **287**: p. 811–818. Copyright 2009 Springer-Verlag.

A comparison of different methods for prediction of T_g of a polyacrylate and a polystyrene common to published group-contribution [2], graft theory [4], and ANN [24] methods is given in Table 13-10. As shown, no method is uniformly successful as is illustrated in the case of the poly(nonyl acrylate), where the best prediction is graph theory, and in the case of poly(4-*sec*-butylstyrene), where the ANN gives the best result. ANN has the advantage that prior parameterization is not necessary; however, obtaining computational data for repeat units is a time-consuming process. The T_g can also be obtained from molecular dynamics simulations as discussed in Section 13.4.3; however, this too is very time-consuming and requires a robust mo-

molecular force field that has been parameterized for the functional groups present in the polymer under study.

Table 13-10 Comparison of Experimental T_g with Values Predicted by ANN, Graph Theory, and Group-Contribution Methods

Polymer	Exp. T_g (K)	ANN [24]	Graph Theory [4]	Group Contribution [2]
Poly(nonyl acrylate)	215	248	220	204
Poly(4- <i>sec</i> -butylstyrene)	359	361	352	344

13.4 Molecular Simulations

Computational (quantum) chemistry provides approximate solutions to the Schrödinger wave equation from which molecular geometries and energies can be obtained. These are called *ab initio* methods. A related approach is density functional theory (DFT). Both approaches require significant computer time and are useful only in the study of small molecules and molecular clusters. In the case of large molecules such as biomolecules or polymers, molecular dynamics (MD) can be used to determine physical, mechanical, and transport properties, including density, self-diffusion coefficients, modulus, phase-equilibrium behavior, X-ray and neutron diffraction spectra, and glass-transition temperatures. Another approach is the use of stochastic methods* such as Monte Carlo (MC) simulations that provide a probabilistic description of events. Monte Carlo techniques represent a statistical sampling process that can be applied to a system with a large number of particles or to explore molecular structure over long time scales or to sample a large region of computational space. MC calculations can be used to determine phase equilibrium and sorption isotherms. Using robust molecular force fields parameterized for polymers as described in the following section, polymer properties can be obtained with considerable accuracy and reliability using MD or MC simulations.

Early MD applications used both atomistic and united-atom (UA) simulations. As illustrated in Figure 13-8, each atom is treated individually in the parameterization and dynamics calculation in atomistic simulations. In UA simulations (Figure 13-8), hydrogen atoms are united with a “heavy” atom such as carbon to form a single species that is separately parameterized. Combined with a simple force field as described in Section 13.4.1, the use of a UA representation reduces the simulation

* A stochastic variable is one that does not depend in a completely definite way upon the independent variable but is subject to random effects that can only be defined in statistical terms.

(CPU) time with some loss in the quality of the results. UA representations have been used in the simulation of large biological systems such as proteins. A related approach that is becoming an important tool in the simulation of both biological and polymeric systems is the use of *coarse-grained* (CG) [25, 26] representation of molecular systems where a chemical grouping such as a methylene linkage or an aromatic ring is represented by one or more CG “beads” as illustrated in Figure 13-9. Force field parameterization for CG systems is much more challenging and more specific to a particular protein or polymer than in atomistic or UA simulations but can greatly accelerate dynamics time and, therefore, extend the temporal and spatial range that can be studied. Specific applications where CG simulations can be useful include simulations of self-assembly of surfactants and block copolymers. CG simulations are beyond the scope of the introductory treatment of molecular simulations given in this chapter and, therefore, the reader is encouraged to consult the excellent journal articles and books [27] in this area. A brief discussion of important CG force fields is given at the end of Section 13.4.1.

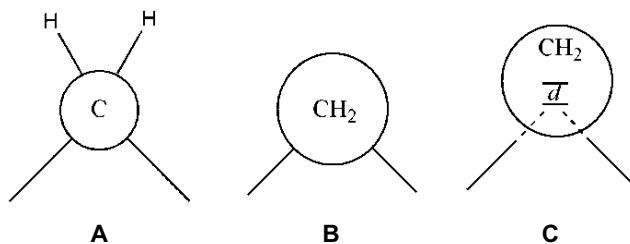


Figure 13-8 Comparison of different atomic representations of a methylene repeat unit. **(A)** Atomistic atom; **(B)** united atom (UA); and **(C)** anisotropic united atom (AUA). In the case of AUA, the parameter d represents the offset of the effective non-bonded center from the atomic center of the carbon atom. UA representation with this adjustable offset was used to improve the quality of UA simulations.

Monte Carlo Simulations. The use of Monte Carlo methods received significant impetus with the development of digital computers in the late 1940s. The most important application of Monte Carlo techniques utilizes statistical sampling procedures, principally the Metropolis or the Monte Carlo Markov chain (MCMC) method [28]. Important applications for Monte Carlo methods in polymer science include the simulation of phase equilibrium and also sorption isotherms as illustrated in Section 13.5.8.

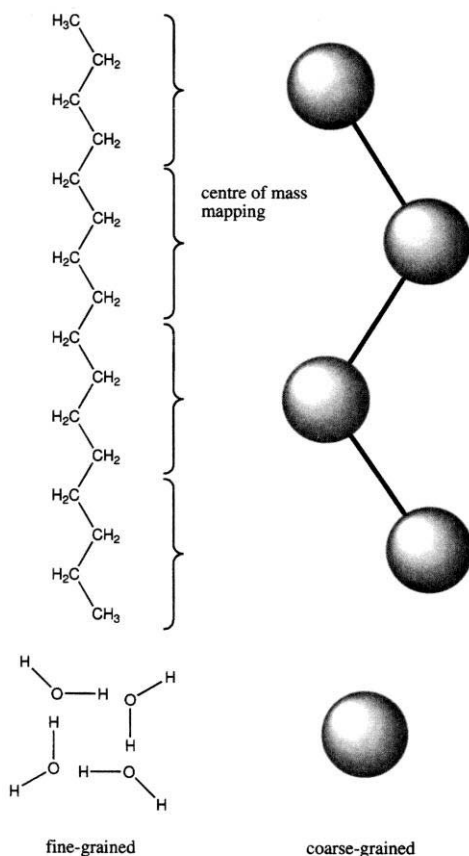


Figure 13-9 Comparison between atomistic (left-hand side) and CG representations of polyethylene and water (right-hand side). In the case of PE, three methylene groups are replaced by a single CG bead while a cluster of three water molecules is represented by one CG bead. Reproduced from M. Christen, and W. F. van Gunsteren, *Multigraining: An Algorithm for Simultaneous Fine-Grained and Coarse-Grained Simulation of Molecular Systems*. *Journal of Chemical Physics*, 2006, **124**(15): p. 154106.

13.4.1 Molecular Mechanics Force Fields

The success of such MD and MC methods depends upon the quality of a force field that describes the potential energy, U , of the molecular system as the sum of all bonded (U^B) and non-bonded (U^{NB}) terms as

$$U(\mathbf{r}) = U^{\text{B}}(\mathbf{r}) + U^{\text{NB}}(\mathbf{r}). \quad (13.36)$$

The bonded terms include potential energy contributions from bond-stretching, angle-bending, and dihedral (or torsional) contributions as

$$V^{\text{B}}(r) = \sum_{\text{bonds}} V^{\text{bond}}(r_{ij}) + \sum_{\text{bends}} V^{\text{bend}}(\theta_{ijk}) + \sum_{\text{dihedral}} V^{\text{tors}}(\phi_{ijkl}) \quad (13.37)$$

where r_{ij} is the distance between two consecutive bonded atoms i and j , θ_{ijk} is the valence angle between three consecutive atoms i, j, k , and ϕ_{ijkl} is the torsional (dihedral) angle between four consecutive atoms i, j, k, l . Each summation is made over all contiguous atoms constituting bonds (i.e., two-body interactions), angles (i.e., three-body interactions), and torsions (i.e., four-body interactions) in the system. Non-bonded terms typically include steric (i.e., Lennard-Jones or LJ) and electrostatic (i.e., Coulombic) terms. Schematic representations of the bonded (i.e., bond-stretching, angle-bending, and torsion or dihedral) and non-bonded (i.e., LJ and Coulombic) contributions to the potential energy of a molecular systems are shown in Figure 13-10.

Force field parameters for each bonded or non-bonded term are obtained by fitting potential energy terms to potentials of small molecules calculated by *ab initio* or DFT methods or by fitting to experimental data such as crystal structure and the heat of vaporization (ΔH_v) for low-molecular-weight compounds. Examples of *bonded* contributions include simple harmonic functions for bond stretching

$$U^{\text{bond}}(r_{ij}) = \frac{1}{2} \sum_{\text{bonds}} k_{ij}^{\text{bond}} (r_{ij} - r_{ij}^{\circ})^2 \quad (13.38)$$

where k_{ij}^{bond} is the bond-stretching parameter and r_{ij}° is the equilibrium bond distance (for which the potential energy contribution is zero). Among alternative forms for the bond-stretching term is the *quartic* expression used in modern force fields

$$U^{\text{bond}}(r_{ij}) = \frac{1}{2} \sum_{\text{bonds}} \left[k_2 (r_{ij} - r_{ij}^{\circ})^2 + k_3 (r_{ij} - r_{ij}^{\circ})^3 + k_4 (r_{ij} - r_{ij}^{\circ})^4 \right] \quad (13.39)$$

where k_2 , k_3 , and k_4 are parameters for individual i - j atom pairs forming covalent bonds. Similar harmonic and quartic terms have been used for angle bending. Torsional contributions to the bonded potential include the form

$$U^{\text{tors}}(\phi_{ijkl}) = \frac{1}{2} \sum_{\text{dihedrals}} \sum_{n=1,2,\dots} k_{ijkl}^{\text{tors}}(n) [1 - \cos(n\phi_{ijkl})] \quad (13.40)$$

where n is the periodicity of the torsional motion and the summation is over all torsional angles for each periodicity. Other forms of torsional terms are available including terms for out-of-plane bending for co-planar structures as illustrated in Figure 13-10.

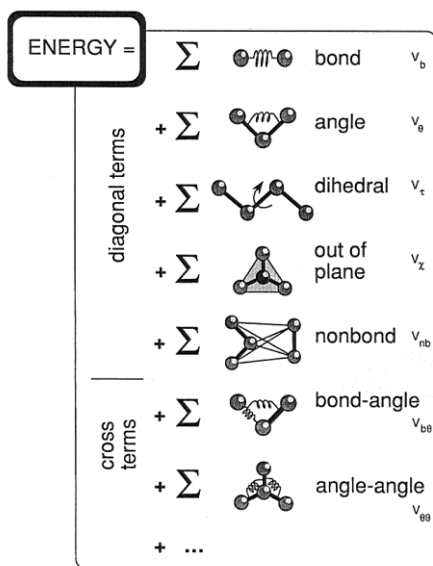


Figure 13-10 Model representation of atoms participating in potential terms found in a typical molecular force field. Diagonal terms refer to interactions that can be expressed as a function of single internal coordinates such as bond stretching or angle bending. Cross-terms represent coupled interactions involving two or more coordinates such as interactions between atoms participating simultaneously in bond stretching and angle bending. Reproduced from U. Dinur and A. T. Hagler, *New Approaches to Empirical Force Field*, in *Reviews in Computational Chemistry*, K. B. Lipkowitz and B. D. Boyd, eds. 1991, New York: VCH Publishers, Inc., p. 99–164. Reprinted by permission of John Wiley & Sons.

Cross-coupling terms are used in many force fields to represent the interrelationship between one type of deformation and another such as between bond stretching and torsional rotation and between bond stretching and angle bending as quantified in eq. (13.41).

$$U^{b,b}(r_{ij}, \theta_{ijk}) = \frac{1}{2} \sum_{\text{bonds}} \sum_{\text{bends}} k^{b,b} (r_{ij} - r_{ij}^o)^2 (\theta_{ijk} - \theta_{ijk}^o)^2 \quad (13.41)$$

Non-bonded terms include intramolecular interactions between pairs of atoms separated by three or more bonds and those belonging to different molecules (i.e., intermolecular interactions). Interactions between pairs of atoms separated by one or two bonds are contained in the bonded energy terms of the bond-stretch and angle-bending terms, respectively. All interactions in a simulation system may be included (i.e., Ewald [31] summation) or distance cutoffs (typically in the range from 8 to 12 Å) may be used. Examples of non-bonded terms include Lennard-Jones (LJ) potential (e.g., LJ 6–12) or the LJ 6–9 potential given as

$$U^{\text{LJ}} = \sum_{i \neq j} \varepsilon_{ij} \left[2 \left(\frac{r_{ij}^0}{r_{ij}} \right)^9 - 3 \left(\frac{r_{ij}^0}{r_{ij}} \right)^6 \right] \quad (13.42)$$

In this case, the sixth order term represents dispersion (i.e., long-range) interactions and the ninth (or twelve) order term represents short-range repulsion. As illustrated by Figure 13-11, the parameters ε_{ij} and r_{ij}^0 appearing in eq. (13.42) are the depth and the distance at the minimum energy of the LJ potential energy function, respectively.

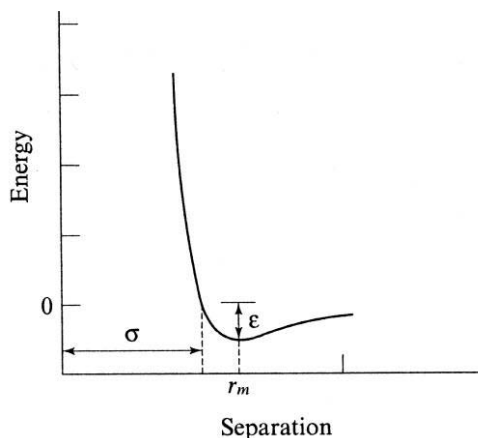


Figure 13-11 The Lennard-Jones potential showing the depth of the potential energy well, ε . Reproduced from A. R. Leach, *Molecular Modelling: Principles and Applications*. 2nd ed. 2001, Upper Saddle River: Prentice Hall.

The other non-bonded contribution is the electrostatic potential represented by a Coulombic expression such as

$$U^{\text{es}} = \sum_{i \neq j} \frac{f q_i q_j}{r_{ij}} \quad (13.43)$$

where q_i represents the charge on atom i of the atom pair $i-j$, r_{ij} is the separation between atoms i and j , and $f = 1/\pi\epsilon_0$ where ϵ_0 is the dielectric constant of the medium.

Force fields can be relatively simple with parameterization suitable for a wide number of different molecular structures. While not as robust as more complete force fields, parameterization of these generic force fields can be easily customized for specific polymers. An example is the DREIDING force field [32] that has been used for molecular simulation of a number of different polymers [33]. DREIDING uses a simple harmonic bond-stretching term eq. (13.38) and a harmonic cosine form of the angle-bending term given by eq. (13.44):

$$U^{\text{bend}}(\theta_{ijk}) = \frac{1}{2} \sum_{\text{bends}} k_{ijk}^{\text{bend}} (\cos \theta_{ijk} - \cos \theta_{ijk}^0)^2. \quad (13.44)$$

As reviewed in detail in another publication [33], additional force fields that have been used in the molecular simulations of polymers include GROMOS* [34], CVFF† [35], PCFF,‡ and COMPASS§ [36]. COMPASS is a robust “Class II” force field that is based upon PCFF and makes extensive use of both anharmonic and cross-coupling terms. Parameterization uses results of *ab initio* calculations of small molecules and condensed-phase experimental properties as is the case for its predecessors CVFF and PCFF. The functional form of COMPASS includes quartic expressions for the bond-stretching and angle-bending terms, four cross-coupling terms, and an LJ 9–6 potential. *Parameterization of COMPASS is especially suited for a wide variety of polymer structures [37].*

Reactive Force Fields. Traditional force fields for MD simulations are unable to model chemical reactions due to their inability to accommodate bond breaking and making. In order to extend the capability of traditional molecular mechanics force fields to chemical events, several reactive force fields have been developed. These include the use of partial bond orders to modify the reactive potential energy surface. One of these is MD_REACT, which has been used to model the thermal degradation of polymers [38, 39]. A more recent approach is ReaxFF [40], which has been used to model the thermal decomposition of polydimethylsiloxane [41] as an example.

CG Force Fields. Several force fields have been used for CG simulations. These include the generic MARTINI [42–44] and the Shinoda [45] force field de-

* GROMINGEN MOLECULAR SIMULATION.

† CONSISTENT VALENCE FORCE FIELD.

‡ POLYMER CONSISTENT FORCE FIELD.

§ CONDENSED-PHASE OPTIMIZED MOLECULAR POTENTIALS FOR ATOMISTIC SIMULATION STUDIES.

veloped to simulate the self-assembly of surfactants, a computationally expensive simulation for fully atomistic simulation. In the case of the MARTINI force field, there is a four-to-one mapping whereby four heavy atoms (excluding hydrogen) are represented by a single interaction center with the exception of ring molecules where there is a two-to-one mapping (e.g., benzene is represented by six beads). In the case of water, four molecules are represented by a single bead. CG force fields can be parameterized and validated from atomistic simulations and experimental data such as pair-correlation functions as discussed in Section 13.5.4. In the case of the MARTINI force field, the *bonded* contribution to the potential energy between connected CG sites includes harmonic bond and dihedral angle terms, which in its simplest form is given as

$$U^B = \frac{1}{2} K_{\text{bond}} (R - R_{\text{bond}})^2 + \frac{1}{2} K_{\text{angle}} [\cos(\theta) - \cos(\theta_0)]^2 \quad (13.45)$$

where K_{bond} and K_{angle} are force constants ($1250 \text{ kJ mol}^{-1} \text{ nm}^{-2}$ and $25 \text{ kJ mol}^{-1} \text{ rad}^{-2}$, respectively), R_{bond} is the equilibrium distance (0.47 nm), and θ_0 is the equilibrium bond angle (180°). The non-bonded contributions include a LJ 6–12 steric potential and a Coulombic electrostatic potential function.

13.4.2 Molecular Dynamics and Monte Carlo Methods

As mentioned earlier, the two principal approaches used in molecular simulations are molecular dynamics (MD) and Monte Carlo (MC) methods. MD methods were used for the first time in the 1970s for molecular simulation of proteins. In MD simulations, an initial position and velocity are assigned for each atom. Forces acting on each atom are then calculated from the potential energy function given by the molecular force field as described in the previous section, and new positions and velocities are calculated at the end of a very small time step, typically a femto-second (10^{-15} s).

In the case of MD simulations, the time step should be at least one order of magnitude smaller than the shortest periodic motion in the system. For example, the shortest periodic motions are stretching vibrations of hydrogen bonds (e.g., C–H and N–H stretching) that fall in the order of ca. 10^{-14} s^{-1} in frequency. This small time step has significant consequences in terms of the computer time required for the simulation of real molecular processes since calculation of 1000 time steps provides only 1 ps of simulation time and 1 million time steps only 1 ns! If it takes 1 sec to compute one dynamics step, then a 1-ns simulation will take 278 h (ca. 12 days) of CPU time. The relatively “large” time scales of natural events such as fluid flow, phase separation, the diffusion of large molecules, and the conformational

folding of even the smallest proteins can extend to milliseconds, which makes atomistic simulation of such events impractical even on the largest computer platforms. As the simulation system increases in size, a single MD step takes greater CPU time following an N^2 rule where N represents the number of atoms in the simulation system. Simulations of systems containing 100,000 or even 1 million atoms are not uncommon. For simulation of such “large” systems and for long simulation times (e.g., >10 ns), non-atomistic approaches such as coarse-grained and dissipative particle dynamics can be used to shorten computer time; but expansion of the simulation time–size scale is achieved at the expense of molecular detail.

Positions within a Cartesian coordinate system may be determined as a function of time from the molecular mechanics potential-energy function (see Section 13.4.1) simply through Newton’s law of motion written in the form

$$F = \frac{dp}{dt} (= ma) \quad (13.46)$$

where F is force, p is momentum ($p = mv$), m is mass, and a is acceleration. Since F is the negative derivative (i.e., the gradient*) of the potential energy, U , while a is obtained as the second derivative of the atomic positions (x_i) with respect to time, we can write for Cartesian coordinates the following form of eq. (13.46):

$$m\ddot{x}_i = -\nabla U_i. \quad (13.47)$$

Equation (13.47) can be numerically integrated with respect to time to find the trajectory (i.e., x_i) of each atom in the system as a function of time. Forces are computed by calculating an analytical derivative over some small time interval or *time step*. At the end of this interval, a new set of coordinates and velocities is obtained. Algorithms include the standard Verlet derivation [46] and the leapfrog algorithm [47]. Two commonly used algorithms for integrating the equations of motion with internal constraints such as fixing specific bond lengths and angles are called SHAKE [48] and RATTLE [49]. These have the advantage of saving computational time by allowing larger time steps (e.g., 2 fs) when performing MD simulations of systems containing large molecules such as proteins and polymers.

Periodic Boundary Conditions. In the simulation of liquids, solutions, and solids, periodic boundary conditions are used to minimize boundary effects associated

* The gradient of the potential energy is given as

$$\nabla V_i = \frac{\partial V}{\partial x_1} + \frac{\partial V}{\partial x_2} + \frac{\partial V}{\partial x_3}.$$

with small simulation cells (often only 30 to 40 Å along a side). The size of the cell strongly affects the computer time required for a given period of dynamics. In fact, simulation time is directly related to the square of the number of atoms in the system if no cutoff is used. Under periodic conditions, a simulation box, typically a cube or orthorhombus, is virtually surrounded by an infinite number of identical cells as shown in Figure 13-12. Macroscopic systems such as a solution or crystalline solid can be simulated by constructing a unit cell with periodic boundary conditions. Properties that can be obtained from simulation include estimation of transport properties such as the diffusion coefficient. The use of periodic conditions is most appropriate in the case of crystalline systems that have ordered, periodic structures. In the case of amorphous systems such as solutions or liquids, periodicity can be an artifact affecting simulation results if sufficient care is not exercised in the specification of the size of the periodic box.

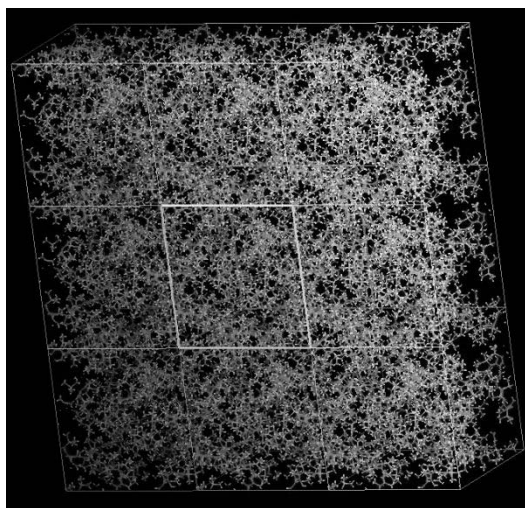


Figure 13-12 Illustration of an amorphous periodic cell containing a polymer chain surrounded by eight identical cells in a periodic structure.

Ensembles. In a molecular simulation, the number of particles and the temperature, pressure, energy, or volume can be held constant. Which variables are held constant and which are allowed to vary define the ensemble. The choice of a particular ensemble is dictated by the property that is the target of the simulation. An example is the *microcanonical* or *NVE* ensemble where *N* indicates that the number of atoms is held constant as are volume and total energy. In the case of the *canonical* or *NVT* ensemble, energy is exchanged with a heat bath in order to maintain a constant (thermodynamic) temperature at constant volume. This ensemble is useful to sample conformational space because energy can be taken from the heat bath to

overcome rotational barriers as well as to calculate diffusion coefficients. Common thermostats used to control temperature include the Nosé [50], Hoover [51], Andersen [52], and Berendsen [53] methods. A third commonly used ensemble is the isothermal–isobaric or *NPT* ensemble where both pressure and temperature are held constant. Berendsen [53] or Andersen [52] *barostats* are often used for *NPT* dynamics. They are also used to obtain density at a fixed temperature or pressure. A fourth ensemble is the *grand canonical* (μVT) for which chemical potential (μ), volume, and temperature are held constant in the simulation. Grand canonical Monte Carlo (GCMC) simulations are used for the simulation of sorption isotherms in zeolites and polymers as will be discussed in Section 13.5.8.

13.5 Applications of Molecular Simulations

Once a fully equilibrated cell is obtained, typically through a series of NVT and NPT dynamics, the simulation cell can be analyzed to provide a number of important properties. As illustrated in the following sections, these include PVT data such as density and thermal-expansion coefficients, X-ray and neutron-scattering spectra, thermal transition temperatures, permeability, modulus, phase behavior, adsorption isotherms, solubility parameters, and the pair-correlation function (PCF), which can be used to identify polymer interactions such as hydrogen bonding in polyamides. When available, experimental data can be used to validate a particular force field for use with a particular class of polymers.

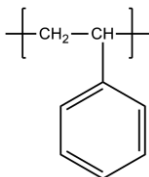
13.5.1 PVT Simulation

PVT data can be obtained from NPT dynamics where the pressure and temperature are held constant and the final volume of a cell is obtained after equilibration. For this purpose, a good thermostat (e.g., Andersen [52]) and barostat (e.g., Berendsen [53]) are required to control temperature and pressure, respectively. Pressure control is the more difficult to control closely, especially when the periodic cells are small. Fortunately, pressure has only a small influence on condensed-phase properties. Results of the analysis of NPT dynamics of an amorphous cell of atactic polystyrene are illustrated in Example 13.7.*

* Example problems shown in this section can be solved by using different force fields and a number of freeware and commercial programs such as Materials Studio (Accelrys, San Diego, CA).

Example 13.7

Using MD solutions, determine the density and solubility parameters of polystyrene (PS) at 298 K.



Solution

For this simulation, the COMPASS force field was selected. Two amorphous cells of PS were constructed. One cell contained a single PS chain having 80 repeat units (RUs) and the other cell contained two PC chains each having 80 RUs. The cell was equilibrated using 25-ps NVT dynamics at 298 K followed by sequential NPT dynamics of 25 ps, 225 ps, and 250 ps, giving a total of 500-ps NPT dynamics. The Andersen [52] thermostat and Berendsen [53] barostat were used for temperature and pressure control, respectively. Ewald [31] summation was used for all non-bonded interactions.

Ball-and-stick and space-filling (CPK) representations of the smaller amorphous cell (one 80-RU chain) are shown in Figure 13-13. Results of simulation values of density for amorphous cells of two different sizes are shown in Table 13-11. As shown, equilibrium values of density appear to be achieved within 250-ps dynamics. The difference in densities between the small cell (23.9 Å on a side) and large cell (30.0 Å on a side) is only about 2% while the computational time for the larger cell is about twice that for the smaller cell. The density of the larger cell averaged over the final 250 ps of NPT dynamics is 1.023 g cm⁻³ (s.d. = 0.007). This value is in reasonable agreement with experimental densities of amorphous PS that have been reported in the range between 1.04 and 1.065 g cm⁻³ [5]. It is possible that using a larger amorphous cell will give even better agreement with experimental data although computational time will significantly increase.

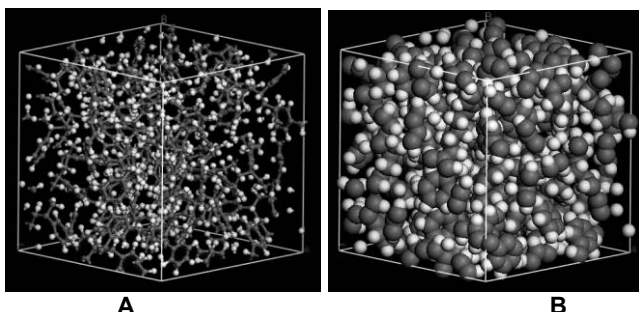


Figure 13-13 Amorphous cell of single PS chain after 500-ps NPT dynamics. **A.** Ball-and-stick representation; **B.** CPK (space-filling) representation (carbon atoms are shown as dark gray spheres).

Table 13–11 Average Densities Obtained from NPT Dynamics of PS Amorphous Cells at 25°C

Avg. Density (g cm ⁻³)	25-ps NPT	250-ps NPT	500-ps NPT
Avg. (s.d.), one chain (80-RU)	0.985 (0.008)	1.001 (0.009)	1.001 (0.009) ^a
Avg. (s.d.), two chains (80-RU)	0.974 (0.007)	1.015 (0.018)	1.023 (0.007) ^b

13.5.2 Cohesive Energy Density and the Solubility Parameter

Cohesive energy density (CED) is another property that can be obtained from MD simulations and used to calculate the solubility parameter (see Sections 3.2.6 and 13.1.4) of a simple liquid or a polymer. Specifically, the CED is obtained by subtracting the average (i.e., intramolecular) energies of the individual molecules in an amorphous cell from the average energy of the total cell and then dividing by the cell volume. The heat of vaporization (ΔH_{vap}) from this energy difference between that of a periodic cell, E_{cell} , and the summation of the energy of the individual molecules, E_i , in the cell is expressed by the equation

$$\Delta H_{\text{vap}} = \left\langle E_{\text{cell}} - \sum_{i=1}^n E_i \right\rangle_p + RT \quad (13.48)$$

where R is the ideal gas constant. Energies are summed over the total number of molecules in the system, n . The brackets indicate that the difference between E_{cell} and E_i is averaged for all ensembles at constant pressure. This average is the *cohesive energy* (E^{coh}). The ΔH_{vap} obtained from simulation on the basis of eq. (13.48) can be compared to the experimental value for small molecules as a method of validating the force field.

The solubility parameter, δ , can be calculated from E^{coh} using the following:

$$\delta = \sqrt{E^{\text{coh}}} = \sqrt{\frac{E}{V}}. \quad (13.49)$$

In this way, simulation provides the opportunity to obtain solubility parameters for polymers for which (1) experimental values are not available and (2) group contributions cannot be used due to the absence of the required group-contribution parameters. As a further validation of the force field, solubility parameters obtained from molecular simulations can be compared with both experimental values (Section 3.2.6) and/or values obtained from group-contribution methods (Section 13.1.4) or topological indices (Section 13.2). As an illustration, the solubility parameter obtained for the larger amorphous cell of polystyrene in Example 13.7 is determined

from simulation to be $13.6 \text{ (J/cm}^3\text{)}^{1/2}$ (s.d. = 0.035) or $13.6 \text{ MPa}^{1/2}$ (averaged over the final 250 ps of NPT dynamics). Experimental values fall within the range of 15.6 to 21.1 $\text{(MPa)}^{1/2}$ [5].

13.5.3 Glass-Transition Temperature

Since density can be obtained from NPT dynamics as described in the previous section, densities obtained at different temperatures and a fixed pressure can be plotted as a function of temperature to obtain the glass-transition temperature (T_g), in a similar fashion to the experimental technique of dilatometry (Section 4.3.2). Values of specific volume ($1/\rho$) calculated from NPT densities obtained for a polyphosphazene (see Section 2.4.2) are plotted against temperature in Figure 13-14. In this example, the T_g corresponding to the intersection of lines obtained from least-square fit of simulation data above and below the T_g is 212 K compared to 198 K from DSC measurements. The use of simulations to determine T_g have been reported for a variety of polymers including polyphosphazenes [54], polysilanes [55], polyethylene [56], polypropylene [56], polyisobutylene [56], polydimethylsiloxane [56], polyoxymethylene [56], and poly(L-lactide) [57] using a variety of force fields. In general, T_g values obtained from NPT dynamics are very similar to values obtained from DSC measurements as shown in Table 13-12.

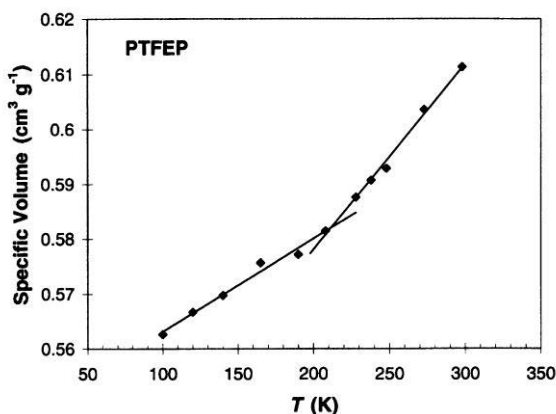


Figure 13-14 Plot of specific volume of a polyphosphazene, poly[bis(2,2,2-trifluoroethoxy)phosphazene], against temperature. As shown by the intersection of the two lines, the T_g is 212 K compared to 198 K from DSC results. Reproduced from J. R. Fried and P. Ren, *Molecular Simulation of Polyphosphazenes*. Computational and Theoretical Polymer Science, 1999, **9**: p. 111–166.

Like dilatometry, NPT dynamics can be very time-consuming to get a statistically sufficient number of data points. Advantages of this approach are that T_g can be obtained for synthetic polymers that decompose at temperatures below T_g and for polymers that have not yet been synthesized. As an additional benefit, thermal-expansion coefficients (α) above and below T_g can be obtained from these plots. In addition, comparison between simulated and experimental values of T_g can be used as a validation of the molecular force field selected for the simulation.

Table 13-12 Comparison of Experimental Density and T_g for a Variety of Different Polymers with Values Obtained from NPT Dynamics

Polymer	Density (g cm ⁻³)		T_g (K)		Ref.
	Exp.	Sim.	Exp.	Sim.	
Poly[bis(<i>n</i> -butoxy)phosphazene]	1.047	1.005	165	162	[54]
Poly[bis(<i>iso</i> -butoxy)phosphazene]	1.055	1.016	178	178	[54]
Poly[bis(<i>sec</i> -butoxy)phosphazene]	1.104	1.077	182	159	[54]
Poly[bis(2,2,2-trifluoroethoxy)phosphazene]	1.71 ^a	1.633 ^b	198	212 ^b	[54]
Poly(di- <i>n</i> -hexylsilane)	0.971	0.955	221	213	[55]
Poly(propylmethylsilane)	1.047	1.051	245	223–273	[55]
Poly(trifluoropropylmethylsilane)	0.913	0.917	270	266–290	[55]
Polyethylene	0.85	0.868	155, 252	178 ^b	[56]
Polyisobutylene	0.88	0.872	200	192	[56]
Polypropylene	0.85	0.767	259	248 ^b	[56]
Polydimethylsiloxane	0.98	0.995	150, 146	181	[56]
Polyoxymethylene	1.25	1.312	190	191 ^b	[56]

^a.60% crystallinity.

^b amorphous.

13.5.4 Pair Correlations

The pair-correlation function (PCF) or radial distribution function (RDF), $g(r)$, is an extremely useful tool for structural analysis and can provide important information concerning molecular packing, ordering behavior, compressibility, and phase transitions. The PCF can be obtained from experimental studies (e.g., neutron scattering) but also can be conveniently obtained from MD simulations. Plots of specific PCFs, such as the intramolecular and intermolecular PCF between oxygen and hydrogen atoms in water versus atomic distance obtained from simulations, can be directly compared to those obtained from experimental data. Such a comparison provides an excellent basis to validate a force field for a particular system.

Pair-correlation functions provide spherically averaged distributions of interatomic vector lengths. A three-dimensional Fourier transform of the PCF will give the *structure factor* from which X-ray, neutron, and electron diffraction distributions can be predicted and compared with experimental data. In the X-ray diffraction pattern, the first peak in the intermolecular part of the PCF between skeletal atoms gives a direct measure of the average distance between chain backbones in the amorphous bulk.

Calculations can include all the atoms in the model or they can be restricted to comparisons between atoms in two selected groups. The atom pairs included in the calculations can also be restructured to specific elements or force field types. This allows the calculation of the structure factor for each atom in the model; each can then be weighed appropriately before making comparisons with X-ray diffraction data. Calculations can be done using trajectory file data or the coordinates of the current model; however, the trajectory file data allow averaging over multiple frames giving statistically more reliable results.

An example of an application of the insight that PCF calculations can provide is the nature of interactions of CO₂ with fluorinated polymers. This results in high selectivity for CO₂ membrane separations. One polymer that has been considered for this application is poly[bis(2,2,2-trifluoroethoxy)phosphazene] (PTFEP), mentioned in the previous section, whose repeat unit structure is shown in Figure 13-15. The PCFs between CO₂ and the backbone atoms of P and N and with O, CH₂, and CF₃ of the trifluoroethoxy-substituent group of PTFEP were determined using the COMPASS force field parameterized for phosphazenes [37]. In this study [58], PCFs were calculated from an amorphous cell containing four CO₂ molecules and a single chain of 120 repeat units and equilibrated with 2-ns NVT dynamics followed by 1.5-ns NPT dynamics. The PCF was calculated from the relationship

$$g_i(r) = \frac{N_i(r)}{\rho_i N_{\text{CO}_2} N_S 4\pi r^2 dr} \quad (13.50)$$

where $N_i(r)$ represents the number of atoms of type i in a spherical shell contained between r and $r + dr$, ρ_i is the bulk density of atoms of type i in PTFEP, N_S is the total number of frames used for the analysis, and N_{CO_2} is the number of CO₂ molecules. As shown, there is a strong peak near 4.3 Å representing an interaction between CO₂ and CF₃. At greater distances, the PCF reaches a limiting value of unity. These results were shown to agree very closely with the conclusions obtained from *ab initio* computational chemistry calculations of CO₂ with trifluoroethane as a model compound. This comparison provides a very good validation of molecular simulation methods.

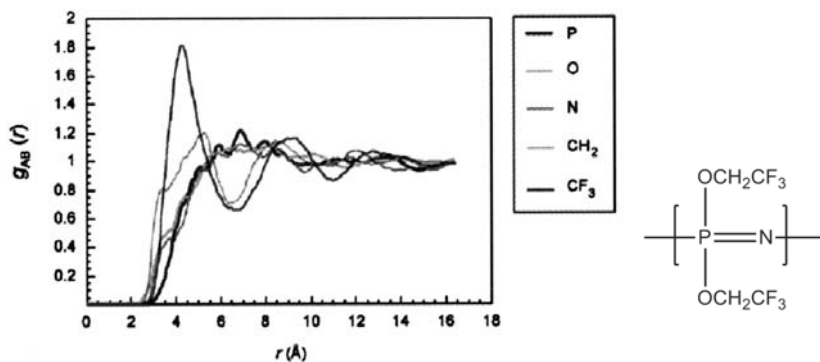


Figure 13-15 Plot of the pair-correlation function, $g_{AB}(r)$, versus the separation distance, $r(\text{\AA})$, between CO_2 and the phosphorus and nitrogen atoms along the chain backbone and between CO_2 and the oxygen atoms, methylene chain groups of the trifluoroethoxy side chains of poly[bis(2,2,2-trifluoroethoxy)phosphazene] (PTFEP). Reproduced from J. R. Fried and N. Hu, *The Molecular Basis of CO_2 Interaction with Polymers Containing Fluorinated Groups; Computational Chemistry of Model Compounds and Molecular Simulation of Poly[bis(2,2,2-trifluoroethoxy)-phosphazene]*. Polymer, 2003. **44**: p. 4363–4372.

13.5.5 Time-Correlation Coefficients

One advantage of molecular dynamics over Monte Carlo methods is the ability to calculate time-dependent properties in the form of time-correlation coefficients. An important example is the *velocity autocorrelation function* (VACF) defined as

$$C(m) = \frac{1}{n} \sum_{i=1}^n v(m+1)v(i) \quad (13.51)$$

where m is the maximum number of points allowed for the VACF calculation, n is the number of data points used for averaging, and i is the step counter (i.e., increment). A Fourier transform of the VACF gives the power spectrum useful for predicting vibrational properties such as thermal effects on IR or Raman spectra. The VAC also can be used to determine the self-diffusion coefficient as shown in Section 13.5.5.

Another time-correlation function is the *vectorial* or orientational autocorrelation function defined as [59]

$$m(t) = \langle \mathbf{u}(0) \cdot \mathbf{u}(t) \rangle \quad (13.52)$$

where $\mathbf{u}(t)$ is a vector characterizing the orientation of a polymer backbone or side chain at a given time, t . Using polyphosphazene as a further example, a main-chain vector was defined as one originating from the phosphorus $P(i)$ atom at position i along the backbone to the adjacent nitrogen atom, $N(i+1)$ in the sequence $P(i)-N(i)-P(i+1)-N(i+1)$. In Figure 13-16, the main-chain vectorial autocorrelation functions are plotted versus time for three polyphosphazenes—poly[bis(*n*-butoxy)phosphazene] (PnBuP), poly[bis(*iso*-butoxy)phosphazene] (PiBuP), and poly[bis(*sec*-butoxy)phosphazene] (PsBuP). A value of unity for the vectorial autocorrelation function indicates a totally rigid backbone chain while decreasing values indicate increasing flexibility. As shown, the most sterically hindered side chains result in the highest backbone rigidity as reflected by the following order of decreasing rigidity: PiBuP>PsBUP>PnBuP.

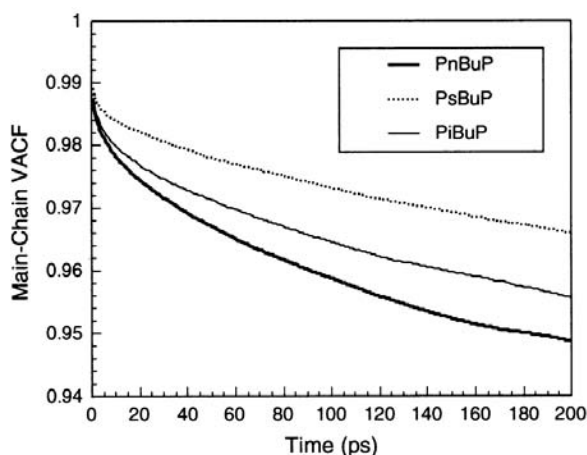


Figure 13-16 Plot of the vectorial autocorrelation function of the backbone chains of three polyphosphazenes over 200 ps of NPT dynamics. Reproduced from J. R. Fried, *Gas Diffusion and Solubility in Poly(organophosphazenes): Results of Molecular Simulation Studies*. Journal of Inorganic and Organometallic Polymers and Materials, 2006, **16**(4): p. 407–418. Copyright 2006 Springer-Verlag.

An additional example of a time-correlation function is the time-dependent *dipole moment*

$$\mu_{\text{tot}}(t) = \sum_{i=1}^N \mu_i(t) \quad (13.53)$$

where $\mu_i(t)$ is the dipole moment of molecule i at time t . The total dipolar correlation function is given by

$$C_{\text{dipole}}(t) = \frac{\langle \mu_{\text{tot}}(t) \cdot \mu_{\text{tot}}(0) \rangle}{\langle \mu_{\text{tot}}(0) \cdot \mu_{\text{tot}}(0) \rangle}. \quad (13.54)$$

The infrared spectra can be obtained from molecular dynamics using a Fourier transform of the dipolar correlation function.

13.5.6 Scattering Functions

Molecular dynamics simulations may be used to reproduce X-ray and neutron scattering spectra that can be compared with experimental data as a test of the validation of the chosen force field for the polymer under study. The intersegmental or d -spacing, an approximate measure of free volume in amorphous polymers, can be obtained from the simulated diffraction patterns through use of the Bragg equation in the form

$$d = \frac{\lambda}{2 \sin \theta} \quad (13.55)$$

where λ is the wavelength (1.5418 Å for CuK α radiation) and θ is the scattering angle corresponding to the maximum of the principal peak in a plot of intensity versus the scattering angle, 2θ . As an illustration, the X-ray diffraction pattern of the high-free-volume polymer, poly[1-(trimethylsilyl)-1-propyne] (PTMSP), is shown in Figure 13-17. As discussed elsewhere [61], the simulated X-ray diffraction pattern and the calculated d -spacing of 9.31 Å agree well with published experimental data.

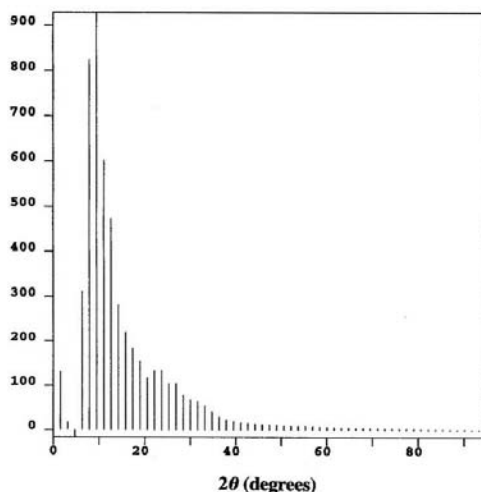


Figure 13-17 Simulated X-ray diffraction pattern of PTMSP. Reproduced from J. R. Fried and D. K. Goyal, *Molecular Simulation of Gas Transport in Poly[1-(trimethylsilyl)-1-Propyne]*. *Journal of Polymer Science: Part B: Polymer Physics*, 1998. **36**: p. 519–536.

13.5.7 Mechanical Properties

Early developments in the use of atomistic modeling to determine mechanical properties have been reported by a number of groups [62–64]. During simulation of an amorphous cell under externally applied stress, pressure and stress may be controlled using the Parrinello–Rahman algorithm [65], which allows both the shape and volume of the cell to change, thereby enabling the internal stress of the system to match the externally applied stress.

The fundamental relationship between the stress ($\boldsymbol{\tau}$) and strain ($\boldsymbol{\epsilon}$) tensors is given by the generalized Hooke's law in the form

$$\boldsymbol{\tau} = \mathbf{C}\boldsymbol{\epsilon}. \quad (13.56)$$

Since both tensors are symmetric, eq. (13.56) can be written in vector notation as

$$\tau_i = C_{ij}\epsilon_j \quad (13.57)$$

where τ_i and ϵ_i are the six components of the stress and strain vectors, respectively, and C_{ij} is the symmetric 6×6 stiffened matrix. In all there are 21 coefficients to fully describe the stress-strain behavior. For totally isotropic material, only two inde-

pendent coefficients—the Lamé constants, λ and μ —can fully describe the stress-strain behavior. These constants are contained in components of the stiffness matrix for an isotropic material, C_{ij} , as

$$\mathbf{C}_{\text{isotropic}} = \begin{pmatrix} \lambda + 2\mu & \lambda & \lambda & 0 & 0 & 0 \\ \lambda & \lambda + 2\mu & \lambda & 0 & 0 & 0 \\ \lambda & \lambda & \lambda + 2\mu & 0 & 0 & 0 \\ 0 & 0 & 0 & \mu & 0 & 0 \\ 0 & 0 & 0 & 0 & \mu & 0 \\ 0 & 0 & 0 & 0 & 0 & \mu \end{pmatrix}. \quad (13.58)$$

The internal stress is obtained from the first derivative of the potential energy with respect to strain and the diagonal and off-diagonal components of the stiffness matrix are obtained from the second derivative of the potential energy as follows:

$$C_{ii} = \frac{1}{V} \frac{\partial^2 U}{\partial \varepsilon_i^2} \quad (13.59)$$

and

$$C_{ij} = \frac{1}{V} \frac{\partial^2 U}{\partial \varepsilon_i \partial \varepsilon_j} = \frac{\partial \sigma_i}{\partial \varepsilon_j}. \quad (13.60)$$

The Lamé constants can be used to determine Young's modulus (E), bulk modulus (B), shear modulus (G), and Poisson's ratio (ν) through the following relationships:

$$E = \frac{3\lambda + 2\mu}{\lambda/\mu + 1} \quad (13.61)$$

$$\nu = \frac{\lambda}{2(\lambda + \mu)} \quad (13.62)$$

$$B = \lambda + \frac{2\mu}{3} \quad (13.63)$$

and

$$G = \mu. \quad (13.64)$$

In the case of an *anisotropic* material such as a crystal, all coefficients of the stiffness matrix are needed.

13.5.8 Sorption Isotherms

Sorption isotherms of solutes in polymers can be obtained at different pressures by a variety of methods including the Grand Canonical Monte Carlo (GCMC) simulations (μ, T, p). This approach uses a Metropolis [28] algorithm for accepting or rejecting configurational moves (i.e., rotation and translation of the sorbate molecule) as well as for sorbate insertion and deletion. GCMC simulations have been used to predict gas adsorption in zeolites [66] but also can be conveniently used to determine sorption isotherms for polymers. In order to accommodate larger gas penetrants such as CH_4 and CO_2 , amorphous cells of at least 40 Å are recommended to achieve a statistically representative distribution of free-volume sites [67].

In GCMC simulation, the first step is a random selection and insertion of a sorbate molecule into a simulation box. The decision whether to translate or reorient the sorbate molecule is based upon the potential energy of the new configuration. Specifically, the decision to accept or reject the move or return to the original configuration is based upon the probability

$$p_{\text{move}} = \min[\exp(-\Delta U/kT); 1] \quad (13.65)$$

where ΔU is the difference in potential energy between the old and new configurations. The decision to accept or reject the new configuration is based on comparing p_{move} with a random number between 0 and 1. The decision to add or subtract is based upon a similar calculation of a probability. For example, the probability for addition can be written as

$$p_{\text{add}} = \min\left[\frac{1}{(N+1)} \frac{pV}{kT} \exp(-\Delta U/kT); 1\right] \quad (13.66)$$

where N is the number of molecules before the addition, p is the pressure of the bulk gas, and V is the volume of the cell. Such calculations may be performed as many as 10 million times at each pressure before an equilibrium state (i.e., a single point on the sorption isotherm) is reached.

Solubility coefficients can be obtained from the limiting slope of the GCMC sorption isotherms for each gas at low pressure as

$$S = \lim_{p \rightarrow \infty} (C/p) \quad (13.67)$$

where C is the concentration of sorbed gas and p is pressure. In simulation, concentration is reported as the number of sorbate molecules that are sorbed per volume of the simulation cell (\AA^3) at a given pressure (or fugacity). Typical units of experimental solubility coefficients are $\text{cm}^3(\text{STP})/\text{cm}^3$ polymer and, therefore, a unit conversion must be made to compare with experimental data. As an example, sorption isotherms of methane in PTMSP at four temperatures are shown in Figure 13.18. Using eq. (13.67), solubility coefficients were obtained and used to calculate the heat of sorption, ΔH_s , from the van't Hoff expression

$$S = S_0 \exp(-\Delta H_s/RT). \quad (13.68)$$

The simulation value was $-3.08 \text{ kcal mol}^{-1}$, which is in very good agreement with the experimental value of $-3.3 \text{ kcal mol}^{-1}$. Example 13.8 illustrates the use of GCMC calculations to determine the sorption isotherm of O_2 in the rubbery polymer polydimethylsiloxane.

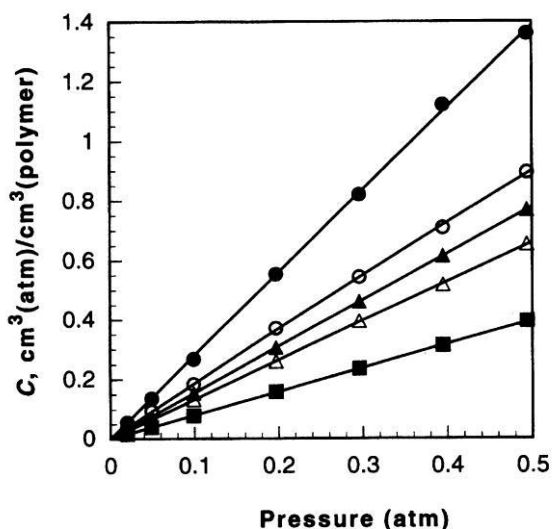


Figure 13-18 Sorption isotherms for CH_4 in PTMSP obtained at 308 K (●), 320 K (▲), 360 K (△) and 400 K (■). Curves represent dual-mode model fit of simulation data (see Section 12.1.3). Reproduced from T. Zheng and J. R. Fried, *Monte Carlo Simulation of the Sorption of Pure and Mixed Alkanes in Poly[1-(trimethylsilyl)-1-Propyne]*, *Separation Science and Technology*, 2001. **36**(5&6), 959–973.

Example 13.8

Using GCMC simulations, calculate the sorption isotherm of O₂ in polydimethylsiloxane (PDMS) at 298 K.

Solution

For this simulation, the COMPASS [36] force field has been selected. An amorphous cell was built using four PDMS chains each containing 80 repeat units (RUs) at 298 K and an initial density of 0.8 g cm⁻³. The cell was then equilibrated using 25-ps NVT dynamics (Andersen [52] thermostat) at 298 K followed by sequential 250-ps NPT dynamics (Andersen thermostat and Berendsen [53] barostat). Average temperature over 250-ps NPT was 298.0 K. Temperature and density over the final 50 ps of NPT dynamics was 297.8 (s.d. = 2.8) K and 1.0170 g cm⁻³ (s.d. = 0.0063). The final amorphous cell at the end of the 250-ps NPT dynamics was 36.5 Å on a side. This structure was used for the O₂ sorption measurements at 298 K from 10 to 1000 total fugacity using GCMC (configurational bias*). Because PDMS is a rubbery polymer ($T_g = 120$ K), the sorption isotherm is linear ($R^2 = 0.9993$) as shown in Figure 13-19.

Experimentally determined densities of silicone rubber fall within the range around 0.97 to 0.98 g cm⁻³. Silicone rubber is not pure PDMS but is lightly crosslinked and may contain some fillers or additives; however, the simulation density of 1.0170 g cm⁻³ is less than 5% higher than reported experimental values. The experimental solubility coefficient obtained from the O₂ isotherm using eq. (13.67) for O₂ has been reported [68] to be 0.18(±0.01) cm³(STP)/cm³ polymer atm at 35°C. Reported simulation values have been in the range from 0.22 to 0.25 cm³(STP)/cm³ polymer atm in reasonable agreement with the GCMC results in this example. The solubility units refer to the volume (cm³) of the gas (O₂) at standard temperature and pressure (i.e., 273 K, 1 bar) while cm³ polymer is the unit of volume of the experimental polymer sample used in the sorption measurements.

* In configurational bias, the solute is inserted into the amorphous cell using different orientations. This is important for accurate simulation of the sorption of asymmetric molecules such as ethanol.

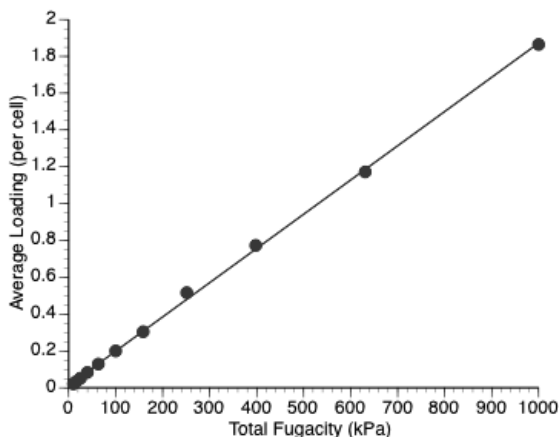


Figure 13-19 Sorption isotherm of O_2 in PDMS at 298 K obtained by GCMC simulation at 298 K. Line represents a least-square fit of the data points.

The slope of the simulated isotherm shown in Figure 13-19 is 1.859×10^{-3} molecules per cell/kPa. To compare with the experimental results, we need to convert from molecules per cell/kPa to the experimental units of $\text{cm}^3(\text{STP})/\text{cm}^3$ polymer atm. This requires several steps. First, the molar volume of an ideal gas at STP is 0.02245 m^3 or $2.242 \times 10^4 \text{ cm}^3$. Second, the volume of the amorphous cell is calculated as $(36.5 \text{ \AA})^3 = 48,630 \text{ \AA}^3 = 4.87 \times 10^{-20} \text{ cm}^3$. The final conversion is given as

$$\frac{1.86 \times 10^{-3} \text{ molecules}}{\text{kPa}} \frac{\text{kPa}}{9.87 \times 10^{-3} \text{ atm}} \frac{2.24 \times 10^4 \text{ cm}^3(\text{STP})}{4.87 \times 10^{-20} \text{ cm}^3 \text{ polymer}} \times \frac{\text{mol}}{6.02 \times 10^{23} \text{ molecules}} = \frac{41.7}{289.4} = 0.144 \frac{\text{cm}^3(\text{STP})}{\text{cm}^3 \text{ polymer atm}}.$$

The value of $0.144 \text{ cm}^3(\text{STP})/\text{cm}^3$ polymer atm obtained at 298 K compares well with reported experimental values of 0.18 and $0.224 \text{ cm}^3(\text{STP})/\text{cm}^3$ polymer atm and other simulation values of 0.22 and $0.25 \text{ cm}^3(\text{STP})/\text{cm}^3$ polymer atm.

13.5.9 Permeability

The permeability coefficient (P) is the product of the diffusion coefficient (D) and the solubility coefficient (S). Both can be obtained from molecular simulations including the use of MD and MC simulations as discussed in the following sections.

Diffusion Coefficients. The self-displacement coefficient, D , can be obtained from MD simulations, typically NVT or NVE dynamics, through two approaches. The most frequently used is the Einstein relationship

$$D_\alpha = \frac{1}{6N_\alpha} \lim_{t \rightarrow \infty} \frac{d}{dt} \left\langle \sum_i^N |\mathbf{r}_i(t) - \mathbf{r}_i(0)|^2 \right\rangle \quad (13.69)$$

where N_α is the number of diffusing species. The term in brackets is the mean-square displacement (MSD) where $\mathbf{r}_i(t)$ is a vector representing the final position of particle i (atom or molecule) at time t and $\mathbf{r}_i(0)$ is the initial position at the start of the dynamics. Equation (13.69) applies in the region of Einstein diffusion where $n = 1$ in the following relationship between the MSD and time:

$$\left\langle |\mathbf{r}_i(t) - \mathbf{r}_i(0)|^2 \right\rangle \propto t^n. \quad (13.70)$$

For very short times, the MSD may be quadratic in time (i.e., $n = 2$) characteristic of “free flight” as may occur in a pore or cage well. In the processing of simulation data, the MSD is plotted as a function of elapsed time and D is calculated as 1/6 of the slope of the best-fit line. Typically, the initial trajectories, where $n = 2$, are discarded from the data used to calculate D . In addition, the MSD versus time plot is typically noisy near the end of the simulation due to the way that trajectories are averaged and, therefore, these data points are also excluded when D is calculated.

An example of a log–log plot of MSD versus time for O_2 and CO_2 diffusing in an amorphous cell of the high-free-volume glassy polymer poly[1-(trimethylsilyl)-1-propyne] (PTMSP) (see Section 12.1.2) is shown in Figure 13-20. The plot shows that Einstein diffusion is reached by 32 ps in this case. Diffusion coefficients at 300 K obtained using a customized DREIDING [32] force field and MSD data in the Einstein region were found to be $2.38 \times 10^{-5} \text{ cm}^2 \text{ s}^{-1}$ for O_2 in good agreement with the experimental value. Procedures for calculating O_2 diffusion in the highly permeable rubbery polymer polydimethylsiloxane (PDMS) are shown next in Example 13.9.

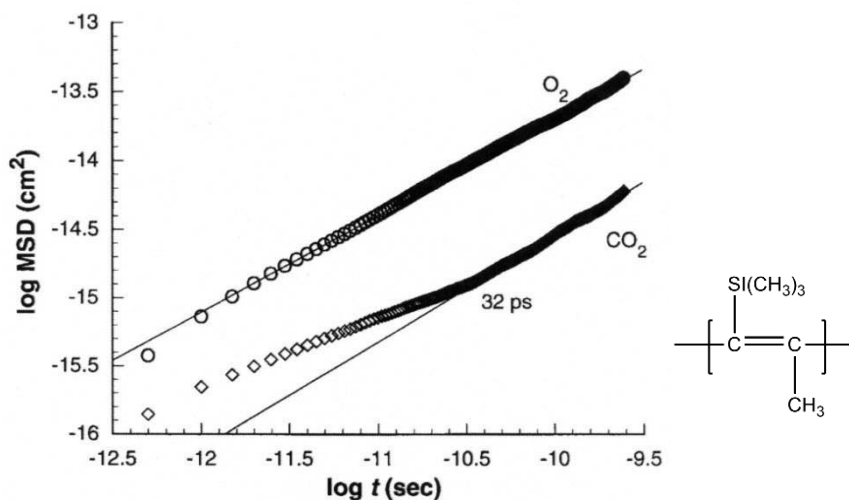


Figure 13-20 Log-log plot of MSD versus NVT simulation time for oxygen and carbon dioxide in poly[1-(trimethylsilyl)-1-propyne] (PTMSP). Reproduced from J. R. Fried and D. K. Goyal, *Molecular Simulation of Gas Transport in Poly[1-(trimethylsilyl)-1-Propyne]*. *Journal of Polymer Science: Part B: Polymer Physics*, 1998. **36**: p. 519–536. Reprinted by permission of John Wiley, Inc.

An alternative approach makes use of the velocity autocorrelation function (VACF) given by the Green–Kubo relation as

$$D = \frac{1}{3} \int \mathbf{v}(t) \cdot \mathbf{v}(0) dt \quad (13.71)$$

where $\mathbf{v}_i(t)$ is the center-of-mass velocity vector of a single molecule at time t . In general, MD simulations can be expected to provide meaningful estimates of the diffusion coefficient for rapid diffusion (i.e., $>10^{-8}$ to 10^{-7} cm s $^{-1}$). In the case of slower diffusion, such as the investigation of diffusion in barrier polymers, an alternative approach using atomistic simulations is the transition state theory (TST) of Suter and Gusev [69].

Example 13.9

Using MD solutions, calculate the diffusion coefficient of O $_2$ (O=O) in polydimethylsiloxane (PDMS) at 298 K.

Solution

Using the COMPASS force field, an amorphous cell was constructed using the same procedures as used in Example 13.8 except four oxygen molecules were built into the cell. As before, 25-ps NVT and 250-ps NPT dynamics were used to equilibrate the cell. The final density at the end of 250-ps NPT dynamics was 1.026 g cm^{-3} at 292.8 K. The amorphous cell, shown in Figure 13-21, was 36.4 \AA on a side (density of 1.026 g cm^{-3}). Figure 13-21 shows the four oxygen molecules (in space-filling representation) in the box containing the PDMS chains shown as line representations. Next, 1.0-ns NVT dynamics were used to obtain trajectories to determine the diffusion coefficient. Average temperature during the 1.0-ns NVT dynamics was 298.4 K (s.d. = 3.2) with an average pressure of 0.017 GPa (s.d. = 0.084 GPa).

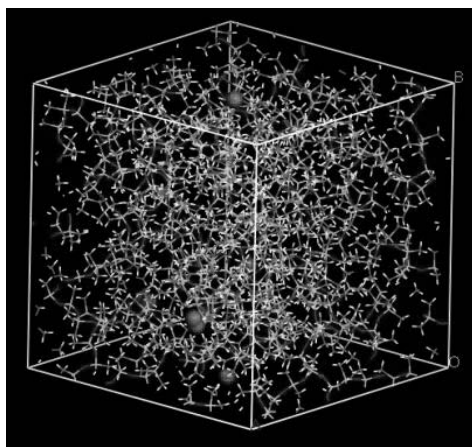


Figure 13-21 Amorphous cell of PDMS containing four O_2 molecules (CPK space-filling representation).

The MSD plot is shown Figure 13-22. As shown in Figure 13-23, a log–log plot of MSD versus time shows reasonable linearity between 125 and 625 ps (slope = 0.95, $R^2 = 0.9988$). The good linearity with a slope of the log–log plot near unity is a good indication that diffusion is within the Einstein region. The slope in the plot of MSD versus time (ps) over this time range gives a slope of $0.7065 \text{ \AA}^2/\text{ps}$ ($R^2 = 0.9974$). The diffusion coefficient at 298 K is then calculated from eq. (13.69) as

$$D = \frac{\text{slope}}{6} = \frac{0.7065 \text{ \AA}^2 (10^{-8}) \text{ cm}^2}{6 \text{ ps}} \frac{\text{ps}}{10^{-12} \text{ s}} = 0.1178 \times 10^{-4} \frac{\text{cm}^2}{\text{s}} = 11.8 \times 10^{-6} \frac{\text{cm}^2}{\text{s}}.$$

The value of $11.8 \times 10^{-6} \text{ cm}^2 \text{ s}^{-1}$ obtained here compares well with experimental values reported in the range from 16 to $41 \times 10^{-6} \text{ cm}^2 \text{ s}^{-1}$ at temperatures up to 308 K. Other simulation studies reported in the literature give diffusion coefficients for O_2 in the range from 4.5 to $35 \times 10^{-6} \text{ cm}^2 \text{ s}^{-1}$.

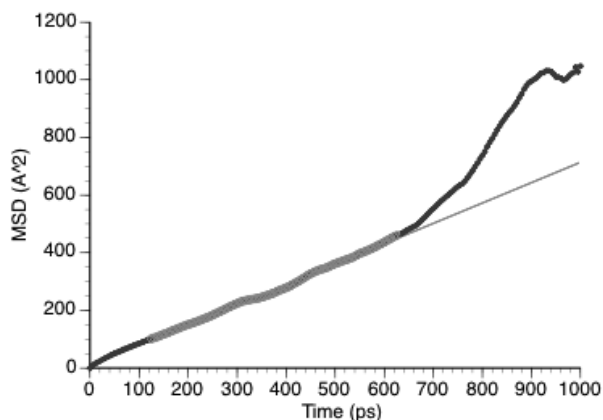


Figure 13-22 Plot of MSD versus NVT simulation time for O₂ in PDMS. Data used in the calculation of the diffusion coefficient are indicated in red. The thin line shown is the least-square fit of that data.

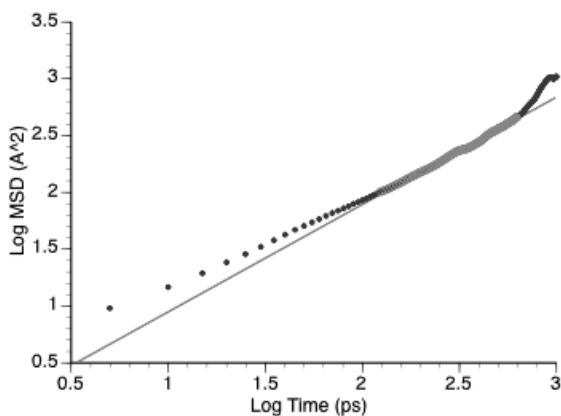


Figure 13-23 Log-log plot of MSD versus NVT simulation time for O₂ in PDMS.

Solubility Coefficients. The solubility coefficient, S , can be obtained from several approaches such as the calculation of excess chemical potential, μ_{ex} , as

$$S = \exp(-\mu_{\text{ex}}/RT) \quad (13.72)$$

where μ_{ex} is obtained from the calculated interaction energy, E , from the Widom insertion method (1963). Alternatively, the solubility coefficient can be obtained from the sorption isotherm obtained using GCMC simulation (Section 13.5.8) from eq. (13.67).

Permeability Coefficients. Once the diffusion and solubility coefficients have been determined from simulation, the permeability coefficient can be estimated as

$$P = DS. \quad (13.73)$$

Using the values of S and D for O_2 in PDMS (Examples 13.7 and 13.8), the permeability coefficient can be estimated as*

$$P(O_2) = \left(11.8 \times 10^{-6} \frac{\text{cm}^2}{\text{s}} \right) 0.144 \frac{\text{cm}^3(\text{STP})}{\text{cm}^3(\text{polymer}) \text{ atm}} =$$

$$1.70 \times 10^{-6} \frac{\text{cm}^3(\text{STP})}{\text{cm}(\text{polymer}) \text{ atm s}} \frac{1 \text{ atm}}{76 \text{ cm Hg}} = \quad (13.74)$$

$$2.24 \times 10^{-8} \frac{\text{cm}^3(\text{STP}) \text{ cm}}{\text{cm}^2(\text{polymer}) \text{ s cm Hg}} = 224 \text{ Barrer.}$$

Considering the errors associated with the simulation of diffusion and particularly solubility using small atomistic cells, this value of 224 Barrer obtained entirely from simulation reasonably compares with values of around 933 Barrer cited for the O_2 permeability of PDMS [70].

13.5.10 Free Volume

Free volume and free-volume distribution control such important properties as gas diffusivity as described previously. Free volume can be obtained from simulation by a variety of methods including geometric methods such as the Voronoi and Delaunay tessellations of space [71, 72], the Voorintholt method [73] that utilizes the van der Waals surface of the polymer chain to determine free volume, the TST method mentioned in the previous section, the phantom bubble method [74], and a more recent approach by Sanchez [75].

Voronoi tessellation produces a distribution of polyhedrals using a procedure that bisects the vectors connecting one atom to all other atoms by a plane perpendicular to itself. A related tessellation procedure is called the Delaunay tessellation whereby all contiguous pairs of atoms (i.e., those whose polyhedrals have a com-

* 1 Barrer = $\frac{10^{-10} \text{ cm}^3(\text{STP}) \text{ cm}}{\text{cm}^2 \text{ s cmHg}}$.

mon face) are joined. A schematic representation of Voronoi and Delaunay tessellation in two dimensions is shown in Figure 13-24.

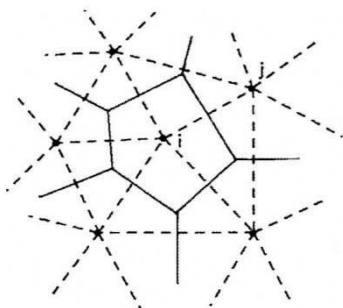


Figure 13-24 Two-dimensional representation of a Voronoi polygon around atom *i*. The network formed by the dashed lines is the result of the Delaunay tessellation. Reproduced from S. Arizzi, P. H. Mott, and U. W. Suter, *Space Available to Small Diffusants in Polymeric Glasses: Analysis of Unoccupied Space and Its Connectivity*. *Journal of Polymer Science: Part B: Polymer Physics*, 1992. **30**: 415–426. Reprinted by permission of John Wiley & Sons, Inc.

SUGGESTED READING

- Bicerano, J., *Prediction of Polymer Properties*. 3rd ed. 2002, New York: Marcel Dekker, Inc.
- Binder, K., *Monte Carlo and Molecular Dynamics Simulations in Polymer Science*. 1995, New York: Oxford University Press.
- Fried, J. R., *Molecular Simulation of Gas and Vapor Transport in Highly Permeable Polymers*, in *Materials Science of Membranes for Gas and Vapor Separation*, B. D. Freeman, I. Pinnau, and Y. Yampolskii, eds. 2006, London: John Wiley & Sons. p. 94.
- Fried, J. R., *Computational Chemistry and Molecular Simulations*. 2014, New York: John Wiley & Sons.
- Kremer, K., *Computer Simulations for Macromolecular Science*. *Macromolecular Chemistry and Physics*, 2003. **204**: p. 247.
- Müller-Plathé, F., *Permeation of Polymer—A Computational Approach*. *Acta Polymerica*, 1994. **45**: p. 259–293.
- Rigby, D., and B. E. Eichinger, *Polymer Modeling*. *Current Opinion in Solid State Material Science*, 2001. **5**: p. 445.
- Sumpter, B. G., D. W. Noid, and B. Wunderlich, *Computer Simulation and Modeling of Polymer Crystal*. *Trends of Polymer Science*, 1993. **1**(6): p. 160.

- Theodorou, D. N., *Principles of Molecular Simulation of Gas Transport in Polymers*, in *Materials Science of Membranes for Gas and Vapor Separation*, B. D. Freeman, I. Pinnau, and Y. Yampolskii, eds. 2006, London: John Wiley & Sons, p. 49.
- van Krevelen, D. W., *Group Contribution Techniques for Correlating Polymer Properties and Chemical Structure*, in *Computational Modeling of Polymers*, J. Bicerano, ed. 1992, New York: Marcel Dekker, Inc., p. 55.
- Voth, G. A., ed. *Coarse-Graining of Condensed Phase and Biomolecular Systems*. 2009, CRC Press: Boca Raton.

PROBLEMS

13.1 Poly(2,6-dimethyl-1,4-phenylene oxide) (PDMPO) can be partially crystallized in solution (i.e., solvent-induced crystallization). **(a)** Calculate the density of 100% crystalline PDMPO using the group-contribution parameters given in Table 13-1. **(b)** If the crystallinity of a semicrystalline sample of PDMPO is 8%, estimate its crystallinity using the relationship

$$V_{sc} = x_c V_c + (1 - x_c) V_a$$

where x_c is the degree of crystallinity, V_c is the molar specific volume of a 100% crystalline polymer, and V_a is the molar specific volume of the totally amorphous polymer.

13.2 Using the values of molar attraction constants given by van Krevelen in Table 13-2, calculate the solubility parameters, units of $(\text{MPa})^{1/2}$, at 25°C of the following polymers whose densities are given within parentheses:

- (a)** Polyisobutylene ($\rho = 0.924 \text{ g cm}^{-3}$)
- (b)** Polystyrene ($\rho = 1.04 \text{ g cm}^{-3}$)
- (c)** Polycarbonate ($\rho = 1.20 \text{ g cm}^{-3}$)

13.3 Using UNIFAC-FV, estimate the activity of toluene in a 50 wt% solution of polydimethylsiloxane in toluene at 298 K.

13.4 Based upon their calculated Permachors, order the following polymers in terms of their expected performance as oxygen barriers: **(a)** amorphous Teflon, **(b)** polyisobutylene, **(c)** polychloroprene, **(d)** polybutadiene, **(e)** nitrile rubber, **(f)** silicone rubber, and **(g)** butyl rubber. Does your result give the correct order based upon experimental permeability values?

REFERENCES

1. Poling, B. E., J. M. Prausnitz, and J. P. O'Connell, *The Properties of Gases and Liquids*. 5th ed. 2001, New York: McGraw-Hill Book Company.
2. van Krevelen, D. W., *Properties of Polymers*. 3rd ed. 1990, Amsterdam: Elsevier.

3. van Krevelen, D. W., *Group Contribution Techniques for Correlating Polymer Properties and Chemical Structure*, in *Computational Modeling of Polymers*, J. Bicerano, ed. 1992, New York: Marcel Dekker, Inc. p. 55–123.
4. Bicerano, J., *Prediction of Polymer Properties*. 3rd ed. 2002, New York: Marcel Dekker, Inc.
5. Mark, J. E., ed., *Polymer Data Handbook*. 2nd ed. 2009, Oxford: Oxford University Press.
6. Bondi, A., *Physical Properties of Molecular Crystals*. 1968, New York: John Wiley & Sons.
7. Thran, A., G. Kroll, and F. Faupel, *Correlation Between Fractional Free Volume and Diffusivity of Gas Molecules in Glassy Polymers*. *Journal of Polymer Science: Part B: Polymer Physics*, 1999. **37**: p. 3344–3358.
8. Fried, J. R., *Correlative Techniques for the Estimation of the Glass-Transition Temperature*. *Computational Polymer Science*, 1993. **3**: p. 47–58.
9. Salame, M., *Transport Properties of Nitrile Polymers*. *Journal of Polymer Science, Polymer Symposium*, 1973. **41**: p. 1–15.
10. Salame, M., *Prediction of Gas Barrier Properties of High Polymers*. *Polymer Engineering and Science*, 1986. **26**(22): p. 1543–1546.
11. Stern, S. A., V. M. Shah, and B. J. Hardy, *Structure-Permeability Relationships in Silicone Polymers*. *Journal of Polymer Science: Part B: Polymer Physics*, 1987. **25**: p. 1263–1298.
12. Small, P. A., *Some Factors Affecting the Solubility of Polymers*. *Journal of Applied Chemistry*, 1953. **3**: p. 71–80.
13. Hoy, K. L., *New Values of the Solubility Parameters from Vapor Pressure Data*. *Journal of Paint Technology*, 1970. **42**: p. 76–118.
14. Barton, A. F. M., *CRC Handbook of Polymer-Liquid Parameters and Solubility Parameters*. 1990, Boca Raton: CRC Press.
15. Brandrup, J., E. H. Immergut, and E. A. Grulke, eds. *Polymer Handbook*. 4th ed. 1999, New York: John Wiley & Sons..
16. Fried, J. R., J. S. Jiang, and E. Yeh, *Group-Contribution Methods in Polymer Thermo-dynamics*. *Computational Polymer Science*, 1992. **2**: p. 95–113.
17. Oishi, T., and J. M. Prausnitz, *Estimation of Solvent Activities in Polymer Solutions Using a Group-Contribution Method*. *Industrial Engineering Chemical Process Design and Development*, 1978. **17**: p. 333–339.
18. Fredenslund, A., R. L. Jones, and J. M. Prausnitz, *Group-Contribution Estimation of Activity Coefficients in Nonideal Liquid Mixtures*. *AIChE Journal*, 1975. **21**(6): p. 1086–1592.
19. Abrams, D. S. and J. M. Prausnitz, *Statistical Thermodynamics of Liquid Mixtures: A New Expression for the Excess Gibbs Energy of Partly or Completely Miscible Systems*. *AIChE Journal*, 1975. **21**(1): p. 116–128.
20. Derr, E. L.. and C. H. Deal, *Predicted Compositions during Mixed Solvent Evaporation from Resin Solutions Using the Analytical Solution of Groups Method*, in *Advances in Chemistry Series*, R. W. Tess, ed., 1973, ACS:Washington DC, vol 124, p. 11–30.
21. Hansen, H. K., et al., *Vapor-Liquid Equilibria by UNIFAC Group Contributions. 5. Revision and Extension*. *Industrial and Engineering Chemistry and Research*, 1991. **30**: p. 2352–2355.
22. Bicerano, J., *Prediction of the Properties of Polymers from Their Structures*. *Journal of Macromolecular Science—Reviews in Macromolecular Chemistry and Physics*, 1996. **C36**(1): p. 161–196.
23. Sumpter, B. G., and D. W. Noid, *Neural Networks and Graph Theory as Computational Tools for Predicting Polymer Properties*. *Macromolecular Theory and Simulation*, 1994. **3**: p. 363–378.
24. Liu, W., and C. Cao, *Artificial Neural Network Prediction of Glass Transition Temperature of Polymers*. *Colloid and Polymer Science*, 2009. **287**: p. 811–818.

25. Nielsen, S. O., et al., *Coarse Grain Models and the Computer Simulation of Soft Material*. Journal of Physics: Condensed Matter, 2004. **16**: p. R481–R512.
26. Girard, S., and F. Müller-Plathe, *Coarse-Graining in Polymer Simulations*. Lecture Notes in Physics, 2004. **640**: p. 327–356.
27. Voth, G. A., ed., *Coarse-Graining of Condensed Phase and Biomolecular Systems*. 2009, Boca Raton: CRC Press.
28. Metropolis, N., et al., *Equation of State Calculations by Fast Computing Machines*. Journal of Chemical Physics, 1953. **21**(6): p. 1087–1092.
29. Christen, M., and W. F. van Gunsteren, *Multigraining: An Algorithm for Simultaneous Fine-Grained and Coarse-Grained Simulation of Molecular Systems*. Journal of Chemical Physics, 2006. **124**: p. 1541061.
30. Dinur, U., and A. T. Hagler, *New Approaches to Empirical Force Fields*, in *Reviews in Computational Chemistry*, K. B. Lipkowitz and B. D. Boyd, eds. 1991, New York: VCH Publishers, Inc. p. 99–164.
31. Ewald, P., *Die Berechnung Optischer und Elektrostatischer Gitterpotentiale*. Annals of Physics, 1921. **64**: p. 253–287.
32. Mayo, S. L., B. D. Olafson, and W. A. Goddard III, *DREIDING: A Generic Force Field for Molecular Simulations*. Journal of Physical Chemistry, 1990. **94**: p. 8897–8909.
33. Fried, J. R., *Computational Parameters*, in *Physical Properties of Polymers Handbook*, J. E. Mark, ed. 2007, Springer. p. 59–65.
34. Scott, W. R. P., et al., *The GROMOS Biomolecular Simulation Program Package*. Journal of Physical Chemistry, 1999. **103**: p. 3596–3607.
35. Hwang, M. J., T. P. Stockfisch, and A. T. Hagler, *Derivation of Class II Force Fields. 2. Derivation and Characterization of a Class II Force Field, CFF03, for the Alkyl Functional Groups and Alkane Molecules*. Journal of the American Chemical Society, 1994. **117**: p. 2515–2525.
36. Sun, H., *COMPASS: An Ab Initio Force-Field Optimized for Condensed-Phase Applications—Overview with Details on Alkane and Benzene Compounds*. Journal of Physical Chemistry B, 1998. **102**: p. 7338–7364.
37. Sun, H., P. Ren, and J. R. Fried, *The COMPASS Force Field: Parameterization and Validation for Phosphazenes*. Computational and Theoretical Polymer Science, 1998. **8**(1/2): p. 229–246.
38. Blaisten-Barojas, E., and M. R. Nyden, *Molecular Dynamics Study of the Depolymerization Reactions in Simple Polymers*. Chemical Physics Letters, 1990. **A205**: p. 499–505.
39. Nyden, M. R., and D. W. Noid, *Molecular Dynamics of Initial Events in the Thermal Degradation of Polymers*. Journal of Physical Chemistry, 1991. **95**(2): p. 940–945.
40. van Duin, A. C. T., et al., *ReaxFF: A Reactive Force Field for Hydrocarbons*. Journal of Physical Chemistry A, 2001. **105**: p. 9396–9409.
41. Chenoweth, K., et al., *Simulations on the Thermal Decomposition of a Poly(dimethyl-siloxane) Polymer Using the ReaxFF Reactive Force Field*. Journal of the American Chemical Society, 2005. **127**: p. 7192–7202.
42. Marrink, S. J., et al., *The MARTINI Force Field*, in *Coarse-Graining of Condensed Phase and Biomolecular Systems*, G. A. Voth, ed. 2009, Boca Raton: CRC Press, p. 5–39.
43. Marrink, S. J., et al., *The MARTINI Force Field: Coarse Grained Model for Biomolecular Simulations*. Journal of Physical Chemistry B, 2007. **111**: p. 7812–7824.
44. Marrink, S. J., A. H. de Vries, and A. E. Mark, *Coarse Grained Model for Semiquantitative Lipid Simulations*. Journal of Physical Chemistry B, 2004. **108**: p. 750–760.
45. Shinoda, W., R. Devane, and N.L. Klein, *Multi-Property Fitting and Parameterization of a Coarse-Grained Model for Aqueous Surfactants*. Molecular Simulation, 2007. **33**: p. 27–36.

46. Verlet, L., *Computer "Experiments" on Classical Fluids. I. Thermodynamical Properties of Lennard-Jones Molecules*. *Physical Review*, 1967. **159**: p. 98-103.
47. Hockney, R. W., and J. W. Eastwood, *Computer Simulations Using Particles*. 1981, New York: McGraw-Hill.
48. Ryckaert, J.-P., G. Ciccotti, and H. J. C. Berendsen, *Numerical Integration of the Cartesian Equations of Motion of a System with Constraints: Molecular Dynamics of n-Alkanes*. *Journal of Computational Physics*, 1977. **23**: p. 327-341.
49. Anderson, H. C., *A "Velocity" Version of the Shake Algorithm for Molecular Dynamics Calculations*. *Journal of Computational Physics*, 1983. **52**: p. 24-34.
50. Nosé, S., *A Unified Formulation of the Constant Temperature Molecular Dynamics Methods*. *Journal of Chemical Physics*, 1984. **81**(1): p. 511-519.
51. Hoover, W. G., *Canonical Dynamics: Equilibrium Phase-Space Distributions*. *Molecular Physics*, 1985. **31**(3): p. 1695-1697.
52. Andersen, H. C., *Molecular Dynamics Simulations at Constant Pressure and/or Temperature*. *Journal of Chemical Physics*, 1980. **72**(4): p. 2384-2383.
53. Berendsen, H. J. C., *Molecular Dynamics with Coupling to an External Bath*. *Journal of Chemical Physics*, 1984. **81**(8): p. 3684-3690.
54. Fried, J. R., and P. Ren, *Molecular Simulation of the Glass Transition of Polyphosphazenes*. *Computational and Theoretical Polymer Science*, 1999. **9**: p. 111-116.
55. Fried, J. R., and B. Li, *Atomistic Simulation of the Glass Transition of Di-Substituted Polysilanes*. *Computational and Theoretical Polymer Science*, 2001. **11**: p. 273-281.
56. Yu, K.-Q., Z.-S. Li, and J. Sun, *Polymer Structures and Glass Transition: A Molecular Dynamics Simulation Study*. *Macromolecular Theory and Simulation*, 2001. **10**(6): p. 624-653.
57. Zhang, J., et al., *Study of the Molecular Weight Dependence of Glass Transition Temperature for Amorphous Poly(L-lactide) by Molecular Dynamics Simulation*. *Polymer*, 2007. **48**: p. 4900-4905.
58. Fried, J. R. and N. Hu, *The Molecular Basis of CO₂ Interaction with Polymers Containing Fluorinated Groups; Computational Chemistry of Model Compounds and Molecular Simulation of Poly[bis(2,2,2-trifluoroethoxy)phosphazene]*. *Polymer*, 2003. **44**: p. 4363-4372.
59. Müller-Plathé, F., *Permeation of Polymer—A Computational Approach*. *Acta Polymerica*, 1994. **45**: p. 259-293.
60. Fried, J. R., *Gas Diffusion and Solubility in Poly(organophosphazenes): Results of Molecular Simulation Studies*. *Journal of Inorganic and Organometallic Polymers and Materials*, 2006. **16**(4): p. 407-418.
61. Fried, J. R., and D. K. Goyal, *Molecular Simulation of Gas Transport in Poly[1-(trimethylsilyl)-1-Propyne]*. *Journal of Polymer Science: Part B: Polymer Physics*, 1998. **36**: p. 519-536.
62. Theodorou, D. H., and U. W. Suter, *Atomistic Modeling of Mechanical Properties of Polymeric Glasses*. *Macromolecules*, 1986. **19**: p. 139-154.
63. Brown, D., and J. H. R. Clarke, *Molecular Dynamics Simulation of an Amorphous Polymer under Tension. I. Phenomenology*. *Macromolecules*, 1991. **24**: p. 2075-2082.
64. Rutledge, G. C., and U. W. Suter, *Calculation of Mechanical Properties of Poly(p-Phenylene terephthalamide) by Atomistic Modelling*. *Polymer*, 1991. **32**(12): p. 2179-2189.
65. Parrinello, M., and A. Rahman, *Strain Fluctuations and Elastic Constants*. *Journal of Chemical Physics*, 1982. **76**: p. 2662-2666.
66. Razmus, D. M., and C. K. Hall, *Prediction of Gas Adsorption in 5A Zeolites Using Monte Carlo Simulation*. *AIChE Journal*, 1991. **37**(5): p. 769-779.

67. Cuthbert, T. R., N. J. Wagner, and M.E. Paulaitis, *Molecular Simulation of Glassy Polystyrene: Size Effects on Gas Solubilities*. *Macromolecules*, 1997. **30**: p. 3058–3065.
68. Merkel, T. C., et al., *Gas Sorption, Diffusion, and Permeation in Poly(dimethylsiloxane)*. *Journal of Polymer Science: Part B: Polymer Physics*, 2000. **38**: p. 415–434.
69. Gusev, A. A., and U. W. Suter, *Dynamics of Small Molecules in Dense Polymer Subject to Thermal Motion*. *Journal of Chemical Physics*, 1993. **99**: p. 2228–2234.
70. Stern, A. A., V. M. Shah, and B. J. Hardy, *Structure-Permeability Relationships in Silicone Polymers*. *Journal of Polymer Science: Polymer Physics Edition*, 1987. **25**: p. 1263–1298.
71. Brostow, W., J.-P. Dussault, and B. L. Fox, *Construction of Voronoi Polyhedra*. *Journal of Computational Chemistry*, 1978. **29**: p. 81–92.
72. Tanemura, M., T. Ogawa, and N. Ogita, *A New Algorithm for Three-Dimensional Voronoi Tessellation*. *Journal of Computational Physics*, 1983. **51**: p. 191–207.
73. Voorintholt, R., et al., *A Very Fast Program for Visualizing Protein Surfaces, Channels and Cavities*. *Journal of Molecular Graphics*, 1989. **7**: p. 243–245.
74. Lee, S., and W. L. Mattice, *A Phantom Bubble Model for the Distribution of Free Volume in Polymers*. *Computational and Theoretical Polymer Science*, 1999. **9**: p. 57–61.
75. in't Veld, P. J., et al., *Liquid Structure via Cavity Size Distributions*. *Journal of Physical Chemistry B*, 2000. **104**: p. 12028–12034.
76. Arizzi, S., P. H. Mott, and U. W. Suter, *Space Available to Small Diffusants in Polymeric Glasses: Analysis of Unoccupied Space and Its Connectivity*. *Journal of Polymer Science: Part B: Polymer Physics*, 1992. **30**: p. 415–426.

Polymer Abbreviations

ABS	acrylonitrile–butadiene–styrene resin
CA	cellulose acetate
CAB	cellulose acetate butyrate
CAP	cellulose acetate propionate
CF	cresol–formaldehyde
CMC	carboxymethylcellulose
CN	cellulose nitrate
CP	cellulose propionate
CPE	chlorinated polyethylene
CTA	cellulose triacetate
CTFE	poly(chlorotrifluoroethylene)
EC	ethylcellulose
EP	epoxy resin
E/P	ethylene–propylene copolymer
EPDM	elastomeric terpolymer of ethylene, propylene, and a nonconjugated diene
EPS	expanded polystyrene (foam)
ETFE	ethylene–tetrafluoroethylene copolymer
EVA	ethylene–vinyl acetate copolymer
FEP	elastomeric copolymer of tetrafluoroethylene and hexafluoroethylene
FF	furan–formaldehyde resin
GP	gutta percha
HDPE	high-density polyethylene
HEC	hydroxyethylcellulose
HIPS	high-impact polystyrene
HMWPE	high-molecular-weight polyethylene
LDPE	low-density polyethylene

LLDPE	linear low-density polyethylene
MBS	methyl methacrylate-butadiene-styrene copolymer
MC	methylcellulose
MDPE	medium-density polyethylene
MF	melamine-formaldehyde resin
MPF	melamine/phenol-formaldehyde resin
NBR	nitrile rubber (elastomeric copolymer of butadiene and acrylonitrile)
NR	natural rubber
PA	polyamide, polyacetylene
PAA	poly(acrylic acid)
PAI	poly(amide-imide)
PAMS	poly(α -methylstyrene)
PAN	polyacrylonitrile
PANI	polyaniline
PAR	polyarylate
PB	polybutene-1
PBA	poly(butyl acrylate)
PBI	polybenzimidazole
PBO	polybenzoxazole
PBT	poly(butylene terephthalate)
PC	polycarbonate
PCTFE	poly(chlorotrifluoroethylene)
PDAP	poly(diallyl phthalate)
PDMS	polydimethylsiloxane
PE	polyethylene
PEEK	poly(aryl ether ether ketone)
PEN	poly(ethylene-2,6-naphthalate)
PEO	poly(ethylene oxide)
PES	polyethersulfone
PET	poly(ethylene terephthalate)
PF	phenol-formaldehyde resin
HEMA	poly(2-hydroxyethyl methacrylate)
PI	polyimide
PIB	polyisobutylene
PMMA	poly(methyl methacrylate)
PMP	poly(4-methyl-1-pentene)
POM	poly(oxymethylene); polyformaldehyde
POP	poly(phenylene oxide)
PP	polypropylene
PPBT	poly(<i>p</i> -phenylene benzobisthiazole)
PPP	poly(<i>p</i> -phenylene)
PPS	poly(<i>p</i> -phenylene sulfide)
PPSU	poly(phenylene sulfone)

PPV	poly(<i>p</i> -phenylene vinylene)
PPy	polypyrrole
PS	polystyrene
PSF	polysulfone
PT	polythiophene
PTFE	polytetrafluoroethylene
PUR	polyurethane
PVAC	poly(vinyl acetate)
PVAL	poly(vinyl alcohol)
PVB	poly(vinyl butyral)
PVC	poly(vinyl chloride)
PVF	poly(vinyl fluoride)
PVDC	poly(vinylidene dichloride)
PVDF	poly(vinylidene difluoride)
PVFM	poly(vinyl formal)
PVK	poly(<i>N</i> -vinylcarbazole)
PVP	poly(<i>N</i> -vinylpyrrolidone)
S/B	styrene–butadiene copolymer
SIN	simultaneous interpenetrating network
SMC	sheet molding compound
UF	urea–formaldehyde resin
UHMW-PE	ultrahigh-molecular-weight polyethylene
UP	unsaturated polyester

This page intentionally left blank

Representative Properties of Some Important Commercial Polymers

Table B-1 Physical and Thermal Properties*

Polymer	ρ (g cm ⁻³) ^a	T_g (°C)	T_m (°C) ^b
Cellulose acetate	1.27–1.34	(49)	—
Nylon-6	1.08–1.23	46–60	223
Nylon-6,6	1.07–1.24	45–57	265
Polycarbonate	1.20–1.31	141–150	227
Polyethylene (all grades)	0.91–1.00	(-120)	98–135
Poly(ethylene terephthalate)	1.33–1.48	69–77	267
Poly(methyl methacrylate)	1.17–1.23	105–126	160
Polyoxymethylene	1.43–1.54	-85 to -30	187
Polypropylene	0.9–0.95	-10 to -18	177
Polysulfone	1.24	190	—
Polystyrene	1.05–1.13	100	240
Polytetrafluoroethylene	2.1–2.35	-73	327–332
Poly(vinyl acetate)	1.19–1.34	28–31	—
Poly(vinyl chloride)	1.39–1.52	81	273
Silicone rubber	1.07	-123	-43

^a Numbers typically indicate a range of reported values for samples with different crystallinity, water content, molecular weight, and thermal histories. Uncertain or controversial values are given within parentheses.

^b In most cases, values indicate the range of densities between that of the glassy amorphous state to that of the fully crystalline polymer as calculated from X-ray data of crystalline domains.

Table B-2 Mechanical Properties

Polymer	E^a (GPa)	σ_b (σ_y) ^b (MPa)	ϵ_b (ϵ_y) ^c %	Izod Impact ^d Strength (J/m)
Cellulose acetate	2	30 (60)	30 (6)	6–133
Nylon-6	1.9	75 (50)	300 (30)	(25)
Nylon-6,6	2.0	80 (57)	200 (25)	110
Polycarbonate	2.5	60 (65)	125 (30)	800
Polyethylene (all grades)	0.2–1	10–30 (8–30)	600–800 (9–20)	130–700
Poly(ethylene terephthalate)	3.0	54	275 (6)	70
Poly(methyl methacrylate)	3.2	65	10	27
Polyoxymethylene	2.7	65	40	80
Polypropylene	1.4	33 (32)	400 (12)	80
Polysulfone	3.4	50	2.5	28
Polystyrene	2.5	65	75	85
Polytetrafluoroethylene	0.5	25 (13)	200 (63)	160
Poly(vinyl acetate)	0.6	29–49	10–20	160
Poly(vinyl chloride)	2.6	50 (48)	30 (3)	43
Silicone rubber	—	4.8–7.0	100–400	—

^a Tensile modulus; to convert GPa to psi, multiply by 1.45×10^5 .

^b Stress at break (yield); to convert MPa to psi, multiply by 145.

^c Elongation at break (yield).

^d To convert $J\ m^{-1}$ to $ft\cdot lb_f\ in^{-1}$, divide by 53.38.

ASTM Standards for Plastics and Rubber

Table C-1 Plastics (Vols. 8.01, 8.02, 8.03)

ASTM	Standards
D 256	Impact resistance of plastics and electrical insulating materials
D 412	Rubber properties in tension
D 542	Index of refraction of transparent organic plastics
D 543	Resistance of plastics to chemical reagents
D 568	Rate of burning and/or extent and time of burning of flexible plastics in a vertical position
D 569	Measuring the flow properties of thermoplastic molding materials
D 570	Water absorption of plastics
D 618	Conditioning plastics and electrical insulating materials for testing
D 621	Deformation of plastics under load
D 635	Rate of burning and/or extent and time of burning of self-supporting plastics in a horizontal position
D 638	Tensile properties of plastics
D 647	Design of molds for test specimens of plastics under flexural load
D 648	Deflection temperature of plastics under flexural load
D 671	Flexural fatigue of plastics under flexural load
D 695	Compressive properties of rigid plastics
D 696	Coefficient of linear thermal expansion of plastics
D 746	Brittleness temperature of linear thermal expansion of plastics
D 785	Rockwell hardness of plastics and electrical insulating materials
D 790	Flexural properties of unreinforced and reinforced plastics and electrical insulating materials
D 792	Specific gravity and density of plastics by displacement
D 882	Tensile properties of thin plastic sheeting

(Continues)

Table C-1 Plastics (Vols. 8.01, 8.02, 8.03) (Continued)

ASTM	Standard
D 1238	Flow rates of thermoplastics by extrusion plastometer
D 1434	Determining gas permeability characteristics of plastic film and sheeting
D 1435	Outdoor weathering of plastics
D 1505	Density of plastics by the density-gradient technique
D 1525	Vicat softening temperature of plastics
D 1637	Tensile heat-distortion temperature of plastic sheeting
D 1708	Tensile properties of plastics by use of microtensile specimens
D 1746	Transparency of plastic sheeting
D 1790	Brittleness temperature of plastic sheeting by impact
D 1822	Tensile-impact energy to break plastics and electrical insulating materials
D 1870	Elevated temperature aging using a tubular oven
D 1894	Static and kinetic coefficients of friction of plastic film and sheeting
D 1895	Apparent density, bulk factor, and pourability of plastic materials
D 1896	Transfer-molding test specimens of thermosetting compounds
D 1897	Injection-molding test specimens of thermoplastic molding and extrusion materials
D 1898	Sampling of plastics
D 1925	Yellowness index of plastics
D 1929	Ignition properties of plastics
D 1938	Tear propagation resistance of plastic film and thin sheeting by a single-tear method
D 2117	Melting point of semicrystalline polymers by the hot stage microscopy method
D 2126	Response of rigid cellular plastics to thermal and humid aging
D 2134	Softening of organic coatings by plastic compositions
D 2236	Dynamic mechanical properties of plastics by means of a torsional pendulum
D 2240	Rubber property—durometer hardness
D 2288	Weight loss of plasticizers on heating
D 2471	Gel time and peak exothermic temperature of reacting thermosetting resins
D 2566	Linear shrinkage of cured thermosetting casting resins during cure
D 2582	Puncture-propagation tear resistance of plastic film and thin sheeting
D 2684	Determining permeability of thermoplastic containers
D 2732	Unrestrained linear thermal shrinkage of plastic film and sheeting
D 2734	Density of smoke from the burning or decomposition of plastics
D 2857	Dilute solution viscosity of polymers
D 2863	Measuring the minimum oxygen concentration to support candle-like combustion of plastics (oxygen index)
D 2990	Tensile, compressive, and flexural creep and creep rupture of plastics
D 3029	Impact resistance of rigid plastic sheeting or parts by means of a tub (falling weight)
D 2856	Open cell content of rigid cellular plastics by the air pycnometer
D 3420	Test method for dynamic ball burst (pendulum) impact resistance of plastic films

(Continues)

Table C-1 Plastics (Vols. 8.01, 8.02, 8.03) (Continued)

ASTM	Standard
D 3593	Test method for molecular-weight averages and molecular weight distribution of certain polymers by liquid size-exclusion chromatography (gel permeation chromatography, GPC) using universal calibration
D 3750	Practice for determination of number-average molecular weight of polymers by membrane osmometry
D 3763	Test method for high-speed puncture properties of plastics using load and displacement sensors
D 3795	Test method for thermal flow and cure properties of thermosetting resins by torque rheometer
D 3845	Test method for the rheological properties of thermoplastics with a capillary rheometer
D 3846	Test method for in-plane shear strength of reinforced plastics
D 4000	Specifying plastic material
D 4001	Practice for determination of weight-average molecular weight of polymers by light scattering
D 4065	Practice for determining and reporting dynamic mechanical properties of plastics
D 4093	Test method for photoelastic measurements of birefringence and residual strains in transparent or translucent plastic materials
D 4272	Test method for impact resistance of plastic film by instrumented dart drop
D 4440	Practice for rheological measurement of polymer melts using dynamic mechanical procedures
D 4473	Practice for measuring the cure behavior of thermosetting resins using dynamic mechanical procedures
D 4526	Determination of volatiles in polymers by headspace chromatography
D 6108	Standard test method for compressive properties of plastic lumber and shapes
D 6109	Standard test method for flexural properties of unreinforced and reinforced plastic lumber
D 6111	Standard test method for bulk density and specific gravity of plastic lumber and shapes by displacement
D 6662	Standard specification for polyolefin-based plastic lumber decking boards

Table C-2 Rubber (Vols. 9.01 and 9.02)

ASTM	Standard
D 297	Methods for rubber products—chemical analysis
D 395	Test methods for rubber property—compression set
D 412	Test methods for rubber properties in tension
D 471	Test methods for rubber property—effect of liquids
D 624	Test methods for rubber property—tear resistance
D 797	Test methods for rubber property—Young's modulus at normal and subnormal temperatures
D 814	Test methods for rubber property—vapor transmission of volatile liquids
D 1349	Recommended practice for rubber—standard temperatures and atmospheres for testing and conditioning
D 1630	Test method for rubber property—abrasion resistance (NBS abrader)

(Continues)

Table C-2 Rubber (Vols. 9.01 and 9.02) (Continued)

ASTM	Standard
D 2084	Test method for rubber property—vulcanization characteristics using oscillating disk cure meter
D 2228	Test method for rubber property—abrasion resistance (Pico abrader)
D 2240	Test method for rubber property—Durometer hardness
D 3137	Test method for rubber property—hydrolytic stability
D 3452	Practice for rubber—identification by pyrolysis-gas chromatography
D 3677	Test methods for rubber—identification by infrared spectrophotometry

SI Units and Physical Constants

Table D-1 Units and Symbols

Quantity	Name	Symbol	CGS Equiv.
Capacity	liter	L	10^{-3} m^3
Electric capacitance	farad	F	A s V^{-1}
Electric current	ampere	A	ampere
Energy, work, heat	joule	J	N m
Force	newton	N	m kg s^{-2}
Frequency	hertz	Hz	s^{-1}
Mass	kilogram	kg	kg
Plane angle	radian	rad	rad
Power	watt	W	J s^{-1}
Pressure, stress	pascal	Pa	N m^{-2}
Viscosity (dynamic)	pascal second	Pa s	N s m^{-2}

Table D-2 Conversion Factors

	Conversion
Density	$1 \text{ g cm}^{-3} = 0.0361 \text{ lb in.}^{-3}$
Energy	$1 \text{ J} = 0.2387 \text{ cal}$
Force	$1 \text{ N} = 10^5 \text{ dynes} = 0.102 \text{ kg}_f = 0.2248 \text{ lb}_f$
Pressure, stress	$1 \text{ Pa} = 10 \text{ dyne cm}^{-2} = 7.5 \times 10^{-3} \text{ mm Hg} = 7.5 \times 10^{-4} \text{ cm Hg} = 10^{-5} \text{ bar} = 1 \text{ kg m}^{-1} \text{ s}^{-2} = 1.45 \times 10^{-4} \text{ psi} = 9.869 \times 10^{-6} \text{ atm}$
Solubility parameter	$1 \text{ (MPa)}^{1/2} = 0.489 \text{ (cal cm}^{-3}\text{)}^{1/2}$
Temperature	$^{\circ}\text{R} = (9/5)\text{K}$ $^{\circ}\text{C} = (5/9)(^{\circ}\text{F} - 32) = \text{K} + 273.15$
Thermal conductivity	$\text{J s}^{-1} \text{ cm}^{-1} \text{ K}^{-1} = 1 \times 10^{-2} \text{ W m}^{-1} \text{ K}^{-1}$
Viscosity	$1 \text{ Pa s} = 10 \text{ poise}$

Table D-3 SI Prefixes

Prefix	Symbol	Equivalent
pico	p	10^{-12}
nano	n	10^{-9}
micro	μ	10^{-6}
milli	m	10^{-3}
centi	c	10^{-2}
deci	d	10^{-1}
kilo	k	10^3
mega	M	10^6
giga	G	10^9

Table D-4 Fundamental Physical Constants

Physical Constant	Symbol	Unit	Value
Avogadro's number	N_A	mol^{-1}	6.0220×10^{23}
Boltzmann constant, R/N_A	k	J K^{-1}	1.3807×10^{-23}
Gas law constant	R	J (mol K)^{-1}	8.3144
		$\text{bar cm}^3 \text{ (mol K)}^{-1}$	83.144
		$\text{psia ft}^2 \text{ (lb mol } ^{\circ}\text{R)}$	10.732
		$\text{atm cm}^3 \text{ (mol K)}^{-1}$	82.057
Gravitational acceleration	g	m s^{-2}	9.80665
Planck constant	h	J s	6.6262×10^{-34}
Permeability of vacuum	μ_0	N A^{-2}	12.566×10^{-7}
Permittivity of vacuum, $1/\mu_0 c^2$	ϵ_0	F m^{-1}	8.85419×10^{-12}
Speed of light in vacuum	c	m s^{-1}	2.9979×10^8

Mathematical Relationships

Trigonometric Functions

$$\sin^2 \theta = \frac{1}{2} - \frac{1}{2} \cos 2\theta$$

$$\sin^2 \theta + \cos^2 \theta = 1$$

$$\sin(\theta \pm \phi) = \sin \theta \cos \phi \pm \cos \theta \sin \phi$$

$$\sin 2\theta = 2 \sin \theta \cos \theta$$

$$\cos 2\theta = \cos^2 \theta - \sin^2 \theta$$

Euler's Identities

$$e^{i\theta} = \cos \theta + i \sin \theta$$

$$e^{-i\theta} = \cos \theta - i \sin \theta$$

Quadratic Equation

$$ax^2 + bx + c = 0$$

$$x = \frac{-b \pm \sqrt{b^2 - 4ac}}{2a}$$

Derivatives

$$\frac{d}{dx}(u^n) = nu^{n-1} \frac{du}{dx}$$

$$\frac{d}{dx}(uv) = u \frac{dv}{dx} + v \frac{du}{dx}$$

$$\frac{d}{dx} \left(\frac{u}{v} \right) = \frac{v(du/dx) - u(dv/dx)}{v^2}$$

$$\frac{d}{dx} \sin \theta = \cos \theta \frac{d\theta}{dx}$$

$$\frac{d}{dx} \cos \theta = -\sin \theta \frac{d\theta}{dx}$$

$$\frac{d}{dx} \ln u = \frac{1}{u} \frac{du}{dx}$$

$$\frac{d}{dx} e^u = e^u \frac{du}{dx}$$

Indefinite Integrals

$$\int u^n du = \frac{u^{n+1}}{n+1} \quad (n \neq -1)$$

$$\int a^u du = \frac{a^u}{\ln a}$$

$$\int u dv = uv - \int v du \quad (\text{integration by parts})$$

$$\int e^u du = e^u$$

$$\int \frac{du}{u} = \ln u$$

$$\int \ln x dx = x \ln x - x$$

$$\int \sin u du = -\cos u$$

$$\int \cos u du = \sin u$$

$$\int \sin ax \cos ax dx = \frac{\sin^2 ax}{2a}$$

$$\int \sin ax \cos ax dx = \frac{\sin^2 ax}{2a}$$

$$\int \cos^2 u du = \frac{u}{2} + \frac{\sin 2u}{4} = \frac{1}{2}(u + \sin u \cos u)$$

Definite Integrals

$$\int_0^\pi \sin mx \cos nx dx = \begin{cases} 0 & m \text{ and } n, \text{ integers } m+n, \text{ odd} \\ 2m/(m^2-n^2) & m \text{ and } n, \text{ integers } m+n, \text{ even} \end{cases}$$

Geometric Series

$$a + ar + ar^2 + ar^3 + \dots + ar^{n-1} = \frac{a(1-rn)}{1-r} = \frac{a-rn}{1-r}$$

where $l = ar^{n-1}$ is the last term and $r \neq 1$

$$a + ar + ar^2 + ar^3 + \dots = \frac{a}{1-r} \quad (-1 < r < 1)$$

Taylor Series

$$e^x = 1 + x + \frac{x^2}{2!} + \frac{x^3}{3!} + \dots \quad (-\infty < x < \infty)$$

$$\ln(1+x) = x - \frac{x^2}{2!} + \frac{x^3}{3!} + \dots \quad (-1 < x \leq 1)$$

$$\ln(1-x) = -x - \frac{x^2}{2} - \frac{x^3}{3} - \dots$$

$$\ln x = 2 \left\{ \left(\frac{x-1}{x+1} \right) + \frac{1}{3} \left(\frac{x-1}{x+1} \right)^3 + \frac{1}{5} \left(\frac{x-1}{x+1} \right)^5 + \dots \right\} \quad (x > 0)$$

$$\ln x = \left(\frac{x-1}{x} \right) + \frac{1}{2} \left(\frac{x-1}{x} \right)^2 + \frac{1}{3} \left(\frac{x-1}{x} \right)^3 + \dots \quad \left(x \geq \frac{1}{2} \right)$$

$$\sin x = x - \frac{x^3}{3!} + \frac{x^5}{5!} - \frac{x^7}{7!} + \dots \quad (-\infty < x < \infty)$$

$$\cos x = 1 - \frac{x^2}{2!} + \frac{x^4}{4!} - \frac{x^4}{6!} + \dots \quad (-\infty < x < \infty)$$

The Gamma Function

$$\Gamma(n) = \int_0^\infty t^{n-1} e^{-t} dt \quad n > 0$$

$$\Gamma(n+1) = \int_0^\infty t^n e^{-t} dt = n\Gamma(n) = n! \quad (n \text{ is a positive integer})$$

Fourier Sine Transforms

$$F_s(\alpha) = \int_0^{\infty} f(x) \sin \alpha x dx$$

Table E-2 Fourier Sine Transforms

$f(x)$	$F_s(\alpha)$
$\begin{cases} 1, & 0 < x < b \\ 0, & x > b \end{cases}$	$\frac{1 - \cos b\alpha}{\alpha}$
x^{-1}	$\pi/2$
$\frac{x}{x^2 + b^2}$	$(\pi/2)e^{-b\alpha}$
e^{-bx}	$\frac{\alpha}{\alpha^2 + b^2}$

Fourier Cosine Transforms

$$F_c(\alpha) = \int_0^{\infty} f(x) \cos \alpha x dx$$

Table E-3 Fourier Cosine Transforms

$f(x)$	$F_c(\alpha)$
$\begin{cases} 1, & 0 < x < b \\ 0, & x > b \end{cases}$	$\frac{\sin b\alpha}{\alpha}$
$\frac{1}{x^2 + b^2}$	$\frac{\pi e^{-b\alpha}}{2b}$
e^{-bx}	$\frac{b}{\alpha^2 + b^2}$

Laplace Transforms

$$L[F(t)] = \int_0^{\infty} e^{-pt} F(t) dt = f(p)$$

$$F(t) = L^{-1}\{f(p)\}$$

Table E-1 Table of Useful Laplace Transforms

$F(t)$	$f(p)$
a	$\frac{a}{p}$
t	$\frac{1}{p^2}$
at	$\frac{a}{p^2}$
e^{at}	$\frac{1}{p-a}$
e^{-at}	$\frac{1}{p+a}$
$\cos at$	$\frac{p}{p^2 + a^2}$
$\frac{\sin at}{a}$	$\frac{1}{s^2 + a^2}$
$F(t-a)$	$e^{-ap}L[F(t)]$
$F'(t)$	$pf(p) - F(0)$
$F''(t)$	$p^2f(p) - pF(0) - F'(0)$
$\int_0^t F(u)G(t-u)du$	$f(p)g(p)$

This page intentionally left blank

The Major Elements

Table F-1 The Elements

Element	Symbol	Atomic Number	Atomic Weight
Aluminum	Al	13	26.98154
Argon	Ar	18	39.948
Arsenic	As	33	74.9216
Barium	Bs	56	137.33
Boron	B	5	10.81
Bromine	Br	35	79.904
Calcium	Ca	20	40.08
Carbon	C	6	12.011
Chlorine	Cl	17	35.453
Chromium	Cr	24	51.996
Cobalt	Co	27	51.9332
Copper	Cu	29	63.546
Fluorine	F	9	18.998404
Germanium	Ge	32	72.59
Gold	Au	79	196.9665
Helium	He	2	4.00260
Hydrogen	H	1	1.00794
Iodine	I	53	126.9045
Iron	Fe	26	55.847
Lead	Pb	82	207.2
Lithium	Li	3	6.941
Magnesium	Mg	12	24.305
Mercury	Hg	80	200.59

(continues)

Table F-1 The Elements (*continued*)

Element	Symbol	Atomic Number	Atomic Weight
Neon	Ne	10	20.1179
Nickel	Ni	28	58.69
Nitrogen	N	7	14.0067
Osmium	Os	76	190.2
Oxygen	O	8	15.9994
Palladium	Pd	46	106.42
Phosphorus	P	15	30.97376
Platinum	Pt	78	195.08
Potassium	K	19	39.0983
Radon	Rn	86	(222)
Rhodium	Rh	45	102.9055
Silicon	Si	14	28.0855
Silver	Ag	47	107.8682
Sodium	Na	11	22.98977
Sulfur	S	16	32.06
Tin	Sn	50	118.69
Titanium	Ti	22	47.88
Tungsten	W	74	183.85
Vanadium	V	23	50.9415
Zinc	Zn	30	65.38

Index

A

- Ab initio methods, 581, 584
- ABA block copolymers, SBS elastomers, 385
- ABA-triblock copolymers, 9
- AB-block copolymers, 9
- Abbreviations, polymer, 14–15, 621–623
- ABS, 401–402
- Acetal, 405–406
- Acrylics
 - medical applications, 526
 - non-cellulosic synthetic fibers of, 353
 - synthetic fibers of, 348
- Acrylonitrile
 - in ABS, 401
 - ABS formulated from, 401
 - acrylic fibers as copolymers of, 353
 - with butadiene for nitrile rubber, 377
 - copolymerization of styrene with, 369
 - free-radical copolymerization, 44–46
 - polymerized in SCFs, 72
 - polymerizing with ATRP, 60
- Activation energies
 - dissociation rate constant, 32
 - dynamic-mechanical analysis, 220–221
- Activity coefficients, predicting, 566–574
- Addition polymers, 4–5, 7
- Additives
 - antiplasticization, 286–287
 - antistatic agents, 292
 - biocides, 291
 - biodegradability and, 278
 - blowing agents, 292–293
 - compatibilizers, 293
 - determining composition of polymer mixture, 284
 - external and internal plasticization, 284–286
 - fillers and reinforcers, 287–288
 - flame retardants, 290–291
 - heat distortion and impact modifiers, 292
 - list of PVC plasticizers, 286
 - lubricants, curing agents, and colorants, 291–292
 - overview of, 281–282
 - plasticizers, 282–284
 - for potable water, 288–289
 - in prevention of degradation, 288
 - references, 293
 - stabilizers, 289–290
- Adenine (A), 337
- Adhesion, improving polymers with, 74
- Advanced technologies
 - biomedical engineering. *See* Biomedical engineering and drug delivery
 - electronics/energy. *See* Electronics and energy applications
 - membranes. *See* Membrane science and technology
 - overview of, 493–494
 - photonic polymers, 541–544
 - references, 550–551
 - review problems, 550
 - sensor applications, 544–546
 - suggested reading, 547–549
- Affine deformation, rubber elasticity, 254
- AFM (atomic force microscopy), 200–201
- Aliphatic polyamides. *See* Nylons (aliphatic polyamides)
- American Chemical Society (ACS), nomenclature, 14
- American Society of Testing Methods (ASTM)
 - D-4000, 14
 - heat-distortion temperature, 176–177
 - standards for plastics and rubber, 627–629
- Amidation, 26
- Amino acids, naturally occurring, 332–335
- Aminoplasts (UF or MF) resins, 389–393, 524
- Amorphous state
 - of atactic polymers, 11
 - critical molecular weight, 154–155
 - defined, 20
 - density measures, 166

- Amorphous state (*continued*)
 glass-transition temperature and, 156–158
 overview of, 154
 reptation, 155–156
 secondary-relaxation processes, 158–159
- Amorphous Teflon (TEFLON-AF), 411
- Anion-exchange resins, 75
- Anionic polymerization
 electron-withdrawing monomers in, 31
 overview of, 49–51
 preparing dienes, 375
- Anions, polymerization in ionic liquids, 73
- ANNs (artificial neural networks), 554, 578–581
- Antimicrobial polymers, 532
- Antioxidants, 268, 288–289
- Antiplasticization, 286–287
- Antistatic agents, as additives, 292
- Antithixotropic fluid, 452
- Apparent shear rate, capillary-rheometry, 470
- Apparent viscosity, 448–451, 470
- a*-PS (atactic PS), 368
- Argon gas, plasma polymerization, 70
- Aromatic polyamides (aramids)
 as engineering plastics, 400–401
 as step-growth polymers, 26
- Arrhenius dependence on temperature
 apparent viscosity, 451
 dissociation rate constant, 32
 propagation/termination rate constants, 36–37
- Artificial neural networks (ANNs), 554, 578–581
- Artificial organs, biomedical engineering, 533
- Association step, free-radical polymerization, 33
- ASTM. *See* American Society of Testing Methods (ASTM)
- Asymmetric-membrane formation, 518–523
- Atactic polymers
 example of amorphous polymer, 154
 geometric isomers as, 12–13
 overview of, 10–12
 producing atactic polypropylene, 367
- Atactic PS (*a*-PS), 368
- Atom transfer radical polymerization (ATRP), 51, 59–61
- Atomic force microscopy (AFM), 200–201
- Atomic indices, topological calculations polymer properties, 575–577
- Atomistic simulations, MD applications, 581–583
- ATRP (atom transfer radical polymerization), 51, 59–61
- Average degree of polymerization, 29
- Averages, molecular-weight, 16–20
- Avrami equation, 164
- Axial annular Couette flow, 467–468
- Azeotropic copolymerization, 47
- Azide-alkyne coupling reaction., click chemistry, 79–80
- Azo (R-N=N-R) compounds, free-radical initiators, 33
- ## B
- Backbone bonds, 575
- Bacterial growth, biocides for, 291
- Bakeland, Leo Hendrik, 2, 438
- Bagley plot of pressure drop, capillary rheometer, 472–473
- Bakelite, 2, 390
- Ball-and-stick representation, PVT simulation, 592
- Band gaps, electrically conductive polymers, 535
- Barostats
 NPT ensembles, 591
 PVT simulation, 591–593
- Barrier polymers, 494–495
- Batteries, polymeric, 535–537
- Becquerel, Edmund, 537
- Benzene, 109–110, 131–132
- Benzoyl peroxide, free-radical polymerizations, 32–34
- BF₃ counterion (gegen ion), isobutylene polymerization, 51
- BHJ (bulk-heterojunction) solar cells, 538–539
- Bicerano's method
 artificial neural network, 578–581
 topological indices and, 574–578
- Bingham fluids, 461–462
- Binodal curve, phase equilibria, 123–125
- Biocidal polymers, 532
- Biocides, additives, 291
- Biocompatibility
 controlled drug delivery and, 526–527
 improving polymer by adding, 74
 protein adsorption and, 526
- Biodegradation
 managing plastics, 275–278
 stability of polymers, 262
- Biomedical engineering and drug delivery
 antimicrobial polymers, 532
 artificial organs, 533
 controlled drug delivery, 527–530
 gene therapy, 530–531
 kidney dialysis, 533
 overview of, 526–527
 review problems, 547–549
 suggested reading, 547–549
 tissue engineering, 532
- Biopolymers
 cellulose as, 76
 naturally occurring elastomers, 344–346
 overview of, 331–332

- polynucleotides, 336–341
- polysaccharides, 341–344
- proteins, 332–336
- references, 359–360
- suggested reading, 358–359
- Bischloroformates, 381–382
- Bisphenol-A
 - nomenclature, 14–15
 - polymerization of, 6
 - synthesizing polycarbonate, 402–403
 - synthesizing polysulfones, 407
- Blade coating operation, 446
- Blends. *See* Polymer blends
- Block copolymers
 - overview of, 306–307
 - self-assembly, 307–309
 - suggested reading, 327
- Blow molding, 443–444
- Blowing agents, additives, 292–293
- BMC (bulk-molding compound), 316
- Boltzmann superposition principle
 - Flory–Huggins theory, 111
 - methods of dielectric analysis, 245–246
 - transient and dynamic properties, 247–248
- Bond indices, topological calculations for properties, 575–576
- Bonded terms, molecular mechanics force fields, 583–584
- Bond-rotation angle, polymer chain bonds, 105, 107–108
- Bound electrons, OPV solar cells, 538
- Bragg equation, 201, 598–599
- Bragg peaks, 167–168
- Branching, low-density polyethylene, 364–365
- Bromination, fire retardancy with, 74
- Buckyballs, nanocomposites, 322–323
- Bulk modulus, mechanical properties, 601–602
- Bulk polymerization, 64–65
- Bulk-heterojunction (BHJ) solar cells, 538–539
- Bulk-molding compound (BMC), 316
- Butadiene, 12–13, 401
- Butadiene-based elastomers, 376–377
- C**
- CA. *See* Cellulose diacetate (CA)
- Calendering, 436, 445
- Calorimetry
 - dynamic, 239–242
 - measuring thermal transitions, 170, 174–176
- Canonical ensemble, molecular simulations, 590–591
- Capillary, flow through a, 464–466
- Capillary modules, UF/MF applications, 524
- Capillary rheometry, 469–473
- Capillary viscometers, 142
- Carbon dioxide, supercritical fluid in polymerization, 71
- Carbon nanofiber (CNF), 319
- Carbon nanotubes (CNTs), 319, 323–324
- Carbonium ion, isobutylene polymerization, 51
- Carothers, Wallace, 4, 331
- Cartesian coordinates
 - equations for, 486
 - incompressible fluids, 462–463
 - polymer conformation/chain dimensions, 102–103
- Cast polymerization, 65
- Catalysts
 - atom transfer radical polymerization, 60
 - cationic polymerization, 51
 - chloromethylation of polystyrene, 74
 - metallocene, 55–56
 - olefin metathesis, 82
 - polyethylene with reduced branching, 364–365
 - RAFT polymerization, 61–63
 - using green chemistry for, 86
 - Ziegler-Natta, 55–56
- Cation-exchange resins, 75
- Cationic polymerization, 31–32, 51–52
- Cationic ring-opening polymerization (CROP), 51–52
- Cations, polymerization in ionic liquids, 73
- Caustic production, 504–505
- CBAs (chemical blowing agents), 292–293
- CED (Cohesive energy density), solubility parameter, 127–129, 593–594
- Ceiling temperatures (T_c), free-radical polymerization, 41–43
- Cellophane, 76
- Celluloid, 2, 440
- Cellulose
 - chemical structure of, 343
 - graft copolymerization using ATRP of, 61
 - as natural and abundant biopolymer, 76
 - polysaccharides, 342
 - preparing cellulose acetate from, 76
- Cellulose diacetate (CA)
 - intrinsic viscosity measurements, 140–143
 - low-angle laser light scattering of, 139–140
 - preparing from cellulose, 76
 - properties of, 347
- Cellulose nitrate development, 2
- Cellulose triacetate (CTA), 349–350
- Cellulosics, 347, 349–350
- CG (coarse-grained) simulations, 582–583, 587–588
- Chain dimensions, polymer conformation, 102–109
- Chain entanglements, 154–156, 202
- Chain expansion factor, 108
- Chain flexibility, 177

- Chain scission reactions, polymer degradation, 263–265
- Chain transfer, cationic polymerization, 52
- Chain-growth polymerization
- chain-extension reaction in, 25
 - controlled radical polymerizations, 57–64
 - coordination polymerization, 53–57
 - free-radical copolymerization, 43–49
 - free-radical polymerization, 32–43
 - free-radical polymerization kinetics, 28
 - ionic copolymerization, 53
 - ionic polymerization, 49–52
 - overview of, 31–32
- Chain-transfer agent
- bulk polymerization, 64–65
 - free-radical polymerization kinetics, 40–41
 - suspension polymerization, 66
- Chain-transfer coefficient, 40
- Characteristic pressure for mixture, Flory equation of state theory, 121
- Characteristic ratios, 108
- Characteristic temperature for mixture, Flory equation of state theory, 121
- Charpy tests, 185, 198
- Chemical blowing agents (CBAs), 292–293
- Chemical modification, reactions of polymers, 74–75
- Chemical structure determination
- nuclear magnetic resonance spectroscopy, 89–92
 - overview of, 86
 - structure–property relationships, 177–179
 - and thermal transitions, 20–22
 - vibrational spectroscopy, 86–89
- Chitin, 343–344
- Chitosan, 343
- Chlor-alkali cell, caustic production, 504–505
- Chlorination, commercial PVC, 370
- Chloromethylation, polystyrene, 74
- 4-chlorostyrene, 44–49
- Cholesteric state, liquid-crystal structures, 425
- cis*-polyacetylene, 427
- Classification of polymers
- mechanism of polymerization, 4–7
 - polymer structure, 7–8
 - thermoplastics and thermosets, 3–4
- Click chemistry, 74, 79–80
- Clot (thrombus) formation, artificial organs, 533
- Cloud-point curve, polymer blends, 295–296
- Clusters, ionic polymers, 421
- CNF (carbon nanofiber), 319
- CNTs (carbon nanotubes), 319, 323–324
- Coarse-grained (CG) simulations, 582–583, 587–588
- Coated asymmetric membranes, 521–523
- Coating, 445–446
- Cohesive energy density (CED), solubility parameter, 127–129, 593–594
- Cold drawing, stress/strain testing, 192
- Colorants, as additives, 291–292
- Combinatorial (entropy) term, UNIFAC-FV, 566–568
- Commercial blends, 300–301
- Commodity thermoplastics
- as largest share of market, 361
 - overview of, 362
 - polyolefins, 362–367
 - thermoplastic polyesters, 372–374
 - vinyl polymers, 367–372
- Common names, nomenclature for polymers, 14
- Comonomer distribution, 90
- COMPASS force field, 587, 592–593
- Compatibilizers, as additives, 293
- Composite membranes, 521–523
- Composites
- benefits of, 282
 - dynamic-mechanical properties, 314–316
 - fabrication of, 316–317
 - filament winding in fabrication of, 317–318
 - interfacial adhesion and coupling agents, 313–314
 - modulus of, 311–312
 - overview of, 310–311
 - pultrusion in fabrication of, 317–318
 - strength of, 312–313
 - suggested reading, 327
- Compressibility coefficient, Flory equation of state theory, 119
- Compression
- molding, 438
 - processing composites, 310
 - as section of extruders, 436–437
 - testing mechanical properties, 190–191
- Condensation polymers
- nomenclature rules, 13–14
 - overview of, 6–7
 - RIM suited only for, 442
 - step growth polymerization of, 7, 26–27
- Conductive polymers, 427–429, 533–535
- Cone-and-plate rheometer, 475
- Configuration
- of polymer chain, 102
 - stereochemical/geometrical arrangement of atoms, 9–11
- Conformation and chain dimensions
- overview of, 102–109
 - references, 150
 - review problems, 146–150
 - suggested reading, 146
- Connectivity indices, 575–576
- Consistency, power-law index and, 461–462
- Constitutive equations, 456–457, 461–468
- Continuity equations
- defined, 462

- for incompressible fluids, 463
- polymer processing, 486–487
- Controlled drug delivery (release), 527–530
- Controlled living radical polymerizations (CRP), 51, 58, 73
- Controlled radical polymerizations
 - atom transfer radical polymerization, 59–61
 - miniemulsion techniques of, 69
 - nitroxide-mediated polymerization, 58–59
 - overview of, 57–58
 - RAFT polymerization, 61–64
- Conversion factors, 632
- Coordination polymerization
 - metallocene polymerizations, 56–57
 - overview of, 53–56
 - for polyethylene with reduced branching, 364–365
- Copolyesters, thermoplastic, 386
- Copolymerization
 - free-radical, 43–49
 - ionic, 53
- Copolymers
 - in low-density polyethylene production, 363–364
 - overview of, 9
 - possible structures of, 9–10
 - scheme for naming, 15
 - of vinyl chloride, 369–371
- Copper halide, 60
- Copper-catalyzed Huisgen Cu(I) 1,3-dipolar cycloaddition, 79
- Correlations and simulations
 - group-contribution. *See* Group-contribution methods
 - molecular simulation applications. *See* Molecular simulation applications
 - molecular simulations. *See* Molecular simulations
 - overview of, 553–554
 - references, 612–616
 - review problems, 612
 - suggested reading, 611–612
 - topological indices and Bicerano's method, 574–581
- Cotton, 346–347
- Couette rheometer, 472–474
- Coulombic expression, 586–587
- Coupling agents, composites, 313–314
- Cox–Merz rule, 230
- Cp₂MX₂ (cyclopentadienyl ligands), as metallocene catalysts, 57
- CPDB (2-cyanoprop-2-yl dithiobenzoate), 62–63
- CPK (space-filling) representation
 - of PVC chain, 11–12
 - of PVT simulation, 592
- CPK (space-filling) representation, PVT simulation, 592
- Cracking, solvent, 269–270
- Crankshaft rotation model, 158
- Crazing, 183–184, 269–270
- Creep resistance, acetal, 405
- Creep tests
 - Maxwell model and, 222
 - overview of, 185
 - time-temperature superposition, 242–245
 - transient tests of mechanical properties, 195–196
 - Voigt model and, 225
- Critical concentration regions, solution viscosity, 452–455
- Critical micelle concentration, emulsions, 67
- Critical molecular weight (M_c), 154–155
- Critical point, phase equilibria, 124
- CROP (cationic ring-opening polymerization), 51–52
- Cross coupling, molecular force fields, 585–586
- Cross talk, dielectrics, 541
- Crosslinks
 - effect on glass-transition temperature, 182
 - hydrogels, 80
 - of polystyrene, 369
 - rubber elasticity and, 254
 - unsaturated polyesters, 387–388
- Cross-terms, molecular force fields, 585
- CRP (controlled living radical polymerizations), 51, 58, 73
- Cryogenic separation, 498
- Crystalline kinetics, 164–165
- Crystalline polyoxymethylene, 70
- Crystalline state
 - crystalline kinetics, 164–165
 - crystalline-melting temperature, 163–164
 - ordering of polymer chains, 159–162
 - overview of, 159
 - techniques for determining crystallinity, 165–167
- Crystalline-melting temperature (T_m)
 - crystalline state and, 160
 - heat-distortion temperature, 176–177
 - overview of, 163–164
 - structure–property relationships, 177–179
 - thermal transitions and, 21–22, 161
- Crystallinity
 - isotactic polypropylene, 54
 - low-density polyethylene, 53
 - Raman spectroscopy studying, 89
 - suggested reading, 202
 - of tactic polymers, 11
 - using FTIR to follow development of, 87–88
- Crystallites, thermal transitions and, 21
- CTA (cellulose triacetate), 349–350
- CTFE (polychlorotrifluoroethylene), 377, 411–412
- Cull, transfer molding process, 438–439
- Curing agents, as additives, 291–292
- CVFF force field, 587

- Cyclic tests. *See* Fatigue tests
- Cycloalkene, 82
- Cyclohexane, 131–132
- Cyclopentadienyl ligands (Cp_2MX_2), as metallocene catalysts, 57
- Cyclopentene, ring-opening metathesis of, 82
- Cylindrical coordinates
- equations for, 487
 - expressing elastic response, 458
 - polymer rheology, 447
 - using Couette rheometer, 473–474
- D**
- D (diffusion coefficient), estimating permeability, 605–610
- de Gennes, Pierre-Gilles, 156
- Debye, Peter, 237
- Debye equation, 139–140
- Definite integrals, 635
- Deformation mechanisms
- crazing, 183–185
 - dynamic, 212–213
 - elastic recovery of solutions after shear, 457–460
 - overview of, 183
 - shear banding, 184
 - testing compression or shear strain, 190–191
 - testing stress or strain, 186–190
- Degradation of polymers
- additives for preventing, 288
 - biodegradation, 275–278
 - chain scission reactions, 263–265
 - environmental strategies for managing plastics, 272–273
 - hydrolytic effects, 269–271
 - incineration of plastics, 274
 - mechanodegradation, 272
 - non-chain scission reactions, 265–266
 - overview of, 261
 - oxidative and UV stability, 267–269
 - radiation effects, 271–272
 - recycling plastics, 273–274
 - references, 279–280
 - solvent crazing and cracking, 269–270
 - stability and, 262
 - strategies for thermal stability, 266–267
 - suggested reading, 279
 - thermal degradation, 262–263
- Degree of polymerization, as molecular weight, 29
- Dehydrohalogenation, in degradation, 265
- Delaunay tessellation, free volume, 610–611
- Dendrimers
- defined, 430
 - in polymeric nanomedicines, 527–528
 - as specialty plastics, 430–431
- Density
- crystallinity measures, 165–166
 - polymerization in ionic liquids and, 73
- Density functional theory (DFT), 581, 584
- Deoxyribonucleic acid (DNA), 336–339
- Depolymerization
- chain scission reactions in degradation, 263–264
 - thermodynamics of free-radical polymerization, 41–42
- Derivatives
- mathematical functions of, 634
 - preparing polymer, 76–77
- Detector, gel-permeation chromatography, 144
- Determination of interaction, 125–126
- Devolatilization process, extrusion, 437
- DFT (density functional theory), 581, 584
- Dialysis, 505, 533
- Die
- extrusion operations, 436–437
 - flow through capillary, 465
 - injection molding process, 440–441
 - modeling extrusion process, 477–479
 - modeling wire coating process, 482–485
- Die swell, elastic response, 457–460
- Dielectrics
- analysis, 237–239
 - overview of, 541
 - relaxational strength, 235
 - suggested reading, 255
- Diels-Alder diene + olefin cycloaddition reaction, 79
- Diene elastomers
- butadiene-based elastomers, 376–377
 - metathesis elastomers, 377
 - polychloroprene, 377
 - polyisoprene, 377
 - polymerization of, 374–376
 - vulcanization, 377–379
- Differential refractometer, gel-permeation chromatography, 144
- Differential scanning calorimetry (DSC), 170, 174–176
- Diffusion coefficient (D), estimating permeability, 605–610
- Diffusion control, of drug release, 529
- Diffusivity, solution-diffusion transport, 509–515
- Diisocyanates, 381–383
- Dilatometry, 169, 172–174
- Dilute polymer solution, Flory-Krigbaum theory, 116–117
- Dimethyl terephthalate (DMT), 273
- Dipolar correlation function, 598–599
- Dissociation of initiator, 32, 37–39
- Dissociation rate constants, free-radical polymerization, 32–33
- Dissolving power, supercritical fluids, 71

- Dissymmetry method, molecular weight, 138–139
- Distribution, molecular weight, 15–16
- DMT (dimethyl terephthalate), 273
- DNA
- in conjugated polymeric nanomedicines, 527–528
 - in gene therapy, 530–531
 - using genetically engineered protein-like polymers, 85
- Double extrapolation, Zimm plot, 137–138
- Drag flow
- axial annular Couette flow, 467–468
 - extrusion process, 477–482
 - plane Couette flow, 467
 - wire coating process, 484–485
- Drag reduction, polymer rheology, 460–461
- Draw stress, 192
- DREIDING force field, 587
- Drug conjugates, polymeric nanomedicines, 527–528
- Drug delivery, controlled, 527–530
- Dry process, asymmetric-membrane formation, 520
- Dry spinning, fibers, 355
- DSC (differential scanning calorimetry), 170, 174–176
- Dual-mode model, solution-diffusion transport, 510–511, 513
- Dynamic calorimetry, 239–242
- Dynamic deformation, 212–213
- Dynamic equations
- defined, 462
 - flow through capillary, 464–465
 - plane Couette flow, 467
 - polymer processing, 486–487
 - solution to flow problems, 462–464
 - wire coating, 485
- Dynamic viscosity, 230
- Dynamic-mechanical analysis, viscoelasticity
- activation energies, 220–221
 - experimental techniques, 213–214
 - forced-vibration methods, 218–220
 - free-vibration methods, 214–218
 - theory, 208–212
 - work in dynamic deformation, 212–213
- Dynamic-mechanical properties, composites, 314–316
- Dynamic-mechanical spectroscopy, 255
- E**
- Eccentric rotating-disk (ERD), 231–232
- Ehrenfest second-order transition, 169
- Einstein coefficient, viscosity of suspensions, 455
- Ejector pin, transfer molding, 438–439
- Elastic properties of polymeric fluids, 457–460
- Elastin, 344–345
- Elastomers. *See also* Rubber elasticity
- birth of polymer science, 2
 - from copolymers of TFE/perfluoroalkyl vinyl ethers, 412
 - diene, 375–379
 - graft copolymers as, 9
 - naturally occurring, 344–346
 - nondiene, 379–384
 - obtained from metathesis, 81–82
 - overview of, 374–375
 - principle feature of, 361–362
 - references, 395
 - review problems, 394
 - RIM-produced polyurethane used for, 442
 - suggested reading, 394
 - suitable polymers for, 1
 - thermoplastic, 384–386
- Electrically conductive polymers, 533–535
- Electrodialysis, 504–505
- Electromagnetic interference (EMI) shielding, 540
- Electron acceptors, OPV solar cells, 538–539
- Electron beams, radiation effects on polymers, 271–272
- Electron spectroscopy for chemical analysis (ESCA), 70
- Electron-donating monomers, polymerizing by cationic pathway, 31–32
- Electronic encapsulation, 541
- Electronic shielding, 540
- Electronics and energy applications
- dielectrics, 541
 - electrically conductive polymers, 533–535
 - electronic encapsulation, 541
 - electronic shielding, 540
 - organic photovoltaic polymers, 537–540
 - overview of, 533
 - polymeric batteries, 535–537
 - review problems, 550
 - suggested reading, 547–549
- Electron-withdrawing monomers, 31
- Electro-osmosis, 505
- Electrospinning, fibers, 357–358
- EMI (electromagnetic interference) shielding, 540
- Emissions, burning plastic, 274
- Emulsion polymerizations, 67–69
- Encapsulation, electronic, 541
- Endurance limits, fatigue tests, 199
- Energy, laws of thermodynamics and, 248–251
- Energy equations, 462
- Engineering plastics
- ABS, 401–402
 - acetal, 405–406
 - engineering polyesters, 409–410
 - fluoropolymers, 411–412
 - modified poly(phenylene oxide), 404–405
 - polyamides, 399–401
 - polycarbonates, 402–403

- Engineering plastics (*continued*)
 poly(*p*-phenylene sulfide) (PPS), 408–409
 polysulfones, 406–408
 properties of important, 398
 references, 433–434
 review problems, 433
 specialty plastics vs., 397–398
 suggested reading, 431–432
- Engineering polyesters, 409–410
- Engineering shear stress, 190
- Engineering strain, 186
- Engineering stress, 186
- Ensembles, molecular simulations, 590–591
- Entanglements
 effect of shear on, 449–450
 solution viscosity, 454–455
- Enthalpy of mixing, Flory–Huggins theory, 114–115
- Entropy, laws of thermodynamics and, 248–251
- Entropy of mixing, 111–115
- Environment
 agents impacting polymers, 262
 biodegradation, 275–278
 green chemistry and hazards of, 86
 incineration of plastics, 274
 recycling plastics, 273–274
 strategies for managing plastics, 272–273
- EOS. *See* Equation of state (EOS), Flory
- Epoxies
 cure of, 387–388
 overview of, 386–387
 producing using RIM, 442
 as thermosets, 4
- EPS (expandable PS), 367
- Equation of state (EOS), Flory
 Flory–Huggins theory, 297–298
 interaction parameter determination, 125–126
 overview of, 118–122
 predicting activity coefficients, 566, 570
 thermodynamics of polymer solutions, 117–118
- ERD (eccentric rotating-disk), 231–232
- ESCA (electron spectroscopy for chemical analysis), 70
- Ester interchange, step-growth polymers, 26
- Esterification, step-growth polymers, 26
- Ethylene
 addition polymers derived from, 4–5
 free-radical polymerization of, 53
 gas-phase polymerization of, 69
 in low-density polyethylene production, 363–364
 polymerizing. *See* Polyethylene (PE)
 and propylene (EPM/EPDM) rubber, 384
 Unipol process for, 366
- Euler's identity, 210–211, 633
- EVA (vinyl acetate), 363, 370–371
- Evaporation process, membranes, 502–503
- EVOH (vinyl alcohol), 363
- Exchange interaction parameter, Flory, 121
- Excitons, OPV solar cells, 538
- Excluded volume, real polymer chain bonds, 106–108
- Expandable PS (EPS), 367
- Explosives detection, chemical sensors, 546
- External degrees of freedom, Flory EOS theory, 118–119
- External plasticization, 284–286
- Extruder
 extrusion blow-molding process, 443–444
 extrusion operations, 436–437
- Extrusion
 blow-molding process, 443–444
 defined, 436
 modeling of, 476–482
 process, 436–437
- ## F
- Fabrication of composites, 316–318
- Facilitated and coupled transport, 515–516
- Failure envelope, testing stress or strain, 193
- Fast-scanning calorimetry (FSC), 176
- Fatigue life, 199
- Fatigue tests, 186, 199–200
- Feed section, extruders, 436–437
- FEP (fluorinated ethylene–propylene copolymer), 412
- Fiberglass, 4, 310
- Fibers
 cellulose, 349–350
 in composite materials, 310
 fiber-reinforced composites, 313
 filler and reinforcer additives, 287–288
 naturally occurring, 346–347
 non-cellulosic, 350–354
 overview of, 331–332, 346
 references, 359–360
 spinning, 354–358
 suggested reading, 359
 synthetic, 1–2, 347–348
 U.S. production of synthetic, 2–3
- Fiber-spinning operations
 dry spinning, 355
 electrospinning, 357–358
 melt spinning, 354
 wet spinning, 356–357
- Fibroin, 347
- Fick's first law, 512–513
- Filament winding, 310, 317–318
- Fillers, as additives, 287–288
- Filtration membranes, 495–498
- Finite (van der Waals) volume, 106
- First (or primary) normal-stress difference, 459
- First-order transitions, thermodynamic relationships, 167–169

- Flame retardants
 as additives, 288, 290–291
 improving polymer by adding, 74
 strategies for thermal stability, 266
- Flash
 compression molding process, 438
 rotational molding producing little/no, 444
- Flexibility, chains, 177
- Flory, Paul
 equation of state theory. *See* Equation of state (EOS), Flory
 Flory–Huggins theory. *See* Flory–Huggins theory
 Fox–Flory parameters, 179–180
 liquid-crystalline polymers and, 424
- Flory constant, 143
- Flory–Huggins theory
 estimating activity of solvents, 566
 membrane osmometry, 130
 modified, 117
 predicting activity coefficients, 567–568
 predicting blend behavior, 296–298
 solution-diffusion transport, 509–510
 thermodynamics of polymer solutions, 110–115
 weaknesses of, 116–118
- Flory–Krigbaum theory, 116–117
- Flowing afterglow plasma reactor, 70
- Fluids
 drag flow, 467–468
 drag reduction, 460–461
 elastic properties of polymeric, 457–460
 generalized Newtonian fluid model, 448–450
 melt instabilities, 460
 modeling polymer-processing operations, 476–485
 rheometry. *See* Rheometry
 supercritical, 71
 thixotropic vs. antithixotropic, 452
- Fluorinated ethylene–propylene copolymer (FEP), 412
- Fluoroelastomers, 380–381
- Fluoropolymers, 411–412
- Flux, asymmetric-membrane formation, 518–519
- Force field parameterization, CG systems, 582, 587–588
- Force fields, molecular, 583–588
- Forced-vibration methods, dynamic-mechanical analysis, 218–220
- Formaldehyde resins
 acetal, 405–406
 aminoplasts, 391–393
 overview of, 389–390
 phenoplasts, 390–391
- Fourier transform infrared (FTIR) spectroscopy, 86–88
- Fox equation, 181–182
- Fox–Flory parameters, 179–180
- Fractional monomer conversion, 29
- Free radical polymerization, with step growth, 28
- Free radicals, oxidative and UV stability, 268
- Free volume, molecular simulation applications, 610–611
- Freely jointed chains, 102–105
- Freely rotating chain models, 107–108
- Free-radical copolymerization, 43–49
- Free-radical polymerization
 of commercial-grade PVC, 370
 controlled. *See* Controlled radical polymerizations
 of ethylene and polyethylene, 53–54
 initiation step, 32–33
 kinetics, 37–41
 of low-density polyethylene, 364–365
 overview of, 32
 propagation step, 34
 termination step, 34–37
 thermodynamics of, 41–43
 using bulk polymerization, 65
- Free-vibration methods, dynamic-mechanical analysis, 214–218
- Free-volume contribution, predicting activity coefficients, 570, 573–574
- FSC (fast-scanning calorimetry), 176
- FTIR (Fourier transform infrared) spectroscopy, 86–88
- Fuel cell membranes, 506–507
- Functional group, macromers, 84
- ## G
- G (guanine), 337
- Gage length (L_g), static testing, 186
- Gamma function, 635
- Gas permeability, predicting, 559–560
- Gas sensors, conjugated polymers as, 546
- Gas separations, polymeric membranes in, 498–501
- Gas-phase polymerization, 69
- Gaussian distribution, 102–103
- Gauss's flux theorem, 233
- GCMC (Grand Canonical Monte Carlo) simulations, 602–605
- Gel effect, 65
- Gel-permeation chromatography (GPC), 129–130, 143–146
- Gene therapy, 530–531
- Generalized Newtonian fluid (GNF) model, 448–450
- General-purpose styrenic polymers (GP-PS), 367–369
- Genetic engineering, 85–86
- Geometric isomerism, 12–13
- Geometric series, 635
- Geometrical arrangement of atoms, conformation, 9
- Gibbs free energy (G)
 first derivative applied to thermal properties, 167–168

- Gibbs free energy (G) (*continued*)
 of mixing, 112, 122–125
 polymer blends and, 294
 second derivative applied to thermal properties,
 169–170
- Glass-transition temperature (T_g)
 crystalline state and, 160
 defined, 154
 heat-distortion temperature, 176–177
 molecular simulation applications, 594–595
 molecular weight, composition, pressure and,
 179–182
 overview of, 20–21
 predicting by group contributions, 558–559
 of sample amorphous polymers, 158
 structure–property relationships and, 157,
 177–179
 suggested reading, 202
 thermal transitions of semicrystalline poly-
 mers, 161
 views of, 156–157
- Glassy domains, SBS elastomers, 385–386
- Glycogen, 341–342
- Glyptal, 2
- GNF (generalized Newtonian fluid) model, 448–450
- Goodyear, Charles, 2
- Gordon–Taylor equation, 283–284
- Gossamer Albatross* aircraft, 26
- Gough–Joule effect, 248
- GPC (gel-permeation chromatography), 129–130,
 143–146
- GP-PS (general-purpose styrenic polymers), 367–369
- γ -radiation, 271–272
- Gradient IPNs, 306
- Graft copolymers, 9, 61, 70
- Graft polymerization, 84
- Graham, Thomas, 498
- Grand Canonical Monte Carlo (GCMC) simulations,
 602–605
- Grand canonical (μVT) ensemble, molecular simula-
 tions, 591
- Graphene, 324–325
- Green chemistry, 86
- Group-contribution methods
 activity coefficients, 566–574
 glass-transition temperature, 558–559
 overview of, 554
 permeability, 559–562
 predicting polymer properties with, 553–554
 solubility parameter, 562–565
 volumetric properties, 554–558
- Group-interaction parameters, UNIFAC, 569–570
- Group-transfer polymerization (GTP), 83–84
- GTP (group-transfer polymerization), 83–84
- Guanine (G), 337
- Guar, as drag-reducing agent, 461
- Guth–Smallwood equation, 253
- ## H
- Hagen–Poiseuille *equation*, 465
- Halogen atom transfer promoter, 60
- Halpin–Tsai equation, 311–312
- HALS (hindered-amine light stabilizers), 405
- HDPE. *See* High-density polyethylene (HDPE)
- HDT. *See* Heat-distortion temperature (HDT)
- Head-to-head monomer placement, 34, 90
- Head-to-tail monomer placement, 34, 90
- Heat capacity, thermal conductivity, 65
- Heat dissipation, in bulk polymerization, 65
- Heat distortion modifiers, as additives, 292
- Heat of polymerization (ΔH_p), 42–43
- Heat-distortion temperature (HDT)
 heat distortion modifiers, 292
 measuring thermal transitions, 176–177
 polymerizing polycarbonates, 403
 PPO, 404
 properties of blends, 303
- Heating rate, effect on T_g , 182
- Helium–neon (He-Ne) lasers, light scattering instru-
 ments, 139–140
- Helmholtz free energy, 252
- Henry’s law, solution–diffusion transport,
 509–511, 513
- Heterochain polymers, backbone structure of, 8
- Heteropolymers, proteins as, 332
- Hevea rubber
 as natural elastomer, 346
 as natural occurring polymer, 1
 synthetic rubber and short supply of, 2
 vulcanization of, 377–379
- High-impact polymers, 9
- High monomer conversion, 29–30
- High monomer purity, 30
- High reaction yield, 29–30
- High yield, of bulk polymerization, 64–65
- High-density polyethylene (HDPE)
 commercial applications, 366
 development of, 54–55
 polypropylene vs., 367
 properties, 362–363
- High-impact polystyrene (HIPS)
 overview of, 302–303
 production of, 369
 properties of, 367
- High-molecular-weight polymers, 25
- High-performance fibers, 429–430
- Hindered-amine light stabilizers (HALS), 405
- HIPS (high-impact polystyrene), 302–303, 369
- Hollow-fiber modules, 524
- Homochain polymers, 7–8

- Hooke's law
 applied to strain rate of elastic spring, 221
 determining mechanical properties, 600–602
 dynamic-mechanical analysis and, 210
 shear deformation, 190
 stress and strain in tensile deformation, 188
- Huggins equation, 141
- Huggins, Maurice. *See* Flory–Huggins theory
- Hyatt, John Wesley, 440, 443
- Hydrogels, controlled drug release, 529
- Hydrolysis, 262, 269–271
- Hydroxyl groups, 76
- Hyper-filtration membranes, 497–498
- I**
- IGC (inverse gas chromatography), 125–126
- Immiscibility, polymer blends and, 296–297
- Impact modifiers, as additives, 292
- Impact tests, 186, 198–199
- Incineration of plastics, 274
- Indefinite integrals, 634
- Infrared spectroscopy, 86–89
- Iniferfers, 58
- Initiation step
 anionic polymerization, 49–50
 free-radical polymerization, 32–33
 free-radical polymerization kinetics, 37–39
- Initiators
 anionic polymerization, 49–50
 bulk polymerization, 64–65
 controlled “living” radical polymerization, 58
 emulsion polymerization water-soluble, 67–69
 free-radical, 32–33
 group-transfer polymerization, 83
 RAFT polymerization, 63
 solution polymerization, 66
 suspension polymerization, 66
- Injection blow-molding process, 443
- Injection molding, 438, 440–441, 452
- Inorganic photovoltaic (IPV) solar cells, 537–538
- Instantaneous copolymerization equation, 44
- Instrumentation
 gel-permeation chromatography, 143–144
 He-Ne lasers in light scattering, 139–140
 light-scattering, 136–137
- Interaction parameter
 determination of, 125–126
 Flory, 115–116
 Flory exchange, 121
- Interfacial adhesion, composites, 313–314
- Internal degrees of freedom, Flory EOS theory, 118–119
- Internal plasticization, 284
- Internal rotational angle, real polymer chain bonds, 105–106
- International Union of Pure and Applied Chemistry (IUPAC), 14–15
- Interpenetrating polymer networks (IPNs), 304–306, 326–327
- Intrinsic viscosity measurements, molecular-weight determination, 140–143
- Inverse emulsion polymerization, 69
- Inverse gas chromatography (IGC), 125–126
- Inverse rule of mixtures, 181
- Ion-exchange resins, 75
- Ionic addition, 28
- Ionic copolymerization, 53
- Ionic liquids, 72–73
- Ionic polymerization
 anionic polymerization, 49–51
 cationic polymerization, 51–52
 overview of, 49
- Ionic polymers, as specialty plastics, 421–422
- Ionization, radiation effects on polymers, 271–272
- Ionomers, 421–422
- IPNs (interpenetrating polymer networks), 304–306, 326–327
- i*-PP (isotactic polypropylene), 54–55, 367–368
- i*-PS (isotactic PS), 368
- IPV (inorganic photovoltaic) solar cells, 537–538
- IR analysis, FTIR spectroscopy, 87
- Isobutylene polymerization, 51
- Isocyanates, elastomeric polyurethane, 381
- Isoentropic state, glass transition, 157
- Isofree volume, glass transition, 157
- Isomeric forms, 12–13
- Isotactic polymers, 10–13
- Isotactic polypropylene (*i*-PP), 54–55, 367–368
- Isotactic PS (*i*-PS), 368
- Isothermal compressibility coefficient (β), 170–172
- Isothermal flow, wire coating, 484–485
- Isothermal-isobaric (NPT) dynamics
 defined, 591
 glass-transition temperature, 594–595
 PVT simulation, 591–593
- Isoviscous state, glass transition, 156–157
- Italicized connective terms, naming copolymers, 15
- IUPAC (International Union of Pure and Applied Chemistry), 14–15
- Izod tests, 185, 198–199
- K**
- K₂SO₄ (persulfate-ferrous) redox initiator, 67
- Kapton (DuPont), 413–414
- Kel (or CTFE), 377, 411–412
- Kelley–Bueche equation, 180–181
- Keratin, in naturally occurring fibers, 347
- Kidney dialysis, 533
- Kinetics
 crystalline, 164–165

Kinetics (*continued*)

- free-radical emulsion polymerization, 68–69
 - free-radical polymerization, 28, 37–41
 - step-growth polymerization, 30–31
- Knudsen flow, 508–509
Knudsen number, 508

L

- Ladder polymers, 418
LALLS (low-angle laser light scattering), 139–140
Lamé constants, 601–602
Lamellae, 159, 164
L-amino acids, 332–335
Langmuir-type hole-filling, solution-diffusion transport, 510–513
Laplace transforms, 247, 636
Latex, 455
Lattice model
 - Flory–Huggins theory, 110–116
 - modified Flory–Huggins, 117
 - weaknesses of, 117–118
LCP (liquid-crystalline polymers), 424–426
LCST (lower critical solution temperature), 125, 294–297
LDPE. *See* Low-density polyethylene (LDPE)
LEDs (light-emitting diodes), 543–544
Lennard-Jones model, 506–508, 511
Letters, nomenclature system, 13–15
Lewis acid, 51, 55
Lewis–Randall law, 112
Light-emitting diodes (LEDs), 543–544
Light-scattering measurements
 - determining molecular-weight with, 17, 134–147
 - dissymmetry method of, 138–139
 - low-angle laser light scattering method of, 139–140
 - Zimm plot for, 137–138
Limiting-property relationships, 179–180
Liquid separation membranes, 502–504
Liquid-crystalline polymers (LCP), 424–426
Liquid–liquid equilibrium (LLE), predicting, 566
Lithium–polymer batteries, 535–537
Living cationic polymerization, 52
Living polymerization, 49–51
LLDPE (low-pressure, low-density PE), 366
LLE (liquid–liquid equilibrium), predicting, 566
Log decrement, dynamic-mechanical analysis, 215–216
Logarithmic rule of mixtures, 182
Low-angle laser light scattering (LALLS), 139–140
Low-density polyethylene (LDPE)
 - commercial applications, 363
 - development of, 53
 - LLDPE advantages over, 366
 - production of, 363–366

properties of, 362–363

- Lower critical solution temperature (LCST), 125, 294–297
Low-pressure, low-density PE (LLDPE), 366
Low-pressure, low-density polyethylene (LLDPE), 366
Lubricants, as additives, 291–292
Lyotropic polymers, 424

M

- Macromers, 84
Magic-angle spinning (MAS) NMR, 91
MAO (methylaluminoxane), 55–56
Market forecasting, using ANNs, 579
Mark–Houwink constants, GPC universal calibration, 145–146
Mark–Houwink–Sakurada equation, 140
MARTINI force field, 587–588
MAS (magic-angle spinning) NMR, 91
Mastication, mechanodegradation, 272
Mathematical relationships
 - definite integrals, 635
 - derivatives, 634
 - Euler’s identity, 633
 - gamma function, 635
 - geometric series, 635
 - indefinite integrals, 634
 - Laplace transforms, 636
 - quadratic equation, 633
 - Taylor series, 635
 - trigonometric functions, 633
Maxwell elements
 - limitations of simple Maxwell model, 225–226
 - Maxwell–Wiechert multielement modeling, 226–228
 - modeling viscoelastic behavior, 221–224
 - relaxation and retardation spectra, 228–229
MC. *See* Monte Carlo (MC) simulations
MCMC (Monte Carlo Markov chain) method, 582
MD. *See* Molecular dynamics (MD)
MD_REACT force field, 587
MDMO-PPV/fullerene BHV, 538–539
Mean free path, through porous media, 508
Mean-square end-to-end distance
 - calculating for polymer chain, 103–104
 - light-scattering measurements, 136
 - in real polymer chain bonds, 104–105
Mean-square radius of gyration, light-scattering, 136
Measurement techniques, thermal transitions
 - calorimetry, 174–176
 - dilatometry, 172–174
 - heat-distortion temperature, 176–177
 - overview of, 172
Mechanical models, viscoelastic behavior
 - Maxwell model, 221–224

- multi-element models, 226–228
 - overview of, 221
 - relaxation and retardation spectra, 228–230
 - simple models, 225–226
 - Voigt model, 225
- Mechanical properties**
- commercial polymers, 626
 - composites, 311–312
 - creep tests, 195–196
 - fatigue testing, 199–200
 - impact testing, 198–199
 - mechanisms of deformation, 183–185
 - molecular simulation applications, 600–602
 - static testing, 186
 - stress-relaxation measurement, 196–198
 - stress-strain behavior curves, 191–194
 - suggested reading, 202–203
 - testing compression or shear strain, 190–191
 - testing methods overview, 185
 - testing stress or strain, 186–190
 - transient testing, 194–197
- Mechanodegradation, 272**
- Mediating nitroxides, 59**
- Medical applications. *See* Biomedical engineering and drug delivery**
- Melamine–formaldehyde (MF) resins, 389–393**
- Melt fracture, 460**
- Melt index, LDPE, 364**
- Melt instabilities, polymer rheology, 460**
- Melt spinning, fibers, 354**
- Melts, rheometry of polymer, 475–476**
- Membrane osmometry, 17, 130–133**
- Membrane preparation**
- asymmetric-membrane formation, 518–521
 - coated asymmetric and composite membranes, 521–523
 - microporous membranes, 517–518
 - module fabrication, 523–526
 - overview of, 517
- Membrane science and technology**
- mechanisms of transport. *See* Transport mechanisms
 - membrane preparation. *See* Membrane preparation
 - membrane separations. *See* Membrane separations
 - overview of, 494
 - review problems, 550
 - suggested reading, 547–549
- Membrane separations**
- barrier polymers, 494–495
 - filtration, 495–498
 - fuel cells, 506–507
 - gas separations, 498–501
 - liquid separations, 502–504
 - mechanisms of transport. *See* Transport mechanisms
 - other separations, 504–505
- Merrifield synthesis of proteins, 74**
- Mesogens, liquid-crystalline polymers, 424–425**
- Metalocene polymerizations**
- coordination polymerization using, 56–57
 - of ethylene, 365–366
 - syndiotactic polypropylene (*s*-PP), 367
- Metals, conductivity of polymers and, 534**
- Metastable region, phase equilibria, 123**
- Metathesis elastomers, 377**
- Metathesis polymerization, 427**
- Metathesis reactions, 81–82**
- Metering section, extruders, 436–437, 476–482**
- (Meth)acrylates, 59–61**
- Methacrylic acid, 363–364, 421–422**
- Methanol crossover, fuel cell membranes, 506**
- Methyl methacrylate**
- as chain-transfer constant, 41
 - group-transfer polymerization of, 83–84
 - heat of polymerization and ceiling temperatures, 43
 - pathways of, 32
- Methylaluminoxane (MAO), 55–56**
- Metropolis algorithm, 582, 602–605**
- MF (melamine–formaldehyde) resins, 389–393, 524**
- Micelles, 67–69, 527–528**
- Microcanonical ensemble, molecular simulations, 590–591**
- Microfiltration membranes, 496–498**
- Microporous membranes**
- for composite membranes, 522–523
 - overview of, 517–518
 - thermally induced phase separation of, 521
- Microscopy, 200–201**
- Miniemulsion polymerization, 69**
- Miscibility**
- and phase equilibria, 122–125
 - of polymer blends, 300–301
- Mixtures, Flory EOS theory for, 120–121**
- MMT (Montmorillonite), 319–322**
- Modeling of polymer-processing operations**
- extrusion, 476–482
 - wire coating, 482–485
- Models. *See* Mechanical models, viscoelastic behavior**
- Modified Flory–Huggins, 117**
- Modified poly(phenylene oxide), 404–405**
- Module fabrication, 523–526**
- Modulus, 301, 311–312**
- Moisture. *See* Hydrolysis**
- Molar attraction constants, solubility parameters, 562–564**

- Molar energy of vaporization of pure liquid (DEv), 127–129
- Molar Gibbs free energy, 112
- Molar volume of liquid (V_l), 127–128
- Molar-mass dispersity (D_M), 17–20
- Molding
 - blow, 443–444
 - compression, 438
 - defined, 436
 - grades of PET, 373–374
 - injection, 440–441
 - reaction injection molding (RIM), 441–443
 - rotational, 444
 - thermoforming, 443
 - transfer, 438–439
- Mole fraction of monomer, free-radical copolymerization, 46–48
- Molecular dynamics (MD)
 - cohesive energy density from, 593–594
 - early applications of, 581–582
 - molecular mechanics force fields in, 583–588
 - Monte Carlo methods of, 588–591
 - obtaining permeability coefficient, 605–610
 - overview of, 581
 - velocity autocorrelation function in, 597
- Molecular mechanics force fields, 583–588
- Molecular sieving, through porous media, 508–509
- Molecular simulation applications
 - cohesive energy density and solubility parameter, 593–594
 - free volume, 610–611
 - glass-transition temperature, 594–595
 - mechanical properties, 600–602
 - overview of, 591
 - pair correlations, 595–597
 - permeability, 605–610
 - PVT simulation, 591–593
 - scattering functions, 599–600
 - sorption isotherms, 602–605
 - time-correlation coefficients, 597–599
- Molecular simulations
 - CG force fields, 587–588
 - molecular dynamics and Monte Carlo methods, 588–591
 - molecular mechanics force fields, 583–588
 - Monte Carlo simulations, 582–583
 - overview of, 581–582
 - predicting polymer properties, 554
 - reactive force fields, 587
- Molecular weight
 - in anionic polymerization, 50
 - critical, 154–155
 - determining, 15–20
 - effect on T_g , 179–180
 - of epoxies, 386–387
 - of isotactic polypropylene, 367–368
 - of low-density polyethylene, 364
 - polymer viscosity and increasing, 450
 - RAFT polymerization and, 63–64
 - references, 150
 - in step-growth polymerization, 28–29
 - ultrahigh-molecular-weight PE, 366
- Molecular weight, measurement
 - gel-permeation chromatography, 143–146
 - intrinsic viscosity, 140–143
 - light-scattering, 134–140
 - osmometry, 130–133
 - overview of, 129–130
 - review problems, 146–150
 - suggested reading, 146
 - vapor-pressure osmometry, 133–134
- Monoethylphenol, phenolic resins, 390
- Monomers
 - of copolymers, 9–10
 - macromers as macromolecular, 84
 - in polymer synthesis. *See* Polymer synthesis
- Monte Carlo Markov chain (MCMC) method, 582
- Monte Carlo (MC) simulations
 - introduction to, 581
 - molecular dynamics and, 588–591
 - molecular dynamics vs., 597
 - molecular mechanics force fields in, 583–588
 - obtaining permeability coefficient, 605
 - obtaining sorption isotherms, 602–605
 - overview of, 582
- Montmorillonite (MMT), 319–322
- Mooney–Rivlin equation, rubber elasticity, 253–255
- Multi-element models, viscoelastic behavior, 226–228
- Multi-impression molds, 440–441
- Multiplets, ionic polymers, 421
- ## N
- Nafion perfluorinated ionomer, 422, 516–517
- Nanocomposites
 - buckyballs, 322–323
 - carbon nanotubes, 323–324
 - graphene, 324–325
 - montmorillonite, 319–320
 - overview of, 318–319
 - polyhedral oligomeric silsesquioxane (POSS), 325–326
 - processing, 321
 - properties of, 321–322
 - suggested reading, 327
- Nanofiltration (NF) membranes, 497–498
- Nanomedicines, polymeric, 527–528
- Naphthalene dicarboxylate (NDC), 410
- Natta, Giulio, 2, 54–55
- Natural polymers, 331–332

- Natural rubber (NR)
 development of elastomer for, 2
 as electrical insulator, 533
 as natural elastomer, 346
 as natural occurring polymer, 1
 polyisoprene in, 377
 synthetic rubber and short supply of, 2
 vulcanization of, 377–379
- Naturally occurring polymers, 1
- Navier–Stokes equations, 463–464
- NBR (nitrile rubber), 377
- Nematic state, liquid-crystal structures, 425
- Neutron scattering, 598–599
- Newton's law of motion, 589
- Newton's law of viscosity, 221, 231, 446–450
- NF (nanofiltration) membranes, 497–498
- Nitrile rubber (NBR), 377
- Nitroaromatic explosives, detecting, 546
- Nitroxide-mediated polymerization (NMP), 51, 58–59
- NLO (nonlinear optical) polymers, 542–543
- NMP (nitroxide-mediated polymerization), 51, 58–59
- NMR (nuclear magnetic resonance) spectroscopy, 89–92
- Nodes, artificial neural networks, 578–581
- Nomenclature system, polymers, 13–15
- Nomex (poly(*m*-phenylene isophthalamide)), 21, 26, 400
- Non-bonded terms, force fields, 583–584, 586–587
- Non-cellulosics, 350–354
- Non-chain scission reactions, polymer degradation, 265–266
- Non-condensation-type, step-growth polymers, 27–28
- Nonadiene elastomers
 fluoroelastomers, 380–381
 overview of, 379
 polyisobutylene or butyl rubber, 379–380
 from polyolefins, 384
 polysiloxanes, 380
 polyurethanes, 381–384
 properties of, 375
- Nonlinear optical (NLO) polymers, 542–543
- Non-Newtonian flow or apparent viscosity
 analysis of simple flow, 461–468
 constitutive equations, 461–462
 overview of, 448–450
 solution viscosity and, 454–455
- Non-Newtonian fluid, capillary rheometry data for, 469–470
- Non-vinyl polymers, nomenclature rules for, 13–14
- Normal stresses, elastic response, 458–460
- Norrish–Smith effect, 65
- Novolac formation, phenolic resins, 390–391
- NR. *See* Natural rubber (NR)
- Nuclear magnetic resonance (NMR) spectroscopy, 89–92
- Nucleation track etching, microporous membranes, 518
- Nuclei, in polymer NMR, 89–92
- Number-average molecular weight (M_n), 129
 determining, 16–20
 membrane osmometry, 133
 vapor-pressure osmometry, 133–134
- Number-average (X_n) degree of polymerization
 free-radical polymerization, 39–40
 RAFT polymerization, 63
 step-growth polymerization, 29
- Numbers, nomenclature system for polymers, 13–15
- NVE ensemble, molecular simulations, 590–591
- Nylons (aliphatic polyamides)
 development of, 331
 improving with aromatic polyamides, 400–401
 nomenclature rules for, 13–14
 non-cellulosic synthetic fibers, 351
 polyamidation of, 6
 as step-growth polymers, 26
 synthetic fibers, 348
- O**
- Olefins
 olefinic elastomers, 386
 olefinic fibers, 353–354
 undergoing metathesis to yield elastomers, 81–82
- Open discharge condition, modeling extrusion, 477
- Optical storage of computer data, photonic polymers, 541–544
- Order–disorder transition, 307
- Organic halide, 60
- Organic light-emitting diodes (OLEDs), 543–544
- Organic photovoltaic (OPV) polymers, 537–540
- Orientation hardening, testing stress or strain, 192
- Osmometry
 membrane, 130–133
 molecular-weight determination, 130
 vapor-pressure, 133–134
- Osmotic pumps, controlled drug release, 529–530
- Ostwald-de Waele–Nutting (power-law index) model, 461–462
- Ostwald-Fenske capillary viscometers, 142–143
- Oxidation, stability of polymers and, 267–269
- Oxidative pyrolysis, 290
- Ozone, 261–262, 268
- Ozonolysis, 268
- P**
- P* (permeability coefficient), 605–610
- PAEK (polyaryletherketones), 419–420
- PAI (poly(amide-imide)), 414, 416–417
- Pair correlation functions (PCFs), 595–597
- PAN (polyacrylonitrile), 265–266, 494

- PANI (polyaniline), 427–428
- PAR (polyarylate), 409
- Parison, blow molding process, 443–444
- Partial immobilization theory, solution-diffusion transport, 513
- Partial-molar Gibbs free energy, 112, 114
- Particle-scattering function, light-scattering, 135–136
- Partition functions, Flory EOS theory, 118–119
- Pattern recognition, using ANNs, 579
- PBD. *See* Polybutadiene (PBD)
- PBI (poly[2,2'-(*m*-phenylene)-5,5'-bibenzimidazole]), 20
- PBI (polybenzimidazole), 417–418, 429–430
- PBO (polybenzobisoxazole), 430
- PBT (polybenzobisthiazole), 430
- PBT (poly(butylene terephthalate)), 373, 409
- PCFF force field, 587
- PCFs (pair correlation functions), 595–597
- PCL (polycaprolactone), 21, 277
- PCT (poly(dimethylene cyclohexane terephthalate)), 409–410
- PE. *See* Polyethylene (PE)
- PEEK (polyimidazopyrrolones), 419–420
- PEG (poly(ethylene glycol)), 527, 530
- PEI (polyetherimide), 414, 416–417
- PEN (poly(ethylene naphthalate)), 410
- PEN (poly(ethylene oxide)), 461
- Perfluorosulfonate ionomers (PFSI)
commercial applications, 422
fuel-cell applications, 506
transport through, 516–517
- Periodic boundary conditions, molecular simulations, 589–590
- Permachor method, predicting permeability, 494, 560–562
- Permeability
barrier polymers and, 494–495
molecular simulation applications, 605–610
polymers for gas-separation applications, 499–500
predicting by group contributions, 559–562
- Permeability coefficient (P), 605–610
- Permeate, liquid separations, 502–503
- Permselectivity, 499–500
- Persulfate-ferrous (K_2SO_4) redox initiator, 67
- Pertraction, liquid separations, 502
- Pervaporation process, membranes, 502–504
- PES (polyethersulfone), 406–407
- PET. *See* Poly(ethylene terephthalate) (PET)
- PFSI. *See* Perfluorosulfonate ionomers (PFSI)
- PGA, in controlled drug delivery, 527
- Phantom chain approximation, rubber elasticity, 254
- Phase equilibria, thermodynamics of solutions, 122–125
- Phase inversion, asymmetric-membrane formation, 519
- Phase-separated blends, 302–304
- PHEMA (poly(2-hydroxyethyl methacrylate)), 529
- Phenol-formaldehyde resins, as thermosets, 4
- Phenomenological model, rubber elasticity, 253–254
- Phenoplasts or (phenolic) PF resins, 389–391
- Philips-type catalysts, PE with reduced branching, 364–365
- Photoconductive polymers, 428–429
- Photooxidative degradation, of polystyrene, 368
- Photovoltaic polymers, organic, 537–540
- Physical constants, symbols and units, 632
- Physical properties, of commercial polymers, 625
- PIB (polyisobutylene), 379–380, 461
- PLA (poly(lactic acid)), 276–277
- PLA, controlled drug delivery using, 527
- Plane Couette flow, 467–468
- Plant oils, polymer synthesis, 86
- Plasma polymerization, 70–71
- Plasticizer efficiency, 284
- Plasticizers
antiplasticization and, 286–287
determining composition of polymer mixture, 284
external and internal plasticization, 284–286
list of common PVC, 286
overview of, 282–284
- Plastics
ASTM standards for, 627–629
high-performance engineering, 2
U.S. production of, 2–3
- Plastisol, 455
- PLF. *See* Power-law fluid (PLF) model
- PLGA (poly(lactide-*co*-glycolide)), 277, 529
- Plunger, transfer molding process, 438–439
- PMAN structure 1 (polymethacrylonitrile), 494
- PMMA. *See* Poly(methyl methacrylate) (PMMA)
- PMP (poly(4-methylpentene-1)), 420
- Poiseuille (pressure) flow, 464–466
- Poisson's ratio, 187–188, 601–602
- Poly (prefix), nomenclature for vinyl polymers, 13
- Poly[1-(trimethylsilyl)-1-propyne] (PTMSP), 500–501
- Poly[2,2'-(*m*-phenylene)-5,5'-bibenzimidazole] (PBI), 20
- Poly(2,6-dimethyl-1,4-phenylene oxide) (PPO), 404–405
- Poly(2-hydroxyethyl methacrylate) (PHEMA), 529
- Poly(4-methylpentene-1) (PMP), 420
- Polyacetal, as engineering plastic, 405–406
- Polyacetylene, 8, 534–535
cis-polyacetylene, 427
- Polyacrylamide, 461
- Polyacrylonitrile (PAN), 265–266, 494
- Polyalkenylenes, 8
- Polyalkylenes (or polyalkylidenes), 7–8
- Polyallomers, 386

- Poly(amide-imide) (PAI), 414, 416–417
- Polyamides
- aromatic, 400–401
 - chemical structures of, 399–400
 - non-cellulosic synthetic fibers, 351–353
 - producing using RIM, 442
- Polyaniline (PANI), 427–428
- Polyarylate (PAR), 409
- Polyaryletherketones (PAEK), 419–420
- Polybenzimidazole (PBI), 417–418, 429–430
- Polybenzobisoxazole (PBO), 430
- Polybenzobisthiazole (PBT), 430
- Polybismaleimides, 417
- Polybutadiene (PBD)
- ABS polystyrene developed from, 401
 - effects of ozone on, 262
 - GPC calibration curve, 145
 - improving impact strength of brittle plastics, 302–303
 - obtaining polystyrene using, 369
 - polymerization of, 374, 376
- Poly(butylene terephthalate) (PBT), 373, 409
- Polycaprolactone (PCL), 21, 277
- Polycarbonates, 26, 402–403
- Polychlorotrifluoroethylene (CTFE), 377, 411–412
- Polycondensations, step-growth, 26–27
- Poly(dichlorophosphazene), 78
- Poly(diethyleneglycol adipate), 382
- Poly(dimethylene cyclohexane terephthalate) (PCT), 409–410
- Polydimethylsiloxane, 20
- Polyelectrolytes, 421
- Polyesters
- engineering, 409–410
 - non-cellulosic synthetic fibers, 350–351
 - polyurethanes based on, 382–383
 - as step-growth polymers, 26
 - synthetic fibers, 348
 - thermoplastic, 372–374
 - unsaturated, 387–389
- Polyetherimide (PEI), 414, 416–417
- Polyethersulfone (PES), 406–407
- Polyethylene (PE)
- as barrier polymer, 494–495
 - as commercial thermoplastic, 3
 - conformation of small chain, 106–107
 - free-radical polymerization of, 53–54
 - high-density (HDPE), 54–55
 - isotactic polypropylene (*i*-PP), 54
 - low-density (LDPE), 53
 - overview of, 363–366
 - as polyalkylene, 7
 - UHMWPE, 420
 - Unipol process for, 69–70
 - U.S. production of, 2–3
- Poly(ethylene glycol) (PEG), 527, 530
- Poly(ethylene naphthalate) (PEN), 410
- Poly(ethylene oxide) (PEO), 461
- Poly(ethylene terephthalate) (PET)
- as barrier polymer, 494
 - commercial production of, 372–374
 - crystalline kinetics, 164–165
 - improving with PEN, 410
 - liquid-crystal polyester properties vs., 426
 - modified grades of, 409
 - recycling plastics, 273–274
- Polyfluorenes, 429
- Polyformaldehyde, 405–406
- Polyfuran, 70
- Polyhedral oligomeric silsesquioxane (POSS), 319, 325–326
- Polyimidazopyrrolones (PEEK), 419–420
- Polyimides
- poly(amide-imide) and polyetherimide, 416–417
 - polybenzimidazole, 417–418
 - polybismaleimides, 417
 - properties of, 414
 - synthesis of, 413–416
- Polyisobutylene (PIB), 379–380, 461
- Polyisoprene, 345–346, 377
- Poly(lactic acid) (PLA), 276–277
- Poly(lactide-*co*-glycolide) (PLGA), 277, 529
- Polymer
- abbreviations, 621–623
 - derivation of term, 1
 - solubility parameters, 129
- Polymer blends
- benefits of, 281–282
 - commercial blends, 300–301
 - Flory–Huggins theory predicting behavior of, 296–298
 - free-energy considerations in, 294
 - immiscibility and, 296–297
 - interpenetrating networks, 304–306
 - LCST and UCST phase behavior, 294–297
 - overview of, 293
 - properties of, 301–302
 - references, 293
 - suggested reading, 326
 - ternary, 299–300
 - thermodynamics and, 293–294
 - toughened plastics and phase-separated, 302–304
- Polymer processing
- analysis of simple flow, 461–466
 - basic operations, 436
 - calendering, 445
 - coating, 445–446
 - dynamic and continuity equations, 486–487
 - extrusion, 436–437
 - extrusion, modeling, 476–482

- Polymer processing (*continued*)
molding. *See* Molding
references, 491
relationship between WLF parameters and free volume, 485–486
review problems, 488–491
rheology. *See* Polymer rheology
rheometry. *See* Rheometry
suggested reading, 487–488
wire coating, modeling, 482–485
- Polymer rheology
constitutive equations, 456–457
drag reduction, 460–461
elastic properties of polymeric fluids, 457–460
introduction to, 446–448
melt instabilities, 460
non-Newtonian flow, 448–452
references, 491
review problems, 488–491
suggested reading, 487–488
viscosity of polymer solutions/suspensions, 452–456
- Polymer science, introduction to
birth of, 2
chemical structure/thermal transitions, 20–22
classifications, 3–8
copolymers, 9
geometric isomerism, 12–13
introduction to, 1–3
molecular weight, 15–20
nomenclature, 13–15
references, 24
review problems, 22–24
structure, 8–15
suggested reading, 22
tacticity, 9–12
- Polymer structure
classification based on, 7–8
copolymers, 9
geometric isomerism, 12–13
nomenclature, 13–15
properties, 8–9
tacticity, 9–12
- Polymer synthesis
chain-growth polymerization. *See* Chain-growth polymerization
chemical structure determination, 86–92
genetic engineering in, 85
green chemistry in, 86
group-transfer polymerization in, 83–84
macromers in, 84
metathesis reactions in, 81–82
overview of, 25
polymerization techniques. *See* Polymerization techniques
reactions of polymers, 74–80
references, 98–100
review problems, 95–98
step-growth polymerization, 26–31
suggested reading, 92–95
- Polymer-assisted membrane formation, 521
- Polymeric batteries, 535–537
- Polymeric solar cells (PSCs), 538
- Polymerization
classifying polymers by, 4–7
determining tactic or atactic polymers, 11
in ionic liquids, 72–73
molecular-weight determination, 15–16
in supercritical fluids, 71–72
- Polymerization rate (R_p)
free-radical polymerization kinetics, 37–41
step-growth polymerization kinetics, 30–31
- Polymerization techniques
bulk polymerization, 64–65
emulsion polymerizations, 67–69
gas-phase polymerization, 69
plasma polymerization, 70–71
polymerization in ionic liquids, 72–73
polymerization in supercritical fluids, 71–72
solid-state polymerization, 69–70
solution polymerization, 66
suspension polymerization, 66–67
- Polymer-sensitive detector, gel-permeation chromatography, 144
- Polymethacrylonitrile (PMAN, structure 1), 494
- Poly(methyl methacrylate) (PMMA)
amorphous in solid state, 20
commercial-grade, 371
properties of, 14
universal GPC calibration curve, 145
using NMR to study tacticity of, 91–92
- Poly(*m*-phenylene isophthalamide) (Nomex), 21, 26, 400
- Polynorbornene, 377
- Polynucleotides
heterocyclic bases, 337
molecular weight/structure of DNA, 338–340
protein synthesis and, 340–341
types of, 336
- Poly(*N*-vinyl-2-pyrrolidinone) (PVP), 372
- Poly(*N*-vinylcarbazole) (PVK), 428–429
- Polyoctamer, 377
- Polyolefins
as barrier polymers, 494–495
as commercial thermoplastic, 3
elastomers from, 384
medical applications of, 526
metallocene polymers, 55–56
as nondiene elastomers, 384
overview of, 362–363

- polyethylene, 363–366
- polypropylene, 366–367
- specialty, 420
- synthetic fibers of, 348
- Poly(organophosphazenes), 78, 422–423
- Polyoxymethylene (POM), 405–406
- Polyphenylsulfone, 406
- Poly(*p*-phenylene) (PPP), 428
- Poly(*p*-phenylene sulfide) (PPS), 408–409
- Poly(*p*-phenylene terephthalamide) (PPT) (Kevlar), 401
- Polypropylene (PP)
 - atactic, 11
 - as barrier polymer, 494–495
 - as commercial thermoplastic, 3
 - development of, 2
 - isotactic polypropylene, 54
 - medical applications of, 526
 - overview of, 366–367
 - as polyalkylene, 7
 - U.S. production of, 2–3
- Poly(propylene glycol), 382
- Polypyrrole (PPy), 428
- Polysaccharides
 - cellulose, 342
 - chitin, 343–344
 - overview of, 341–342
 - reactions of, 344
 - starch, 342–343
- Polysilanes or polysilylenes, 423
- Polysilastyrene, 423–424
- Polysiloxanes, 8, 380
- Polystyrene (PS)
 - abbreviation for, 14
 - ABS as high-HDT grade of, 401–402
 - as addition polymer, 4
 - amorphous in solid state, 20
 - chloromethylation of, 74
 - commercial applications, 367
 - as commercial thermoplastic, 3
 - GPC chromatogram of, 144–145
 - HIPS as high impact, 302–303, 367, 369
 - medical applications, 526–527
 - as polyalkylene, 7
 - syndiotactic, 11
 - topological calculations for properties, 574–578
 - universal GPC calibration curve, 145
 - U.S. production of, 2–3
- Polysulfones (PSF), 26, 406–408
- Polysulfurnitride (SN), 534
- Polytetrafluoroethylene (PTFE or Teflon)
 - dielectric constants of, 541
 - engineering plastic, 411
 - as good electrical insulator, 533
- Polythiophene (PT), 70, 428
- Polyurethane (PUR)
 - producing using RIM, 442
 - as step-growth polymer, 26
 - synthesizing elastomeric, 381–384
- Poly(vinyl acetate) (PVAC), 76, 371
- Poly(vinyl alcohol) (PVAL), 76, 371
- Poly(vinyl butyral) (PVB), 76, 371
- Poly(vinyl chloride) (PVC)
 - calendering process for, 445
 - commercial grades of, 369–370
 - commercial production/properties of, 370–371
 - as commercial thermoplastic, 3
 - dehydrohalogenation, 265–266
 - development of crystallinity, 87–88
 - electronic shielding applications, 540
 - imperfect tactic structure of, 11–12
 - list of common plasticizers, 286
 - medical applications of, 526
 - plasticizers for, 282
 - recycling plastics, 273
 - softening temperature/blending properties, 74
 - universal GPC calibration curve, 145
 - U.S. production of, 2–3
- Poly(vinyl fluoride) (PVF), 412
- Poly(vinylidene chloride) (Saran), 494
- Poly(vinylidene fluoride) (PVDF), 412
- POM (polyoxymethylene), 405–406
- Pore structure, microporous membranes, 518
- Porous media transport, 508–509
- POSS (polyhedral oligomeric silsesquioxane), 319, 325–326
- Potable water, 288–289
- Power-law fluid (PLF) model
 - analysis of simple flow, 462
 - axial annular Couette flow, 467–468
 - constitutive equations and, 456–457
 - extrusion process, 482
 - flow through capillary, 464–466
 - wire coating process, 483
- Power-law index (Ostwald-de Waele-Nutting) model, 461–462
- PP. *See* Polypropylene (PP)
- PPO (poly(2,6-dimethyl-1,4-phenylene oxide)), 404–405
- PPP (Poly(*p*-phenylene)), 428
- PPS (Poly(*p*-phenylene sulfide)), 408–409
- PPT (Poly(*p*-phenylene terephthalamide)) (Kevlar), 401
- PPy (polypyrrole), 428
- Precipitation threshold, supercritical fluids, 71
- Predictions of solubilities, thermodynamics of polymer solutions, 126–129
- Pressure, effect on T_g , 182
- Pressure dependence, and viscosity, 452

- Pressure flow
 capillary rheometer determining, 469–473
 drag flow, 467–468
 modeling extrusion process, 477–482
 modeling wire coating process, 484–485
 through capillary, 464–466
- Pressure-swing adsorption (PSA), 498
- Primary (first) normal-stress difference, 459
- Process modeling, using ANNs, 579
- Processing. *See* Polymer processing
- Processing agents, as additives, 291
- Propagation step
 free-radical copolymerization, 43–44
 free-radical polymerization, 34, 36–37
 free-radical polymerization thermodynamics, 41–43
- Properties
 atomistic modeling determining mechanical, 600–602
 of blends, 301–302
 of important commercial polymers, 625–626
 predicting polymer. *See* Correlations and simulations
 of supercritical fluids, 71
- Proportional limit, stress-strain relations, 188
- Protein synthesis
 overview of, 336
 polynucleotides and, 340–341
- Proteins
 biocompatibility depending on adsorption of, 526
 biological functions of, 334
 cell structure and, 334–335
 in conjugated polymeric nanomedicines, 527–528
 fibrous and globular, 335
 naturally occurring amino acids, 332–336
 proteomics, 335–336
 synthesizing, 336
- PSA (pressure-swing adsorption), 498
- PSCs (polymeric solar cells), 538
- PSF (polysulfones), 26, 406–408
- PT (polythiophene), 70, 428
- PTFE or Teflon (polytetrafluoroethylene)
 dielectric constants of, 541
 engineering plastic, 411
 as good electrical insulator, 533
- PTMSP (poly[1-(trimethylsilyl)-1-propyne]), 500–501
- Pultrusion, 310, 317–318
- PUR. *See* Polyurethane (PUR)
- Purines, in nucleic acids, 337
- PVAC (poly(vinyl acetate)), 76, 371
- PVAL (poly(vinyl alcohol)), 76, 371
- PVB (poly(vinyl butyral)), 76, 371
- PVC. *See* Poly(vinyl chloride) (PVC)
- PVDF (poly(vinylidene fluoride)), 412
- PVK (poly(*N*-vinylcarbazole)), 428–429
- PVP (poly(*N*-vinyl-2-pyrrolidinone)), 372
- PVT simulation, 591–593
- Pyrimidines, nucleic acids, 337–339
- Pyrolysis, flame retardant, 290
- Q**
- Q*-*e* values, 45–46
- Quadratic equation, 633
- Quality of polymer–solvent interactions, membrane osmometry, 131
- Quartic expression, modern force fields, 584
- R**
- Radial distribution function (RDF), 103–104, 594–595
- Radiation, degradation of polymers, 271–272
- Radiation stabilizers, as additives, 290
- Radio frequency (RF)
 energy, 70
 shielding, 540
- Radiolysis, 271–272
- RAFT (reversible addition-fragmentation chain transfer) polymerization, 51, 61–64
- Raleigh ratio, light-scattering measurements, 135
- Raman spectroscopy, 89
- Random degradation, 263
- Random flight chain, conformation, 102
- Random reactions, step-growth polymerization, 25
- Raoult's ideal solution law, 109–110
- RATTLE algorithm, MD simulations, 589
- Rayleigh scattering, 89
- Rayon (as cellulose fiber)
 processes in making, 344
 synthetic fibers, 347–348
 viscose process of obtaining, 76
- RDF (radial distribution function), 103–104, 594–595
- RDRP (reversible deactivation radical polymerization), 58
- Reaction injection molding (RIM), 381, 441–443
- Reaction-controlled systems, drug release, 529
- Reactions of polymers
 chemical modification, 74–75
 click chemistry, 79–80
 overview of, 74
 preparation of polymer derivatives, 76–78
 in step-growth vs. chain-growth polymerization, 25
- Reactive force fields, 587
- Reactivity ratios, free-radical copolymerization, 44–45
- ReaxFF force field, 587
- Receptor sites, sensor applications, 545
- Reciprocating-screw injection-molding machine, 440–441
- Recycled PET, 373–374

- Recycled plastics, 273–274
Reduced viscosity, 141
Reinforcers, as additives, 287–288
Relative viscosity increment, 141
Relaxation-time distribution function, viscoelastic behavior, 228–230
Repeating units of identical structure, polymers, 1
Reptation, theory of, 155–156
Residual (enthalpic) term, UNIFAC-FV, 568–569
Resins
 ABS, 401–402
 epoxy, 386–388
 formaldehyde, 389–393
 molding. *See* Molding
 unsaturated polyester, 387–389
Resin-transfer molding, composites, 310
Resole formation, phenolic resins, 390–391
Retardation spectrum function, 229–230
Retentate, liquid separations, 502
Reverse osmosis membranes, 497–498
Reversible addition-fragmentation chain transfer (RAFT) polymerization, 51, 61–64
Reversible deactivation radical polymerization (RDRP), 58
RF (radio frequency)
 energy, 70
 shielding, 540
Rheology. *See* Polymer rheology
Rheometry
 capillary rheometer, 469–473
 cone-and-plate rheometer, 475
 Couette rheometer, 473–474
 overview of, 468–469
 of polymer solutions and melts, 475–476
Ribonucleic acid (RNA), 336–339
RIM (reaction injection molding), 381, 441–443
Ring-opening metathesis polymerization (ROMP), 81–82
Ring-opening polymerization of trioxane, 4
RNA (ribonucleic acid), 336–339
Roll coating operation, 445–446
ROMP (ring-opening metathesis polymerization), 81–82
Root-mean-square end-to-end distance, polymer chains, 104, 107–108
Rotatable side-group bonds, polymer properties, 575
Rotational molding (rotomolding), 444
Rotations of polymer chains, steric interference with, 105
Rubber. *See also* Natural rubber (NR)
 ASTM standards for, 629
 development of synthetic, 2
 ethylene and propylene (EPM/EPDM), 384
 slush molding of, 444
 thermodynamics of polymer solutions, 109–110
Rubber elasticity. *See also* Elastomers
 development of elastomer, 2
 introduction to, 248
 phenomenological model, 253–254
 recent developments in, 254–255
 references, 259
 review problems, 256–259
 statistical theory, 252–253
 suggested reading, 255–256
 thermodynamics and, 248–251
Rubbery plateau, stress-strain relation, 189–190
Rule of mixtures, 180–182
Runners, injection molding, 441
- S**
S. *See* Solubility coefficient (S)
Salts
 ionic liquids as, 72–73
 in polymeric batteries, 535–536
SAN (styrene-acrylonitrile copolymer), developing
 ABS, 401–402
Saran (Poly(vinylidene chloride)), 494
SAXS (small-angle X-ray scattering), 167
SBR (styrene-butadiene rubber). *See* Styrene-butadiene rubber (SBR)
SBS elastomers
 commercial applications/properties, 385–386
 glassy domains in, 385
 introduction to, 385–386
 overview of, 375
SBS triblock copolymer, 53–54
Scaffold structure, tissue engineering, 532
Scanning electron microscopy (SEM), 200
Scanning tunneling microscopy (STM), 200
Scatchard-Hildebrand equation, 128
Scattered light. *See* Light-scattering measurements
Scattering functions, molecular simulation, 599–600
SCFs (supercritical fluids), polymerization in, 71–72
Schering impedance bridge, dielectric analysis, 237–238
Schönbein, Christian F., 2
Screw characteristic, flow through capillaries, 466
Screw pot, injection molding, 441
Screw-driven extruders, 436–437, 477–482
SEC (size-exclusion chromatography), 129–130, 143
Secant modulus, stress-strain relations, 188
Second normal-stress difference, 459
Secondary methods, molecular-weight determination, 129–130
Secondary-relaxation processes
 amorphous glassy state, 158–159
 defined, 154
 thermal transitions, 20–22

- Second-order transitions, thermodynamic relationships, 169–172
- SEM (scanning electron microscopy), 200
- Semi-IPNs, 306
- Sensor applications, 544–546
- Separations. *See* Membrane separations
- SHAKE algorithm, MD simulations, 589
- Sharkskin, melt fracture, 460
- Shear
- Boltzmann superposition principle, 245–246
 - mechanodegradation due to, 262, 272
 - testing mechanical properties, 190–191
- Shear banding, 184–185
- Shear flow
- analysis of simple, 461–468
 - apparent viscosity, 448–450
 - melt instabilities, 460
 - modeling extrusion process, 477
 - Newton's law of viscosity for, 446–448
- Shear strain rate (or shear rate)
- analysis of simple flow, 461–468
 - apparent viscosity, 448–450
 - determining with rheometry. *See* Rheometry
 - Newton's law of viscosity, 447–448
 - solution viscosity and, 454–455
- Shear-thickening behavior, 449, 452
- Shear-thinning behavior
- apparent viscosity, 449
 - molecular-weight dependence and, 450
 - solution viscosity and, 454–455
 - time dependence and, 452
- Sheet-molding compound (SMC), composites, 316–317
- Shielding, electronic, 540
- Shinoda force field, 587–588
- SI units, 631–632
- Silicon dioxide (SiO₂), dielectrics, 541
- Simple flows
- analysis of, 461–464
 - constitutive equations for modeling, 456–457
 - drag flow, 467–468
 - Newton's law of viscosity, 447–448
 - pressure (Poiseuille) flow, 464–466
- SIMS (static secondary ion mass spectroscopy), 70
- Simultaneous interpenetrating networks (SINs), 306
- SINs (simultaneous interpenetrating networks), 306
- SiO₂ (silicon dioxide), dielectrics, 541
- Site fraction, Flory EOS theory, 121
- Site-directed drug delivery, 527, 530
- Size exclusion, transport mode in membrane separations, 506
- Size-exclusion chromatography (SEC), 129–130, 143
- Slush molding, 444
- Small-angle X-ray scattering (SAXS), 167
- Small's method, 562–565
- SMC (sheet-molding compound), composites, 316–317
- Smectic state, liquid-crystal structures, 425
- SN (polysulfurnitride), 534
- Sodium naphthalenide, ionic copolymerization, 53–54
- SOG concept, UNIFAC, 569
- Solar cells, 537–540
- Solid-state NMR, 91
- Solid-state polymerization, 69–70
- Solid-state properties
- amorphous state, 154
 - calorimetry measurements, 174–176
 - creep tests, 195–196
 - critical molecular weight, 154–155
 - crystalline kinetics, 164–165
 - crystalline state, 159
 - crystalline-melting temperature, 163–164
 - determining crystallinity, 165–167
 - dilatometry, 172–174
 - fatigue tests, 199–200
 - first-order transitions in thermodynamics, 167–169
 - glass-transition temperature, 156–158
 - heat-distortion temperature, 176–177
 - impact tests, 198–199
 - measurement techniques, 172
 - mechanisms of deformation, 183–185
 - microscopy characterizing, 200–201
 - molecular weight, composition, pressure on T_g , 179–182
 - ordering of polymer chains, 159–162
 - overview of, 153–154
 - reptation, 155–156
 - review problems, 203–204
 - scattering methods in characterizing, 201
 - secondary-relaxation processes, 158–159
 - second-order transitions in thermodynamics, 169–172
 - static tests, 186
 - stress-relaxation measurement, 196–198
 - stress-strain behavior curves, 191–194
 - structure–property relationships, 177–179
 - suggested reading, 202–203
 - testing compression or shear strain, 190–191
 - testing mechanical performance, 185
 - testing stress or strain, 186–190
 - transient tests, 194
- Solubility
- predictions of, 126–129
 - solution-diffusion transport, 509–515
- Solubility coefficient (S)
- estimating permeability coefficient, 605, 609–610
 - obtaining sorption isotherms, 602–603
- Solubility parameter (δ)
- cohesive energy density and, 593–594

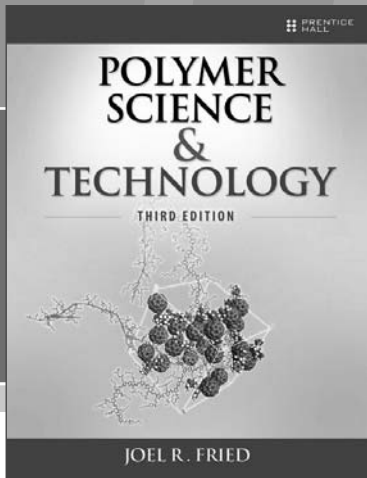
- predicting by group contributions, 562–565
- predictions of solubilities, 127–129
- Solution polymerization, 66
- Solution–diffusion transport, 509–515
- Solutions
 - analysis of simple flow, 461–468
 - drag flow, 467–468
 - drag reduction, 460–461
 - elastic properties of polymeric, 457–460
 - melt instabilities, 460
 - references, 150
 - rheometry of polymer, 475–476
 - thermodynamics of. *See* Thermodynamics of polymer solutions
 - viscosity of, 452–455
- Solvent-controlled delivery, drug release, 529
- Solvents
 - cationic polymerizations, 52
 - gel-permeation chromatography, 143–144
 - group-transfer polymerization, 84
 - ionic liquid as, for polymerization, 73
 - membrane osmometry, 130–133
 - solubility parameters of, 129, 564
 - in solution polymerization, 66
 - vapor-pressure osmometry, 133–134
- Sorption
 - isotherms, 602–605
 - solution-diffusion transport, 510
- Space-filling (CPK) representation of PVC chain, 11–12
- of PVT simulation, 592
- Spatial arrangement, determining properties, 9
- Specialty plastics
 - conductive polymers, 427–429
 - dendritic polymers, 430–431
 - engineering plastics vs., 397–398
 - high-performance fibers, 429–430
 - inorganic polymers, 422–424
 - ionic polymers, 421–422
 - ladder polymers, 418
 - liquid-crystalline polymers, 424–426
 - poly(amide-imide) and polyetherimide, 416–417
 - polyaryletherketones, 419–420
 - polybenzimidazole, 417–418
 - polybismaleimides, 417
 - polyimides, 413–416
 - polyolefins, 420
 - references, 433–434
 - review problems, 433
 - suggested reading, 432
- Spectroscopic methods
 - of chemical structure determination, 86
 - nuclear magnetic resonance spectroscopy, 89–92
 - suggested reading, 255
 - vibrational spectroscopy, 86–89
- Speech recognition, using ANNs, 579
- Spherulites, 160–161, 164–165
- Spinneret, fibers, 354
- Spinning, fibers, 354–358
- Spinodal curve, phase equilibria, 124–125
- Spinodal decomposition, asymmetric-membranes, 520–521
- Spiral-wound membranes, 525
- Sprue, injection molding process, 441
- s-PS (stereospecific polystyrene), 368
- Stability
 - degradation of polymers and, 262
 - oxidative and UV, 267–269
 - thermal, 266–267
- Stabilizers, as additives, 289–290
- Standards. *See* American Society of Testing Methods (ASTM)
- Starch, 278, 342–343
- Static secondary ion mass spectroscopy (SIMS), 70
- Static tests, 186
- Statistical theory, rubber elasticity, 252–253
- Steady-shear viscosity, 230
- Steady-state concentration, free-radical polymerization kinetics, 37–39
- Step-growth polymerization
 - with bulk polymerization, 65
 - kinetics, 30–31
 - molecular weight in, 28–29
 - overview of, 26–28
 - random reaction in, 25
- Stereochemistry
 - arrangement of atoms, 9
 - controlling in metathesis, 82
- Stereospecific polystyrene (s-PS), 368
- Stereo-styrene-butadiene copolymers (stereo SBR), 377
- Steric interference, rotations of polymer chains, 105
- Stirling approximation, Flory-Huggins theory, 111
- STM (scanning tunneling microscopy), 200
- Strain
 - analysis of simple flow, 461–468
 - Boltzmann superposition principle, 245–246
 - crazing, cracking and, 269–270
 - determining mechanical properties, 600–601
 - dynamic-mechanical analysis, 208–209
 - stress-strain behavior curves, 191–194
 - testing mechanical properties, 186–190
 - work expressed as stress and, 212–213
- Strain softening, 192
- Strength
 - properties of blends, 301
 - properties of composites, 312–313
- Stress
 - analysis of simple flow, 461–468
 - Boltzmann superposition principle, 245–246

- Stress (*continued*)
crazing, cracking and, 269–270
determining for polymer solutions and melts, 231–232
determining mechanical properties, 600–601
determining with rheometry. *See* Rheometry
dynamic-mechanical analysis, 208–209
elastic response of polymeric fluids, 457–460
mechanodegradation, 272
stress-strain behavior curves, 191–194
testing mechanical properties, 186–190
tests, 187–190
work expressed as strain and, 212–213
- Stress-at-break (σ_b), 192
- Stress-relaxation measurement
experiment in, 223
overview of, 185
time-temperature superposition, 242–245
transient tests of mechanical properties, 196–198
- Structure factor, PCF, 596
- Structure–property relationships, 157, 177–179
- Styrene
atom transfer radical polymerization of, 59–61
in controlled drug delivery, 527–528
in free-radical copolymerization, 44–49
in free-radical polymerization. *See* Free-radical polymerization
nitroxide-mediated polymerization of, 58–59
pathways of, 32
polymerization of, 4
- Styrene copolymers, 368–369
- Styrene-acrylonitrile copolymer (SAN), developing
ABS, 401–402
- Styrene-butadiene rubber (SBR)
commercial applications/properties, 376–377
producing high-impact PS, 369
YSBR vs., 385–386
- Sulfonyl chlorides, 407
- Sulfur, 377–378
- Sunlight, stability of polymers and, 262
- Supercritical fluids (SCFs), polymerization in, 71–72
- Surface area, Flory EOS theory, 121
- Surface modification, 70–71, 74
- Surface properties, in plasma polymerization, 70
- Surlyn, 421–422
- Suspension polymerization, 66–67
- Suspensions, viscosity of, 455
- Symbols, units and, 631
- Syndiotactic polymers, 10–13
- Synthetic fibers, 347–348
- Synthetic polymers, 1
- Synthetic rubbers
development of, 2
types of, 374
- U.S. production of, 3
- Synthia software program, 574
- ## T
- Tacticity, 9–12, 90–91
- Taylor series, 635
- TBA (torsional-braid analysis), 216–218
- Technologies. *See* Advanced technologies
- Teflon or PFTE (polytetrafluoroethylene), 411, 533, 541
- TEFLON-AF (amorphous Teflon), 411
- TEM (transmission electron microscopy), 200
- Temperature dependence. *See* Arrhenius dependence on temperature
- Temperature-modulated DSC (TMDSC)
dynamic calorimetry, 239–242
measuring thermal transitions, 176
suggested reading, 256
- Termination step
cationic polymerizations, 52
free-radical polymerization, 34–37
“living” polymerization, 49–50
rate of termination, 38–41
termination by chain transfer, 36
termination by combination, 34–35
termination by disproportionation, 35–36
- Ternary blends, polymer blends, 299–300
- Terpolymer, 9
- Tertiary recycling, 273
- Testing methods, mechanical properties
creep tests, 195–196
fatigue tests, 199–200
impact tests, 198–199
overview of, 185
static tests, 186
stress-relaxation measurement, 196–198
stress-strain behavior curves, 191–194
testing compression or shear strain, 190–191
testing stress or strain, 186–190
transient tests, 194
- Tetrabromobisphenol-A polycarbonate (TMBPC), 403
- Tetrafluoroethylene (TFE), in PFTE, 411
- Tetramethylbisphenol-A polycarbonate (TMPC), 403
- Textiles, polymers suitable for, 1
- TFE (tetrafluoroethylene), in PFTE, 411
- T_g . *See* Glass-transition temperature (T_g)
- Thermal conductivity
heat capacity and, 65
in solution polymerization, 66
in suspension polymerization, 66–67
- Thermal degradation
chain scission reactions, 263–265
non-chain scission reactions, 265–266
overview of, 262–263

- Thermal process, asymmetric-membrane formation, 520
- Thermal properties, of commercial polymers, 625
- Thermal stability, 266–267
- Thermal stabilizers, as additives, 288
- Thermal transitions, and chemical structure, 20–22
- Thermal transitions and properties
- calorimetry measurement, 174–176
 - dilatometry measurement, 172–174
 - first-order transitions, 167–169
 - heat-distortion temperature measurement, 176–177
 - measurement techniques, 172
 - molecular weight, composition, pressure and T_g , 179–182
 - second-order transitions, 169–172
 - of semicrystalline polymers, 161
 - structure–property relationships, 177–179
- Thermal-expansion coefficient, 119, 170–172
- Thermally induced phase separation (TIPS), asymmetric-membrane formation, 520
- Thermally stimulated current (TSC) analysis, dielectrics, 238–239
- Thermal-oxidative degradation, flame retardants, 290
- Thermal-pressure coefficient, Flory EOS theory, 119
- Thermid resin, 415
- Thermistors
- calorimetry measurements, 174
 - vapor-pressure osmometry, 133–134
- Thermodynamic relationships, 167–172
- Thermodynamics
- of crystalline polymers, 161
 - free-radical polymerization, 41–43
 - polymer blends and, 293–294
 - rubber elasticity and, 248–251
- Thermodynamics of polymer solutions
- determination of interaction parameter, 125–126
 - equation of state theories, 117–122
 - Flory–Huggins theory, 110–116
 - Flory–Krigbaum theory, 116–117
 - modified Flory–Huggins, 117
 - overview of, 109–110
 - phase equilibria, 122–125
 - predictions of solubilities, 126–129
- Thermoforming process, 443
- Thermoplastic copolyesters, 386
- Thermoplastic elastomers
- copolyesters, 386
 - olefinic elastomers, 386
 - overview of, 384–385
 - properties of, 375
 - SBS elastomers, 385–386
- Thermoplastic polyesters, 372–374
- Thermoplastics. *See also* Commodity thermoplastics
- condensation, 6–7
 - overview of, 362
 - polyolefins, 53
 - references, 395
 - review problems, 394
 - suggested reading, 393–394
 - thermosets vs., 3–4
- Thermoset PIs, 415
- Thermosets
- composites and, 310
 - epoxies, 386–387
 - formaldehyde resins, 389–393
 - molding resins, 439
 - principle feature of, 361–362
 - references, 395
 - thermoplastics vs., 3–4
 - unsaturated polyesters, 387–389
- Thermostats
- for ensembles, 591
 - PVT simulation, 591–593
- Thermotropic polymers, 424
- Thiol-ene reaction, click chemistry, 79
- Thixotropic fluid, 452
- Thomson formula, crystallinity, 166
- Thrombus (clot) formation, artificial organs, 533
- Time dependence, and viscosity, 452
- Time-correlation coefficients, 597–599
- Time-temperature superposition, 197, 242–245
- TIPS (thermally induced phase separation), asymmetric-membrane formation, 520
- Tissue engineering, 532
- TMBPC (tetrabromobisphenol-A polycarbonate), 403
- TMDSC. *See* Temperature-modulated DSC (TMDSC)
- TMPC (tetramethylbisphenol-A polycarbonate), 403
- TNT (trinitrotoluene), detection of, 546
- Topological indices and Bicerano's method
- artificial neural network, 578–581
 - overview of, 574–578
 - predicting polymer properties with, 554
- Torsion pendulum, 214–216
- Torsional-braid analysis (TBA), 216–218
- Tortoise shells, thermoforming, 443
- Toughened plastics, 302–304
- Transfer (or plunger) molding, 438–439
- Transient tests
- creep tests, 195–196
 - overview of, 186
 - stress-relaxation, 196–198
 - testing mechanical properties, 194
- Transition State Theory (TST) method, 607, 610
- Transition-metal catalyst, 60
- Transmission electron microscopy (TEM), 200
- Transport mechanisms
- facilitated and coupled, 515–516

- Transport mechanisms (*continued*)
 in membrane separations, 506–508
 solution-diffusion, 509–515
 through perfluorosulfonate ionomers, 516–517
 through porous media, 508–509
- Trinitrotoluene (TNT), detection of, 546
- Trommsdorff effect, 65
- True strain, 187
- True stress, 187
- TSC (thermally stimulated current) analysis, dielectrics, 238–239
- TST (Transition State Theory) method, 607, 610
- Tubular-membrane modules, 525–526
- Twin-screw extruders, 436–437
- Two-stage screw, injection molding, 441
- U**
- Ubbelohde capillary viscometers, 142–143
- UDEL polysulfone, 408
- UF (Urea–formaldehyde) resins, 389–393, 524
- Ultimate stress, 192
- Ultrafiltration membranes, 496–498
- Ultrahigh-molecular-weight PE (UHMWPE), 366, 420
- Ultraporous membranes, preparation of, 517–518
- Ultraviolet (UV) light, 261–262, 267–269
- UNIFAC-FV method, 566–574
- Unipol process, ethylene, 366
- UNQUAC Functional-group Activity Coefficients, 566
- United-atom (UA) simulations, MD applications, 581–582
- Units, and symbols, 631
- Universal calibration curve, GPC, 144–146
- Unsaturated polyesters, 387–389
- Upper critical solution temperature (UCST)
 phase equilibria, 123, 125
 polymer blends and, 294–297
- Urea–formaldehyde (UF) resins, 389–393, 524
- UV degradation, stabilizing acetal against, 405–406
- UV stabizers, as additives, 288, 290
- V**
- VACF (velocity autocorrelation function), 597
- Vacuum-forming operation, 443
- Valence angles, chain bonds, 104–105
- Valence atomic indices, topological calculations, 575–577
- van der Waals volume
 calculating properties of molecule, 556–558
 as finite in real chain bonds, 106
 free volume, 610–611
 predicting activity coefficients, 566–567
- van Krevelen
 glass-transition temperature, 558–559
 predicting volumetric properties, 553–556
 values for van der Waals volume increments, 557–558
- van't Hoff equation
 membrane osmometry, 130
 sorption isotherms, 603
- Vapor–liquid equilibrium (VLE), 566
- Vapor-pressure osmometry, 133–134
- Vectorial or orientational autocorrelation function, 597–598
- Vectors, in gene therapy, 530–531
- Velocity
 analysis of simple flow, 463–464
 drag flow, 467–468
 flow through capillary, 464–466
- Velocity autocorrelation function (VACF), 597
- Vibrational spectroscopy, 86–89
- Vinyl acetate (EVA), 363, 370–371
- Vinyl alcohol (EVOH), 363
- Vinyl monomers, polymerization of, 31
- Vinyl polymers
 nomenclature rules for, 13
 poly(methyl methacrylate), 371
 poly(*N*-vinyl-2-pyrrolidinone), 372
 polystyrene, 367–368
 poly(vinyl acetate), 371
 poly(vinyl chloride), 369–371
 stereospecific polystyrene, 368
 styrene copolymers, 368–369
- Viral coefficients, membrane osmometry, 131
- Viruses, as vectors in gene therapy, 530
- Viscoelasticity
 activation energies, 220–221
 Boltzmann superposition principle, 245–246
 dynamic calorimetry, 239–242
 experimental methods of dielectric analysis, 237–238
 experimental techniques, 213–214, 231–232
 forced-vibration methods, 218–220
 free-vibration methods, 214–218
 introduction to, 208
 Maxwell model, 221–224
 mechanical models, 221
 multi-element models, 226–228
 of polymer solutions and melts, 230
 references, 259
 relaxation and retardation spectra, 228–230
 review problems, 256–259
 simple models, 225–226
 suggested reading, 256
 theory of dielectric analysis, 233–237
 theory of dynamic-mechanical analysis, 208–212
 thermally stimulated current analysis, 238–239

- time-temperature superposition, 242–245
 - transient and dynamic properties, 247–248
 - viscoelastic properties of polymer solutions and melts, 230
 - Voigt model, 225
 - work in dynamic deformation, 212–213
 - Viscometric flow, 467–468
 - Viscose process, 76
 - Viscosity
 - capillary rheometer determining, 471
 - cone-and-plate rheometer determining, 475
 - Couette rheometer determining, 473–474
 - of dilute suspensions in Newtonian liquid, 455
 - dynamic viscosity, 230
 - increasing molecular weight and polymer, 450
 - measuring intrinsic, 140–143
 - modeling wire coating process, 482–485
 - Newton's law of, 221, 231, 446–448
 - non-Newtonian flow or apparent, 448–450
 - of polymer solutions/suspensions, 452–456
 - polymerization in ionic liquids and, 73
 - pressure dependence and, 452
 - temperature dependence and, 451–452
 - time dependence and, 452
 - viscous flow region, 189
 - Viscosity-average molecular weight (M_v), 17, 130
 - Viscous flow, 189, 508–509
 - VLE (vapor-liquid equilibrium), 566
 - Voigt elements
 - limitations of simple Voigt model, 225–226
 - modeling viscoelastic behavior, 225
 - relaxation and retardation spectra, 229–230
 - Voigt–Kelvin approach to multielement modeling, 228
 - Volume
 - finite (van der Waals), 106
 - Flory–Huggins theory, 113, 117–118
 - thermodynamics of polymer solutions, 109–110
 - Volumeless chain, conformation, 102
 - Volumetric properties, group contributions, 554–558
 - Voorinholtholt method, 610–611
 - Voronoi tessellation, 610–611
 - Vulcanization process, 377–379, 384–386
- W**
- Waste thermoplastics, refabricating, 3
 - Water-soluble initiator, emulsion polymerization, 67
 - WAXS (wide-angle X-ray scattering), 167–168, 201
 - Weak-link degradation, 263
 - Weathering, 262
 - Webster, Owen, 83
 - Weight-average molecular weight (M_w), 129
 - determining, 16–20
 - light-scattering measurements, 134–140
 - Weight-average degree of polymerization (X_w), 29
 - Weighting, artificial neural networks, 579
 - Wet process, asymmetric-membrane formation, 520
 - Wet spinning, fibers, 356–357
 - Wheatstone bridge, 237–238
 - Wide-angle X-ray scattering (WAXS), 167–168, 201
 - Wire coating, 482–485
 - WLF equation
 - free volume and, 485–486
 - temperature dependence of melt viscosity, 451–452
 - time-temperature superposition, 242–245
 - Work (W)
 - expressed in terms of stress and strain, 212–213
 - laws of thermodynamics and, 248–251
 - naturally occurring fibers, 346–347
- X**
- Xanthan, as drag-reducing agent, 461
 - X-ray
 - diffraction, 166–167, 598–599
 - radiation effects on polymers, 271–272
 - scattering in polymer characterization, 201
- Y**
- Yield stress, 192
 - Young's modulus
 - determining mechanical properties, 601–602
 - of layered silicate-elastomer nanocomposites, 321, 323
 - time-temperature superposition, 244–245
 - YSBR, and SBS elastomers, 385–386
- Z**
- z-average, 16–20, 129
 - Ziegler, Karl, 2, 54
 - Ziegler–Natta (Z-N) catalysts, 55–56
 - Ziegler-type catalysts, 364–365, 367
 - Zimm plot, 137–138



FREE Online Edition

Your purchase of ***Polymer Science and Technology, Third Edition*** includes access to a free online edition for 45 days through the **Safari Books Online** subscription service. Nearly every Prentice Hall book is available online through **Safari Books Online**, along with thousands of books and videos from publishers such as Addison-Wesley Professional, Cisco Press, Exam Cram, IBM Press, O'Reilly Media, Que, Sams, and VMware Press.

Safari Books Online is a digital library providing searchable, on-demand access to thousands of technology, digital media, and professional development books and videos from leading publishers. With one monthly or yearly subscription price, you get unlimited access to learning tools and information on topics including mobile app and software development, tips and tricks on using your favorite gadgets, networking, project management, graphic design, and much more.

Activate your FREE Online Edition at informit.com/safarifree

- STEP 1:** Enter the coupon code: YYFPFDB.
- STEP 2:** New Safari users, complete the brief registration form. Safari subscribers, just log in.

If you have difficulty registering on Safari or accessing the online edition, please e-mail customer-service@safaribooksonline.com



Adobe Press



Cisco Press



IBM Press

Microsoft Press



O'REILLY



QUE



SAMS



vmware PRESS

